

# HANDBOOK OF MARINE CRAFT HYDRODYNAMICS AND MOTION CONTROL

Vademecum de Navium Motu Contra Aquas et de  
Motu Gubernando

2nd edition

Final manuscript to be published in 2020

**Thor I. Fossen**

*Norwegian University of Science and Technology  
Trondheim, Norway*

DRAFT MANUSCRIPT

This edition first published 2020  
© 2020, John Wiley & Sons, Ltd

*Registered office*

John Wiley & Sons Ltd, The Atrium, Southern Gate, Chichester, West Sussex, PO19 8SQ, United Kingdom

For details of our global editorial offices, for customer services and for information about how to apply for permission to reuse the copyright material in this book please see our website at [www.wiley.com](http://www.wiley.com).

The right of the author to be identified as the author of this work has been asserted in accordance with the Copyright, Designs and Patents Act 1988.

All rights reserved. No part of this publication may be reproduced, stored in a retrieval system, or transmitted, in any form or by any means, electronic, mechanical, photocopying, recording or otherwise, except as permitted by the UK Copyright, Designs and Patents Act 1988, without the prior permission of the publisher.

Wiley also publishes its books in a variety of electronic formats. Some content that appears in print may not be available in electronic books.

Designations used by companies to distinguish their products are often claimed as trademarks. All brand names and product names used in this book are trade names, service marks, trademarks or registered trademarks of their respective owners. The publisher is not associated with any product or vendor mentioned in this book. This publication is designed to provide accurate and authoritative information in regard to the subject matter covered.

It is sold on the understanding that the publisher is not engaged in rendering professional services. If professional advice or other expert assistance is required, the services of a competent professional should be sought.

MATLAB® is a trademark of The MathWorks, Inc. and is used with permission. The MathWorks does not warrant the accuracy of the text or exercises in this book. This book's use or discussion of MATLAB® software or related products does not constitute endorsement or sponsorship by The MathWorks of a particular pedagogical approach or particular use of the MATLAB® software.

*Library of Congress Cataloguing-in-Publication Data*

Fossen, Thor I.

Handbook of Marine Craft Hydrodynamics and Motion Control / Thor Fossen.

p. cm.

Includes bibliographical references and index.

ISBN 978-1-119-99149-6 (hardback)

1. Ships—Hydrodynamics.
  2. Stability of ships.
  3. Motion control devices.
  4. Automatic pilot (Ships).
  5. Steering-gear.
  6. Ships—Electronic equipment.
- I. Title.  
VM156.F67 2011  
623.8'1—dc22

2010054228

A catalogue record for this book is available from the British Library.

Print ISBN: 9781119991496  
E-PDF ISBN: 9781119994121  
O-Book ISBN: 9781119994138  
E-Pub ISBN: 9781119998686  
Mobi ISBN: 9781119998693

Set in 9/11pt Times by Thomson Digital, Noida, India.

*This book is dedicated to my parents Gerd Kristine and Ole Johan Fossen and my family Heidi,  
Sindre and Lone Moa who have always been there for me.*

Thor I. Fossen

# Contents

<b>About the Author</b>	<b>xi</b>
<b>Preface</b>	<b>xiii</b>
<b>Tables</b>	<b>xv</b>
<b>I Marine Craft Hydrodynamics</b>	<b>1</b>
<b>1 Introduction</b>	<b>1</b>
1.1 Classification of Models . . . . .	5
1.2 The Classical Models in Naval Architecture . . . . .	6
1.2.1 Maneuvering theory . . . . .	7
1.2.2 Seakeeping theory . . . . .	10
1.2.3 Unified theory . . . . .	11
1.3 Fossen's Robot-Inspired Model for Marine Craft . . . . .	12
<b>2 Kinematics</b>	<b>15</b>
2.1 Kinematic Preliminaries . . . . .	16
2.1.1 Reference frames . . . . .	16
2.1.2 Body-Fixed reference points . . . . .	19
2.1.3 Generalized coordinates . . . . .	20
2.2 Transformations between BODY and NED . . . . .	22
2.2.1 Euler angle transformation . . . . .	24
2.2.2 Unit quaternions . . . . .	30
2.2.3 Unit Quaternion from Euler angles . . . . .	34
2.2.4 Euler angles from a unit quaternion . . . . .	35
2.3 Transformations between ECEF and NED . . . . .	36
2.3.1 Longitude and latitude rotation matrix . . . . .	36
2.3.2 Longitude, latitude and height from ECEF coordinates . . . . .	37
2.3.3 ECEF coordinates from longitude, latitude and height . . . . .	40
2.4 Transformations between ECEF and Flat-Earth Coordinates . . . . .	41
2.4.1 Longitude, latitude and height from flat-Earth coordinates . . . . .	41
2.4.2 Flat-Earth coordinates from longitude, latitude and height . . . . .	42

2.5	Transformations between BODY and FLOW . . . . .	42
2.5.1	Definitions of heading, course and crab angles . . . . .	43
2.5.2	Definitions of angle of attack and sideslip angle . . . . .	44
2.5.3	Flow-axes rotation matrix . . . . .	47
<b>3</b>	<b>Rigid-Body Kinetics</b>	<b>51</b>
3.1	Newton–Euler Equations of Motion about CG . . . . .	52
3.1.1	Translational motion about CG . . . . .	53
3.1.2	Rotational motion about CG . . . . .	54
3.1.3	Equations of motion about CG . . . . .	55
3.2	Newton–Euler Equations of Motion about CO . . . . .	55
3.2.1	Translational motion about CO . . . . .	56
3.2.2	Rotational motion about CO . . . . .	57
3.3	Rigid-Body Equations of Motion . . . . .	58
3.3.1	Nonlinear 6-DOF rigid-body equations of motion . . . . .	58
3.3.2	Linearized 6-DOF rigid-body equations of motion . . . . .	63
<b>4</b>	<b>Hydrostatics</b>	<b>65</b>
4.1	Restoring Forces for Underwater Vehicles . . . . .	65
4.1.1	Hydrostatics of submerged vehicles . . . . .	65
4.2	Restoring Forces for Surface Vessels . . . . .	68
4.2.1	Hydrostatics of floating vessels . . . . .	68
4.2.2	Linear (small angle) theory for boxed-shaped vessels . . . . .	70
4.2.3	Computation of metacenter heights for surface vessels . . . . .	73
4.3	Load Conditions and Natural Periods . . . . .	75
4.3.1	Decoupled computation of natural periods . . . . .	75
4.3.2	Computation of natural periods in a 6-DOF coupled system .	77
4.3.3	Natural periods as a function of load condition . . . . .	79
4.3.4	Free-surface effects . . . . .	82
4.3.5	Payload effects . . . . .	82
4.4	Seakeeping Analysis . . . . .	83
4.4.1	Harmonic oscillator with sinusoidal forcing . . . . .	83
4.4.2	Steady-state heave, roll and pitch responses in regular waves .	84
4.4.3	Explicit formulae for boxed-shaped vessels in regular waves .	86
4.4.4	Resonances in the heave, roll and pitch modes . . . . .	88
4.5	Ballast Systems . . . . .	89
4.5.1	Static conditions for trim and heel . . . . .	91
4.5.2	Automatic ballast control systems . . . . .	93
<b>5</b>	<b>Seakeeping Models</b>	<b>97</b>
5.1	Hydrodynamic Concepts and Potential Theory . . . . .	98
5.1.1	Numerical approaches and hydrodynamic codes . . . . .	100
5.2	Seakeeping and Maneuvering Kinematics . . . . .	102
5.2.1	Seakeeping reference frame . . . . .	102
5.2.2	Transformation between BODY and SEAKEEPING . . . . .	103
5.3	The Classical Frequency-Domain Model . . . . .	106

---

5.3.1	Frequency-dependent hydrodynamic coefficients . . . . .	107
5.3.2	Viscous damping . . . . .	111
5.3.3	Response amplitude operators . . . . .	113
5.4	Time-Domain Models including Fluid Memory Effects . . . . .	114
5.4.1	Cummins equation in SEAKEEPING coordinates . . . . .	114
5.4.2	Linear time-domain seakeeping equations in BODY coordinates	117
5.4.3	Nonlinear unified seakeeping and maneuvering model with fluid memory effects . . . . .	121
5.5	Identification of Fluid Memory Effects . . . . .	122
5.5.1	Frequency-domain identification using the MSS FDI toolbox .	123
<b>6</b>	<b>Maneuvering Models</b>	<b>127</b>
6.1	Rigid-Body Kinetics . . . . .	128
6.2	Potential Coefficients . . . . .	129
6.2.1	Frequency-independent added mass and potential damping .	131
6.2.2	Extension to 6-DOF models . . . . .	132
6.3	Added Mass Forces in a Rotating Coordinate System . . . . .	133
6.3.1	Lagrangian mechanics . . . . .	133
6.3.2	Kirchhoff's equations in vector form . . . . .	135
6.3.3	Added mass and Coriolis–centripetal matrices . . . . .	135
6.4	Dissipative Forces . . . . .	140
6.4.1	Linear viscous damping . . . . .	141
6.4.2	Nonlinear surge damping . . . . .	142
6.4.3	Cross-flow drag principle . . . . .	144
6.5	Ship Maneuvering Models (3 DOF) . . . . .	145
6.5.1	Nonlinear equations of motion . . . . .	146
6.5.2	Nonlinear maneuvering model based on surge resistance and cross-flow drag . . . . .	149
6.5.3	Nonlinear maneuvering model based on second-order modulus functions . . . . .	149
6.5.4	Nonlinear maneuvering model based on odd functions . . . .	151
6.5.5	Linear maneuvering model . . . . .	153
6.6	Ship Maneuvering Models including Roll (4 DOF) . . . . .	155
6.6.1	The nonlinear model of Son and Nomoto . . . . .	161
6.6.2	The nonlinear model of Blanke and Christensen . . . . .	162
6.7	Low-Speed Maneuvering Models for Dynamic Positioning (3 DOF)	163
6.7.1	Current coefficients . . . . .	163
6.7.2	Nonlinear DP model based on current coefficients . . . .	167
6.7.3	Linear DP model . . . . .	168
<b>7</b>	<b>Autopilot Models for Course and Heading Control</b>	<b>171</b>
7.1	Autopilot Models for Course Control . . . . .	172
7.1.1	State-space model . . . . .	172
7.1.2	Transfer function model . . . . .	173
7.2	Autopilot Models for Heading Control . . . . .	173
7.2.1	Second-order Nomoto model . . . . .	174

7.2.2	First-order Nomoto model . . . . .	175
7.2.3	Nonlinear extensions of Nomoto's model . . . . .	177
7.2.4	Pivot point . . . . .	178
<b>8</b>	<b>Models for Underwater Vehicles</b>	<b>181</b>
8.1	6-DOF Models for AUVs and ROVs . . . . .	181
8.1.1	Equations of motion expressed in BODY . . . . .	181
8.1.2	Equations of motion expressed in NED . . . . .	183
8.1.3	Properties of the 6-DOF model . . . . .	184
8.1.4	Symmetry considerations of the system inertia matrix . . . . .	186
8.2	Longitudinal and Lateral Models for Submarines . . . . .	187
8.2.1	Longitudinal subsystem . . . . .	188
8.2.2	Lateral subsystem . . . . .	189
8.3	Decoupled Models for "Flying Underwater Vehicles" . . . . .	191
8.3.1	Forward speed subsystem . . . . .	191
8.3.2	Course subsystem . . . . .	192
8.3.3	Pitch-depth subsystem . . . . .	192
8.4	Cylinder-Shaped Vehicles and Myring-Type Hulls . . . . .	193
8.4.1	Spheroid approximation . . . . .	194
8.5	Spherical-Shaped Vehicles . . . . .	199
<b>9</b>	<b>Control Forces and Moments</b>	<b>201</b>
9.1	Propellers as Thrust Devices . . . . .	201
9.1.1	Fixed-pitch propeller . . . . .	201
9.1.2	Controllable-pitch propeller . . . . .	204
9.2	Ship Propulsion Systems . . . . .	206
9.2.1	Podded propulsion units . . . . .	206
9.2.2	Prime mover system . . . . .	208
9.3	USV and Underwater Vehicle Propulsion Systems . . . . .	210
9.3.1	Propeller shaft speed models . . . . .	210
9.3.2	Motor armature current control . . . . .	212
9.3.3	Motor RPM control . . . . .	213
9.4	Thrusters . . . . .	214
9.4.1	Tunnel thrusters . . . . .	214
9.4.2	Azimuth thrusters . . . . .	215
9.5	Rudder in Propeller Slipstream . . . . .	218
9.5.1	Rudder forces and moment . . . . .	218
9.5.2	Steering machine dynamics . . . . .	221
9.6	Fin Stabilizers . . . . .	224
9.6.1	Fin stabilizers lift and drag forces . . . . .	224
9.6.2	Linear theory for roll moment . . . . .	225
9.7	Underwater Vehicle Control Surfaces . . . . .	226
9.7.1	Rudder . . . . .	227
9.7.2	Dive planes . . . . .	229
9.8	Control Moment Gyroscope . . . . .	229
9.8.1	Ship roll gyrostabilizer . . . . .	230

9.8.2 Control moment gyros for underwater vehicles . . . . .	232
9.9 Moving Mass . . . . .	236
<b>10 Environmental Forces and Moments</b>	<b>241</b>
10.1 Wind Forces and Moments . . . . .	242
10.1.1 Wind forces and moments on marine craft at rest . . . . .	243
10.1.2 Wind forces and moments on moving marine craft . . . . .	245
10.1.3 Wind coefficients based on flow over a Helmholtz–Kirchhoff plate . . . . .	246
10.1.4 Wind coefficients for merchant ships . . . . .	248
10.1.5 Wind coefficients for very large crude carriers . . . . .	249
10.1.6 Wind coefficients for large tankers and medium-sized ships . .	250
10.1.7 Wind coefficients for moored ships and floating structures .	251
10.2 Wave Forces and Moments . . . . .	251
10.2.1 Sea-state descriptions . . . . .	255
10.2.2 Wave spectra . . . . .	256
10.2.3 Wave amplitude response model . . . . .	267
10.2.4 Force RAOs . . . . .	269
10.2.5 Motion RAOs . . . . .	272
10.2.6 State-space models for wave response simulation . . . . .	277
10.3 Ocean Current Forces and Moments . . . . .	279
10.3.1 3-D irrotational ocean current model . . . . .	282
10.3.2 2-D irrotational ocean current model . . . . .	282
<b>Appendices</b>	<b>283</b>
<b>A Nonlinear Stability Theory</b>	<b>601</b>
A.1 Lyapunov Stability for Autonomous Systems . . . . .	601
A.1.1 Stability and convergence . . . . .	601
A.1.2 Lyapunov’s direct method . . . . .	603
A.1.3 Krasovskii–LaSalle’s theorem . . . . .	604
A.1.4 Global exponential stability . . . . .	605
A.2 Lyapunov Stability of Nonautonomous Systems . . . . .	606
A.2.1 Barbălat’s lemma . . . . .	606
A.2.2 LaSalle–Yoshizawa’s theorem . . . . .	606
A.2.3 UGAS when backstepping with integral action . . . . .	607
<b>B Numerical Methods</b>	<b>609</b>
B.1 Discretization of Continuous-Time Systems . . . . .	609
B.1.1 State-space models . . . . .	609
B.1.2 Computation of the transition matrix . . . . .	611
B.2 Numerical Integration Methods . . . . .	611
B.2.1 Euler’s method . . . . .	611
B.2.2 Adams–Bashford’s second-order method . . . . .	613
B.2.3 Runge–Kutta second-order method . . . . .	613

B.2.4	Runge–Kutta fourth-order method . . . . .	614
B.3	Numerical Differentiation . . . . .	614
<b>C</b>	<b>Model Transformations</b>	<b>615</b>
C.1	Transforming the Equations of Motion to an Arbitrarily Point . . . . .	615
C.1.1	System transformation matrix . . . . .	615
C.1.2	Equations of motion about an arbitrarily point . . . . .	617
C.1.3	Matrix and vector transformations . . . . .	617
<b>D</b>	<b>Nondimensional Equations of Motion</b>	<b>619</b>
D.1	Nondimensionalization . . . . .	619
D.1.1	Nondimensional hydrodynamic coefficients . . . . .	620
D.1.2	Nondimensional Nomoto models . . . . .	621
D.1.3	Nondimensional maneuvering models . . . . .	621
D.2	6-DOF Procedure for Nondimensionalization . . . . .	622
<b>References</b>		<b>627</b>
<b>Index</b>		<b>661</b>

# About the Author

Professor Thor I. Fossen received an MTech degree in Marine Technology in 1987 and a PhD in Engineering Cybernetics both from the Norwegian University of Science and Technology (NTNU). He has studied aerodynamics and flight control as a Fulbright Scholar at the University of Washington, Seattle.

His expertise is in the fields of robotics, autonomous systems, unmanned vehicles, hydrodynamics, naval architecture, marine and flight control systems, guidance systems, navigation systems and nonlinear control theory. He was appointed professor of guidance, navigation and control at NTNU at age 30. He has been visiting professor at University of California, San Diego (UCSD), University of California, Santa Barbara (UCSB) and the Technical University of Denmark (DTU). Professor Fossen has been elected to the Norwegian Academy of Technological Sciences (1998) and elevated to IEEE Fellow (2016). He is one of the founders of the company Marine Cybernetics (2002), which was acquired by DNV GL in 2014. He is also one of the founders of the company SCOUT Drone Inspection (2017). Professor Fossen is the author of the textbooks:

Fossen, T. I (2020). *Handbook of Marine Craft Hydrodynamics and Motion Control*, 2nd ed. John Wiley & Sons, Ltd. Chichester, UK.

Fossen, T. I (2011). *Handbook of Marine Craft Hydrodynamics and Motion Control*, 1st edition. John Wiley & Sons, Ltd. Chichester, UK.

Fossen, T. I (1994). *Guidance and Control of Ocean Vehicles*, John Wiley & Sons, Ltd. Chichester, UK.

and co-author of the editorials:

Fossen, T. I, K. Y. Pettersen and H. Nijmeijer (2017). *Sensing and Control for Autonomous Vehicles*, Springer Verlag.

Fossen, T. I and H. Nijmeijer (2012). *Parametric Resonance in Dynamical Systems*, Springer Verlag.

Nijmeijer, H. and T. I. Fossen (1999). *New Directions in Nonlinear Observer Design*, Springer Verlag.

Professor Fossen has been instrumental in the development of several industrial autopilot, path-following and dynamic positioning (DP) systems. He has also experience in nonlinear state estimators for marine craft and automotive systems as well as strapdown

GNSS/INS navigation systems for ships and aerial vehicles. He received the Automatica Prize Paper Award in 2002 for a concept for weather optimal positioning control of marine craft. In 2008 he received the Arch T. Colwell Merit Award at the SAE 2008 World Congress.

He is currently professor of guidance, navigation and control in the Department of Engineering Cybernetics, NTNU.

# Preface

The main motivation for writing the second edition of this book was to include recent results on hydrodynamic modeling, guidance, navigation and control of marine craft.

The Wiley book from 1994 was the first attempt to bring hydrodynamic modeling and control system design into a unified notation for modeling, simulation and control. My first book also contains state-of-the-art linear and nonlinear design methods for ships and underwater vehicles up to 1994. In the period 1994–2011 a great deal of work was done on nonlinear control of marine craft. This work resulted in many useful results and lecture notes, which have been collected and included in the *Handbook of Marine Craft Hydrodynamics and Motion Control*. The first edition was published in 2011 and it was used as the main textbook in my course on “Guidance and Control of Vehicles” at the Norwegian University of Science and Technology (NTNU) until 2020. Then it was replaced by the second edition, which contains many updates and new sections on line-of-sight guidance, propulsion systems, inertial navigation, sensor fusion and feedback control. The second edition of the book contains new chapters on autopilot models, underwater vehicle modeling and control forces as well as two appendices.

## Accompanying Matlab software and lecture notes

In 2019 the Marine Systems Simulator (MSS), which is an open source Matlab toolbox, was migrated to *GitHub* in order to improve version control and support incremental software updates. The Matlab software accompanying the book can be downloaded from the repository:

MSS toolbox: <http://github.com/cybergalactic/MSS>

The second edition of the book is fully compliant with the new features of the MSS toolbox and the book contains many examples using the MSS toolbox. A complete set of lecture notes using examples from the MSS toolbox is complementary. The lecture notes can be downloaded from:

Lecture notes: <http://www.fossen.biz/wiley>

## Preview of the book

Part I of the book covers maneuvering and seakeeping theory and it is explained in detail how the equations of motion can be derived for both cases using both frequency- and time-domain formulations. This includes transformations from the frequency to

the time domain and the explanation of fluid-memory effects. A great effort has been made in the development of kinematic equations for effective representation of the equations of motion in seakeeping, body, inertial and geographical coordinates. This is very confusing in the existing literature on hydrodynamics and the need to explain this properly motivated me to find a unifying notation for marine and mechanical systems. This was done in the period 2002–2010 and it is inspired by the elegant formulation used in robotics where systems are represented in a matrix-vector notation. The unified notation dates back to my PhD thesis, which was published in 1991.

Part II of the book covers guidance systems, navigation systems, state estimators and control of marine craft. This second part of the book focuses on state-of-the-art methods for feedback control such as PID control design for linear and nonlinear systems as well as control allocation methods. A chapter with more advanced topics, such as optimal control theory, backstepping, feedback linearization and sliding-mode control, is included for the advanced reader. Case studies and applications are treated at the end of each chapter. The control systems based on PID and optimal control theory are designed with a complexity similar to those used in many industrial systems. The more advanced methods using nonlinear theory are included so the user can compare linear and nonlinear design techniques before a final implementation is made. Many references to existing systems are included so control system vendors can easily find articles describing state-of-the art design methods for marine craft.

### Acknowledgments

Most of the results in the book have been developed at the Department of Engineering Cybernetics, NTNU, in close cooperation with a large number of my former doctoral students. Our joint efforts have resulted in several patents, industrial implementations and spin-off companies.

The results on maneuvering and seakeeping are joint work with *Dr. Tristan Perez*, Boeing Research and Technology, Australia. The work with Dr. Perez has resulted in several joint publications and I am grateful to him for numerous interesting discussions on hydrodynamic modeling and control.

I am particular grateful to *Professor Tor Arne Johansen* who have co-authored a large number of my publications. Many of our joint results are included in the second edition of the book. *Dr. Morten Breivik* and *Ass. Professor Anastasios Lekkas* have contributed with many important results on guidance systems. *Professor Mogens Blanke* was instrumental in the development of the sections on maneuvering, roll damping and propulsion theory. *Ass. Professor Torleiv H. Bryne* should be thanked for important contributions on ship control and inertial navigation systems, while *Bjarne Stenberg* should be thanked for creating the artistic front and back covers of the book and many other graphical illustrations. Finally, *Stewart Clark* should be thanked for his assistance with the English language. The book project has been sponsored by the Norwegian Research Council through the author's affiliation as key scientist at the Center of Ships and Ocean Structures (2002-2012) and co-director of the Center of Autonomous Marine Operations and Systems since 2012.

**Thor I. Fossen**

# List of Tables

2.1	The notation of SNAME (1950) for marine vessels . . . . .	16
2.2	WGS-84 parameters . . . . .	38
7.1	Parameters for a cargo ship and a fully loaded oil tanker . . . . .	176
10.1	Air density as a function of temperature . . . . .	244
10.2	Definition of Beaufort numbers (Price and Bishop, 1974) . . . . .	245
10.3	Coefficients of lateral and longitudinal resistance, cross-force and rolling moment (Blendermann, 1994). . . . .	246
10.4	Wind force parameters in surge, sway and yaw (Isherwood, 1972) . .	252
10.4	(Continued) . . . . .	253
10.5	Definition of sea-state (SS) codes (Price and Bishop, 1974). Notice that the percentage probability for SS codes 0, 1 and 2 is summarized.	255
A.1	Classification of theorems for stability and convergence . . . . .	602
D.1	Prime and Bis system variables used for nondimensionalization. . . .	620
D.2	Variables used for nondimensionalization of 6-DOF models. . . . .	623



## Part I

# Marine Craft Hydrodynamics

*De Navium Motu Contra Aquas*

DRAFT MANUSCRIPT

# Chapter 1

## Introduction

The subject of this book is *motion control and hydrodynamics of marine craft*. The term marine craft includes ships, high-speed craft, semi-submersibles, floating rigs, submarines, remotely operated and autonomous underwater vehicles, torpedoes, and other propelled and powered structures, for instance a floating air field. Offshore operations involve the use of many marine craft, as shown in Figure 1.1. Vehicles that do not travel on land (ocean and flight vehicles) are usually called craft, such as watercraft, sailcraft, aircraft, hovercraft and spacecraft. The term vessel can be defined as follows:

*Vessel*: “hollow structure made to float upon the water for purposes of transportation and navigation; especially, one that is larger than a row-boat.”

The words *vessel*, *ship* and *boat* are often used interchangeably. In *Encyclopedia Britannica*, a ship and a boat are distinguished by their size through the following definition:

*Ship*: “any large floating vessel capable of crossing open waters, as opposed to a boat, which is generally a smaller craft. The term formerly was applied to sailing vessels having three or more masts; in modern times it usually denotes a vessel of more than 500 tons of displacement. Submersible ships are generally called boats regardless of their size.”

Similar definitions are given for submerged vehicles:

*Submarine*: “any naval vessel that is capable of propelling itself beneath the water as well as on the water’s surface. This is a unique capability among warships, and submarines are quite different in design and appearance from surface ships.”

*Underwater Vehicle*: “small vehicle that is capable of propelling itself beneath the water surface as well as on the water’s surface. This includes unmanned underwater vehicles (UUV), remotely operated vehicles (ROV), autonomous underwater vehicles (AUV) and underwater robotic vehicles (URV). Underwater vehicles are used both commercially and by the navy.”



Figure 1.1: Marine craft in operation. Illustration Bjarne Stenberg.

From a hydrodynamic point of view, marine craft can be classified according to their maximum operating speed. For this purpose it is common to use the *Froude number*

$$F_n := \frac{U}{\sqrt{gL}} \quad (1.1)$$

where  $U$  is the craft speed,  $L$  is the overall submerged length of the craft and  $g$  is the acceleration of gravity. The pressure carrying the craft can be divided into *hydrostatic* and *hydrodynamic* pressure. The corresponding forces are:

- Buoyancy force due to the hydrostatic pressure (proportional to the displacement of the ship).
- Hydrodynamic force due to the hydrodynamic pressure (approximately proportional to the square of the relative speed to the water).

For a marine craft sailing at constant speed  $U$ , the following classifications can be made (Faltinsen, 2005):

**Displacement Vessel ( $F_n < 0.4$ ):** The buoyancy force (restoring terms) dominates relative to the hydrodynamic forces (added mass and damping).

**Semi-displacement Vessel ( $0.4-0.5 < F_n < 1.0-1.2$ ):** The buoyancy force is not dominant at the maximum operating speed for a high-speed submerged hull type of craft.

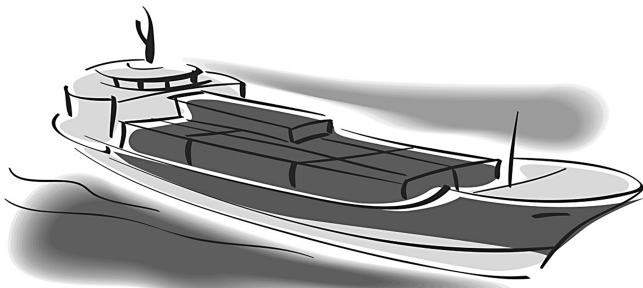


Figure 1.2: Displacement vessel.

**Planing Vessel ( $F_n > 1.0 - 1.2$ ):** The hydrodynamic force mainly carries the weight.

There will be strong flow separation and the aerodynamic lift and drag forces start playing a role.

In this book only displacement vessels are covered; see Figure 1.2.

The Froude number has influence on the hydrodynamic analysis. For displacement vessels, the waves radiated by different parts of the hull do not influence other parts of the hull. For semi-displacement vessels, waves generated at the bow influence the hydrodynamic pressure along the hull towards the stern. These characteristics give rise to different modeling hypotheses, which lead to different hydrodynamic theories.

For displacement ships it is widely accepted to use two- and three-dimensional potential theory programs to compute the potential coefficients and wave loads; see Section 5.1. For semi-displacement vessels and planing vessels it is important to include the lift and drag forces in the computations (Faltinsen, 2005).

### Degrees of freedom and motion of a marine craft

In maneuvering, a marine craft experiences motion in 6 degrees of freedom (DOFs); see Section 9.4. The DOFs are the set of independent displacements and rotations that specify completely the displaced position and orientation of the craft. The motion in the horizontal plane is referred to as *surge* (longitudinal motion, usually superimposed on the steady propulsive motion) and *sway* (sideways motion). *Yaw* (rotation about the vertical axis) describes the heading of the craft. The remaining three DOFs are *roll* (rotation about the longitudinal axis), *pitch* (rotation about the transverse axis) and *heave* (vertical motion); see Figure 1.3.

Roll motion is probably the most influential DOF with regards to human performance, since it produces the highest accelerations and, hence, is the principal villain in seasickness. Similarly, pitching and heaving feel uncomfortable to people. When designing ship autopilots, yaw is the primary mode for feedback control. Stationkeeping of a marine craft implies stabilization of the surge, sway and yaw motions.

When designing feedback control systems for marine craft, reduced-order models are often used since most craft do not have actuation in all DOF. This is usually done by decoupling the motions of the craft according to:

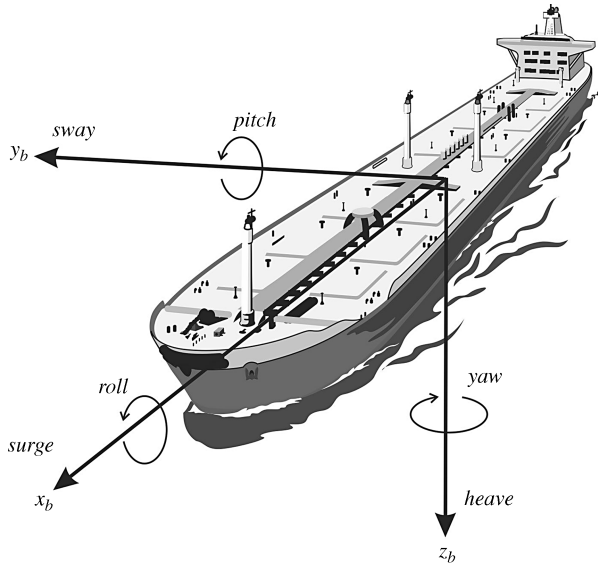


Figure 1.3: Motion in 6 degrees of freedom (DOF).

**1-DOF** models can be used to design forward speed controllers (*surge*), heading autopilots (*yaw*) and roll damping systems (*roll*).

**3-DOF** models are usually:

- Horizontal-plane models (*surge*, *sway* and *yaw*) for ships, semisubmersibles and underwater vehicles that are used in dynamic positioning systems, trajectory-tracking control systems and path-following systems. For slender bodies such as submarines, it is also common to assume that the motions can be decoupled into *longitudinal* and *lateral* motions.
- Longitudinal models (*surge*, *heave* and *pitch*) for forward speed, diving and pitch control.
- Lateral models (*sway*, *roll* and *yaw*) for turning and heading control.

**4-DOF** models (*surge*, *sway*, *roll* and *yaw*) are usually formed by adding the roll equation to the 3-DOF horizontal-plane model. These models are used in maneuvering situations where it is important to include the rolling motion, usually in order to reduce roll by active control of fins, rudders or stabilizing liquid tanks.

**6-DOF** models (*surge*, *sway*, *heave*, *roll*, *pitch* and *yaw*) are fully coupled equations of motion used for simulation and prediction of coupled vehicle motions. These models can also be used in advanced control systems for underwater vehicles that are actuated in all DOF.

## 1.1 Classification of Models

The models in this book can be used for prediction, real-time simulation, decision support systems, situational awareness as well as controller-observer design. The complexity and number of differential equations needed for the various purposes will vary. Consequently, one can distinguish between three types of models (see Figure 1.4):

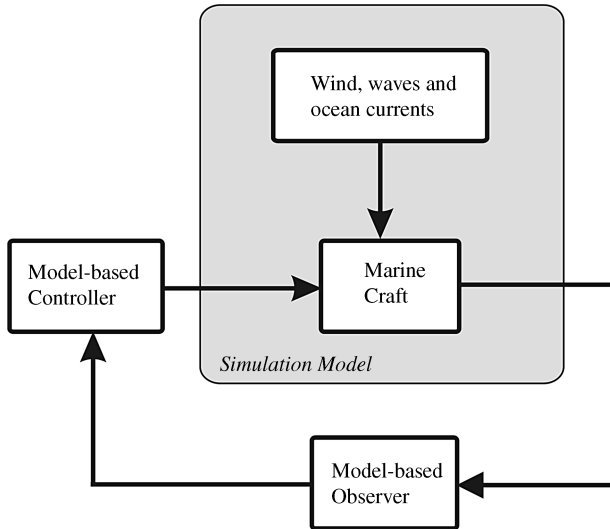


Figure 1.4: Models used in guidance, navigation and control.

**Simulation model:** This model is the most accurate description of a system, for instance a 6-DOF *high-fidelity model* for simulation of coupled motions in the time domain. It includes the marine craft dynamics, propulsion system, measurement system and the environmental forces due to wind, waves and ocean currents. It also includes other features not used for control and observer design that have a direct impact on model accuracy. The simulation model should be able to reconstruct the time responses of the real system and it should also be possible to trigger failure modes to simulate events such as accidents and erroneous signals. Simulation models where the fluid-memory effects are included due to frequency-dependent added mass and potential damping typically consist of 50–200 ordinary differential equations (ODEs) while a maneuvering model can be represented in 6 DOF with 12 ODEs for generalized position and velocity. In addition, some states are needed to describe the environmental forces and actuators, but still the number of states will be less than 50 for a marine craft.

**Control design model:** The controller model is a reduced-order or simplified version of the simulation model that is used to design the *motion control system*. In its simplest form, this model is used to compute a set of constant gains for a proportional, integral, derivative (PID) controller. More sophisticated control systems

use a dynamic model to generate feedforward and feedback signals. This is referred to as *model-based control*. The number of ODEs used in conventional model-based ship control systems is usually less than 20. A PID controller typically requires two states: one for the integrator and one for the low-pass filter used to limit noise amplification. Consequently, setpoint regulation in 6 DOF can be implemented by using 12 ODEs. However, trajectory-tracking controllers require additional states for feedforward as well as filtering so higher-order control laws are not uncommon.

**Observer design model:** The observer model will in general be different from the model used in the controller since the purpose is to capture the additional dynamics associated with the sensors and navigation systems as well as disturbances. It is a simplified version of the simulation model where attention is given to accurate modeling of measurement noise, failure situations including dead-reckoning capabilities, filtering and motion prediction. For marine craft, the *model-based observer* often includes a disturbance model where the goal is to estimate wave, wind and ocean current forces by treating these as colored noise. For marine craft the number of ODEs in the state estimator will typically be 20 for a dynamic positioning (DP) system while a basic heading autopilot is implemented with less than five states.

## 1.2 The Classical Models in Naval Architecture

The motions of a marine craft exposed to wind, waves and ocean currents takes place in 6 DOF. The equations of motion can be derived using the Newton–Euler or Lagrange equations. The equations of motion are used to simulate ships, high-speed craft, underwater vehicles and floating structures operating under or on the water surface, as shown in Figure 1.5. In Section 3.3 it is shown that a rigid body with constant mass  $m$  and center of gravity ( $x_g, y_g, z_g$ ) relative to a fixed point on the hull can be described by the following coupled differential equations

$$\begin{aligned} m [\dot{u} - vr + wq - x_g(q^2 + r^2) + y_g(pq - \dot{r}) + z_g(pr + \dot{q})] &= X \\ m [\dot{v} - wp + ur - y_g(r^2 + p^2) + z_g(qr - \dot{p}) + x_g(qp + \dot{r})] &= Y \\ m [\dot{w} - uq + vp - z_g(p^2 + q^2) + x_g(rp - \dot{q}) + y_g(rq + \dot{p})] &= Z \\ I_x \ddot{p} + (I_z - I_y)qr - (\dot{r} + pq)I_{xz} + (r^2 - q^2)I_{yz} + (pr - \dot{q})I_{xy} \\ &\quad + m [y_g(\dot{w} - uq + vp) - z_g(\dot{v} - wp + ur)] = K \quad (1.2) \\ I_y \ddot{q} + (I_x - I_z)rp - (\dot{p} + qr)I_{xy} + (p^2 - r^2)I_{zx} + (qp - \dot{r})I_{yz} \\ &\quad + m [z_g(\dot{u} - vr + wq) - x_g(\dot{w} - uq + vp)] = M \\ I_z \ddot{r} + (I_y - I_x)pq - (\dot{q} + rp)I_{yz} + (q^2 - p^2)I_{xy} + (rq - \dot{p})I_{zx} \\ &\quad + m [x_g(\dot{v} - wp + ur) - y_g(\dot{u} - vr + wq)] = N \end{aligned}$$

where  $X, Y, Z, K, M$  and  $N$  denote the external forces and moments. This model is the basis for time-domain simulation of marine craft. The external forces and moments acting on a marine craft are usually modeled by using:



Figure 1.5: Ship and semi-submersibles operating offshore. Illustration Bjarne Stenberg.

**Maneuvering theory:** The study of a ship moving at constant positive speed  $U$  in calm water within the framework of maneuvering theory is based on the assumption that the maneuvering (hydrodynamic) coefficients are *frequency independent* (no wave excitation). The maneuvering model will in its simplest representation be linear while nonlinear representations can be derived using methods such as cross-flow drag, quadratic damping or Taylor-series expansions; see Chapter 6.

**Seakeeping theory:** The motions of ships at zero or constant speed in waves can be analyzed using seakeeping theory where the hydrodynamic coefficients and wave forces are computed as a function of the wave excitation frequency using the hull geometry and mass distribution. The seakeeping models are usually derived within a linear framework (Chapter 5) while the extension to nonlinear theory is an important field of research.

For underwater vehicles operating below the wave-affected zone, the wave excitation frequency will not affect the hydrodynamic mass and damping coefficients. Consequently, it is common to model underwater vehicles with constant hydrodynamic coefficients similar to a maneuvering ship.

### 1.2.1 Maneuvering theory

Maneuvering theory assumes that the ship is moving in restricted calm water, that is in sheltered waters or in a harbor. Hence, the maneuvering model is derived for a ship

moving at positive speed  $U$  under a zero-frequency wave excitation assumption such that added mass and damping can be represented by using hydrodynamic derivatives (constant parameters). The zero-frequency assumption is only valid for *surge*, *sway* and *yaw* since the natural periods of a PD-controlled ship will be in the range of 100–150 s. For 150 s the natural frequency is close to zero, that is

$$\omega_n = \frac{2\pi}{T} \approx 0.04 \text{ rad/s} \quad (1.3)$$

This clearly gives support for the zero-frequency assumption. The natural frequencies in *heave*, *roll* and *pitch* are much higher so it is recommended to use the zero-frequency potential coefficients in these modes. For instance, a ship with a roll period of 10 s will have a natural frequency of 0.628 rad/s which clearly violates the zero-frequency assumption. This means that hydrodynamic added mass and potential damping should be evaluated at a frequency of 0.628 rad/s in roll if a pure rolling motion is considered. As a consequence of this, it is common to formulate the ship maneuvering model (1.2) as a coupled *surge–sway–yaw* model and thus neglect heave, roll and pitch motions. Moreover,

$$\begin{aligned} m(\dot{u} - vr - x_g r^2 - y_g \dot{r}) &= X \\ m(\dot{v} + ur - y_g r^2 + x_g \dot{r}) &= Y \\ I_z \ddot{r} + m(x_g(\dot{v} + ur) - y_g(\dot{u} - vr)) &= N \end{aligned} \quad (1.4)$$

The rigid-body kinetics (1.4) can be expressed in vectorial form according to (Fossen, 1994)

$$\boldsymbol{M}_{RB}\dot{\boldsymbol{\nu}} + \boldsymbol{C}_{RB}(\boldsymbol{\nu})\boldsymbol{\nu} = \boldsymbol{\tau}_{RB} \quad (1.5)$$

$$\boldsymbol{\tau}_{RB} = \underbrace{\boldsymbol{\tau}_{\text{hyd}} + \boldsymbol{\tau}_{\text{hs}}}_{\substack{\text{hydrodynamic and} \\ \text{hydrostatic forces}}} + \underbrace{\boldsymbol{\tau}_{\text{wind}} + \boldsymbol{\tau}_{\text{wave}}}_{\substack{\text{environmental forces}}} + \boldsymbol{\tau}_{\text{control}} \quad (1.6)$$

where  $\boldsymbol{M}_{RB}$  is the rigid-body inertia matrix,  $\boldsymbol{C}_{RB}(\boldsymbol{\nu})$  is a matrix of rigid-body Coriolis and centripetal forces and  $\boldsymbol{\tau}_{RB}$  is a vector of generalized forces.

The generalized velocity is

$$\boldsymbol{\nu} = [u, v, w, p, q, r]^\top \quad (1.7)$$

where the first three components ( $u, v, w$ ) are the linear velocities in surge, sway and heave and ( $p, q, r$ ) are the angular velocities in roll, pitch and yaw. The generalized force acting on the craft is

$$\boldsymbol{\tau}_i = [X_i, Y_i, Z_i, K_i, M_i, N_i]^\top, \quad i \in \{\text{hyd, hs, wind, wave, control}\} \quad (1.8)$$

where the subscripts stand for

- Hydrodynamic added mass, potential damping due to wave radiation and viscous damping
- Hydrostatic forces (spring stiffness)
- Wind forces

- Wave forces (first and second order)
- Control and propulsion forces

This model is motivated by Newton's second law:  $F = ma$ , where  $F$  represents force,  $m$  is the mass and  $a$  is the acceleration. The Coriolis and centripetal term is due to the rotation of the body-fixed reference frame with respect to the inertial reference frame. The model (1.5) is used in most textbooks on hydrodynamics and the generalized hydrodynamic force  $\tau_{hyd}$  can be represented by linear or nonlinear theory.

### Linearized models

In the linear 6-DOF case there will be a total of 36 mass and 36 damping elements proportional to velocity and acceleration. In addition to this, there will be restoring forces, propulsion forces and environmental forces. If the generalized hydrodynamic force  $\tau_{hyd}$  is written in component form using the SNAME (1950) notation, the linear added mass and damping forces become

$$\begin{aligned} X_1 &= X_u u + X_v v + X_w w + X_p p + X_q q + X_r r \\ &\quad + X_{\dot{u}} \dot{u} + X_{\dot{v}} \dot{v} + X_{\dot{w}} \dot{w} + X_{\dot{p}} \dot{p} + X_{\dot{q}} \dot{q} + X_{\dot{r}} \dot{r} \end{aligned} \quad (1.9)$$

⋮

$$\begin{aligned} N_1 &= N_u u + N_v v + N_w w + N_p p + N_q q + N_r r \\ &\quad + N_{\dot{u}} \dot{u} + N_{\dot{v}} \dot{v} + N_{\dot{w}} \dot{w} + N_{\dot{p}} \dot{p} + N_{\dot{q}} \dot{q} + N_{\dot{r}} \dot{r} \end{aligned} \quad (1.10)$$

where  $X_u, X_v, \dots, N_r$  are the linear damping coefficients and  $X_{\dot{u}}, X_{\dot{v}}, \dots, N_{\dot{r}}$  represent hydrodynamic added mass.

### Nonlinear models

Application of nonlinear theory implies that many elements must be included in addition to the 36 linear elements. This is usually done by one of the following methods:

- *Truncated Taylor-series expansions* using *odd terms* (first and third order) which are fitted to experimental data, for instance (Abkowitz 1964)

$$X_1 = X_{\dot{u}} \dot{u} + X_u u + X_{uuu} u^3 + X_{\dot{v}} \dot{v} + X_v v + X_{vvv} v^3 + \dots \quad (1.11)$$

⋮

$$N_1 = N_{\dot{u}} \dot{u} + N_u u + N_{uuu} u^3 + N_{\dot{v}} \dot{v} + N_v v + N_{vvv} v^3 + \dots \quad (1.12)$$

In this approach added mass is assumed to be linear and damping is modeled by a third order odd function. Alternatively, *second-order modulus terms* can be used (Fedyaevsky and Sobolev 1963), for instance

$$X_1 = X_{\dot{u}} \dot{u} + X_u u + X_{|u|u} |u| u + X_{\dot{v}} \dot{v} + X_v v + X_{|v|v} |v| v + \dots \quad (1.13)$$

⋮

$$N_1 = N_{\dot{u}} \dot{u} + N_u u + N_{|u|u} |u| u + N_{\dot{v}} \dot{v} + N_v v + N_{|v|v} |v| v + \dots \quad (1.14)$$

This is motivated by the square-law damping terms in fluid dynamics and aerodynamics. When applying Taylor-series expansions in model-based control design, the system (1.5) becomes relatively complicated due to the large number of hydrodynamic coefficients on the right-hand side needed to represent the hydrodynamic forces. This approach is quite common when deriving maneuvering models and many of the coefficients are difficult to determine with sufficient accuracy since the model can be overparametrized. Taylor-series expansions are frequently used in commercial planar motion mechanism (PMM) tests where the purpose is to derive the maneuvering coefficients experimentally.

- *First principles* where hydrodynamic effects such as lift and drag are modeled using well established models. This results in physically sound Lagrangian models that preserve energy properties. Models based on first principles usually require a much smaller number of parameters than models based on third order Taylor-series expansions.

### 1.2.2 Seakeeping theory

As explained above, maneuvering refers to the study of ship motion in the absence of wave excitation (calm water). Seakeeping, on the other hand, is the study of motion when there is wave excitation and the craft keeps its heading  $\psi$  and its speed  $U$  constant (which includes the case of zero speed). This introduces a dissipative force (Cummins 1962) known as *fluid-memory effects*. Although both areas are concerned with the same issues, study of motion, stability and control, the separation allows different assumptions to be made that simplify the study in each case. Seakeeping analysis is used in capability analysis and operability calculations to obtain operability diagrams according to the adopted criteria.

The seakeeping theory is formulated using seakeeping axes  $\{s\}$  where the state vector  $\xi = [\xi_1, \xi_2, \xi_3, \xi_4, \xi_5, \xi_6]^\top$  represents perturbations with respect to a fixed equilibrium state; see Figure 1.6. These perturbations can be related to motions in the body frame  $\{b\}$  and North-East-Down frame  $\{n\}$  by using kinematic transformations; see Section 5.2. The governing model is formulated in the time domain using the *Cummins equation* in the following form (see Section 5.4):

$$[\mathbf{M}_{RB} + \mathbf{A}(\infty)]\ddot{\xi} + \mathbf{B}_{total}(\infty)\dot{\xi} + \int_0^t \mathbf{K}(t-\tau)\dot{\xi}(\tau)d\tau + \mathbf{C}\xi = \boldsymbol{\tau}_{wind} + \boldsymbol{\tau}_{wave} + \delta\boldsymbol{\tau} \quad (1.15)$$

where  $\delta\boldsymbol{\tau}$  is the perturbed control input due to propulsion and control surfaces,  $\mathbf{A}(\infty)$  is the infinite-frequency added mass matrix,  $\mathbf{B}_{total}(\infty) = \mathbf{B}(\infty) + \mathbf{B}_V(\infty)$  is the infinite-frequency damping matrix containing potential and viscous damping terms,  $\mathbf{C}$  is the spring stiffness matrix and  $\mathbf{K}(t)$  is a time-varying matrix of *retardation functions* given by

$$\mathbf{K}(t) = \frac{2}{\pi} \int_0^\infty [\mathbf{B}_{total}(\omega) - \mathbf{B}_{total}(\infty)] \cos(\omega t) d\omega \quad (1.16)$$

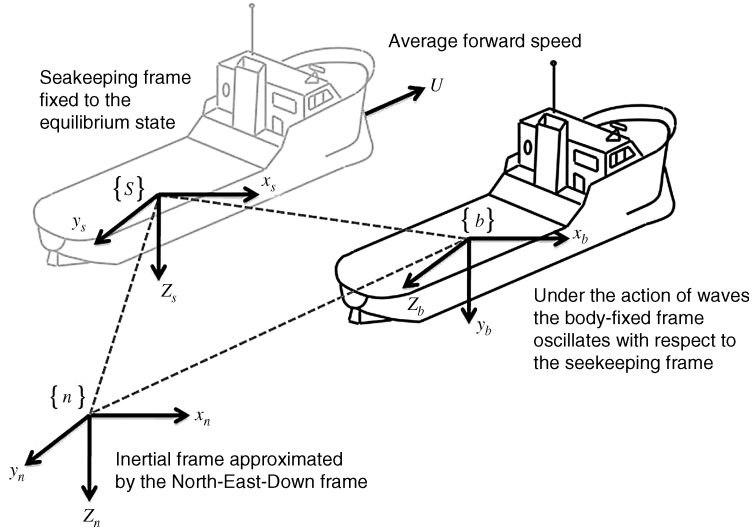


Figure 1.6: Coordinate systems used in seakeeping analysis.

The frequency-domain representation of (1.15) is (Newman, 1977; Faltinsen, 1990)

$$(-\omega^2[M_{RB} + A(\omega)] - j\omega B_{\text{total}}(\omega) + C)\xi(j\omega) = \tau_{\text{wind}}(j\omega) + \tau_{\text{wave}}(j\omega) + \delta\tau(j\omega) \quad (1.17)$$

where  $\xi(j\omega)$  is a complex vector

$$\xi(j\omega) = \bar{\xi} e^{(j\omega t)} \quad (1.18)$$

Similarly, the external signals  $\tau_{\text{wind}}(j\omega)$ ,  $\tau_{\text{wave}}(j\omega)$  and  $\delta\tau(j\omega)$  are complex vectors.

Naval architects often write the seakeeping model as a *pseudo-differential equation*:

$$[M_{RB} + A(\omega)]\ddot{\xi} + B_{\text{total}}(\omega)\dot{\xi} + C\xi = \tau_{\text{wind}} + \tau_{\text{wave}} + \delta\tau \quad (1.19)$$

mixing time and frequency. Unfortunately this is deeply rooted in the literature of hydrodynamics even though it is not correct to mix time and frequency in one single equation. Consequently, it is recommended to use the time- and frequency-domain representations (1.15) and (1.17).

Computer simulations are done under the assumptions of linear theory and harmonic motions such that the resulting response is linear in the time domain. This approach dates back to Cummins (1962) and the necessary derivations are described in Chapter 5.

### 1.2.3 Unified theory

A unified theory for maneuvering and seakeeping is useful since it allows for time-domain simulation of a marine craft in a seaway. This is usually done by using the seakeeping representation (1.19) as described in Chapter 5. The next step is to assume

linear superposition such that wave-induced forces can be added for different speeds  $U$  and sea states. A similar assumption is used to add nonlinear damping and restoring forces so that the resulting model is a unified nonlinear model combining the most important terms from both maneuvering and seakeeping. Care must be taken with respect to “double counting.” This refers to the problem that hydrodynamic effects can be modeled twice when merging the results from two theories. The procedure is described in details by Fossen (2005).

### 1.3 Fossen’s Robot-Inspired Model for Marine Craft

In order to exploit the physical properties of the maneuvering and seakeeping models, the equations of motion are represented in a vectorial setting which dates back to Fossen (1991). The matrix-vector model is expressed in  $\{b\}$  and  $\{n\}$  so appropriate kinematic transformations between the reference frames  $\{b\}$ ,  $\{n\}$  and  $\{s\}$  must be derived. This is done in Chapters 2 and 5. The matrix-vector model is well suited for computer implementation and control systems design.

#### Component form

The classical model (1.2) is often combined with expressions such as (1.9)–(1.10) or (1.11)–(1.14) to describe the hydrodynamic forces. This often results in complicated models with hundreds of elements. In most textbooks the resulting equations of motion are on component form. The following introduces a compact notation using matrices and vectors that will simplify the representation of the equations of motion considerably.

#### Matrix-vector representation

In order to exploit the physical properties of the models, the equations of motion are represented in a matrix-vector setting. It is often beneficial to exploit physical system properties to reduce the number of coefficients needed for control. This is the main motivation for developing a vectorial representation of the equations of motion. In Fossen (1991) the robot model (Craig, 1989; Sciavicco and Siciliano, 1996)

$$\mathbf{M}(\mathbf{q})\ddot{\mathbf{q}} + \mathbf{C}(\mathbf{q}, \dot{\mathbf{q}})\mathbf{q} = \boldsymbol{\tau} \quad (1.20)$$

was used as motivation to derive a compact marine craft model in 6 DOFs using a vectorial setting. In the robot model  $\mathbf{q}$  is a vector of joint angles,  $\boldsymbol{\tau}$  is the torque, while  $\mathbf{M}$  and  $\mathbf{C}$  denote the system inertia and Coriolis matrices, respectively. It is found that similar quantities can be identified for marine craft and aircraft. In Fossen (1991) a complete 6-DOF vectorial setting for marine craft was derived based on these ideas. These results were further refined by Sagatun and Fossen (1991), Fossen (1994) and Fossen and Fjellstad (1995). The 6-DOF models considered in this book use the following representation

$$\mathbf{M}\dot{\boldsymbol{\nu}} + \mathbf{C}(\boldsymbol{\nu})\boldsymbol{\nu} + \mathbf{D}(\boldsymbol{\nu})\boldsymbol{\nu} + \mathbf{g}(\boldsymbol{\eta}) + \mathbf{g}_0 = \boldsymbol{\tau} + \boldsymbol{\tau}_{\text{wind}} + \boldsymbol{\tau}_{\text{wave}} \quad (1.21)$$

where

$$\boldsymbol{\eta} = [x^n, y^n, z^n, \phi, \theta, \psi]^\top \quad (1.22)$$

$$\boldsymbol{\nu} = [u, v, w, p, q, r]^\top \quad (1.23)$$

are vectors of velocities and position/Euler angles, respectively. In fact  $\boldsymbol{\nu}$  and  $\boldsymbol{\eta}$  are generalized velocities and positions used to describe motions in 6 DOF. Similarly,  $\boldsymbol{\tau}$  is a vector of forces and moments or the generalized forces in 6 DOF. The model matrices  $\mathbf{M}$ ,  $\mathbf{C}(\boldsymbol{\nu})$  and  $\mathbf{D}(\boldsymbol{\nu})$  denote inertia, Coriolis and damping, respectively, while  $\mathbf{g}(\boldsymbol{\eta})$  is a vector of generalized gravitational and buoyancy forces. Static restoring forces and moments due to ballast systems and water tanks are collected in the term  $\mathbf{g}_0$ .

### Component form versus matrix-vector representation

When designing control systems, there are clear advantages using the vectorial model (1.21) instead of (1.5)–(1.6) and the component forms of the Taylor-series expansions (1.11)–(1.14). The main reasons are that system properties such as symmetry, skew-symmetry and positiveness of matrices can be incorporated into the stability analysis. In addition, these properties are related to passivity of the hydrodynamic and rigid-body models (Berge and Fossen 2000). The system properties represent physical properties of the system, which should be exploited when designing controllers and observers for marine craft. As a consequence, Equation (1.21) is chosen as the foundation for this textbook and the previous book *Guidance and Control of Ocean Vehicles* (Fossen, 1994). Equation (1.21) has also been adopted by the international community as a “standard model” for marine control systems design (controller and observer design models) while the “classical model” (1.5)–(1.6) is mostly used in hydrodynamic modeling where isolated effects often are studied in more detail.

It should be noted that the classical model with hydrodynamic forces in component form and the vectorial model (1.21) are equivalent. Therefore it is possible to combine the best of both approaches, that is hydrodynamic component-based modeling and control design models based on vectors and matrices. However, it is much easier to construct multiple input multiple output (MIMO) controllers and observers when using the vectorial representation, since the model properties and model reduction follow from the basic matrix properties. This also applies to system analysis since there are many tools for MIMO systems. Finally, it should be pointed out that the vectorial models are beneficial from a computational point of view and in order to perform algebraic manipulations. Readability is also significantly improved thanks to the compact notation.



# Chapter 2

## Kinematics

The study of *dynamics* can be divided into two parts: *kinematics*, which treats only geometrical aspects of motion, and *kinetics*, which is the analysis of the forces causing the motion. In this chapter kinematics with application to local and terrestrial navigation is discussed. Kinetics is dealt with in Chapters 3–10.

The interested reader is advised to consult Britting (1971), Maybeck (1979), Savage (1990), Forsell (1991), Lin (1992), Hofmann-Wellenhof *et al.* (1994), Parkinson and Spilker (1995), Titterton and Weston (1997), and Farrell (2008) for a discussion of navigation kinematics and kinematics in general. The development of the kinematic equations of motion are also found in Kane *et al.* (1983) and Hughes (1986). Both of these references use spacecraft systems for illustration. An alternative derivation of the Euler angle representation in the context of ship steering is given by Abkowitz (1964). A more recent discussion of quaternions is found in Chou (1992). An analogy to robot manipulators is given by Craig (1989) or Sciavicco and Siciliano (1996), while a more detailed discussion of kinematics is found in Goldstein (1980), and Egeland and Gravdahl (2002).

### 6-DOF marine craft equations of motion

The overall goal of Chapters 2–10 is to show that the marine craft equations of motion can be written in the following *matrix-vector form* (Fossen 1991)

$$\dot{\boldsymbol{\eta}} = \mathbf{J}_\Theta(\boldsymbol{\eta})\boldsymbol{\nu} \quad (2.1)$$

$$\mathbf{M}\dot{\boldsymbol{\nu}} + \mathbf{C}(\boldsymbol{\nu})\boldsymbol{\nu} + \mathbf{D}(\boldsymbol{\nu})\boldsymbol{\nu} + \mathbf{g}(\boldsymbol{\eta}) + \mathbf{g}_0 = \boldsymbol{\tau} + \boldsymbol{\tau}_{\text{wind}} + \boldsymbol{\tau}_{\text{wave}} \quad (2.2)$$

where the different matrices and vectors and their properties will be defined in the forthcoming sections. This model representation is used as a foundation for model-based control design and stability analysis in Part II.

### Motion variables

For marine craft moving in six *degrees of freedom* (DOFs), six independent coordinates are necessary to determine the position and orientation. The first three coordinates, and

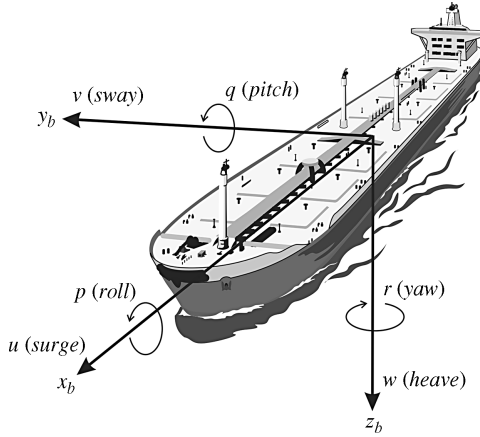


Figure 2.1: The six body-fixed velocities  $u, v, w, p, q$  and  $r$  and their interpretation in the body-fixed reference frame  $\{b\} = (x_b, y_b, z_b)$ .

their time derivatives, correspond to the position and translational motion along the  $x$ ,  $y$  and  $z$  axes, while the last three coordinates and their time derivatives are used to describe orientation and rotational motion. For marine craft, the six different motion components are conveniently defined as *surge*, *sway*, *heave*, *roll*, *pitch* and *yaw* (see Figure 2.1 and Table 2.1).

## 2.1 Kinematic Preliminaries

### 2.1.1 Reference frames

When analyzing the motion of marine craft in 6 DOF, it is convenient to define two Earth-centered coordinate frames as indicated in Figure 2.2. In addition several geographic reference frames are needed.

Table 2.1: The notation of SNAME (1950) for marine vessels

DOF		Forces and moments	Linear and angular velocities	Positions and Euler angles
1	motions in the $x$ -direction (surge)	$X$	$u$	$x^n$
2	motions in the $y$ -direction (sway)	$Y$	$v$	$y^n$
3	motions in the $z$ -direction (heave)	$Z$	$w$	$z^n$
4	rotation about the $x$ -axis (roll)	$K$	$p$	$\phi$
5	rotation about the $y$ -axis (pitch)	$M$	$q$	$\theta$
6	rotation about the $z$ -axis (yaw)	$N$	$r$	$\psi$

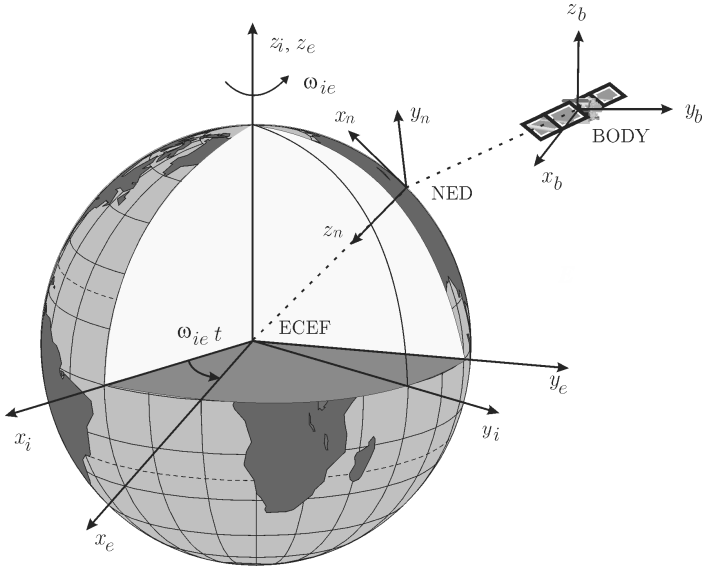


Figure 2.2: The Earth-centered Earth-fixed (ECEF) frame  $x_e y_e z_e$  is rotating with angular rate  $\omega_{ie}$  with respect to an Earth-centered inertial (ECI) frame  $x_i y_i z_i$  fixed in space.

### Earth-centered reference frames

**ECI:** The Earth-centered inertial (ECI) frame  $\{i\} = (x_i, y_i, z_i)$  is an inertial frame for terrestrial navigation, that is a nonaccelerating reference frame in which Newton's laws of motion apply. This is exploited when designing inertial navigation systems. The origin of  $\{i\}$  is located at the center  $o_i$  of the Earth with axes as shown in Figure 2.2.

**ECEF:** The Earth-centered Earth-fixed (ECEF) reference frame  $\{e\} = (x_e, y_e, z_e)$  has its origin  $o_e$  fixed to the center of the Earth but the axes rotate relative to the inertial frame ECI, which is fixed in space. Moreover

- $x_e$  - axis in the equatorial plane pointing towards the zero/prime meridian; same longitude as the Greenwich observatory
- $y_e$  - axis in the equatorial plane completing the right-hand frame
- $z_e$  - axis pointing along the Earth's rotational axis

The Earth rotation is  $\omega_{ie} = 7.2921 \times 10^{-5}$  rad/s and the Earth's rotational vector is  $\omega_{ie}^e = [0, 0, \omega_{ie}]^\top$ . For marine craft moving at relatively low speed, the Earth rotation can be neglected and hence  $\{e\}$  can be considered to be inertial. Drifting ships, however, should not neglect the Earth rotation. The coordinate system  $\{e\}$  is usually used for global navigation applications, for instance to describe the motion and location of ships in transit between different continents.

### Geographic reference frames (tangent planes)

Geographical reference frames are usually chosen as tangent planes on the surface of the Earth. Tangent planes can be used for both local and terrestrial navigation.

- *Terrestrial navigation:* The tangent plane on the surface of the Earth moves with the craft and its location is specified by time-varying longitude-latitude values  $(l, \mu)$ . The tangent frame is usually rotated such that its axes points in the North-East-Down (NED) directions.
- *Local navigation:* The tangent plane is fixed at constant values  $(l_0, \mu_0)$  and the position is computed with respect to a local coordinate origin. The axes of the tangent plane are usually chosen to coincide with the NED axes. This is also referred to as “flat Earth navigation” and the position is accurate to a smaller geographical area, typically  $10\text{ km} \times 10\text{ km}$ .

**NED:** The *North-East-Down* (NED) coordinate system is denoted  $\{n\} = (x_n, y_n, z_n)$  where

- $x_n$  - axis points towards true *North*
- $y_n$  - axis points towards *East*
- $z_n$  - axis points *downwards* normal to the Earth’s surface

The coordinate origin  $o_n$  is defined relative to the Earth’s reference ellipsoid (World Geodetic System 1984), usually as the tangent plane to the ellipsoid<sup>1</sup>. The location of  $\{n\}$  relative to  $\{e\}$  is determined by using two angles  $l$  and  $\mu$  denoting the *longitude* and *latitude*, respectively. This is the coordinate system we refer to in our everyday life and it is used for local navigation.

### Body-fixed reference frames

**BODY:** The body-fixed reference frame  $\{b\} = (x_b, y_b, z_b)$  with origin  $o_b$  is a moving coordinate frame that is fixed to the craft. The position and orientation of the craft are described relative to the inertial reference frame (approximated by  $\{e\}$  or  $\{n\}$  for marine craft) while the linear and angular velocities of the craft should be expressed in the body-fixed coordinate system. The origin  $o_b$  is usually chosen to coincide with a point midships in the water line. For marine craft, the body axes  $x_b$ ,  $y_b$  and  $z_b$  are chosen to coincide with the *principal axes of inertia*, and they are usually defined as (see Figure 2.3):

- $x_b$  - longitudinal axis (directed from aft to fore)
- $y_b$  - transversal axis (directed to starboard)
- $z_b$  - normal axis (directed from top to bottom)

<sup>1</sup>An alternative right-handed variant is the East-North-Up (ENU) reference frame. Both the NED and ENU reference frames are commonly used in GNC applications.

**FLOW:** Flow axes (see Section 2.5) are used to align the  $x$ -axis with the craft's velocity vector such that lift is perpendicular to the relative flow and drag is parallel. The transformation from FLOW to BODY axes is defined by two principal rotations where the rotation angles are the angle of attack  $\alpha$  and the sideslip angle  $\beta$ . The main purpose of the flow axes is to simplify the computations of lift and drag forces when a marine craft is exposed to ocean currents. Other applications are line-of-sight (LOS) path-following control systems, which must take into account that the angle of attack and sideslip angle may be time varying in a flow (ocean current).

**SEAKEEPING:** The seakeeping reference frame  $\{s\} = (x_s, y_s, z_s)$  is not fixed to the craft (see Section 5.2). It represents the equilibrium state of a marine craft moving in waves. Hence, in the absence of wave excitation, the  $\{s\}$ -frame origin  $o_s$  coincides with the location of the  $\{b\}$ -frame origin  $o_b$ , which is a fixed point in the ship. Under the action of the waves, the hull is disturbed from its equilibrium and the point  $o_s$  oscillates, with respect to its equilibrium position.

## 2.1.2 Body-Fixed reference points

When designing guidance, navigation and control (GNC) systems for marine craft several reference points are needed to express the equations of motion. The most important reference point is

**CO** - coordinate origin  $\{b\}$  of the body-fixed frame. CO also represents the coordinate origin of the feedback control, navigation and guidance systems.

The main idea is that CO should be body fixed with location specified by the operator, while other reference points can be allowed to have time-varying coordinates with respect to CO. This is the case for the following reference points, which all are time varying

**CG** - Center of gravity located at  $\mathbf{r}_g^b = [x_g, y_g, z_g]^\top$  with respect to CO

**CB** - Center of buoyancy located at  $\mathbf{r}_b^b = [x_b, y_b, z_b]^\top$  with respect to CO

**CF** - Center of flotation located at  $\mathbf{r}_f^b = [x_f, y_f, z_f]^\top$  with respect to CO. If CO is located midships in the waterline  $\mathbf{r}_f^b = [\text{LCF}, 0, 0]^\top$

In general, the locations of CG, CB and CF depend on loading conditions, fuel burning rate, ballast tank levels, weather conditions and ship motions. This is in contrast with CO, which has a constant location.

The CF is the centroid of the water plane area  $A_{wp}$  in calm water. A craft will roll and pitch about the  $x_f$  and  $y_f$  axes through the CF if the displacement is constant (small angle assumption). Consequently, this point can be used to compute the pitch and roll periods for moderate sea states. Notice that the eigenvalues of the 6-DOF linear model are independent of the reference points (CF, CB, CG and CO) but decoupled equations in heave, roll and pitch will produce incorrect results if they are formulated in a point different from CF (see Section 4.3).

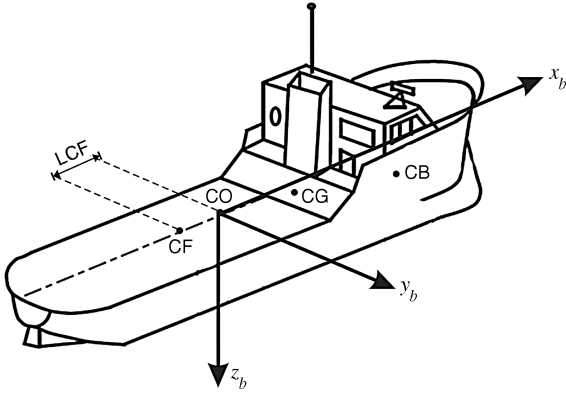


Figure 2.3: Body-fixed reference points.

### 2.1.3 Generalized coordinates

For a marine craft not subject to any motion constraints, the number of independent (generalized) coordinates will be equal to the degrees of freedom (DOFs). The term generalized coordinates refers to the parameters that describe the configuration of the craft relative to some reference configuration. For marine craft, the generalized position is chosen as

$$\boldsymbol{\eta} = [x^n, y^n, z^n, \phi, \theta, \psi]^\top \quad (2.3)$$

The generalized velocities are the time derivatives of the generalized coordinates of the system. Moreover,

$$\dot{\boldsymbol{\eta}} = [\dot{x}^n, \dot{y}^n, \dot{z}^n, \dot{\phi}, \dot{\theta}, \dot{\psi}]^\top \quad (2.4)$$

These quantities are all formulated in NED. It is advantageous to express the velocities of the craft in the BODY frame. Moreover,

$$\boldsymbol{\nu} = [u, v, w, p, q, r]^\top \quad (2.5)$$

We will use the notation  $\vec{u}$  to refer to a *coordinate free vector*, that is a *directed line segment*. When a vector is described relative to a coordinate system  $\{n\}$ , the following notation will be used:

$$\vec{u} = u_1^n \vec{n}_1 + u_2^n \vec{n}_2 + u_3^n \vec{n}_3 \quad (2.6)$$

where  $\vec{n}_i$  ( $i = 1, 2, 3$ ) are the unit vectors that define  $\{n\}$ ,  $u_i^n$  are the measures of  $\vec{u}$  along  $\vec{n}_i$  and  $u_i^n \vec{n}_i$  are the components of  $\vec{u}$  in  $\{n\}$ . We will also use the *coordinate form*  $\boldsymbol{u}^n$  of  $\vec{u}$  in  $\{n\}$  which is represented by a *column vector* in  $\mathbb{R}^3$ :

$$\boldsymbol{u}^n = [u_1^n, u_2^n, u_3^n]^\top \quad (2.7)$$

For marine craft the following notation will be adopted for vectors in the coordinate

systems  $\{b\}$ ,  $\{e\}$  and  $\{n\}$ :

$v_{nb}^e$	linear velocity of the point $o_b$ in $\{b\}$ with respect to $\{n\}$ expressed in $\{e\}$
$\omega_{en}^b$	angular velocity of $\{n\}$ with respect to $\{e\}$ expressed in $\{b\}$
$f_b^n$	force with line of action through the point $o_b$ in $\{b\}$ expressed in $\{n\}$
$m_b^n$	moment about the point $o_b$ in $\{b\}$ expressed in $\{n\}$
$\Theta_{nb}$	Euler angles from $\{b\}$ to $\{n\}$
$q_b^n$	Unit quaternion from $\{b\}$ to $\{n\}$

The different quantities in Table 2.1, as defined by SNAME (1950), can now be conveniently expressed in a vectorial setting according to

ECEF position	$p_{eb}^e = \begin{bmatrix} x^e \\ y^e \\ z^e \end{bmatrix} \in \mathbb{R}^3$	Longitude and latitude	$\Theta_{en} = \begin{bmatrix} l \\ \mu \end{bmatrix} \in \mathcal{S}^2$
NED position	$p_{nb}^n = \begin{bmatrix} x^n \\ y^n \\ z^n \end{bmatrix} \in \mathbb{R}^3$	Attitude (Euler angles)	$\Theta_{nb} = \begin{bmatrix} \phi \\ \theta \\ \psi \end{bmatrix} \in \mathcal{S}^3$
Body-fixed linear velocity	$v_{nb}^b = \begin{bmatrix} u \\ v \\ w \end{bmatrix} \in \mathbb{R}^3$	Body-fixed angular velocity	$\omega_{nb}^b = \begin{bmatrix} p \\ q \\ r \end{bmatrix} \in \mathbb{R}^3$
Body-fixed force	$f_b^b = \begin{bmatrix} X \\ Y \\ Z \end{bmatrix} \in \mathbb{R}^3$	Body-fixed moment	$m_b^b = \begin{bmatrix} K \\ M \\ N \end{bmatrix} \in \mathbb{R}^3$

where  $\mathbb{R}^3$  is the *Euclidean space* of dimension three and  $\mathcal{S}^2$  denotes a *torus* of dimension two (shape of a donut), implying that there are two angles defined on the interval  $[0, 2\pi]$ . In the three-dimensional (3-D) case the set  $\mathcal{S}^3$  is a sphere. Hence, the general motion of a marine craft in 6 DOF with  $o_b$  as coordinate origin is described by the following vectors for generalized position, velocity and force

$$\boldsymbol{\eta} = \begin{bmatrix} p_{nb}^n \text{ (or } p_{nb}^e) \\ \Theta_{nb} \end{bmatrix}, \quad \boldsymbol{\nu} = \begin{bmatrix} v_{nb}^b \\ \omega_{nb}^b \end{bmatrix}, \quad \boldsymbol{\tau} = \begin{bmatrix} f_b^b \\ m_b^b \end{bmatrix} \quad (2.8)$$

where  $\boldsymbol{\eta} \in \mathbb{R}^3 \times \mathcal{S}^3$  denotes the position and orientation vector where the position vector  $p_{nb}^n \in \mathbb{R}^3$  is the distance from NED to BODY expressed in NED coordinates,  $\Theta_{nb} \in \mathcal{S}^3$  is a vector of Euler angles,  $\boldsymbol{\nu} \in \mathbb{R}^6$  denotes the linear and angular velocity vectors that are decomposed in the body-fixed reference frame and  $\boldsymbol{\tau} \in \mathbb{R}^6$  is used to describe the forces and moments acting on the craft in the body-fixed frame.

In many applications, such as flat Earth navigation, the position vector  $p_{nb}^n \in \mathbb{R}^3$  from NED to BODY is expressed in NED coordinates. For terrestrial navigation it is convenient to express the position of the BODY origin  $o_b$  with respect to ECEF, that is  $p_{eb}^e \in \mathbb{R}^3$ . The orientation of the marine craft with respect to NED will be represented by means of the Euler angles  $\Theta_{nb}$  or the unit quaternions  $q_b^n \in \mathbb{R}^4$ . In the next sections, the kinematic equations relating the BODY, NED and ECEF reference frames will be presented.

## 2.2 Transformations between BODY and NED

The rotation matrix  $\mathbf{R}$  between two frames  $a$  and  $b$  is denoted as  $\mathbf{R}_b^a$ , and it is an element in  $SO(3)$ , that is the *special orthogonal group of order 3*:

$$SO(3) = \{\mathbf{R} | \mathbf{R} \in \mathbb{R}^{3 \times 3}, \quad \mathbf{R} \text{ is orthogonal and } \det \mathbf{R} = 1\} \quad (2.9)$$

The group  $SO(3)$  is a subset of all *orthogonal matrices of order 3*, that is  $SO(3) \subset O(3)$  where  $O(3)$  is defined as

$$O(3) := \{\mathbf{R} | \mathbf{R} \in \mathbb{R}^{3 \times 3}, \quad \mathbf{R}\mathbf{R}^\top = \mathbf{R}^\top\mathbf{R} = \mathbf{I}_3\} \quad (2.10)$$

Rotation matrices are useful when deriving the kinematic equations of motion for a marine craft. As a consequence of (2.9) and (2.10), the following properties can be stated:

**Property 2.1 (Rotation Matrix)**

A rotation matrix  $\mathbf{R} \in SO(3)$  satisfies

$$\mathbf{R}\mathbf{R}^\top = \mathbf{R}^\top\mathbf{R} = \mathbf{I}_3, \quad \det \mathbf{R} = 1$$

which implies that  $\mathbf{R}$  is orthogonal. Consequently, the inverse rotation matrix is given by  $\mathbf{R}^{-1} = \mathbf{R}^\top$ .

In this book, the following notation is adopted when transforming a vector from one coordinate frame to another:

$$\nu^{\text{to}} = \underbrace{\mathbf{R}_{\text{from}}^{\text{to}}}_{\text{rotation matrix}} \nu^{\text{from}} \quad (2.11)$$

Here  $\nu^{\text{from}} \in \mathbb{R}^3$  denotes a velocity vector that can be transformed to a new reference frame by applying the rotation matrix  $\mathbf{R}_{\text{from}}^{\text{to}}$ . The result is the vector  $\nu^{\text{to}} \in \mathbb{R}^3$ .

A frequently used rotation matrix in guidance, navigation and control is the rotation matrix  $\mathbf{R}_b^n$  between  $\{n\}$  and  $\{b\}$ . When deriving the expression for  $\mathbf{R}_b^n$  we will make use of the following matrix properties:

**Definition 2.1 (Skew-Symmetry of a Matrix)**

A matrix  $\mathbf{S} \in \text{SS}(n)$ , that is the set of skew-symmetric matrices of order  $n$ , is said to be *skew-symmetric* if

$$\mathbf{S} = -\mathbf{S}^\top$$

This implies that the off-diagonal elements of  $\mathbf{S}$  satisfy  $s_{ij} = -s_{ji}$  for  $i \neq j$  while the diagonal elements are zero.

**Definition 2.2 (Cross-Product Operator)**

The vector cross product  $\times$  is defined by

$$\boldsymbol{\lambda} \times \mathbf{a} := \mathbf{S}(\boldsymbol{\lambda})\mathbf{a} \quad (2.12)$$

where  $\mathbf{S} \in \text{SS}(3)$  is defined as

$$\mathbf{S}(\boldsymbol{\lambda}) = -\mathbf{S}^\top(\boldsymbol{\lambda}) = \begin{bmatrix} 0 & -\lambda_3 & \lambda_2 \\ \lambda_3 & 0 & -\lambda_1 \\ -\lambda_2 & \lambda_1 & 0 \end{bmatrix}, \quad \boldsymbol{\lambda} = \begin{bmatrix} \lambda_1 \\ \lambda_2 \\ \lambda_3 \end{bmatrix} \quad (2.13)$$

The inverse operator is denoted  $\text{vex}(\cdot)$ , such that

$$\boldsymbol{\lambda} = \text{vex}(\mathbf{S}(\boldsymbol{\lambda})) \quad (2.14)$$

**Matlab:**

The cross-product operator is included in the MSS toolbox as `Smtx.m`. Hence, the cross-product  $\mathbf{b} = \mathbf{S}(\boldsymbol{\lambda})\mathbf{a}$  can be computed as

```
S = Smtx(lambda);
b = S * a;
```

The inverse operation is

```
lambda = vex(S);
```

**Definition 2.3 (Simple Rotation)**

The motion of a rigid body or reference frame  $\mathcal{B}$  relative to a rigid body or reference frame  $\mathcal{A}$  is called a simple rotation of  $\mathcal{B}$  in  $\mathcal{A}$  if there exists a line  $L$ , called an axis of rotation, whose orientation relative to both  $\mathcal{A}$  and  $\mathcal{B}$  remains unaltered throughout the motion.

Based on this definition, Euler stated the following theorem for rotation of two rigid bodies or reference frames (Euler 1776).

**Theorem 2.1 (Euler's Theorem on Rotation)**

Every change in the relative orientation of two rigid bodies or reference frames  $\{\mathcal{A}\}$  and  $\{\mathcal{B}\}$  can be produced by means of a simple rotation of  $\{\mathcal{B}\}$  in  $\{\mathcal{A}\}$ .

Let  $\mathbf{v}_{nb}^b$  be a vector fixed in BODY and  $\mathbf{v}_{nb}^n$  be a vector fixed in NED. Hence, the vector  $\mathbf{v}_{nb}^n$  can be expressed in terms of the vector  $\mathbf{v}_{nb}^b$ , the unit vector  $\boldsymbol{\lambda} = [\lambda_1, \lambda_2, \lambda_3]^\top$ ,  $\|\boldsymbol{\lambda}\| = 1$ , parallel to the axis of rotation and  $\beta$  the angle NED is rotated. This rotation is described by (see Hughes 1986, Kane *et al.* 1983)

$$\mathbf{v}_{nb}^n = \mathbf{R}_b^n \mathbf{v}_{nb}^b, \quad \mathbf{R}_b^n := \mathbf{R}_{\lambda, \beta} \quad (2.15)$$

Here,  $\mathbf{R}_{\lambda, \beta}$  is the rotation matrix corresponding to a rotation  $\beta$  about the  $\boldsymbol{\lambda}$  axis:

$$\mathbf{R}_{\lambda, \beta} = \mathbf{I}_3 + \sin(\beta) \mathbf{S}(\boldsymbol{\lambda}) + [1 - \cos(\beta)] \mathbf{S}^2(\boldsymbol{\lambda}) \quad (2.16)$$

where  $\mathbf{S}(\boldsymbol{\lambda})$  is the skew-symmetric matrix according to Definition 2.2. Consequently,  $\mathbf{S}^2(\boldsymbol{\lambda}) = \boldsymbol{\lambda} \boldsymbol{\lambda}^\top - \mathbf{I}_3$  since  $\boldsymbol{\lambda}$  is a unit vector.

Expanding (2.16) yields the following expressions for the matrix elements:

$$\begin{aligned}
 R_{11} &= [1 - \cos(\beta)] \lambda_1^2 + \cos(\beta) \\
 R_{22} &= [1 - \cos(\beta)] \lambda_2^2 + \cos(\beta) \\
 R_{33} &= [1 - \cos(\beta)] \lambda_3^2 + \cos(\beta) \\
 R_{12} &= [1 - \cos(\beta)] \lambda_1 \lambda_2 - \lambda_3 \sin(\beta) \\
 R_{21} &= [1 - \cos(\beta)] \lambda_2 \lambda_1 + \lambda_3 \sin(\beta) \\
 R_{23} &= [1 - \cos(\beta)] \lambda_2 \lambda_3 - \lambda_1 \sin(\beta) \\
 R_{32} &= [1 - \cos(\beta)] \lambda_3 \lambda_2 + \lambda_1 \sin(\beta) \\
 R_{31} &= [1 - \cos(\beta)] \lambda_3 \lambda_1 - \lambda_2 \sin(\beta) \\
 R_{13} &= [1 - \cos(\beta)] \lambda_1 \lambda_3 + \lambda_2 \sin(\beta)
 \end{aligned} \tag{2.17}$$

### 2.2.1 Euler angle transformation

The Euler angles, roll ( $\phi$ ), pitch ( $\theta$ ) and yaw ( $\psi$ ), can now be used to decompose the body-fixed velocity vector  $v_{nb}^b$  in the NED reference frame.

Let  $\mathbf{R}(\Theta_{nb}) : \mathcal{S}^3 \rightarrow SO(3)$  denote the Euler angle rotation matrix with argument  $\Theta_{nb} = [\phi, \theta, \psi]^\top$ . Hence,

$$v_{nb}^n = \mathbf{R}_b^n v_{nb}^b \tag{2.18}$$

where

$$\mathbf{R}_b^n := \mathbf{R}(\Theta_{nb}) \tag{2.19}$$

#### Principal rotations

The principal rotation matrices (one-axis rotations) can be obtained by setting  $\boldsymbol{\lambda} = [1, 0, 0]^\top$ ,  $\boldsymbol{\lambda} = [0, 1, 0]^\top$  and  $\boldsymbol{\lambda} = [0, 0, 1]^\top$  corresponding to the  $x$ ,  $y$  and  $z$  axes, and  $\beta = \phi$ ,  $\beta = \theta$  and  $\beta = \psi$ , respectively, in the formula for  $\mathbf{R}_{\lambda, \beta}$  given by (2.16). This yields

$$\mathbf{R}_{x,\phi} = \begin{bmatrix} 1 & 0 & 0 \\ 0 & c\phi & -s\phi \\ 0 & s\phi & c\phi \end{bmatrix}, \quad \mathbf{R}_{y,\theta} = \begin{bmatrix} c\theta & 0 & s\theta \\ 0 & 1 & 0 \\ -s\theta & 0 & c\theta \end{bmatrix}, \quad \mathbf{R}_{z,\psi} = \begin{bmatrix} c\psi & -s\psi & 0 \\ s\psi & c\psi & 0 \\ 0 & 0 & 1 \end{bmatrix} \tag{2.20}$$

where  $s \cdot = \sin(\cdot)$  and  $c \cdot = \cos(\cdot)$ .

#### Linear velocity transformation

It is customary to describe  $\mathbf{R}_b^n = \mathbf{R}(\Theta_{nb})$  by three *principal* rotations about the  $z$ ,  $y$  and  $x$  axes ( $zyx$  convention). Note that the order in which these rotations is carried out is not arbitrary. In guidance, navigation and control applications it is common to use the  $zyx$  convention from  $\{n\}$  to  $\{b\}$  specified in terms of the Euler angles  $\phi$ ,  $\theta$  and  $\psi$  for the rotations. This rotation sequence is mathematically equivalent to

$$\mathbf{R}_b^n := \mathbf{R}_{z,\psi} \mathbf{R}_{y,\theta} \mathbf{R}_{x,\phi} \tag{2.21}$$

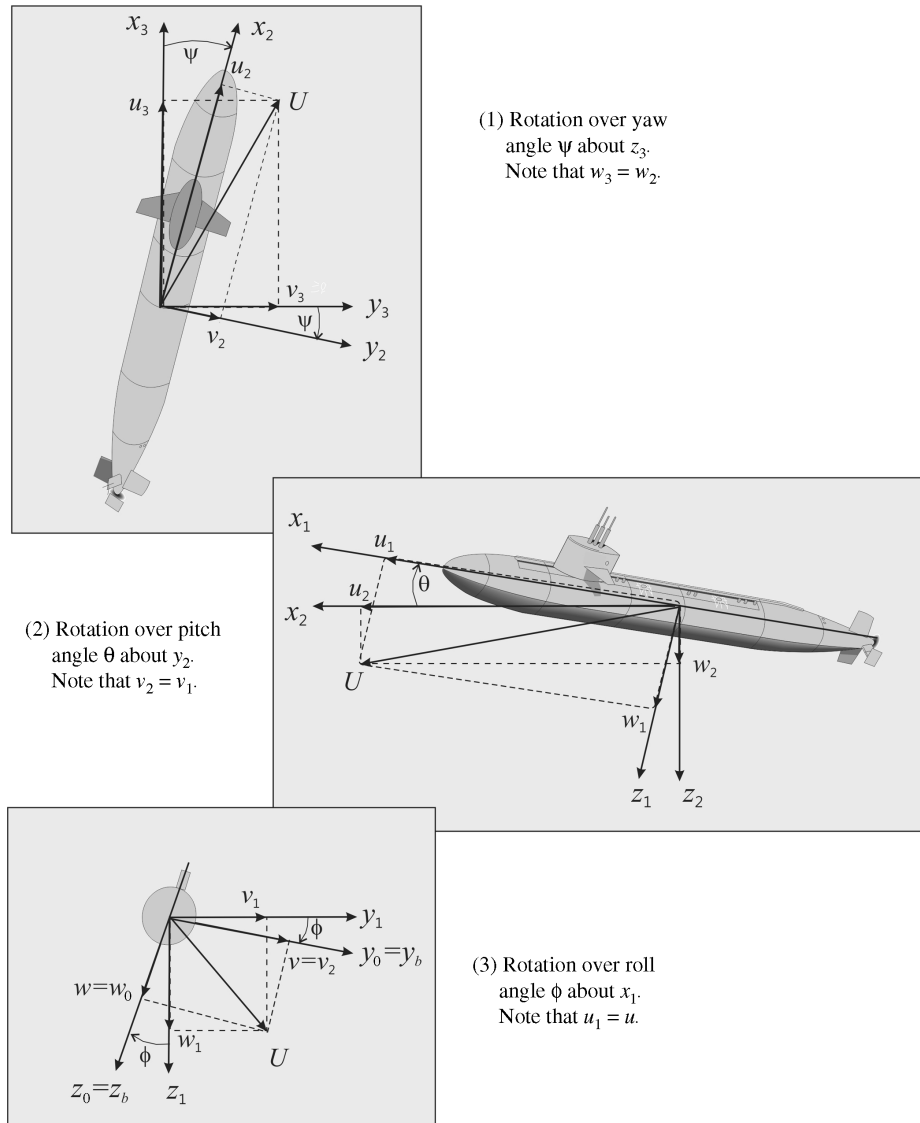


Figure 2.4: Euler angle rotation sequence (zyx convention). The submarine is rotated from  $\{n\}$  to  $\{b\}$  by using three principal rotations.

and the inverse transformation is then written

$$(\mathbf{R}_b^n)^{-1} = \mathbf{R}_n^b = \mathbf{R}_{x,\phi}^\top \mathbf{R}_{y,\theta}^\top \mathbf{R}_{z,\psi}^\top \quad (2.22)$$

where we have used the result of Property 2.1. This can also be verified by studying Figure 2.4.

Let  $x_3y_3z_3$  be the coordinate system obtained by translating the NED coordinate system  $x_ny_nz_n$  parallel to itself until its origin coincides with the origin of the body-fixed coordinate system. The coordinate system  $x_3y_3z_3$  is rotated a *yaw* angle  $\psi$  about the  $z_3$  axis. This yields the coordinate system  $x_2y_2z_2$ . The coordinate system  $x_2y_2z_2$  is rotated a *pitch* angle  $\theta$  about the  $y_2$  axis. This yields the coordinate system  $x_1y_1z_1$ . Finally, the coordinate system  $x_1y_1z_1$  is rotated a *roll* angle  $\phi$  about the  $x_1$  axis. This yields the body-fixed coordinate system  $x_b y_b z_b$ .

Expanding (2.21) yields

$$\mathbf{R}(\Theta_{nb}) = \begin{bmatrix} c\psi c\theta & -s\psi c\phi + c\psi s\theta s\phi & s\psi s\phi + c\psi c\phi s\theta \\ s\psi c\theta & c\psi c\phi + s\phi s\theta s\psi & -c\psi s\phi + s\theta s\psi c\phi \\ -s\theta & c\theta s\phi & c\theta c\phi \end{bmatrix} \quad (2.23)$$

### Matlab:

The rotation matrix  $\mathbf{R}(\Theta_{nb})$  is implemented in the MSS toolbox as

```
R = Rzyx(phi,theta,psi)
```

For small angles  $\delta\phi$ ,  $\delta\theta$  and  $\delta\psi$  the expression (2.23) simplifies to

$$\mathbf{R}(\delta\Theta_{nb}) \approx \mathbf{I}_3 + \mathbf{S}(\delta\Theta_{nb}) = \begin{bmatrix} 1 & -\delta\psi & \delta\theta \\ \delta\psi & 1 & -\delta\phi \\ -\delta\theta & \delta\phi & 1 \end{bmatrix} \quad (2.24)$$

which is quite useful when applying linear theory.

The body-fixed velocity vector  $\mathbf{v}_{nb}^b$  can be expressed in  $\{n\}$  as

$$\dot{\mathbf{p}}_{nb}^n = \mathbf{R}(\Theta_{nb}) \mathbf{v}_{nb}^b \quad (2.25)$$

where  $\dot{\mathbf{p}}_{nb}^n$  is the NED velocity vector. Expanding (2.25) yields

$$\begin{aligned} \dot{x}^n &= u \cos(\psi) \cos(\theta) + v [\cos(\psi) \sin(\theta) \sin(\phi) - \sin(\psi) \cos(\phi)] \\ &\quad + w [\sin(\psi) \sin(\phi) + \cos(\psi) \cos(\phi) \sin(\theta)] \end{aligned} \quad (2.26)$$

$$\begin{aligned} \dot{y}^n &= u \sin(\psi) \cos(\theta) + v [\cos(\psi) \cos(\phi) + \sin(\phi) \sin(\theta) \sin(\psi)] \\ &\quad + w [\sin(\theta) \sin(\psi) \cos(\phi) - \cos(\psi) \sin(\phi)] \end{aligned} \quad (2.27)$$

$$\dot{z}^n = -u \sin(\theta) + v \cos(\theta) \sin(\phi) + w \cos(\theta) \cos(\phi) \quad (2.28)$$

The inverse velocity transformation is obtained by Definition 2.1 as

$$\mathbf{v}_{nb}^b = \mathbf{R}^{-1}(\Theta_{nb})\dot{\mathbf{p}}_{nb}^n = \mathbf{R}^\top(\Theta_{nb})\dot{\mathbf{p}}_{nb}^n \quad (2.29)$$

**Example 2.1 (Numerical Computation of Position Trajectory)**

The flight path or position trajectory  $\mathbf{p}_{nb}^n$  of the craft relative to the NED coordinate system is found by numerical integration of (2.25), for instance by using Euler's method

$$\mathbf{p}_{nb}^n[k+1] = \mathbf{p}_{nb}^n[k] + h\mathbf{R}(\Theta_{nb}[k])\mathbf{v}_{nb}^b[k] \quad (2.30)$$

where  $h > 0$  is the sampling time and  $k$  is the sample index.

### Angular velocity transformation

The body-fixed angular velocity vector  $\omega_{nb}^b = [p, q, r]^\top$  and the Euler rate vector  $\dot{\Theta}_{nb} = [\dot{\phi}, \dot{\theta}, \dot{\psi}]^\top$  are related through a transformation matrix  $\mathbf{T}(\Theta_{nb})$  according to

$$\dot{\Theta}_{nb} = \mathbf{T}(\Theta_{nb})\omega_{nb}^b \quad (2.31)$$

It should be noted that the angular body velocity vector  $\omega_{nb}^b = [p, q, r]^\top$  cannot be integrated directly to obtain actual angular coordinates. This is due to the fact that  $\int_0^t \omega_{nb}^b(\tau) d\tau$  does not have any immediate physical interpretation; however, the vector  $\Theta_{nb} = [\phi, \theta, \psi]^\top$  does represent proper generalized coordinates. The transformation matrix  $\mathbf{T}(\Theta_{nb})$  can be derived in several ways, for instance:

$$\omega_{nb}^b = \begin{bmatrix} \dot{\phi} \\ 0 \\ 0 \end{bmatrix} + \mathbf{R}_{x,\phi}^\top \begin{bmatrix} 0 \\ \dot{\theta} \\ 0 \end{bmatrix} + \mathbf{R}_{x,\phi}^\top \mathbf{R}_{y,\theta}^\top \begin{bmatrix} 0 \\ 0 \\ \dot{\psi} \end{bmatrix} := \mathbf{T}^{-1}(\Theta_{nb})\dot{\Theta}_{nb} \quad (2.32)$$

This relationship is verified by inspection of Figure 2.4. Expanding (2.32) yields

$$\mathbf{T}^{-1}(\Theta_{nb}) = \begin{bmatrix} 1 & 0 & -s\theta \\ 0 & c\phi & c\theta s\phi \\ 0 & -s\phi & c\theta c\phi \end{bmatrix} \implies \mathbf{T}(\Theta_{nb}) = \begin{bmatrix} 1 & s\phi t\theta & c\phi t\theta \\ 0 & c\phi & -s\phi \\ 0 & s\phi/c\theta & c\phi/c\theta \end{bmatrix} \quad (2.33)$$

where  $s \cdot = \sin(\cdot)$ ,  $c \cdot = \cos(\cdot)$  and  $t \cdot = \tan(\cdot)$ . Expanding (2.31) yields the Euler angle attitude equations in component form

$$\dot{\phi} = p + q \sin(\phi) \tan(\theta) + r \cos(\phi) \tan(\theta) \quad (2.34)$$

$$\dot{\theta} = q \cos(\phi) - r \sin(\phi) \quad (2.35)$$

$$\dot{\psi} = q \frac{\sin(\phi)}{\cos(\theta)} + r \frac{\cos(\phi)}{\cos(\theta)}, \quad \theta \neq \pm 90^\circ \quad (2.36)$$

Notice that  $\mathbf{T}(\Theta_{nb})$  is undefined for a pitch angle of  $\theta = \pm 90^\circ$  and that  $\mathbf{T}(\Theta_{nb})$  does not satisfy Property 2.1. Consequently,  $\mathbf{T}^{-1}(\Theta_{nb}) \neq \mathbf{T}^\top(\Theta_{nb})$ . For surface vessels this is not a problem whereas both underwater vehicles and aircraft may operate

close to this singularity. In this case, the kinematic equations can be described by two Euler angle representations with different singularities and the singular point can be avoided by switching between them. Another possibility is to use the unit quaternion representation; see Section 2.2.2.

**Matlab:**

The transformation matrix  $\mathbf{T}(\Theta_{nb})$  is implemented in the MSS toolbox as

```
T = Tzyx(phi,theta)
```

For small angles  $\delta\phi$ ,  $\delta\theta$  and  $\delta\psi$  the transformation matrix  $\mathbf{T}(\Theta_{nb})$  simplifies to

$$\mathbf{T}(\delta\Theta_{nb}) \approx \begin{bmatrix} 1 & 0 & \delta\theta \\ 0 & 1 & -\delta\phi \\ 0 & \delta\phi & 1 \end{bmatrix} \quad (2.37)$$

The differential equation for the rotation matrix is given by Theorem 2.2.

**Theorem 2.2 (Rotation Matrix Differential Equation)**

*The differential equation for the rotation matrix between the BODY and NED reference frames is*

$$\dot{\mathbf{R}}_b^n = \mathbf{R}_b^n \mathbf{S}(\omega_{nb}^b) \quad (2.38)$$

where

$$\mathbf{S}(\omega_{nb}^b) = \begin{bmatrix} 0 & -r & q \\ r & 0 & -p \\ -q & p & 0 \end{bmatrix} \quad (2.39)$$

This can be written in component form as nine differential equations:

$$\begin{bmatrix} \dot{R}_{11} & \dot{R}_{12} & \dot{R}_{13} \\ \dot{R}_{21} & \dot{R}_{22} & \dot{R}_{23} \\ \dot{R}_{31} & \dot{R}_{23} & \dot{R}_{33} \end{bmatrix} = \begin{bmatrix} R_{12}r - R_{13}q & -R_{11}r + R_{13}p & R_{11}q - R_{12}p \\ R_{22}r - R_{23}q & -R_{21}r + R_{23}p & R_{21}q - R_{22}p \\ R_{23}r - R_{33}q & -R_{31}r + R_{33}p & R_{31}q - R_{23}p \end{bmatrix} \quad (2.40)$$

**Proof.** For a small time increment  $\Delta t$  the rotation matrix  $\mathbf{R}_b^n$  satisfies

$$\mathbf{R}_b^n(t + \Delta t) \approx \mathbf{R}_b^n(t) \mathbf{R}_b^n(\Delta t) \quad (2.41)$$

since  $\sin(\Delta t) \approx \Delta t$  and  $\cos(\Delta t) \approx 1$ . Assume that after time  $t + \Delta t$  there has been an infinitesimal increment  $\Delta\beta$  in the rotation angle. From (2.16) we have

$$\begin{aligned} \mathbf{R}_b^n(\Delta t) &= \mathbf{I}_3 + \sin(\Delta\beta) \mathbf{S}(\lambda) + [1 - \cos(\Delta\beta)] \mathbf{S}^2(\lambda) \\ &\approx \mathbf{I}_3 + \Delta\beta \mathbf{S}(\lambda) \end{aligned} \quad (2.42)$$

From (2.41), it follows that

$$\mathbf{R}_b^n(t + \Delta t) = \mathbf{R}_b^n(t) [\mathbf{I}_3 + \Delta\beta \mathbf{S}(\lambda)] \quad (2.43)$$

Defining the vector  $\Delta\beta^b := \Delta\beta\lambda$ , the time derivative of  $\mathbf{R}_b^n$  is found as

$$\begin{aligned}\dot{\mathbf{R}}_b^n(t) &= \lim_{\Delta t \rightarrow 0} \frac{\mathbf{R}_b^n(t + \Delta t) - \mathbf{R}_b^n(t)}{\Delta t} \\ &= \lim_{\Delta t \rightarrow 0} \frac{\mathbf{R}_b^n(t) \Delta\beta \mathbf{S}(\lambda)}{\Delta t} \\ &= \lim_{\Delta t \rightarrow 0} \frac{\mathbf{R}_b^n(t) \mathbf{S}(\Delta\beta^b)}{\Delta t} \\ &= \mathbf{R}_b^n(t) \mathbf{S}(\omega_{nb}^b)\end{aligned}\quad (2.44)$$

where  $\omega_{nb}^b = \lim_{\Delta t \rightarrow 0} (\Delta\beta^b / \Delta t)$ .

### 6-DOF kinematic equations

Summarizing the results from this section, the 6-DOF kinematic equations can be expressed in matrix-vector form as

$$\begin{aligned}\dot{\boldsymbol{\eta}} &= \mathbf{J}_\Theta(\boldsymbol{\eta})\boldsymbol{\nu} \\ \Updownarrow \\ \begin{bmatrix} \dot{\mathbf{p}}_{nb}^n \\ \dot{\boldsymbol{\Theta}}_{nb} \end{bmatrix} &= \begin{bmatrix} \mathbf{R}(\boldsymbol{\Theta}_{nb}) & \mathbf{0}_{3 \times 3} \\ \mathbf{0}_{3 \times 3} & \mathbf{T}(\boldsymbol{\Theta}_{nb}) \end{bmatrix} \begin{bmatrix} \mathbf{v}_{nb}^b \\ \omega_{nb}^b \end{bmatrix}\end{aligned}\quad (2.45)$$

where  $\boldsymbol{\eta} \in \mathbb{R}^3 \times \mathcal{S}^3$  and  $\boldsymbol{\nu} \in \mathbb{R}^6$ .

#### Matlab:

The transformation matrix  $\mathbf{J}_\Theta(\boldsymbol{\eta})$  and its diagonal elements  $\mathbf{J}_{11}(\boldsymbol{\eta}) = \mathbf{R}(\boldsymbol{\Theta}_{nb})$  and  $\mathbf{J}_{22}(\boldsymbol{\eta}) = \mathbf{T}(\boldsymbol{\Theta}_{nb})$  can be computed by using the MSS toolbox command

```
[J, J11, J22] = eulerang(phi,theta,psi)
```

The differential equations are then found by

```
p_dot = J1 * v
theta_dot = J2 * w_nb
```

Alternatively, (2.45) can be written in component form as

$$\begin{aligned}\dot{x}^n &= u \cos(\psi) \cos(\theta) + v [\cos(\psi) \sin(\theta) \sin(\phi) - \sin(\psi) \cos(\phi)] \\ &\quad + w [\sin(\psi) \sin(\phi) + \cos(\psi) \cos(\phi) \sin(\theta)]\end{aligned}\quad (2.46)$$

$$\begin{aligned}\dot{y}^n &= u \sin(\psi) \cos(\theta) + v [\cos(\psi) \cos(\phi) + \sin(\phi) \sin(\theta) \sin(\psi)] \\ &\quad + w [\sin(\theta) \sin(\psi) \cos(\phi) - \cos(\psi) \sin(\phi)]\end{aligned}\quad (2.47)$$

$$\dot{z}^n = -u \sin(\theta) + v \cos(\theta) \sin(\phi) + w \cos(\theta) \cos(\phi)\quad (2.48)$$

$$\dot{\phi} = p + q \sin(\phi) \tan(\theta) + r \cos(\phi) \tan(\theta)\quad (2.49)$$

$$\dot{\theta} = q \cos(\phi) - r \sin(\phi)\quad (2.50)$$

$$\dot{\psi} = q \frac{\sin(\phi)}{\cos(\theta)} + r \frac{\cos(\phi)}{\cos(\theta)}, \quad \theta \neq \pm 90^\circ\quad (2.51)$$

### 3-DOF model for surface vessels

A frequently used simplification of (2.45) is the 3-DOF (surge, sway and yaw) representation for marine craft. This is based on the assumption that  $\phi$  and  $\theta$  are small during normal operation of ships, underwater vehicles and rigs. Hence,  $\mathbf{R}(\Theta_{nb}) = \mathbf{R}_{z,\psi}\mathbf{R}_{y,\theta}\mathbf{R}_{x,\phi} \approx \mathbf{R}_{z,\psi}$  and  $\mathbf{T}(\Theta_{nb}) \approx \mathbf{I}_3$ . Moreover, neglecting the elements corresponding to heave, roll and pitch finally yields

$$\dot{\boldsymbol{\eta}} = \mathbf{R}(\psi)\boldsymbol{\nu} \quad (2.52)$$

where  $\mathbf{R}(\psi) := \mathbf{R}_{z,\psi}$  with  $\boldsymbol{\nu} = [u, v, r]^\top$  and  $\boldsymbol{\eta} = [x^n, y^n, \psi]^\top$ .

## 2.2.2 Unit quaternions

An alternative to the Euler angle representation is a four-parameter method based on *unit quaternions* or *Euler parameters*. The main motivation for using four parameters is to avoid the representation singularity of the Euler angles.

A quaternion  $\mathbf{q}$  is defined as a complex number (Chou 1992) with one real part  $\eta$  and three imaginary parts given by the vector

$$\boldsymbol{\varepsilon} = [\varepsilon_1, \varepsilon_2, \varepsilon_3]^\top \quad (2.53)$$

A unit quaternion satisfies  $\mathbf{q}^\top \mathbf{q} = 1$ . The set  $Q$  of unit quaternions is therefore defined as

$$Q := \{\mathbf{q} | \mathbf{q}^\top \mathbf{q} = 1, \mathbf{q} = [\eta, \boldsymbol{\varepsilon}^\top]^\top, \boldsymbol{\varepsilon} \in \mathbb{R}^3 \text{ and } \eta \in \mathbb{R}\} \quad (2.54)$$

The motion of the body-fixed reference frame relative to the inertial frame will now be expressed in terms of unit quaternions.

From (2.16) it is seen that

$$\mathbf{R}_{\beta, \lambda} = \mathbf{I}_3 + \sin(\beta)\mathbf{S}(\lambda) + [1 - \cos(\beta)]\mathbf{S}^2(\lambda) \quad (2.55)$$

The real and imaginary parts of the unit quaternions are defined as (Chou 1992)

$$\eta := \cos\left(\frac{\beta}{2}\right) \quad (2.56)$$

$$\boldsymbol{\varepsilon} = [\varepsilon_1, \varepsilon_2, \varepsilon_3]^\top := \lambda \sin\left(\frac{\beta}{2}\right) \quad (2.57)$$

where  $\lambda = [\lambda_1, \lambda_2, \lambda_3]^\top$  is a unit vector satisfying

$$\lambda = \pm \frac{\boldsymbol{\varepsilon}}{\sqrt{\boldsymbol{\varepsilon}^\top \boldsymbol{\varepsilon}}} \quad \text{if} \quad \sqrt{\boldsymbol{\varepsilon}^\top \boldsymbol{\varepsilon}} \neq 0 \quad (2.58)$$

Consequently, the unit quaternions can be expressed in the form

$$\mathbf{q} = \begin{bmatrix} \eta \\ \varepsilon_1 \\ \varepsilon_2 \\ \varepsilon_3 \end{bmatrix} = \begin{bmatrix} \cos\left(\frac{\beta}{2}\right) \\ \lambda \sin\left(\frac{\beta}{2}\right) \end{bmatrix} \in Q, \quad 0 \leq \beta \leq 2\pi \quad (2.59)$$

This parametrization implies that the unit quaternions satisfy the constraint  $\mathbf{q}^\top \mathbf{q} = 1$ , that is

$$\eta^2 + \varepsilon_1^2 + \varepsilon_2^2 + \varepsilon_3^2 = 1 \quad (2.60)$$

The product of two quaternions is defined as

$$\mathbf{q}_1 \otimes \mathbf{q}_2 = \begin{bmatrix} \eta_1\eta_2 - \varepsilon_1^\top \varepsilon_2 \\ \eta_1\varepsilon_2 + \eta_2\varepsilon_1 + \mathbf{S}(\varepsilon_1)\varepsilon_2 \end{bmatrix} \quad (2.61)$$

### Unit quaternion rotation matrix from BODY to NED

From (2.55) with (2.56) and (2.57), the following rotation matrix for the unit quaternions is obtained

$$\mathbf{R}(\mathbf{q}_b^n) := \mathbf{I}_3 + 2\eta\mathbf{S}(\varepsilon) + 2\mathbf{S}^2(\varepsilon) \quad (2.62)$$

### Linear velocity transformation

The transformation relating the linear velocity vector in an inertial reference frame to a velocity in the body-fixed reference frame can now be expressed as

$$\dot{\mathbf{p}}_{nb}^n = \mathbf{R}(\mathbf{q}_b^n) \mathbf{v}_{nb}^b \quad (2.63)$$

where

$$\mathbf{R}(\mathbf{q}_b^n) = \begin{bmatrix} 1 - 2(\varepsilon_2^2 + \varepsilon_3^2) & 2(\varepsilon_1\varepsilon_2 - \varepsilon_3\eta) & 2(\varepsilon_1\varepsilon_3 + \varepsilon_2\eta) \\ 2(\varepsilon_1\varepsilon_2 + \varepsilon_3\eta) & 1 - 2(\varepsilon_1^2 + \varepsilon_3^2) & 2(\varepsilon_2\varepsilon_3 - \varepsilon_1\eta) \\ 2(\varepsilon_1\varepsilon_3 - \varepsilon_2\eta) & 2(\varepsilon_2\varepsilon_3 + \varepsilon_1\eta) & 1 - 2(\varepsilon_1^2 + \varepsilon_2^2) \end{bmatrix} \quad (2.64)$$

Expanding (2.63) yields

$$\dot{x}^n = u(1 - 2\varepsilon_2^2 - 2\varepsilon_3^2) + 2v(\varepsilon_1\varepsilon_2 - \varepsilon_3\eta) + 2w(\varepsilon_1\varepsilon_3 + \varepsilon_2\eta) \quad (2.65)$$

$$\dot{y}^n = 2u(\varepsilon_1\varepsilon_2 + \varepsilon_3\eta) + v(1 - 2\varepsilon_1^2 - 2\varepsilon_3^2) + 2w(\varepsilon_2\varepsilon_3 - \varepsilon_1\eta) \quad (2.66)$$

$$\dot{z}^n = 2u(\varepsilon_1\varepsilon_3 - \varepsilon_2\eta) + 2v(\varepsilon_2\varepsilon_3 + \varepsilon_1\eta) + w(1 - 2\varepsilon_1^2 - 2\varepsilon_2^2) \quad (2.67)$$

As for the Euler angle representation, Property 2.1 implies that the inverse transformation matrix satisfies  $\mathbf{R}^{-1}(\mathbf{q}_b^n) = \mathbf{R}^\top(\mathbf{q}_b^n)$ .

#### Matlab:

The quaternion rotation matrix is easily computed by using the MSS toolbox commands

```
q = [eta,eps1,eps2,eps3];
R = Rquat(q);
```

Notice that  $(\mathbf{q}_b^n)^\top \mathbf{q}_b^n = 1$  must be true for `Rquat.m` to return a solution. One way to ensure this is to use the transformation

```
q = euler2q(phi,theta,psi);
```

transforming the three Euler angles  $\phi, \theta$  and  $\psi$  to the unit quaternion vector  $\mathbf{q}_b^n$ ; see Section 2.2.3 for details.

### Angular velocity transformation

The angular velocity transformation can be derived by substituting the expressions for  $R_{ij}$  from (2.64) into the differential equation  $\dot{\mathbf{R}}_b^n = \mathbf{R}_b^n \mathbf{S}(\boldsymbol{\omega}_{nb}^b)$ ; see Theorem 2.2. Some calculations yield

$$\dot{\mathbf{q}}_b^n = \frac{1}{2} \mathbf{q}_b^n \otimes \begin{bmatrix} 0 \\ \boldsymbol{\omega}_{nb}^b \end{bmatrix} \quad (2.68)$$

An alternative formulation is the vector representation (Kane *et al.* 1983)

$$\begin{aligned} \dot{\mathbf{q}}_b^n &= \frac{1}{2} \begin{bmatrix} -\boldsymbol{\varepsilon}^\top \\ \eta \mathbf{I}_3 + \mathbf{S}(\boldsymbol{\varepsilon}) \end{bmatrix} \boldsymbol{\omega}_{nb}^b \\ &:= \mathbf{T}(\mathbf{q}_b^n) \boldsymbol{\omega}_{nb}^b \end{aligned} \quad (2.69)$$

where

$$\mathbf{T}(\mathbf{q}_b^n) = \frac{1}{2} \begin{bmatrix} -\varepsilon_1 & -\varepsilon_2 & -\varepsilon_3 \\ \eta & -\varepsilon_3 & \varepsilon_2 \\ \varepsilon_3 & \eta & -\varepsilon_1 \\ -\varepsilon_2 & \varepsilon_1 & \eta \end{bmatrix}, \quad \mathbf{T}^\top(\mathbf{q}_b^n) \mathbf{T}(\mathbf{q}_b^n) = \frac{1}{4} \mathbf{I}_3 \quad (2.70)$$

Hence,

$$\dot{\eta} = -\frac{1}{2}(\varepsilon_1 p + \varepsilon_2 q + \varepsilon_3 r) \quad (2.71)$$

$$\dot{\varepsilon}_1 = \frac{1}{2}(\eta p - \varepsilon_3 q + \varepsilon_2 r) \quad (2.72)$$

$$\dot{\varepsilon}_2 = \frac{1}{2}(\varepsilon_3 p + \eta q - \varepsilon_1 r) \quad (2.73)$$

$$\dot{\varepsilon}_3 = \frac{1}{2}(-\varepsilon_2 p + \varepsilon_1 q + \eta r) \quad (2.74)$$

#### Matlab:

The transformation matrix  $\mathbf{T}(\mathbf{q}_b^n)$  is implemented in the MSS toolbox as

```
T = Tquat(q)
```

## 6-DOF kinematic equations

The 6-DOF kinematic equations based on unit quaternions result in seven differential equations with  $\boldsymbol{\eta} = [x^n, y^n, z^n, \eta, \varepsilon_1, \varepsilon_2, \varepsilon_3]^\top$  as state vector (recall that only six differential equations are needed when using the Euler angle representation). The additional differential equation is needed because of the unity constraint of the unit quaternions. Consequently, unit quaternions do not represent generalized coordinates. The resulting model is

$$\begin{aligned}\dot{\boldsymbol{\eta}} &= \mathbf{J}_q(\boldsymbol{\eta})\boldsymbol{\nu} \\ \Downarrow \\ \begin{bmatrix} \dot{\mathbf{p}}_{nb}^n \\ \dot{\mathbf{q}}_b^n \end{bmatrix} &= \begin{bmatrix} \mathbf{R}(\mathbf{q}_b^n) & \mathbf{0}_{3 \times 3} \\ \mathbf{0}_{4 \times 3} & \mathbf{T}(\mathbf{q}_b^n) \end{bmatrix} \begin{bmatrix} \mathbf{v}_{nb}^b \\ \boldsymbol{\omega}_{nb}^b \end{bmatrix}\end{aligned}\quad (2.75)$$

where  $\boldsymbol{\eta} \in \mathbb{R}^7$  and  $\boldsymbol{\nu} \in \mathbb{R}^6$ , and  $\mathbf{J}_q(\boldsymbol{\eta}) \in \mathbb{R}^{7 \times 6}$  is a nonquadratic transformation matrix. Equation (2.75) in component form is given by (2.65)–(2.67) and (2.71)–(2.74).

### Matlab:

The transformation matrix  $\mathbf{J}_q(\boldsymbol{\eta})$  and its elements  $\mathbf{J}_{11} = \mathbf{R}(\mathbf{q}_b^n)$  and  $\mathbf{J}_{22} = \mathbf{T}(\mathbf{q}_b^n)$  can be computed directly in the MSS toolbox by using the following commands

```
q = [eta, eps1, eps2, eps3]';
[J,J11,J22] = quatern(q);
```

The corresponding differential equations are

```
p_dot = J11 * v;
q_dot = J22 * w_bn;
```

### Implementation considerations: unit quaternion normalization

When integrating (2.69), a normalization procedure is necessary to ensure that the constraint

$$(\mathbf{q}_b^n)^\top \mathbf{q}_b^n = \varepsilon_1^2 + \varepsilon_2^2 + \varepsilon_3^2 + \eta^2 = 1 \quad (2.76)$$

is satisfied in the presence of measurement noise and numerical round-off errors. For this purpose, the following discrete-time algorithm can be applied.

#### Algorithm 2.1 (Discrete-Time Unit Quaternion Normalization)

1.  $k = 0$ . Compute the initial value of  $\mathbf{q}_b^n[0]$ .
2. Euler's method implies that

$$\mathbf{q}_b^n[k+1] = \mathbf{q}_b^n[k] + h \mathbf{T}(\mathbf{q}_b^n[k]) \boldsymbol{\omega}_{nb}^b[k] \quad (2.77)$$

where  $h$  is the sampling time.

3. *Normalization:*

$$\dot{\mathbf{q}}_b^n[k+1] = \frac{\mathbf{q}_b^n[k+1]}{\|\mathbf{q}_b^n[k+1]\|} = \frac{\mathbf{q}_b^n[k+1]}{\sqrt{\mathbf{q}_b^n[k+1]^\top \mathbf{q}_b^n[k+1]}}$$

4. Let  $k = k + 1$  and return to Step 2.

A continuous-time algorithm for unit quaternion normalization can be implemented by noting that

$$\frac{d}{dt} ((\mathbf{q}_b^n)^\top \mathbf{q}_b^n) = 2(\mathbf{q}_b^n)^\top \mathbf{T}(\mathbf{q}_b^n) \boldsymbol{\omega}_{nb}^b = 0 \quad (2.78)$$

This shows that if  $\mathbf{q}_b^n$  is initialized as a unit vector, then it will remain a unit vector. Since integration of the quaternion vector  $\mathbf{q}_b^n$  from the differential equation (2.69) will introduce numerical errors that will cause the length of  $\mathbf{q}_b^n$  to deviate from unity, a non-linear feedback or normalization term is suggested. This can be achieved by replacing the kinematic differential equation (2.69) with

$$\dot{\mathbf{q}}_b^n = \mathbf{T}(\mathbf{q}_b^n) \boldsymbol{\omega}_{nb}^b + \frac{\gamma}{2} (1 - (\mathbf{q}_b^n)^\top \mathbf{q}_b^n) \mathbf{q}_b^n \quad (2.79)$$

where  $\gamma \geq 0$  (typically 100) is a design parameter reflecting the convergence rate of the normalization. This results in

$$\begin{aligned} \frac{d}{dt} ((\mathbf{q}_b^n)^\top \mathbf{q}_b^n) &= \underbrace{2(\mathbf{q}_b^n)^\top \mathbf{T}(\mathbf{q}_b^n) \boldsymbol{\omega}_{nb}^b}_{0 \text{ since } \mathbf{q}_b^n(0) \text{ is a unit vector}} + \gamma (1 - (\mathbf{q}_b^n)^\top \mathbf{q}_b^n) (\mathbf{q}_b^n)^\top \mathbf{q}_b^n \\ &= \gamma (1 - (\mathbf{q}_b^n)^\top \mathbf{q}_b^n) (\mathbf{q}_b^n)^\top \mathbf{q}_b^n \end{aligned} \quad (2.80)$$

A change of coordinates  $x = 1 - (\mathbf{q}_b^n)^\top \mathbf{q}_b^n$  and  $\dot{x} = -d/dt ((\mathbf{q}_b^n)^\top \mathbf{q}_b^n)$  yields

$$\dot{x} = -\gamma x(1 - x) \quad (2.81)$$

Linearization about  $x = 0$  results in  $\dot{x} = -\gamma x$ . Consequently, the normalization algorithm converges with a time constant  $T = \gamma^{-1}$ .

### 2.2.3 Unit Quaternion from Euler angles

If the Euler angles  $\Theta_{nb} = [\phi, \theta, \psi]^\top$  are known the corresponding unit quaternion can be computed using the transformation (NASA 2013):

$$\mathbf{q}_b^n = \begin{bmatrix} \cos(\psi) \cos(\theta) \cos(\phi) + \sin(\psi) \sin(\theta) \sin(\phi) \\ \cos(\psi) \cos(\theta) \sin(\phi) - \sin(\psi) \sin(\theta) \cos(\phi) \\ \sin(\psi) \cos(\theta) \sin(\phi) + \cos(\psi) \sin(\theta) \cos(\phi) \\ \sin(\psi) \cos(\theta) \cos(\phi) - \cos(\psi) \sin(\theta) \sin(\phi) \end{bmatrix} \quad (2.82)$$

Formula (2.82) is implemented in the MSS toolbox as `euler2q.m` and it is only valid for the *zyx* convention of the Euler angles. This formula can also be used to compute the initial values of the Euler parameters corresponding to Step 1 of Algorithm 2.1.

**Example 2.2 (Unit Quaternion from Euler Angles)**

Consider a marine craft with attitude  $\phi = 10.0^\circ$ ,  $\theta = -20.0^\circ$  and  $\psi = 30.0^\circ$ . The unit quaternion is computed in Matlab by using the commands:

```
phi=10*(pi/180); psi = 30*(pi/180); theta=-20*(pi/180);
q = euler2q(phi,theta,psi)
q =
    0.9437
    0.1277
   -0.1449
    0.2685
>> norm(q)           % normalization test
ans =
    1
```

**2.2.4 Euler angles from a unit quaternion**

The relationship between the Euler angles  $\phi, \theta$  and  $\psi$  ( $zyx$  convention) and the unit quaternion  $q_b^n$  ( $i = 1, \dots, 4$ ) can be established by requiring that the rotation matrices of the two kinematic representations are equal

$$\mathbf{R}(\Theta_{nb}) := \mathbf{R}(q_b^n) \quad (2.83)$$

Let the elements of  $\mathbf{R}(q_b^n)$  be denoted by  $R_{ij}$  where the superscripts  $i$  and  $j$  denote the  $i$ -th row and  $j$ -th column. Writing expression (2.83) in component form yields a system of nine equations with three unknowns ( $\phi, \theta$  and  $\psi$ ) given by

$$\begin{bmatrix} c\psi c\theta & -s\psi c\phi + c\psi s\theta s\phi & s\psi s\phi + c\psi c\phi s\theta \\ s\psi c\theta & c\psi c\phi + s\phi s\theta s\psi & -c\psi s\phi + s\theta s\psi c\phi \\ -s\theta & c\theta s\phi & c\theta c\phi \end{bmatrix} = \begin{bmatrix} R_{11} & R_{12} & R_{13} \\ R_{21} & R_{22} & R_{23} \\ R_{31} & R_{32} & R_{33} \end{bmatrix} \quad (2.84)$$

One solution to (2.84) is

$$\phi = \text{atan2}(R_{32}, R_{33}) \quad (2.85)$$

$$\theta = -\text{asin}(R_{31}), \quad \theta \neq \pm 90^\circ \quad (2.86)$$

$$\psi = \text{atan2}(R_{21}, R_{11}) \quad (2.87)$$

where  $\text{atan2}(y, x)$  is the 4-quadrant inverse tangent confining the result to  $(-\pi, \pi]$ . Precautions must be taken against computational errors in the vicinity of  $\theta = \pm 90^\circ$ . The MSS toolbox script `[phi, theta, psi] = q2euler(q)` is based on Formulas (2.85)–(2.87). A singularity test is included in order to avoid numerical problems for  $\theta = \pm 90^\circ$ .

**Example 2.3 (Euler Angles from a Unit Quaternion)**

Consider the marine vessel in Example 2.2 where the Euler angles were converted into a unit quaternion. The inverse transformation `q2euler.m` results in:

```

q =[0.9437, 0.1277, -0.1449, 0.2685]';
[phi,theta,psi] = q2euler(q/norm(q))
phi =
    0.1746
theta =
   -0.3491
psi =
    0.5235

```

corresponding to  $\phi = 10.0^\circ$ ,  $\theta = -20.0^\circ$  and  $\psi = 30.0^\circ$ .

## 2.3 Transformations between ECEF and NED

Wide area or terrestrial guidance and navigation implies that the position should be related to the Earth center instead of a local frame on the Earth's surface. This section describes the kinematic transformation between ECEF and NED parametrized in terms of *longitude*, *latitude* and *height*. The NED reference frame can be represented as a tangent plane on the Earth's surface moving with the craft or an Earth-fixed tangent plane with constant longitude and latitude used for local navigation.

### 2.3.1 Longitude and latitude rotation matrix

The transformation between the ECEF and NED velocity vectors is

$$\dot{\mathbf{p}}_{eb}^e = \mathbf{R}_n^e \dot{\mathbf{p}}_{eb}^n = \mathbf{R}_n^e \mathbf{R}_b^n \mathbf{v}_{eb}^b \quad (2.88)$$

where  $\mathbf{R}_n^e = \mathbf{R}(\Theta_{en})$  and  $\mathbf{R}_b^n = \mathbf{R}(\Theta_{nb})$ . Let  $\Theta_{en} = [l, \mu]^\top \in \mathcal{S}^2$  denote the vector formed by longitude  $l$  and latitude  $\mu$  (see Figure 2.5) and  $\mathbf{R}_n^e: \mathcal{S}^2 \rightarrow SO(3)$  is a rotation matrix between ECEF and NED.

The rotation matrix  $\mathbf{R}_n^e$  is found by performing two principal rotations: (1) a rotation  $l$  about the  $z$  axis and (2) a rotation  $(-\mu - \pi/2)$  about the  $y$  axis. This gives

$$\begin{aligned} \mathbf{R}_n^e &:= \mathbf{R}_{z,l} \mathbf{R}_{y,-\mu-\frac{\pi}{2}} \\ &= \begin{bmatrix} \cos(l) & -\sin(l) & 0 \\ \sin(l) & \cos(l) & 0 \\ 0 & 0 & 1 \end{bmatrix} \begin{bmatrix} \cos(-\mu-\frac{\pi}{2}) & 0 & \sin(-\mu-\frac{\pi}{2}) \\ 0 & 1 & 0 \\ -\sin(-\mu-\frac{\pi}{2}) & 0 & \cos(-\mu-\frac{\pi}{2}) \end{bmatrix} \end{aligned} \quad (2.89)$$

Using the trigonometric formulae  $\cos(-\mu - \frac{\pi}{2}) = -\sin(\mu)$  and  $\sin(-\mu - \frac{\pi}{2}) = -\cos(\mu)$  yields

$$\mathbf{R}_n^e = \mathbf{R}(\Theta_{en}) = \begin{bmatrix} -\cos(l)\sin(\mu) & -\sin(l) & -\cos(l)\cos(\mu) \\ -\sin(l)\sin(\mu) & \cos(l) & -\sin(l)\cos(\mu) \\ \cos(\mu) & 0 & -\sin(\mu) \end{bmatrix} \quad (2.90)$$

Hence, the ECEF positions  $\mathbf{p}_{eb}^e = [x^e, y^e, z^e]^\top$  can be found by numerical integration of (2.88).

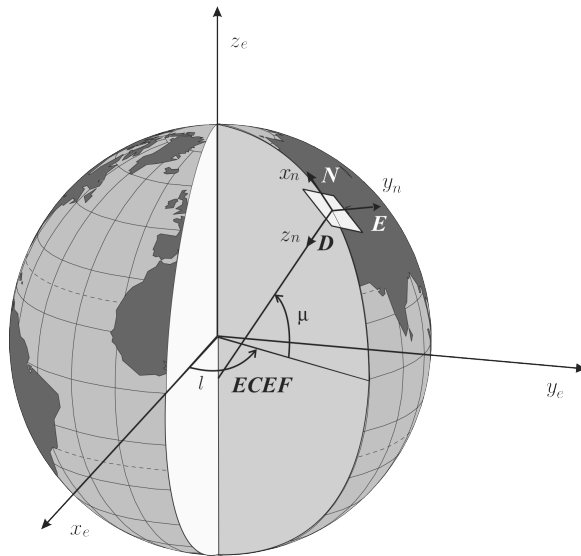


Figure 2.5: Definitions of longitude  $l$  and latitude  $\mu$  and the NED reference frame on the surface of the Earth. The  $D$  axis points in the normal direction to the Earth's surface.

**Matlab:**

The rotation matrix  $R_n^e$  is computed using the MSS toolbox command

```
R = Rll(l,mu)
```

### 2.3.2 Longitude, latitude and height from ECEF coordinates

The measurements of global navigation satellite systems (BeiDou, Galileo, GLONASS and GPS) are given in the Cartesian ECEF frame, but these are measurements that do not make much sense to a human operator. The presentation of terrestrial position data  $p_{eb}^e = [x^e, y^e, z^e]^\top$  is therefore made in terms of the ellipsoidal parameters longitude  $l$ , latitude  $\mu$  and height  $h$ .

The reference ellipsoid used for satellite navigation systems, WGS-84, is found by rotating an ellipse around the polar axis. Because of symmetry about the polar axis, it is only necessary to look at the meridian plane (latitude) equations. The origin of the ellipsoid coincides with the mass center of the Earth. The most important parameters of the WGS-84 ellipsoid are listed in Table 2.2.

In Figure 2.6,  $\mu$  is the *geodetic* latitude,  $h$  is the ellipsoidal height and  $N$  is the radius of curvature in the prime vertical.  $N$  is calculated by

$$N = \frac{r_e^2}{\sqrt{r_e^2 \cos^2(\mu) + r_p^2 \sin^2(\mu)}} \quad (2.91)$$

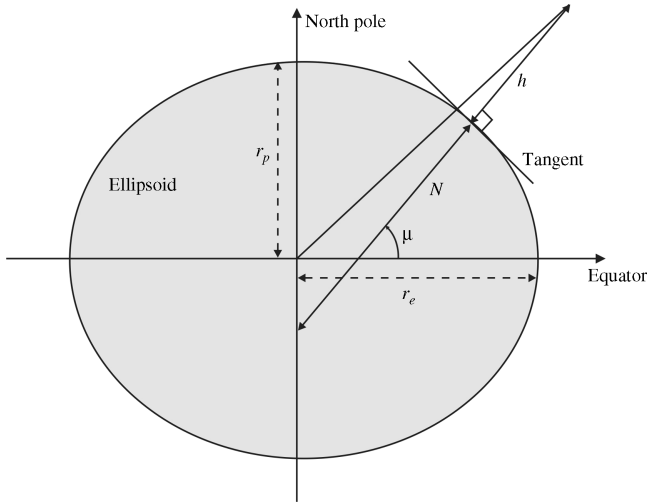


Figure 2.6: Definitions of the ellipsoidal parameters.

where the equatorial and polar earth radii,  $r_e$  and  $r_p$ , are the semi-axes of the ellipsoid. Longitude  $l$  is easily computed as

$$l = \text{atan} \left( \frac{y^e}{x^e} \right) \quad (2.92)$$

while latitude  $\mu$  and height  $h$  are implicitly computed by

$$\tan(\mu) = \frac{z^e}{p} \left( 1 - e^2 \frac{N}{N + h} \right)^{-1} \quad (2.93)$$

$$h = \frac{p}{\cos(\mu)} - N \quad (2.94)$$

where  $e$  is the eccentricity of the Earth given by

$$e = \sqrt{1 - \left( \frac{r_p}{r_e} \right)^2} \quad (2.95)$$

Since these two equations are implicit, they can be solved iteratively by using Algorithm 2.2 (Hofmann-Wellenhof *et al.* 1994).

Table 2.2: WGS-84 parameters

Parameters	Comments
$r_e = 6\,378\,137 \text{ m}$	Equatorial radius of ellipsoid (semi-major axis)
$r_p = 6\,356\,752 \text{ m}$	Polar axis radius of ellipsoid (semi-minor axis)
$\omega_{ie} = 7.292115 \times 10^{-5} \text{ rad/s}$	Angular velocity of the Earth
$e = 0.0818$	Eccentricity of ellipsoid

**Algorithm 2.2 (Transformation of  $(x^e, y^e, z^e)$  to  $(l, \mu, h)$ )**

1. Compute  $p = \sqrt{(x^e)^2 + (y^e)^2}$ .
2. Compute the approximate value  $\mu_{(0)}$  from

$$\tan(\mu_{(0)}) = \frac{z^e}{p}(1 - e^2)^{-1}$$

3. Compute an approximate value  $N$  from

$$N = \frac{r_e^2}{\sqrt{r_e^2 \cos^2(\mu_{(0)}) + r_p^2 \sin^2(\mu_{(0)})}}$$

4. Compute the ellipsoidal height by

$$h = \frac{p}{\cos(\mu_{(0)})} - N_{(0)}$$

5. Compute an improved value for the latitude by

$$\tan(\mu) = \frac{z^e}{p} \left(1 - e^2 \frac{N_{(0)}}{N_{(0)} + h}\right)^{-1}$$

6. Check for another iteration step: if  $|\mu - \mu_{(0)}| < \varepsilon$ , where  $\varepsilon$  is a small number, then the iteration is complete. Otherwise set  $\mu_{(0)} = \mu$  and continue with Step 3.

**Matlab:**

Algorithm 2.2 is programmed in the MSS toolbox as a function

```
[l,mu,h] = ecef2llh(x,y,z)
```

Several other algorithms can be used for this purpose; see Farrell (2008) and references therein. An approximate solution can also be found in Hofmann-Wellenhof *et al.* (1994) and an exact explicit solution is given by Zhu (1993).

**Height transformation**

The WGS-84 ellipsoid is a global ellipsoid, which is only an approximation of the mean sea level of the Earth. It can deviate from the real mean sea level by as much as 100 meters at certain locations. The Earth's geoid, on the other hand, is defined physically and its center is coincident with the center of the Earth. It is an equipotential surface so that it has the same gravitational magnitude all over the surface, and the gravity vector is always perpendicular to the geoid.

The geoid is the surface chosen as a zero level reference. The ellipsoidal height  $h$  in Figure 2.7 must therefore be transformed to the *orthometric* height  $H$  in Figure 2.7 through the relation

$$h \approx H + M$$

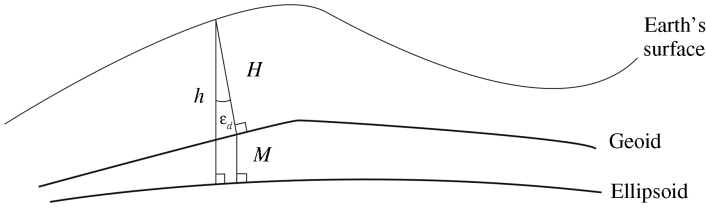


Figure 2.7: Illustration of ellipsoidal and orthometric heights  $h$  and  $H$  where  $\varepsilon_d$  is the deflection of gravity and  $M$  is the geoidal height (undulation).

where  $M$  is called the *geoidal height*. The angle  $\varepsilon_d$  is small enough for the above approximation to be sufficiently accurate for all practical purposes. The angle  $\varepsilon_d$  is known as the deflection of the vertical, and does not exceed 30 arcseconds in most of the world. In fact the largest deflection encountered over the entire earth is in the order of 1 arcminutes (Britting 1971). The geoidal height  $M$  is found through a *datum transformation* (Hofmann-Wellenhof *et al.* 1994).

### 2.3.3 ECEF coordinates from longitude, latitude and height

The transformation from  $\Theta_{en} = [l, \mu]^\top$  for given heights  $h$  to  $p_{eb}^e = [x^e, y^e, z^e]^\top$  is given by (Heiskanen and Moritz 1967)

$$\begin{bmatrix} x^e \\ y^e \\ z^e \end{bmatrix} = \begin{bmatrix} (N + h) \cos(\mu) \cos(l) \\ (N + h) \cos(\mu) \sin(l) \\ \left(\frac{r_p^2}{r_e^2} N + h\right) \sin(\mu) \end{bmatrix} \quad (2.96)$$

For a ship  $h$  is the vertical distance from the sea level to the coordinate origin of  $\{b\}$ .

#### Matlab:

The transformation from  $\Theta_{en} = [l, \mu]^\top$  to  $p_{eb}^e = [x^e, y^e, z^e]^\top$ . Equation (2.96), is programmed in the MSS toolbox function

```
[x, y, z] = llh2ecef(l, mu, h)
```

Assume that  $l = 10.3^\circ$ ,  $\mu = 63.0^\circ$  and  $h = 0$  m. Hence, the ECEF coordinates are computed to be

$$\begin{bmatrix} x^e \\ y^e \\ z^e \end{bmatrix} = \begin{bmatrix} 2\,856\,552 & \text{m} \\ 519\,123 & \text{m} \\ 5\,659\,978 & \text{m} \end{bmatrix}$$

using the MSS Matlab command

```
[x, y, z] = llh2ecef(10.3*(pi/180), 63.0*(pi/180), 0)
```

## 2.4 Transformations between ECEF and Flat-Earth Coordinates

For local flat-Earth navigation it can be assumed that the NED tangent plane is fixed on the surface of the Earth. Assume that the NED tangent plane is located at  $l_0$  and  $\mu_0$  such that

$$\mathbf{R}_n^e = \mathbf{R}(\theta_{en}) = \text{constant} \quad (2.97)$$

where  $\theta_{en} = [l_0, \mu_0]^\top$ . The ECEF coordinates satisfy the differential equation

$$\dot{\mathbf{p}}_{eb}^e = \mathbf{R}_n^e \mathbf{R}_b^n \mathbf{v}_{eb}^b \quad (2.98)$$

When designing dynamic positioning (DP) systems for offshore vessels this is a good approximation. However, when designing global waypoint tracking control systems for ships, “flat Earth” is not a good approximation since  $(l, \mu)$  will vary largely for ships in transit between the different continents.

### 2.4.1 Longitude, latitude and height from flat-Earth coordinates

Assume that a flat-Earth coordinate system is defined as the tangent plan to the WGS-84 ellipsoid. The coordinate origin is located at  $(l_0, \mu_0)$  with reference height  $h_{\text{ref}}$  in meters above the surface of the Earth. The NED positions with respect to the coordinate origin are denoted as  $(x^n, y^n, z^n)$  with  $z^n$  positive downwards.

The Earth radius of curvature in the prime vertical  $R_N$  and the radius of curvature in the meridian  $R_M$  are (Farrell 2008)

$$R_N = \frac{r_e}{\sqrt{1 - e^2 \sin^2(\mu_0)}} \quad (2.99)$$

$$R_M = R_N \frac{1 - e^2}{\sqrt{1 - e^2 \sin^2(\mu_0)}} \quad (2.100)$$

where  $r_e = 6\,378\,137$  m is the semi-minor axis (equatorial radius) and  $e = 0.0818$  is the Earth eccentricity. It follows that

$$\Delta l = y^n \text{atan2}(1, R_M \cos(\mu_0)) \quad (2.101)$$

$$\Delta \mu = x^n \text{atan2}(1, R_N) \quad (2.102)$$

where  $\text{atan2}(y, x)$  is the 4-quadrant inverse tangent confining the result to  $(-\pi, \pi]$ . The triplet  $(l, \mu, h)$  is computed as

$$l = \text{ssa}(l_0 + \Delta l) \quad (2.103)$$

$$\mu = \text{ssa}(\mu_0 + \Delta \mu) \quad (2.104)$$

$$h = h_{\text{ref}} - z^n \quad (2.105)$$

where  $\text{ssa}(\cdot)$  is the *smallest signed angle* confining the argument to the interval  $[-\pi, \pi]$ .

**Matlab:**

The `ssa(·)` function is implemented in the MSS toolbox as

```
angle = ssa(angle,type)
```

where `type` can be chosen as '`'rad'` or '`'deg'`'.

**Matlab:**

The triplet  $(l, \mu, h)$  corresponding to the NED coordinates  $(x^n, y^n, z^n)$  in a flat-Earth coordinate origin located at  $(l_0, \mu_0)$  with reference height  $h_{\text{ref}}$  in meters above the surface of the Earth is computed as

```
[l,mu,h] = flat2llh(x,y,z,10,mu0,h_ref)
```

### 2.4.2 Flat-Earth coordinates from longitude, latitude and height

The NED positions  $(x^n, y^n, z^n)$  with respect to a flat-Earth coordinate system with origin  $(l_0, \mu_0)$  and reference height  $h_{\text{ref}}$  are computed as (Farrell 2008)

$$x^n = \frac{\Delta\mu}{\text{atan}2(1, R_M)} \quad (2.106)$$

$$y^n = \frac{\Delta l}{\text{atan}2(1, R_N \cos(\mu_0))} \quad (2.107)$$

$$z^n = h_{\text{ref}} - h \quad (2.108)$$

where

$$\Delta l := l - l_0 \quad (2.109)$$

$$\Delta\mu := \mu - \mu_0 \quad (2.110)$$

**Matlab:**

For a marine craft operating on the sea surface ( $h = 0$ ) or submerged ( $h < 0$ ) with longitude and latitude  $(l, \mu)$  and a local coordinate origin at  $(l_0, \mu_0, h_{\text{ref}})$ , the NED positions can be computed using the MSS toolbox command

```
[x,y,z] = llh2flat(l,mu,h,10,mu0,h_ref)
```

## 2.5 Transformations between BODY and FLOW

The FLOW frame  $\{f\} = (x_f, y_f, z_f)$  is a convenient frame to express the hydrodynamic forces and moments acting on a marine craft. The FLOW axes are found by rotating the BODY axis system such that the resulting  $x_f$  axis is parallel to the freestream flow. Moreover, in FLOW axes, the  $x_f$  axis points directly into the relative flow while

the  $z_f$  axis remains in the reference plane, but rotates so that it remains perpendicular to the  $x_f$  axis. The  $y_f$  axis completes the right-handed system. The transformation is outlined in Section 2.5.3.

The main reason for the FLOW axis system is that it is more convenient for calculating hydrodynamic forces. For instance, lift is, by definition, perpendicular to the relative flow, while drag is parallel. With FLOW axes, both lift and drag resolve into a force that is parallel to one of the axes.

### 2.5.1 Definitions of heading, course and crab angles

The relationship between the angular variables *course*, *heading* and *sideslip* is important for maneuvering of a marine craft in the horizontal plane (3 DOF). The terms *course* and *heading* are used interchangeably in much of the literature on guidance, navigation and control of marine craft, and this leads to confusion. Consequently, definitions utilizing a consistent symbolic notation will now be established.

**Definition 2.4 (Heading (Yaw) Angle  $\psi$ )**

*The angle  $\psi$  from the  $x_n$  axis of  $\{n\}$  to the  $x_b$  axis of  $\{b\}$ , positive rotation about the  $z_n$  axis of  $\{n\}$  by the right-hand screw convention (see Figure 2.8).*

The heading angle is usually measured by using a magnetic compass, gyrocompass or two GNSS receivers; see Gade (2016) for a discussion on methods. The heading angle is well defined for zero speed such that it is possible to design a *heading autopilot* to maintain constant heading during stationkeeping and transit. However, during transit it is common to use a *course autopilot* for path following.

**Definition 2.5 (Course Angle  $\chi$ )**

*The angle  $\chi$  from the  $x_n$  axis of  $\{n\}$  to the velocity vector of the craft, positive rotation about the  $z_n$  axis of  $\{n\}$  by the right-hand screw convention (see Figure 2.8).*

Notice that the course angle is only defined for positive speed. For surface vessels both the course and speed over ground (COG and SOG) can be measured by GNSS. For underwater vehicles it is common to use hydroacoustic reference systems.

From (2.28) it follows that the horizontal motion of a marine craft can be described by

$$\dot{x}^n = u \cos(\psi) - v \sin(\psi) \quad (2.111)$$

$$\dot{y}^n = u \sin(\psi) + v \cos(\psi) \quad (2.112)$$

These equations can be expressed in *amplitude-phase* form

$$\dot{x}^n = U \cos(\psi + \beta_c) := U \cos(\chi) \quad (2.113)$$

$$\dot{y}^n = U \sin(\psi + \beta_c) := U \sin(\chi) \quad (2.114)$$

where

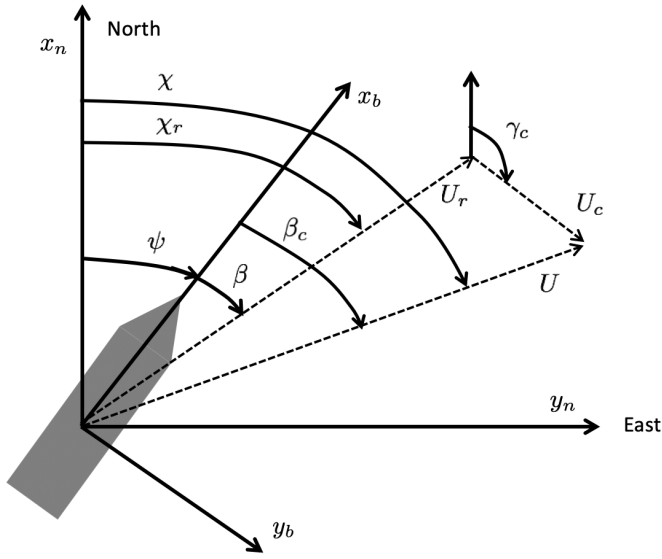


Figure 2.8: Ocean current triangle. Horizontal plane.

$$\chi = \psi + \beta_c \quad (2.115)$$

The amplitude  $U$  is recognized as the horizontal-plane speed

$$U = \sqrt{u^2 + v^2} \quad (2.116)$$

and the phase variable  $\beta_c = \text{atan}(v/u)$  is the crab angle. The relationship between the angular variables is shown in Figure 2.8.

#### **Definition 2.6 (Crab Angle $\beta_c$ )**

*The angle  $\beta_c$  from the  $x_b$  axis of  $\{b\}$  to the velocity vector of the vehicle, positive rotation about the  $z_b$  axis of  $\{b\}$  by the right-hand screw convention.*

$$\beta_c = \text{atan} \left( \frac{v}{u} \right) = \sin^{-1} \left( \frac{v}{U} \right) \xrightarrow{\beta_c \text{ small}} \beta_c \approx \frac{v}{U} \quad (2.117)$$

#### **2.5.2 Definitions of angle of attack and sideslip angle**

A marine craft is exposed to ocean currents. Let  $(u_c, v_c, w_c)$  denote the velocity components of the current. Hence, the current speed is

$$U_c = \sqrt{u_c^2 + v_c^2 + w_c^2} \quad (2.118)$$

and the *relative speed* is

$$U_r = \sqrt{u_r^2 + v_r^2 + w_r^2} \quad (2.119)$$

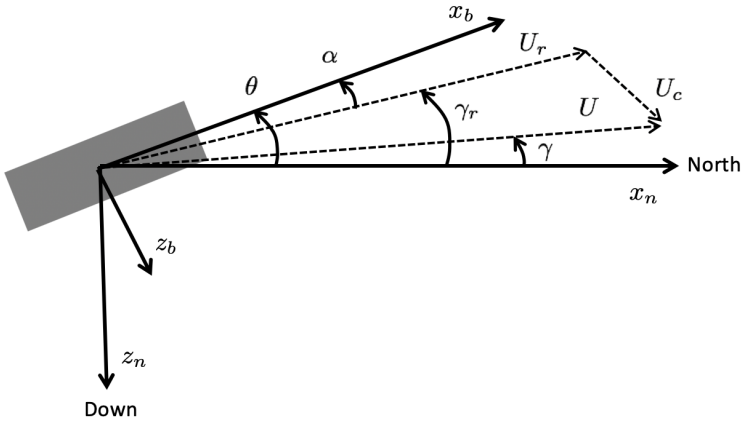


Figure 2.9: Ocean current triangle. Vertical plane.

where

$$u_r = u - u_c \quad (2.120)$$

$$v_r = v - v_c \quad (2.121)$$

$$w_r = w - w_c \quad (2.122)$$

It is possible to generalize the results of Section 2.5.1 to incorporate the effects of ocean currents. Figures 2.8 and 2.9 show the angle of attack  $\alpha$  and sideslip angle  $\beta$  for a marine craft. The mathematical definitions are given below.

#### **Definition 2.7 (Angle of Attack $\alpha$ )**

*The angle  $\alpha$  from the velocity vector of the vehicle to the  $x_b$  axis of  $\{b\}$ , positive rotation about the  $y_b$  axis of  $\{b\}$  by the right-hand screw convention.*

$$\alpha = \tan^{-1} \left( \frac{w_r}{u_r} \right) \quad \alpha \underset{\text{small}}{\Rightarrow} \quad \alpha \approx \frac{w_r}{u_r} \quad (2.123)$$

#### **Definition 2.8 (Sideslip (Drift) Angle $\beta$ )**

*The angle  $\beta$  from the  $x_b$  axis of  $\{b\}$  to the velocity vector of the vehicle, positive rotation about the  $z_b$  axis of  $\{b\}$  by the right-hand screw convention.*

$$\beta = \sin^{-1} \left( \frac{v_r}{U_r} \right) \quad \beta \underset{\text{small}}{\Rightarrow} \quad \beta \approx \frac{v_r}{U_r} \quad (2.124)$$

These relationships are easily verified from Figures 2.8 and 2.9 where it is observed that the angle of attack and sideslip angle satisfy

$$\gamma_r = \theta - \alpha \quad (2.125)$$

$$\chi_r = \psi + \beta \quad (2.126)$$

Here  $\gamma_r$  and  $\chi_r$  are recognized as the relative flight-path and course angles.

**Remark 2.1**

In SNAME (1950) and Lewis (1989) the sideslip angle for marine craft is defined according to

$$\beta_{\text{SNAME}} := -\beta$$

Note that the sideslip angle definition in this section follows the sign convention used by the aircraft community, for instance as in Nelson (1998) and Stevens and Lewis (1992). This definition is more intuitive from a guidance point of view, as shown in Figure 2.8.

Time differentiation of  $\beta$  under the assumption that  $\beta$  is small and  $U_r > 0$  is constant gives

$$\dot{\nu}_r = U_r \cos(\beta) \dot{\beta} \quad (2.127)$$

Consequently, the differential equation for  $\beta$  becomes

$$\dot{\beta} = \frac{1}{U_r \cos(\beta)} \dot{\nu}_r \quad (2.128)$$

This relationship is exploited when designing path-following control systems (see Section 10.3).

**Example 2.4 (Sideslip Angle: No Ocean Currents)**

Consider a ship moving at  $U = 10 \text{ m/s}$  with constant turning rate  $r = 0.1 \text{ rad/s}$  under the assumption of no ocean currents. The steady-state sway velocity during turning is  $v = 0.8 \text{ m/s}$ . For this case the crab and sideslip angles are equal

$$\beta_c = \beta = \sin^{-1} \left( \frac{v}{U} \right) = \sin^{-1} \left( \frac{0.8}{10} \right) \approx 4.6^\circ \quad (2.129)$$

Consequently, the heading and course angles satisfy

$$\chi = \psi + 4.6^\circ \quad (2.130)$$

**Example 2.5 (Sideslip Angle: Stationkeeping)**

Consider a marine craft at rest and exposed for an ocean current  $u_c = v_c = 0.5 \text{ m/s}$ . Since  $u = v = 0$  it follows that  $U_r = \sqrt{u_c^2 + v_c^2}$  and

$$\beta_c = 0 \quad (2.131)$$

$$\beta = \sin^{-1} \left( \frac{-v_c}{U_r} \right) \approx -20.7^\circ \quad (2.132)$$

**Example 2.6 (Sideslip Angle: Straight-Line Motion)**

Consider a marine craft moving at  $u = 10 \text{ m/s}$  on a straight line under the assumption of zero sway velocity ( $v = 0$ ). For an ocean current  $u_c = v_c = 0.5 \text{ m/s}$  it follows that  $U_r = \sqrt{(u - u_c)^2 + v_c^2}$  and

$$\beta_c = 0 \quad (2.133)$$

$$\beta = \sin^{-1} \left( \frac{-v_c}{U_r} \right) \approx -3.0^\circ \quad (2.134)$$

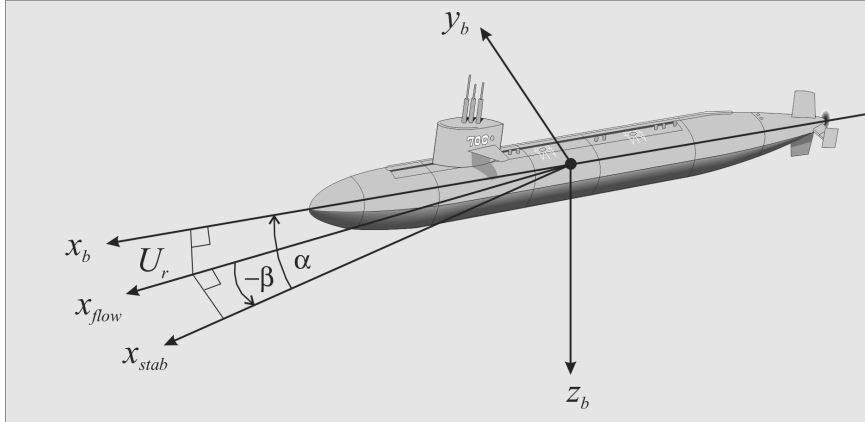


Figure 2.10: Illustration of stability and flow axes in terms of the angle of attack  $\alpha$ , sideslip angle  $\beta$  and relative speed  $U_r$ .

### 2.5.3 Flow-axes rotation matrix

The transformation from FLOW to BODY axes is defined by two principal rotations. First, the flow axes are rotated by a *negative* sideslip angle  $-\beta$  about the  $z$  axis and the new coordinate system is called *stability axes*. Second, the stability axes are rotated by a *positive* angle  $\alpha$  about the new  $y$  axis. This angle  $\alpha$  is called the *angle of attack*.

The names *stability* and *wind axes* are commonly used in aerodynamics to model lift and drag forces, which both are nonlinear functions of  $\alpha$ ,  $\beta$  and  $U_r$ . This convention has been adopted by the marine community and SNAME to describe lift and drag forces on submerged vehicles (SNAME 1950). For marine craft, *wind axes* correspond to *flow axes*.

The main reason for the FLOW axis system is that it is more convenient for calculation of the hydrodynamic forces. Assume that the lift and drag coefficients  $C_L(\alpha)$  and  $C_D(\alpha)$  are known for a marine craft such that the forces in FLOW axes become

$$F_{\text{drag}} = \frac{1}{2} \rho V_r^2 S C_D(\alpha) \quad (2.135)$$

$$F_{\text{lift}} = \frac{1}{2} \rho V_r^2 S C_L(\alpha) \quad (2.136)$$

where  $\rho$  is the density of water and  $S$  is the area of the wetted surface of the hull. Since lift is perpendicular to the relative flow and drag is parallel, the longitudinal forces in BODY axes become

$$\begin{bmatrix} X \\ Z \end{bmatrix} = \begin{bmatrix} \cos(\alpha) & -\sin(\alpha) \\ \sin(\alpha) & \cos(\alpha) \end{bmatrix} \begin{bmatrix} -F_{\text{drag}} \\ -F_{\text{lift}} \end{bmatrix} \quad (2.137)$$

For surface ships it is common to assume that  $\alpha = 0$  such that  $X = -F_{\text{drag}}$  and  $Z = -F_{\text{lift}}$ , while submerged vehicles operate at nonzero angles of attack.

Stability and flow axes are also used in path following. For instance, a ship equipped with a single rudder and a main propeller can follow a path even though only two controls are available by simply steering the vessel to the path using the rudder. The speed is controlled by an independent propeller feedback loop (Fossen *et al.* 2003). This means that we control the  $x^n y^n$  coordinates and yaw angle  $\psi$  of the ship (3 DOF). When doing this, it is optimal to have a zero sideslip angle when there are no ocean currents, wave and wind loads. If the environmental forces are nonzero, it is optimal to have a nonzero sideslip angle, as shown in Figure 2.10 (Breivik and Fossen 2005a). This is referred to as weathervaning. However, it is extremely difficult to track the desired path given by  $x^n$  and  $y^n$ , and at the same time maintain a constant heading angle  $\psi$  unless three controls are available for feedback since this is an underactuated control problem.

The transformation between BODY, STABILITY and FLOW axes can be mathematically expressed as

$$\mathbf{v}_r^{\text{stab}} = \mathbf{R}_{y,\alpha} \mathbf{v}_r^b \quad (2.138)$$

$$\mathbf{v}_r^{\text{flow}} = \mathbf{R}_{z,-\beta} \mathbf{v}_r^{\text{stab}} \quad (2.139)$$

where the subscript  $r$  denotes the relative velocities and

$$\mathbf{R}_{y,\alpha} = \begin{bmatrix} \cos(\alpha) & 0 & \sin(\alpha) \\ 0 & 1 & 0 \\ -\sin(\alpha) & 0 & \cos(\alpha) \end{bmatrix} \quad (2.140)$$

$$\mathbf{R}_{z,-\beta} = \mathbf{R}_{z,\beta}^\top = \begin{bmatrix} \cos(\beta) & \sin(\beta) & 0 \\ -\sin(\beta) & \cos(\beta) & 0 \\ 0 & 0 & 1 \end{bmatrix} \quad (2.141)$$

The transformation matrix from BODY to FLOW axes then becomes

$$\mathbf{R}_b^{\text{flow}} = \mathbf{R}_{z,-\beta} \mathbf{R}_{y,\alpha} = \begin{bmatrix} \cos(\beta) \cos(\alpha) & \sin(\beta) & \cos(\beta) \sin(\alpha) \\ -\sin(\beta) \cos(\alpha) & \cos(\beta) & -\sin(\beta) \sin(\alpha) \\ -\sin(\alpha) & 0 & \cos(\alpha) \end{bmatrix} \quad (2.142)$$

The velocity transformation

$$\mathbf{v}_r^{\text{flow}} = \mathbf{R}_b^{\text{flow}} \mathbf{v}_r^b \quad (2.143)$$

can now be rewritten as

$$\mathbf{v}_r^b = (\mathbf{R}_b^{\text{flow}})^\top \mathbf{v}_r^{\text{flow}} \quad (2.144)$$

$$\Downarrow$$

$$\begin{bmatrix} u_r \\ v_r \\ w_r \end{bmatrix} = \mathbf{R}_{y,\alpha}^\top \mathbf{R}_{z,-\beta}^\top \begin{bmatrix} U_r \\ 0 \\ 0 \end{bmatrix} \quad (2.145)$$

Writing this expression in component form yields

$$u_r = U_r \cos(\alpha) \cos(\beta) \quad (2.146)$$

$$v_r = U_r \sin(\beta) \quad (2.147)$$

$$w_r = U_r \sin(\alpha) \cos(\beta) \quad (2.148)$$

From this it follows that

$$\alpha = \tan^{-1} \left( \frac{w_r}{u_r} \right) \quad (2.149)$$

$$\beta = \sin^{-1} \left( \frac{v_r}{U_r} \right) \quad (2.150)$$

For small angles of  $\alpha$  and  $\beta$  (linear theory), the following expressions are obtained

$$u_r \approx U_r, \quad v_r \approx \beta U_r, \quad w_r \approx \alpha U_r \quad (2.151)$$



## Chapter 3

# Rigid-Body Kinetics

In order to derive the marine craft equations of motion, it is necessary to study the motion of rigid bodies, hydrodynamics and hydrostatics. The overall goal of Chapter 3 is to show that the rigid-body kinetics can be expressed in a vectorial setting according to (Fossen 1991)

$$\boldsymbol{M}_{RB}\dot{\boldsymbol{\nu}} + \boldsymbol{C}_{RB}(\boldsymbol{\nu})\boldsymbol{\nu} = \boldsymbol{\tau}_{RB} \quad (3.1)$$

where  $\boldsymbol{M}_{RB}$  is the rigid-body mass matrix,  $\boldsymbol{C}_{RB}$  is the rigid-body Coriolis and centripetal matrix due to the rotation of  $\{b\}$  about the approximative inertial frame  $\{n\}$ ,  $\boldsymbol{\nu} = [u, v, w, p, q, r]^\top$  is the generalized velocity vector expressed in  $\{b\}$  and  $\boldsymbol{\tau}_{RB} = [X, Y, Z, K, M, N]^\top$  is a generalized vector of external forces and moments expressed in  $\{b\}$ .

The rigid-body equations of motion will be derived using the *Newton–Euler formulation* and *vectorial mechanics*. In this context it is convenient to define the vectors without reference to a coordinate frame (*coordinate free vector*). The velocity of the origin  $o_b$  with respect to  $\{n\}$  is a vector  $\vec{v}_{nb}$  that is defined by its magnitude and the direction. The vector  $\vec{v}_{nb}$  decomposed in the inertial reference frame is denoted as  $\boldsymbol{v}_{nb}^i$ , which is also referred to as a *coordinate vector* (see Section 2.1.1).

The equations of motion will be represented in two body-fixed reference points:

**CO** - coordinate origin  $o_b$  of  $\{b\}$

**CG** - center of gravity, located at  $\boldsymbol{r}_g^b = [x_g, y_g, z_g]^\top$  with respect to CO

These points coincide if the vector  $\boldsymbol{r}_g^b = \mathbf{0}$  (see Figure 3.1). The point CO is usually specified by the control engineer and it is the reference point used to design the guidance, navigation and control systems. For marine craft, it is common to locate this point on the centerline midships. It is advantageous to use a fixed reference point CO for controller–observer design since CG will depend on the load condition (see Section 4.3).

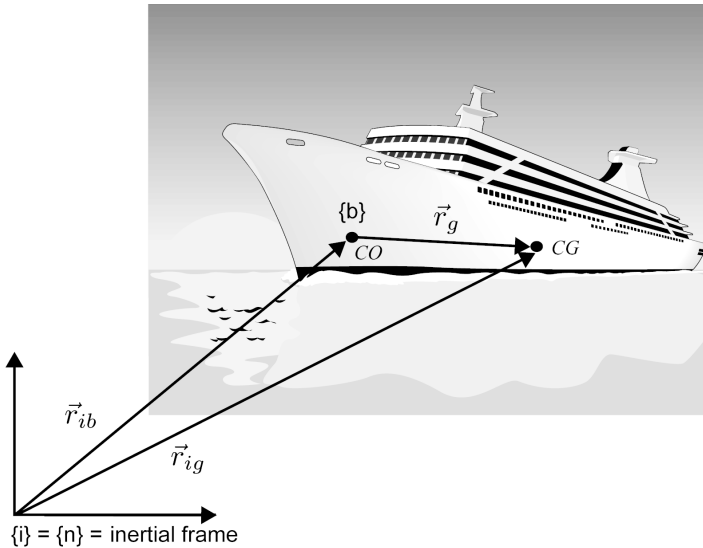


Figure 3.1: Definition of the distance vectors from  $\{i\}$  to CO and CG.

### 3.1 Newton–Euler Equations of Motion about CG

The *Newton–Euler formulation* is based on *Newton’s second law*, which relates mass  $m$ , acceleration  $\dot{\vec{v}}_{ig}$  and force  $\vec{f}_g$  according to

$$m\dot{\vec{v}}_{ig} = \vec{f}_g \quad (3.2)$$

where  $\vec{v}_{ig}$  is the velocity of the CG with respect to the *inertial frame*  $\{i\}$ .

If no force is acting ( $\vec{f}_g = \vec{0}$ ), then the rigid body is moving with constant speed ( $\vec{v}_{ig} = \text{constant}$ ) or the body is at rest ( $\vec{v}_{ig} = \vec{0}$ )—a result known as *Newton’s first law*. Newton’s laws were published in 1687 by Isaac Newton (1643–1727) in *Philosophia Naturalis Principia Mathematica*.

#### Euler’s first and second axioms

Leonhard Euler (1707–1783) showed in his *Novi Commentarii Academiae Scientiarum Imperialis Petropolitane* that Newton’s second law can be expressed in terms of conservation of both linear momentum  $\vec{p}_g$  and angular momentum  $\vec{h}_g$ . These results are known as *Euler’s first and second axioms*, respectively:

$$\frac{i}{dt} \vec{p}_g = \vec{f}_g \quad \vec{p}_g = m\vec{v}_{ig} \quad (3.3)$$

$$\frac{i}{dt} \vec{h}_g = \vec{m}_g \quad \vec{h}_g = I_g \vec{\omega}_{ig} \quad (3.4)$$

where  $\vec{f}_g$  and  $\vec{m}_g$  are the forces and moments acting on the body's CG and  $I_g$  is the inertia dyadic about the body's CG (to be defined later). For a rigid body, the angular velocities of CO and CG with respect to  $\{i\}$  are equal

$$\vec{\omega}_{ig} = \vec{\omega}_{ib} \quad (3.5)$$

Time differentiation in the inertial frame  $\{i\}$  is denoted by  ${}^i d/dt$ . The application of these equations is often referred to as *vectorial mechanics* since both conservation laws are expressed in terms of vectors.

When deriving the equations of motion it will be assumed: (1) that the craft is rigid and (2) that the NED frame  $\{n\}$  is inertial; see Section 2.1.1. The first assumption eliminates the consideration of forces acting between individual elements of mass while the second eliminates forces due to the Earth's motion relative to a star-fixed inertial reference system. Consequently,

$$\vec{v}_{ig} \approx \vec{v}_{ng} \quad (3.6)$$

$$\vec{\omega}_{ig} = \vec{\omega}_{ib} \approx \vec{\omega}_{nb} \quad (3.7)$$

Time differentiation of a vector  $\vec{a}$  in a rotating reference frame  $\{b\}$  satisfies

$$\frac{{}^i d}{dt} \vec{a} = \frac{{}^b d}{dt} \vec{a} + \vec{\omega}_{ib} \times \vec{a} \quad (3.8)$$

where time differentiation in  $\{b\}$  is denoted as

$$\dot{\vec{a}} := \frac{{}^b d}{dt} \vec{a} \quad (3.9)$$

For guidance and navigation applications in space it is usual to use a star-fixed reference frame or a reference frame rotating with the Earth. Marine craft are, on the other hand, usually related to  $\{n\}$ . This is a good assumption since the forces on marine craft due to the Earth's rotation:

$$\omega_{ie} = 7.2921 \times 10^{-5} \text{ rad/s} \quad (3.10)$$

are quite small compared to the hydrodynamic forces. The Earth's rotation should, however, not be neglected in global navigation or if the equations of motion of a drifting ship are analyzed.

### 3.1.1 Translational motion about CG

From Figure 3.1 it follows that

$$\vec{r}_{ig} = \vec{r}_{ib} + \vec{r}_g \quad (3.11)$$

where  $\vec{r}_g$  (short for  $\vec{r}_{bg}$ ) is the distance vector from CO to CG. Consequently, the assumption that  $\{n\}$  is inertial implies that (3.11) can be rewritten as

$$\vec{r}_{ng} = \vec{r}_{nb} + \vec{r}_g \quad (3.12)$$

Time differentiation of  $\vec{r}_{ng}$  in a moving reference frame  $\{b\}$  using (3.8) gives

$$\vec{v}_{ng} = \vec{v}_{nb} + \left( \frac{^b d}{dt} \vec{r}_g + \vec{\omega}_{nb} \times \vec{r}_g \right) \quad (3.13)$$

For a rigid body, CG satisfies

$$\frac{^b d}{dt} \vec{r}_g = \vec{0} \quad (3.14)$$

such that

$$\vec{v}_{ng} = \vec{v}_{nb} + \vec{\omega}_{nb} \times \vec{r}_g \quad (3.15)$$

From Euler's first axiom (3.3) it follows that

$$\begin{aligned} \vec{f}_g &= \frac{^i d}{dt} (m \vec{v}_{ig}) \\ &= \frac{^i d}{dt} (m \vec{v}_{ng}) \\ &= \frac{^b d}{dt} (m \vec{v}_{ng}) + m \vec{\omega}_{nb} \times \vec{v}_{ng} \\ &= m (\dot{\vec{v}}_{ng} + \vec{\omega}_{nb} \times \vec{v}_{ng}) \end{aligned} \quad (3.16)$$

Finally, the vectors can be expressed in  $\{b\}$  such that the translational motion in CG becomes

$$m [\dot{\vec{v}}_{ng}^b + \mathbf{S}(\vec{\omega}_{nb}^b) \vec{v}_{ng}^b] = \vec{f}_g^b \quad (3.17)$$

where the cross-product is written in matrix form using the skew-symmetric matrix (2.13), that is  $\mathbf{S}(\vec{\omega}_{nb}^b) \vec{v}_{ng}^b = \vec{\omega}_{nb}^b \times \vec{v}_{ng}^b$ .

### 3.1.2 Rotational motion about CG

The rotational dynamics (attitude dynamics) follows a similar approach. From Euler's second axiom (3.4), it is seen that

$$\begin{aligned} \vec{m}_g &= \frac{^i d}{dt} (I_g \vec{\omega}_{ib}) \\ &= \frac{^i d}{dt} (I_g \vec{\omega}_{nb}) \\ &= \frac{^b d}{dt} (I_g \vec{\omega}_{nb}) + \vec{\omega}_{nb} \times (I_g \vec{\omega}_{nb}) \\ &= I_g \dot{\vec{\omega}}_{nb} - (I_g \vec{\omega}_{nb}) \times \vec{\omega}_{nb} \end{aligned} \quad (3.18)$$

From this it follows that

$$I_g^b \dot{\vec{\omega}}_{nb}^b - \mathbf{S}(I_g^b \vec{\omega}_{nb}^b) \vec{\omega}_{nb}^b = \vec{m}_g^b \quad (3.19)$$

since  $\mathbf{S}(I_g^b \vec{\omega}_{nb}^b) \vec{\omega}_{nb}^b = (I_g^b \vec{\omega}_{nb}^b) \times \vec{\omega}_{nb}^b$ . This expression is also referred to as *Euler's equations*.

**Definition 3.1 (Inertia Dyadic)**

The inertia dyadic  $\mathbf{I}_g^b \in \mathbb{R}^{3 \times 3}$  about CG is defined as

$$\mathbf{I}_g^b := \begin{bmatrix} I_x & -I_{xy} & -I_{xz} \\ -I_{yx} & I_y & -I_{yz} \\ -I_{zx} & -I_{zy} & I_z \end{bmatrix}, \quad \mathbf{I}_g^b = (\mathbf{I}_g^b)^\top > 0 \quad (3.20)$$

where  $I_x$ ,  $I_y$  and  $I_z$  are the moments of inertia about the  $x_b$ ,  $y_b$  and  $z_b$  axes, and  $I_{xy} = I_{yx}$ ,  $I_{xz} = I_{zx}$  and  $I_{yz} = I_{zy}$  are the products of inertia defined as

$$\begin{aligned} I_x &= \int_V (y^2 + z^2) \rho_m dV; & I_{xy} &= \int_V xy \rho_m dV = \int_V yx \rho_m dV = I_{yx} \\ I_y &= \int_V (x^2 + z^2) \rho_m dV; & I_{xz} &= \int_V xz \rho_m dV = \int_V zx \rho_m dV = I_{zx} \\ I_z &= \int_V (x^2 + y^2) \rho_m dV; & I_{yz} &= \int_V yz \rho_m dV = \int_V zy \rho_m dV = I_{zy} \end{aligned}$$

### 3.1.3 Equations of motion about CG

The Newton–Euler equations (3.17) and (3.19) can be represented in matrix form according to

$$\mathbf{M}_{RB}^{CG} \begin{bmatrix} \dot{\mathbf{v}}_{ng}^b \\ \dot{\boldsymbol{\omega}}_{nb}^b \end{bmatrix} + \mathbf{C}_{RB}^{CG} \begin{bmatrix} \mathbf{v}_{ng}^b \\ \boldsymbol{\omega}_{nb}^b \end{bmatrix} = \begin{bmatrix} \mathbf{f}_g^b \\ \mathbf{m}_g^b \end{bmatrix} \quad (3.21)$$

or

$$\underbrace{\begin{bmatrix} m\mathbf{I}_3 & \mathbf{0}_{3 \times 3} \\ \mathbf{0}_{3 \times 3} & \mathbf{I}_g^b \end{bmatrix}}_{\mathbf{M}_{RB}^{CG}} \begin{bmatrix} \dot{\mathbf{v}}_{ng}^b \\ \dot{\boldsymbol{\omega}}_{nb}^b \end{bmatrix} + \underbrace{\begin{bmatrix} m\mathbf{S}(\boldsymbol{\omega}_{nb}^b) & \mathbf{0}_{3 \times 3} \\ \mathbf{0}_{3 \times 3} & -\mathbf{S}(\mathbf{I}_g^b \boldsymbol{\omega}_{nb}^b) \end{bmatrix}}_{\mathbf{C}_{RB}^{CG}} \begin{bmatrix} \mathbf{v}_{ng}^b \\ \boldsymbol{\omega}_{nb}^b \end{bmatrix} = \begin{bmatrix} \mathbf{f}_g^b \\ \mathbf{m}_g^b \end{bmatrix} \quad (3.22)$$

## 3.2 Newton–Euler Equations of Motion about CO

For marine craft it is desirable to derive the equations of motion for an arbitrary origin CO to take advantage of the craft’s geometric properties. Since the hydrodynamic forces and moments often are computed in CO, Newton’s laws will be formulated in CO as well.

In order to do this, we will start with the equations of motion about CG and transform these expressions to CO using a coordinate transformation. The needed coordinate transformation is derived from (3.15). Moreover,

$$\begin{aligned} \mathbf{v}_{ng}^b &= \mathbf{v}_{nb}^b + \boldsymbol{\omega}_{nb}^b \times \mathbf{r}_g^b \\ &= \mathbf{v}_{nb}^b - \mathbf{r}_g^b \times \boldsymbol{\omega}_{nb}^b \\ &= \mathbf{v}_{nb}^b + \mathbf{S}^\top(\mathbf{r}_g^b) \boldsymbol{\omega}_{nb}^b \end{aligned} \quad (3.23)$$

From this it follows that

$$\begin{bmatrix} \mathbf{v}_{ng}^b \\ \boldsymbol{\omega}_{nb}^b \end{bmatrix} = \mathbf{H}(\mathbf{r}_g^b) \begin{bmatrix} \mathbf{v}_{nb}^b \\ \boldsymbol{\omega}_{nb}^b \end{bmatrix} \quad (3.24)$$

where  $\mathbf{r}_g^b = [x_g, y_g, z_g]^\top$  and  $\mathbf{H}(\mathbf{r}_g^b) \in \mathbb{R}^{3 \times 3}$  is a transformation matrix

$$\mathbf{H}(\mathbf{r}_g^b) := \begin{bmatrix} \mathbf{I}_3 & \mathbf{S}^\top(\mathbf{r}_g^b) \\ \mathbf{0}_{3 \times 3} & \mathbf{I}_3 \end{bmatrix}, \quad \mathbf{H}^\top(\mathbf{r}_g^b) = \begin{bmatrix} \mathbf{I}_3 & \mathbf{0}_{3 \times 3} \\ \mathbf{S}(\mathbf{r}_g^b) & \mathbf{I}_3 \end{bmatrix} \quad (3.25)$$

Notice that angular velocity is unchanged during this transformation. The next step is to transform (3.21) from CG to CO using (3.24). This gives

$$\mathbf{H}^\top(\mathbf{r}_g^b) \mathbf{M}_{RB}^{CG} \mathbf{H}(\mathbf{r}_g^b) \begin{bmatrix} \dot{\mathbf{v}}_{nb}^b \\ \dot{\boldsymbol{\omega}}_{nb}^b \end{bmatrix} + \mathbf{H}^\top(\mathbf{r}_g^b) \mathbf{C}_{RB}^{CG} \mathbf{H}(\mathbf{r}_g^b) \begin{bmatrix} \mathbf{v}_{nb}^b \\ \boldsymbol{\omega}_{nb}^b \end{bmatrix} = \mathbf{H}^\top(\mathbf{r}_g^b) \begin{bmatrix} \mathbf{f}_g^b \\ \mathbf{m}_g^b \end{bmatrix} \quad (3.26)$$

We now define two new matrices in CO according to (see Appendix C)

$$\mathbf{M}_{RB} := \mathbf{H}^\top(\mathbf{r}_g^b) \mathbf{M}_{RB}^{CG} \mathbf{H}(\mathbf{r}_g^b) \quad (3.27)$$

$$\mathbf{C}_{RB} := \mathbf{H}^\top(\mathbf{r}_g^b) \mathbf{C}_{RB}^{CG} \mathbf{H}(\mathbf{r}_g^b) \quad (3.28)$$

Expanding these expressions gives

$$\mathbf{M}_{RB} = \begin{bmatrix} m\mathbf{I}_3 & -m\mathbf{S}(\mathbf{r}_g^b) \\ m\mathbf{S}(\mathbf{r}_g^b) & \mathbf{I}_g^b - m\mathbf{S}^2(\mathbf{r}_g^b) \end{bmatrix} \quad (3.29)$$

$$\mathbf{C}_{RB} = \begin{bmatrix} m\mathbf{S}(\boldsymbol{\omega}_{nb}^b) & -m\mathbf{S}(\boldsymbol{\omega}_{nb}^b)\mathbf{S}(\mathbf{r}_g^b) \\ m\mathbf{S}(\mathbf{r}_g^b)\mathbf{S}(\boldsymbol{\omega}_{nb}^b) & -\mathbf{S}(\mathbf{I}_g^b - m\mathbf{S}^2(\mathbf{r}_g^b))\boldsymbol{\omega}_{nb}^b \end{bmatrix} \quad (3.30)$$

where we have used the fact that

$$m\mathbf{S}(\mathbf{r}_g^b)\mathbf{S}(\boldsymbol{\omega}_{nb}^b)\mathbf{S}^\top(\mathbf{r}_g^b)\boldsymbol{\omega}_{nb}^b - \mathbf{S}(\mathbf{I}_g^b\boldsymbol{\omega}_{nb}^b)\boldsymbol{\omega}_{nb}^b \equiv \mathbf{S}(\mathbf{I}_g^b - m\mathbf{S}^2(\mathbf{r}_g^b))\boldsymbol{\omega}_{nb}^b \quad (3.31)$$

### 3.2.1 Translational motion about CO

From the first row in (3.26) with matrices (3.29) and (3.30) it is seen that the translational motion about CO satisfies

$$m[\dot{\mathbf{v}}_{nb}^b + \mathbf{S}^\top(\mathbf{r}_g^b)\dot{\boldsymbol{\omega}}_{nb}^b + \mathbf{S}(\boldsymbol{\omega}_{nb}^b)\mathbf{v}_{nb}^b + \mathbf{S}(\boldsymbol{\omega}_{nb}^b)\mathbf{S}^\top(\mathbf{r}_g^b)\boldsymbol{\omega}_{nb}^b] = \mathbf{f}_g^b \quad (3.32)$$

Since the translational motion is independent of the attack point of the external force  $\mathbf{f}_g^b = \mathbf{f}_b^b$  it follows that

$$m[\dot{\mathbf{v}}_{nb}^b + \mathbf{S}(\dot{\boldsymbol{\omega}}_{nb}^b)\mathbf{r}_g^b + \mathbf{S}(\boldsymbol{\omega}_{nb}^b)\mathbf{v}_{nb}^b + \mathbf{S}^2(\boldsymbol{\omega}_{nb}^b)\mathbf{r}_g^b] = \mathbf{f}_b^b \quad (3.33)$$

where we have exploited the fact that  $\mathbf{S}^\top(\mathbf{a})\mathbf{b} = -\mathbf{S}(\mathbf{a})\mathbf{b} = \mathbf{S}(\mathbf{b})\mathbf{a}$ . An alternative representation of (3.33) using vector cross-products is

$$m[\dot{\mathbf{v}}_{nb}^b + \dot{\boldsymbol{\omega}}_{nb}^b \times \mathbf{r}_g^b + \boldsymbol{\omega}_{nb}^b \times \mathbf{v}_{nb}^b + \boldsymbol{\omega}_{nb}^b \times (\boldsymbol{\omega}_{nb}^b \times \mathbf{r}_g^b)] = \mathbf{f}_b^b \quad (3.34)$$

### 3.2.2 Rotational motion about CO

In order to express the rotational motion (attitude dynamics) about CO we will make use of the parallel-axis theorem that transforms the inertia matrix to an arbitrarily point.

**Theorem 3.1 (Parallel-Axis Theorem or Huygens–Steiner Theorem)**

The inertia dyadic  $\mathbf{I}_b^b = (\mathbf{I}_b^b)^\top \in \mathbb{R}^{3 \times 3}$  about an arbitrary origin  $o_b$  is given by

$$\mathbf{I}_b^b = \mathbf{I}_g^b - m\mathbf{S}^2(\mathbf{r}_g^b) = \mathbf{I}_g^b + m((\mathbf{r}_g^b)^\top \mathbf{r}_g^b \mathbf{I}_3 - \mathbf{r}_g^b (\mathbf{r}_g^b)^\top) \quad (3.35)$$

where  $\mathbf{I}_g^b = (\mathbf{I}_g^b)^\top \in \mathbb{R}^{3 \times 3}$  is the inertia dyadic about the body's center of gravity. Expanding (3.35) gives

$$\mathbf{I}_b^b = \mathbf{I}_g^b + m \begin{bmatrix} y^2 + z^2 & -xy & -xz \\ -yx & x^2 + z^2 & -yz \\ -zx & -zy & x^2 + y^2 \end{bmatrix} \quad (3.36)$$

**Proof.** See Egeland and Gravdahl (2002).

The lower-right elements in (3.29) and (3.30) can be reformulated by using the parallel-axes theorem. For instance,

$$\begin{aligned} \mathbf{I}_g^b + m\mathbf{S}(\mathbf{r}_g^b)\mathbf{S}^\top(\mathbf{r}_g^b) &= \mathbf{I}_g^b - m\mathbf{S}^2(\mathbf{r}_g^b) \\ &= \mathbf{I}_b^b \end{aligned} \quad (3.37)$$

while the quadratic term in (3.30) satisfies (follows from the Jacobi identity)

$$\mathbf{S}(\mathbf{r}_g^b)\mathbf{S}(\boldsymbol{\omega}_{nb}^b)\mathbf{S}^\top(\mathbf{r}_g^b)\boldsymbol{\omega}_{nb}^b = -\mathbf{S}(\boldsymbol{\omega}_{nb}^b)\mathbf{S}^2(\mathbf{r}_g^b)\boldsymbol{\omega}_{nb}^b \quad (3.38)$$

such that

$$m\mathbf{S}(\mathbf{r}_g^b)\mathbf{S}(\boldsymbol{\omega}_{nb}^b)\mathbf{S}^\top(\mathbf{r}_g^b)\boldsymbol{\omega}_{nb}^b + \mathbf{S}(\boldsymbol{\omega}_{nb}^b)\mathbf{I}_g^b\boldsymbol{\omega}_{nb}^b = \mathbf{S}(\boldsymbol{\omega}_{nb}^b)\mathbf{I}_b^b\boldsymbol{\omega}_{nb}^b \quad (3.39)$$

Consequently, the rotational motion about CO is given by the last row in (3.26):

$$\mathbf{I}_b^b\dot{\boldsymbol{\omega}}_{nb}^b + \mathbf{S}(\boldsymbol{\omega}_{nb}^b)\mathbf{I}_b^b\boldsymbol{\omega}_{nb}^b + m\mathbf{S}(\mathbf{r}_g^b)\dot{\mathbf{v}}_{nb}^b + m\mathbf{S}(\mathbf{r}_g^b)\mathbf{S}(\boldsymbol{\omega}_{nb}^b)\mathbf{v}_{nb}^b = \mathbf{m}_b^b \quad (3.40)$$

where the moment about CO is

$$\begin{aligned} \mathbf{m}_b^b &= \mathbf{m}_g^b + \mathbf{r}_g^b \times \mathbf{f}_g^b \\ &= \mathbf{m}_g^b + \mathbf{S}(\mathbf{r}_g^b)\mathbf{f}_g^b \end{aligned} \quad (3.41)$$

Equation (3.40) can be written in cross-product form as

$$\mathbf{I}_b^b\dot{\boldsymbol{\omega}}_{nb}^b + \boldsymbol{\omega}_{nb}^b \times \mathbf{I}_b^b\boldsymbol{\omega}_{nb}^b + m\mathbf{r}_g^b \times (\dot{\mathbf{v}}_{nb}^b + \boldsymbol{\omega}_{nb}^b \times \mathbf{v}_{nb}^b) = \mathbf{m}_b^b \quad (3.42)$$

### 3.3 Rigid-Body Equations of Motion

In the previous sections it was shown how the rigid-body kinetics can be derived by applying *Newtonian* mechanics. In this section, useful properties of the equations of motion are discussed and it is also demonstrated how these properties considerably simplify the representation of the nonlinear equations of motion.

#### 3.3.1 Nonlinear 6-DOF rigid-body equations of motion

Equations (3.34) and (3.42) are usually written in component form according to the SNAME (1950) notation by defining:

$\mathbf{f}_b^b = [X, Y, Z]^\top$	force through $o_b$ expressed in $\{b\}$
$\mathbf{m}_b^b = [K, M, N]^\top$	moment about $o_b$ expressed in $\{b\}$
$\mathbf{v}_{nb}^b = [u, v, w]^\top$	linear velocity of $o_b$ relative $o_n$ expressed in $\{b\}$
$\boldsymbol{\omega}_{nb}^b = [p, q, r]^\top$	angular velocity of $\{b\}$ relative to $\{n\}$ expressed in $\{b\}$
$\mathbf{r}_g^b = [x_g, y_g, z_g]^\top$	vector from $o_b$ to CG expressed in $\{b\}$

Applying this notation, (3.34) and (3.42) become

$$\begin{aligned}
 m[\dot{u} - vr + wq - x_g(q^2 + r^2) + y_g(pq - \dot{r}) + z_g(pr + \dot{q})] &= X \\
 m[\dot{v} - wp + ur - y_g(r^2 + p^2) + z_g(qr - \dot{p}) + x_g(qp + \dot{r})] &= Y \\
 m[\dot{w} - uq + vp - z_g(p^2 + q^2) + x_g(rp - \dot{q}) + y_g(rq + \dot{p})] &= Z \\
 I_x \dot{p} + (I_z - I_y)qr - (\dot{r} + pq)I_{xz} + (r^2 - q^2)I_{yz} + (pr - \dot{q})I_{xy} \\
 + m[y_g(\dot{w} - uq + vp) - z_g(\dot{v} - wp + ur)] &= K \\
 I_y \dot{q} + (I_x - I_z)rp - (\dot{p} + qr)I_{xy} + (p^2 - r^2)I_{zx} + (qp - \dot{r})I_{yz} \\
 + m[z_g(\dot{u} - vr + wq) - x_g(\dot{w} - uq + vp)] &= M \\
 I_z \dot{r} + (I_y - I_x)pq - (\dot{q} + rp)I_{yz} + (q^2 - p^2)I_{xy} + (rq - \dot{p})I_{zx} \\
 + m[x_g(\dot{v} - wp + ur) - y_g(\dot{u} - vr + wq)] &= N
 \end{aligned} \tag{3.43}$$

The first three equations represent the translational motion, while the last three equations represent the rotational motion.

#### Matrix-vector representation

The rigid-body kinetics (3.43) can be expressed in a vectorial setting as (Fossen 1991)

$$\mathbf{M}_{RB}\dot{\boldsymbol{\nu}} + \mathbf{C}_{RB}(\boldsymbol{\nu})\boldsymbol{\nu} = \boldsymbol{\tau}_{RB} \tag{3.44}$$

where  $\boldsymbol{\nu} = [u, v, w, p, q, r]^\top$  is the generalized velocity vector expressed in  $\{b\}$  and  $\boldsymbol{\tau}_{RB} = [X, Y, Z, K, M, N]^\top$  is a generalized vector of external forces and moments.

#### Property 3.1 (Rigid-Body System Inertia Matrix $\mathbf{M}_{RB}$ )

The representation of the rigid-body system inertia matrix  $\mathbf{M}_{RB}$  is unique and satisfies

$$\mathbf{M}_{RB} = \mathbf{M}_{RB}^\top > 0, \quad \dot{\mathbf{M}}_{RB} = \mathbf{0}_{6 \times 6} \tag{3.45}$$

where

$$\begin{aligned} \mathbf{M}_{RB} &= \begin{bmatrix} m\mathbf{I}_3 & -m\mathbf{S}(\mathbf{r}_g^b) \\ m\mathbf{S}(\mathbf{r}_g^b) & \mathbf{I}_b^b \end{bmatrix} \\ &= \begin{bmatrix} m & 0 & 0 & 0 & mz_g & -my_g \\ 0 & m & 0 & -mz_g & 0 & mx_g \\ 0 & 0 & m & my_g & -mx_g & 0 \\ 0 & -mz_g & my_g & I_x & -I_{xy} & -I_{xz} \\ mz_g & 0 & -mx_g & -I_{yx} & I_y & -I_{yz} \\ -my_g & mx_g & 0 & -I_{zx} & -I_{zy} & I_z \end{bmatrix} \quad (3.46) \end{aligned}$$

Here,  $\mathbf{I}_3$  is the identity matrix,  $\mathbf{I}_b^b = (\mathbf{I}_b^b)^\top > 0$  is the inertia dyadic according to Definition 3.1 and  $\mathbf{S}(\mathbf{r}_g^b)$  is a skew-symmetric matrix according to Definition 2.2.

### Matlab:

The rigid-body system inertia matrix  $\mathbf{M}_{RB}$  can be computed in Matlab as

```
r_g = [10 0 1]'; % location of CG with respect to CO
R44 = 10; % radius of gyration in roll
R55 = 20; % radius of gyration in pitch
R66 = 5; % radius of gyration in yaw
m = 1000; % mass
I_g = m * diag([R44^2 R55^2 R66^2]); % inertia dyadic in CG

% rigid-body system inertia matrix
S = Smtrix(r_g);
MRB = [ m * eye(3) -m * S
        m * S I_g - m * S^2 ];

MRB =
1000 0 0 0 1000 0
0 1000 0 -1000 0 10000
0 0 1000 0 -10000 0
0 -1000 0 101000 0 -10000
1000 0 -10000 0 501000 0
0 10000 0 -10000 0 125000
```

The rigid-body system inertia matrix can also be computed using the command

```
MRB = rbody(m,R44,R55,R66,zeros(3,1),r_g)
```

The matrix  $\mathbf{C}_{RB}$  in (3.44) represents the Coriolis vector term  $\omega_{nb}^b \times v_{nb}^b$  and the centripetal vector term  $\omega_{nb}^b \times (\omega_{nb}^b \times \mathbf{r}_g^b)$ . Contrary to the representation of  $\mathbf{M}_{RB}$ , it is possible to find a large number of representations for the matrix  $\mathbf{C}_{RB}$ .

### Theorem 3.2 (Coriolis–Centripetal Matrix from System Inertia Matrix)

Let  $\mathbf{M}$  be a  $6 \times 6$  system inertia matrix defined as

$$\mathbf{M} = \mathbf{M}^\top = \begin{bmatrix} \mathbf{M}_{11} & \mathbf{M}_{12} \\ \mathbf{M}_{21} & \mathbf{M}_{22} \end{bmatrix} > 0 \quad (3.47)$$

where  $\mathbf{M}_{21} = \mathbf{M}_{12}^\top$ . Then the Coriolis–centripetal matrix can always be parameterized such that  $\mathbf{C}(\boldsymbol{\nu}) = -\mathbf{C}^\top(\boldsymbol{\nu})$  by choosing (Sagatun and Fossen 1991)

$$\mathbf{C}(\boldsymbol{\nu}) = \begin{bmatrix} \mathbf{0}_{3 \times 3} & -\mathbf{S}(\mathbf{M}_{11}\boldsymbol{\nu}_1 + \mathbf{M}_{12}\boldsymbol{\nu}_2) \\ -\mathbf{S}(\mathbf{M}_{11}\boldsymbol{\nu}_1 + \mathbf{M}_{12}\boldsymbol{\nu}_2) & -\mathbf{S}(\mathbf{M}_{21}\boldsymbol{\nu}_1 + \mathbf{M}_{22}\boldsymbol{\nu}_2) \end{bmatrix} \quad (3.48)$$

where  $\boldsymbol{\nu}_1 := \mathbf{v}_{nb}^b = [u, v, w]^\top$ ,  $\boldsymbol{\nu}_2 := \boldsymbol{\omega}_{nb}^b = [p, q, r]^\top$  and  $\mathbf{S}$  is the cross-product operator according to Definition 2.2.

**Proof.** The kinetic energy  $T$  is written in the quadratic form

$$T = \frac{1}{2} \boldsymbol{\nu}^\top \mathbf{M} \boldsymbol{\nu}, \quad \mathbf{M} = \mathbf{M}^\top > 0 \quad (3.49)$$

Expanding this expression yields

$$T = \frac{1}{2} (\boldsymbol{\nu}_1^\top \mathbf{M}_{11} \boldsymbol{\nu}_1 + \boldsymbol{\nu}_1^\top \mathbf{M}_{12} \boldsymbol{\nu}_2 + \boldsymbol{\nu}_2^\top \mathbf{M}_{21} \boldsymbol{\nu}_1 + \boldsymbol{\nu}_2^\top \mathbf{M}_{22} \boldsymbol{\nu}_2) \quad (3.50)$$

where  $\mathbf{M}_{12} = \mathbf{M}_{21}^\top$  and  $\mathbf{M}_{21} = \mathbf{M}_{12}^\top$ . This gives

$$\frac{\partial T}{\partial \boldsymbol{\nu}_1} = \mathbf{M}_{11}\boldsymbol{\nu}_1 + \mathbf{M}_{12}\boldsymbol{\nu}_2 \quad (3.51)$$

$$\frac{\partial T}{\partial \boldsymbol{\nu}_2} = \mathbf{M}_{21}\boldsymbol{\nu}_1 + \mathbf{M}_{22}\boldsymbol{\nu}_2 \quad (3.52)$$

Using Kirchhoff's equations (Kirchhoff 1869):

$$\frac{d}{dt} \left( \frac{\partial T}{\partial \boldsymbol{\nu}_1} \right) + \mathbf{S}(\boldsymbol{\nu}_2) \frac{\partial T}{\partial \boldsymbol{\nu}_1} = \boldsymbol{\tau}_1 \quad (3.53)$$

$$\frac{d}{dt} \left( \frac{\partial T}{\partial \boldsymbol{\nu}_2} \right) + \mathbf{S}(\boldsymbol{\nu}_2) \frac{\partial T}{\partial \boldsymbol{\nu}_2} + \mathbf{S}(\boldsymbol{\nu}_1) \frac{\partial T}{\partial \boldsymbol{\nu}_2} = \boldsymbol{\tau}_2 \quad (3.54)$$

where  $\mathbf{S}$  is the skew-symmetric cross-product operator in Definition 2.2, it is seen that there are some terms dependent on acceleration, that is  $(d/dt)(\partial T/\partial \boldsymbol{\nu}_1)$  and  $(d/dt)(\partial T/\partial \boldsymbol{\nu}_2)$ . The remaining terms are due to Coriolis–centripetal forces. Consequently,

$$\mathbf{C}(\boldsymbol{\nu})\boldsymbol{\nu} := \begin{bmatrix} \mathbf{S}(\boldsymbol{\nu}_2) \frac{\partial T}{\partial \boldsymbol{\nu}_1} \\ \mathbf{S}(\boldsymbol{\nu}_2) \frac{\partial T}{\partial \boldsymbol{\nu}_2} + \mathbf{S}(\boldsymbol{\nu}_1) \frac{\partial T}{\partial \boldsymbol{\nu}_1} \end{bmatrix} = \begin{bmatrix} \mathbf{0}_{3 \times 3} & -\mathbf{S}(\frac{\partial T}{\partial \boldsymbol{\nu}_1}) \\ -\mathbf{S}(\frac{\partial T}{\partial \boldsymbol{\nu}_1}) & -\mathbf{S}(\frac{\partial T}{\partial \boldsymbol{\nu}_2}) \end{bmatrix} \begin{bmatrix} \boldsymbol{\nu}_1 \\ \boldsymbol{\nu}_2 \end{bmatrix} \quad (3.55)$$

which after substitution of (3.51) and (3.52) gives (3.48); see Sagatun and Fossen (1991) for the original proof of this theorem.

We next state some useful properties of the Coriolis and centripetal matrix  $\mathbf{C}_{RB}(\boldsymbol{\nu})$ .

### Property 3.2 (Rigid-Body Coriolis and Centripetal Matrix $\mathbf{C}_{RB}$ )

According to Theorem 3.2 the rigid-body Coriolis and centripetal matrix  $\mathbf{C}_{RB}(\boldsymbol{\nu})$  can always be represented such that  $\mathbf{C}_{RB}(\boldsymbol{\nu})$  is skew-symmetric. Moreover,

$$\mathbf{C}_{RB}(\boldsymbol{\nu}) = -\mathbf{C}_{RB}^\top(\boldsymbol{\nu}), \quad \forall \boldsymbol{\nu} \in \mathbb{R}^6 \quad (3.56)$$

The skew-symmetric property is very useful when designing a nonlinear motion control system since the quadratic form  $\boldsymbol{\nu}^\top \mathbf{C}_{RB}(\boldsymbol{\nu})\boldsymbol{\nu} \equiv 0$ . This is exploited in energy-based designs where Lyapunov functions play a key role. The same property is also used in nonlinear observer design. There exist several parametrizations that satisfy Property 3.2. Two of them are presented below:

**Lagrangian parametrization:** Application of Theorem 3.2 with  $\mathbf{M} = \mathbf{M}_{RB}$  yields the following expression

$$\mathbf{C}_{RB}(\boldsymbol{\nu}) = \begin{bmatrix} \mathbf{0}_{3 \times 3} & -m\mathbf{S}(\boldsymbol{\nu}_1) - m\mathbf{S}(\mathbf{S}(\boldsymbol{\nu}_2)\mathbf{r}_g^b) \\ -m\mathbf{S}(\boldsymbol{\nu}_1) - m\mathbf{S}(\mathbf{S}(\boldsymbol{\nu}_2)\mathbf{r}_g^b) & m\mathbf{S}(\mathbf{S}(\boldsymbol{\nu}_1)\mathbf{r}_g^b) - \mathbf{S}(\mathbf{I}_b^b\boldsymbol{\nu}_2) \end{bmatrix} \quad (3.57)$$

This is not a unique parametrization. There are other parametrizations giving the same product  $\mathbf{C}_{RB}(\boldsymbol{\nu})\boldsymbol{\nu}$ . For instance

$$\mathbf{C}_{RB}(\boldsymbol{\nu}) = \begin{bmatrix} \mathbf{0}_{3 \times 3} & -m\mathbf{S}(\boldsymbol{\nu}_1) - m\mathbf{S}(\boldsymbol{\nu}_2)\mathbf{S}(\mathbf{r}_g^b) \\ -m\mathbf{S}(\boldsymbol{\nu}_1) + m\mathbf{S}(\mathbf{r}_g^b)\mathbf{S}(\boldsymbol{\nu}_2) & -\mathbf{S}(\mathbf{I}_b^b\boldsymbol{\nu}_2) \end{bmatrix} \quad (3.58)$$

To illustrate the complexity of 6-DOF modeling, the rigid-body Coriolis and centripetal terms in expression (3.57) are expanded to give

$$\mathbf{C}_{RB}(\boldsymbol{\nu}) = \begin{bmatrix} 0 & 0 & 0 \\ 0 & 0 & 0 \\ 0 & 0 & 0 \\ -m(y_g q + z_g r) & m(y_g p + w) & m(z_g p - v) \\ m(x_g q - w) & -m(z_g r + x_g p) & m(z_g q + u) \\ m(x_g r + v) & m(y_g r - u) & -m(x_g p + y_g q) \\ m(y_g q + z_g r) & -m(x_g q - w) & -m(x_g r + v) \\ -m(y_g p + w) & m(z_g r + x_g p) & -m(y_g r - u) \\ -m(z_g p - v) & -m(z_g q + u) & m(x_g p + y_g q) \\ 0 & -I_{yz}q - I_{xz}p + I_zr & I_{yz}r + I_{xy}p - I_yq \\ I_{yz}q + I_{xz}p - I_zr & 0 & -I_{xz}r - I_{xy}q + I_xp \\ -I_{yz}r - I_{xy}p + I_yq & I_{xz}r + I_{xy}q - I_xp & 0 \end{bmatrix} \quad (3.59)$$

**Linear velocity-independent parametrization:** By using the property  $\mathbf{S}(\boldsymbol{\nu}_1)\boldsymbol{\nu}_2 = -\mathbf{S}(\boldsymbol{\nu}_2)\boldsymbol{\nu}_1$ , it is possible to move the  $-m\mathbf{S}(\boldsymbol{\nu}_1)$  term from  $\mathbf{C}_{RB}^{\{12\}}$  to  $\mathbf{C}_{RB}^{\{11\}}$  in (3.58). Since  $\mathbf{S}(\boldsymbol{\nu}_1)\boldsymbol{\nu}_1 = \mathbf{0}$  this gives an expression for  $\mathbf{C}_{RB}(\boldsymbol{\nu})$  that is independent of linear velocity  $\boldsymbol{\nu}_1$  (Fossen and Fjellstad 1995)

$$\mathbf{C}_{RB}(\boldsymbol{\nu}) = \begin{bmatrix} m\mathbf{S}(\boldsymbol{\nu}_2) & -m\mathbf{S}(\boldsymbol{\nu}_2)\mathbf{S}(\mathbf{r}_g^b) \\ m\mathbf{S}(\mathbf{r}_g^b)\mathbf{S}(\boldsymbol{\nu}_2) & -\mathbf{S}(\mathbf{I}_b^b\boldsymbol{\nu}_2) \end{bmatrix} \quad (3.60)$$

Notice that this expression is similar to (3.30) which was derived using Newton–Euler equations. Formula (3.60) can also be expressed in terms of  $\mathbf{H}(\mathbf{r}_g)$  for nonzero values of  $\mathbf{r}_g$  (see (C.19) in Appendix C.1.3). This gives

$$C_{RB}(\boldsymbol{\nu}) = \mathbf{H}^\top(\mathbf{r}_g) \begin{bmatrix} 0 & -mr & mq & 0 & 0 & 0 \\ mr & 0 & -mp & 0 & 0 & 0 \\ -mq & mp & 0 & 0 & 0 & 0 \\ 0 & 0 & 0 & 0 & I_z r & -I_y q \\ 0 & 0 & 0 & -I_z r & 0 & I_x p \\ 0 & 0 & 0 & I_y q & -I_x p & 0 \end{bmatrix} \mathbf{H}(\mathbf{r}_g) \quad (3.61)$$

**Remark 3.1.**

Formulae (3.60) and (3.61) are useful when irrotational ocean currents

$$\boldsymbol{\nu}_c = [u_c, v_c, w_c, 0, 0, 0]^\top \quad (3.62)$$

enter the equations of motion. The main reason for this is that  $C_{RB}(\boldsymbol{\nu})$  does not depend on linear velocity  $\boldsymbol{\nu}_1$  (uses only angular velocity  $\boldsymbol{\nu}_2$  and lever arm  $\mathbf{r}_g^b$ ). According to Property 10.1 in Section 10.3

$$M_{RB}\dot{\boldsymbol{\nu}} + C_{RB}(\boldsymbol{\nu})\boldsymbol{\nu} \equiv M_{RB}\dot{\boldsymbol{\nu}}_r + C_{RB}(\boldsymbol{\nu}_r)\boldsymbol{\nu}_r \quad (3.63)$$

if the relative velocity vector  $\boldsymbol{\nu}_r = \boldsymbol{\nu} - \boldsymbol{\nu}_c$ . Since the ocean current (3.62) is assumed to be irrotational, Equation (3.63) can be proven using (3.60). The details are outlined in Section 10.3.

**Matlab:**

The Lagrangian parametrization (Theorem 3.2) is implemented in the Matlab MSS toolbox in the function `m2c.m`, while the linear-velocity independent parametrization (3.60) is implemented in the more generic functions `rbody.m`. The following example demonstrates how  $C_{RB}(\boldsymbol{\nu})$  can be computed numerically

```

r_g = [10 0 1]'; % location of CG with respect to CO
R44 = 10; % radius of gyration in roll
R55 = 20; % radius of gyration in pitch
R66 = 5; % radius of gyration in yaw
m = 1000; % mass
nu = [8 0.5 0.1 0.2 -0.3 0.2]'; % velocity vector

% Method 1: Linear velocity-independent parametrization
nu2 = nu(4:6);
[MRB, CRB] = rbody(m, R44, R55, R66, nu2, r_g)

MRB =
    1000      0      0      0     1000      0
        0    1000      0   -1000      0   10000
        0      0   1000      0   -10000      0
        0   -1000      0  101000      0  -10000
    1000      0  -10000      0  501000      0
        0  10000      0  -10000      0  125000

CRB =
        0   -200   -300     200    3000   -2000
    200      0   -200      0   2200      0

```

```

300      200      0     -200      300     2000
-200      0      200       0    2800 120000
-3000   -2200   -300   -2800       0   -2000
2000      0   -2000  -120000    2000       0
% Method 2: Lagrangian parametrization
CRB = m2c(MRB, nu)

CRB =
      0      0      0      0    3100   -2300
      0      0      0   -3100       0    7700
      0      0      0    2300   -7700       0
      0    3100   -2300       0   28000 143300
   -3100      0    7700  -28000       0   17700
    2300   -7700       0  -143300  -17700       0

```

Even though the numerical values for the two  $\mathbf{C}_{RB}(\boldsymbol{\nu})$  matrices are different, they both produce the same product  $\mathbf{C}_{RB}(\boldsymbol{\nu})\boldsymbol{\nu}$ .

### 3.3.2 Linearized 6-DOF rigid-body equations of motion

The rigid-body equations of motion (3.44) can be linearized about  $\boldsymbol{\nu}_0 = [U, 0, 0, 0, 0, 0]^\top$  for a marine craft moving at forward speed  $U$ . This gives

$$\mathbf{M}_{RB}\dot{\boldsymbol{\nu}} + \mathbf{C}_{RB}^*\boldsymbol{\nu} = \boldsymbol{\tau}_{RB} \quad (3.64)$$

where

$$\mathbf{C}_{RB}^* = \mathbf{M}_{RB}\mathbf{L}U, \quad \mathbf{C}_{RB}^* \neq -(\mathbf{C}_{RB}^*)^\top \quad (3.65)$$

and  $\mathbf{L}$  is a selection matrix

$$\mathbf{L} = \begin{bmatrix} 0 & 0 & 0 & 0 & 0 & 0 \\ 0 & 0 & 0 & 0 & 0 & 1 \\ 0 & 0 & 0 & 0 & -1 & 0 \\ 0 & 0 & 0 & 0 & 0 & 0 \\ 0 & 0 & 0 & 0 & 0 & 0 \\ 0 & 0 & 0 & 0 & 0 & 0 \end{bmatrix} \quad (3.66)$$

The linearized Coriolis and centripetal forces are recognized as

$$\mathbf{f}_c = \mathbf{C}_{RB}^*\boldsymbol{\nu} = \begin{bmatrix} 0 \\ mUr \\ -mUq \\ -my_gUq - mz_gUr \\ mx_gUq \\ mx_gUr \end{bmatrix} \quad (3.67)$$

**Matlab:**

The linearized model (3.64) is computed using the following Matlab commands

```

U = 1;
MRB = [
    1000      0      0      0     1000      0
    0     1000      0     -1000      0    10000
    0      0     1000      0    -10000      0
    0    -1000      0   101000      0   -10000
   1000      0   -10000      0   501000      0
    0   10000      0   -10000      0   125000];

L = zeros(6,6); L(2,6) = 1; L(3,5) = -1;
CRB = MRB * L * U;

CRB =
    0      0      0      0      0      0
    0      0      0      0      0    1000
    0      0      0      0    -1000      0
    0      0      0      0      0   -1000
    0      0      0      0   10000      0
    0      0      0      0      0   10000

```

Notice that the skew-symmetric property is destroyed by linearization. Moreover,  
 $\mathbf{C}_{\text{RB}}^* \neq -(\mathbf{C}_{\text{RB}}^*)^\top$

# Chapter 4

## Hydrostatics

Archimedes (287–212 BC) derived the basic laws of fluid statics that are the fundamentals of hydrostatics today. In hydrostatic terminology, the gravitational and buoyancy forces are called *restoring forces* and are equivalent to the spring forces in a *mass-damper-spring* system. In the derivation of the restoring forces and moments it will be distinguished between submersibles and surface vessels:

- Section 4.1: underwater vehicles (ROVs, AUVs and submarines).
- Section 4.2: surface vessels (ships, semisubmersibles, structures and USVs).

For a floating or submerged vessel, the restoring forces are determined by the volume of the displaced fluid, the location of the center of buoyancy (CB), the area of the waterplane and its associated moments. The forthcoming sections show how these quantities determine the heaving, rolling and pitching motions of a marine craft.

### 4.1 Restoring Forces for Underwater Vehicles

Consider the submarine in Figure 4.1 where the gravitational force  $\mathbf{f}_g^b$  acts through the CG defined by the vector  $\mathbf{r}_g^b := [x_g, y_g, z_g]^\top$  with respect to CO. Similarly, the buoyancy force  $\mathbf{f}_b^b$  acts through the CB defined by the vector  $\mathbf{r}_b^b := [x_b, y_b, z_b]^\top$  (see Section 2.1.1). Both vectors are referred to the body-fixed reference point CO.

#### 4.1.1 Hydrostatics of submerged vehicles

Let  $m$  be the mass of the vehicle including water in free floating space,  $\nabla$  the volume of fluid displaced by the vehicle,  $g$  the acceleration of gravity (positive downwards) and  $\rho$  the water density. According to the SNAME (1950) notation, the submerged weight of the body and buoyancy force are written as

$$W = mg, \quad B = \rho g \nabla \quad (4.1)$$

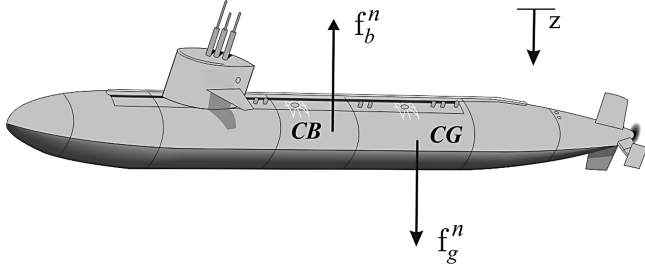


Figure 4.1: Gravitational and buoyancy forces acting on the center of gravity (CG) and center of buoyancy (CB) of a submarine.

These forces act in the vertical plane of  $\{n\}$ . Hence,

$$\mathbf{f}_g^n = \begin{bmatrix} 0 \\ 0 \\ W \end{bmatrix} \quad \text{and} \quad \mathbf{f}_b^n = -\begin{bmatrix} 0 \\ 0 \\ B \end{bmatrix} \quad (4.2)$$

Notice that the  $z$  axis is taken to be positive downwards such that gravity is positive and buoyancy is negative. By applying the results from Section 2.2.1, the weight and buoyancy force can be expressed in  $\{b\}$  by

$$\mathbf{f}_g^b = \mathbf{R}^\top(\Theta_{nb}) \mathbf{f}_g^n \quad (4.3)$$

$$\mathbf{f}_b^b = \mathbf{R}^\top(\Theta_{nb}) \mathbf{f}_b^n \quad (4.4)$$

where  $\mathbf{R}_b^n = \mathbf{R}(\Theta_{nb})$  is the Euler angle coordinate transformation matrix defined in Section 2.2.1. According to (2.2), the sign of the restoring forces and moments  $\mathbf{f}_i^b$  and  $\mathbf{m}_i^b = \mathbf{r}_i^b \times \mathbf{f}_i^b$ ,  $i \in \{g, b\}$ , must be changed when moving these terms to the left-hand side of (2.2), that is the vector  $\mathbf{g}(\eta)$ . Consequently, the restoring force and moment vector expressed in  $\{b\}$  is

$$\begin{aligned} \mathbf{g}(\eta) &= - \left[ \mathbf{r}_g^b \times \mathbf{f}_g^b + \mathbf{r}_b^b \times \mathbf{f}_b^b \right] \\ &= - \left[ \mathbf{r}_g^b \times \mathbf{R}^\top(\Theta_{nb}) (\mathbf{f}_g^n + \mathbf{f}_b^n) + \mathbf{r}_b^b \times \mathbf{R}^\top(\Theta_{nb}) \mathbf{f}_b^n \right] \end{aligned} \quad (4.5)$$

Expanding this expression yields

$$\mathbf{g}(\eta) = \left[ \begin{array}{l} (W - B) \sin(\theta) \\ -(W - B) \cos(\theta) \sin(\phi) \\ -(W - B) \cos(\theta) \cos(\phi) \\ -(y_g W - y_b B) \cos(\theta) \cos(\phi) + (z_g W - z_b B) \cos(\theta) \sin(\phi) \\ (z_g W - z_b B) \sin(\theta) + (x_g W - x_b B) \cos(\theta) \cos(\phi) \\ -(x_g W - x_b B) \cos(\theta) \sin(\phi) - (y_g W - y_b B) \sin(\theta) \end{array} \right] \quad (4.6)$$

**Matlab:**

The restoring forces  $\mathbf{g}(\boldsymbol{\eta})$  for an underwater vehicle can be computed with the CO as coordinate origin by using the MSS toolbox commands:

```
r_g = [0, 0, 0]; % location of CG with respect to CO
r_b = [0, 0, -10]; % location of CB with respect to CO
m = 1000; % mass
g = 9.81; % acceleration of gravity
W = m * g; % weight
B = W; % buoyancy

% pitch and roll angles
theta = 10 * (180/pi); phi = 30 * (pi/180);

% g vector in CO
g = gvect(W,B,theta,phi,r_g,r_b)

g =
1.0e+04 *
0
0
0
1.8324
9.0997
0
```

Equation (4.6) is the Euler angle representation of the hydrostatic forces and moments. An alternative representation can be found by applying *unit quaternions*. Then  $\mathbf{R}(\mathbf{q}_b^n)$  replaces  $\mathbf{R}(\Theta_{nb})$  in (4.3); see Section 2.2.2.

A neutrally buoyant underwater vehicle will satisfy

$$W = B \quad (4.7)$$

It is convenient to design underwater vehicles with  $B > W$  (positive buoyancy) such that the vehicle will surface automatically in the case of an emergency situation, for instance power failure. In this case, the magnitude of  $B$  should only be slightly larger than  $W$ . If the vehicle is designed such that  $B \gg W$ , too much control energy is needed to keep the vehicle submerged. Hence, a trade-off between positive buoyancy and controllability must be made.

**Example 4.1 (Neutrally Buoyant Underwater Vehicles)**

Let the distance from the CB to CG be defined by the vector

$$[BG_x, BG_y, BG_z]^\top := [x_g - x_b, y_g - y_b, z_g - z_b]^\top \quad (4.8)$$

For neutrally buoyant vehicles  $W = B$ , (4.6) therefore simplifies to

$$\mathbf{g}(\boldsymbol{\eta}) = \begin{bmatrix} 0 \\ 0 \\ 0 \\ -BG_y W \cos(\theta) \cos(\phi) + BG_z W \cos(\theta) \sin(\phi) \\ BG_z W \sin(\theta) + BG_x W \cos(\theta) \cos(\phi) \\ -BG_x W \cos(\theta) \sin(\phi) - BG_y W \sin(\theta) \end{bmatrix} \quad (4.9)$$

An even simpler representation is obtained for vehicles where the CG and CB are located vertically on the  $z$  axis, that is  $x_b = x_g$  and  $y_g = y_b$ . This yields

$$\mathbf{g}(\eta) = [0, 0, 0, BG_z W \cos(\theta) \sin(\phi), BG_z W \sin(\theta), 0]^\top \quad (4.10)$$

## 4.2 Restoring Forces for Surface Vessels

Formula (4.6) should only be used for completely submerged vehicles. Static stability considerations due to restoring forces are usually referred to as *metacentric stability* in the hydrostatic literature. A metacentric stable vessel will resist inclinations away from its steady state or equilibrium points in heave, roll and pitch.

For surface vessels, the restoring forces will depend on the vessel's metacentric height, the location of the CG and the CB, as well as the shape and size of the waterplane. Let  $A_{wp}$  denote the waterplane area and

$$\begin{aligned} GM_T &= \text{transverse metacentric height} \\ GM_L &= \text{longitudinal metacentric height} \end{aligned} \quad (4.11)$$

The metacentric height  $GM_i$ , where  $i \in \{T, L\}$ , is the distance between the metacenter  $M_i$  and the CG, as shown in Figures 4.2 and 4.3.

### Definition 4.1 (Metacenter)

*The theoretical point at which an imaginary vertical line through the CB intersects another imaginary vertical line through a new CB created when the body is displaced, or tilted, in the water (see Figure 4.2).*

### 4.2.1 Hydrostatics of floating vessels

For a floating vessel at rest, Archimedes stated that buoyancy and weight are in balance

$$mg = \rho g \nabla \quad (4.12)$$

Let  $z$  denote the displacement in heave and let  $z = 0$  denote the equilibrium position corresponding to the nominal displaced water volume  $\nabla$ . Hence, the hydrostatic force in heave will be the difference between the gravitational and the buoyancy forces

$$\begin{aligned} Z_{hs} &= mg - \rho g (\nabla + \delta \nabla(z)) \\ &= -\rho g \delta \nabla(z) \end{aligned} \quad (4.13)$$

where the change in displaced water  $\delta \nabla(z)$  is due to variations in heave position  $z$ . This can be written

$$\delta \nabla(z) = \int_0^z A(\zeta) d\zeta \quad (4.14)$$

where  $A(\zeta)$  is the waterplane area of the vessel as a function of the heave position. For conventional ships and floating structures, however, it is common to assume that the waterplane area  $A(\zeta) \approx A(0) := A_{wp}$  is constant for small perturbations in  $z$ . Hence, the hydrostatic restoring force  $Z_{hs}$  will be linear in  $z$ , that is

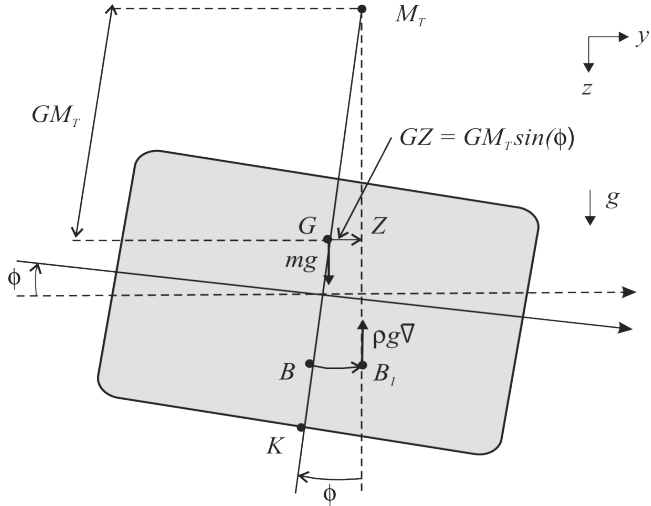


Figure 4.2: Transverse metacentric stability. Notice that  $mg = \rho g \nabla$ . A similar figure can be drawn to illustrate lateral metacentric stability by simply replacing  $M_T$  and  $\phi$  with  $M_L$  and  $\theta$ .

$$Z_{hs} \approx -\rho g A_{wp} z := Z_z z \quad (4.15)$$

where  $Z_z = -\rho g A_{wp} > 0$  is recognized as the spring stiffness or restoring coefficient in heave. This gives rise to a mass-damper-spring system

$$\dot{z} = w \quad (4.16)$$

$$(m - Z_w) \dot{w} - Z_w w - Z_z z = Z_{ext} \quad (4.17)$$

Recall that if a floating vessel is forced downwards by an external force  $Z_{ext}$  such that  $z > 0$ , the buoyancy force becomes larger than the constant gravitational force since the submerged volume  $\nabla$  increases by  $\delta\nabla$  to  $\nabla + \delta\nabla$ . Consequently, the buoyancy force vector due to variations in displaced volume is

$$\delta \mathbf{f}_b^n = \begin{bmatrix} 0 \\ 0 \\ -\rho g \int_0^z A(\zeta) d\zeta \end{bmatrix} \quad (4.18)$$

From this it follows that the restoring force vector is

$$\begin{aligned} \mathbf{f}_r^b &= \mathbf{R}^\top(\Theta_{nb}) (\mathbf{f}_g^n + \mathbf{f}_b^n + \delta \mathbf{f}_b^n) \\ &= -\rho g \begin{bmatrix} -\sin(\theta) \\ \cos(\theta) \sin(\phi) \\ \cos(\theta) \cos(\phi) \end{bmatrix} \int_0^z A(\zeta) d\zeta \end{aligned} \quad (4.19)$$

where we have exploited that  $\mathbf{f}_g^n = -\mathbf{f}_b^n$ .

From Figure 4.2 it is seen that the moment arms in roll and pitch for the force pair  $\mathbf{f}_g^n = -\mathbf{f}_b^n$  are  $GM_T \sin(\phi)$  and  $GM_L \sin(\theta)$ , respectively. Neglecting the moment contribution due to  $\delta \mathbf{f}_b^n$  (only considering  $\mathbf{f}_b^n$ ) implies that

$$\mathbf{r}_{GM}^b = \begin{bmatrix} -GM_L \sin(\theta) \\ GM_T \sin(\phi) \\ 0 \end{bmatrix} \quad (4.20)$$

$$\mathbf{f}_b^b = \mathbf{R}^\top(\Theta_{nb}) \begin{bmatrix} 0 \\ 0 \\ -\rho g \nabla \end{bmatrix} = -\rho g \nabla \begin{bmatrix} -\sin(\theta) \\ \cos(\theta) \sin(\phi) \\ \cos(\theta) \cos(\phi) \end{bmatrix} \quad (4.21)$$

The restoring moment becomes

$$\begin{aligned} \mathbf{m}_r^b &= \mathbf{r}_{GM}^b \times \mathbf{f}_b^b \\ &= -\rho g \nabla \begin{bmatrix} GM_T \sin(\phi) \cos(\theta) \cos(\phi) \\ GM_L \sin(\theta) \cos(\theta) \cos(\phi) \\ -GM_L \cos(\theta) + GM_T \sin(\phi) \sin(\theta) \end{bmatrix} \end{aligned} \quad (4.22)$$

The assumption that  $\mathbf{r}_{GM}^b \times \delta \mathbf{f}_b^b = \mathbf{0}$  (no moments due to heave motions) is a good assumption since this term is small compared to  $\mathbf{r}_{GM}^b \times \mathbf{f}_b^b$ . The restoring forces and moments are finally written

$$\mathbf{g}(\boldsymbol{\eta}) = - \begin{bmatrix} \mathbf{f}_r^b \\ \mathbf{m}_r^b \end{bmatrix} \quad (4.23)$$

Expanding this expression gives

$$\mathbf{g}(\boldsymbol{\eta}) = \begin{bmatrix} -\rho g \int_0^z A(\zeta) d\zeta \sin(\theta) \\ \rho g \int_0^z A(\zeta) d\zeta \cos(\theta) \sin(\phi) \\ \rho g \int_0^z A(\zeta) d\zeta \cos(\theta) \cos(\phi) \\ \rho g \nabla GM_T \sin(\phi) \cos(\theta) \cos(\phi) \\ \rho g \nabla GM_L \sin(\theta) \cos(\theta) \cos(\phi) \\ \rho g \nabla (-GM_L \cos \theta + GM_T) \sin(\phi) \sin(\theta) \end{bmatrix} \quad (4.24)$$

## 4.2.2 Linear (small angle) theory for boxed-shaped vessels

For surface vessels it is common to use linear theory

$$\mathbf{M}\dot{\boldsymbol{\nu}} + \mathbf{N}\boldsymbol{\nu} + \mathbf{G}\boldsymbol{\eta} + \mathbf{g}_o = \boldsymbol{\tau} + \boldsymbol{\tau}_{\text{wind}} + \boldsymbol{\tau}_{\text{wave}} \quad (4.25)$$

implying that (4.24) is approximated by a matrix  $\mathbf{G}$  of restoring coefficients

$$\mathbf{g}(\boldsymbol{\eta}) \approx \mathbf{G}\boldsymbol{\eta} \quad (4.26)$$

This is based on the assumption that

$$\int_0^z A(\zeta) d\zeta \approx A_{wp} z$$

and the assumptions that  $\phi$ ,  $\theta$  and  $z$  are small. Moreover,

$$\begin{aligned}\sin(\theta) &\approx \theta; & \cos(\theta) &\approx 1 \\ \sin(\phi) &\approx \phi; & \cos(\phi) &\approx 1\end{aligned}$$

From this it follows that (4.24) can be written

$$\mathbf{g}(\boldsymbol{\eta}) \approx \begin{bmatrix} -\rho g A_{wp} z \theta \\ \rho g A_{wp} z \phi \\ \rho g A_{wp} z \\ \rho g \nabla GM_T \phi \\ \rho g \nabla GM_L \theta \\ \rho g \nabla (-GM_L + GM_T) \phi \theta \end{bmatrix} \approx \begin{bmatrix} 0 \\ 0 \\ \rho g A_{wp} z \\ \rho g \nabla GM_T \phi \\ \rho g \nabla GM_L \theta \\ 0 \end{bmatrix} \quad (4.27)$$

where we have neglected second-order terms. Consequently,

$$\mathbf{G}^{CF} = \text{diag}\{0, 0, \rho g A_{wp}, \rho g \nabla GM_T, \rho g \nabla GM_L, 0\} \quad (4.28)$$

The superscript CF (see Section 2.1.1) denotes the center of flotation. The first moment of areas are zero in the CF

$$\frac{1}{A_{wp}} \iint_{A_{wp}} x dA = 0, \quad \frac{1}{A_{wp}} \iint_{A_{wp}} y dA = 0 \quad (4.29)$$

since the integrals are computed about the centroid  $\{f\} = (x_f, y_f, z_f)$ , that is the geometric center of  $A_{wp}$ . This is the point of rotation for a freely rotating body subject to an applied horizontal moment. The second moment of areas are both positive

$$I_L := \iint_{A_{wp}} x^2 dA, \quad I_T := \iint_{A_{wp}} y^2 dA \quad (4.30)$$

For conventional ships the CG and the CB lies on the same vertical line ( $x_b = x_g$  and  $y_b = y_g$ ) such that (Newman, 1977)

$$\nabla GM_T = \frac{I_T}{\nabla} + z_g - z_b \quad (4.31)$$

$$\nabla GM_L = \frac{I_L}{\nabla} + z_g - z_b \quad (4.32)$$

It is convenient to represent the equations of motion about the CO usually midships on the centerline with CG and the CB on the same vertical line. For this case both the first and second moments of area of the waterplane have to be computed about the origin  $\{b\} = (x_b, y_b, z_b)$  which is located a distance LCF in the  $x_f$  direction. This introduces nonzero coupling terms  $G_{35}$  and  $G_{53}$  and the expression for  $\mathbf{G}$  takes the following form

$$\mathbf{G} = \mathbf{G}^\top = \begin{bmatrix} 0 & 0 & 0 & 0 & 0 & 0 \\ 0 & 0 & 0 & 0 & 0 & 0 \\ 0 & 0 & -Z_z & 0 & -Z_\theta & 0 \\ 0 & 0 & 0 & -K_\phi & 0 & 0 \\ 0 & 0 & -M_z & 0 & -M_\theta & 0 \\ 0 & 0 & 0 & 0 & 0 & 0 \end{bmatrix} > 0 \quad (4.33)$$

The numerical value for  $\mathbf{G}$  can be computed directly from the expression  $\mathbf{G}^{\text{CF}}$  by using the transformation (C.12) with distance vector  $\mathbf{r}_f^b = [\text{LCF}, 0, 0]^\top$  where LCF is the distance from the CO to the CF (negative for conventional ships). Moreover

$$\begin{aligned} \mathbf{G} &= \mathbf{H}^\top(\mathbf{r}_f^b) \mathbf{G}^{\text{CF}} \mathbf{H}(\mathbf{r}_f^b) \\ &= \begin{bmatrix} 0 & 0 & 0 & 0 & 0 & 0 \\ 0 & 0 & 0 & 0 & 0 & 0 \\ 0 & 0 & \rho g A_{wp} & 0 & -\rho g A_{wp} \text{LCF} & 0 \\ 0 & 0 & 0 & \rho g \nabla GM_T & 0 & 0 \\ 0 & 0 & -\rho g A_{wp} \text{LCF} & 0 & \rho g (A_{wp} \text{LCF}^2 + \nabla GM_L) & 0 \\ 0 & 0 & 0 & 0 & 0 & 0 \end{bmatrix} \end{aligned} \quad (4.34)$$

### Matlab:

The  $6 \times 6$  system spring stiffness matrix  $\mathbf{G}$  is computed by using the MSS toolbox function Gmtrx.m:

```
A_wp = 1000; % waterplane area
nabla = 8000; % volume displacement
GMT = 1; % transverse metacentric height
GML = 10; % longitudinal metacentric heights
LCF = -8; % location of CF w.r.t. CO
r_p = [0 0 0]', % location of P w.r.t. CO

% Spring stiffness matrix in CO
G = Gmtrx(nabla,A_wp,GMT,GML,LCF,r_p)

G =
1.0e+09 *
0 0 0 0 0 0
0 0 0 0 0 0
0 0 0.0101 0 0.0804 0
0 0 0 0.0804 0 0
0 0 0.0804 0 1.4480 0
0 0 0 0 0 0
```

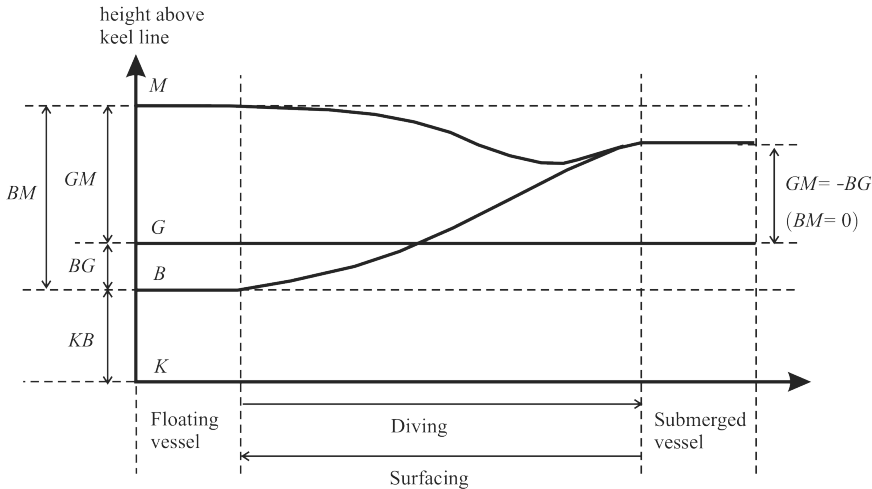


Figure 4.3: Metacenter  $M_T$ , center of gravity  $G$  and center of buoyancy  $B$  for a submerged and a floating vessel.  $K$  is the keel line.

#### 4.2.3 Computation of metacenter heights for surface vessels

The metacenter height can be computed by using basic hydrostatics

$$GM_T = BM_T - BG, \quad GM_L = BM_L - BG \quad (4.35)$$

This relationship is verified directly from Figure 4.3, where  $M_T$  and  $M_L$  denote the transverse and longitudinal metacenters (intersections between the vertical lines through  $B$  and  $B_1$  when  $\phi$  and  $\theta$  approaches zero). The symbol  $K$  is used to denote the keel line. For small inclinations  $\phi$  and  $\theta$  the transverse and longitudinal radii of curvature can be approximated by

$$BM_T = \frac{I_T}{\nabla}, \quad BM_L = \frac{I_L}{\nabla} \quad (4.36)$$

where the second moments of area  $I_T$  and  $I_L$  are defined by (4.30). For conventional ships an upper bound on these integrals can be found by considering a rectangular waterplane area  $A_{wp} = BL$  where  $B$  and  $L$  are the beam and length of the hull, respectively. This implies that

$$I_T < \frac{1}{12}B^3L, \quad I_L < \frac{1}{12}L^3B \quad (4.37)$$

At an early stage in the ship design process it is necessary to ensure that the ship will have an adequate  $GM_T$  for all reasonable loading conditions. This requires that  $KB$  and  $BM_T$  are estimated. For this purpose, the *Munro-Smith formula* for estimating  $BM_T$  is quite useful (Wilson 2018, pp. 89–90)

$$I_T = \frac{1}{12}B^3L \frac{6C_w^3}{(1 + C_w)(1 + 2C_w)} \quad (4.38)$$

where  $C_w = A_{wp}/(LB)$  is the waterplane area coefficient.

The following method, known as *Morrish's formula*, gives a reasonably accurate estimate of KB (Wilson 2018, pp. 88–89)

$$KB = \frac{1}{3} \left( \frac{5T}{2} - \frac{\nabla}{A_{wp}} \right) \quad (4.39)$$

The formulae for KB and  $BM_T$  are very useful when simulating the vessel dynamics at an early stage.

#### **Example 4.2 (Computation of GM Values)**

Consider a floating barge with length 100 m and width 8 m. The draft is 5 m while CG is located 3 m above the keel line ( $KG = 3.0$  m). Since  $KB = 2.5$  m, it follows that

$$BG = KG - KB = 3 - 2.5 = 0.5 \text{ m} \quad (4.40)$$

Hence,

$$I_T = \frac{1}{12} B^3 L = \frac{1}{12} 8^3 \times 100 = 4\ 266.7 \text{ m}^4 \quad (4.41)$$

$$I_L = \frac{1}{12} L^3 B = \frac{1}{12} 100^3 \times 8 = 666\ 666.7 \text{ m}^4 \quad (4.42)$$

The volume displacement is

$$\nabla = 100 \times 8 \times 5 = 4\ 000 \text{ m}^3 \quad (4.43)$$

Consequently,

$$BM_T = \frac{I_T}{\nabla} = 2.08 \text{ m} \quad (4.44)$$

$$BM_L = \frac{I_L}{\nabla} = 166.7 \text{ m} \quad (4.45)$$

Finally,

$$GM_T = BM_T - BG = 2.08 - 0.5 = 1.58 \text{ m} \quad (4.46)$$

$$GM_L = BM_L - BG = 166.7 - 0.5 = 166.2 \text{ m} \quad (4.47)$$

The corresponding metacentric heights are

$$KM_T = KG + GM_T = 3 + 1.58 = 4.58 \text{ m} \quad (4.48)$$

$$KM_L = KG + GM_L = 3 + 166.2 = 169.2 \text{ m} \quad (4.49)$$

#### **Definition 4.2 (Metacenter Stability)**

A floating vessel is said to be transverse metacentrically stable if

$$GM_T \geq GM_{T,\min} > 0 \quad (4.50)$$

and longitudinal metacentrically stable if

$$GM_L \geq GM_{L,\min} > 0 \quad (4.51)$$

The longitudinal stability requirement (4.51) is easy to satisfy for ships since the pitching motion is quite limited. The transverse requirement, however, is an important design criterion used to predescribe sufficient stability in roll to avoid the craft rolling around. For most ships  $GM_{T,\min} > 0.5$  m while  $GM_{L,\min}$  usually is much larger (more than 100 m).

If the transverse metacentric height  $GM_T$  is large, the spring is stiff in roll and it is quite uncomfortable for passengers onboard the vessel. However, the stability margin and robustness to large transverse waves are good in this case. Consequently, a trade-off between stability and comfort should be made. Another point to consider is that all ships have varying load conditions. This implies that the pitch and roll periods will vary with the loads since  $GM_T$  varies with the load. This is the topic for the next section.

## 4.3 Load Conditions and Natural Periods

The chosen load condition or weight distribution will determine the heave, roll and pitch periods of a marine craft. Hydrodynamic codes (see Section 6.2) can be used to compute a linear seakeeping model

$$(M_{RB} + A(\omega)) \ddot{\xi} + (B(\omega) + B_V(\omega)) \dot{\xi} + C\xi = \tau_{\text{ext}} \quad (4.52)$$

This is a linear mass-damper-spring system where the seakeeping coordinates  $\xi = [\zeta_1, \zeta_2, \zeta_3, \zeta_4, \zeta_5, \zeta_6]^\top$  are zero-mean wave-induced perturbations in  $\{s\}$  from an equilibrium state defined by a ship moving at constant heading  $\psi$  and speed  $U$ . In calm water  $\xi = \mathbf{0}$  and  $\{s\}$  coincides with  $\{b\}$ .

The outputs from the hydrodynamic codes are frequency-dependent added mass  $A(\omega)$  and potential damping  $B(\omega)$ . Viscous damping  $B_V(\omega)$  is usually added using semi-empirical methods while the restoring matrix is  $C = G$ .

If the decoupled heave, roll and pitch equations are used to compute the natural periods it is important to transform the hydrodynamic data to the CF, which is the point of rotation of a free-floating body. However, in a linear system the natural periods will be independent of the coordinate origin if they are computed using the 6-DOF coupled equations of motion. This is due to the fact that the eigenvalues of a linear system do not change when applying a similarity transformation. However, it is not straightforward to use the linear equations of motion since the potential coefficients depend on the wave frequency. This section presents methods for computation of the natural periods using coupled and decoupled equations in heave, roll and pitch.

### 4.3.1 Decoupled computation of natural periods

Consider the linear decoupled heave, roll and pitch equations

$$(m + A_{33}^{\text{CF}}(\omega_3)) \ddot{z} + (B_{33}^{\text{CF}}(\omega_3) + B_{v,33}^{\text{CF}}(\omega_3)) \dot{z} + C_{33}^{\text{CF}} z = 0 \quad (4.53)$$

$$(I_x^{\text{CF}} + A_{44}^{\text{CF}}(\omega_4)) \ddot{\phi} + (B_{44}^{\text{CF}}(\omega_4) + B_{v,44}^{\text{CF}}(\omega_4)) \dot{\phi} + C_{44}^{\text{CF}} \phi = 0 \quad (4.54)$$

$$(I_y^{\text{CF}} + A_{55}^{\text{CF}}(\omega_5)) \ddot{\theta} + (B_{55}^{\text{CF}}(\omega_5) + B_{v,55}^{\text{CF}}(\omega_5)) \dot{\theta} + C_{55}^{\text{CF}} \theta = 0 \quad (4.55)$$

where the potential coefficients  $A_{ii}^{\text{CF}}$  and  $B_{ii}^{\text{CF}}$ , viscous damping  $B_{v,ii}^{\text{CF}}$ , spring stiffness  $C_{ii}^{\text{CF}}$  ( $i = 3, 4, 5$ ) and moments of inertia  $I_x^{\text{CF}}$  and  $I_y^{\text{CF}}$  are computed in the CF, which is the vessel rotation point for a pure rolling or pitching motion under assumption of constant volume displacement. In the coupled case, the point of rotation as well as the rotation axes will change. If CF is unknown, a good approximation is to use the midships origin CO and an estimate for LCF. This will only affect the pitching frequency, which is not very sensitive to small translations along the  $x$  axis. If the natural frequencies are computed in a point far from CF using the decoupled equations (4.53)–(4.55), the results can be erroneous since the eigenvalues of the decoupled equations depend on the coordinate origin as opposed to the 6-DOF coupled system.

From (4.53)–(4.55) it follows that the natural frequencies and periods of heave, roll and pitch in the CF are given by the implicit equations

$$\omega_3 = \sqrt{\frac{C_{33}^{\text{CF}}}{m + A_{33}^{\text{CF}}(\omega_3)}}, \quad T_3 = \frac{2\pi}{\omega_3} \quad (4.56)$$

$$\omega_4 = \sqrt{\frac{C_{44}^{\text{CF}}}{I_x^{\text{CF}} + A_{44}^{\text{CF}}(\omega_4)}}, \quad T_4 = \frac{2\pi}{\omega_4} \quad (4.57)$$

$$\omega_5 = \sqrt{\frac{C_{55}^{\text{CF}}}{I_y^{\text{CF}} + A_{55}^{\text{CF}}(\omega_5)}}, \quad T_5 = \frac{2\pi}{\omega_5} \quad (4.58)$$

which can be solved in Matlab by using `fsoolve.m` (requires optimization toolbox) or `fzero.m`.

### Matlab:

1-DOF decoupled analysis for computation of natural periods for the MSS tanker and supply vessel. The hydrodynamic data have been computed using WAMIT and ShipX.

```
% w_n = natfrequency(vessel,dof,w_0,speed,LCF)
% vessel = MSS vessel data (computed in CO)
% dof = degree of freedom (3,4,5), use -1 for 6-DOF analysis
% w_0 = initial natural frequency (typical 0.5)
% speed = index 1,2,3... for hydrodynamic data set
% LCF = (optionally) x coordinate from CO to CF (negative)

load tanker;      % WAMIT data file
T_3 = 2 * pi / natfrequency(vessel,3,0.5,1)
T_4 = 2 * pi / natfrequency(vessel,4,0.5,1)
T_5 = 2 * pi / natfrequency(vessel,5,0.5,1)

T_3 =
    9.6814
T_4 =
   12.5074
T_5 =
    9.0851
```

```

load supply; % shipX data file
T_3 = 2 * pi / natfrequency(vessel,3,0.5,1)
T_4 = 2 * pi / natfrequency(vessel,4,0.5,1)
T_5 = 2 * pi / natfrequency(vessel,5,0.5,1)

T_3 =
    6.3617
T_4 =
   10.8630
T_5 =
    6.0988

```

### 4.3.2 Computation of natural periods in a 6-DOF coupled system

A 6-DOF coupled analysis of the frequency-dependent data can be done by using modal analysis. The coupled system can be transformed to six decoupled systems and the natural frequencies can be computed for each of them. This involves solving a generalized eigenvalue problem at each frequency.

Let CO be the coordinate origin of the linear seakeeping model

$$(\mathbf{M}_{RB} + \mathbf{A}(\omega)) \ddot{\boldsymbol{\xi}} + (\mathbf{B}(\omega) + \mathbf{B}_V(\omega) + \mathbf{K}_d) \dot{\boldsymbol{\xi}} + (\mathbf{C} + \mathbf{K}_p) \boldsymbol{\xi} = \mathbf{0} \quad (4.59)$$

where  $\mathbf{K}_p$  and  $\mathbf{K}_d$  are optional positive definite matrices due to feedback control,  $\mathbf{A}(\omega)$  and  $\mathbf{B}(\omega)$  are frequency-dependent added mass and potential damping (see Section 5.3) while  $\mathbf{B}_V(\omega)$  denotes additional viscous damping. The effect of feedback control can be included in the analysis by specifying three PD controllers in surge, sway and heave using

$$\mathbf{K}_p = \text{diag}(K_{p_{11}}, K_{p_{22}}, 0, 0, 0, K_{p_{66}}) \quad (4.60)$$

$$\mathbf{K}_d = \text{diag}(K_{d_{11}}, K_{d_{22}}, 0, 0, 0, K_{d_{66}}) \quad (4.61)$$

The gain selection represents a standard feedback control system for stationkeeping. Let

$$\mathbf{M}(\omega) = \mathbf{M}_{RB} + \mathbf{A}(\omega) \quad (4.62)$$

$$\mathbf{D}(\omega) = \mathbf{B}(\omega) + \mathbf{B}_V(\omega) + \mathbf{K}_d \quad (4.63)$$

$$\mathbf{G} = \mathbf{C} + \mathbf{K}_p \quad (4.64)$$

where  $\mathbf{M}(\omega) = \mathbf{M}(\omega)^\top > 0$  and  $\mathbf{D}(\omega) = \mathbf{D}(\omega)^\top > 0$  such that

$$\mathbf{M}(\omega) \ddot{\boldsymbol{\xi}} + \mathbf{D}(\omega) \dot{\boldsymbol{\xi}} + \mathbf{G} \boldsymbol{\xi} = \mathbf{0} \quad (4.65)$$

For surface vessels, the restoring matrix takes the following form (see Section 4.2):

$$\mathbf{G} = \mathbf{G}^\top = \begin{bmatrix} K_{p_{11}} & 0 & 0 & 0 & 0 & 0 \\ 0 & K_{p_{22}} & 0 & 0 & 0 & 0 \\ 0 & 0 & C_{33} & 0 & C_{35} & 0 \\ 0 & 0 & 0 & C_{44} & 0 & 0 \\ 0 & 0 & C_{53} & 0 & C_{55} & 0 \\ 0 & 0 & 0 & 0 & 0 & K_{p_{66}} \end{bmatrix} \quad (4.66)$$

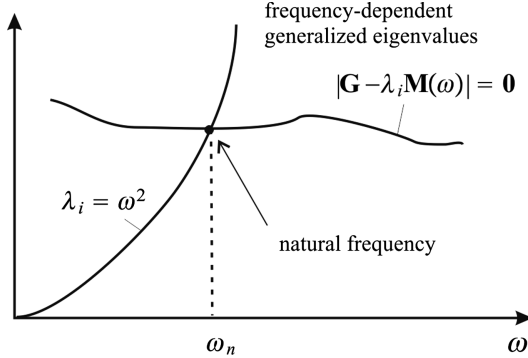


Figure 4.4: Generalized eigenvalue problem.

Notice that  $K_{p11}$ ,  $K_{p22}$  and  $K_{p66}$  must be positive to guarantee that  $\mathbf{G} > 0$ . Assume that the floating vessel under PD control carries out oscillations in 6 DOF

$$\boldsymbol{\xi} = \mathbf{a} \cos(\omega t) \quad (4.67)$$

where  $\mathbf{a} = [a_1, \dots, a_6]^\top$  is a vector of amplitudes. Then,

$$[\mathbf{G} - \omega^2 \mathbf{M}(\omega) - j\omega \mathbf{D}(\omega)] \mathbf{a} = \mathbf{0} \quad (4.68)$$

The natural frequencies can be computed for the undamped system  $\mathbf{D}(\omega) = \mathbf{0}$  by solving

$$[\mathbf{G} - \omega^2 \mathbf{M}(\omega)] \mathbf{a} = \mathbf{0} \quad (4.69)$$

The natural frequencies of a marine craft are usually shifted less than 1.0 % when damping is added. Hence, the undamped system (4.69) gives an accurate estimate of the frequencies of oscillation.

Equation (4.69) represents a frequency-dependent *generalized eigenvalue problem*

$$\mathbf{G}\mathbf{x}_i = \lambda_i \mathbf{M}(\omega)\mathbf{x}_i \quad (i = 1, \dots, 6) \quad (4.70)$$

where  $\mathbf{x}_i$  is the eigenvector and  $\lambda_i = \omega^2$  are the eigenvalues. This is recognized as an algebraic equation

$$\|\mathbf{G} - \lambda_i \mathbf{M}(\omega)\| = 0 \quad (4.71)$$

where  $\lambda_i$  is an eigenvalue satisfying (see Figure 4.4)

$$\lambda_i = \omega^2 \quad (4.72)$$

The characteristic equation of (4.71) is of sixth order:

$$\lambda^6 + a_5\lambda^5 + a_4\lambda^4 + a_3\lambda^3 + a_2\lambda^2 + a_1\lambda + a_0 = 0 \quad (4.73)$$

Let the solutions of the eigenvalue problem (4.71) as a function of  $\omega$  be denoted  $\lambda_i^*(\omega)$ . Then we can use the *Newton–Raphson method*:

$$\omega_{i,k+1} = \omega_{i,k} - \frac{f_i(\omega_{i,k})}{f'_i(\omega_{i,k})} \quad (i = 1, \dots, 6, k = 1, \dots, n) \quad (4.74)$$

where  $k$  denotes the number of iterations,  $i$  is the DOF considered and

$$f_i(\omega_{i,k}) = \lambda_i^*(\omega_{i,k}) - \omega_{i,k}^2 \quad (4.75)$$

to satisfy the constraint (4.72). After solving  $f_i(\omega_{i,k}) = 0$  for all DOFs to obtain  $\omega_{i,n}$ , the natural periods in 6 DOF follow from

$$T_i = \frac{2\pi}{\omega_{i,n}} \quad (4.76)$$

### Matlab:

The 6-DOF coupled eigenvalue analysis in Section 4.3.2 is implemented in the MSS toolbox. The natural periods for tanker is computed by using the following commands:

```
dof = -1; % use -1 for 6-DOF analysis
load tanker; % load WAMIT tanker data
T = 2 * pi ./ natfrequency(vessel,dof,0.5,1)

T =
    9.8261
   12.4543
   8.9536

load supply; % load ShipX supply ship data
T = 2 * pi ./ natfrequency(vessel,dof,0.5,1)

T =
    6.5036
   10.4205
   6.0210
```

Notice that that natural periods for the coupled analysis are quite close to the numbers obtained in the decoupled analysis in Section 4.3.1.

### 4.3.3 Natural periods as a function of load condition

The roll and pitch periods will depend strongly on the load condition while heave is less affected. From (4.56)–(4.58) it follows that

$$T_3 = 2\pi \sqrt{\frac{m + A_{33}^{\text{CF}}(\omega_3)}{\rho g A_{wp}}} \quad (4.77)$$

$$T_4 = 2\pi \sqrt{\frac{I_x^{\text{CF}} + A_{44}^{\text{CF}}(\omega_4)}{\rho g \nabla \text{GM}_T}} \quad (4.78)$$

$$T_5 = 2\pi \sqrt{\frac{I_y^{\text{CF}} + A_{55}^{\text{CF}}(\omega_5)}{\rho g \nabla \text{GM}_L}} \quad (4.79)$$

An estimate of the heave period can be computed by assuming that  $A_{33}^{\text{CF}} \approx m = \rho \nabla$  and  $\nabla \approx A_{wp} T$  where  $T$  is the draft. This implies that (4.77) can be approximated as

$$T_3 \approx 2\pi \sqrt{\frac{2T}{g}} \quad (4.80)$$

Formula (4.80) indicates that the natural period in heave mainly depends on the draft  $T$ , which again depends on the vessel load condition.

For roll and pitch one can compute the moments of inertia about CG according to

$$I_x^{\text{CG}} = mR_{44}^2 \quad (4.81)$$

$$I_y^{\text{CG}} = mR_{55}^2 \quad (4.82)$$

where  $R_{44}$  and  $R_{55}$  are the radii of gyration with respect to CG. For offshore vessels  $R_{44} \approx 0.35B$  while tankers have  $R_{44} \approx 0.37B$ . Semisubmersibles have two or more pontoons so  $0.40B$  is not uncommon for these vessels. In pitch and yaw it is common to use  $R_{55} = R_{66} \approx 0.25L_{pp}$  for smaller vessels while tankers use  $R_{55} = R_{66} \approx 0.27L_{pp}$ .

Assume that  $\mathbf{r}_f^b = [\text{LCF}, 0, 0]^\top$  and  $\mathbf{r}_g^b = [x_g, 0, z_g]^\top$  such that CO is on the centerline midships. Application of the parallel-axes theorem (3.36) gives

$$I_x^{\text{CF}} = mR_{44}^2 + mz_g^2 := m(R_{44}^{\text{CF}})^2 \quad (4.83)$$

$$I_y^{\text{CF}} = mR_{55}^2 + m((x_g - \text{LCF})^2 + z_g^2) := m(R_{55}^{\text{CF}})^2 \quad (4.84)$$

Assume that the added mass matrix  $\mathbf{A}$  is computed in CO. The transformations between CO and CF are (see Appendix C.1.3)

$$\mathbf{A} = \mathbf{H}^\top(\mathbf{r}_f^b) \mathbf{A}^{\text{CF}} \mathbf{H}(\mathbf{r}_f^b) \quad (4.85)$$

$$\mathbf{A}^{\text{CF}} = \mathbf{H}^{-\top}(\mathbf{r}_f^b) \mathbf{A} \mathbf{H}^{-1}(\mathbf{r}_f^b) \quad (4.86)$$

Define  $\kappa_4$  and  $\kappa_5$  as the ratios

$$\kappa_4 := \frac{A_{44}^{\text{CF}}(\omega_4)}{I_x^{\text{CF}}} \quad (4.87)$$

$$\kappa_5 := \frac{A_{55}^{\text{CF}}(\omega_5)}{I_y^{\text{CF}}} \quad (4.88)$$

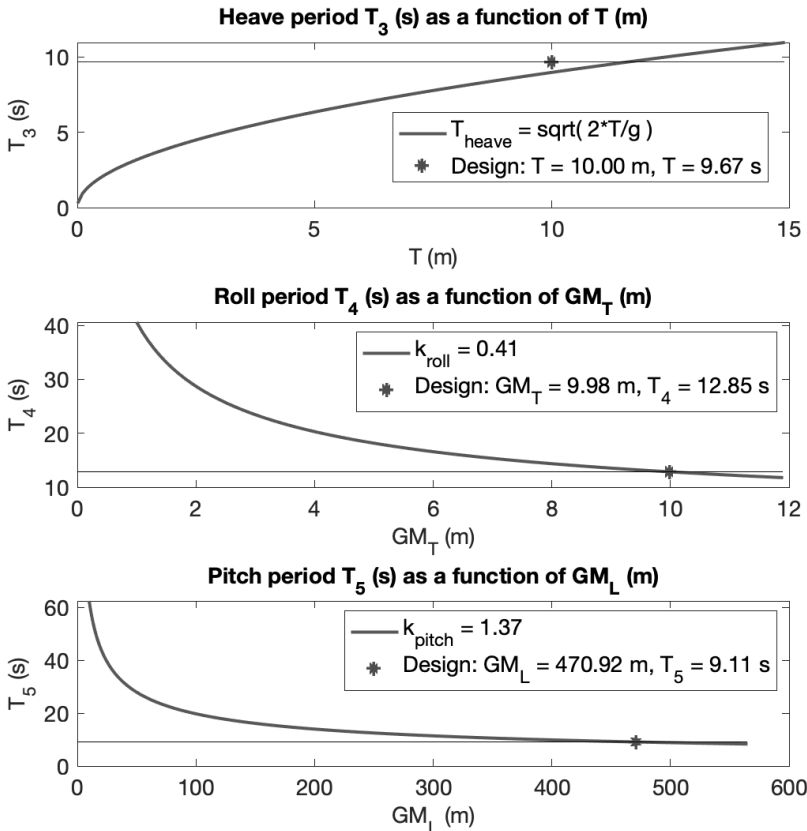


Figure 4.5: Heave, roll and pitch periods for varying draft and metacenter heights using formulae (4.78)–(4.79) for roll and pitch. The heave period is approximated by formula (4.80). The design values (asterisks) are computed using the WAMIT data for the operational condition.

Typical values for  $\kappa_4$  are 0.1–0.3 for ships and 1.0 or more for semisubmersibles. In pitch  $\kappa_5$  will be in the range 1.0–2.0. This implies that the roll and pitch periods (4.78)–(4.79) can be approximated as

$$T_4 = 2\pi R_{44}^{\text{CF}} \sqrt{\frac{1 + \kappa_4}{g GM_T}} \quad (4.89)$$

$$T_5 = 2\pi R_{55}^{\text{CF}} \sqrt{\frac{1 + \kappa_5}{g GM_L}} \quad (4.90)$$

Formulae (4.89)–(4.90) show that the natural periods in roll and pitch mainly depend on  $GM_T$  and  $GM_L$ , which again depend on the vessel load condition.

**Matlab:**

The heave, roll and pitch design periods for the MSS tanker are plotted together with formulae (4.78)–(4.79) and (4.80). using the MSS toolbox command:

```
load tanker; % load WAMIT tanker data
loadcond(vessel); % periods as a function of load condition
```

The roll and pitch periods as a function of  $GM_T$  and  $GM_L$  for tanker are shown in Figure 4.5. It is seen that  $T_{\text{roll}}$  is reduced if  $GM_T$  is increased and vice versa. The same effect is observed in pitch. The heave period  $T_{\text{heave}}$  is proportional to  $\sqrt{T}$  as expected.

#### 4.3.4 Free-surface effects

Many ships are equipped liquid tanks such as ballast and anti-roll tanks. A partially filled tank is known as a slack tank and in these tanks the liquid can move and endanger the ship's stability. The reduction of metacentric height caused by the liquids in slack tanks is known as the *free-surface effect*. The mass of the liquid or the location of the tanks have no role; it is only the moment of inertia of the surface that affects stability. The effective metacentric height corrected for slack tanks filled with sea water is (Brian 2003)

$$GM_{T,\text{eff}} = GM_T - FSC \quad (4.91)$$

where the *free-surface correction* (FSC) is

$$FSC = \sum_{r=1}^N \frac{\rho}{m} i_r \quad (4.92)$$

where  $i_r$  is the moment of inertia of the water surface. For a rectangular tank with length  $l$  in the  $x$  direction and width  $b$  in the  $y$  direction, the moment of inertia of the surface about an axis through the centroid is

$$i_r = \frac{lb^3}{12} \quad (4.93)$$

#### 4.3.5 Payload effects

A reduction in  $GM_T$  is observed if a payload with mass  $m_p$  is lifted up and suspended at the end of a rope of length  $h$ . Then the effective metacentric height becomes

$$GM_{T,\text{eff}} = GM_T - h \frac{m_p}{m} \quad (4.94)$$

Consequently, it is important to notice that a reduction in  $GM_T$  due to slack tanks or lift operations increases the roll period/passenger comfort to the cost of a less stable ship. These effects are also observed in pitch, but pitch is much less affected since  $GM_L \gg GM_T$ .

## 4.4 Seakeeping Analysis

In the design of ships and ocean structures, the wave-induced motions are of great importance to the assessment of the comfort and safety of the crew and the passengers. Seakeeping analyses should be performed to estimate seakeeping ability or seaworthiness, that is how well-suited a marine craft is to conditions when underway. In this context the watercraft's response to wave-induced forces is of great importance.

This section presents methods for computation of the heave, roll and pitch responses in regular waves. This also includes resonance analyses, that is the phenomenon that occurs when the frequency of a sinusoidal wave is equal or nearly equal to one of the natural frequencies of the watercraft. This causes the craft to heave, roll and pitch with larger amplitudes than when the wave-induced force is applied at other frequencies. Resonance can cause a marine craft to roll to very large angles in moderate sea states, leading to cargo damage, loss of containers and, in extreme cases, capsizing of the craft.

### 4.4.1 Harmonic oscillator with sinusoidal forcing

The heave, roll and pitch motions of a marine craft can be described by a second-order mass–damper–spring system

$$m\ddot{x} + d\dot{x} + kx = F \sin(\omega t) \quad (4.95)$$

where  $F$  is the amplitude of the sinusoidal driving force and  $\omega$  is the driving frequency. It is convenient to rewrite (4.95) as

$$\ddot{x} + 2\zeta\omega_n\dot{x} + \omega_n^2x = \frac{F}{m} \sin(\omega t) \quad (4.96)$$

where  $\zeta$  is the relative damping ratio and  $\omega_n$  is the natural frequency given by

$$\zeta = \frac{d}{2}\sqrt{\frac{1}{mk}}, \quad \omega_n = \sqrt{\frac{k}{m}} \quad (4.97)$$

This is a linear system where the general solution is a sum of a transient solution that depends on the initial conditions, and a steady-state solution that is independent of initial conditions and depends only on the driving amplitude  $F$ . The transient solution is a short-lived burst of energy caused by a sudden change of the state. Hence, we only consider the steady-state solution

$$x = \frac{F}{mZ_m\omega} \sin(\omega t + \varepsilon) \quad (4.98)$$

with

$$Z_m = \sqrt{(2\zeta\omega_n)^2 + \frac{1}{\omega^2}(\omega_n^2 - \omega^2)^2} \quad (4.99)$$

$$\varepsilon = \text{atan} \left( \frac{2\zeta\omega_n\omega}{\omega^2 - \omega_n^2} \right) \quad (4.100)$$

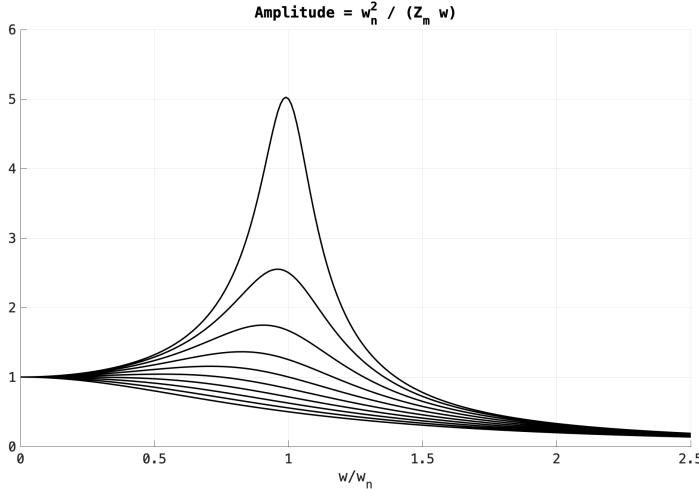


Figure 4.6: Steady-state variation of amplitude  $\omega_n^2 / (Z_m \omega)$  with relative frequency  $\omega/\omega_n$  for relative damping ratios  $\zeta = 0.1, 0.2, \dots, 1.0$ .

Here  $Z_m$  is the absolute value of the *impedance* and  $\varepsilon$  is the *phase* of the oscillation relative to the driving force. Impedance is a measure of how much the craft resists motion when subjected to a sinusoidal force. It represents the ratio of the applied force  $F$  to the velocity  $\dot{x}$ .

### Resonant frequency

The solution (4.98) does not exist for  $Z_m = 0$ . This is when resonance occurs. Solving  $Z_m = 0$  for the driving frequency  $\omega$  gives the resonant frequency

$$\omega_r = \omega_n \sqrt{1 - 2\zeta^2} \quad (4.101)$$

Since the expression in the square root has to be nonnegative, resonance only occurs when  $\zeta < 1/\sqrt{2} \approx 0.707$ . This corresponds to significantly underdamped systems. For marine craft both roll and pitch are underdamped. Figure 4.6 shows the steady-state variation of the amplitude  $\omega_n^2 / (Z_m \omega)$  corresponding to  $F = m\omega_n^2$  for varying relative damping ratios  $\zeta$ .

### 4.4.2 Steady-state heave, roll and pitch responses in regular waves

Consider the linear decoupled heave, roll and pitch equations (4.53)–(4.53) with harmonic forcing

$$(m + A_{33}^{\text{CF}}(\omega_3)) \ddot{z} + (B_{33}^{\text{CF}}(\omega_3) + B_{v,33}^{\text{CF}}(\omega_3)) \dot{z} + C_{33}^{\text{CF}} z = F_3 \cos(\omega_e t) \quad (4.102)$$

$$(I_x^{\text{CF}} + A_{44}^{\text{CF}}(\omega_4)) \ddot{\phi} + (B_{44}^{\text{CF}}(\omega_4) + B_{v,44}^{\text{CF}}(\omega_4)) \dot{\phi} + C_{44}^{\text{CF}} \phi = F_4 \cos(\omega_e t) \quad (4.103)$$

$$(I_y^{\text{CF}} + A_{55}^{\text{CF}}(\omega_5)) \ddot{\theta} + (B_{55}^{\text{CF}}(\omega_5) + B_{v,55}^{\text{CF}}(\omega_5)) \dot{\theta} + C_{55}^{\text{CF}} \theta = F_5 \sin(\omega_e t) \quad (4.104)$$

where the phase shift of pitch is 90 degrees relative heave and roll. The frequency of encounter is

$$\omega_e = \omega - kU \cos(\beta) \quad (4.105)$$

where  $\beta$  is the encounter angle, that is the angle between the heading angle  $\psi$  and the direction  $\gamma_w$  of the wave. This implies that head sea corresponds to 180 degrees, see Figure 10.14. The wave frequency  $\omega$  satisfies the dispersion relation

$$\omega^2 = kg \tanh(kd) \quad (4.106)$$

where  $k$  is the wave number and  $d$  is the water depth. For large water depths  $\omega^2 = kg$ .

The natural frequencies and relative damping factors are found from (4.97)

$$\begin{aligned} \omega_3 &= \sqrt{\frac{C_{33}^{\text{CF}}}{m + A_{33}^{\text{CF}}(\omega_3)}}, \quad \zeta_3 = \frac{B_{33}^{\text{CF}}(\omega_3) + B_{v,33}^{\text{CF}}(\omega_3)}{2} \sqrt{\frac{1}{(m + A_{33}^{\text{CF}}(\omega_3)) C_{33}^{\text{CF}}}} \\ \omega_4 &= \sqrt{\frac{C_{44}^{\text{CF}}}{I_x^{\text{CF}} + A_{44}^{\text{CF}}(\omega_4)}}, \quad \zeta_4 = \frac{B_{44}^{\text{CF}}(\omega_4) + B_{v,44}^{\text{CF}}(\omega_4)}{2} \sqrt{\frac{1}{(I_x^{\text{CF}} + A_{44}^{\text{CF}}(\omega_4)) C_{44}^{\text{CF}}}} \\ \omega_5 &= \sqrt{\frac{C_{55}^{\text{CF}}}{I_y^{\text{CF}} + A_{55}^{\text{CF}}(\omega_5)}}, \quad \zeta_5 = \frac{B_{55}^{\text{CF}}(\omega_5) + B_{v,55}^{\text{CF}}(\omega_5)}{2} \sqrt{\frac{1}{(I_y^{\text{CF}} + A_{55}^{\text{CF}}(\omega_5)) C_{55}^{\text{CF}}}} \end{aligned}$$

From (4.98) it follows that

$$z = \frac{F_3}{(m + A_{33}^{\text{CF}}(\omega_3)) Z_{m,3} \omega_e} \cos(\omega_e t + \varepsilon_3) \quad (4.107)$$

$$\phi = \frac{F_4}{(I_x^{\text{CF}} + A_{44}^{\text{CF}}(\omega_4)) Z_{m,4} \omega_e} \cos(\omega_e t + \varepsilon_4) \quad (4.108)$$

$$\theta = \frac{F_5}{(I_y^{\text{CF}} + A_{55}^{\text{CF}}(\omega_5)) Z_{m,5} \omega_e} \sin(\omega_e t + \varepsilon_5) \quad (4.109)$$

where the impedances and phase shifts are

$$Z_{m,3} = \sqrt{(2\zeta_3 \omega_3)^2 + \frac{1}{\omega_e^2} (\omega_3^2 - \omega_e^2)^2}, \quad \varepsilon_3 = \tan^{-1} \left( \frac{2\zeta_3 \omega_3 \omega_e}{\omega_e^2 - \omega_3^2} \right) \quad (4.110)$$

$$Z_{m,4} = \sqrt{(2\zeta_4 \omega_4)^2 + \frac{1}{\omega_e^2} (\omega_4^2 - \omega_e^2)^2}, \quad \varepsilon_4 = \tan^{-1} \left( \frac{2\zeta_4 \omega_4 \omega_e}{\omega_e^2 - \omega_4^2} \right) \quad (4.111)$$

$$Z_{m,5} = \sqrt{(2\zeta_5 \omega_5)^2 + \frac{1}{\omega_e^2} (\omega_5^2 - \omega_e^2)^2}, \quad \varepsilon_5 = \tan^{-1} \left( \frac{2\zeta_5 \omega_5 \omega_e}{\omega_e^2 - \omega_5^2} \right) \quad (4.112)$$

### Data from hydrodynamic codes

The heave, roll and pitch responses with respect to the CF can be computed using data from hydrodynamic codes. The necessary terms are the added mass coefficient  $A_{ii}^{\text{CF}}(\omega_i)$ , potential damping coefficient  $B_{ii}^{\text{CF}}(\omega_i)$  viscous damping coefficient  $B_{v,ii}^{\text{CF}}(\omega_i)$  and restoring coefficients  $C_{ii}^{\text{CF}}$  ( $i = 3, 4, 5$ ); see Chapter 5. Hydrodynamic codes also computes the wave loads for varying frequencies and encounter angles.

#### 4.4.3 Explicit formulae for boxed-shaped vessels in regular waves

A semi-analytical approach can be used to derive frequency response functions for the wave-induced motions of monohull ships.

Jensen *et al.* (2004) have derived closed-form expressions for the heave, roll and pitch responses in regular waves where the required input information for the method is restricted to the main dimensions: length  $L$ , breadth  $B$ , draught  $T$ , block coefficient  $C_b = LBT/\nabla$  and waterplane area  $A_w$  together with speed  $U$  and wave encounter angle  $\beta$ . The formulas make it simple to obtain quick estimates of the wave-induced motions and accelerations in the conceptual design phase and to perform a sensitivity study of the variation with main dimensions and operational profile. The method is based on linear strip theory where the coupling terms between heave and pitch are neglected and by assuming a constant sectional added mass equal to the displaced water. Faltinsen (1990, pp. 89–90) presents a similar approach based on strip theory in which explicit formulae for the expressions  $F_3$  and  $F_5$  in (4.107)–(4.109) are derived.

#### Steady-state heave and pitch responses

Consider the two harmonic oscillators (Jensen *et al.* 2004)

$$\ddot{z} + 2\zeta\omega_n\dot{z} + \omega_n^2 z = \omega_n^2 \zeta_a F \cos(\omega_e t) \quad (4.113)$$

$$\ddot{\theta} + 2\zeta\omega_n\dot{\theta} + \omega_n^2 \theta = \omega_n^2 \zeta_a G \sin(\omega_e t) \quad (4.114)$$

where the wave amplitude  $\zeta_a$  is the driving term. The oscillators have common relative damping ratio and natural frequency

$$\zeta = \frac{A^2}{B\alpha^3 \sqrt{8k^3 T}}, \quad \omega_n = \sqrt{\frac{g}{2T}} \quad (4.115)$$

where  $A$  is the sectional hydrodynamic damping

$$A = 2 \sin\left(\frac{1}{2}kB\alpha^2\right) \exp(-kT\alpha^2) \quad (4.116)$$

and  $\alpha = \omega_e/\omega = 1 - \sqrt{kg} U \cos(\beta)$  is the ratio between the frequency of encounter  $\omega_e$  and the wave frequency  $\omega$ . Let  $k_e$  denote the effective wave number

$$k_e = k|\cos(\beta)| \quad (4.117)$$

and

$$f = \sqrt{(1 - kT)^2 + \left(\frac{A^2}{kB\alpha^3}\right)^2} \quad (4.118)$$

Then the forcing functions  $F$  and  $G$  can be expressed as

$$F = \kappa f \frac{\sin(\sigma)}{\sigma} \quad (4.119)$$

$$G = \kappa f \frac{6}{L_{pp}\sigma} \left( \frac{\sin(\sigma)}{\sigma} - \cos(\sigma) \right) \quad (4.120)$$

where  $\sigma = k_e L_{pp}/2$  and  $\kappa = \exp(-k_e T)$ . The steady-state heave and pitch responses become

$$z = \zeta_a \frac{w_n^2}{Z_m w_e} F \cos(w_e t + \varepsilon) \quad (4.121)$$

$$\theta = \zeta_a \frac{w_n^2}{Z_m w_e} G \sin(w_e t + \varepsilon) \quad (4.122)$$

where  $Z_m$  and  $\varepsilon$  are given by (4.99)–(4.100). The heave and pitch responses (4.121)–(4.122) can be plotted in Matlab by using MSS toolbox script `waveresponse345.m`.

### Steady-state roll response

The roll motion is assumed to be decoupled from the other transverse motions such that the equation of motion for roll in regular waves with unit wave amplitude is (Jensen *et al.* 2004)

$$\left(\frac{T_4}{2\pi}\right)^2 C_{44} \ddot{\phi} + B_{44} \dot{\phi} + C_{44} \phi = M \cos(\omega_e t) \quad (4.123)$$

where

$$C_{44} = \rho \nabla G M_T \quad (4.124)$$

The natural period  $T_4$  replaces the mass moment of inertia and the added mass in the equation of motion. Consequently, the variation in the added mass with frequency is neglected. Jensen *et al.* (2004) assumes that the ship can be described as two prismatic beams with the same draught, but different breadths and cross-sectional areas. Under these assumptions a formulae for the 2-D sectional inviscid hydrodynamic damping coefficient is derived. An even simpler approach could be to specify the relative damping ratio  $\zeta_4$  such that

$$B_{44} = 2\zeta_4 \left(\frac{T_4}{2\pi}\right) C_{44} \quad (4.125)$$

An estimate of  $M$  for varying encounter angles  $\beta$  will then be

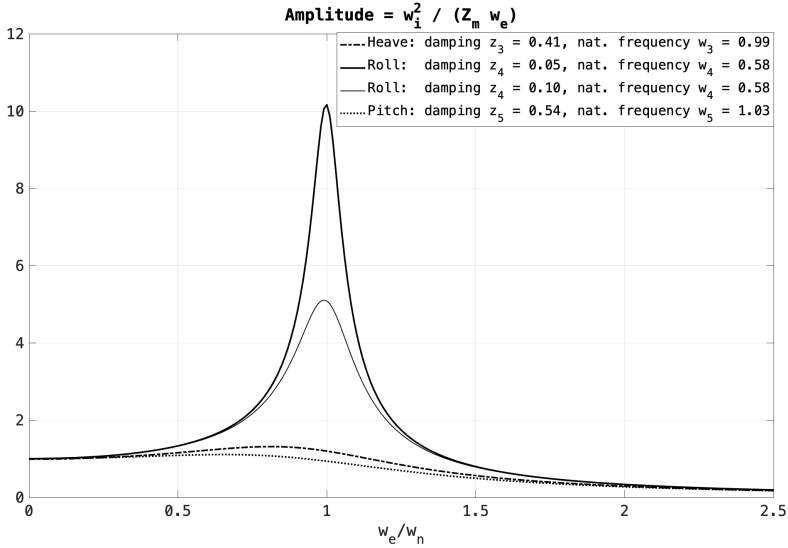


Figure 4.7: Steady-state variation of amplitudes  $\omega_i^2 / (Z_{m,i} \omega_e)$  with relative frequency  $\omega_e/\omega_i$  ( $i = 3, 4, 5$ ) corresponding to heave, roll and pitch. The numerical analysis is based on the MSS supply vessel. The vessel is underdamped in roll and this gives rise to significant magnification of roll amplitudes when  $\omega_e/\omega_4 = 1.0$ .

$$M = \sqrt{\frac{\rho g^2}{\omega_e} B_{44} \sin(\beta)} \quad (4.126)$$

Finally, the steady-state roll response becomes

$$\phi = \frac{w_4^2}{\rho \nabla G M_T Z_{m,4} \omega_e} M \cos(w_e t + \varepsilon_4) \quad (4.127)$$

where  $Z_{m,4}$  and  $\varepsilon_4$  are given by (4.111). The roll response (4.127) can be plotted in Matlab by using the MSS script `waveresponse345.m`.

#### 4.4.4 Resonances in the heave, roll and pitch modes

The MSS supply vessel is used in the resonance analysis. The wave excitation amplitudes are chosen as

$$F_3 = (m + A_{33}^{\text{CF}}(\omega_3)) \omega_3^2 \quad (4.128)$$

$$F_4 = (I_x^{\text{CF}} + A_{44}^{\text{CF}}(\omega_4)) \omega_4^2 \quad (4.129)$$

$$F_5 = (I_y^{\text{CF}} + A_{55}^{\text{CF}}(\omega_5)) \omega_5^2 \quad (4.130)$$

such that the steady-state amplitudes of (4.107)–(4.109) become  $\omega_i^2/(Z_{m,i} \omega_e)$  for  $i = 3, 4, 5$ .

Figure 4.7 shows the amplitudes in heave, roll and pitch for variation in relative frequencies  $\omega_e/\omega_i$  for  $i = 3, 4, 5$ . The numerical example is included in the MSS Matlab script ExResonance.m. As expected roll is the critical DOF for which the amplitude of the roll angle  $\phi$  is significantly amplified at the resonant frequency  $\omega_4 = 0.58$  rad/s for incoming sinusoidal waves  $F_4 \cos(\omega_e t)$  when  $\omega_e = \omega_4$ . This corresponds to regular waves with a period  $T_4 = 10.9$  s, which are likely to happen. The relative damping ratio  $\zeta_4 = 0.05$  in roll for the MSS supply vessel is quite low, while  $GM_T = 2.14$  m gives sufficient stability. Hydrodynamic codes usually compute the potential damping terms  $B_{ii}^{CF}$  and leaves to the user to add viscous damping  $B_{v,ii}^{CF}$ . Hence, the data set should be calibrated by increasing the viscous damping term  $B_{v,44}^{CF}$  if roll is to little damped (Ikeda *et al.* 1976). The positive effect of increasing  $\zeta_4$  from 0.05 to 0.10 is clearly seen in the plot. From a physical point of view, roll damping can be increased by adding bilge keels or fins.

Figure 4.7 shows that the heave and pitch motions are well damped for the supply vessel. The relative damping ratios are  $\zeta_3 = 0.41$  and  $\zeta_5 = 0.54$ . This gives a moderate amplification of the heave and pitch amplitudes.

## 4.5 Ballast Systems

In addition to the metacentric restoring forces  $\mathbf{g}(\boldsymbol{\eta})$  described in Section 4.1, the equilibrium point can be changed by pretrimming, for instance by pumping water between the ballast tanks of the vessel. The vessel can only be trimmed in *heave*, *pitch* and *roll* where restoring forces are present.

Let the equilibrium point be

$$z = z_d, \quad \phi = \phi_d \quad \text{and} \quad \theta = \theta_d$$

where  $z_d, \phi_d$  and  $\theta_d$  are the desired states. The equilibrium states corresponding to these values are found by considering the steady-state solution of

$$\mathbf{M}\dot{\boldsymbol{\nu}} + \mathbf{C}(\boldsymbol{\nu})\boldsymbol{\nu} + \mathbf{D}(\boldsymbol{\nu})\boldsymbol{\nu} + \mathbf{g}(\boldsymbol{\eta}) + \mathbf{g}_o = \boldsymbol{\tau} + \underbrace{\boldsymbol{\tau}_{\text{wind}} + \boldsymbol{\tau}_{\text{wave}}}_{\mathbf{w}} \quad (4.131)$$

which under assumption of zero acceleration/velocity ( $\dot{\boldsymbol{\nu}} = \boldsymbol{\nu} = \mathbf{0}$ ) and no control forces ( $\boldsymbol{\tau} = \mathbf{0}$ ) reduces to

$$\mathbf{g}(\boldsymbol{\eta}_d) + \mathbf{g}_o = \mathbf{w} \quad (4.132)$$

where  $\boldsymbol{\eta}_d = [-, -, z_d, \phi_d, \theta_d, -]^\top$ ; that is only three states are used for pretrimming.

The forces and moments  $\mathbf{g}_o$  due to the ballast tanks are computed using hydrostatic analyses. Consider a marine craft with  $n$  ballast tanks of volumes  $V_i \leq V_{i,\max}$  for  $i = 1, \dots, n$ . For each ballast tank the water volume is

$$V_i(h_i) = \int_o^{h_i} A_i(h)dh \approx A_i h_i; \quad A_i(h) = \text{constant} \quad (4.133)$$

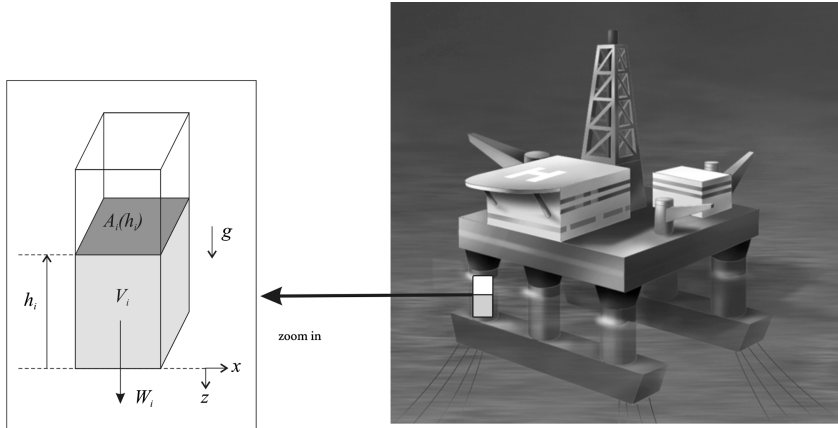


Figure 4.8: Semisubmersible ballast tanks. Illustration by Bjarne Stenberg.

where  $A_i(h)$  is the area of the ballast tank at height  $h$ . Hence, the volume of the water column in each ballast tank can be computed by measuring the water heights  $h_i$ . Next, assume that the ballast tanks are located at

$$\mathbf{r}_i^b = [x_i, y_i, z_i]^\top \quad (i = 1, \dots, n) \quad (4.134)$$

where  $\mathbf{r}_i^b$  is the vector from the coordinate origin CO to the geometric center of tank  $i$ . The gravitational forces  $W_i$  in heave are summed up according to (see Figure 4.8)

$$\begin{aligned} Z_{\text{ballast}} &= \sum_{i=1}^n W_i \\ &= \rho g \sum_{i=1}^n V_i \end{aligned} \quad (4.135)$$

The moments due to the ballast heave force  $\rho g V_i$  are then found from

$$\begin{aligned} \mathbf{m}_i^b &= \mathbf{r}_i^b \times \mathbf{f}_i^b \\ &= \begin{bmatrix} x_i \\ y_i \\ z_i \end{bmatrix} \times \begin{bmatrix} 0 \\ 0 \\ \rho g V_i \end{bmatrix} \\ &= \begin{bmatrix} y_i \rho g V_i \\ -x_i \rho g V_i \\ 0 \end{bmatrix} \end{aligned} \quad (4.136)$$

implying that the roll and pitch moments due to ballast are

$$K_{\text{ballast}} = \rho g \sum_{i=1}^n y_i V_i \quad (4.137)$$

$$M_{\text{ballast}} = -\rho g \sum_{i=1}^n x_i V_i \quad (4.138)$$

Finally, this gives

$$\mathbf{g}_o = \begin{bmatrix} 0 \\ 0 \\ -Z_{\text{ballast}} \\ -K_{\text{ballast}} \\ -M_{\text{ballast}} \\ 0 \end{bmatrix} = \rho g \begin{bmatrix} 0 \\ 0 \\ -\sum_{i=1}^n V_i \\ -\sum_{i=1}^n y_i V_i \\ \sum_{i=1}^n x_i V_i \\ 0 \end{bmatrix} \quad (4.139)$$

### Metacentric height correction

Since ballast tanks are partially filled tanks of liquids, the restoring roll moment will be affected. The formulae for the free-surface correction (4.91)–(4.92) can, however, be applied to correct the transverse metacentric height  $GM_T$  in roll.

#### 4.5.1 Static conditions for trim and heel

Distribution of water between the ballast tanks can be done manually by pumping water until the desired water levels  $h_i$  in each tank are reached or automatically by using feedback control. For manual operation, the steady-state relationships between water levels  $h_i$  and the desired pretrimming values  $z_d$ ,  $\phi_d$  and  $\theta_d$  are needed. Trimming is usually done under the assumptions that  $\phi_d$  and  $\theta_d$  are small such that linear theory can be applied

$$\mathbf{g}(\boldsymbol{\eta}_d) \approx G\boldsymbol{\eta}_d \quad (4.140)$$

Since we are only concerned with the heave, roll and pitch modes it is convenient to use the 3-DOF reduced-order system

$$\mathbf{G}^{\{3,4,5\}} = \begin{bmatrix} -Z_z & 0 & -Z_\theta \\ 0 & -K_\phi & 0 \\ -M_z & 0 & -M_\theta \end{bmatrix}$$

$$\mathbf{g}_o^{\{3,4,5\}} = \rho g \begin{bmatrix} -\sum_{i=1}^n V_i \\ -\sum_{i=1}^n y_i V_i \\ \sum_{i=1}^n x_i V_i \end{bmatrix}$$

$$\boldsymbol{\eta}_d^{\{3,4,5\}} = [z_d, \phi_d, \theta_d]^\top$$

$$\mathbf{w}^{\{3,4,5\}} = [w_3, w_4, w_5]^\top$$

The key assumption for open-loop pretrimming is that  $\mathbf{w}^{\{3,4,5\}} = [w_3, w_4, w_5]^\top = \mathbf{0}$ , that is no disturbances in heave, roll and pitch. From (4.132) and (4.33) it follows that

$$\mathbf{G}^{\{3,4,5\}} \boldsymbol{\eta}_d^{\{3,4,5\}} + \mathbf{g}_o^{\{3,4,5\}} = \mathbf{0} \quad (4.141)$$

⇓

$$\begin{bmatrix} -Z_z & 0 & -Z_\theta \\ 0 & -K_\phi & 0 \\ -M_z & 0 & -M_\theta \end{bmatrix} \begin{bmatrix} z_d \\ \phi_d \\ \theta_d \end{bmatrix} + \rho g \begin{bmatrix} -\sum_{i=1}^n V_i \\ -\sum_{i=1}^n y_i V_i \\ \sum_{i=1}^n x_i V_i \end{bmatrix} = \mathbf{0}$$

This can be rewritten as

$$\mathbf{H}\mathbf{v} = \mathbf{y} \quad (4.142)$$

⇓

$$\rho g \begin{bmatrix} 1 & \dots & 1 & 1 \\ y_1 & \dots & y_{n-1} & y_n \\ -x_1 & \dots & -x_{n-1} & -x_n \end{bmatrix} \begin{bmatrix} V_1 \\ V_2 \\ \vdots \\ V_n \end{bmatrix} = \begin{bmatrix} -Z_z z_d - Z_\theta \theta_d \\ -K_\phi \phi_d \\ -M_z z_d - M_\theta \theta_d \end{bmatrix} \quad (4.143)$$

where  $\mathbf{v}$  is a vector of tank volumes:

$$\mathbf{v} = [V_1, V_2, \dots, V_n]^\top \quad (4.144)$$

The tank volumes are computed from (4.142) by using the *Moore–Penrose pseudo-inverse*

$$\begin{aligned} \mathbf{v} &= \mathbf{H}^\dagger \mathbf{y} \\ &= \mathbf{H}^\top (\mathbf{H} \mathbf{H}^\top)^{-1} \mathbf{y} \end{aligned} \quad (4.145)$$

where it is assumed that  $n \geq 3$  and that  $\mathbf{H} \mathbf{H}^\top$  has full rank. Finally, the desired water heights can be computed from

$$V_i(h_i) = \int_o^{h_i} A_i(h) dh \quad (4.146)$$

$$\Downarrow \quad (A_i(h) = A_i)$$

$$h_i = \frac{V_i}{A_i} \quad (4.147)$$

### Example 4.3 (Semisubmersible Ballast Control)

Consider the semisubmersible shown in Figure 4.9 with four ballast tanks located at  $\mathbf{r}_1^b = [-x, -y]$ ,  $\mathbf{r}_2^b = [x, -y]$ ,  $\mathbf{r}_3^b = [x, y]$  and  $\mathbf{r}_4^b = [-x, y]$ . In addition,  $yz$  symmetry implies that  $Z_\theta = M_z = 0$  while the diagonal elements in  $\mathbf{G}^{\{3,4,5\}}$  are nonzero.

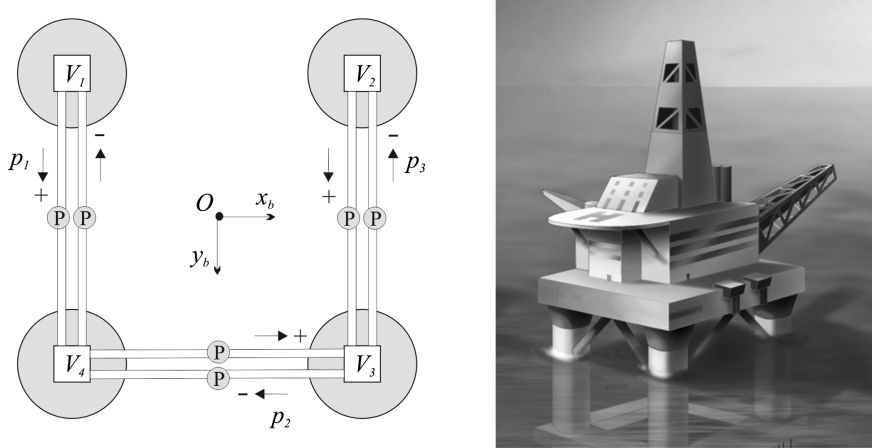


Figure 4.9: Semisubmersible with four ballast tanks.  $V_i$  is the water volume in leg  $i = 1, \dots, 4$  and  $p_j$  is the volume flow for water pump  $j = 1, \dots, 3$ . Illustration by Bjarne Stenberg.

Consequently,

$$\begin{aligned} \mathbf{H} &= \rho g \begin{bmatrix} 1 & 1 & 1 & 1 \\ -y & -y & y & y \\ x & -x & -x & x \end{bmatrix} \\ \mathbf{y} &= \begin{bmatrix} -Z_z z_d \\ -K_\phi \phi_d \\ -M_\theta \theta_d \end{bmatrix} = \rho g \begin{bmatrix} A_{wp} z_d \\ \nabla \text{GM}_T \phi_d \\ \nabla \text{GM}_L \theta_d \end{bmatrix} \end{aligned}$$

The right pseudo-inverse of  $\mathbf{H}$  is

$$\mathbf{H}^\dagger = \mathbf{H}^\top (\mathbf{H} \mathbf{H}^\top)^{-1} = \frac{1}{4\rho g} \begin{bmatrix} 1 & -\frac{1}{y} & \frac{1}{x} \\ 1 & -\frac{1}{y} & -\frac{1}{x} \\ 1 & \frac{1}{y} & -\frac{1}{x} \\ 1 & \frac{1}{y} & \frac{1}{x} \end{bmatrix}$$

which finally gives the water volumes  $V_i$  corresponding to the desired values  $z_d, \phi_d$  and  $\theta_d$

$$\mathbf{v} = \begin{bmatrix} V_1 \\ V_2 \\ V_3 \\ V_4 \end{bmatrix} = \frac{1}{4\rho g} \begin{bmatrix} 1 & -\frac{1}{y} & \frac{1}{x} \\ 1 & -\frac{1}{y} & -\frac{1}{x} \\ 1 & \frac{1}{y} & -\frac{1}{x} \\ 1 & \frac{1}{y} & \frac{1}{x} \end{bmatrix} \begin{bmatrix} \rho g A_{wp} z_d \\ \rho g \nabla \text{GM}_T \phi_d \\ \rho g \nabla \text{GM}_L \theta_d \end{bmatrix}$$

## 4.5.2 Automatic ballast control systems

In the manual pretrimming case it was assumed that  $\mathbf{w}^{\{3,4,5\}} = \mathbf{0}$ . This assumption can be removed by using feedback from  $z, \phi$  and  $\theta$ . The closed-loop dynamics of a

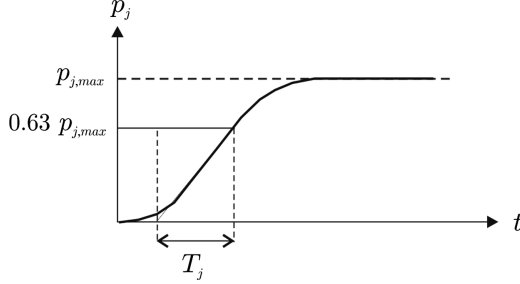


Figure 4.10: The time constant  $T_j$  for pump  $j$  is found by commanding a step  $p_{d_j} = p_{j,\max}$  as shown in the plot.

PID-controlled water pump can be described by a first-order model with amplitude saturation

$$T_j \dot{p}_j + p_j = \text{sat}(p_{d_j}) \quad (4.148)$$

where  $T_j$  is a positive time constant,  $p_j$  is the volumetric flow rate  $\text{m}^3/\text{s}$  produced by pump  $j = 1, \dots, m$  and  $p_{d_j}$  is the pump setpoint. As shown in Figure 4.9, one separate water pump can be used to pump water in each direction. This implies that the water pump capacity is different for positive and negative flow directions. Moreover,

$$\text{sat}(p_{d_j}) = \begin{cases} p_{j,\max}^+ & p_j > p_{j,\max}^+ \\ p_{d_j} & p_{j,\max}^- \leq p_{d_j} \leq p_{j,\max}^+ \\ p_{j,\max}^- & p_{d_j} < p_{j,\max}^- \end{cases} \quad (4.149)$$

The pump time constant  $T_j$  is found from a step response, as shown in Figure 4.10. The volume flow  $\dot{V}_i$  to tank  $i$  is given by linear combinations of flows corresponding to the pumps/pipelines supporting tank  $i$ . For the semisubmersible shown in Figure 4.9, we obtain

$$\dot{V}_1 = -p_1 \quad (4.150)$$

$$\dot{V}_2 = -p_3 \quad (4.151)$$

$$\dot{V}_3 = p_2 + p_3 \quad (4.152)$$

$$\dot{V}_4 = p_1 - p_2 \quad (4.153)$$

More generally, the water flow model can be written

$$T\dot{\mathbf{p}} + \mathbf{p} = \text{sat}(\mathbf{p}_d) \quad (4.154)$$

$$\dot{\mathbf{v}} = \mathbf{L}\mathbf{p} \quad (4.155)$$

where  $\text{sat}(\mathbf{p}_d) = [\text{sat}(p_{d_1}), \dots, \text{sat}(p_{d_m})]^\top$ ,  $\mathbf{p} = [p_1, \dots, p_m]^\top$  and  $\mathbf{v} = [V_1, \dots, V_n]^\top$  ( $m \geq n$ ). The mapping from the water volume vector  $\mathbf{v}$  to  $\eta^{\{3,4,5\}}$  is given by the steady-state condition (see Figure 4.11)

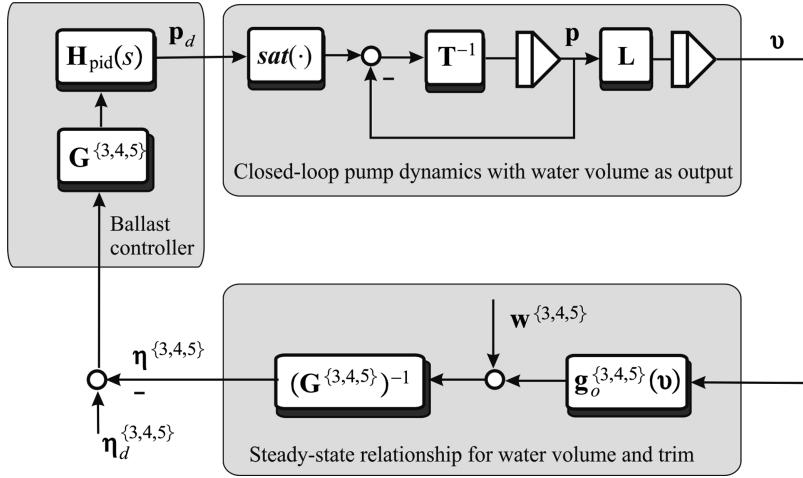


Figure 4.11: Ballast control system using feedback from  $z, \phi$  and  $\theta$ .

$$G^{\{3,4,5\}} \eta^{\{3,4,5\}} = g_o^{\{3,4,5\}}(v) + w^{\{3,4,5\}} \quad (4.156)$$

#### Example 4.4 (Semisubmersible Ballast Control, Continued)

Consider the semisubmersible in Example 4.3. The water flow model corresponding to Figure 4.9 becomes

$$\mathbf{v} = \begin{bmatrix} V_1 \\ V_2 \\ V_3 \\ V_4 \end{bmatrix}, \quad \mathbf{p} = \begin{bmatrix} p_1 \\ p_2 \\ p_3 \end{bmatrix}, \quad \mathbf{L} = \begin{bmatrix} -1 & 0 & 0 \\ 0 & 0 & -1 \\ 0 & 1 & 1 \\ 1 & -1 & 0 \end{bmatrix} \quad (4.157)$$

reflecting that there are three pumps and four water volumes connected through the configuration matrix  $\mathbf{L}$ .

A feedback control system for automatic trimming is presented in Figure 4.11. The ballast controllers can be chosen to be of PID type, for instance

$$\mathbf{p}_d = \mathbf{H}_{\text{pid}}(s) \mathbf{G}^{\{3,4,5\}} \left( \boldsymbol{\eta}_d^{\{3,4,5\}} - \boldsymbol{\eta}^{\{3,4,5\}} \right) \quad (4.158)$$

where  $\boldsymbol{\eta}_d^{\{3,4,5\}} = [z_d, \phi_d, \theta_d]^\top$  and

$$\mathbf{H}_{\text{pid}}(s) = \text{diag}\{h_{1,\text{pid}}(s), h_{2,\text{pid}}(s), \dots, h_{m,\text{pid}}(s)\} \quad (4.159)$$

is a diagonal transfer matrix containing  $m$  PID controllers. Integral action in the controllers is needed to compensate for nonzero environmental disturbances  $\mathbf{w}^{\{3,4,5\}}$ .



# Chapter 5

## Seakeeping Models

The study of ship dynamics has traditionally been covered by two main theories: *maneuvering* and *seakeeping*. Maneuvering refers to the study of ship motion in the absence of wave excitation (calm water). The maneuvering equations of motion are derived in Chapter 6 under the assumption that the hydrodynamic potential coefficients and radiation-induced forces are frequency independent. Seakeeping, on the other hand, refers to the study of motion of marine craft on constant course and speed when there is wave excitation. This includes the trivial case of zero speed. In seakeeping analysis, a dissipative force (Cummins 1962) known as *fluid memory effects* is introduced. Although both areas are concerned with the same issues, study of motion, stability and control, the separation allows us to make different assumptions that simplify the study in each case. A chief distinguishing characteristic of these theories is the use of different coordinates and reference systems to express the equations of motion.

In maneuvering theory, the equations of motion are described relative to  $\{b\}$ , which is fixed to the marine craft, whereas in seakeeping the motion is described relative to a coordinate system  $\{s\}$  fixed to an equilibrium virtual craft that moves at a constant speed and heading corresponding to the average motion of the actual craft. Most hydrodynamic programs compute radiation and wave excitation forces in  $\{s\}$ .

This chapter presents the seakeeping theory and the classical equation in naval architecture

$$[\mathbf{M}_{RB} + \mathbf{A}(\omega)]\ddot{\boldsymbol{\xi}} + [\mathbf{B}(\omega) + \mathbf{B}_V(\omega)]\dot{\boldsymbol{\xi}} + \mathbf{C}\boldsymbol{\xi} = \boldsymbol{\delta\tau} + \boldsymbol{\tau}_{\text{wind}} + \boldsymbol{\tau}_{\text{wave}} \quad (5.1)$$

which is transformed from *equilibrium axes*  $\{s\}$  to body-fixed axes  $\{b\}$  using the time-domain solution known as the *Cummins equation*. The radiation-induced forces and moment are represented as impulse response functions and state-space models. This is done within a linear framework so viscous damping can be added under the assumption of linear superposition. The main results are the  $\{b\}$ -frame seakeeping equations of motion in the following form

$$\dot{\boldsymbol{\eta}} = \mathbf{J}_\Theta(\boldsymbol{\eta})\boldsymbol{\nu} \quad (5.2)$$

$$\mathbf{M}_{RB}\dot{\boldsymbol{\nu}} + \mathbf{C}_{RB}^*\boldsymbol{\nu} + \mathbf{M}_A\dot{\boldsymbol{\nu}}_r + \mathbf{C}_A^*\boldsymbol{\nu}_r + \mathbf{D}\boldsymbol{\nu}_r + \boldsymbol{\mu} + \mathbf{G}\boldsymbol{\eta} = \boldsymbol{\tau} + \boldsymbol{\tau}_{\text{wind}} + \boldsymbol{\tau}_{\text{wave}} \quad (5.3)$$

where  $\boldsymbol{\mu}$  is an additional term representing the fluid memory effects. This model is valid in the body-fixed reference frame and describes a maneuvering ship in a seaway. When designing model-based control systems or simulating marine craft motions it is important to have good estimates of the inertia, damping and restoring coefficients. In Chapter 3, formulae for computation of the rigid-body matrices  $\mathbf{M}_{RB}$  and  $\mathbf{C}_{RB}^*$  were given while the restoring and ballast forces  $\mathbf{G}\boldsymbol{\eta} + \mathbf{g}_0$  were derived in Chapter 4. In this chapter, we will derive formulae for hydrodynamic added mass  $\mathbf{M}_A$ , linear Coriolis–centripetal forces  $\mathbf{C}_A^*$  due to the rotation of the seakeeping reference frame  $\{s\}$  about  $\{n\}$  and linear potential damping  $\mathbf{D}_P$ . Linear viscous damping  $\mathbf{D}_V$  will be added manually to obtain a more accurate model.

The terms in (5.3) can be grouped according to:

Inertia forces:	$\mathbf{M}_{RB}\dot{\boldsymbol{\nu}} + \mathbf{C}_{RB}^*\boldsymbol{\nu} + \mathbf{M}_A\dot{\boldsymbol{\nu}}_r + \mathbf{C}_A^*\boldsymbol{\nu}_r$
Damping forces:	$+ (\mathbf{D}_P + \mathbf{D}_V)\boldsymbol{\nu}_r + \boldsymbol{\mu}$
Restoring forces:	$+ \mathbf{G}\boldsymbol{\eta} + \mathbf{g}_0$
Wind and wave forces:	$= \boldsymbol{\tau}_{\text{wind}} + \boldsymbol{\tau}_{\text{wave}}$
Propulsion forces:	$+ \boldsymbol{\tau}$

The matrices  $\mathbf{M}_A$ ,  $\mathbf{C}_A$  and  $\mathbf{D}_P$ , the fluid memory function  $\boldsymbol{\mu}$  as well as transfer functions for  $\boldsymbol{\tau}_{\text{wave}}$  can be computed using hydrodynamics programs. This requires postprocessing of hydrodynamic data and methods for this are discussed later in this chapter. The environmental forces,  $\boldsymbol{\tau}_{\text{wave}}$  and  $\boldsymbol{\tau}_{\text{wind}}$ , are treated separately in Chapter 10.

Different principles for the computation of the hydrodynamic coefficients can be used. The main tool is *potential theory* where it is assumed that the flow is constant, irrotational and incompressible such that time becomes unimportant. Hence, the discrepancies between real and idealized flow must be compensated by adding dissipative forces, for instance viscous damping.

## 5.1 Hydrodynamic Concepts and Potential Theory

In order to describe most fluid flow phenomena associated with the waves and the motion of ships in waves, we need to know the velocity of the fluid and the pressure at different locations. The velocity of the fluid at the location  $\mathbf{x} = [x_1, x_2, x_3]^\top$  is given by the *fluid flow velocity vector*

$$\mathbf{v}(\mathbf{x}, t) = [v_1(\mathbf{x}, t), v_2(\mathbf{x}, t), v_3(\mathbf{x}, t)]^\top \quad (5.4)$$

For the flow velocities involved in ship motion, the fluid can be considered *incompressible*, that is of constant density  $\rho$ . Under this assumption, the net volume rate at a

volume  $V$  enclosed by a closed surface  $S$  is

$$\iint_S \mathbf{v} \cdot \mathbf{n} \, ds = \iiint_V \operatorname{div}(\mathbf{v}) \, dV = 0 \quad (5.5)$$

Since (5.5) should be valid for all the regions  $V$  in the fluid, then by assuming that  $\nabla \cdot \mathbf{v}$  is continuous we obtain

$$\operatorname{div}(\mathbf{v}) = \nabla \cdot \mathbf{v} = \frac{\partial v_1}{\partial x} + \frac{\partial v_2}{\partial y} + \frac{\partial v_3}{\partial z} = 0 \quad (5.6)$$

which is the *continuity equation* for incompressible flows.

The conservation of momentum in the flow is described by the *Navier–Stokes equations*; see, for example, Acheson (1990):

$$\rho \left( \frac{\partial \mathbf{v}}{\partial t} + \mathbf{v} \cdot \nabla \mathbf{v} \right) = \rho \mathbf{F} - \nabla p + \mu \nabla^2 \mathbf{v} \quad (5.7)$$

where  $\mathbf{F} = [0, 0, -g]^\top$  are accelerations due to volumetric forces, from which only gravity is considered,  $p = p(\mathbf{x}, t)$  is the pressure and  $\mu$  is the viscosity coefficient of the fluid.

To describe the real flow of ships, it is then necessary to solve the Navier–Stokes equations (5.7) together with the continuity equation (5.6). These form a system of nonlinear partial differential equations, which unfortunately do not have analytical solutions and the numerical solutions are still far from being feasible with current computing power.

If viscosity is neglected, the fluid is said to be an *ideal fluid*. This is a common assumption that is made to calculate ship flows because viscosity often matters only in a thin layer close to the ship hull. By disregarding the last term in (5.7), the *Euler equations* of fluid motion are obtained

$$\rho \left( \frac{\partial \mathbf{v}}{\partial t} + \mathbf{v} \cdot \nabla \mathbf{v} \right) = \rho \mathbf{F} - \nabla p \quad (5.8)$$

A further simplification of the flow description is obtained by assuming that the flow is *irrotational*:

$$\operatorname{curl}(\mathbf{v}) = \nabla \times \mathbf{v} = 0 \quad (5.9)$$

The term *potential flow* is used to describe irrotational flows of inviscid-incompressible fluids. Under this assumption, there exists a scalar function  $\Phi(t, x, y, z)$  called *potential* such that

$$\mathbf{v} = \nabla \Phi \quad (5.10)$$

Hence, if the potential is known the velocities can be calculated as

$$v_1 = \frac{\partial \Phi}{\partial x}, \quad v_2 = \frac{\partial \Phi}{\partial y}, \quad v_3 = \frac{\partial \Phi}{\partial z} \quad (5.11)$$

Using the potential  $\Phi$ , the continuity equation (5.6) reverts to the *Laplace equation* of the potential

$$\nabla^2 \Phi = \frac{\partial^2 \Phi}{\partial x^2} + \frac{\partial^2 \Phi}{\partial y^2} + \frac{\partial^2 \Phi}{\partial z^2} = 0 \quad (5.12)$$

The potential can then be obtained by solving the Laplace equation (5.12) subject to appropriate boundary conditions, that is by solving a boundary value problem.

The pressure in the fluid can be obtained by integrating the *Euler equation* of fluid motion (5.8). This results in the *Bernoulli equation*:

$$\frac{p}{\rho} + \frac{\partial \Phi}{\partial t} + \frac{1}{2}(\nabla \Phi)^2 + gz = C \quad (5.13)$$

By setting the constant  $C = p_0/\rho$ , the relative pressure can be computed from

$$p - p_0 = -\rho gz - \rho \frac{\partial \Phi}{\partial t} - \frac{1}{2}\rho(\nabla \Phi)^2 \quad (5.14)$$

For simplicity, the atmospheric pressure  $p_0$  is often considered zero.

To summarize, *potential theory* makes two assumptions:

1. Inviscid fluid (no viscosity)
2. Irrotational flow

The assumption of irrotational flow leads to the description of the fluid velocity vector as the gradient of a potential function, which has no physical meaning. However, this is a large simplification because the potential is scalar while the velocity is a vector quantity. The potential satisfies the Laplace equation (5.12), which needs to be solved subject to appropriate boundary conditions (on the free surface, sea floor and ship hull). This is another large simplification because the Laplace equation is linear; therefore, superposition holds and the problem can also be solved in the frequency domain, which is the basis of most hydrodynamic programs. Once we have the potential and thus the velocities, the pressure can be computed using Bernoulli's equation. Then, by integrating the pressure over the surface of the hull, the hydrodynamic forces are obtained.

For most problems related to ship motion in waves, potential theory is sufficient to obtain results with appropriate accuracy for engineering purposes. However, because of the simplifying assumptions in some cases we need to complement the results by adding the effects of viscosity. This is important, for example, when considering maneuvering and propeller–rudder–hull interactions. For further discussions on the topics presented in this section, see Newman (1977), Faltinsen (1990), Acheson (1990), Journée and Massie (2001) and Bertram (2004).

### 5.1.1 Numerical approaches and hydrodynamic codes

In order to evaluate the potentials a boundary value problem needs to be solved. There are different approaches to do this, which lead to different formulations.

#### Strip theory (2-D potential theory)

In some problems, the motion of the fluid can be approximated as two-dimensional (2-D). This is characteristic for slender bodies. In this case a good estimate of the

hydrodynamic forces can be obtained by applying *strip theory* (Newman 1977; Faltinsen 1990; Journée and Massie 2001). The 2-D theory takes into account the fact that variation of the flow in the cross-directional plane is much larger than the variation in the longitudinal direction of the ship. The principle of strip theory involves dividing the submerged part of the craft into a finite number of strips. Hence, 2-D hydrodynamic coefficients for added mass can be computed for each strip and then summed over the length of the body to yield the 3-D coefficients. The 2-D hydrodynamic coefficients can be calculated from boundary element methods or via conformal mapping and analytical expressions. This principle is also used to compute viscous quadratic damping from 2-D drag coefficients, as explained in Section 6.4.

Several strip theory programs can be used to compute hydrodynamic added mass  $M_A$ , potential damping  $D_p$  and the hydrostatic matrix  $G$ . Commonly used 2-D programs are *Octopus Office* (Journée and Adegeest 2003) and *ShipX (Veres)* (Fathi 2004). These programs can be used at both zero speed and forward speed and they calculate frequency-dependent added mass and potential damping coefficients, restoring terms, first- and second-order wave load transfer functions (amplitudes and phases) between the marine craft and the waves for given wave directions and frequencies as well as other hydrodynamic data. Processing of the data is explained later in this chapter.

In this context it will be shown how frequency-dependent added mass and damping can be used to derive the equations of motion where these effects are included as fluid memory effects using retardation functions. In order to compute the retardation functions, asymptotic values for zero and infinite added mass must be used.

### Panel methods (3-D potential theory)

For potential flows, the integrals over the fluid domain can be transformed to integrals over the boundaries of the fluid domain. This allows the application of panel or boundary element methods to solve the 3-D potential theory problem. Panel methods divide the surface of the ship and the surrounding water into discrete elements (panels). On each of these elements, a distribution of sources and sinks is defined that fulfill the Laplace equation. The problem then amounts to finding the strength of these distributions and identifying the potential.

Computer codes based on this approach provide suitable performance for offshore applications at zero-forward speed in either the frequency or time domain. A commercial program such as WAMIT (2010) has become the de facto industry standard among oil and engineering companies. This program computes frequency-dependent added mass  $M_A$ , potential damping coefficients  $D_P$ , restoring terms  $G$ , and first- and second-order wave load transfer functions (amplitudes and phases) between the marine craft and the waves for given wave directions and frequencies, and much more. One special feature of WAMIT is that the program solves a boundary value problem for zero and infinite added mass. These boundary values are particularly useful when computing the retardation functions describing the fluid memory effects.

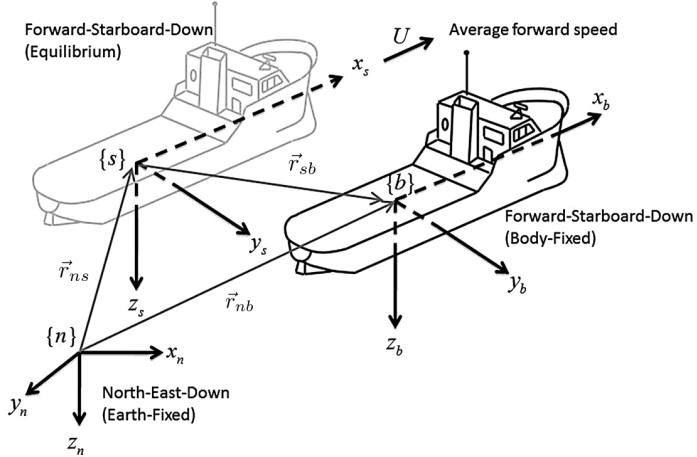


Figure 5.1: The seakeeping coordinate system  $\{s\}$  and distance vectors to the reference frames  $\{b\}$  and  $\{n\}$ .

### Semi-empirical methods

An alternative and less accurate approach to hydrodynamic programs is to use semi-empirical methods to compute the added mass derivatives; see, for instance, Imlay (1961), Humphreys and Watkinson (1978) and Triantafyllou and Amzallag (1984).

## 5.2 Seakeeping and Maneuvering Kinematics

This section derives the kinematics needed to transform the equations of motion from the seakeeping reference frame  $\{s\}$  to the body-fixed reference frame  $\{b\}$  and the NED reference frame  $\{n\}$ . This is based on Perez and Fossen (2007).

### 5.2.1 Seakeeping reference frame

In seakeeping theory the study of ship motion is performed under the assumption that it can be described as the superposition of an equilibrium state of motion plus perturbations. The equilibrium is determined by a constant heading angle  $\bar{\psi}$  and speed  $U$ , and the perturbations are zero-mean oscillatory components induced by first-order wave excitations. Note that the case of zero forward speed  $U = 0$  is also contemplated as an equilibrium of motion. Due to this, the motion is often described using an equilibrium or seakeeping reference frame.

**Seakeeping frame:** The seakeeping reference frame  $\{s\} = (x_s, y_s, z_s)$  is not fixed to the marine craft; it is fixed to the equilibrium state. Hence, in the absence of wave excitation, the  $\{s\}$ -frame origin  $o_s$  coincides with the location of the  $\{b\}$ -frame origin  $o_b$  (also denoted as CO) which is a fixed point in the ship. Under the action

of the waves, the hull is disturbed from its equilibrium and the point  $o_s$  oscillates, with respect to its equilibrium position. This is illustrated in Figure 5.1.

The  $\{s\}$  frame is considered *inertial* and therefore it is nonaccelerating and fixed in orientation with respect to the  $\{n\}$  frame (or must vary very slowly). This assumption implies that the  $\{s\}$ -frame equations of motion are linear. The equilibrium state is defined by a constant heading and speed

$$\mathbf{v}_{ns}^n = [U \cos(\bar{\psi}), U \sin(\bar{\psi}), 0]^\top \quad (5.15)$$

$$\boldsymbol{\omega}_{ns}^n = [0, 0, 0]^\top \quad (5.16)$$

$$\boldsymbol{\Theta}_{ns} = [0, 0, \bar{\psi}]^\top \quad (5.17)$$

where  $U = \|\mathbf{v}_{ns}^n\|$  is the average forward speed and  $\bar{\psi}$  is the equilibrium heading. Hence, the velocity of  $\{s\}$  with respect to  $\{n\}$  expressed in  $\{s\}$  is

$$\mathbf{v}_{ns}^s = \mathbf{R}_n^s \mathbf{v}_{ns}^n = [U, 0, 0]^\top \quad (5.18)$$

where  $\mathbf{R}_n^s = \mathbf{R}(\boldsymbol{\Theta}_{ns})$ . The equilibrium heading  $\bar{\psi}$  can be computed by averaging the gyro compass measurements  $\psi$  over a fixed period (moving horizon) of time.

### Seakeeping (perturbation) coordinates

The *seakeeping or perturbation coordinates* are defined as (Perez and Fossen 2007)

$$\delta\boldsymbol{\eta} := \begin{bmatrix} \mathbf{r}_{sb}^s \\ \boldsymbol{\Theta}_{sb} \end{bmatrix} \quad (5.19)$$

$$\delta\boldsymbol{\nu} := \begin{bmatrix} \mathbf{v}_{sb}^b \\ \boldsymbol{\omega}_{sb}^b \end{bmatrix} \quad (5.20)$$

In hydrodynamic textbooks it is common to denote the perturbation coordinates by

$$\boldsymbol{\xi} := \delta\boldsymbol{\eta} \quad (5.21)$$

where  $\boldsymbol{\xi} = [\xi_1, \xi_2, \xi_3, \xi_4, \xi_5, \xi_6]^\top$ . The first three coordinates  $(\xi_1, \xi_2, \xi_3)$  are translational motion perturbations and

$$\boldsymbol{\Theta}_{sb} = [\xi_4, \xi_5, \xi_6]^\top = [\delta\phi, \delta\theta, \delta\psi]^\top \quad (5.22)$$

are the angular motion perturbations (roll, pitch and yaw).

### 5.2.2 Transformation between BODY and SEAKEEPING

From the definition of  $\{s\}$  and the coordinates  $\delta\boldsymbol{\eta}$  and  $\delta\boldsymbol{\nu}$  it follows that

$$\delta\dot{\boldsymbol{\eta}} = \mathbf{J}_\Theta(\delta\boldsymbol{\eta})\delta\boldsymbol{\nu} \quad (5.23)$$

where  $\mathbf{J}_\Theta(\delta\boldsymbol{\eta})$  is the transformation matrix between  $\{b\}$  and  $\{s\}$

$$\mathbf{J}_\Theta(\delta\boldsymbol{\eta}) = \begin{bmatrix} \mathbf{R}(\boldsymbol{\Theta}_{sb}) & \mathbf{0}_{3 \times 3} \\ \mathbf{0}_{3 \times 3} & \mathbf{T}(\boldsymbol{\Theta}_{sb}) \end{bmatrix} \quad (5.24)$$

This expression is similar to the transformation between  $\{b\}$  and  $\{n\}$ . This is an expected result since both  $\{n\}$  and  $\{s\}$  are assumed inertial while  $\{b\}$  rotates about the inertial frame. In addition to position and attitude it is necessary to derive the relationship between the perturbed velocities and accelerations  $(\delta\nu, \delta\dot{\nu})$  and  $(\nu, \dot{\nu})$ . To obtain these expressions consider the distance vector; see Figure 5.1:

$$\vec{r}_{nb} = \vec{r}_{ns} + \vec{r}_{sb} \quad (5.25)$$

which can be expressed in  $\{n\}$  as

$$\vec{r}_{nb}^n = \vec{r}_{ns}^n + \mathbf{R}_s^n \vec{r}_{sb}^s \quad (5.26)$$

Time differentiation gives

$$\dot{\vec{r}}_{nb}^n = \dot{\vec{r}}_{ns}^n + \mathbf{R}_s^n \dot{\vec{r}}_{sb}^s + \dot{\mathbf{R}}_s^n \vec{r}_{sb}^s \quad (5.27)$$

where

$$\mathbf{R}_s^n = \mathbf{R}_{z,\bar{\psi}} = \begin{bmatrix} \cos(\bar{\psi}) & -\sin(\bar{\psi}) & 0 \\ \sin(\bar{\psi}) & \cos(\bar{\psi}) & 0 \\ 0 & 0 & 1 \end{bmatrix}, \quad \dot{\mathbf{R}}_s^n = \mathbf{0} \quad (5.28)$$

Note that the time derivative of  $\mathbf{R}_s^n$  is zero because  $\{s\}$  does not rotate with respect to  $\{n\}$ . The expression for  $\dot{\vec{r}}_{nb}^n$  can be rewritten as

$$\begin{aligned} \dot{\vec{r}}_{nb}^n &= \dot{\vec{r}}_{ns}^n + \mathbf{R}_s^n \mathbf{R}_s^b \dot{\vec{r}}_{sb}^b \\ &= \dot{\vec{r}}_{ns}^n + \mathbf{R}_s^n \vec{v}_{sb}^b \end{aligned} \quad (5.29)$$

Both sides of (5.29) can be multiplied by  $\mathbf{R}_n^b$  to obtain

$$\vec{v}_{nb}^b = \mathbf{R}_n^b \vec{v}_{ns}^n + \vec{v}_{sb}^b \quad (5.30)$$

For notational simplicity, the linear and angular velocity vectors are grouped according to

$$\boldsymbol{\nu} = \begin{bmatrix} \boldsymbol{\nu}_1 \\ \boldsymbol{\nu}_2 \end{bmatrix} = \begin{bmatrix} [u, v, w]^\top \\ [p, q, r]^\top \end{bmatrix} \quad (5.31)$$

$$\delta\boldsymbol{\nu} = \begin{bmatrix} \delta\boldsymbol{\nu}_1 \\ \delta\boldsymbol{\nu}_2 \end{bmatrix} = \begin{bmatrix} [\delta u, \delta v, \delta w]^\top \\ [\delta p, \delta q, \delta r]^\top \end{bmatrix} \quad (5.32)$$

Then it follows from (5.30) that

$$\boldsymbol{\nu}_1 = \bar{\boldsymbol{\nu}}_1 + \delta\boldsymbol{\nu}_1 \quad (5.33)$$

where

$$\bar{\boldsymbol{\nu}}_1 := \mathbf{R}_n^b \begin{bmatrix} U \cos(\bar{\psi}) \\ U \sin(\bar{\psi}) \\ 0 \end{bmatrix} = \mathbf{R}_s^b \begin{bmatrix} U \\ 0 \\ 0 \end{bmatrix} \quad (5.34)$$

To obtain the angular velocity transformation, we make use of

$$\vec{\omega}_{nb} = \vec{\omega}_{ns} + \vec{\omega}_{sb} = \vec{\omega}_{sb} \quad (5.35)$$

since  $\vec{\omega}_{ns} = \vec{0}$ . Moreover,  $\{s\}$  does not rotate with respect to  $\{n\}$ . This leads to

$$\boldsymbol{\omega}_{nb}^b = \boldsymbol{\omega}_{sb}^b \Rightarrow \boldsymbol{\nu}_2 = \delta\boldsymbol{\nu}_2 \quad (5.36)$$

The Euler angle transformation matrices  $\mathbf{R}(\Theta_{sb})$  and  $\mathbf{T}(\Theta_{sb})$  for  $\Theta_{sb} = [\delta\phi, \delta\theta, \delta\psi]^\top$  are similar to those used in Section 2.2. Moreover,

$$\mathbf{R}(\Theta_{sb}) = \begin{bmatrix} c_{\delta\psi}c_{\delta\theta} & -s_{\delta\psi}c_{\delta\phi} + c_{\delta\psi}s_{\delta\theta}s_{\delta\phi} & s_{\delta\psi}s_{\delta\phi} + c_{\delta\psi}c_{\phi}s_{\delta\theta} \\ s_{\delta\psi}c_{\delta\theta} & c_{\delta\psi}c_{\delta\phi} + s_{\delta\phi}s_{\delta\theta}s_{\delta\psi} & -c_{\delta\psi}s_{\delta\phi} + s_{\delta\theta}s_{\delta\psi}c_{\delta\phi} \\ -s_{\delta\theta} & c_{\delta\theta}s_{\delta\phi} & c_{\delta\theta}c_{\delta\phi} \end{bmatrix} \quad (5.37)$$

$$\mathbf{T}(\Theta_{sb}) = \begin{bmatrix} 1 & s_{\delta\phi}t_{\delta\theta} & c_{\delta\phi}t_{\delta\theta} \\ 0 & c_{\delta\phi} & -s_{\delta\phi} \\ 0 & s_{\delta\phi}/c_{\delta\theta} & c_{\delta\phi}/c_{\delta\theta} \end{bmatrix}, \quad c_{\delta\theta} \neq 0 \quad (5.38)$$

Computing  $\bar{\boldsymbol{\nu}}_1$  under the assumption of small angles gives

$$\begin{aligned} \bar{\boldsymbol{\nu}}_1 &= \mathbf{R}^\top(\Theta_{sb}) \begin{bmatrix} U \\ 0 \\ 0 \end{bmatrix} \\ &= U \begin{bmatrix} c_{\delta\psi}c_{\delta\theta} \\ -s_{\delta\psi}c_{\delta\phi} + c_{\delta\psi}s_{\delta\theta}s_{\delta\phi} \\ s_{\delta\psi}s_{\delta\phi} + c_{\delta\psi}c_{\phi}s_{\delta\theta} \end{bmatrix} \\ &\approx U \begin{bmatrix} 1 \\ -\delta\psi \\ \delta\theta \end{bmatrix} \end{aligned} \quad (5.39)$$

Finally,

$$\boldsymbol{\nu} = \bar{\boldsymbol{\nu}} + \delta\boldsymbol{\nu} \quad (5.40)$$

where

$$\bar{\boldsymbol{\nu}} \approx U[1, -\delta\psi, \delta\theta, 0, 0, 0]^\top \quad (5.41)$$

This can written as

$$\boldsymbol{\nu} \approx U(\boldsymbol{e}_1 - \mathbf{L}\delta\boldsymbol{\eta}) + \delta\boldsymbol{\nu} \quad (5.42)$$

$$\boldsymbol{e}_1 := \begin{bmatrix} 1 \\ 0 \\ 0 \\ 0 \\ 0 \\ 0 \end{bmatrix}, \quad \mathbf{L} := \begin{bmatrix} 0 & 0 & 0 & 0 & 0 & 0 \\ 0 & 0 & 0 & 0 & 0 & 1 \\ 0 & 0 & 0 & 0 & -1 & 0 \\ 0 & 0 & 0 & 0 & 0 & 0 \\ 0 & 0 & 0 & 0 & 0 & 0 \\ 0 & 0 & 0 & 0 & 0 & 0 \end{bmatrix} \quad (5.43)$$

Differentiation of (5.42) with respect to time gives

$$\dot{\boldsymbol{\nu}} = -U\mathbf{L}\delta\boldsymbol{\nu} + \delta\dot{\boldsymbol{\nu}} \quad (5.44)$$

Hence, the linear transformations needed to transform a system from seakeeping coordinates  $(\delta\boldsymbol{\eta}, \delta\boldsymbol{\nu})$  to body-fixed coordinates  $(\boldsymbol{\eta}, \boldsymbol{\nu})$  are

$$\delta\nu \approx \nu + U(L\delta\eta - e_1) \quad (5.45)$$

$$\delta\dot{\nu} \approx \dot{\nu} + UL\nu \quad (5.46)$$

The Euler angles are related through the following equation

$$\Theta_{nb} = \Theta_{ns} + \Theta_{sb} \quad (5.47)$$

which gives

$$\begin{bmatrix} \phi \\ \theta \\ \psi \end{bmatrix} = \begin{bmatrix} 0 \\ 0 \\ \bar{\psi} \end{bmatrix} + \begin{bmatrix} \delta\phi \\ \delta\theta \\ \delta\psi \end{bmatrix} \quad (5.48)$$

### 5.3 The Classical Frequency-Domain Model

Frequency-dependent hydrodynamic forces can be determined experimentally or computed using potential theory programs or seakeeping codes. This section describes the transformations needed to obtain what is called the *frequency-domain model* and a method known as *forced oscillations*, which can be used to obtain frequency-dependent added mass and damping experimentally.

The seakeeping equations of motion are considered to be inertial. Hence, the rigid-body kinetics in terms of perturbed coordinates  $\delta\eta$  and  $\delta\nu$  becomes (see Section 3.3)

$$\delta\dot{\eta} = J_\Theta(\delta\eta)\delta\nu \quad (5.49)$$

$$M_{RB}\delta\ddot{\eta} + C_{RB}(\delta\nu)\delta\dot{\eta} = \delta\tau_{RB} \quad (5.50)$$

Linear theory suggests that second-order terms can be neglected. Consequently, the rigid-body kinetics in seakeeping coordinates  $\xi = \delta\eta$  and  $\dot{\xi} = \delta\nu$  reduces to

$$\begin{aligned} M_{RB}\ddot{\xi} &= \delta\tau_{RB} \\ &= \tau_{hyd} + \tau_{hs} + \tau_{exc} \end{aligned} \quad (5.51)$$

The rigid-body kinetics is forced by the term  $\delta\tau_{RB}$  which can be used to model hydrodynamic forces  $\tau_{hyd}$ , hydrostatic forces  $\tau_{hs}$  and other external forces  $\tau_{exc}$ . Cummins (1962) showed that the radiation-induced hydrodynamic forces in an ideal fluid can be related to frequency-dependent added mass  $A(\omega)$  and potential damping  $B(\omega)$  according to

$$\tau_{hyd} = -\bar{A}\ddot{\xi} - \int_0^t \bar{K}(t-\tau)\dot{\xi}(\tau)d\tau \quad (5.52)$$

where  $\bar{A} = A(\infty)$  is the constant infinite-frequency added mass matrix and  $\bar{K}(t)$  is a matrix of *retardation functions* given by

$$\bar{K}(t) = \frac{2}{\pi} \int_0^\infty B(\omega) \cos(\omega t) d\omega \quad (5.53)$$

If linear restoring forces  $\tau_{hs} = -C\xi$  are included in the model, this results in the time-domain model

$$(\mathbf{M}_{RB} + \mathbf{A}(\infty))\ddot{\xi} + \int_0^t \bar{\mathbf{K}}(t-\tau)\dot{\xi}(\tau)d\tau + C\xi = \tau_{exc} \quad (5.54)$$

This is a vector *integro-differential equation* formulated in the time domain even though the potential coefficients are frequency dependent. In order to understand this, we will consider a floating body forced to oscillate at a given frequency.

### 5.3.1 Frequency-dependent hydrodynamic coefficients

Consider the motions of a floating or submerged body given by

$$\mathbf{M}_{RB}\ddot{\xi} = \tau_{hyd} + \tau_{hs} + \tau_{exc} \quad (5.55)$$

where  $\tau_{hyd}$  and  $\tau_{hs}$  denote the hydrodynamic and hydrostatic forces due to the surrounding water. The vector  $\tau_{exc} = \mathbf{f} \cos(\omega t)$  where  $\mathbf{f} = [f_1, \dots, f_6]^\top$  contains the excitation force amplitudes. In an experimental setup with a restrained scale model, it is then possible to vary the wave excitation frequency  $\omega$  and the amplitudes  $f_i$  for  $i = 1, \dots, 6$  of the excitation force. Hence, by measuring the position and attitude vector  $\xi$ , the response of the second-order system (5.55) can be fitted to a linear model

$$[\mathbf{M}_{RB} + \mathbf{A}(\omega)]\ddot{\xi} + \mathbf{B}_{total}(\omega)\dot{\xi} + C\xi = \tau_{exc} \quad (5.56)$$

for each frequency  $\omega$ . The total damping matrix is the sum of the potential and viscous damping matrices

$$\mathbf{B}_{total}(\omega) = \mathbf{B}(\omega) + \mathbf{B}_V(\omega) \quad (5.57)$$

By closer inspection of (5.56), the hydrodynamic and hydrostatic forces are recognized as a frequency-dependent mass–damper–spring system with elements

$$\tau_{hyd} = \underbrace{-\mathbf{A}(\omega)\ddot{\xi} - \mathbf{B}(\omega)\dot{\xi}}_{\text{radiation force}} - \underbrace{\mathbf{B}_V(\omega)\dot{\xi}}_{\text{viscous damping force}} \quad (5.58)$$

$$\tau_{hs} = \underbrace{-C\xi}_{\text{restoring force}} \quad (5.59)$$

The *radiation force* is due to the energy carried away by generated surface waves and it is formed by two components, hydrodynamic inertia forces  $\mathbf{A}(\omega)\ddot{\xi}$  and potential damping  $\mathbf{B}(\omega)\dot{\xi}$ . The physical interpretations of the matrices are

- $\mathbf{A}(\omega)$  added mass matrix
- $\mathbf{B}(\omega)$  potential damping matrix
- $\mathbf{B}_V(\omega)$  viscous damping matrix
- $\mathbf{C}$  spring stiffness or hydrostatic matrix

If the experiment is repeated for several frequencies  $\omega_i$  ( $i = 1, \dots, N$ ), added mass  $\mathbf{A}(\omega_i)$  and damping  $\mathbf{B}_{\text{total}}(\omega_i)$  can be computed at different frequencies. Added mass and damping for a conventional ship is plotted as a function of  $\omega$  in Figures 5.2 and 5.3.

The matrices  $\mathbf{A}(\omega)$ ,  $\mathbf{B}_{\text{total}}(\omega)$  and  $\mathbf{C}$  in (5.56) represent a *hydrodynamic mass-damper-spring system* which varies with the frequency of the forced oscillation. The added mass matrix  $\mathbf{A}(\omega)$  should not be understood as additional mass due to a finite amount of water that is dragged with the vessel. A more precise definition is:

### **Definition 5.1 (Added Mass)**

*Hydrodynamic added mass can be seen as a virtual mass added to a system because an accelerating or decelerating body must move some volume of the surrounding fluid as it moves through it. Moreover, the object and fluid cannot occupy the same physical space simultaneously.*

The model (5.56) is rooted deeply in the literature of hydrodynamics and the abuse of notation of this false time-domain model has been discussed eloquently in the literature. This is in fact not a time-domain model but rather a different way of writing (5.73), which is the frequency response function. The corresponding time-domain model is given by (5.54).

The potential coefficients  $\mathbf{A}(\omega)$  and  $\mathbf{B}(\omega)$  are usually computed using a seakeeping program but the frequency response will not be accurate unless viscous damping is included. The viscous matrix  $\mathbf{B}_V(\omega)$  is an optional matrix that can be used to model viscous damping such as skin friction, surge resistance and viscous roll damping.

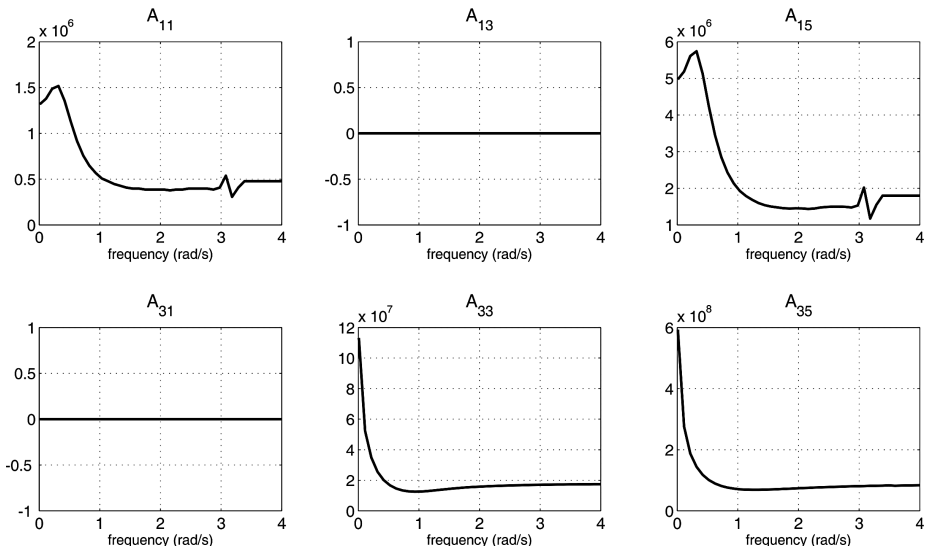


Figure 5.2: Longitudinal added mass and potential damping coefficients as a function of frequency. Exponential decaying viscous damping is included for  $B_{11}(\omega)$ .

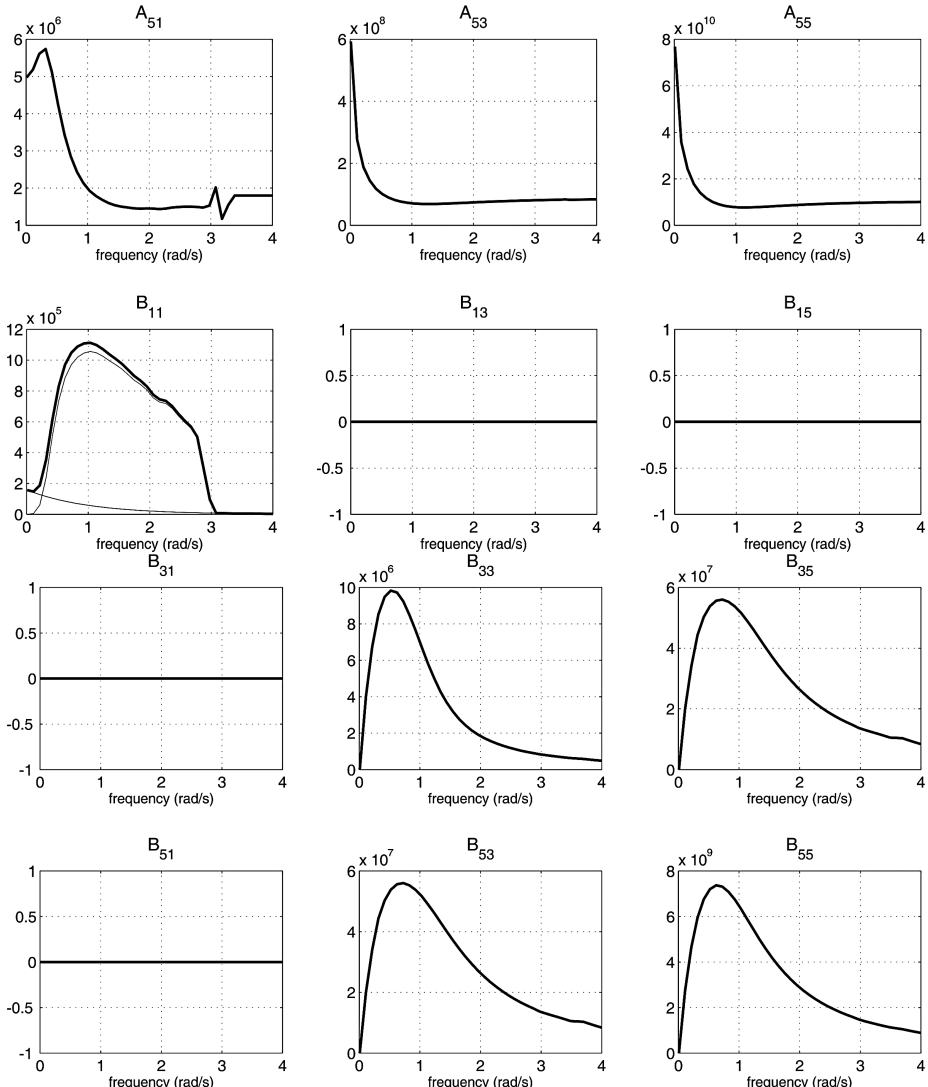


Figure 5.2: (Continued)

The pressure supporting a marine craft can be separated into hydrostatic and hydrodynamic forces. The hydrostatic pressure gives the buoyancy force, which is proportional to the displaced volume. Thus, the *hydrostatic force*,  $C\xi$ , represents the restoring forces due to gravity buoyancy that tend to bring the marine craft back to its upright equilibrium position.

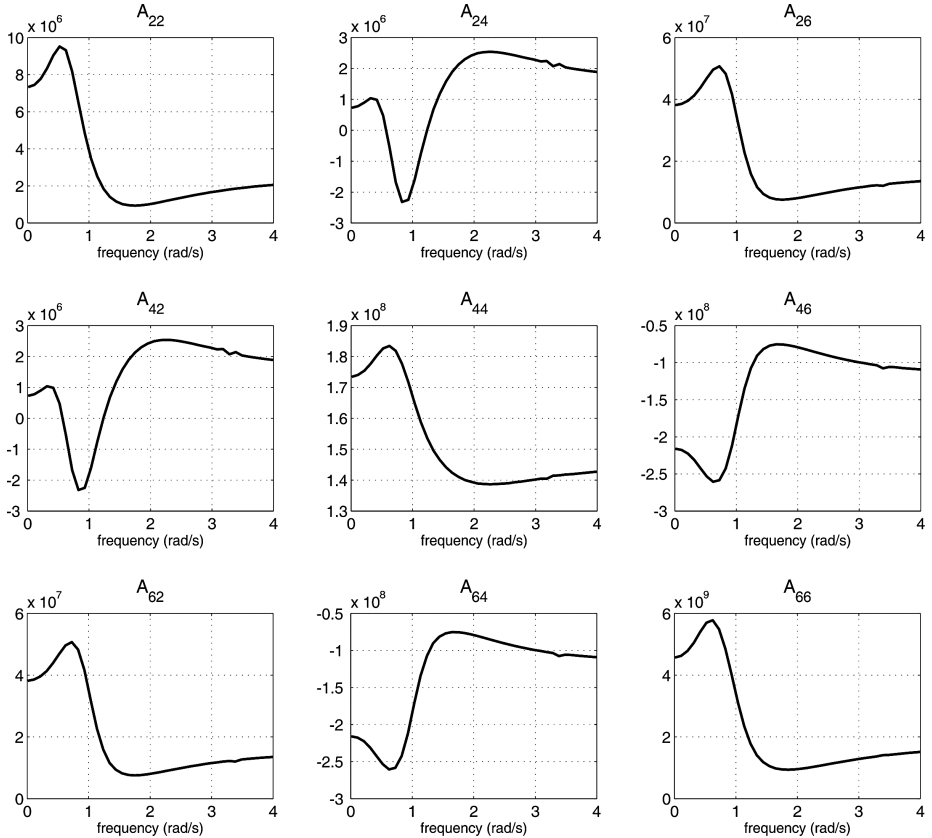


Figure 5.3: Lateral added mass and potential damping coefficients as a function of frequency. Exponential decaying viscous damping is included for  $B_{22}(\omega)$  and  $B_{66}(\omega)$  while viscous IKEDA damping is included in  $B_{44}(\omega)$  (shown as a peak).

The *wave excitation forces*,  $\tau_{\text{wave}}$ , arise due to changes in pressure due to waves. These have one component that varies linearly with the wave elevation and another that varies nonlinearly. The linear forces are oscillatory forces with a zero mean; these forces are called *first-order wave forces* – Froude–Krylov and diffraction forces. The energy of these forces is distributed at the same frequencies as the wave elevation seen from the moving ship (encounter frequencies). The nonlinear components give rise to nonoscillatory forces – *mean wave drift forces* – and also oscillatory forces, which have energy at frequencies that are both lower and higher than the range of first-order wave forces.

The components at lower frequencies are called second-order *slow wave drift forces*, and together with the mean wave drift and the first-order wave forces constitute the main disturbances for ship motion control. The high-frequency forces are usually of no concern for ship motion control, but can produce oscillation in the structure of the vessel; this effect is known as springing. For further details on wave loads see Faltinsen (1990; 2005).

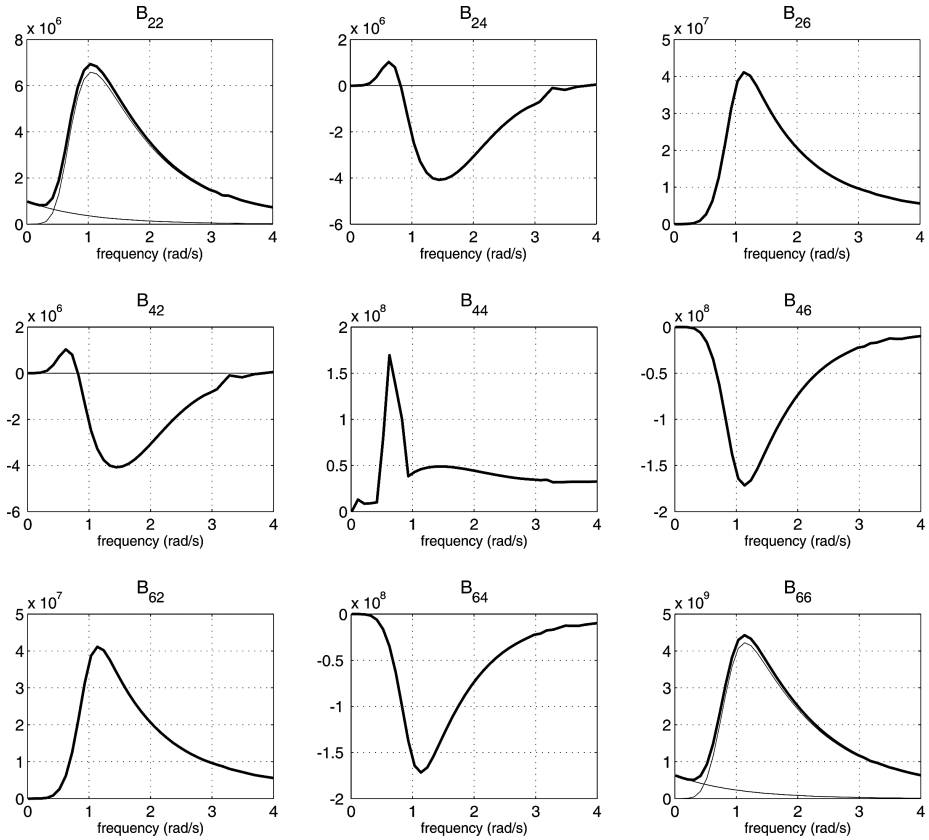


Figure 5.3: (Continued)

### 5.3.2 Viscous damping

When running seakeeping codes it is important to include an *external viscous damping matrix*  $\mathbf{B}_V(\omega)$  in order to obtain accurate estimates of the response amplitude operators (RAOs), which are used to compute the motions due to first- and second-order wave forces. The viscous damping coefficients will give additional contributions to the potential damping matrix  $\mathbf{B}(\omega)$ , as shown in the plots for  $B_{11}(\omega)$ ,  $B_{22}(\omega)$ ,  $B_{44}(\omega)$  and  $B_{66}(\omega)$  in Figures 5.2 and 5.3.

In maneuvering theory, it is standard to use the zero-frequency added mass and damping coefficients in surge, sway and yaw to describe the ship motions. When applying a feedback control system to stabilize the motions in surge, sway and yaw, the natural periods will be in the range of 100–200 s. This implies that the natural frequencies are in the range of 0.03–0.10 rad/s, which is quite close to the zero wave excitation frequency. Since the potential damping coefficients  $B_{11}(\omega)$ ,  $B_{22}(\omega)$  and  $B_{66}(\omega)$  are zero for  $\omega = 0$ , a ship maneuvering model should include viscous damping terms at low frequencies.

Bailey *et al.* (1998) suggest using ramps in surge, sway and yaw to describe the viscous part of the damping forces. However, in the framework of linear theory exponential functions are well suited for this purpose. For instance,  $\mathbf{B}_V(\omega)$  can be chosen as a diagonal matrix

$$\mathbf{B}_V(\omega) = \text{diag} \left\{ \beta_1 e^{-\alpha\omega} + N_{\text{ITTC}}(A_1), \beta_2 e^{-\alpha\omega}, \beta_3, \beta_{\text{IKEDA}}(\omega), \beta_5, \beta_6 e^{-\alpha\omega} \right\} \quad (5.60)$$

where  $\alpha > 0$  is the exponential rate,  $\beta_i > 0$  ( $i = 1, 2, 6$ ) are linear viscous skin friction coefficients,  $N_{\text{ITTC}}(A_1)$  is equivalent linear surge resistance depending on the surge velocity amplitude  $A_1$  and  $\beta_{\text{IKEDA}}(\omega)$  is frequency-dependent roll damping based on the theory of Ikeda *et al.* (1976). Other models for viscous roll damping can also be used.

One useful property of the exponential function  $\beta_i e^{-\alpha\omega}$  is that linear skin friction only affects low-frequency motions. It is also possible to add a frequency-independent linear damper  $D_{ii} = \beta_i \xi_i$  directly to the equations of motion in the time domain and obtain the same effect as solving the frequency-domain equation with  $B_{ii}(\omega) = \beta_i e^{-\alpha\omega}$  (Ross and Fossen 2005).

A rule of thumb for choosing  $\beta_i$  ( $i = 1, 2, 6$ ) can be to specify the time constants  $T_i$  in surge, sway and yaw corresponding to the three mass-damper systems. Since,

$$T_1 = \frac{m + A_{11}(0)}{B_{v,11}(0)}, \quad T_2 = \frac{m + A_{22}(0)}{B_{v,22}(0)}, \quad T_6 = \frac{I_z + A_{66}(0)}{B_{v,66}(0)} \quad (5.61)$$

it follows that

$$\beta_1 = \frac{m + A_{11}(0)}{T_1}, \quad \beta_2 = \frac{m + A_{22}(0)}{T_2}, \quad \beta_6 = \frac{I_z + A_{66}(0)}{T_6} \quad (5.62)$$

Viscous damping  $\beta_3$  in heave is usually added as a constant value to increase damping at the natural frequency  $\omega_3$ . The relative damping ratio  $\zeta_3$  satisfies

$$2\zeta_3\omega_3 = \frac{B_{33}(\omega_3) + \beta_3}{m + A_{33}(\omega_3)} \quad (5.63)$$

Consequently, damping can be increased by specifying a percentage increase in damping e.g.  $\beta_3 = pB_{33}(\omega_3)$  where  $p > 0$ . A similar approach can be used in pitch to determine  $\beta_5$ . Moreover,

$$2\zeta_5\omega_5 = \frac{B_{55}(\omega_5) + \beta_5}{I_y + A_{55}(\omega_5)} \quad (5.64)$$

### Equivalent linearization method and describing functions

The surge resistance  $N_{\text{ITTC}}(A_1)$  can be found by *equivalent linearization* of the quadratic damping (6.70). Equivalent linearization is a *Fourier-series approximation* where the work done over one period  $T$  is the same for the nonlinear and linear terms. This is similar to a sinusoidal-input *describing function* that is frequently used in control engineering. Consider a sinusoidal input

$$u = A \sin(\omega t) \quad (5.65)$$

For static linearities, displaying no dependence upon the derivatives, the describing function for the particular odd polynomial nonlinearity

$$y = c_1 x + c_2 x|x| + c_3 x^3 \quad (5.66)$$

is (Gelb and Vander Velde 1968)

$$N(A) = c_1 + \frac{8A}{3\pi} c_2 + \frac{3A^2}{4} c_3 \quad (5.67)$$

Consequently, the amplitude-dependent linear mapping

$$y = N(A)u \quad (5.68)$$

approximates the nonlinear polynomial (5.66) if the input is a harmonic function. This result is very useful for marine craft since it allows for linear approximation of nonlinear dissipative forces under the assumption of regular waves. For instance, the quadratic damping in surge due to the ITTC surge resistance formulation results in an expression (see Section 6.4.2)

$$\begin{aligned} X &= -X_{|u|u}|u|u \\ &\approx N_{\text{ITTC}}(A_1)u \end{aligned} \quad (5.69)$$

where the surge velocity  $u = A_1 \cos(\omega t)$  is assumed to be harmonic. Then it follows from (5.67) that

$$N_{\text{ITTC}}(A_1) = -\frac{8A_1}{3\pi} X_{|u|u} \quad (5.70)$$

Viscous damping can also be added in sway and yaw using a similar approach. The diagonal terms from the cross-flow drag analysis (see Section 6.4.3) result in similar terms depending on the sway and yaw amplitudes  $A_2$  and  $A_6$ . Moreover,

$$Y = N_{Y, \text{crossflow}}(A_2)v, \quad N_{Y, \text{crossflow}}(A_2) = -\frac{8A_2}{3\pi} Y_{|v|v} \quad (5.71)$$

$$N = N_{N, \text{crossflow}}(A_6)r, \quad N_{N, \text{crossflow}}(A_6) = -\frac{8A_6}{3\pi} N_{|r|r} \quad (5.72)$$

For a ship moving at high speed, the amplitudes  $A_2$  and  $A_6$  will be much smaller than  $A_1$ . Hence, it is common to neglect these terms in seakeeping analysis.

### 5.3.3 Response amplitude operators

Equation (5.56) can be transformed to the frequency domain by using the Laplace transformation. Moreover, application of  $\mathcal{L}\{\ddot{\xi}(t)\} = s^2\xi(s)$  and  $\mathcal{L}\{\dot{\xi}\} = s\xi(s)$  together with  $s = j\omega$  gives

$$(-\omega^2[M_{RB} + A(\omega)] - j\omega B_{\text{total}}(\omega) + C)\xi(j\omega) = \tau_{\text{exc}}(j\omega) \quad (5.73)$$

Assume that  $\tau_{\text{exc}}(\text{j}\omega) = F_i \zeta$  for  $i = 1, 2, \dots, 6$  are harmonic excitation forces proportional to an incoming regular wave  $\zeta = \zeta_a e^{\text{j}\omega t}$  where  $\zeta_a$  is the wave amplitude and  $F_i$  denotes the proportional gain. Linear theory implies that  $\xi_i = \bar{\xi}_i e^{\text{j}\omega t}$  where  $\bar{\xi}_i$  denotes the amplitudes. Consequently,

$$(\mathbf{C} - \omega^2[\mathbf{M}_{RB} + \mathbf{A}(\omega)] - \text{j}\omega \mathbf{B}_{\text{total}}(\omega)) \bar{\boldsymbol{\xi}} e^{\text{j}\omega t} = F_i \zeta_a e^{\text{j}\omega t} \quad (5.74)$$

Let  $\text{RAO}_i(\omega)$  denote the *response amplitude operator* between  $\zeta_a$  and  $\bar{\xi}_i$  for  $i = 1, 2, \dots, 6$ . Hence, the decoupled transfer functions become

$$\text{RAO}_i(\omega) = \frac{\bar{\xi}_i}{\zeta_a} = \frac{F_i}{C_{ii} - \omega^2[M_{RB,ii} + A_{ii}(\omega)] + \text{j}B_{\text{total},ii}(\omega)\omega} \quad (5.75)$$

Notice that  $\text{RAO}_i(\omega)$  is a frequency-dependent and complex function. It is common to only consider the absolute value of the response amplitude operator

$$|\text{RAO}_i(\omega)| = \frac{F_i}{\sqrt{(C_{ii} - \omega^2[M_{RB,ii} + A_{ii}(\omega)])^2 + (\omega B_{\text{total},ii}(\omega))^2}} \quad (5.76)$$

The phase between the wave excitation and the ship motions is

$$\angle \text{RAO}_i(\omega) = -\text{atan} \left( \frac{\omega B_{\text{total},ii}(\omega)}{C_{ii} - \omega^2[M_{RB,ii} + A_{ii}(\omega)]} \right) \quad (5.77)$$

Note the similarity to *Bode* magnitude and phase plots, for which magnitude is logarithmic and given in decibels while phase is plotted in degrees using a common logarithmic frequency axis. The advantage of the logarithmic scale is that asymptotic properties of magnitude and phase are preserved. This is exploited when designing feedback control systems in the frequency domain.

## 5.4 Time-Domain Models including Fluid Memory Effects

The time-domain models are useful both for simulation and control systems design. In particular it is convenient to add nonlinear terms directly in the time domain to describe coupled maneuvers at high speed. Fluid memory effects and wave force terms are kept from the seakeeping theory. Hence, this can be seen as a *unified* approach where seakeeping and maneuvering theory are combined. The basis for the time-domain transformations are the famous papers by Cummins (1962) and Ogilvie (1964), and recent results by Fossen (2005) and Perez and Fossen (2007).

### 5.4.1 Cummins equation in SEAKEEPING coordinates

Cummins (1962) considered the behavior of the fluid and the ship in the time domain *ab initio*. He made the assumption of linearity and considered impulses in the components of motion. This resulted in a boundary value problem in which the potential was

separated into two parts: one valid during the duration of the impulses and the other valid after the impulses are extinguished. By expressing the pressure as a function of these potentials and integrating it over the wetted surface of the marine craft, he obtained a vector integro-differential equation, which is known as the *Cummins equation*; see (5.52) in Section 5.3. If we add viscous damping, restoring forces, wave-induced forces and wind forces, the time-domain seakeeping model becomes

$$(\mathbf{M}_{RB} + \bar{\mathbf{A}}) \ddot{\boldsymbol{\xi}} + \int_{-\infty}^t \bar{\mathbf{K}}(t - \tau) \dot{\boldsymbol{\xi}}(\tau) d\tau + \bar{\mathbf{C}} \boldsymbol{\xi} = \boldsymbol{\tau}_{\text{wind}} + \boldsymbol{\tau}_{\text{wave}} + \delta \boldsymbol{\tau} \quad (5.78)$$

In this expression,  $\delta \boldsymbol{\tau}$  is the perturbed control input,  $\bar{\mathbf{A}}$  and  $\bar{\mathbf{C}}$  are constant matrices to be determined and  $\bar{\mathbf{K}}(t)$  is a matrix of *retardation functions* given by

$$\bar{\mathbf{K}}(t) = \frac{2}{\pi} \int_0^\infty \mathbf{B}_{\text{total}}(\omega) \cos(\omega t) d\omega \quad (5.79)$$

Equation (5.78) is a time-domain equation that reveals the structure of the linear equations of motion in  $\{s\}$  and it is valid for any excitation, provided the linear assumption is not violated; that is the forces produce small displacements from a state of equilibrium. The terms proportional to the accelerations due to the change in momentum of the fluid have constant coefficients. Moreover,  $\bar{\mathbf{A}}$  is constant and independent of the frequency of motion as well as forward speed.

Due to the motion of the ship, waves are generated in the free surface. These waves will, in principle, persist at all subsequent times, affecting the motion of the ship. This is known as fluid memory effects, and they are captured by the convolution integral in (5.78). The convolution integral is a function of  $\dot{\boldsymbol{\xi}}$  and the retardation functions  $\bar{\mathbf{K}}(t)$ . These functions depend on the hull geometry and the forward speed. This effect appears due to the free surface. For sinusoidal motions, these integrals have components in phase with the motion and 90 degrees out of phase. The latter components contribute to damping, whereas the components in phase with the motion can be added as a frequency-dependent added mass.

### The Ogilvie (1964) transformation

In order to relate the Cummins equation and the matrices  $\bar{\mathbf{A}}$ ,  $\bar{\mathbf{C}}$  and  $\bar{\mathbf{K}}$  to the frequency-domain equation, we will rely on a result from Ogilvie (1964). Assume that the floating vessel carries out harmonic oscillations

$$\boldsymbol{\xi} = \bar{\boldsymbol{\xi}} e^{j\omega t} \quad (5.80)$$

with amplitude vector  $\bar{\boldsymbol{\xi}}$ . Substituting (5.80) into the Cummins equation (5.78) yields

$$-\omega^2 [\mathbf{M}_{RB} + \bar{\mathbf{A}}] \bar{\boldsymbol{\xi}} e^{j\omega t} + j\omega \int_{-\infty}^t \bar{\mathbf{K}}(\tau) \bar{\boldsymbol{\xi}} e^{j(\omega t - \omega \tau)} d\tau + \bar{\mathbf{C}} \bar{\boldsymbol{\xi}} e^{j\omega t} = \boldsymbol{\tau}_{\text{wind}} + \boldsymbol{\tau}_{\text{wave}} + \delta \boldsymbol{\tau}$$

where we have replaced  $\tau$  by  $t - \tau$  in the integral. This gives

$$\begin{aligned} & -\omega^2 \left\{ [M_{RB} + \bar{A}] - \frac{1}{\omega} \int_0^\infty \bar{K}(\tau) \sin(\omega\tau) d\tau \right\} \bar{\xi} e^{j\omega t} \\ & - j\omega \left\{ \int_0^\infty \bar{K}(\tau) \cos(\omega\tau) d\tau \right\} \bar{\xi} e^{j\omega t} + \bar{C} \bar{\xi} e^{j\omega t} = \boldsymbol{\tau}_{\text{wind}} + \boldsymbol{\tau}_{\text{wave}} + \delta \boldsymbol{\tau} \end{aligned} \quad (5.81)$$

The frequency-domain model (5.74) is written

$$-\omega^2 [M_{RB} + \mathbf{A}(\omega)] \bar{\xi} e^{j\omega t} - j\omega \mathbf{B}_{\text{total}}(\omega) \bar{\xi} e^{j\omega t} + \mathbf{C} \bar{\xi} e^{j\omega t} = \boldsymbol{\tau}_{\text{wind}} + \boldsymbol{\tau}_{\text{wave}} + \delta \boldsymbol{\tau} \quad (5.82)$$

By comparing the terms in (5.81) and (5.82), it is seen that

$$\mathbf{A}(\omega) = \bar{A} - \frac{1}{\omega} \int_0^\infty \bar{K}(\tau) \sin(\omega\tau) d\tau \quad (5.83)$$

$$\mathbf{B}_{\text{total}}(\omega) = \int_0^\infty \bar{K}(\tau) \cos(\omega\tau) d\tau \quad (5.84)$$

$$\mathbf{C} = \bar{C} \quad (5.85)$$

Equation (5.83) must be valid for all  $\omega$ . Hence, we choose to evaluate (5.83) at  $\omega = \infty$ , implying that

$$\bar{A} = \mathbf{A}(\infty) \quad (5.86)$$

Equation (5.84) is rewritten using the inverse Fourier transform

$$\bar{K}(t) = \frac{2}{\pi} \int_0^\infty \mathbf{B}_{\text{total}}(\omega) \cos(\omega t) d\omega \quad (5.87)$$

This expression is recognized as a matrix of *retardation functions*. From a numerical point of view is it better to integrate the difference

$$\mathbf{K}(t) = \frac{2}{\pi} \int_0^\infty [\mathbf{B}_{\text{total}}(\omega) - \mathbf{B}_{\text{total}}(\infty)] \cos(\omega t) d\omega \quad (5.88)$$

than to use (5.87), since  $\mathbf{B}_{\text{total}}(\omega) - \mathbf{B}_{\text{total}}(\infty)$  will be exact zero at  $\omega = \infty$ . Figure 5.4 shows a typical retardation function that is converging to zero in 15–20 s. The tail will oscillate if (5.87) is used instead of (5.88) in the numerical integration.

The relationship between  $\bar{K}(t)$  and  $\mathbf{K}(t)$  follows from

$$\begin{aligned} \bar{K}(t) &= \frac{2}{\pi} \int_0^\infty [\mathbf{B}_{\text{total}}(\omega) - \mathbf{B}_{\text{total}}(\infty) + \mathbf{B}_{\text{total}}(\infty)] \cos(\omega t) d\omega \\ &= \mathbf{K}(t) + \frac{2}{\pi} \int_0^\infty \mathbf{B}_{\text{total}}(\infty) \cos(\omega t) d\omega \end{aligned} \quad (5.89)$$

Then it follows that

$$\begin{aligned} \int_{-\infty}^t \bar{K}(t - \tau) \dot{\xi}(\tau) d\tau &= \int_{-\infty}^t \mathbf{K}(t - \tau) \dot{\xi}(\tau) d\tau + \mathbf{B}_{\text{total}}(\infty) \dot{\xi} \\ &\stackrel{\text{causal}}{=} \int_0^t \mathbf{K}(t - \tau) \dot{\xi}(\tau) d\tau + \mathbf{B}_{\text{total}}(\infty) \dot{\xi} \end{aligned} \quad (5.90)$$

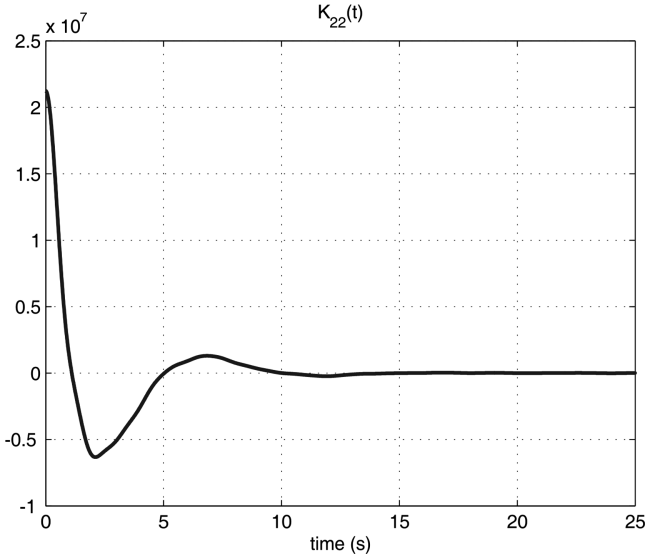


Figure 5.4: Typical plot of the retardation function  $K_{22}(t)$  in sway.

We are now ready to state the main result.

#### Time-domain seakeeping equations of motion in $\{s\}$

The relationship between the time-domain equation (5.78) and the frequency-domain equation (5.74) is established through (5.83)–(5.85) and (5.90). This gives

$$[M_{RB} + A(\infty)]\ddot{\xi} + B_{\text{total}}(\infty)\dot{\xi} + \int_0^t K(t-\tau)\dot{\xi}(\tau)d\tau + C\xi = \tau_{\text{wind}} + \tau_{\text{wave}} + \delta\tau \quad (5.91)$$

where  $K(t-\tau)$  is defined by (5.88). The equations of motion (5.91) describe the perturbed motion  $\xi$  of a marine craft in 6 DOF using seakeeping coordinates. We will now transform this result to the rotating frame  $\{b\}$ .

#### 5.4.2 Linear time-domain seakeeping equations in BODY coordinates

Two representations in  $\{b\}$  are available: one using zero-speed potential coefficients and one using speed-dependent matrices. Motion control systems are usually formulated in  $\{b\}$ . Consequently, we need to transform the time-domain representation of the Cummins equation (5.91) from  $\{s\}$  to  $\{b\}$ . When transforming the equations of motion to the rotating frame  $\{b\}$ , Coriolis and centripetal forces between  $\{s\}$  and  $\{b\}$  appear; see Figure 5.5. To illustrate this, consider

$$[M_{RB} + A(\infty)]\ddot{\xi} + B_{\text{total}}(\infty)\dot{\xi} + \int_0^t K(t-\tau)\dot{\xi}(\tau)d\tau + C\xi = \tau_{\text{wind}} + \tau_{\text{wave}} + \delta\tau \quad (5.92)$$

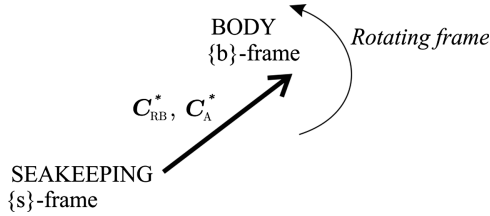


Figure 5.5: Coriolis matrices due to the rotation of the body-fixed frame  $\{b\}$  about the inertial frame  $\{s\}$ .

which can be transformed from  $\{s\}$  to  $\{b\}$  by using the kinematic transformations (5.21) and (5.45)–(5.46) derived in Section 5.2.2. This gives

$$\begin{aligned} & [\mathbf{M}_{RB} + \mathbf{A}(\infty)][\dot{\boldsymbol{\nu}} + U\mathbf{L}\boldsymbol{\nu}] + \mathbf{B}_{\text{total}}(\infty)[\boldsymbol{\nu} + U(\mathbf{L}\delta\boldsymbol{\eta} - \mathbf{e}_1)] \\ & + \int_0^t \mathbf{K}(t-\tau)\delta\boldsymbol{\nu}(\tau)d\tau + \mathbf{C}\delta\boldsymbol{\eta} = \boldsymbol{\tau}_{\text{wind}} + \boldsymbol{\tau}_{\text{wave}} + (\boldsymbol{\tau} - \bar{\boldsymbol{\tau}}) \end{aligned} \quad (5.93)$$

The steady-state control force  $\bar{\boldsymbol{\tau}}$  needed to obtain the forward speed  $U$  when  $\boldsymbol{\tau}_{\text{wind}} = \boldsymbol{\tau}_{\text{wave}} = \mathbf{0}$  and  $\delta\boldsymbol{\eta} = \mathbf{0}$  is

$$\bar{\boldsymbol{\tau}} = \mathbf{B}_{\text{total}}(\infty)U\mathbf{e}_1 \quad (5.94)$$

Hence, (5.93) can be rewritten as

$$\begin{aligned} & [\mathbf{M}_{RB} + \mathbf{A}(\infty)][\dot{\boldsymbol{\nu}} + U\mathbf{L}\boldsymbol{\nu}] + \mathbf{B}_{\text{total}}(\infty)[\boldsymbol{\nu} + U\mathbf{L}\delta\boldsymbol{\eta}] \\ & + \int_0^t \mathbf{K}(t-\tau)\delta\boldsymbol{\nu}(\tau)d\tau + \mathbf{C}\delta\boldsymbol{\eta} = \boldsymbol{\tau}_{\text{wind}} + \boldsymbol{\tau}_{\text{wave}} + \boldsymbol{\tau} \end{aligned} \quad (5.95)$$

In this expression, the linearized Coriolis–centripetal forces due to rigid-body mass and hydrodynamic added mass are recognized as  $\mathbf{M}_{RB}U\mathbf{L}\boldsymbol{\nu}$  and  $\mathbf{A}(\infty)U\mathbf{L}\boldsymbol{\nu}$ , respectively.

When computing the damping and retardation functions, it is common to neglect the influence of  $\delta\boldsymbol{\eta}$  on the forward speed such that

$$\delta\boldsymbol{\nu} \approx \boldsymbol{\nu} + U(\mathbf{L}\delta\boldsymbol{\eta} - \mathbf{e}_1) \approx \boldsymbol{\nu} - U\mathbf{e}_1 \quad (5.96)$$

Hence, we can present the linear seakeeping equations expressed in the  $\{b\}$  frame.

### Linear equations of motion using zero-speed potential coefficients

The kinematic equation between  $\{b\}$  and  $\{n\}$  is

$$\dot{\boldsymbol{\eta}} = \mathbf{J}_\Theta(\boldsymbol{\eta})\boldsymbol{\nu} \quad (5.97)$$

From (5.95)–(5.96) it follows that

$$\begin{aligned} \mathbf{M}\dot{\boldsymbol{\nu}} + \mathbf{C}_{RB}^*\boldsymbol{\nu} + \mathbf{C}_A^*\boldsymbol{\nu}_r + \mathbf{D}\boldsymbol{\nu}_r \\ + \int_0^t \mathbf{K}(t-\tau)[\boldsymbol{\nu}(\tau) - U\mathbf{e}_1]d\tau + \mathbf{G}\boldsymbol{\eta} = \boldsymbol{\tau}_{\text{wind}} + \boldsymbol{\tau}_{\text{wave}} + \boldsymbol{\tau} \end{aligned} \quad (5.98)$$

where  $\boldsymbol{\nu}$  has been replaced by the relative velocity  $\boldsymbol{\nu}_r$  to include ocean currents,  $\mathbf{M} = \mathbf{M}_{RB} + \mathbf{M}_A$  and

$$\begin{aligned} \mathbf{M}_A &= \mathbf{A}(\infty) \\ \mathbf{C}_A^* &= U\mathbf{A}(\infty)\mathbf{L} \\ \mathbf{C}_{RB}^* &= U\mathbf{M}_{RB}\mathbf{L} \\ \mathbf{D} &= \mathbf{B}_{\text{total}}(\infty) \\ \mathbf{G} &= \mathbf{C} \end{aligned}$$

We have here exploited the fact that  $\mathbf{C}\delta\boldsymbol{\eta} = \mathbf{G}\boldsymbol{\eta}$ . Notice that  $\mathbf{C}_{RB}^*$  and  $\mathbf{C}_A^*$  are linearized Coriolis and centripetal forces due to the rotation of  $\{b\}$  about  $\{s\}$ . At zero speed, these terms vanish.

### Linear equations of motion using speed-dependent potential coefficients

Some potential theory programs compute the potential coefficients as functions of speed and frequency

$$\mathbf{A}_U(\omega, U) = \mathbf{A}(\omega) + \boldsymbol{\alpha}(\omega, U) \quad (5.99)$$

$$\mathbf{B}_U(\omega, U) = \mathbf{B}(\omega) + \boldsymbol{\beta}(\omega, U) \quad (5.100)$$

where  $\boldsymbol{\alpha}(\omega, U)$  and  $\boldsymbol{\beta}(\omega, U)$  denote the speed-dependent terms. For these codes,  $\boldsymbol{\beta}(\omega, U)$  can include the matrix  $\mathbf{C}_A^* = U\mathbf{A}(\infty)\mathbf{L}$  as well as other effects. A frequently used representation is

$$\boldsymbol{\beta}(\omega, U) = \underbrace{\mathbf{C}_A^*}_{\mathbf{C}_A^*} + \mathbf{B}_{\text{ITTC}}(\omega, U) + \mathbf{B}_{\text{IKEDA}}(\omega, U) + \mathbf{B}_{\text{transom}}(\omega, U) \quad (5.101)$$

where the subscripts denote linearized ITTC resistance, IKEDA damping and transom stern effects. If the speed-dependent matrices (5.99) and (5.100) are used instead of the zero-speed matrices in (5.98), the equations of motion for each speed,  $U = \text{constant}$ , take the following form

$$\begin{aligned} \mathbf{M}_U\dot{\boldsymbol{\nu}} + \mathbf{C}_{RB}^*\boldsymbol{\nu} + \mathbf{D}_U\boldsymbol{\nu}_r \\ + \int_0^t \mathbf{K}_U(t-\tau, U)[\boldsymbol{\nu}(\tau) - U\mathbf{e}_1]d\tau + \mathbf{G}\boldsymbol{\eta} = \boldsymbol{\tau}_{\text{wind}} + \boldsymbol{\tau}_{\text{wave}} + \boldsymbol{\tau} \end{aligned} \quad (5.102)$$

where the matrix  $\mathbf{C}_A^*$  is superfluous and

$$\begin{aligned}\mathbf{M}_U &= \mathbf{M}_{RB} + \mathbf{A}_U(\infty, U) \\ \mathbf{C}_{RB}^* &= U\mathbf{M}_{RB}\mathbf{L} \\ \mathbf{D}_U &= \mathbf{B}_{\text{total},U}(\infty, U) \\ \mathbf{G} &= \mathbf{C}\end{aligned}$$

and

$$\mathbf{K}_U(t, U) = \frac{2}{\pi} \int_0^\infty [\mathbf{B}_{\text{total},U}(\omega, U) - \mathbf{B}_{\text{total},U}(\infty, U)] \cos(\omega t) d\omega \quad (5.103)$$

The speed-dependent equations of motion (5.102) are computed at each speed  $U = \text{constant}$  while (5.98) is valid for any  $U(t)$  provided that  $U(t)$  is slowly varying. It is advantageous to use (5.98) since only the zero-speed potential coefficients  $\mathbf{A}(\omega)$  and  $\mathbf{B}(\omega)$  are needed in the implementation. This is based on the assumption that the  $\mathbf{C}_A$  matrix is the only element in  $\mathbf{B}_U(\omega, U)$ . Moreover, it is assumed that

$$\begin{aligned}\beta(\omega, U) &:= \mathbf{C}_A^* \\ &= U\mathbf{A}(\infty)\mathbf{L}\end{aligned} \quad (5.104)$$

When using (5.98) instead of (5.102), it is necessary to add the remaining damping terms directly in the time-domain equations, as explained in Section 5.4.3.

### Properties of $\mathbf{A}$ , $\mathbf{B}$ and $\mathbf{K}$

The following properties are useful when processing the hydrodynamic data:

- Asymptotic values for  $\omega = 0$ :

$$\mathbf{B}(0) = \mathbf{0}$$

- Asymptotic values for  $\omega \rightarrow \infty$ :

$$\begin{aligned}\mathbf{A}_U(\infty, U) &= \mathbf{0} \\ \mathbf{A}_U(\infty, U) &= \mathbf{A}(\infty)\end{aligned}$$

These properties can be exploited when computing  $\mathbf{K}(t)$  numerically since most sea-keeping codes only return values on an interval  $\omega = [\omega_{\min}, \omega_{\max}]$ .

Some useful properties of the retardation functions are:

- Asymptotic value for  $t = 0$ :

$$\lim_{t \rightarrow 0} \mathbf{K}(t) \neq \mathbf{0} < \infty \quad (5.105)$$

- Asymptotic value for  $t \rightarrow \infty$ :

$$\lim_{t \rightarrow \infty} \mathbf{K}(t) = \mathbf{0} \quad (5.106)$$

A plot illustrating the retardation function in sway is shown in Figure 5.4.

### 5.4.3 Nonlinear unified seakeeping and maneuvering model with fluid memory effects

Consider the seakeeping model (5.98) based on the zero-speed potential coefficients

$$\begin{aligned} M\dot{\nu} + C_{RB}^*\nu + C_A^*\nu_r + D\nu_r \\ + \int_0^t \mathbf{K}(t-\tau)[\nu(\tau) - Ue_1]d\tau + G\eta = \tau_{\text{wind}} + \tau_{\text{wave}} + \tau \end{aligned} \quad (5.107)$$

For this model, the linearized Coriolis and centripetal matrices  $C_{RB}^*$  and  $C_A^*$  can be replaced by their nonlinear counterparts  $C_{RB}(\nu)$  and  $C_A(\nu_r)$ ; see Section 6.3.1. In addition, the nonlinear damping  $D(\nu_r)\nu_r$  or maneuvering coefficients can be added directly in the time domain.

#### Unified seakeeping and maneuvering model

Some authors refer to (5.107) as a *unified model* when nonlinear maneuvering terms are included since it merges the maneuvering and seakeeping theories (see Bailey *et al.*, 1998; Fossen, 2005). This gives a *unified* seakeeping and maneuvering model in the following form

$$\dot{\eta} = J_\Theta(\eta)\nu \quad (5.108)$$

$$M\dot{\nu}_r + C_{RB}(\nu)\nu + C_A(\nu_r)\nu_r + D(\nu_r)\nu_r + \mu + G\eta = \tau_{\text{wind}} + \tau_{\text{wave}} + \tau \quad (5.109)$$

The seakeeping *fluid memory effects* are captured in the term

$$\mu := \int_0^t \mathbf{K}(t-\tau) \underbrace{[\nu(\tau) - Ue_1]}_{\delta\nu} d\tau \quad (5.110)$$

#### Constant and irrotational ocean currents

The model (5.109) can be simplified if the *ocean currents* are assumed to be *constant* and *irrotational* in  $\{n\}$  such that Property 10.1 is satisfied. Following the approach in Section 10.3 this gives

$$M\dot{\nu}_r + C(\nu_r)\nu_r + D(\nu_r)\nu_r + \mu + G\eta = \tau_{\text{wind}} + \tau_{\text{wave}} + \tau \quad (5.111)$$

#### Example 5.1 (Zero-Speed Model for DP with Fluid Memory Effects)

For stationkeeping ( $U = 0$  and  $r = 0$ ), the model (5.111) reduces to

$$\dot{\eta} = J_\Theta(\eta)\nu \quad (5.112)$$

$$M\dot{\nu}_r + D\nu_r + \mu + G\eta = \tau_{\text{wind}} + \tau_{\text{wave}} + \tau \quad (5.113)$$

under the assumptions that  $C_{RB}(\nu) = C_A(\nu_r) = \mathbf{0}$  and  $D(\nu_r) = D$ . This is similar to the result of Fossen and Smogeli (2004).

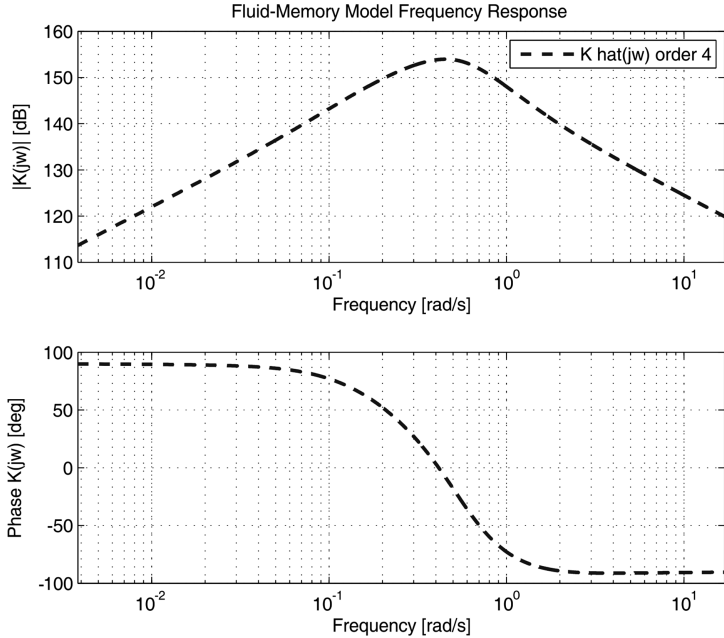


Figure 5.6: Bode plot showing the identified transfer function  $h_{33}(s)$  of an FPSO when  $A_{33}(\infty)$  is treated as an unknown to be estimated.

## 5.5 Identification of Fluid Memory Effects

Kristiansen and Egeland (2003) and Kristiansen *et al.* (2005) have developed a state-space approximation for  $\mu$  using realization theory. Other methods such as the impulse response LS fitting can also be used (see Yu and Falnes, 1995, 1998). The time-domain methods are usually used in conjunction with model reduction in order to obtain a state-space model of smaller dimension suited for feedback control and time-domain simulation. This often results in a state-space model  $(A_r, B_r, C_r, D_r)$  where the  $D_r$  matrix is nonzero (Perez and Fossen 2008). This is nonphysical since potential damping should not amplify signals at low frequencies. Hence, care must be taken when using time-domain methods. As a consequence of this, frequency-domain identification methods are much more accurate and they do have the advantage that a transfer function of correct relative degree can be chosen prior to the identification process. Hence, model reduction in the time domain can be avoided since the estimated transfer function can be converted into a  $(A_r, B_r, C_r)$  state-space model exploiting the structural constraint  $D_r = \mathbf{0}$  directly. A more detailed discussion of the identification methods are found in Perez and Fossen (2008) while practical aspects are reported in Perez and Fossen (2011).

### 5.5.1 Frequency-domain identification using the MSS FDI toolbox

This section illustrates how the fluid memory effects can be accurately approximated using frequency-domain identification. The main tool for this is the MSS FDI toolbox (Perez and Fossen 2009). When using the frequency-domain approach, the property that the mapping

$$\delta\nu \rightarrow \mu \quad (5.114)$$

has relative degree one is exploited. Hence, the fluid memory effects  $\mu$  can be approximated by a matrix  $\mathbf{H}(s)$  containing relative degree one transfer functions (see Figure 5.6)

$$h_{ij}(s) = \frac{p_r s^r + p_{r-1} s^{r-1} + \cdots + p_0}{s^n + q_{n-1} s^{n-1} + \cdots + q_0}, \quad r = n - 1, \quad n \geq 2 \quad (5.115)$$

such that

$$\mu = \mathbf{H}(s)\delta\nu \quad (5.116)$$

with

$$\mathbf{H}(s) = \mathbf{C}_r(s\mathbf{I} - \mathbf{A}_r)^{-1}\mathbf{B}_r \quad (5.117)$$

Consequently, the corresponding state-space model is in the form

$$\begin{aligned} \dot{\mathbf{x}} &= \mathbf{A}_r \mathbf{x} + \mathbf{B}_r \delta\nu \\ \mu &= \mathbf{C}_r \mathbf{x} \end{aligned} \quad (5.118)$$

The states  $\mathbf{x}$  in (5.118) reflect the fact that once the marine craft changes the momentum of the fluid, this will affect the forces in the future. In other words, the radiation forces at a particular time depend on the history of the velocity of the marine craft up to the present time. The dimension of  $\mathbf{x}$  and the matrices  $\mathbf{A}_r$ ,  $\mathbf{B}_r$  and  $\mathbf{C}_r$  depend on the order of the identified transfer functions (usually 2 to 20).

#### Matlab:

The fluid memory transfer function (5.115) can be computed using the MSS toolbox, which includes the FDI toolbox for frequency-domain identification (Perez and Fossen 2009). The toolbox includes two demo files for the cases where infinite added mass is unknown (2-D strip theory codes) or computed by the hydrodynamic code, for instance the 3-D code by WAMIT.

#### *Example 5.2 (Computation of Fluid Memory Effects)*

*Consider the FPSO data set in the MSS toolbox and assume that the infinite-frequency added mass matrix is unknown. Hence, we can estimate the fluid transfer function  $h_{33}(s)$  by using the following Matlab code*

```
load fpso
Dof = [3, 3]; % Use coupling 3-3 heave-heave
Nf = length(vessel.freqs);
w = vessel.freqs(1:Nf-1);
```

```

Ainf = vessel.A(Dof(1),Dof(2),Nf) % Ainf computed by WAMIT
Ainf =
    1.7283e+08

A = reshape(vessel.A(Dof(1),Dof(2),1:Nf-1),1,length(w))';
B = reshape(vessel.B(Dof(1),Dof(2),1:Nf-1),1,length(w))';

```

A fourth-order transfer function of relative degree 1 is found by using the following options (see Perez and Fossen (2009) for a more detailed explanation).

```

FDIopt.OrdMax = 20;
FDIopt.AinfFlag = 0;
FDIopt.Method = 2;
FDIopt.Iterations = 20;
FDIopt.PlotFlag = 0;
FDIopt.LogLin = 1;
FDIopt.wsFactor = 0.1;
FDIopt.wminFactor = 0.1;
FDIopt.wmaxFactor = 5;

[Krad,Ainf_hat] = FDIRadMod(W,A,0,B,FDIopt,Dof)

```

```

Krad =
-----  

1.647e07 s^3 + 2.358e07 s^2 + 2.122e06 s  

-----  

s^4 + 1.253 s^3 + 0.7452 s^2 + 0.2012 s + 0.01686

Ainf_hat =
    1.7265e+08

```

The state-space model (5.118) is obtained by calling

```

[num,den] = tfdata(Krad, 'v');
[A_r, B_r, C_r, D_r] = tf2ss(num,den)

A_r =
-1.2529   -0.7452   -0.2012   -0.0169
 1.0000       0       0       0
 0       1.0000       0       0
 0           0       1.0000       0

B_r =
 1
 0
 0
 0

C_r =
 1.0e+07 *
 1.6472     2.3582     0.2122       0
D_r =
 0

```

The identified transfer function  $h_{33}(s)$  is plotted in Figure 5.6 while curve fitting of amplitude, phase, added mass and potential damping are shown in Figure 5.7. The estimated transfer function and potential coefficients are matching the exper-

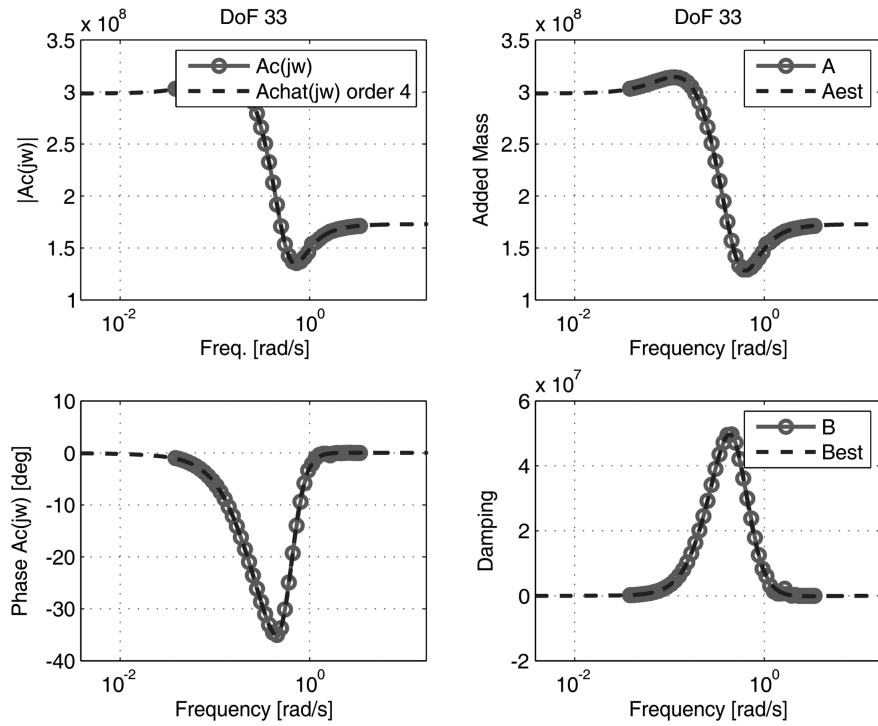


Figure 5.7: FPSO identification results for  $h_{33}(s)$  without using the infinite added mass  $A_{33}(\infty)$ . The left-hand-side plots show the complex coefficient and its estimate while added mass and damping are plotted on the right-hand-side plots.

*perimental data with good accuracy. Notice that the asymptotic behavior satisfies the properties of added mass  $A_{33}(\omega)$  and potential damping  $B_{33}(\omega)$  as expected.*



## Chapter 6

# Maneuvering Models

In Chapter 5 the 6-DOF seakeeping equations of motion for a ship in a seaway were presented. The seakeeping model is based on linear theory and a potential theory program is used to compute the frequency-dependent hydrodynamic forces for varying wave excitation frequencies. The time-domain representation of the seakeeping model is very useful for accurate prediction of motions and sealoads of floating structures offshore. The seakeeping theory can also be applied to displacement ships moving at constant speed. Seakeeping time-domain models are limited to linear theory since it is necessary to approximate the fluid memory effects by impulse responses or transfer functions.

An alternative to the seakeeping formalism is to use maneuvering theory to describe the motions of marine craft in 3 DOF, that is *surge*, *sway* and *yaw*. Sometimes roll is augmented to the horizontal plane model to describe more accurately the coupled lateral motions, that is *sway-roll-yaw* couplings while *surge* is left decoupled; see Section 6.6. In maneuvering theory, frequency-dependent added mass and potential damping are approximated by constant values and thus it is not necessary to compute the fluid-memory effects. The main results of this chapter are based on the assumption that the hydrodynamic forces and moments can be approximated at one frequency of oscillation such that the fluid-memory effects can be neglected. The result is a nonlinear mass–damper–spring system with constant coefficients.

In the following sections, it is shown that the maneuvering equations of motion can be represented by (Fossen, 1991, 1994)

$$\mathbf{M}\dot{\boldsymbol{\nu}} + \mathbf{C}(\boldsymbol{\nu})\boldsymbol{\nu} + \mathbf{D}(\boldsymbol{\nu})\boldsymbol{\nu} + \mathbf{g}(\boldsymbol{\eta}) + \mathbf{g}_o = \boldsymbol{\tau} + \boldsymbol{\tau}_{\text{wind}} + \boldsymbol{\tau}_{\text{wave}} \quad (6.1)$$

In the case of *irrotational ocean currents*, the relative velocity vector

$$\boldsymbol{\nu}_r = \boldsymbol{\nu} - \boldsymbol{\nu}_c, \quad \boldsymbol{\nu}_c = [u_c, v_c, w_c, 0, 0, 0]^\top$$

contributes to the hydrodynamic terms such that

$$\underbrace{\mathbf{M}_{RB}\dot{\boldsymbol{\nu}} + \mathbf{C}_{RB}(\boldsymbol{\nu})\boldsymbol{\nu}}_{\text{rigid-body forces}} + \underbrace{\mathbf{M}_A\dot{\boldsymbol{\nu}}_r + \mathbf{C}_A(\boldsymbol{\nu}_r)\boldsymbol{\nu}_r + \mathbf{D}(\boldsymbol{\nu}_r)\boldsymbol{\nu}_r}_{\text{hydrodynamic forces}} \\
 + \underbrace{\mathbf{g}(\boldsymbol{\eta}) + \mathbf{g}_o}_{\text{hydrostatic forces}} = \boldsymbol{\tau} + \boldsymbol{\tau}_{\text{wind}} + \boldsymbol{\tau}_{\text{wave}} \quad (6.2)$$

The model (6.2) can be simplified if the *ocean currents* are assumed to be *constant* and *irrotational* in  $\{\mathbf{n}\}$  such that (see Section 10.3)

$$\dot{\boldsymbol{\nu}}_c = \begin{bmatrix} -S(\boldsymbol{\omega}_{nb}^b) & \mathbf{0}_{3 \times 3} \\ \mathbf{0}_{3 \times 3} & \mathbf{0}_{3 \times 3} \end{bmatrix} \boldsymbol{\nu}_c \quad (6.3)$$

According to Property 10.1, it is then possible to represent the equations of motion by relative velocities only

$$\mathbf{M}\dot{\boldsymbol{\nu}}_r + \mathbf{C}(\boldsymbol{\nu}_r)\boldsymbol{\nu}_r + \mathbf{D}(\boldsymbol{\nu}_r)\boldsymbol{\nu}_r + \mathbf{g}(\boldsymbol{\eta}) + \mathbf{g}_o = \boldsymbol{\tau} + \boldsymbol{\tau}_{\text{wind}} + \boldsymbol{\tau}_{\text{wave}} \quad (6.4)$$

where

$\mathbf{M} = \mathbf{M}_{RB} + \mathbf{M}_A$  - system inertia matrix (including added mass)

$\mathbf{C}(\boldsymbol{\nu}_r) = \mathbf{C}_{RB}(\boldsymbol{\nu}_r) + \mathbf{C}_A(\boldsymbol{\nu}_r)$  - Coriolis–centripetal matrix (including added mass)

$\mathbf{D}(\boldsymbol{\nu}_r)$  - damping matrix

$\mathbf{g}(\boldsymbol{\eta})$  - vector of gravitational/buoyancy forces and moments

$\mathbf{g}_o$  - vector used for pretrimming (ballast control)

$\boldsymbol{\tau}$  - vector of control inputs

$\boldsymbol{\tau}_{\text{wind}}$  - vector of wind forces

$\boldsymbol{\tau}_{\text{wave}}$  - vector of wave-induced forces

The expressions for  $\mathbf{M}$ ,  $\mathbf{C}(\boldsymbol{\nu}_r)$ ,  $\mathbf{D}(\boldsymbol{\nu}_r)$ ,  $\mathbf{g}(\boldsymbol{\eta})$  and  $\mathbf{g}_o$  are derived in the forthcoming sections while the environmental forces  $\boldsymbol{\tau}_{\text{wind}}$  and  $\boldsymbol{\tau}_{\text{wave}}$  are treated separately in Chapter 10. The maneuvering model presented in this chapter is mainly intended for controller–observer design, prediction and computer simulations in combination with system identification and parameter estimation.

Hydrodynamic programs compute mass, inertia, potential damping and restoring forces while a more detailed treatment of viscous dissipative forces (damping) are found in the extensive literature on hydrodynamics; see Faltinsen (1990, 2005), Newman (1977), Sarpkaya (1981) and Triantafyllou and Hover (2002). Other useful references on marine craft modeling are Lewandowski (2004) and Perez (2005).

## 6.1 Rigid-Body Kinetics

Recall from Chapter 3 that the rigid-body kinetics can be expressed as

$$\mathbf{M}_{RB}\dot{\boldsymbol{\nu}} + \mathbf{C}_{RB}(\boldsymbol{\nu})\boldsymbol{\nu} = \boldsymbol{\tau}_{RB} \quad (6.5)$$

where  $M_{RB} = M_{RB}^\top > 0$  is the rigid-body mass matrix and  $C_{RB}(\boldsymbol{\nu}) = -C_{RB}^\top(\boldsymbol{\nu})$  is the rigid-body Coriolis and centripetal matrix due to the rotation of  $\{b\}$  about the inertial frame  $\{n\}$ . The horizontal motion of a maneuvering ship or semisubmersible is given by the motion components in surge, sway and yaw. Consequently, the state vectors are chosen as  $\boldsymbol{\nu} = [u, v, r]^\top$  and  $\boldsymbol{\eta} = [x^n, y^n, \psi]^\top$ . It is also common to assume that the craft has homogeneous mass distribution and  $xz$ -plane symmetry so that

$$I_{xy} = I_{yz} = 0 \quad (6.6)$$

Let the  $\{b\}$ -frame coordinate origin be set in the centerline of the craft in the point CO, such that  $y_g = 0$ . Under the previously stated assumptions, the matrices (3.46) and (3.59) associated with the rigid-body kinetics reduce to

$$\mathbf{M}_{RB} = \begin{bmatrix} m & 0 & 0 \\ 0 & m & mx_g \\ 0 & mx_g & I_z \end{bmatrix}, \quad C_{RB}(\boldsymbol{\nu}) = \begin{bmatrix} 0 & -mr & -mx_gr \\ mr & 0 & 0 \\ mx_gr & 0 & 0 \end{bmatrix} \quad (6.7)$$

Notice that surge is decoupled from sway and yaw in  $\mathbf{M}_{RB}$  due to symmetry considerations of the system inertia matrix (see Section 3.3).

The linear approximation to (6.5) about  $u = U = \text{constant}$ ,  $v = 0$  and  $r = 0$  is

$$\mathbf{M}_{RB}\dot{\boldsymbol{\nu}} + \mathbf{C}_{RB}^*\boldsymbol{\nu} = \boldsymbol{\tau}_{RB} \quad (6.8)$$

where

$$\mathbf{C}_{RB}^* = \begin{bmatrix} 0 & 0 & 0 \\ 0 & 0 & mU \\ 0 & 0 & mx_gU \end{bmatrix} \quad (6.9)$$

## 6.2 Potential Coefficients

Hydrodynamic potential theory programs can be used to compute the added mass and damping matrices by integrating the pressure of the fluid over the wetted surface of the hull; see Section 5.1. These programs assume that viscous effects can be neglected. Consequently, it is necessary to add viscous forces manually. The programs are also based on the assumptions that first- and second-order wave forces can be linearly superimposed.

The potential coefficients are usually represented as frequency-dependent matrices for 6-DOF motions. The matrices are:

- $\mathbf{A}(\omega)$  added mass
- $\mathbf{B}(\omega)$  potential damping

where  $\omega$  is the wave excitation frequency of a sinusoidal (regular) wave generated by a wave maker or the ocean. Figure 6.1 illustrates the components in sway.

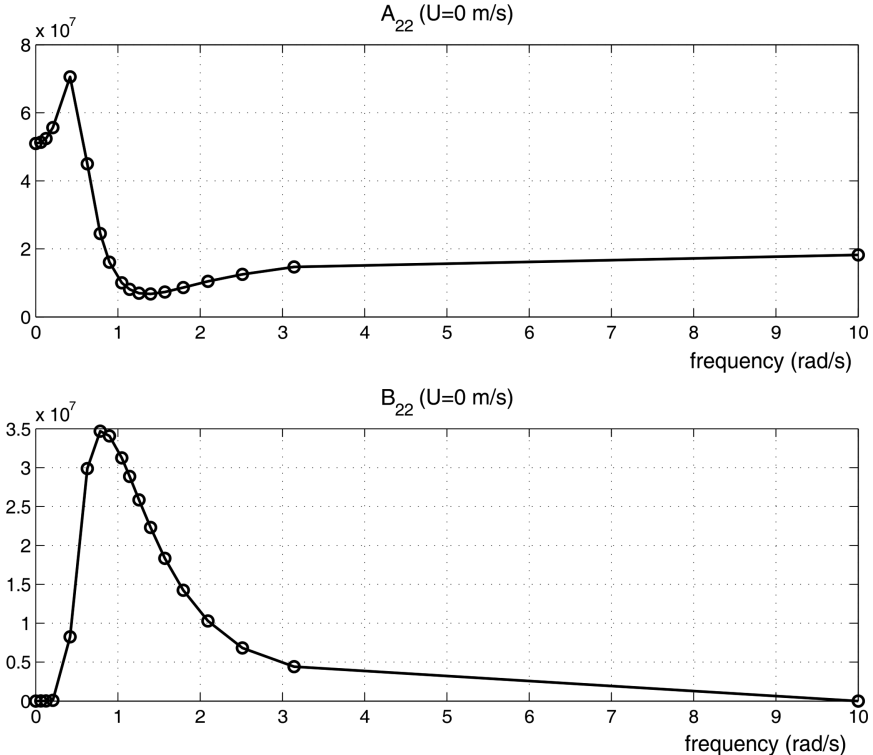


Figure 6.1: Added mass  $A_{22}(\omega)$  and potential damping  $B_{22}(\omega)$  in sway as a function of wave frequency  $\omega$  for a large tanker.

In seakeeping analysis, the equations of motion (see Chapter 5)

$$[M_{RB} + A(\omega)]\ddot{\xi} + [B(\omega) + B_V(\omega)]\dot{\xi} + C\xi = \delta\tau + \tau_{wind} + \tau_{wave} \quad (6.10)$$

are perturbations  $\xi = [\delta x^n, \delta y^n, \delta z^n, \delta\phi, \delta\theta, \delta\psi]^\top$  about an inertial equilibrium frame.

Equation (6.10) should not be used in computer simulations. As earlier mentioned, (6.10) is not an ordinary differential equation since it combines time and frequency. As stressed in Chapter 5, the time-domain seakeeping model should be represented by the Cummins equation, which is an integro-differential equation (Cummins 1962). For surface vessels it is common to solve the Cummins equation in the time domain under the assumption of linear theory (see Section 5.4)

$$(M_{RB} + M_A)\dot{\nu} + C_{RB}^*\nu + C_A^*\nu_r + D\nu + \mu + G\eta = \tau_{wind} + \tau_{wave} + \tau \quad (6.11)$$

where the hydrostatic and hydrodynamic terms are

$$\begin{aligned}\mathbf{M}_A &= \mathbf{A}(\infty) \\ \mathbf{C}_A^* &= U\mathbf{A}(\infty)\mathbf{L} \\ \mathbf{D} &= \mathbf{B}(\infty) + \mathbf{B}_V(\infty) \\ \mathbf{G} &= \mathbf{C}\end{aligned}$$

This introduces *fluid-memory effects*  $\mu$ , which can be interpreted as filtered potential damping forces. These forces are retardation functions that can be approximated by transfer functions and state-space models, as shown in Section 5.4.

### 6.2.1 Frequency-independent added mass and potential damping

The classical maneuvering model makes use of the following assumption:

**Definition 6.1 (Zero-Frequency Models for Surge, Sway and Yaw)**

The horizontal motions (surge, sway and yaw) of a marine craft moving at forward speed can be described by a zero-frequency model where:

$$\mathbf{M}_A = \mathbf{A}^{\{1,2,6\}}(0) = \begin{bmatrix} A_{11}(0) & 0 & 0 \\ 0 & A_{22}(0) & A_{26}(0) \\ 0 & A_{62}(0) & A_{66}(0) \end{bmatrix} \quad (6.12)$$

$$\mathbf{D}_p = \mathbf{B}^{\{1,2,6\}}(0) = \mathbf{0} \quad (6.13)$$

are constant matrices.

When applying a feedback control system to stabilize the motions in surge, sway and yaw, the natural periods will be in the range of 100–200 s. This implies that the natural frequencies are in the range of 0.03–0.10 rad/s, which is quite close to the zero wave excitation frequency. Also note that viscous damping forces will dominate the potential damping terms at low frequency and that fluid memory effects can be neglected at higher speeds.

Definition 6.1 implies that (6.11) can be approximated at a single frequency  $\omega = 0$  in surge, sway and yaw and thus avoid the fluid memory effects ( $\mu = \mathbf{0}$ ). This gives

$$(\mathbf{M}_{RB} + \mathbf{M}_A)\dot{\nu} + \mathbf{C}_{RB}^*\nu + \mathbf{C}_A^*\nu + \mathbf{D}\nu = \tau_{wind} + \tau_{wave} + \tau \quad (6.14)$$

where

$$\begin{aligned}\mathbf{M}_A &= \mathbf{A}^{\{1,2,6\}}(0) \\ \mathbf{C}_A^* &= U\mathbf{A}^{\{1,2,6\}}(0)\mathbf{L}^{\{1,2,6\}} \\ \mathbf{D} &= \mathbf{B}_V^{\{1,2,6\}}(0)\end{aligned}$$

and

$$\mathbf{L}^{\{1,2,6\}} = \begin{bmatrix} 0 & 0 & 0 \\ 0 & 0 & 1 \\ 0 & 0 & 0 \end{bmatrix} \quad (6.15)$$

The viscous damping matrix  $\mathbf{B}_V^{\{1,2,6\}}(0)$  can be computed using the methods in Section 5.3.2.

## Underwater vehicles

For vehicles operating at water depths below the wave-affected zone, the hydrodynamic coefficients will be independent of the wave excitation frequency. Consequently,

$$\mathbf{A}(\omega) = \text{constant} \quad \forall \omega \quad (6.16)$$

$$\mathbf{B}(\omega) = \mathbf{0} \quad (6.17)$$

This means that if a seakeeping code is used to compute the potential coefficients, only one frequency is needed to obtain an estimate of the added mass matrix. In addition, there will be no potential damping. However, viscous damping  $\mathbf{B}_V(\omega)$  will be present.

### 6.2.2 Extension to 6-DOF models

One limitation of Definition 6.1 is that it cannot be applied to *heave*, *roll* and *pitch*. These modes are second-order mass–damper–spring systems where the dominating frequencies are the natural frequencies. Hence, the constant frequency models in heave, roll and pitch should be formulated at their respective natural frequencies and not at the zero frequency.

The natural frequencies for the decoupled motions in heave, roll and pitch are given by the implicit equations

$$\omega_3 = \sqrt{\frac{C_{33}^{CF}}{m + A_{33}^{CF}(\omega_3)}} \quad (6.18)$$

$$\omega_4 = \sqrt{\frac{C_{44}^{CF}}{I_x^{CF} + A_{44}^{CF}(\omega_4)}} \quad (6.19)$$

$$\omega_5 = \sqrt{\frac{C_{55}^{CF}}{I_y^{CF} + A_{55}^{CF}(\omega_5)}} \quad (6.20)$$

where the potential coefficients  $A_{ii}(\omega)$  and  $B_{ii}(\omega)$  ( $i = 3, 4, 5$ ) are computed in the center of flotation (CF).

The potential coefficients  $\mathbf{A}(\omega)$  and  $\mathbf{B}(\omega)$  can be computed using a hydrodynamic code. If we rely on Definition 6.1 to approximate  $\mathbf{M}_A$  and  $\mathbf{D} = \mathbf{D}_P + \mathbf{D}_V$  in surge, sway and yaw it is necessary to assume that there are no couplings between the surge, heave–roll–pitch and the sway–yaw subsystems. Hence, added mass and

potential damping can be approximated by two constant matrices

$$\mathbf{M}_A \approx \begin{bmatrix} A_{11}(0) & 0 & & & & 0 \\ 0 & A_{22}(0) & & & & A_{26}(0) \\ & \dots & & \dots & & \dots \\ & & \boxed{A_{33}(\omega_3) & 0 & 0} & & \\ & & 0 & A_{44}(\omega_4) & 0 & \\ & & 0 & 0 & A_{55}(\omega_5) & \\ & 0 & A_{62}(0) & & \dots & A_{66}(0) \end{bmatrix} \quad (6.21)$$

$$\mathbf{D}_p \approx \begin{bmatrix} 0 & 0 & & & & 0 \\ 0 & 0 & & & & 0 \\ & \dots & & \dots & & \dots \\ & & \boxed{B_{33}(\omega_3) & 0 & 0} & & \\ & & 0 & B_{44}(\omega_4) & 0 & \\ & & 0 & 0 & B_{55}(\omega_5) & \\ & 0 & 0 & & \dots & 0 \end{bmatrix} \quad (6.22)$$

The natural frequencies  $\omega_3, \omega_4$  and  $\omega_5$  can be computed using the methods in Sections 4.3.1–4.3.2. The linear viscous damping terms are usually approximated by a diagonal matrix

$$\mathbf{D}_V \approx \text{diag}\{B_{11v}, B_{22v}, B_{33v}, B_{44v}, B_{55v}, B_{66v}\} \quad (6.23)$$

where the elements  $B_{iiv}$  ( $i = 1, \dots, 6$ ) can be computed using the methods in Section 5.3.2.

## 6.3 Added Mass Forces in a Rotating Coordinate System

In seakeeping theory, the body frame  $\{b\}$  rotates about  $\{s\}$ , which is assumed to be inertial. This results in two linear Coriolis and centripetal matrices  $\mathbf{C}_{RB}^*$  and  $\mathbf{C}_A^*$ . In maneuvering theory it is assumed that  $\{b\}$  rotates about the  $\{n\}$  as illustrated in Figure 6.2. This suggests that the linear terms  $\mathbf{C}_{RB}^*$  and  $\mathbf{C}_A^*$  can be replaced by their nonlinear counterparts  $\mathbf{C}_{RB}(\boldsymbol{\nu})$  and  $\mathbf{C}_A(\boldsymbol{\nu})$ , which gives

$$(\mathbf{M}_{RB} + \mathbf{M}_A)\dot{\boldsymbol{\nu}} + \mathbf{C}_{RB}(\boldsymbol{\nu})\boldsymbol{\nu} + \mathbf{C}_A(\boldsymbol{\nu})\boldsymbol{\nu} + \mathbf{D}\boldsymbol{\nu} = \boldsymbol{\tau}_{\text{wind}} + \boldsymbol{\tau}_{\text{wave}} + \boldsymbol{\tau} \quad (6.24)$$

The nonlinear Coriolis and centripetal matrix  $\mathbf{C}_{RB}(\boldsymbol{\nu})$  for a rigid-body is given by (6.7), while  $\mathbf{C}_A(\boldsymbol{\nu})$  depends on the added mass terms. This is in general a complicated function but it is straightforward to find the formulae by using Lagrangian mechanics.

### 6.3.1 Lagrangian mechanics

In Section 3.1, it was shown that the rigid-body kinetics of a marine craft can be derived by applying the *Newtonian* formulation. As for the rigid-body kinetics, it is advantageous to separate the added mass forces and moments in terms that belong to the *added mass matrix*  $\mathbf{M}_A$  and a matrix of hydrodynamic Coriolis and centripetal terms denoted

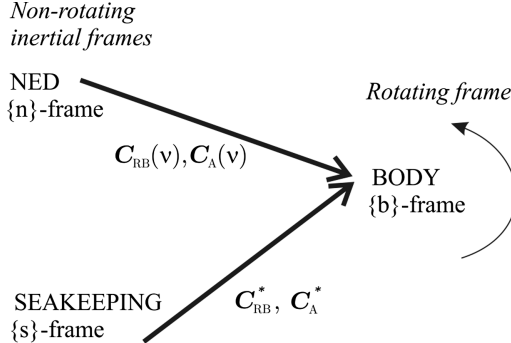


Figure 6.2: Coriolis matrices due to the rotation of the body-fixed frame  $\{b\}$  about the inertial frames  $\{n\}$  or  $\{s\}$ .

$C_A(\nu)$ . To derive the expressions for these two matrices, an *energy approach* based on Kirchhoff's equations will now be presented. Detailed discussions of Newtonian and Lagrangian mechanics are found in Goldstein (1980), Hughes (1986), Kane *et al.* (1983), Meirovitch (1990) and Egeland and Gravdahl (2002).

The Lagrangian  $L$  is formed by using kinetic energy  $T$  and potential energy  $V$ , according to

$$L = T - V \quad (6.25)$$

The *Euler–Lagrange equation* is

$$\frac{d}{dt} \left( \frac{\partial L}{\partial \dot{\eta}} \right) - \frac{\partial L}{\partial \eta} = J_{\Theta}^{-\top}(\eta) \tau \quad (6.26)$$

which in component form corresponds to a set of six second-order differential equations. From the above formula it is seen that the Lagrangian mechanics describes the system dynamics in terms of energy. Formula (6.26) is valid in any reference frame, inertial and body-fixed, as long as *generalized coordinates* are used.

For a marine craft not subject to any motion constraints, the number of independent (*generalized*) coordinates is equal to the number of DOF. For a marine craft moving in 6-DOF the generalized coordinates in  $\{n\}$  can be chosen as

$$\boldsymbol{\eta} = [x^n, y^n, z^n, \phi, \theta, \psi]^{\top} \quad (6.27)$$

It should be noted that the alternative representation

$$\boldsymbol{\eta} = [x^n, y^n, z^n, \eta, \varepsilon_1, \varepsilon_2, \varepsilon_3]^{\top} \quad (6.28)$$

using unit quaternions cannot be used in a Lagrangian approach since this representation is defined by seven parameters. Hence, these parameters are not *generalized coordinates*. It is not straightforward to formulate the equations of motion in  $\{b\}$  since

$$\boldsymbol{\nu} = [u, v, w, p, q, r]^{\top} \quad (6.29)$$

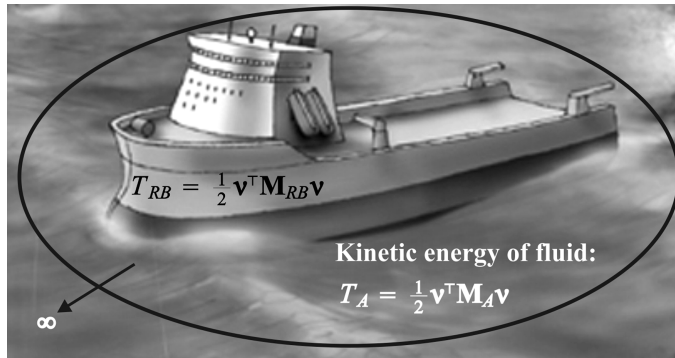


Figure 6.3: Rigid-body and fluid kinetic energy (ocean surrounding the ship). Illustration by Bjarne Stenberg.

*cannot* be integrated to yield a set of generalized coordinates in terms of position and orientation. In fact  $\int_0^t \nu d\tau$  has no immediate physical interpretation. Consequently, the Lagrange equation cannot be directly used to formulate the equations of motion in  $\{b\}$ . However, this problem is circumvented by applying Kirchhoff's equations of motion, or the so-called *quasi-Lagrangian* approach; see Meirowitch and Kwak (1989) for details.

### 6.3.2 Kirchhoff's equations in vector form

Consider a marine craft with linear velocity  $\nu_1 := [u, v, w]^\top$  and angular velocity  $\nu_2 := [p, q, r]^\top$  expressed in  $\{b\}$ . Hence, the force  $\tau_1 := [X, Y, Z]^\top$  and moment  $\tau_2 := [K, M, N]^\top$  are related to the kinetic energy (Kirchhoff 1869)

$$T = \frac{1}{2} \nu^\top M \nu \quad (6.30)$$

by the vector equations

$$\frac{d}{dt} \left( \frac{\partial T}{\partial \nu_1} \right) + S(\nu_2) \frac{\partial T}{\partial \nu_1} = \tau_1 \quad (6.31)$$

$$\frac{d}{dt} \left( \frac{\partial T}{\partial \nu_2} \right) + S(\nu_2) \frac{\partial T}{\partial \nu_2} + S(\nu_1) \frac{\partial T}{\partial \nu_1} = \tau_2 \quad (6.32)$$

where  $S$  is the skew-symmetric cross-product operator in Definition 2.2. *Kirchhoff's equations* will prove to be very useful in the derivation of the expression for added inertia. Notice that Kirchhoff's equations do not include the gravitational forces.

### 6.3.3 Added mass and Coriolis–centripetal matrices

The matrix  $C_A^*$  in (6.11) represents linearized forces due to a rotation of  $\{b\}$  about the seakeeping frame  $\{s\}$ . Instead of using  $\{s\}$  as the inertial frame, we will assume

that  $\{n\}$  is the inertial frame and that  $\{b\}$  rotates about  $\{n\}$ . The nonlinear Coriolis and centripetal matrix  $C_A(\nu)$  due to a rotation of  $\{b\}$  about the inertial frame  $\{n\}$  can be derived using an energy formulation based on the constant matrix  $M_A$ . Since any motion of the marine craft will induce a motion in the otherwise stationary fluid, the fluid must move aside and then close behind the craft in order to let the craft pass through the fluid. As a consequence, the fluid motion possesses kinetic energy that it would lack otherwise (see Figure 6.3). The expression for the fluid kinetic energy  $T_A$  is written as a quadratic form (Lamb 1932)

$$T_A = \frac{1}{2} \nu^\top M_A \nu, \quad \dot{M}_A = \mathbf{0} \quad (6.33)$$

where  $M_A = M_A^\top \geq 0$  is the  $6 \times 6$  system inertia matrix of added mass terms:

$$M_A = - \begin{bmatrix} X_{\dot{u}} & X_{\dot{v}} & X_{\dot{w}} & X_{\dot{p}} & X_{\dot{q}} & X_{\dot{r}} \\ Y_{\dot{u}} & Y_{\dot{v}} & Y_{\dot{w}} & Y_{\dot{p}} & Y_{\dot{q}} & Y_{\dot{r}} \\ Z_{\dot{u}} & Z_{\dot{v}} & Z_{\dot{w}} & Z_{\dot{p}} & Z_{\dot{q}} & Z_{\dot{r}} \\ K_{\dot{u}} & K_{\dot{v}} & K_{\dot{w}} & K_{\dot{p}} & K_{\dot{q}} & K_{\dot{r}} \\ M_{\dot{u}} & M_{\dot{v}} & M_{\dot{w}} & M_{\dot{p}} & M_{\dot{q}} & M_{\dot{r}} \\ N_{\dot{u}} & N_{\dot{v}} & N_{\dot{w}} & N_{\dot{p}} & N_{\dot{q}} & N_{\dot{r}} \end{bmatrix} \quad (6.34)$$

The notation of SNAME (1950) for the hydrodynamic derivatives is used in this expression; for instance the hydrodynamic added mass force  $Y$  along the  $y$  axis due to an acceleration  $\dot{u}$  in the  $x$  direction is written as

$$Y = -Y_{\dot{u}} \dot{u}, \quad Y_{\dot{u}} := \frac{\partial Y}{\partial \dot{u}} \quad (6.35)$$

This implies that  $\{M_A\}_{21} = -Y_{\dot{u}}$  in the example above.

#### **Property 6.1 (Hydrodynamic System Inertia Matrix $M_A$ )**

For a rigid body at rest or moving at forward speed  $U \geq 0$  in ideal fluid, the hydrodynamic system inertia matrix  $M_A$  is positive semidefinite

$$M_A = M_A^\top \geq 0$$

**Proof.** Newman (1977) has shown this for zero speed. The results extend to forward speed by using the approach presented in Chapter 5.

#### **Remark 6.1**

In a real fluid the 36 elements of  $M_A$  may all be distinct but still  $M_A \geq 0$ . Experience has shown that the numerical values of the added mass derivatives in a real fluid are usually in good agreement with those obtained from ideal theory (see Wendel 1956).

#### **Remark 6.2**

If experimental data are used, the inertia matrix can be symmetrized by using

$$M_A = \frac{1}{2} (M_{A,\text{exp}} + M_{A,\text{exp}}^\top) \quad (6.36)$$

where  $M_{A,\text{exp}}$  contains the experimentally data.

### Added mass forces and moments

Based on the kinetic energy  $T_A$  of the fluid, it is straightforward to derive the added mass forces and moments. Substituting (6.33) into (6.31)–(6.32) gives the following expressions for the added mass terms (Imlay 1961):

$$\begin{aligned}
 X_A &= X_{\dot{u}}\dot{u} + X_{\dot{w}}(\dot{w} + uq) + X_{\dot{q}}\dot{q} + Z_{\dot{w}}wq + Z_{\dot{q}}q^2 \\
 &\quad + X_{\dot{v}}\dot{v} + X_{\dot{p}}\dot{p} + X_{\dot{r}}\dot{r} - Y_{\dot{v}}vr - Y_{\dot{p}}rp - Y_{\dot{r}}r^2 \\
 &\quad - X_{\dot{v}}ur - Y_{\dot{w}}wr \\
 &\quad + Y_{\dot{w}}vq + Z_{\dot{p}}pq - (Y_{\dot{q}} - Z_{\dot{r}})qr \\
 Y_A &= X_{\dot{v}}\dot{u} + Y_{\dot{w}}\dot{w} + Y_{\dot{q}}\dot{q} \\
 &\quad + Y_{\dot{v}}\dot{v} + Y_{\dot{p}}\dot{p} + Y_{\dot{r}}\dot{r} + X_{\dot{v}}vr - Y_{\dot{w}}vp + X_{\dot{r}}r^2 + (X_{\dot{p}} - Z_{\dot{r}})rp - Z_{\dot{p}}p^2 \\
 &\quad - X_{\dot{w}}(up - wr) + X_{\dot{u}}ur - Z_{\dot{w}}wp \\
 &\quad - Z_{\dot{q}}pq + X_{\dot{q}}qr \\
 Z_A &= X_{\dot{w}}(\dot{u} - wq) + Z_{\dot{w}}\dot{w} + Z_{\dot{q}}\dot{q} - X_{\dot{u}}uq - X_{\dot{q}}q^2 \\
 &\quad + Y_{\dot{w}}\dot{v} + Z_{\dot{p}}\dot{p} + Z_{\dot{r}}\dot{r} + Y_{\dot{v}}vp + Y_{\dot{r}}rp + Y_{\dot{p}}p^2 \\
 &\quad + X_{\dot{v}}up + Y_{\dot{w}}wp \\
 &\quad - X_{\dot{v}}vq - (X_{\dot{p}} - Y_{\dot{q}})pq - X_{\dot{r}}qr \\
 K_A &= X_{\dot{p}}\dot{u} + Z_{\dot{p}}\dot{w} + K_{\dot{q}}\dot{q} - X_{\dot{v}}wu + X_{\dot{r}}uq - Y_{\dot{w}}w^2 - (Y_{\dot{q}} - Z_{\dot{r}})wq + M_{\dot{r}}q^2 \\
 &\quad + Y_{\dot{p}}\dot{v} + K_{\dot{p}}\dot{p} + K_{\dot{r}}\dot{r} + Y_{\dot{w}}v^2 - (Y_{\dot{q}} - Z_{\dot{r}})vr + Z_{\dot{p}}vp - M_{\dot{r}}r^2 - K_{\dot{q}}rp \\
 &\quad + X_{\dot{w}}uv - (Y_{\dot{v}} - Z_{\dot{w}})vw - (Y_{\dot{r}} + Z_{\dot{q}})wr - Y_{\dot{p}}wp - X_{\dot{q}}ur \\
 &\quad + (Y_{\dot{r}} + Z_{\dot{q}})vq + K_{\dot{r}}pq - (M_{\dot{q}} - N_{\dot{r}})qr \\
 M_A &= X_{\dot{q}}(\dot{u} + wq) + Z_{\dot{q}}(\dot{w} - uq) + M_{\dot{q}}\dot{q} - X_{\dot{w}}(u^2 - w^2) - (Z_{\dot{w}} - X_{\dot{u}})wu \\
 &\quad + Y_{\dot{q}}\dot{v} + K_{\dot{q}}\dot{p} + M_{\dot{r}}\dot{r} + Y_{\dot{p}}vr - Y_{\dot{r}}vp - K_{\dot{r}}(p^2 - r^2) + (K_{\dot{p}} - N_{\dot{r}})rp \\
 &\quad - Y_{\dot{w}}uv + X_{\dot{v}}vw - (X_{\dot{r}} + Z_{\dot{p}})(up - wr) + (X_{\dot{p}} - Z_{\dot{r}})(wp + ur) \\
 &\quad - M_{\dot{r}}pq + K_{\dot{q}}qr \\
 N_A &= X_{\dot{r}}\dot{u} + Z_{\dot{r}}\dot{w} + M_{\dot{r}}\dot{q} + X_{\dot{v}}u^2 + Y_{\dot{w}}wu - (X_{\dot{p}} - Y_{\dot{q}})uq - Z_{\dot{p}}wq - K_{\dot{q}}q^2 \\
 &\quad + Y_{\dot{r}}\dot{v} + K_{\dot{r}}\dot{p} + N_{\dot{r}}\dot{r} - X_{\dot{v}}v^2 - X_{\dot{r}}vr - (X_{\dot{p}} - Y_{\dot{q}})vp + M_{\dot{r}}rp + K_{\dot{q}}p^2 \\
 &\quad - (X_{\dot{u}} - Y_{\dot{v}})uv - X_{\dot{w}}vw + (X_{\dot{q}} + Y_{\dot{p}})up + Y_{\dot{r}}ur + Z_{\dot{q}}wp \\
 &\quad - (X_{\dot{q}} + Y_{\dot{p}})vq - (K_{\dot{p}} - M_{\dot{q}})pq - K_{\dot{r}}qr
 \end{aligned} \tag{6.37}$$

Imlay (1961) arranged the equations in four lines with longitudinal components on the first line and lateral components on the second. The third line consists of mixed terms involving  $u$  or  $w$  as one factor. If one or both of these velocities are large enough to be treated as constants, the third line may be treated as an additional term to the lateral equations of motion. The fourth line contains mixed terms that usually can be neglected as second-order terms.

It should be noted that the off-diagonal elements of  $M_A$  will be small compared to the diagonal elements for most practical applications. A more detailed discussion on the different added mass derivatives can be found in Humphreys and Watkinson (1978).

**Property 6.2 (Hydrodynamic Coriolis–Centripetal Matrix  $C_A(\nu)$ )**

For a rigid body moving through an ideal fluid the hydrodynamic Coriolis and centripetal matrix  $C_A(\nu)$  can always be parameterized such that it is skew-symmetric:

$$C_A(\nu) = -C_A^\top(\nu), \quad \forall \nu \in \mathbb{R}^6 \quad (6.38)$$

One parametrization satisfying (6.38) is

$$C_A(\nu) = \begin{bmatrix} \mathbf{0}_{3 \times 3} & -S(A_{11}\nu_1 + A_{12}\nu_2) \\ -S(A_{11}\nu_1 + A_{12}\nu_2) & -S(A_{21}\nu_1 + A_{22}\nu_2) \end{bmatrix} \quad (6.39)$$

where  $A_{ij} \in \mathbb{R}^{3 \times 3}$  is given by

$$M_A = \begin{bmatrix} A_{11} & A_{12} \\ A_{21} & A_{22} \end{bmatrix} \quad (6.40)$$

**Proof.** Substituting  $M_A$  for  $M$  in (3.48) in Theorem 3.2 directly proves (6.39).

Formula (6.39) can be written in component form according to

$$C_A(\nu) = \begin{bmatrix} 0 & 0 & 0 & 0 & -a_3 & a_2 \\ 0 & 0 & 0 & a_3 & 0 & -a_1 \\ 0 & 0 & 0 & -a_2 & a_1 & 0 \\ 0 & -a_3 & a_2 & 0 & -b_3 & b_2 \\ a_3 & 0 & -a_1 & b_3 & 0 & -b_1 \\ -a_2 & a_1 & 0 & -b_2 & b_1 & 0 \end{bmatrix} \quad (6.41)$$

where

$$\begin{aligned} a_1 &= X_{\dot{u}}u + X_{\dot{v}}v + X_{\dot{w}}w + X_{\dot{p}}p + X_{\dot{q}}q + X_{\dot{r}}r \\ a_2 &= Y_{\dot{u}}u + Y_{\dot{v}}v + Y_{\dot{w}}w + Y_{\dot{p}}p + Y_{\dot{q}}q + Y_{\dot{r}}r \\ a_3 &= Z_{\dot{u}}u + Z_{\dot{v}}v + Z_{\dot{w}}w + Z_{\dot{p}}p + Z_{\dot{q}}q + Z_{\dot{r}}r \\ b_1 &= K_{\dot{u}}u + K_{\dot{v}}v + K_{\dot{w}}w + K_{\dot{p}}p + K_{\dot{q}}q + K_{\dot{r}}r \\ b_2 &= M_{\dot{u}}u + M_{\dot{v}}v + M_{\dot{w}}w + M_{\dot{p}}p + M_{\dot{q}}q + M_{\dot{r}}r \\ b_3 &= N_{\dot{u}}u + N_{\dot{v}}v + N_{\dot{w}}w + N_{\dot{p}}p + N_{\dot{q}}q + N_{\dot{r}}r \end{aligned} \quad (6.42)$$

Properties 6.2 and 10.1 imply that the marine craft dynamics can be represented in terms of nonlinear Coriolis and centripetal forces using relative velocity:

$$M\dot{\nu}_r + C(\nu_r)\nu_r + D(\nu_r)\nu_r + g(\eta) = \tau + \tau_{\text{wind}} + \tau_{\text{wave}} \quad (6.43)$$

where

$$M = M_{RB} + M_A \quad (6.44)$$

$$C(\nu_r) = C_{RB}(\nu_r) + C_A(\nu_r) \quad (6.45)$$

while classical seakeeping theory uses linear matrices  $C_{RB}^*$  and  $C_A^*$  as explained in Section 6.2.

**Example 6.1 (Added Mass for Surface Vessels)**

For surface ships such as tankers, cargo ships and cruise-liners it is common to decouple the surge mode from the steering dynamics due to  $xz$ -plane symmetry. Similarly, the heave, pitch, and roll modes are neglected under the assumption that these motion variables are small. Hence,  $\boldsymbol{\nu}_r = [u_r, v_r, r]^\top$  implies that the added mass derivatives for a surface ship are

$$\mathbf{M}_A = \mathbf{M}_A^\top = - \begin{bmatrix} X_{\dot{u}} & 0 & 0 \\ 0 & Y_{\dot{v}} & Y_{\dot{r}} \\ 0 & Y_{\dot{r}} & N_{\dot{r}} \end{bmatrix} \quad (N_{\dot{v}} = Y_{\dot{r}}) \quad (6.46)$$

$$\mathbf{C}_A(\boldsymbol{\nu}_r) = -\mathbf{C}_A^\top(\boldsymbol{\nu}_r) = \begin{bmatrix} 0 & 0 & Y_{\dot{v}}v_r + Y_{\dot{r}}r \\ 0 & 0 & -X_{\dot{u}}u_r \\ -Y_{\dot{v}}v_r - Y_{\dot{r}}r & X_{\dot{u}}u_r & 0 \end{bmatrix} \quad (6.47)$$

The Coriolis and centripetal forces are recognized as

$$\mathbf{C}_A(\boldsymbol{\nu}_r)\boldsymbol{\nu}_r = \begin{bmatrix} Y_{\dot{v}}v_r r + Y_{\dot{r}}r^2 \\ -X_{\dot{u}}u_r r \\ \underbrace{(X_{\dot{u}} - Y_{\dot{v}})u_r v_r}_{\text{Munk moment}} - Y_{\dot{r}}u_r r \end{bmatrix} \quad (6.48)$$

where the first term in the yaw moment is the nonlinear Munk moment, which is known to have destabilizing effects.

**Example 6.2 (Added Mass for Underwater Vehicles)**

In general, the motion of an underwater vehicle moving in 6 DOF at high speed will be highly nonlinear and coupled. However, in many AUV and ROV applications the vehicle will only be allowed to move at low speed. If the vehicle also has three planes of symmetry, this suggests that the contribution from the off-diagonal elements in the matrix  $\mathbf{M}_A$  can be neglected. Hence, the following simple expressions for the matrices  $\mathbf{M}_A$  and  $\mathbf{C}_A$  are obtained:

$$\mathbf{M}_A = \mathbf{M}_A^\top = -\text{diag}\{X_{\dot{u}}, Y_{\dot{v}}, Z_{\dot{w}}, K_{\dot{p}}, M_{\dot{q}}, N_{\dot{r}}\} \quad (6.49)$$

$$\mathbf{C}_A(\boldsymbol{\nu}_r) = -\mathbf{C}_A^\top(\boldsymbol{\nu}_r) = \begin{bmatrix} 0 & 0 & 0 & 0 & -Z_{\dot{w}}w_r & Y_{\dot{v}}v_r \\ 0 & 0 & 0 & Z_{\dot{w}}w_r & 0 & -X_{\dot{u}}u_r \\ 0 & 0 & 0 & -Y_{\dot{v}}v_r & X_{\dot{u}}u_r & 0 \\ 0 & -Z_{\dot{w}}w_r & Y_{\dot{v}}v_r & 0 & -N_{\dot{r}}r & M_{\dot{q}}q \\ Z_{\dot{w}}w_r & 0 & -X_{\dot{u}}u_r & N_{\dot{r}}r & 0 & -K_{\dot{p}}p \\ -Y_{\dot{v}}v_r & X_{\dot{u}}u_r & 0 & -M_{\dot{q}}q & K_{\dot{p}}p & 0 \end{bmatrix} \quad (6.50)$$

The diagonal structure is often used since it is time consuming to determine the off-diagonal elements from experiments as well as theory. In practice, the diagonal approximation is found to be quite good for many applications. This is due to the fact that the off-diagonal elements of a positive inertia matrix will be much smaller than their diagonal counterparts.

## 6.4 Dissipative Forces

Hydrodynamic damping for marine craft is mainly caused by:

**Potential Damping:** We recall from the beginning of Section 6.2 that *added mass*, *damping* and *restoring* forces and moments are encountered when a body is forced to oscillate with the wave excitation frequency in the absence of incident waves. The radiation-induced damping term is usually referred to as *linear frequency-dependent potential damping*  $\mathbf{B}(\omega)$ .

**Skin Friction:** Linear frequency-dependent skin friction  $\mathbf{B}_v(\omega)$  due to laminar boundary layer theory is important when considering the low-frequency motion of marine craft (Faltinsen and Sortland 1987). In addition to linear skin friction, there will be a high-frequency contribution due to a turbulent boundary layer. This is usually referred to as a quadratic or nonlinear skin friction.

**Wave Drift Damping:** Wave drift damping can be interpreted as added resistance for surface vessels advancing in waves. This type of damping is derived from second-order wave theory. Wave drift damping is the most important damping contribution to surge for higher sea states. This is due to the fact that the wave drift forces are proportional to the square of the significant wave height  $H_s$ . Wave drift damping in sway and yaw is small relative to eddy-making damping (vortex shedding). A rule of thumb is that second-order wave drift forces are less than 1 % of the first-order wave forces when the significant wave height is equal to 1 m and 10 % when the significant wave height is equal to 10 m.

**Damping Due to Vortex Shedding:** *D'Alambert's paradox* states that no hydrodynamic forces act on a solid moving completely submerged with constant velocity in a nonviscous fluid. In a viscous fluid, frictional forces are present such that the system is not conservative with respect to energy. This is commonly referred to as *interference drag*. It arises due to the shedding of vortex sheets at sharp edges. The viscous damping force due to vortex shedding can be modeled as

$$f(u) = -\frac{1}{2} \rho C_D(R_n) A|u|u \quad (6.51)$$

where  $u$  is the velocity of the craft,  $A$  is the projected cross-sectional area under water,  $C_D(R_n)$  is the drag coefficient based on the representative area and  $\rho$  is the water density. This expression is recognized as one of the terms in *Morison's equation* (see Faltinsen 1990). The drag coefficient  $C_D(R_n)$  is a function of the *Reynolds number*  $R_n = uD/\nu$  where  $D$  is the characteristic length of the body and  $\nu$  is the kinematic viscosity coefficient ( $\nu = 1.56 \times 10^{-6}$  for salt water at 5 °C with salinity 3.5 %).

**Lifting Forces:** Hydrodynamic lift forces arise from two physical mechanisms. The first is due to the linear circulation of water around the hull. The second is a nonlinear effect, commonly called cross-flow drag, which acts from a momentum transfer from the body to the fluid. This secondary effect is closely linked to vortex shedding.

The different damping terms contribute to both linear and quadratic damping. However, it is in general difficult to separate these effects. In many cases, it is convenient to write total hydrodynamic damping as

$$\mathbf{D}(\boldsymbol{\nu}_r) = \mathbf{D} + \mathbf{D}_n(\boldsymbol{\nu}_r) \quad (6.52)$$

where  $\mathbf{D}$  is the *linear damping matrix* due to potential damping and possible skin friction and  $\mathbf{D}_n(\boldsymbol{\nu}_r)$  is the *nonlinear damping matrix* due to quadratic damping and higher-order terms. Hydrodynamic damping satisfies the following dissipative property:

**Property 6.3 (Hydrodynamic Damping Matrix  $\mathbf{D}(\boldsymbol{\nu}_r)$ )**

For a rigid body moving through an ideal fluid the hydrodynamic damping matrix,

$$\mathbf{D}(\boldsymbol{\nu}_r) = \frac{1}{2} [\mathbf{D}(\boldsymbol{\nu}_r) + \mathbf{D}(\boldsymbol{\nu}_r)^\top] + \frac{1}{2} [\mathbf{D}(\boldsymbol{\nu}_r) - \mathbf{D}(\boldsymbol{\nu}_r)^\top] \quad (6.53)$$

will be real, nonsymmetric and strictly positive

$$\mathbf{D}(\boldsymbol{\nu}_r) > 0, \quad \forall \boldsymbol{\nu} \in \mathbb{R}^6 \quad (6.54)$$

or

$$\mathbf{x}^\top \mathbf{D}(\boldsymbol{\nu}_r) \mathbf{x} = \frac{1}{2} \mathbf{x}^\top [\mathbf{D}(\boldsymbol{\nu}_r) + \mathbf{D}(\boldsymbol{\nu}_r)^\top] \mathbf{x} > 0 \quad \forall \mathbf{x} \neq \mathbf{0} \quad (6.55)$$

Some of the damping terms can be determined by using well-established methods from the literature and experimental techniques.

### 6.4.1 Linear viscous damping

For surface ships such as tankers, cargo ships and cruise-liners it is common to decouple the surge mode from the steering dynamics due to  $xz$ -plane symmetry. Hence, the linear damping matrix in CO with decoupled surge dynamics can be written

$$\begin{aligned} \mathbf{D} &= \mathbf{D}_P + \mathbf{D}_V \\ &= - \begin{bmatrix} X_u & 0 & 0 & 0 & 0 & 0 \\ 0 & Y_v & 0 & Y_p & 0 & Y_r \\ 0 & 0 & Z_w & 0 & Z_q & 0 \\ 0 & K_v & 0 & K_p & 0 & K_r \\ 0 & 0 & M_w & 0 & M_q & 0 \\ 0 & N_v & 0 & N_p & 0 & N_r \end{bmatrix} \end{aligned} \quad (6.56)$$

**Example 6.3 (Linear Damping for Surface Vessels)**

In maneuvering theory, the heave, pitch, and roll modes are neglected under the assumption that these motion variables are small. Hence, the linear damping matrix for a surface vessel becomes

$$\mathbf{D} = - \begin{bmatrix} X_u & 0 & 0 \\ 0 & Y_v & Y_r \\ 0 & N_v & N_r \end{bmatrix} \quad (6.57)$$

The diagonal terms relate to seakeeping theory according to

$$-X_u = B_{11v}(0) \quad (6.58)$$

$$-Y_v = B_{22v}(0) \quad (6.59)$$

$$-N_r = B_{66v}(0) \quad (6.60)$$

where the expressions for  $B_{iiv}$  ( $i = 1, 2, 6$ ) are given by (5.60).

#### **Example 6.4 (Linear Damping for Underwater Vehicles)**

In general, the motion of an underwater vehicle moving in 6 DOF at high speed will be highly nonlinear and coupled. However, in many AUV and ROV applications the vehicle will only be allowed to move at low speed. If the vehicle also has three planes of symmetry, this suggests that the contribution from the off-diagonal elements in the matrix  $\mathbf{D}$  can be neglected. Consequently,

$$\mathbf{D} = -\text{diag}\{X_u, Y_v, Z_w, K_p, M_q, N_r\} \quad (6.61)$$

The diagonal structure is often used since it is time consuming to determine the off-diagonal elements from experiments as well as theory.

For heave, roll and pitch it is common to approximate

$$-Z_w = B_{33v}(\omega_3) \quad (6.62)$$

$$-K_p = B_{44v}(\omega_4) \quad (6.63)$$

$$-M_q = B_{55v}(\omega_5) \quad (6.64)$$

using (5.60) or by specifying the relative damping ratios  $\zeta_3$ ,  $\zeta_4$  and  $\zeta_5$  in the formula

$$D_{ii} = 2\zeta_i \omega_i M_{ii} \quad (6.65)$$

for  $i = 3, 4, 5$ . Here  $M_{ii}$  denotes the sum of rigid-body and hydrodynamic added mass while  $\omega_i$  are given by (6.18)–(6.20).

#### **6.4.2 Nonlinear surge damping**

In surge, the viscous damping for ships may be modeled as (Lewis 1989)

$$X = -\frac{1}{2}\rho S(1+k)C_f(u_r)|u_r|u_r \quad (6.66)$$

$$C_f(u_r) = \underbrace{\frac{0.075}{(\log_{10}(R_n) - 2)^2}}_{C_F} + C_R \quad (6.67)$$

where  $\rho$  is the density of water,  $S$  is the wetted surface of the hull,

$$\begin{aligned} u_r &= u - u_c \\ &= u - V_c \cos(\beta_c - \psi) \end{aligned} \quad (6.68)$$

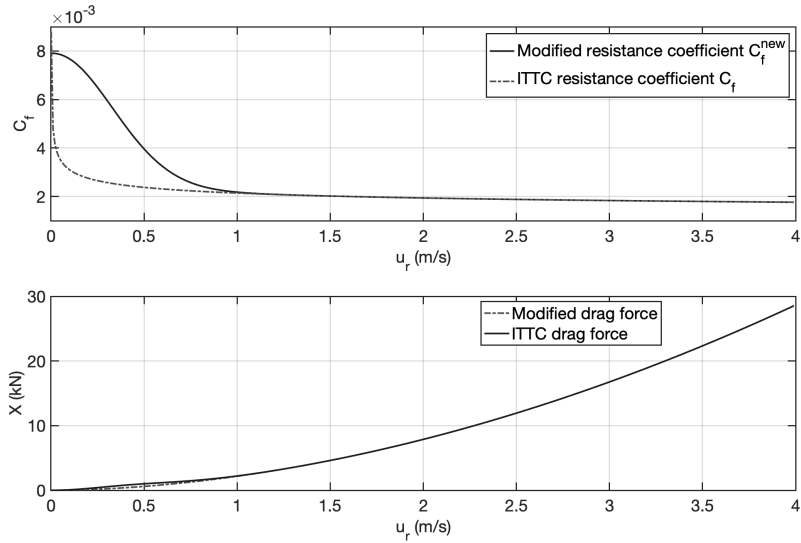


Figure 6.4: Modified resistance curve  $C_f^{\text{new}}(u_r)$  and  $C_f(u_r)$  as a function of  $u_r$  when  $C_R = 0$  and  $\sigma(u_r) = e^{-5u_r^2}$ . Here  $C_f^{\text{new}}(0) = -(A_{F_c}/S(1+k))C_X(0) = 0.008$  where  $C_X(0) = -0.16$  is the current coefficient.

is the relative surge velocity (see Section 10.3),  $k$  is the form factor giving a viscous correction,  $C_F$  is the flat plate friction from the ITTC 1957 line and  $C_R$  represents *residual friction* due to hull roughness, pressure resistance, wave-making resistance and wave-breaking resistance. For ships in transit  $k$  is typically 0.1 whereas this value is much higher in DP, typically  $k = 0.25$  (Hoerner 1965). The friction coefficient  $C_F$  depends on the *Reynolds number*

$$R_n = \frac{L_{pp}}{\nu} |u_r| \geq 0 \quad (6.69)$$

where  $\nu = 1 \times 10^{-6} \text{ m/s}^2$  is the *kinematic viscosity* at 20 °C. Notice that the Reynolds number is nonnegative since it is independent of the flow direction. From a numerical point of view, the denominator of  $C_F$  should be replaced with,  $(\log_{10}(R_n) - 2)^2 + \epsilon$ , where  $\epsilon$  is a small number to ensure that (6.66)–(6.67) are well defined at  $u_r = 0$ .

The damping model in surge can also be expressed in terms of the hydrodynamic derivative  $X_{|u|u}$  since

$$X = X_{|u|u} |u_r| u_r \quad (6.70)$$

$$X_{|u|u} = -\frac{1}{2} \rho S(1+k) C_f(u_r) < 0 \quad (6.71)$$

### Low-speed calibration

For DP applications (low-speed maneuvering), the ITTC formulae (6.66)–(6.67) give too little damping compared to what is observed in a wind tunnel experiment with a scale model. For a ship at zero speed, the current force is (see Section 6.7.1)

$$X = \frac{1}{2} \rho A_{F_c} C_X(\gamma_c) V_c^2 \quad (6.72)$$

where  $V_c$  and  $\gamma_c$  are the current speed and angle of attack, respectively. The frontal projected current area is denoted  $A_{F_c}$  while  $\rho$  is the density of water. The current coefficient  $C_X(\gamma_c)$  is shown in Figure 6.11. Assume that the ship is facing the current such that  $\gamma_c = 0$  and  $u_c = -V_c$ . Formulae (6.70)–(6.71) with  $u_r = 0 - u_c = V_c$  can be rewritten as

$$X = -\frac{1}{2} \rho S(1+k) C_f(u_r) V_c^2 \quad (6.73)$$

Comparing Formula (6.73) with (6.72) at  $u_r = 0$  gives

$$C_f(0) = -\frac{A_{F_c}}{S(1+k)} C_X(0) \quad (6.74)$$

where  $C_X(0) < 0$  as shown in Figure 6.11. Hence, one way to obtain sufficient damping at low speed is to modify the resistance curve  $C_f(u_r)$  according to

$$C_f^{\text{new}}(u_r) = (1 - \sigma(u_r)) C_f(u_r) + \sigma(u_r) \left( -\frac{A_{F_c}}{S(1+k)} C_X(0) \right) \quad (6.75)$$

where  $\sigma(u_r)$  is a blending function

$$\sigma(u_r) = e^{-\alpha u_r^2} \quad (6.76)$$

with  $\alpha > 0$  (typically 5.0). The modified resistance curve  $C_f^{\text{new}}(u_r)$  is plotted together with  $C_f(u_r)$  in Figure 6.4. Notice that the resistance curve is increased at lower velocities due to the contribution of the current coefficient  $C_X(0)$ . The second plot shows the current force for the original and modified resistance curves. Notice that the effect of the current coefficient vanishes at higher speeds thanks to the exponentially decaying weight  $e^{-\alpha u_r^2}$ .

### 6.4.3 Cross-flow drag principle

For relative current angles  $|\beta_c - \psi| \gg 0$ , where  $\beta_c$  is the current direction, the cross-flow drag principle may be applied to calculate the nonlinear damping force in sway and the yaw moment (Faltinsen 1990)

$$Y = -\frac{1}{2} \rho \int_{-\frac{L_{pp}}{2}}^{\frac{L_{pp}}{2}} T(x) C_d^{2D}(x) |v_r + xr| (v_r + xr) dx \quad (6.77)$$

$$N = -\frac{1}{2} \rho \int_{-\frac{L_{pp}}{2}}^{\frac{L_{pp}}{2}} T(x) C_d^{2D}(x) x |v_r + xr| (v_r + xr) dx \quad (6.78)$$

where  $C_d^{2D}(x)$  is the 2-D drag coefficient,  $T(x)$  is the draft and

$$\begin{aligned} v_r &= v - v_c \\ &= v - V_c \sin(\beta_c - \psi) \end{aligned} \quad (6.79)$$

is the relative sway velocity (see Section 10.3). This is a strip theory approach where each hull section contributes to the integral. Drag coefficients for different hull forms are found in Hooft (1994). A constant 2-D current coefficient can also be estimated using Hoerner's curve (see Figure 6.5).

#### Matlab:

The 2-D drag coefficients  $C_d^{2D}$  can be computed as a function of beam  $B$  and length  $T$  using Hoerner's curve. This is implemented in the Matlab MSS toolbox as

```
Cd = Hoerner(B, T)
```

A 3-D representation of (6.77)–(6.78) eliminating the integrals can be found by curve fitting formula (6.77) and (6.78) to *second-order modulus terms* to obtain a maneuvering model similar to that of Fedyaevsky and Sobolev (1963)

$$Y = Y_{|v|v}|v_r|v_r + Y_{|v|r}|v_r|r + Y_{|v|r}|v_r|r + Y_{|r|r}|r|r \quad (6.80)$$

$$N = N_{|v|v}|v_r|v_r + N_{|v|r}|v_r|r + N_{|v|r}|v_r|r + N_{|r|r}|r|r \quad (6.81)$$

where  $Y_{|v|v}, Y_{|v|r}, Y_{|v|r}|r|r, N_{|v|v}, N_{|v|r}, N_{|v|r}|r|r$ , and  $N_{|r|r}|r|r$  are maneuvering coefficients defined using the SNAME notation. In the next section, this approach will be used to derive maneuvering models in 3 DOF.

## 6.5 Ship Maneuvering Models (3 DOF)

This section summarizes the linear and nonlinear maneuvering equations using the results in Sections 6.1–6.4.

#### Matlab:

Several MSS maneuvering models are located under the toolbox catalog MSS/VESSELS:

```
[xdot,U] = container(x,tau)    % Container ship L = 175 m
[xdot,U] = Lcontainer(x,tau)   % Linearized container ship
[xdot,U] = mariner(x,ui,U0)    % Mariner class vessel L = 161 m
[xdot,U] = navalvessel(x,tau)  % Naval vessel L = 51.5 m
[xdot,U] = tanker(x,ui)        % Tanker L = 304.8 m
```

The models can be simulated under feedback control using the user editable scripts

```
Sim<model name>.m
```

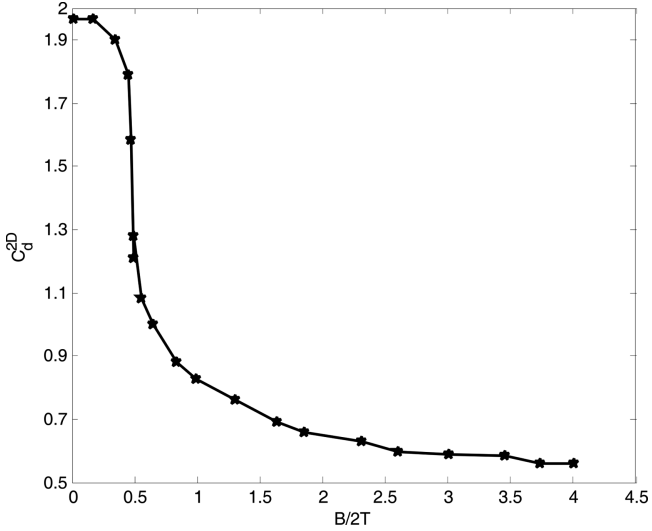


Figure 6.5: 2-D cross-flow coefficient  $C_d^{2D}$  as a function of  $B/2T$  (Hoerner, 1965).

### 6.5.1 Nonlinear equations of motion

The matrix-vector representation for a surface vessel with generalized position vector  $\boldsymbol{\eta} = [x^n, y^n, \psi]^\top$  and velocity vector  $\boldsymbol{\nu} = [u, v, r]^\top$  is

$$\dot{\boldsymbol{\eta}} = \mathbf{R}(\psi)\boldsymbol{\nu} \quad (6.82)$$

$$\underbrace{\mathbf{M}_{RB}\dot{\boldsymbol{\nu}} + \mathbf{C}_{RB}(\boldsymbol{\nu})\boldsymbol{\nu} + \mathbf{M}_A\dot{\boldsymbol{\nu}}_r + \mathbf{N}(\boldsymbol{\nu}_r)\boldsymbol{\nu}_r}_{\text{rigid-body forces}} = \boldsymbol{\tau} + \boldsymbol{\tau}_{\text{wind}} + \boldsymbol{\tau}_{\text{wave}} \quad (6.83)$$

where  $\boldsymbol{\nu}_r = \boldsymbol{\nu} - \boldsymbol{\nu}_c$  is the relative velocity vector,  $\boldsymbol{\nu}_c = [u_c, v_c, 0]^\top$  is the current velocity vector and

$$\mathbf{N}(\boldsymbol{\nu}_r) := \mathbf{C}_A(\boldsymbol{\nu}_r) + \mathbf{D} + \mathbf{D}_n(\boldsymbol{\nu}_r) \quad (6.84)$$

Moreover, added mass Coriolis and centripetal terms together with hydrodynamic damping terms are collected into the matrix  $\mathbf{N}(\boldsymbol{\nu}_r)$ . This is convenient since it is difficult to distinguish terms in  $\mathbf{C}_A(\boldsymbol{\nu}_r)$  with similar terms in  $\mathbf{D}_n(\boldsymbol{\nu}_r)$ . Hence, only the sum of these terms is used in the model in order to avoid overparametrization.

The model matrices are

$$\mathbf{R}(\psi) = \begin{bmatrix} \cos(\psi) & -\sin(\psi) & 0 \\ \sin(\psi) & \cos(\psi) & 0 \\ 0 & 0 & 1 \end{bmatrix} \quad (6.85)$$

$$\mathbf{M}_{RB} = \begin{bmatrix} m & 0 & 0 \\ 0 & m & mx_g \\ 0 & mx_g & I_z \end{bmatrix} \quad (6.86)$$

$$\mathbf{C}_{RB}(\boldsymbol{\nu}) = \begin{bmatrix} 0 & -mr & -mx_gr \\ mr & 0 & 0 \\ mx_gr & 0 & 0 \end{bmatrix} \quad (6.87)$$

$$\mathbf{M}_A = - \begin{bmatrix} X_{\dot{u}} & 0 & 0 \\ 0 & Y_{\dot{v}} & Y_{\dot{r}} \\ 0 & N_{\dot{v}} & N_{\dot{r}} \end{bmatrix} = \begin{bmatrix} A_{11}(0) & 0 & 0 \\ 0 & A_{22}(0) & A_{26}(0) \\ 0 & A_{26}(0) & A_{66}(0) \end{bmatrix} \quad (6.88)$$

$$\begin{aligned} \mathbf{C}_A(\boldsymbol{\nu}_r) &= \begin{bmatrix} 0 & 0 & Y_{\dot{v}}v_r + Y_{\dot{r}}r \\ 0 & 0 & -X_{\dot{u}}u_r \\ -Y_{\dot{v}}v_r - Y_{\dot{r}}r & X_{\dot{u}}u_r & 0 \end{bmatrix} \\ &= \begin{bmatrix} 0 & 0 & -A_{22}(0)v_r - A_{26}(0)r \\ 0 & 0 & A_{11}(0)u_r \\ A_{22}(0)v_r + A_{26}(0)r & -A_{11}(0)u_r & 0 \end{bmatrix} \end{aligned} \quad (6.89)$$

$$\mathbf{D} = - \begin{bmatrix} X_u & 0 & 0 \\ 0 & Y_v & Y_r \\ 0 & N_v & N_r \end{bmatrix} \approx \begin{bmatrix} B_{11v}(0) & 0 & 0 \\ 0 & B_{22v}(0) & 0 \\ 0 & 0 & B_{66v}(0) \end{bmatrix} \quad (6.90)$$

$$\mathbf{D}_n(\boldsymbol{\nu}_r) = - \begin{bmatrix} X_{|u|u}|u_r| & 0 & 0 \\ 0 & Y_{|v|v}|v_r| + Y_{|r|r}|r| & Y_{|v|r}|v_r| + Y_{|r|r}|r| \\ 0 & N_{|v|v}|v_r| + N_{|r|r}|r| & N_{|v|r}|v_r| + N_{|r|r}|r| \end{bmatrix} \quad (6.91)$$

In the case of ocean currents it is possible to express (6.83) using only the relative velocity vector  $\boldsymbol{\nu}_r$  and thus avoiding terms in  $\boldsymbol{\nu}$ . Since  $\mathbf{C}_{RB}(\boldsymbol{\nu})$  is parametrized independent of linear velocity it follows from Property 10.1 in Section 10.3 that (6.83) can be rewritten as

$$\mathbf{M}\dot{\boldsymbol{\nu}}_r + \underbrace{\mathbf{C}(\boldsymbol{\nu}_r)\boldsymbol{\nu}_r + \mathbf{D}\boldsymbol{\nu}_r + \mathbf{D}_n(\boldsymbol{\nu}_r)\boldsymbol{\nu}_r}_{\mathbf{N}(\boldsymbol{\nu}_r)\boldsymbol{\nu}_r} = \boldsymbol{\tau} + \boldsymbol{\tau}_{\text{wind}} + \boldsymbol{\tau}_{\text{wave}} \quad (6.92)$$

where

$$\mathbf{M} = \mathbf{M}_A + \mathbf{M}_{RB} \quad (6.93)$$

$$\mathbf{C}(\boldsymbol{\nu}_r) = \mathbf{C}_A(\boldsymbol{\nu}_r) + \mathbf{C}_{RB}(\boldsymbol{\nu}_r) \quad (6.94)$$

In this representation the generalized velocity  $\boldsymbol{\nu}_r$  is the only velocity vector while (6.83) uses both  $\boldsymbol{\nu}$  and  $\boldsymbol{\nu}_r$ .



Figure 6.6: Displacement vessel where the horizontal plane model can be used for DP and maneuvering.

### State-space model including ocean currents

For an ocean current with constant speed  $V_c$  and direction  $\beta_c$  the components of the ocean current velocity vector  $\nu_c = [u_c, v_c, 0]^\top$  are computed as (see Section 10.3)

$$u_c = V_c \cos(\beta_c - \psi) \quad (6.95)$$

$$v_c = V_c \sin(\beta_c - \psi) \quad (6.96)$$

Time differentiation of  $u_c$  and  $v_c$  gives the accelerations

$$\dot{u}_c = rV_c \sin(\beta_c - \psi) = rv_c \quad (6.97)$$

$$\dot{v}_c = -rV_c \cos(\beta_c - \psi) = -ru_c \quad (6.98)$$

The state-space model for (6.94) in terms of generalized position and relative velocity becomes (Fossen 2012)

$$\dot{\eta} = \mathbf{R}(\psi) \left( \nu_r + \begin{bmatrix} u_c \\ v_c \\ 0 \end{bmatrix} \right) \quad (6.99)$$

$$\dot{\nu}_r = \mathbf{M}^{-1} (\boldsymbol{\tau} + \boldsymbol{\tau}_{\text{wind}} + \boldsymbol{\tau}_{\text{wave}} - \mathbf{C}(\nu_r)\nu_r - \mathbf{D}\nu_r - \mathbf{D}_n(\nu_r)\nu_r) \quad (6.100)$$

Alternatively, the state-space model can be expressed using absolute velocities

$$\dot{\boldsymbol{\eta}} = \mathbf{R}(\psi)\boldsymbol{\nu} \quad (6.101)$$

$$\dot{\boldsymbol{\nu}} = \begin{bmatrix} rv_c \\ -ru_c \\ 0 \end{bmatrix} + \mathbf{M}^{-1} (\boldsymbol{\tau} + \boldsymbol{\tau}_{\text{wind}} + \boldsymbol{\tau}_{\text{wave}} - \mathbf{C}(\boldsymbol{\nu}_r)\boldsymbol{\nu}_r - \mathbf{D}\boldsymbol{\nu}_r - \mathbf{D}_n(\boldsymbol{\nu}_r)\boldsymbol{\nu}_r) \quad (6.102)$$

where  $\boldsymbol{\nu}_r = \boldsymbol{\nu} - [u_c, v_c, 0]^\top$ .

### 6.5.2 Nonlinear maneuvering model based on surge resistance and cross-flow drag

If we use the surge resistance and cross-flow drag models in Section 6.4, the  $\mathbf{N}(\boldsymbol{\nu}_r)$  matrix in the maneuvering model (6.84) can be redefined according to

$$\mathbf{N}(\boldsymbol{\nu}_r)\boldsymbol{\nu}_r = \mathbf{C}_A(\boldsymbol{\nu}_r)\boldsymbol{\nu}_r + \mathbf{D}\boldsymbol{\nu}_r + \mathbf{d}(\boldsymbol{\nu}_r) \quad (6.103)$$

where

$$\mathbf{C}_A(\boldsymbol{\nu}_r) = \begin{bmatrix} 0 & 0 & Y_{\dot{v}}v_r + Y_{\dot{r}}r \\ 0 & 0 & -X_{\dot{u}}u_r \\ -Y_{\dot{v}}v_r - Y_{\dot{r}}r & X_{\dot{u}}u_r & 0 \end{bmatrix} \quad (6.104)$$

$$\mathbf{D} = \begin{bmatrix} -X_u & 0 & 0 \\ 0 & -Y_v & -Y_r \\ 0 & -N_v & -N_r \end{bmatrix} \quad (6.105)$$

$$\mathbf{d}(\boldsymbol{\nu}_r) = \begin{bmatrix} \frac{1}{2}\rho S(1+k)C_f^{\text{new}}(u_r)|u_r|u_r \\ \frac{1}{2}\rho \int_{-L_{pp}/2}^{L_{pp}/2} T(x)C_d^{2D}(x)|v_r+xr|(v_r+xr) dx \\ \frac{1}{2}\rho \int_{-L_{pp}/2}^{L_{pp}/2} T(x)C_d^{2D}(x)x|v_r+xr|(v_r+xr) dx \end{bmatrix} \quad (6.106)$$

The linear damper  $\mathbf{D}$  in this expression is important for low-speed maneuvering and stationkeeping while the term  $\mathbf{d}(\boldsymbol{\nu}_r)$  dominates at higher speeds. Linear damping also guarantees that the velocity converges exponentially to zero.

### 6.5.3 Nonlinear maneuvering model based on second-order modulus functions

The idea of using second-order *modulus functions* to describe the nonlinear dissipative terms in  $\mathbf{N}(\boldsymbol{\nu}_r)$  dates back to Fedyaevsky and Sobolev (1963). Within this framework, a simplified form of Norrbin's nonlinear model (Norrbin 1970), which retains the most important terms for steering and propulsion loss assignment, has been proposed by

Blanke (1981). This model corresponds to fitting the cross-flow drag integrals (6.77) and (6.78) to second-order modulus functions:<sup>1</sup>

$$\begin{aligned} \mathbf{N}(\boldsymbol{\nu}_r)\boldsymbol{\nu}_r &= \mathbf{C}_A(\boldsymbol{\nu}_r)\boldsymbol{\nu}_r + \mathbf{D}(\boldsymbol{\nu}_r)\boldsymbol{\nu}_r \\ &= \begin{bmatrix} Y_{\dot{v}}v_r r + Y_{\dot{r}}r^2 \\ -X_{\dot{u}}u_r r \\ (X_{\dot{u}} - Y_{\dot{v}})u_r v_r - Y_{\dot{r}}u_r r \end{bmatrix} \left( \begin{array}{l} \text{altern-} \\ \text{atively:} \end{array} \right) \begin{bmatrix} X_{vr}v_r r + X_{rr}r^2 \\ Y_{ur}u_r r \\ N_{uv}u_r v_r + N_{ur}u_r r \end{bmatrix} \\ &+ \begin{bmatrix} -X_{|u|u}|u_r|u_r \\ -Y_{|v|v}|v_r|v_r - Y_{|v|r}|v_r|r - Y_{v|r}|v_r|r - Y_{|r|r}|r|r \\ -N_{|v|v}|v_r|v_r - N_{|v|r}|v_r|r - N_{v|r}|v_r|r - N_{|r|r}|r|r \end{bmatrix} \end{aligned}$$

or

$$\mathbf{N}(\boldsymbol{\nu}_r)\boldsymbol{\nu}_r = \begin{bmatrix} -X_{|u|u}|u_r|u_r + Y_{\dot{v}}v_r r + Y_{\dot{r}}r^2 \\ -X_{\dot{u}}u_r r - Y_{|v|v}|v_r|v_r - Y_{|v|r}|v_r|r - Y_{v|r}|v_r|r - Y_{|r|r}|r|r \\ (X_{\dot{u}} - Y_{\dot{v}})u_r v_r - Y_{\dot{r}}u_r r - N_{|v|v}|v_r|v_r \\ -N_{|v|r}|v_r|r - N_{v|r}|v_r|r - N_{|r|r}|r|r \end{bmatrix} \quad (6.107)$$

From this expression it is seen that

$$\mathbf{C}_A(\boldsymbol{\nu}_r) = \begin{bmatrix} 0 & 0 & Y_{\dot{v}}v_r + Y_{\dot{r}}r \\ 0 & 0 & -X_{\dot{u}}u_r \\ -Y_{\dot{v}}v_r - Y_{\dot{r}}r & X_{\dot{u}}u_r & 0 \end{bmatrix} \quad (6.108)$$

$$\mathbf{D}(\boldsymbol{\nu}_r) = \begin{bmatrix} -X_{|u|u}|u_r| & 0 & 0 \\ 0 & -Y_{|v|v}|v_r| - Y_{|r|r}|r| & -Y_{|v|r}|v_r| - Y_{|r|r}|r| \\ 0 & -N_{|v|v}|v_r| - N_{|r|r}|r| & -N_{|v|r}|v_r| - N_{|r|r}|r| \end{bmatrix} \quad (6.109)$$

Recall that  $\mathbf{D}(\boldsymbol{\nu}_r) = \mathbf{D} + \mathbf{D}_n(\boldsymbol{\nu}_r)$ . However, linear potential damping and skin friction  $\mathbf{D}$  are neglected in (6.107) since the nonlinear quadratic terms  $\mathbf{D}_n(\boldsymbol{\nu}_r)$  dominate at higher speeds (see Figure 6.7). This is a good assumption for maneuvering while stationkeeping models should include a nonzero  $\mathbf{D}$ .

Figure 6.7 shows the significance of the linear and quadratic terms for different ship speeds. It is recommended to use different damping models depending on the regime of the control system. In many cases, it is important to include both linear and quadratic damping, since only quadratic damping in the model will cause oscillatory behavior at low speed. The main reason is that linear damping is needed for exponential convergence to zero. For marine craft operating in waves, linear damping will always be present due to potential damping and linear skin friction (Faltinsen and Sortland 1987). For large ships Blanke (1981) suggests simplifying (6.109) according to

$$\mathbf{D}_n(\boldsymbol{\nu}_r) = \begin{bmatrix} -X_{|u|u}|u_r| & 0 & 0 \\ 0 & -Y_{|v|v}|v_r| & -Y_{|v|r}|v_r| \\ 0 & -N_{|v|v}|v_r| & -N_{|v|r}|v_r| \end{bmatrix} \quad (6.110)$$

<sup>1</sup>The  $\mathbf{C}_A$  terms can also be denoted as  $X_{vr}v_r r$ ,  $X_{rr}r^2$ ,  $Y_{ur}u_r r$ ,  $N_{uv}u_r v_r$  and  $N_{ur}u_r r$ . If these terms are experimentally obtained, viscous effects will be included in addition to the potential coefficients  $Y_{\dot{v}}$ ,  $X_{\dot{u}}$  and  $Y_{\dot{r}}$ .

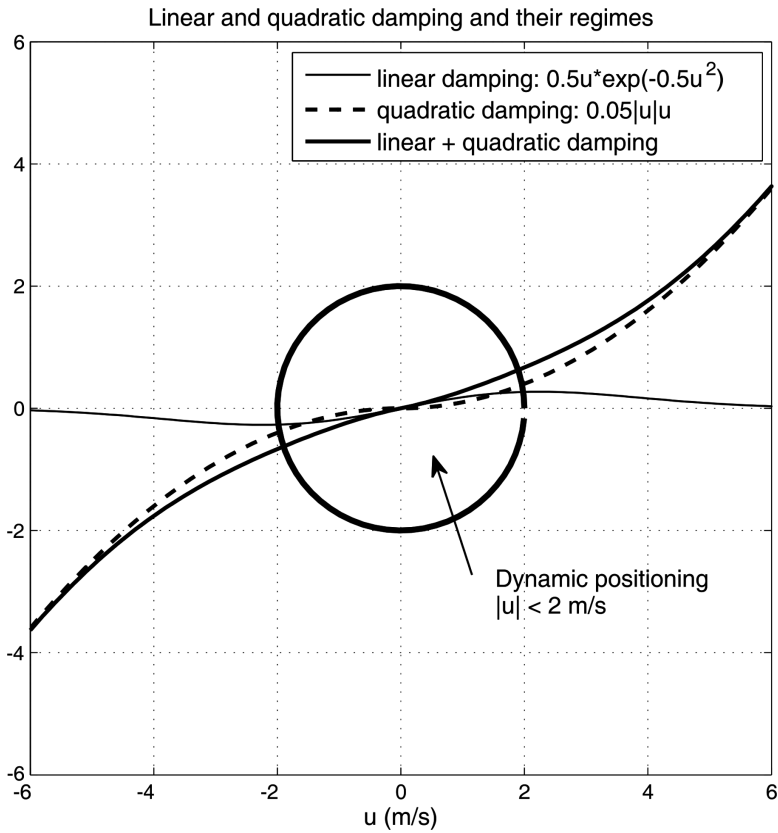


Figure 6.7: Linear and quadratic damping and their speeds regimes. Notice that the linear part goes to zero for higher speeds.

This gives

$$\begin{aligned} \mathbf{N}(\boldsymbol{\nu}_r) &= \mathbf{C}_A(\boldsymbol{\nu}_r) + \mathbf{D}(\boldsymbol{\nu}_r) \\ &= \begin{bmatrix} -X_{|u|u} |u_r| & 0 & Y_{\dot{v}} v_r + Y_{\dot{r}} r \\ 0 & -Y_{|v|v} |v_r| & -X_{\dot{u}} u_r - Y_{|v|r} |v_r| \\ -Y_{\dot{v}} v_r - Y_{\dot{r}} r & X_{\dot{u}} u_r - N_{|v|v} |v_r| & -N_{|v|r} |v_r| \end{bmatrix} \quad (6.111) \end{aligned}$$

### 6.5.4 Nonlinear maneuvering model based on odd functions

So far, we have discussed nonlinear maneuvering models based on first principles such as surge resistance and cross-flow drag, which have been approximated by second-order *modulus functions* (see Fedyaevsky and Sobolev, 1963; Norrin, 1970).

In many cases a more pragmatic approach is used for curve fitting of experimental data (Clarke 2003). This is typically done by using *Taylor series* of first- and second-order terms (Abkowitz 1964) to describe the nonlinear terms in  $\mathbf{N}(\boldsymbol{\nu}_r)$ .

### The nonlinear model of Abkowitz (1964)

One of the standard nonlinear ship models in the literature is that of Abkowitz (1964). Consider the nonlinear rigid-body kinetics

$$\boldsymbol{M}_{RB}\dot{\boldsymbol{\nu}} + \boldsymbol{C}_{RB}(\boldsymbol{\nu})\boldsymbol{\nu} = \boldsymbol{\tau}_{RB} \quad (6.112)$$

with external forces and moment:

$$\boldsymbol{\tau}_{RB} = [X(\boldsymbol{x}), Y(\boldsymbol{x}), N(\boldsymbol{x})]^\top \quad (6.113)$$

where  $\boldsymbol{x} = [u, v, r, \dot{u}, \dot{v}, \dot{r}, \delta]^\top$  and  $\delta$  is the rudder angle. Based on these equations, Abkowitz (1964) proposed a third-order truncated *Taylor-series* expansion of the functions  $X(\boldsymbol{x})$ ,  $Y(\boldsymbol{x})$  and  $N(\boldsymbol{x})$  at  $\boldsymbol{x}_0 = [U, 0, 0, 0, 0, 0, 0]^\top$ . This gives

$$\begin{aligned} X(\boldsymbol{x}) &\approx X(\boldsymbol{x}_0) + \sum_{i=1}^n \left( \frac{\partial X(\boldsymbol{x})}{\partial x_i} \Big|_{\boldsymbol{x}_0} \Delta x_i + \frac{1}{2} \frac{\partial^2 X(\boldsymbol{x})}{\partial (x_i)^2} \Big|_{\boldsymbol{x}_0} \Delta x_i^2 + \frac{1}{6} \frac{\partial^3 X(\boldsymbol{x})}{\partial (x_i)^3} \Big|_{\boldsymbol{x}_0} \Delta x_i^3 \right) \\ Y(\boldsymbol{x}) &\approx Y(\boldsymbol{x}_0) + \sum_{i=1}^n \left( \frac{\partial Y(\boldsymbol{x})}{\partial x_i} \Big|_{\boldsymbol{x}_0} \Delta x_i + \frac{1}{2} \frac{\partial^2 Y(\boldsymbol{x})}{\partial (x_i)^2} \Big|_{\boldsymbol{x}_0} \Delta x_i^2 + \frac{1}{6} \frac{\partial^3 Y(\boldsymbol{x})}{\partial (x_i)^3} \Big|_{\boldsymbol{x}_0} \Delta x_i^3 \right) \\ N(\boldsymbol{x}) &\approx Z(\boldsymbol{x}_0) + \sum_{i=1}^n \left( \frac{\partial N(\boldsymbol{x})}{\partial x_i} \Big|_{\boldsymbol{x}_0} \Delta x_i + \frac{1}{2} \frac{\partial^2 N(\boldsymbol{x})}{\partial (x_i)^2} \Big|_{\boldsymbol{x}_0} \Delta x_i^2 + \frac{1}{6} \frac{\partial^3 N(\boldsymbol{x})}{\partial (x_i)^3} \Big|_{\boldsymbol{x}_0} \Delta x_i^3 \right) \end{aligned}$$

where  $\Delta\boldsymbol{x} = \boldsymbol{x} - \boldsymbol{x}_0 = [\Delta x_1, \Delta x_2, \dots, \Delta x_7]^\top$ . Unfortunately, a third-order Taylor-series expansion results in a large number of terms. By applying some physical insight, the complexity of these expressions can be reduced. Abkowitz (1964) makes the following assumptions:

1. *Most ship maneuvers can be described by a 3rd-order truncated Taylor expansion about the steady state condition  $u = u_0$ .*
2. *Only 1st-order acceleration terms are considered.*
3. *Standard port/starboard symmetry simplifications except terms describing the constant force and moment arising from single-screw propellers.*
4. *The coupling between the acceleration and velocity terms is negligible.*

Simulations of standard ship maneuvers show that these assumptions are quite good. Applying these assumptions to the expressions  $X(\boldsymbol{x})$ ,  $Y(\boldsymbol{x})$  and  $N(\boldsymbol{x})$  yields

$$\begin{aligned}
X &= X^* + X_{\dot{u}}\dot{u} + X_u\Delta u + X_{uu}\Delta u^2 + X_{uuu}\Delta u^3 + X_{vv}v^2 + X_{rr}r^2 + X_{\delta\delta}\delta^2 \\
&\quad + X_{rv\delta}rv\delta + X_{r\delta r}\delta + X_{v\delta v}\delta + X_{vvu}v^2\Delta u + X_{rru}r^2\Delta u + X_{\delta\delta u}\delta^2\Delta u \\
&\quad + X_{rvvru}v + X_{r\delta u}r\delta\Delta u + X_{v\delta u}v\delta\Delta u \\
Y &= Y^* + Y_u\Delta u + Y_{uu}\Delta u^2 + Y_r r + Y_v v + Y_{\dot{r}}\dot{r} + Y_{\dot{v}}\dot{v} + Y_\delta\delta + Y_{rrr}r^3 + Y_{vvv}v^3 \\
&\quad + Y_{\delta\delta\delta}\delta^3 + Y_{rr\delta}r^2\delta + Y_{\delta\delta r}\delta^2 r + Y_{rrv}r^2 v + Y_{vvr}v^2 r + Y_{\delta\delta v}\delta^2 v + Y_{vv\delta}v^2 \delta \\
&\quad + Y_{\delta vr}\delta vr + Y_{vu}v\Delta u + Y_{vuu}v\Delta u^2 + Y_{ru}r\Delta u + Y_{ruu}r\Delta u^2 + Y_{\delta u}\delta\Delta u \\
&\quad + Y_{\delta uu}\delta\Delta u^2 \\
N &= N^* + N_u\Delta u + N_{uu}\Delta u^2 + N_{rr}r + N_{vv}v + N_{\dot{r}}\dot{r} + N_{\dot{v}}\dot{v} + N_\delta\delta + N_{rrr}r^3 \\
&\quad + N_{vvv}v^3 + N_{\delta\delta\delta}\delta^3 + N_{rr\delta}r^2\delta + N_{\delta\delta r}\delta^2 r + N_{rrv}r^2 v + N_{vvr}v^2 r + N_{\delta\delta v}\delta^2 v \\
&\quad + N_{vv\delta}v^2 \delta + N_{\delta vr}\delta vr + N_{vu}v\Delta u + N_{vuu}v\Delta u^2 + N_{ru}r\Delta u + N_{ruu}r\Delta u^2 \\
&\quad + N_{\delta u}\delta\Delta u + N_{\delta uu}\delta\Delta u^2
\end{aligned} \tag{6.114}$$

The hydrodynamic derivatives (6.114) are defined using the notation

$$\begin{aligned}
F^* &= F(\mathbf{x}_0), & F_{x_i} &= \frac{\partial F(\mathbf{x})}{\partial x_i} \Big|_{\mathbf{x}_0} \\
F_{x_i x_j} &= \frac{1}{2} \frac{\partial^2 F(\mathbf{x})}{\partial x_i \partial x_j} \Big|_{\mathbf{x}_0}, & F_{x_i x_j x_k} &= \frac{1}{6} \frac{\partial^3 F(\mathbf{x})}{\partial x_i \partial x_j \partial x_k} \Big|_{\mathbf{x}_0}
\end{aligned}$$

where  $F \in \{X, Y, N\}$ .

### PMM models

The hydrodynamic coefficients can be experimentally determined by using a planar-motion-mechanism (PMM) system, which is a device for experimentally determining the hydrodynamic derivatives required in the equations of motion. This includes coefficients usually classified into the three categories of static stability, rotary stability and acceleration derivatives. The PMM device is capable of oscillating a ship (or submarine) model while it is being towed in a testing tank. The forces are measured on the scale model and fitted to odd functions based on Taylor-series expansions. The resulting model is usually referred to as the PMM model and this model is scaled up to a full-scale ship by using Froude number similarity. This ensures that the ratio between the inertial and gravitational forces is kept constant.

#### 6.5.5 Linear maneuvering model

The linearized maneuvering equations in *surge*, *sway* and *yaw* is a special case of the nonlinear model (6.92). Consider

$$\underbrace{(M_{RB} + M_A)}_M \dot{\nu}_r + \underbrace{(C_{RB}^* + C_A^* + D)}_N \nu_r = \tau + \tau_{\text{wind}} + \tau_{\text{wave}} \tag{6.115}$$

where nonlinear Coriolis, centripetal and damping forces are linearized about the velocities  $v = r = 0$  and the cruise speed

$$U = \sqrt{u^2 + v^2} \approx u \quad (6.116)$$

Linearization is performed under the assumption that the unknown current velocities are negligible, that is  $u_c = v_c = 0$ . The expressions for  $\mathbf{C}_{RB}^*$ ,  $\mathbf{C}_A^*$  and  $\mathbf{D}$  are

$$\mathbf{C}_{RB}^* = \begin{bmatrix} 0 & 0 & 0 \\ 0 & 0 & mU \\ 0 & 0 & mx_g U \end{bmatrix} \quad (6.117)$$

$$\mathbf{C}_A^* = \begin{bmatrix} 0 & 0 & 0 \\ 0 & 0 & -X_{\dot{u}} U \\ 0 & (X_{\dot{u}} - Y_{\dot{v}}) U & -Y_{\dot{r}} U \end{bmatrix} \quad (6.118)$$

$$\mathbf{D} = - \begin{bmatrix} X_u & 0 & 0 \\ 0 & Y_v & Y_r \\ 0 & N_v & N_r \end{bmatrix} \quad (6.119)$$

Starboard–port symmetry implies that surge is decoupled from sway and yaw. Equation (6.115) can be expanded as

$$\left[ \begin{array}{ccc} m - X_{\dot{u}} & 0 & 0 \\ 0 & m - Y_{\dot{v}} & (m - X_{\dot{u}})U - Y_r \\ 0 & (X_{\dot{u}} - Y_{\dot{v}})U - N_v & I_z - N_{\dot{r}} \end{array} \right] \begin{bmatrix} \dot{u}_r \\ \dot{v}_r \\ \dot{r} \end{bmatrix} + \left[ \begin{array}{ccc} -X_u & 0 & 0 \\ 0 & -Y_v & (m - X_{\dot{u}})U - Y_r \\ 0 & (X_{\dot{u}} - Y_{\dot{v}})U - N_v & (mx_g - Y_{\dot{r}})U - N_r \end{array} \right] \begin{bmatrix} u_r \\ v_r \\ r \end{bmatrix} = \begin{bmatrix} \tau_1 \\ \tau_2 \\ \tau_6 \end{bmatrix} \quad (6.120)$$

### Linear forward speed model (surge subsystem)

The first row in (6.115) is recognized as the linear surge equation

$$(m - X_{\dot{u}})\dot{u}_r - X_u u_r = \tau_1 \quad (6.121)$$

where  $\tau_1$  is the sum of control and external forces in surge and the linear damping coefficient is approximated by equivalent linearization (see Section 6.4.2). Moreover,

$$X_u = \frac{8A_1}{3\pi} X_{|u|u} \quad (6.122)$$

where the surge velocity  $u_r = A_1 \cos(\omega t)$  is assumed to be harmonic.

### Linear maneuvering model (sway–yaw subsystem)

The second and third rows in (6.115) are the sway–yaw subsystem. This model is also known as the *potential theory representation* (Fossen, 1994, Clarke and Horn, 1997)

$$\mathbf{M}\dot{\boldsymbol{\nu}}_r + \mathbf{N}\boldsymbol{\nu}_r = \mathbf{b}\delta \quad (6.123)$$

where  $\boldsymbol{\nu}_r = [v_r, r]^\top$  and  $\delta$  is the rudder angle. Hence,

$$\mathbf{M} = \begin{bmatrix} m - Y_{\dot{v}} & mx_g - Y_{\dot{r}} \\ mx_g - Y_{\dot{r}} & I_z - N_{\dot{r}} \end{bmatrix} \quad (6.124)$$

$$\mathbf{N} = \begin{bmatrix} -Y_v & (m - X_{\dot{u}})U - Y_r \\ (X_{\dot{u}} - Y_{\dot{v}})U - N_v & (mx_g - Y_{\dot{r}})U - N_r \end{bmatrix} \quad (6.125)$$

$$\mathbf{b} = \begin{bmatrix} -Y_\delta \\ -N_\delta \end{bmatrix} \quad (6.126)$$

**Comment 6.1** Davidson and Schiff (1946) assumed that the hydrodynamic forces  $\tau_{RB}$  are linear in  $\delta$ ,  $\dot{\boldsymbol{\nu}}_r$  and  $\boldsymbol{\nu}_r$  (linear strip theory) such that

$$\tau_{RB} = \underbrace{\begin{bmatrix} Y_{\dot{v}} & Y_{\dot{r}} \\ N_{\dot{v}} & N_{\dot{r}} \end{bmatrix}}_{\mathbf{M}_A} \dot{\boldsymbol{\nu}}_r + \underbrace{\begin{bmatrix} Y_v & Y_r \\ N_v & N_r \end{bmatrix}}_{\mathbf{D}} \boldsymbol{\nu}_r - \underbrace{\begin{bmatrix} Y_\delta \\ N_\delta \end{bmatrix}}_{\mathbf{b}} \delta \quad (6.127)$$

This gives

$$\mathbf{N} = \begin{bmatrix} -Y_v & mU - Y_r \\ -N_v & mx_g U - N_r \end{bmatrix} \quad (6.128)$$

Notice that the Munk moment  $(X_{\dot{u}} - Y_{\dot{v}})Uv_r$  is missing in the yaw equation when compared to (6.125). This is a destabilizing moment known from aerodynamics which tries to turn the craft; see Faltinsen (1990, pp. 188–189). Also notice that the less important terms  $X_{\dot{u}}Ur$  and  $Y_{\dot{r}}Ur$  are removed from  $\mathbf{N}$  when compared to (6.125). All missing terms are due to the  $\mathbf{C}_A(\boldsymbol{\nu}_r)$  matrix, which is omitted in the linear expression (6.127). Consequently, it is recommended to use (6.125), which includes the terms from the  $\mathbf{C}_A(\boldsymbol{\nu}_r)$  matrix.

## 6.6 Ship Maneuvering Models including Roll (4 DOF)

The maneuvering models presented in Section 6.5.1 only describe the horizontal motions (*surge*, *sway* and *yaw*). These models are intended for the design and simulation of DP systems, heading autopilots, trajectory-tracking and path-following control systems. Many vessels, however, are equipped with actuators that can reduce the rolling motion. This could be anti-rolling tanks, rudders and fin stabilizers (see Part II). In order to design a control system for roll damping, it is necessary to add the roll equation to the horizontal plane model. Inclusion of roll means that the restoring moment due to buoyancy and gravity must be included. The resulting model is a 4-DOF maneuvering model that includes roll (*surge*, *sway*, *roll* and *yaw*).

The speed equation (6.121) can be decoupled from the sway, roll and yaw modes. The resulting model takes the form

$$\mathbf{M}\dot{\boldsymbol{\nu}}_r + \mathbf{N}\boldsymbol{\nu}_r + \mathbf{G}\boldsymbol{\eta} = \boldsymbol{\tau} \quad (6.129)$$

where  $\boldsymbol{\nu} = [v_r, p, r]^\top$  and  $\boldsymbol{\eta} = [y^n, \phi, \psi]^\top$  are the states while  $\boldsymbol{\tau}$  is the control vector. For a ship with homogeneous mass distribution and  $xz$ -plane symmetry,  $I_{xy} = I_{yz} = 0$  and  $y_g = 0$ .

From the general expressions (3.46) and (6.34) in Sections 3.3 and 6.3.1, respectively, we get (with nonzero  $I_{xz}$ )

$$\mathbf{M} = \begin{bmatrix} m - Y_v & -mz_g - Y_p & mx_g - Y_r \\ -mz_g - K_v & I_x - K_p & -I_{xz} - K_r \\ mx_g - N_v & -I_{xz} - N_p & I_z - N_r \end{bmatrix} \quad (6.130)$$

The expression for  $\mathbf{N}(u_o)$  is obtained by linearization of  $\mathbf{C}(\boldsymbol{\nu})$  and  $\mathbf{D}(\boldsymbol{\nu})$  about  $u = U$  which gives

$$\mathbf{N} = \begin{bmatrix} -Y_v & -Y_p & mU - Y_r \\ -K_v & -K_p & -mz_g U - K_r \\ -N_v & -N_p & mx_g U - N_r \end{bmatrix} \quad (6.131)$$

Recall from Section 4.1 that the linear restoring forces and moments for a surface vessel can be written

$$\mathbf{G} = \text{diag}\{0, WGM_T, 0\} \quad (6.132)$$

where  $W = mg$  is the weight and  $GM_T$  is the transverse metacenter height.

In addition to these equations, the kinematic equations (assuming  $q = \theta = 0$ )

$$\dot{\phi} = p \quad (6.133)$$

$$\dot{\psi} = r \quad (6.134)$$

must be augmented to the system model. The general kinematic expressions are found in Section 2.2.1.

### State-space model

The linearized model (6.129) together with (6.133)–(6.134) can be written in state-space form by defining the state vector as  $\mathbf{x} := [v_r, p, r, \phi, \psi]^\top$ . The elements associated with the matrices  $\mathbf{A}$  and  $\mathbf{B}$  are given by

$$\dot{\mathbf{x}} = \underbrace{\begin{bmatrix} a_{11} & a_{12} & a_{13} & a_{14} & 0 \\ a_{21} & a_{22} & a_{23} & a_{24} & 0 \\ a_{31} & a_{32} & a_{33} & a_{34} & 0 \\ 0 & 1 & 0 & 0 & 0 \\ 0 & 0 & 1 & 0 & 0 \end{bmatrix}}_{\mathbf{A}} \mathbf{x} + \underbrace{\begin{bmatrix} b_{11} & b_{12} & \cdots & b_{1r} \\ b_{21} & b_{22} & \cdots & b_{2r} \\ b_{31} & b_{32} & \cdots & b_{3r} \\ 0 & 0 & \cdots & 0 \\ 0 & 0 & \cdots & 0 \end{bmatrix}}_{\mathbf{B}} \mathbf{u} \quad (6.135)$$

where the elements  $a_{ij}$  are found from

$$\begin{bmatrix} a_{11} & a_{12} & a_{13} \\ a_{21} & a_{22} & a_{23} \\ a_{31} & a_{32} & a_{33} \end{bmatrix} = -\mathbf{M}^{-1}\mathbf{N}, \quad \begin{bmatrix} * & a_{14} & * \\ * & a_{24} & * \\ * & a_{34} & * \end{bmatrix} = -\mathbf{M}^{-1}\mathbf{G} \quad (6.136)$$

while the elements  $b_{ij}$  depend on what type of actuators are in use. Finally, the roll and yaw outputs are chosen as

$$\phi = \underbrace{[0, 0, 0, 1, 0]}_{\mathbf{c}_{\text{roll}}^{\top}} \mathbf{x}, \quad \psi = \underbrace{[0, 0, 0, 0, 1]}_{\mathbf{c}_{\text{yaw}}^{\top}} \mathbf{x} \quad (6.137)$$

### Decompositions in roll and sway–yaw subsystems

To simplify the system for further analysis, the state vector is reorganized such that state variables associated with the steering and roll dynamics are separated. Consequently, (6.135) is rewritten as

$$\begin{bmatrix} \dot{v}_r \\ \dot{r} \\ \dot{\psi} \\ \dot{p} \\ \dot{\phi} \end{bmatrix} = \left[ \begin{array}{ccc|cc} a_{11} & a_{13} & 0 & a_{12} & a_{14} \\ a_{31} & a_{33} & 0 & a_{32} & a_{34} \\ 0 & 1 & 0 & 0 & 0 \\ \hline a_{21} & a_{23} & 0 & a_{22} & a_{24} \\ 0 & 0 & 0 & 1 & 0 \end{array} \right] \begin{bmatrix} v_r \\ r \\ \psi \\ p \\ \phi \end{bmatrix} + \begin{bmatrix} b_{11} & b_{12} & \cdots & b_{1r} \\ b_{31} & b_{32} & \cdots & b_{3r} \\ 0 & 0 & \cdots & 0 \\ b_{21} & b_{22} & \cdots & b_{2r} \\ 0 & 0 & \cdots & 0 \end{bmatrix} \mathbf{u} \quad (6.138)$$

Let

$$\begin{bmatrix} \dot{x}_{\psi} \\ \dot{x}_{\phi} \end{bmatrix} = \begin{bmatrix} \mathbf{A}_{\psi\psi} & \mathbf{A}_{\psi\phi} \\ \mathbf{A}_{\phi\psi} & \mathbf{A}_{\phi\phi} \end{bmatrix} \begin{bmatrix} x_{\psi} \\ x_{\phi} \end{bmatrix} + \begin{bmatrix} \mathbf{B}_{\psi} \\ \mathbf{B}_{\phi} \end{bmatrix} \mathbf{u} \quad (6.139)$$

where  $\mathbf{x}_{\psi} = [v_r, r, \psi]^{\top}$  and  $\mathbf{x}_{\phi} = [p, \phi]^{\top}$ .

If the coupling matrices are small, that is  $\mathbf{A}_{\psi\phi} = \mathbf{A}_{\phi\psi} = \mathbf{0}$ , the following subsystems

$$\begin{bmatrix} \dot{p} \\ \dot{\phi} \end{bmatrix} = \begin{bmatrix} a_{22} & a_{24} \\ 1 & 0 \end{bmatrix} \begin{bmatrix} p \\ \phi \end{bmatrix} + \begin{bmatrix} b_{21} & b_{22} & \cdots & b_{2r} \\ 0 & 0 & \cdots & 0 \end{bmatrix} \mathbf{u} \quad (6.140)$$

and

$$\begin{bmatrix} \dot{v}_r \\ \dot{r} \\ \dot{\psi} \end{bmatrix} = \begin{bmatrix} a_{11} & a_{13} & 0 \\ a_{31} & a_{33} & 0 \\ 0 & 1 & 0 \end{bmatrix} \begin{bmatrix} v_r \\ r \\ \psi \end{bmatrix} + \begin{bmatrix} b_{11} & b_{12} & \cdots & b_{1r} \\ b_{31} & b_{32} & \cdots & b_{3r} \\ 0 & 0 & \cdots & 0 \end{bmatrix} \mathbf{u} \quad (6.141)$$

will describe the ship dynamics. The last expression is recognized as the second-order Nomoto model (7.23) with  $r$  control inputs.

### Transfer functions for steering and rudder-roll damping

The linearized model (6.138) is useful for frequency analysis of rudder-roll damping (RRD) systems. For simplicity consider a ship with one rudder  $u = \delta$  and  $\mathbf{b} = [b_{11}, b_{21}, b_{31}, 0, 0]^{\top}$ . For the state-space model (6.138) the transfer functions  $\phi(s)/\delta(s) = \mathbf{c}_{\text{roll}}^{\top}(s\mathbf{I} - \mathbf{A})^{-1}\mathbf{b}$  and  $\psi(s)/\delta(s) = \mathbf{c}_{\text{yaw}}^{\top}(s\mathbf{I} - \mathbf{A})^{-1}\mathbf{b}$  become

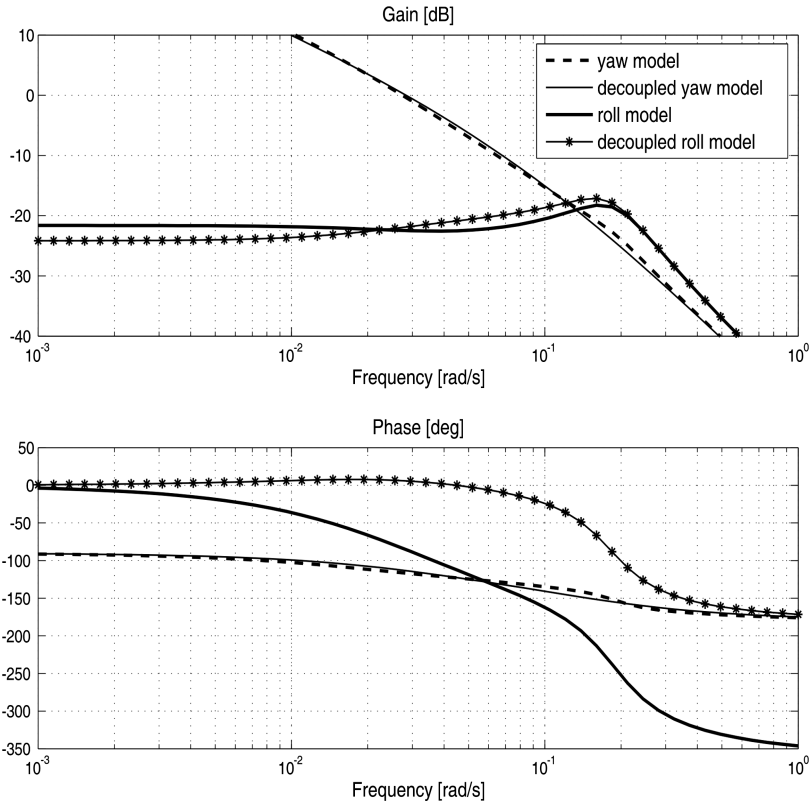


Figure 6.8: Transfer functions for the roll and sway–yaw subsystems corresponding to the Son and Nomoto container ship.

$$\frac{\phi}{\delta}(s) = \frac{b_2 s^2 + b_1 s + b_0}{s^4 + a_3 s^3 + a_2 s^2 + a_1 s + a_0} \approx \underbrace{\frac{K_{\text{roll}} \omega_{\text{roll}}^2 (1 + T_5 s)}{(1 + T_4 s)(s^2 + 2\zeta\omega_{\text{roll}}s + \omega_{\text{roll}}^2)}}_{\text{no coupling between roll and sway-yaw}} \quad (6.142)$$

$$\frac{\psi}{\delta}(s) = \frac{c_3 s^3 + c_2 s^2 + c_1 s + c_0}{s(s^4 + a_3 s^3 + a_2 s^2 + a_1 s + a_0)} \approx \underbrace{\frac{K_{\text{yaw}} (1 + T_3 s)}{s(1 + T_1 s)(1 + T_2 s)}}_{\text{no coupling between roll and sway-yaw}} \quad (6.143)$$

where the decoupled models (6.140) and (6.141) have been applied. In most cases, this approximation is only rough so care should be taken. In Figure 6.8 it is seen that

the phase of the roll transfer function is inaccurate for the decoupled model. This can be improved by using a model reduction via a balanced state-space realization (see `modred.m` and `ssbal.m` in Matlab).

Also, parametric investigations show that cross-couplings between steering and roll might give robust performance problems of RRD control systems (Blanke and Christensen 1993). This is also documented in Blanke (1996), who has identified the ship parameters for several loading conditions during sea trials with a series of ships. The results clearly reveal changes in the dynamics between the different ships in the series, indicating that there is a robustness problem due to changes in load conditions and rudder shape. Nonlinear effects also give rise to the same problem. Identification of ship steering-roll models are discussed by Blanke and Tiano (1997). The interested reader is also advised to consult Van der Klugt (1987) for a discussion of decoupled linear models for RRD, while nonlinear models are presented in Section 6.6.1.

### **Example 6.5 (Roll and Sway–Yaw Transfer Functions)**

The roll and yaw transfer functions corresponding to the model of Son and Nomoto (1981) are plotted in Figure 6.8 using the MSS toolbox script `ExRRD1.m`. The plots show both the full state-space model (6.135) and the decoupled models (6.140)–(6.141). The model considered is a container ship of length  $L = 175$  m and with a displacement volume of  $21\,222\text{ m}^3$ . The ship is moving at service speed  $U = 7.0$  m/s. The model of Son and Nomoto (1981) is based on a third-order Taylor-series expansion (see Section 6.5.4) of the hydrodynamic forces including higher-order restoring terms replacing (6.132). The nonlinear model is included in the MSS toolbox under the file name `container.m` while a linearized version of this model is found in `Lcontainer.m`. The nonlinear model is described more closely in the next section. The numerical values for the transfer functions are

$$\begin{aligned}\frac{\phi}{\delta}(s) &= \frac{0.0032(s - 0.036)(s + 0.077)}{(s + 0.026)(s + 0.116)(s^2 + 0.136s + 0.036)} \\ &\approx \frac{0.083(1 + 49.1s)}{(1 + 31.5s)(s^2 + 0.134s + 0.033)}\end{aligned}\quad (6.144)$$

and

$$\begin{aligned}\frac{\psi}{\delta}(s) &= \frac{0.0024(s + 0.0436)(s^2 + 0.162s + 0.035)}{s(s + 0.0261)(s + 0.116)(s^2 + 0.136s + 0.036)} \\ &\approx \frac{0.032(1 + 16.9s)}{s(1 + 24.0s)(1 + 9.2s)}\end{aligned}\quad (6.145)$$

corresponding to

$$\omega_{\text{roll}} = 0.189 \text{ rad/s} \quad (6.146)$$

$$\zeta = 0.36 \quad (6.147)$$

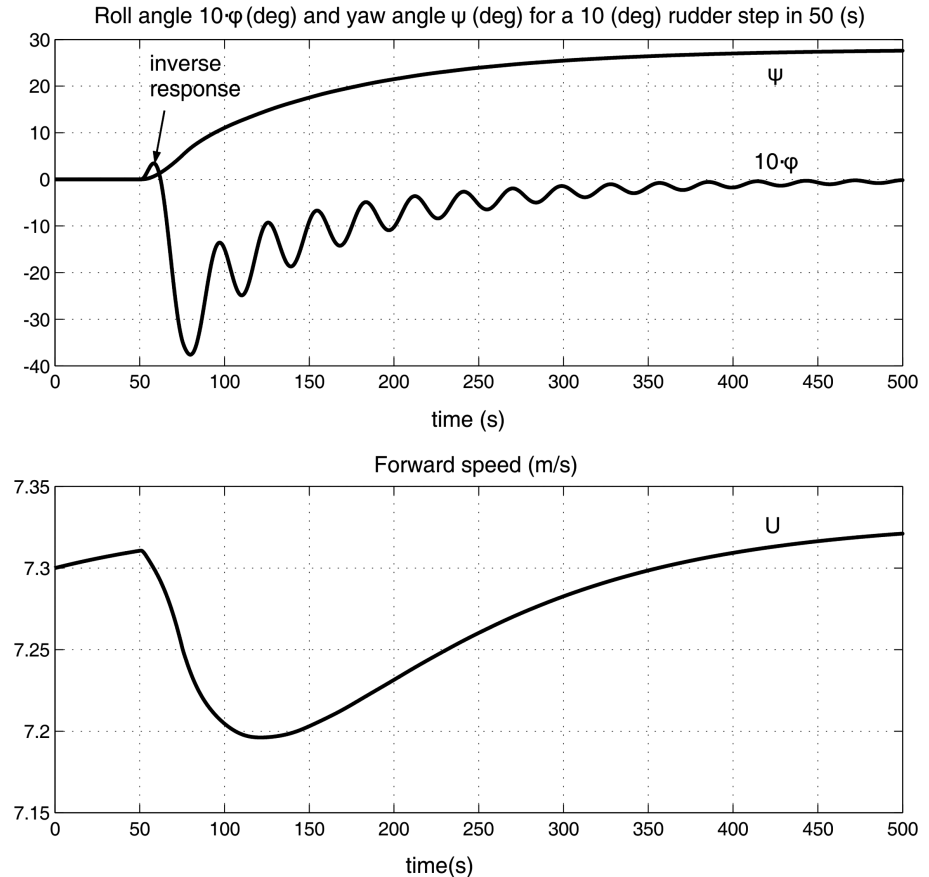


Figure 6.9: Roll angle  $10\dot{\phi}$  and yaw angle  $\dot{\psi}$  versus time for a 10 degree rudder step in 50 s. Notice the inverse response in roll and speed reduction during turning.

*It is seen that the amplitudes of the roll and yaw models are quite close. However, the decoupled model in roll does not describe the phase with sufficient accuracy, so stability problems could be an issue when designing a model-based RRD. The main reason for this is that one pole–zero pair is omitted in the decoupled roll model. Since this is a right-half-plane zero,*

$$z = 0.036 \text{ rad/s} \quad (6.148)$$

*the pole–zero pair gives an additional phase lag of  $-180$  degrees, as observed in the plot of the full model. This will of course result in serious stability problems when trying to damp the roll motion.*

*In practice it will be difficult to design an RRD for this system since the controller should reduce the energy at the peak frequency which is much higher than the right-half-plane zero  $z = 0.036$  rad/s. This is a nonminimum phase property which cannot be changed with feedback (recall that only poles and not zeros can be moved using*

*feedback control). The nonminimum phase characteristic is observed as an inverse response in roll when a step input is applied (see Figure 6.9).*

The plots in Figure 6.9 are generated by simulating the nonlinear model of Son and Nomoto (see EXRRD3.m). The nonminimum phase behavior due to the right-half-plane zero is discussed in more detail by Fossen and Lauvdal (1994), where both linear and nonlinear analyses of the models of Son and Nomoto are considered. The nonlinear equivalent to a right-half-plane zero is unstable zero dynamics.

### 6.6.1 The nonlinear model of Son and Nomoto

A nonlinear model including roll for a high-speed container ship has been proposed by Son and Nomoto (1981, 1982)

$$(m + m_x)\ddot{u} - (m + m_y)vr = X + \tau_1 \quad (6.149)$$

$$(m + m_y)\dot{v} + (m + m_x)ur + m_y\alpha_y\dot{r} - m_yl_y\dot{p} = Y + \tau_2 \quad (6.150)$$

$$(I_x + J_x)\dot{p} - m_yl_y\dot{v} - m_xl_xur = K - WGM_T\phi + \tau_4 \quad (6.151)$$

$$(I_z + J_z)\dot{r} + m_y\alpha_y\dot{v} = N - x_gY + \tau_6 \quad (6.152)$$

where  $m_x = A_{11}(0)$ ,  $m_y = A_{22}(0)$ ,  $J_x = A_{44}(\omega_4)$  and  $J_z = A_{66}(0)$  denote the added mass and added moments of inertia. The control inputs are recognized as  $\boldsymbol{\tau} = [\tau_1, \tau_2, \tau_4, \tau_6]^\top$ . The added mass  $x$  coordinates of  $m_x$  and  $m_y$  are denoted by  $\alpha_x$  and  $\alpha_y$ , while  $l_x$  and  $l_y$  are the added mass  $z$  coordinates of  $m_x$  and  $m_y$ , respectively.

The terms on the right-hand side of (6.149)–(6.152) are defined in terms of a third-order Taylor series expansion where small coefficients are neglected. The remaining terms are

$$\begin{aligned} X &= X(u) + (1-t)T + X_{vr}vr + X_{vv}v^2 + X_{rr}r^2 + X_{\phi\phi}\phi^2 \\ &\quad + X_\delta \sin \delta + X_{\text{ext}} \end{aligned} \quad (6.153)$$

$$\begin{aligned} Y &= Y_vv + Y_{rr}r + Y_{\phi\phi}\phi + Y_pp + Y_{vvv}v^3 + Y_{rrr}r^3 + Y_{vvr}v^2r + Y_{vrr}vr^2 \\ &\quad + Y_{vv\phi}v^2\phi + Y_{v\phi\phi}v\phi^2 + Y_{rr\phi}r^2\phi + Y_{r\phi\phi}r\phi^2 + Y_\delta \cos \delta + Y_{\text{ext}} \end{aligned} \quad (6.154)$$

$$\begin{aligned} K &= K_vv + K_{rr}r + K_{\phi\phi}\phi + K_pp + K_{vvv}v^3 + K_{rrr}r^3 + K_{vvr}v^2r + K_{vrr}vr^2 \\ &\quad + K_{vv\phi}v^2\phi + K_{v\phi\phi}v\phi^2 + K_{rr\phi}r^2\phi + K_{r\phi\phi}r\phi^2 + K_\delta \cos \delta + K_{\text{ext}} \end{aligned} \quad (6.155)$$

$$\begin{aligned} N &= N_vv + N_{rr}r + N_{\phi\phi}\phi + N_pp + N_{vvv}v^3 + N_{rrr}r^3 + N_{vvr}v^2r + N_{vrr}vr^2 \\ &\quad + N_{vv\phi}v^2\phi + N_{v\phi\phi}v\phi^2 + N_{rr\phi}r^2\phi + N_{r\phi\phi}r\phi^2 + N_\delta \cos \delta + N_{\text{ext}} \end{aligned} \quad (6.156)$$

where  $X(u)$  is usually modeled as quadratic drag  $X(u) = X_{|u|u}|u|u$  and the subscript ext denotes external forces and moments due to wind, waves and ocean currents.

#### Matlab:

The nonlinear container ship model is implemented in the MSS toolbox as

```
[xdot, U] = container(x, ui)
```

The linearized model for  $U = U_0$  is accessed as

```
[xdot,U] = Lcontainer(x,ui,U0)
```

where  $x = [u \ v \ r \ x \ y \ \psi \ p \ \phi \ \delta]'$  and  $ui = [\delta_{c\_n} \ n_c]'$ . In the linear case only one input,  $\delta_{c\_n}$ , is used since the forward speed  $U_0$  is constant. For the nonlinear model, propeller rpm,  $n_c$ , should be positive.

### 6.6.2 The nonlinear model of Blanke and Christensen

An alternative model formulation describing the steering and roll motions of ships has been proposed by Blanke and Christensen (1993). This model is written as

$$M\dot{\nu} + C_{RB}(\nu)\nu + G\eta = \tau_{hyd} + \tau_{wind} + \tau_{wave} + \tau \quad (6.157)$$

where  $\nu = [v, p, r]^\top$ ,  $\tau_{hyd} = [Y, K, N]^\top$  and

$$M = \begin{bmatrix} m - Y_v & -mz_g - Y_p & mx_g - Y_r \\ -mz_g - K_v & I_x - K_p & 0 \\ mx_g - N_v & 0 & I_z - N_r \end{bmatrix} \quad (6.158)$$

$$C_{RB}(\nu) = \begin{bmatrix} 0 & 0 & mu \\ 0 & 0 & 0 \\ -mu & 0 & 0 \end{bmatrix} \quad (6.159)$$

$$G = \begin{bmatrix} 0 & 0 & 0 \\ 0 & WGM_T & 0 \\ 0 & 0 & 0 \end{bmatrix} \quad (6.160)$$

The hydrodynamic forces in  $\tau_{hyd}$  include both damping and hydrodynamic Coriolis and centripetal terms

$$\begin{aligned} Y &= Y_{|u|v}|u|v + Y_{ur}ur + Y_{v|v}|v|v + Y_{v|r}|v|r + Y_{|v|r}|v|r \\ &\quad + Y_{\phi|uv}|\phi|uv| + Y_{\phi|ur}|\phi|ur| + Y_{\phi uu}\phi u^2 + Y_{ext} \end{aligned} \quad (6.161)$$

$$\begin{aligned} K &= K_{|u|v}|u|v + K_{ur}ur + K_{v|v}|v|v + K_{v|r}|v|r + K_{|v|r}|v|r \\ &\quad + K_{\phi|uv}|\phi|uv| + K_{\phi|ur}|\phi|ur| + K_{\phi uu}\phi u^2 + K_{|u|p}|u|p \\ &\quad + K_{p|p}|p|p| + K_{p|p}|p|p + K_{\phi\phi\phi}\phi^3 + K_{ext} \end{aligned} \quad (6.162)$$

$$\begin{aligned} N &= N_{|u|v}|u|v + N_{|u|r}|u|r + N_{r|r}|r|r + N_{v|r}|v|r + N_{|v|r}|v|r \\ &\quad + N_{\phi|uv}|\phi|uv| + N_{\phi|ur}|\phi|ur| + N_p p + N_{|p|p}|p|p + N_{|u|p}|u|p \\ &\quad + N_{\phi u|u}|\phi|u|u| + N_{ext} \end{aligned} \quad (6.163)$$

where the forces and moments associated with the roll motion are assumed to involve the square terms of the surge speed  $u^2$  and  $|u|u$ . The terms  $Y_{ext}$ ,  $K_{ext}$  and  $N_{ext}$  consist of possible contributions from external disturbances while control inputs such as rudders, propellers and bow thrusters are included in  $\tau$ .

**Matlab:**

A nonlinear naval ship model is implemented in the MSS toolbox as

```
[xdot, U] = navalvessel(x, tau)
```

where  $x = [u \ v \ p \ r \ phi \ psi]'$  and  $\tau = [X_{ext} \ Y_{ext} \ K_{ext} \ N_{ext}]'$ .

## 6.7 Low-Speed Maneuvering Models for Dynamic Positioning (3 DOF)

Models for dynamic positioning (DP) are derived under the assumption of low speed. The DP models are valid for stationkeeping and low-speed maneuvering up to approximately 2 m/s, as indicated by the speed regions shown in Figure 6.7. This section presents a nonlinear DP model based on current coefficients and linear exponential damping that can be used for accurate simulation and prediction. In addition to this, a linearized model intended for controller–observer design is derived.

Consider the nonlinear maneuvering model (6.83) in surge, sway and yaw

$$\dot{\eta} = R(\psi)\nu \quad (6.164)$$

$$M\dot{\nu} + C_{RB}(\nu)\nu + N(\nu_r)\nu_r = \tau + \tau_{wind} + \tau_{wave} \quad (6.165)$$

where  $\eta = [x^n, y^n, \psi]^\top$  and  $\nu = [u, v, r]^\top$ . This implies that the dynamics associated with the motion in heave, roll and pitch are neglected, that is  $w = p = q = 0$ . The nonlinear terms are reorganized as

$$N(\nu_r)\nu_r := C_A(\nu_r)\nu_r + D(\nu_r)\nu_r \quad (6.166)$$

### 6.7.1 Current coefficients

For low-speed applications such as DP, ocean currents and damping can be modeled by three *current coefficients*  $C_X$ ,  $C_Y$  and  $C_N$ . These can be experimentally obtained using scale models in wind tunnels. The resulting forces are measured on the model, which is restrained from moving ( $U = 0$ ). The current coefficients can also be related to the surge resistance, cross-flow drag and the Munk moment used in maneuvering theory. For a ship moving at forward speed  $U > 0$ , quadratic damping will be embedded in the current coefficients if relative speed is used.

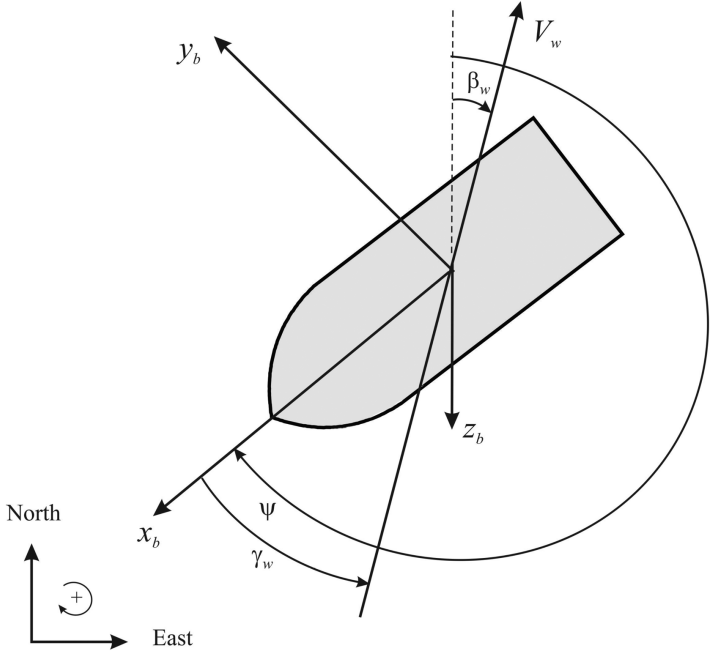


Figure 6.10: Current speed  $V_c$ , current direction  $\beta_c$  and current angle of attack  $\gamma_c$  relative to the bow.

In many textbooks and papers, for instance Blendermann (1994), wind and current coefficients are defined in  $\{b\}$  relative to the bow using a *counter clockwise rotation*  $\gamma_c$  (see Figure 6.10). The current forces on a marine craft at rest ( $U = 0$ ) can be expressed in terms of the area-based current coefficients  $C_X(\gamma_c)$ ,  $C_Y(\gamma_c)$  and  $C_N(\gamma_c)$  as

$$X_{\text{current}} = \frac{1}{2} \rho A_{Fc} C_X(\gamma_c) V_c^2 \quad (6.167)$$

$$Y_{\text{current}} = \frac{1}{2} \rho A_{Lc} C_Y(\gamma_c) V_c^2 \quad (6.168)$$

$$N_{\text{current}} = \frac{1}{2} \rho A_{Lc} L_{oa} C_N(\gamma_c) V_c^2 \quad (6.169)$$

where  $V_c$  is the speed of the ocean current. The frontal and lateral projected currents areas are denoted  $A_{Fc}$  and  $A_{Lc}$ , respectively, while  $L_{oa}$  is the length overall and  $\rho$  is the density of water. Typical experimental current coefficients are shown in Figure 6.11.

Equations (6.167)–(6.169) only add zero-speed current forces (no damping) to the equations of motion since they only depend on the current speed  $V_c$ . For a ship moving at relative forward speed,  $U_r > 0$ , current forces and quadratic damping in surge and sway are given by

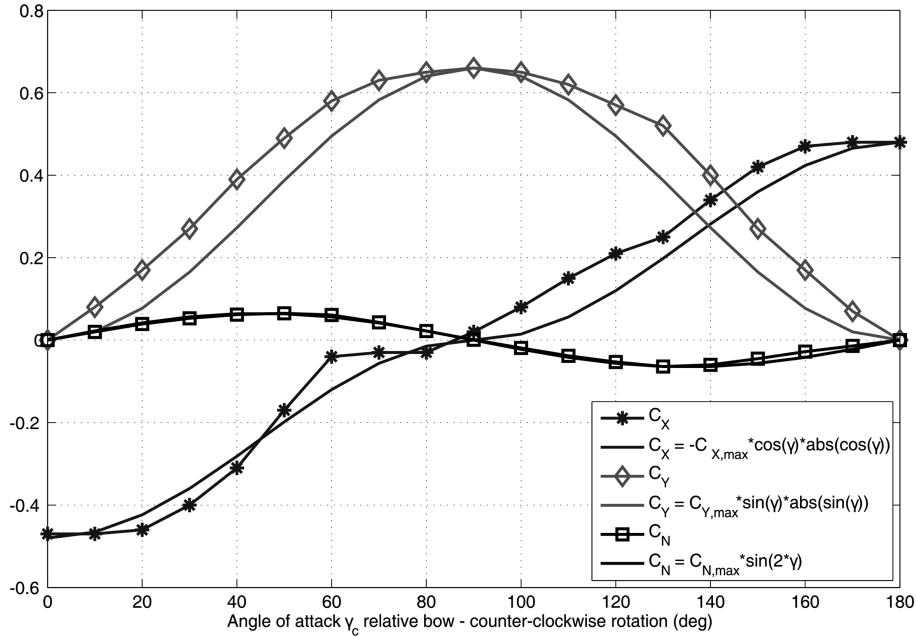


Figure 6.11: Experimental current coefficients  $C_X$ ,  $C_Y$  and  $C_N$  for a tanker. Notice that  $\gamma_c$  is a counter clockwise rotation and the angle of attack  $\gamma_c = 0^\circ$  for a current in the bow.

$$X_{\text{current}} = \frac{1}{2} \rho A_{Fc} C_X(\gamma_{rc}) V_{rc}^2 \quad (6.170)$$

$$Y_{\text{current}} = \frac{1}{2} \rho A_{Lc} C_Y(\gamma_{rc}) V_{rc}^2 \quad (6.171)$$

$$N_{\text{current}} = \frac{1}{2} \rho A_{Lc} L_{oa} C_N(\gamma_{rc}) V_{rc}^2 \quad (6.172)$$

These expressions are functions of the relative speed  $V_{rc}$  and angle of attack  $\gamma_{rc}$  given by the equations

$$V_{rc} = \sqrt{u_{rc}^2 + v_{rc}^2} = \sqrt{(u - u_c)^2 + (v - v_c)^2} \quad (6.173)$$

$$\gamma_{rc} = -\text{atan2}(v_{rc}, u_{rc}) \quad (6.174)$$

where

$$u_c = V_c \cos(\beta_c - \psi) \quad (6.175)$$

$$v_c = V_c \sin(\beta_c - \psi) \quad (6.176)$$

are the current velocities (see Section 10.3).

### Ocean current angle of attack

From Figure 6.10, it is seen that the angles associated with an ocean current in the horizontal plane for a marine craft at rest satisfy

$$\gamma_c = \psi - \beta_c - \pi \quad (6.177)$$

where  $\beta_c$  is the direction of the ocean current and  $\gamma_c$  is specified relative to the bow. Hence, the velocity components (6.175) and (6.176) can be written

$$u_c = -V_c \cos(\gamma_c) \quad (6.178)$$

$$v_c = V_c \sin(\gamma_c) \quad (6.179)$$

The magnitude of the ocean current is

$$V_c = \sqrt{u_c^2 + v_c^2} \quad (6.180)$$

Notice that for zero speed the expressions (6.173) and (6.174) become

$$V_{rc} = \sqrt{(u - u_c)^2 + (v - v_c)^2} \stackrel{u=v=0}{=} V_c \quad (6.181)$$

$$\tan(\gamma_{rc}) = -\frac{v - v_c}{u - u_c} \stackrel{u=v=0}{=} -\frac{v_c}{u_c} = \tan(\gamma_c) \quad (6.182)$$

This means that the angles  $\gamma_{rc}$  and  $\gamma_c$  as well as the speeds  $V_{rc}$  and  $V_c$  in general are different for  $U > 0$ . Consequently, the geometrical relationship (6.177) shown in Figure 6.10 only holds for  $U = 0$ .

DRAFT MANUSCRIPT

### Relationship between current coefficients and quadratic drag

The current coefficients can be related to the surge resistance (6.70) and cross-flow drag (6.80)–(6.81) coefficients by assuming low speed such that  $u \approx 0$  and  $v \approx 0$ . This is a good assumption for DP. From (6.178)–(6.179) it follows that the quadratic terms are

$$\begin{aligned} u_r |u_r| &\approx -u_c |-u_c| \\ &= V_c^2 \cos(\gamma_c) |\cos(\gamma_c)| \end{aligned} \quad (6.183)$$

$$\begin{aligned} v_r |v_r| &\approx -v_c |-v_c| \\ &= -V_c^2 \sin(\gamma_c) |\sin(\gamma_c)| \end{aligned} \quad (6.184)$$

$$\begin{aligned} u_r v_r &\approx u_c v_c \\ &= -\frac{1}{2} V_c^2 \sin(2\gamma_c) \end{aligned} \quad (6.185)$$

The next step is to neglect terms in  $r$  (no rotations during stationkeeping) in (6.80)–(6.81) and require that  $C_X$ ,  $C_Y$  and  $C_N$  in (6.167)–(6.169) satisfy

$$X_{\text{current}} = \frac{1}{2} \rho A_{Fc} C_X(\gamma_c) V_c^2 := X_{|u|u} |u_r| u_r \quad (6.186)$$

$$Y_{\text{current}} = \frac{1}{2} \rho A_{Lc} C_Y(\gamma_c) V_c^2 := Y_{|v|v} |v_r| v_r \quad (6.187)$$

$$N_{\text{current}} = \frac{1}{2} \rho A_{Lc} L_{oa} C_N(\gamma_c) V_c^2 := N_{|v|v} |v_r| v_r - \underbrace{(X_u - Y_v) u_r v_r}_{\text{Munk moment}} \quad (6.188)$$

for  $u = v = r = 0$ . Notice that the Munk moment  $(Y_v - X_u) u_r v_r$  in the yaw equation is included in the expression for  $N_{\text{current}}$  (see Section 6.5.5). The other terms are recognized as diagonal quadratic damping terms in  $\mathbf{D}(\boldsymbol{\nu}_r)$ .

This gives the following analytical expressions for the area-based current coefficients

$$C_X(\gamma_c) = -2 \left( \frac{-X_{|u|u}}{\rho A_{Fc}} \right) \cos(\gamma_c) |\cos(\gamma_c)| \quad (6.189)$$

$$C_Y(\gamma_c) = 2 \left( \frac{-Y_{|v|v}}{\rho A_{Lc}} \right) \sin(\gamma_c) |\sin(\gamma_c)| \quad (6.190)$$

$$C_N(\gamma_c) = \frac{2}{\rho A_{Lc} L_{oa}} (-N_{|v|v} \sin(\gamma_c) |\sin(\gamma_c)| + \underbrace{\frac{1}{2} (X_u - Y_v) \sin(2\gamma_c)}_{A_{22} - A_{11}}) \quad (6.191)$$

These results are similar to Faltinsen (1990, pp. 187–188). The trigonometric functions in (6.189)–(6.191) will be quite close to the shape of the experimental current coefficients shown in Figure 6.11. For tankers, the current coefficients can be computed using the formulae of Leite *et al.* (1998) whereas the ITTC and cross-flow drag principles are commonly used for other hull forms.

### 6.7.2 Nonlinear DP model based on current coefficients

The nonlinear DP model based on current coefficients takes the following form

$$\dot{\boldsymbol{\eta}} = \mathbf{R}(\psi) \boldsymbol{\nu} \quad (6.192)$$

$$\mathbf{M} \dot{\boldsymbol{\nu}} + \mathbf{C}_{RB}(\boldsymbol{\nu}) \boldsymbol{\nu} + \mathbf{D} \exp(-\alpha V_{rc}) \boldsymbol{\nu}_r + \mathbf{d}(V_{rc}, \gamma_{rc}) = \boldsymbol{\tau} + \boldsymbol{\tau}_{\text{wind}} + \boldsymbol{\tau}_{\text{wave}} \quad (6.193)$$

where

$$\mathbf{d}(V_{rc}, \gamma_{cr}) = \begin{bmatrix} -\frac{1}{2} \rho A_{Fc} C_X(\gamma_{rc}) V_{rc}^2 \\ -\frac{1}{2} \rho A_{Lc} C_Y(\gamma_{rc}) V_{rc}^2 \\ -\frac{1}{2} \rho A_{Lc} L_{oa} C_N(\gamma_{rc}) V_{rc}^2 - N_{|r|r} r |r| \end{bmatrix} \quad (6.194)$$

and  $-N_{|r|r} > 0$  is an optional quadratic damping coefficient used to counteract the destabilizing Munk moment in yaw since the current coefficients do not include nonlinear damping in yaw. The model also includes an optional linear damping matrix

$$\mathbf{D} = \begin{bmatrix} -X_u & 0 & 0 \\ 0 & -Y_v & -Y_r \\ 0 & -N_v & -N_r \end{bmatrix} \quad (6.195)$$

to ensure exponential convergence at low relative speed  $V_r$ . This is done by tuning  $\alpha > 0$ . At higher speeds  $V_{rc} \gg 0$  and the nonlinear term  $\mathbf{d}(V_{rc}, \gamma_{rc})$  dominates over the linear term, which vanishes at higher speeds.

It is also possible to eliminate  $\nu$  in (6.193) by using Property 10.1 in Section 10.3. The key assumption is that  $\mathbf{C}_{RB}(\nu)$  must be parametrized according to (3.60). Hence, it follows that

$$\mathbf{M}\dot{\boldsymbol{\nu}}_r + \mathbf{C}_{RB}(\boldsymbol{\nu}_r)\boldsymbol{\nu}_r + \mathbf{D} \exp(-\alpha V_{rc})\boldsymbol{\nu}_r + \mathbf{d}(V_{rc}, \gamma_{rc}) = \boldsymbol{\tau} + \boldsymbol{\tau}_{\text{wind}} + \boldsymbol{\tau}_{\text{wave}} \quad (6.196)$$

where  $\boldsymbol{\nu}_r$  is the state vector.

### 6.7.3 Linear DP model

As shown in Section 6.4, linear damping is a good assumption for low-speed applications. Similarly, the quadratic velocity terms given by  $\mathbf{C}(\boldsymbol{\nu}_r)\boldsymbol{\nu}_r$  and  $\mathbf{d}(V_{rc}, \gamma_{rc})$  can be neglected when designing DP control systems if the ocean currents (drift) are properly compensated for by using integral action. One way to do this is to treat the ocean currents as a slowly varying bias vector  $\mathbf{b}$  expressed in  $\{n\}$ . Hence, the relative velocity vector  $\boldsymbol{\nu}_r$  is superfluous.

The generalized position  $\boldsymbol{\eta} = [x^n, y^n, \psi]^\top$  is usually measured using GNSS and a gyrocompass. Since the heading angle  $\psi = \psi(t)$  is accurately measured, the kinematic nonlinearity due to the rotation matrix can be removed by assuming that

$$\mathbf{R}(\psi(t)) := \mathbf{R}(t) \quad (6.197)$$

is known for all  $t \geq 0$ . Consequently, the resulting DP model will be a linear time-varying (LTV) model

$$\dot{\boldsymbol{\eta}} = \mathbf{R}(t)\boldsymbol{\nu} \quad (6.198)$$

$$\mathbf{M}\dot{\boldsymbol{\nu}} + \mathbf{D}\boldsymbol{\nu} = \mathbf{R}^\top(t)\mathbf{b} + \boldsymbol{\tau} + \boldsymbol{\tau}_{\text{wind}} + \boldsymbol{\tau}_{\text{wave}} \quad (6.199)$$

$$\dot{\mathbf{b}} = \mathbf{0} \quad (6.200)$$

Notice that the currents are assumed constant in  $\{n\}$  and therefore transformed to  $\{b\}$  by  $\mathbf{R}^\top(t)\mathbf{b}$ . The generalized control force vector  $\boldsymbol{\tau} \in \mathbf{R}^3$  is assumed to be linear in the control inputs  $\mathbf{u} \in \mathbb{R}^r$  such that

$$\boldsymbol{\tau} = \mathbf{B}\mathbf{u} \quad (6.201)$$

where  $\mathbf{B}$  is the input matrix. The resulting state-space model is a 9-state LTV system

$$\dot{\boldsymbol{x}} = \underbrace{\begin{bmatrix} \mathbf{0}_{3 \times 3} & \mathbf{R}(t) & \mathbf{0}_{3 \times 3} \\ \mathbf{0}_{3 \times 3} & -\mathbf{M}^{-1}\mathbf{D} & \mathbf{M}^{-1}\mathbf{R}^\top(t) \\ \mathbf{0}_{3 \times 3} & \mathbf{0}_{3 \times 3} & \mathbf{0}_{3 \times 3} \end{bmatrix}}_{\mathbf{A}(t)} \boldsymbol{x} + \underbrace{\begin{bmatrix} \mathbf{0}_{3 \times r} \\ \mathbf{M}^{-1}\mathbf{B} \\ \mathbf{0}_{3 \times r} \end{bmatrix}}_{\mathbf{B}} \boldsymbol{u} + \underbrace{\begin{bmatrix} \mathbf{0}_{3 \times 3} \\ \mathbf{M}^{-1} \\ \mathbf{0}_{3 \times 3} \end{bmatrix}}_{\mathbf{E}} \boldsymbol{w} \quad (6.202)$$

where  $\boldsymbol{x} = [\boldsymbol{\eta}^\top, \boldsymbol{\nu}^\top, \boldsymbol{b}^\top]^\top$  and

$$\boldsymbol{w} = \boldsymbol{\tau}_{\text{wind}} + \boldsymbol{\tau}_{\text{wave}} \quad (6.203)$$

This model is intended for controller–observer design.

**Matlab:**

A linear model of a supply vessel is included in the MSS toolbox

```
[xdot,U] = supply(x,tau) % Supply vessel L = 76.2 m
```



## Chapter 7

# Autopilot Models for Course and Heading Control

This chapter presents mathematical models of marine craft for *course* and *heading* control. The presented models are state-of-the art models used to design autopilot systems for ships and underwater vehicles. In *Encyclopedia Britannica*, an autopilot is defined as follows:

*Automatic pilot*, “also called autopilot, or autohelmsman, device for controlling an aircraft or other vehicle without constant human intervention.”

The earliest automatic pilots could do no more than maintain an aircraft in straight and level flight by controlling *roll*, *pitch* and *yaw* movements; and they are still used most often to relieve the pilot during routine cruising. Modern automatic pilots can, however, execute complex maneuvers such as 3-D attitude control and path-following control and they are used for aircraft, marine craft, automotive systems, etc.

It is important to stress the concepts for course and heading control since there are many conceptual misunderstandings regarding the course and heading of a marine craft. The course angle  $\chi$  of a marine craft is the cardinal direction in which the craft is moving. Hence, the course angle is to be distinguished from the heading angle  $\psi$ , which is the compass direction in which the craft's bow or nose is pointed. The difference between the course and heading angles is the crab angle

$$\beta_c = \text{asin}(v/u) \quad (7.1)$$

which satisfies (see Section 2.5.2)

$$\chi = \psi + \beta_c \quad (7.2)$$

Notice that the course angle is not defined for zero speed while the yaw angle (compass direction) is well-defined for zero and forward speed.

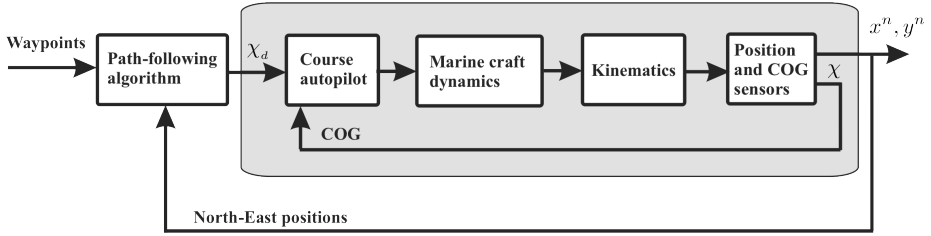


Figure 7.1: Course angle autopilot and path-following control systems.

## 7.1 Autopilot Models for Course Control

Surface craft are usually equipped with a global navigation satellite system (GNSS) receiver, which measures:

**COG** course over ground ( $\chi$ )

**SOG** speed over ground ( $U$ )

Underwater vehicles, however, use hydroacoustic reference systems to determine their position, velocity and course.

Path-following controllers are usually implemented using a course autopilot as shown in Figure 7.1. The path that a marine craft follows over the ground is called COG or *track*. Furthermore, the intended track is referred to as a *route*. For ships and aircraft, routes are typically straight-line segments between waypoints.

### 7.1.1 State-space model

If the course angle  $\chi$  is available as a direct measurement it is straightforward to design a PID controller for course control. Alternatively, the course angle can be computed from the North-East positions according to

$$\chi[k] = \text{atan2}(y^n[k] - y^n[k-1], x^n[k] - x^n[k-1]) \quad (7.3)$$

The PID controller gains are usually tuned using the maneuvering models presented in Section 6.5 to verify the responses. Let the generalized position and velocity vectors be denoted  $\boldsymbol{\eta} = [x^n, y^n, \psi]^\top$  and  $\boldsymbol{\nu} = [u, v, r]^\top$ , respectively. From (6.92) we have

$$M\dot{\boldsymbol{\nu}}_r + C(\boldsymbol{\nu}_r)\boldsymbol{\nu}_r + D\boldsymbol{\nu}_r + D_n(\boldsymbol{\nu}_r)\boldsymbol{\nu}_r = \boldsymbol{\tau} + \boldsymbol{\tau}_{\text{wind}} + \boldsymbol{\tau}_{\text{wave}} \quad (7.4)$$

Assume that North-East positions ( $x^n, y^n$ ), SOG and COG are measured. The state-space model corresponding to these measurements is

$$\dot{\boldsymbol{\eta}} = \mathbf{R}(\psi)\boldsymbol{\nu} \quad (7.5)$$

$$\dot{\boldsymbol{\nu}} = \begin{bmatrix} rv_c \\ -ru_c \\ 0 \end{bmatrix} + \mathbf{M}^{-1} (\boldsymbol{\tau} + \boldsymbol{\tau}_{\text{wind}} + \boldsymbol{\tau}_{\text{wave}} - \mathbf{C}(\boldsymbol{\nu}_r)\boldsymbol{\nu}_r - \mathbf{D}\boldsymbol{\nu}_r - \mathbf{D}_n(\boldsymbol{\nu}_r)\boldsymbol{\nu}_r) \quad (7.6)$$

$$y_1 = x^n \quad (7.7)$$

$$y_2 = y^n \quad (7.8)$$

$$y_3 = \sqrt{u^2 + v^2} \quad (7.9)$$

$$y_4 = \psi + \arcsin\left(\frac{v}{u}\right) \quad (7.10)$$

where  $\boldsymbol{\nu}_r = \boldsymbol{\nu} - [u_c, v_c, 0]^\top$ .

The control objective of the course autopilot system in Figure 7.1 is to ensure that the inner loop satisfies

$$\frac{\chi}{\chi_d} \approx 1 \quad (7.11)$$

### 7.1.2 Transfer function model

For a marine craft moving on a straight line at forward speed  $U$  the crab angle  $\beta_c = 0$ . During turning, the crab angle will be nonzero and act as a disturbance when controlling the course angle. A linear design model for PID control can be found by differentiating the course angle (7.2) with respect to time and approximate the yaw dynamics by a mass-damper system

$$\dot{\chi} = r + \dot{\beta}_c \quad (7.12)$$

$$(I_z - N_{\dot{r}})\ddot{r} - N_r r = \tau_6 \quad (7.13)$$

where  $\tau_6$  is the control input and  $\beta_c$  is treated as a disturbance, which need to be canceled by integral action. The yaw rate transfer function becomes

$$\frac{r}{\tau_6}(s) = \frac{K}{Ts + 1} \quad (7.14)$$

where  $K = 1/(-N_r)$  and  $T = (I_z - N_{\dot{r}})/(-N_r)$ . Consequently,

$$\chi(s) = \frac{K}{s(Ts + 1)}\tau_6(s) + \beta_c(s) \quad (7.15)$$

## 7.2 Autopilot Models for Heading Control

Ships are usually equipped with a gyrocompass, which is nonmagnetic compass based on a fast-spinning disc. A North-seeking gyro gives a highly accurate measurement of

the yaw angle and this is the preferred sensor from a safety point of view. Magnetic compasses are not used on-board commercial ships as navigational devices since they are very sensitive to magnetic disturbances. An alternative measurement could be to use two GNSS antennas on the same receiver with a known offset vector to compute the heading angle. This solution is, however, sensitive to ionospheric disturbances, multipath, loss of signals, the number of available satellites, etc.

If the heading angle  $\psi$  is available as a direct measurement, it is straightforward to design a PID controller for heading control. The PID controller gains can be computed as a function of the model parameters if the yaw dynamics is known. Models for this are presented in Section 7.2.1–7.2.3 and heading autopilot design is discussed in Section 12.2.5. Figure 7.2 shows a heading autopilot system.

Model-based heading autopilots for marine craft are usually based on the model representation of Nomoto *et al.* (1957) for which the sway force and yaw moment (see Section 9.5.1)

$$\tau_2 = -Y_\delta \delta \quad (7.16)$$

$$\tau_6 = -N_\delta \delta \quad (7.17)$$

are generated by a single rudder with deflection  $\delta$ . It is straightforward to modify  $\tau_2$  and  $\tau_6$  to include other control inputs as shown in Chapter 9.

### 7.2.1 Second-order Nomoto model

A linear autopilot model for heading control can be derived from the maneuvering model

$$M\dot{\nu}_r + N\nu_r = b\delta \quad (7.18)$$

where  $\nu_r = [v_r, r]^\top$  and

$$M = \begin{bmatrix} m - Y_{\dot{v}} & mx_g - Y_{\dot{r}} \\ mx_g - Y_{\dot{r}} & I_z - N_{\dot{r}} \end{bmatrix} \quad (7.19)$$

$$N = \begin{bmatrix} -Y_v & (m - X_{\dot{u}})U - Y_r \\ (X_{\dot{u}} - Y_{\dot{v}})U - N_v & (mx_g - Y_{\dot{r}})U - N_r \end{bmatrix} \quad (7.20)$$

$$b = \begin{bmatrix} -Y_\delta \\ -N_\delta \end{bmatrix} \quad (7.21)$$

Choosing the yaw rate  $r$  as output

$$r = c^\top \nu_r, \quad c^\top = [0, 1] \quad (7.22)$$

and application of the *Laplace transformation* yields

$$\frac{r}{\delta}(s) = \frac{K(T_3 s + 1)}{(T_1 s + 1)(T_2 s + 1)} \quad (7.23)$$

A similar expression is obtained for the sway motion

$$\frac{v_r}{\delta}(s) = \frac{K_v(T_v s + 1)}{(T_1 s + 1)(T_2 s + 1)} \quad (7.24)$$

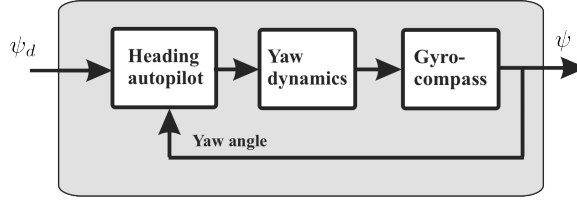


Figure 7.2: Heading autopilot system where the yaw angle is measured by using a gyrocompass.

where  $K_v$  and  $T_v$  differ from  $K$  and  $T_3$  in the yaw equation. Equation (7.23) is referred to as *Nomoto's second-order model* (Nomoto *et al.* 1957). The time-domain representation becomes

$$T_1 T_2 \psi^{(3)} + (T_1 + T_2) \ddot{\psi} + \dot{\psi} = K(T_3 \dot{\delta} + \delta) \quad (7.25)$$

This model can be normalized using speed  $U$  and length  $L$  (see Appendix D)

$$\left(\frac{L}{U}\right)^2 T'_1 T'_2 \psi^{(3)} + \left(\frac{L}{U}\right) (T'_1 + T'_2) \ddot{\psi} + \dot{\psi} = K' T'_3 \dot{\delta} + \left(\frac{U}{L}\right) K' \delta \quad (7.26)$$

The normalized model can be used as basis for gain-scheduling control by choosing  $U$  as scheduling variable. Consequently, the PID controller gains will be functions of the model parameters and the direct measurement  $U$ . Parameter adaption based on classical methods will in general be slower than gain scheduling.

## 7.2.2 First-order Nomoto model

The *first-order Nomoto model* is obtained by defining the *equivalent time constant*

$$T := T_1 + T_2 - T_3 \quad (7.27)$$

Consequently, (7.25) can be approximated as

$$\frac{r}{\delta}(s) = \frac{K}{Ts + 1} \quad (7.28)$$

Using,  $\dot{\psi} = r$  yields

$$\frac{\psi}{\delta}(s) = \frac{K}{s(Ts + 1)} \quad (7.29)$$

which is the transfer function that is used in most commercial autopilot systems. The time-domain representation is

$$T \ddot{\psi} + \dot{\psi} = K \delta \quad (7.30)$$

The first-order Nomoto model can be normalized using speed  $U$  and length  $L$  according to (see Appendix D)

$$\left(\frac{L}{U}\right) T' \ddot{\psi} + \psi = \left(\frac{U}{L}\right) K' \delta \quad (7.31)$$

The normalized model is used to design a gain-scheduled autopilot where  $U$  is treated as a time-varying measurement.

The accuracy of the first-order Nomoto model when compared to the second-order model is illustrated in Example 7.1 where a course stable cargo ship and a course unstable oil tanker are considered (see Section 12.1.1).

**Example 7.1 (Frequency Responses for Nomoto First- and Second-Order Models)**  
Consider a Mariner class cargo ship (Chislett and Strøm-Tøjsen, 1965a) and a fully loaded tanker (Dyne and Trägårdh 1975) given by the parameters in Table 7.1.

Table 7.1: Parameters for a cargo ship and a fully loaded oil tanker

	$L$ (m)	$u_0$ (m/s)	$\nabla$ (dwt)	$K$ (1/s)	$T_1$ (s)	$T_2$ (s)	$T_3$ (s)
Cargo ship	161	7.7	16622	0.185	118.0	7.8	18.5
Oil tanker	350	8.1	389100	-0.019	-124.1	16.4	46.0

### Matlab:

The Bode diagram is generated by using the MSS toolbox commands:

```

T1=118; T2=7.8; T3=18.5; K=0.185;
nomoto(T1, T2, T3, K)

T1=-124.1; T2=16.4; T3=46.0; K=-0.019;
nomoto(T1, T2, T3, K);

function nomoto(T1,T2,T3,K);
% NOMOTO(T1,T2,T3,K) generates the Bode plots for
%           K           K (1+T3s)
% H1(s) = -----      H2(s) = -----
%           s (1+Ts)           s (1+T1s) (1+T2s)

T = T1+T2-T3;
d1 = [T 1 0]; n1 = K;
d2 = [T1*T2 T1+T2 1 0]; n2 = K*[T3 1];
[mag1,phase1,w] = bode(n1,d1);
[mag2,phase2] = bode(n2,d2,w);

% shift phase with 360 deg for course-unstable ship
if K < 0
    phase1 = phase1-360;
    phase2 = phase2-360;
end

subplot(211), semilogx(w,20*log10(mag1)), grid;
xlabel('Frequency [rad/s]'), title('Gain [dB]');

```

```

hold on, semilogx(w, 20*log10(mag2), '--'), hold off;

subplot(212), semilogx(w, phase1), grid;
xlabel('Frequency [rad/s]'), title('Phase [deg]');
hold on, semilogx(w, phase2, '--'), hold off;

```

It is seen from Figure 7.3 that the first-order approximation is quite accurate up to 0.1 rad/s for the cargo ship and the tanker. A small deviation in the phase around 0.5 rad/s is observed. This is due to the cancellation of the sway dynamics.

### 7.2.3 Nonlinear extensions of Nomoto's model

The linear Nomoto model can be extended to include nonlinear effects by adding a *static nonlinearity* to describe the *maneuvering characteristics*.

#### Nonlinear extension of Nomoto's first-order model

In Norrbin (1963) the following first-order model was proposed

$$T\dot{r} + H_N(r) = K\delta \quad (7.32)$$

$$H_N(r) = n_3r^3 + n_2r^2 + n_1r + n_0 \quad (7.33)$$

where  $H_N(r)$  is a nonlinear function. For  $H_N(r) = r$ , the linear model (7.30) is obtained.

#### Nonlinear extension of Nomoto's second-order model

Bech and Wagner Smith (1969) propose a second-order model

$$T_1 T_2 \ddot{r} + (T_1 + T_2)\dot{r} + K H_B(r) = K(\delta + T_3\dot{\delta}) \quad (7.34)$$

$$H_B(r) = b_3r^3 + b_2r^2 + b_1r + b_0 \quad (7.35)$$

where  $H_B(r)$  can be found from Bech's reverse spiral maneuver. The linear equivalent (7.25) is obtained for  $H_B(r) = r$ .

The linear and nonlinear maneuvering characteristics are shown in Figure 12.12 in Section 12.1.2. They are generated by solving for  $r$  as a function of  $\delta$  using the steady-state solutions of (7.32) or (7.34)

$$H_N(r) = K\delta, \quad H_B(r) = \delta \quad (7.36)$$

The nonlinear maneuvering characteristics can also be generated from full-scale maneuvering tests. For stable ships both the *Bech* and *Dieudonne spiral tests* can be applied, while the Bech spiral is the only one avoiding the hysteresis effect for course-unstable ships; see Section 12.1.2 for details.

For a course-unstable ship,  $b_1 < 0$ , whereas a course-stable ship satisfies  $b_1 > 0$ . A single-screw propeller or asymmetry in the hull will cause a nonzero value of  $b_0$ .

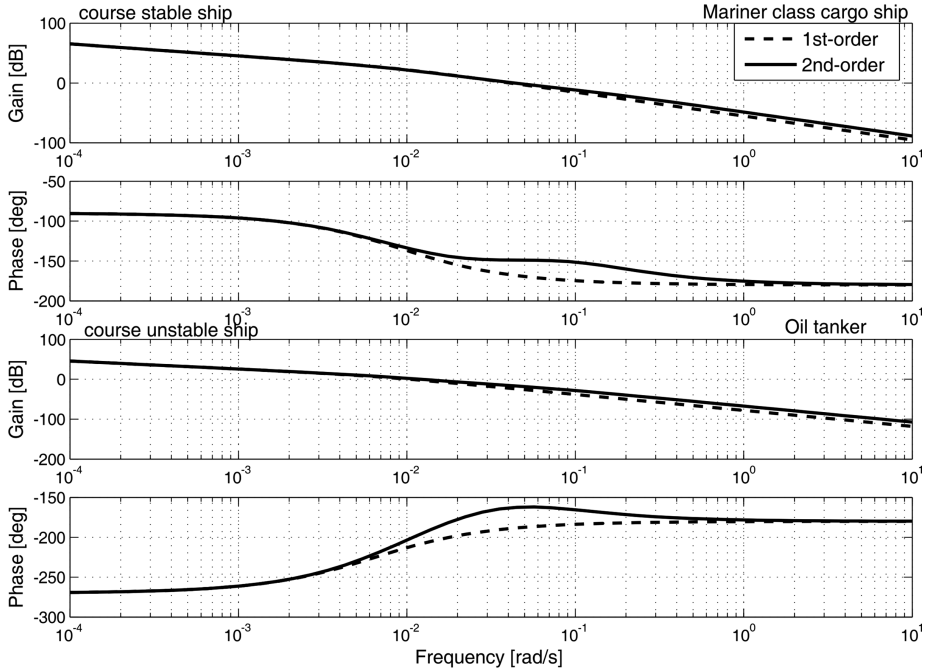


Figure 7.3: First-order and second-order Nomoto transfer functions for a course-stable Mariner class cargo ship and a course-unstable oil tanker.

Similarly, symmetry in the hull implies that  $b_2 = 0$ . Since a constant rudder angle is required to compensate for constant steady-state wind and current forces, the bias term  $b_0$  could conveniently be treated as an additional rudder off set. This in turn implies that a large number of ships can be described by the polynomial

$$H_B(r) = b_3r^3 + b_1r \quad (7.37)$$

The coefficients  $b_i$  for  $i = 0, \dots, 3$  are related to those in Norrbom's model  $n_i$  by

$$n_i = \frac{b_i}{|b_1|} \quad (7.38)$$

resulting in

$$H_N(r) = n_3r^3 + n_1r \quad (7.39)$$

This implies that  $n_1 = 1$  for a course-stable ship and  $n_1 = -1$  for a course-unstable ship.

#### 7.2.4 Pivot point

The pivot point is a useful tool in ship handling and the location of the pivot point in a maneuvering situations is of great importance for the ship handler. The *pivot point* in yaw is defined as follows:

**Definition 7.1 (Pivot Point)**

A ship's pivot point  $x_p$  is a point on the centerline measured from the CG at which sway and yaw completely cancel each other (Tzeng 1998a)

$$v_{np} = v_{ng} + x_p r \equiv 0 \quad (7.40)$$

where  $v_{ng}$  is the sway velocity of CG with respect to  $\{n\}$ . The pivot point will scribe the ship's turning circle and all other points appear to be turning about this point.

It is possible to compute the pivot point for a turning ship online by measuring the velocity  $v_{ng}(t)$  in the CG and the turning rate  $r(t)$ . From (7.40) it follows that

$$x_p(t) = -\frac{v_{ng}(t)}{r(t)}, \quad r(t) \neq 0 \quad (7.41)$$

This expression is not defined for a zero yaw rate corresponding to a straight-line motion. This means that the pivot point is located at infinity when moving on a straight line or in a pure sway motion.

It is well known to the pilots that the pivot point of a turning ship is located at about 1/5 to 1/4 ship length aft of bow (Tzeng 1998a). The location of the pivot point of a rudder controlled ship is related to the ratio of the *sway-rudder* and *yaw-rudder* gain coefficients. This can be explained by considering the linearized maneuvering equations in the steady state. From (7.23) and (7.24) we have

$$\begin{aligned} \frac{v}{r} &= \frac{K_v(T_v s + 1)}{K(T_3 s + 1)} \\ &\stackrel{s=0}{=} \frac{K_v}{K} \end{aligned} \quad (7.42)$$

Consequently, the steady-state location of the pivot point is given by

$$x_{p,ss} = -\frac{K_v}{K} \quad (7.43)$$

This expression can also be related to the hydrodynamic derivatives according to

$$x_{p,ss} = -\frac{N_r Y_\delta - (Y_r - mU) N_\delta}{Y_v N_\delta - N_v Y_\delta} \quad (7.44)$$

Notice that  $x_{p,ss}$  depends on the forward speed  $U$ . The nondimensional form becomes (see Appendix D)

$$\begin{aligned} x'_{p,ss} &= \frac{x_{p,ss}}{L_{pp}} \\ &= -\frac{N'_r Y'_\delta - (Y'_r - m') N'_\delta}{Y'_v N'_\delta - N'_v Y'_\delta} \end{aligned} \quad (7.45)$$

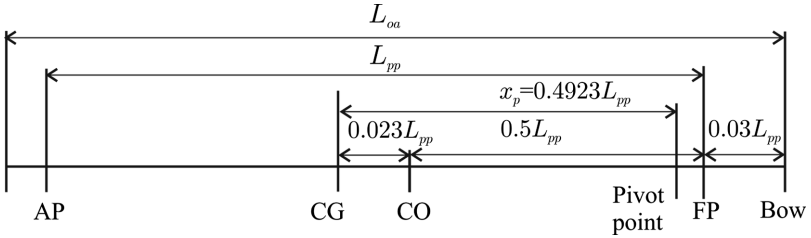


Figure 7.4: Location of the pivot point for the Mariner Class vessel.

### Example 7.2 (Pivot Point for the Mariner Class Vessel)

Consider the Mariner Class vessel (Chislett and Strøm-Tejsen, 1965b) where the nondimensional linear maneuvering coefficients for  $u_0 = 7.175 \text{ m/s}$  (15 knots) are given as

$$\begin{aligned} Y'_v &= -1160 \times 10^{-5} & N'_v &= -264 \times 10^{-5} \\ Y'_r - m' &= -499 \times 10^{-5} & N'_r &= -166 \times 10^{-5} \\ Y'_\delta &= 278 \times 10^{-5} & N'_\delta &= -139 \times 10^{-5} \end{aligned}$$

The Mariner Class vessel is programmed in the MSS toolbox file `mariner.m`. The nondimensional pivot point is computed from (7.45). This gives

$$x'_{p,ss} = 0.4923 \quad \Rightarrow \quad x_{p,ss} = 0.4923 L_{pp} \quad (7.46)$$

where  $L_{pp} = 160.93 \text{ m}$  is the length between the perpendiculars AP and FP. The overall length is  $L_{oa} = 171.8 \text{ m}$ . The pivot point  $x_{p,ss}$  is located ahead of the CG. Since the CG is located at  $x_g = -0.023 L_{pp}$  and the bow is approximately  $0.03 L_{pp}$  fore of FP, the pivot point is  $0.06 L_{pp}$  aft of the bow (see Figure 7.4).

## Chapter 8

# Models for Underwater Vehicles

This chapter presents models for underwater vehicles. The foundation for the models are the kinematic equations (Chapter 2), rigid-body kinetics (Chapter 3), hydrostatics (Chapter 4) and maneuvering theory (Chapter 6). Results from these chapters are combined to obtain forward speed models, horizontal-plane models for steering, vertical-plane models for diving and 6-DOF coupled models for advanced maneuvers.

### 8.1 6-DOF Models for AUVs and ROVs

Ship models are usually reduced-order models for control of the horizontal plane motions (*surge*, *sway* and *yaw*) in combination with *roll* if roll damping is an issue. In this section we will discuss 6-DOF models, which are useful for underwater vehicles with actuation in all DOFs. Such vehicles can control the position and attitude in 6 DOFs by using thrusters, moving weights, spinning rotors and control surfaces.

A 6-DOF model is usually implemented in a computer to describe all dynamic effects as accurately as possible. This is referred to as the *simulation model*; see Figure 1.4 in Section 1.1. The simulation model should be able to reconstruct the time responses of the physical system. Model-based controllers and state estimators, however, can be designed using reduced-order or simplified models.

When designing feedback control systems it can be advantageous to formulate the equations of motion in both the  $\{b\}$  and  $\{n\}$  frames in order to exploit physical properties of the model. This section includes nonlinear transformations that can be used to represent the equations of motion in both reference frames.

#### 8.1.1 Equations of motion expressed in BODY

Consider the nonlinear equations of motion expressed in the following form

$$\dot{\boldsymbol{\eta}} = \mathbf{J}_k(\boldsymbol{\eta})(\boldsymbol{\nu}_r + \boldsymbol{\nu}_c) \quad (8.1)$$

$$\mathbf{M}\dot{\boldsymbol{\nu}}_r + \mathbf{C}(\boldsymbol{\nu}_r)\boldsymbol{\nu}_r + \mathbf{D}(\boldsymbol{\nu}_r)\boldsymbol{\nu}_r + \mathbf{g}(\boldsymbol{\eta}) + \mathbf{g}_o = \boldsymbol{\tau} \quad (8.2)$$

where  $\boldsymbol{\nu}_c = [u_c, v_c, w_c, 0, 0, 0]^\top$  is the current velocity vector and

$$\boldsymbol{M} = \boldsymbol{M}_{RB} + \boldsymbol{M}_A \quad (8.3)$$

$$\boldsymbol{C}(\boldsymbol{\nu}_r) = \boldsymbol{C}_{RB}(\boldsymbol{\nu}_r) + \boldsymbol{C}_A(\boldsymbol{\nu}_r) \quad (8.4)$$

$$\boldsymbol{D}(\boldsymbol{\nu}_r) = \boldsymbol{D} + \boldsymbol{D}_n(\boldsymbol{\nu}_r) \quad (8.5)$$

The expressions for  $\boldsymbol{\eta}$  and  $\boldsymbol{J}_k(\boldsymbol{\eta})$  depend on the kinematic representation. Two different choices for  $\boldsymbol{J}_k(\boldsymbol{\eta})$  will be presented where the subscript  $k \in \{\Theta, q\}$  denotes the Euler angle and unit quaternion representation, respectively. Moreover,

$$\boldsymbol{J}_\Theta(\boldsymbol{\eta}) = \begin{bmatrix} \boldsymbol{R}(\boldsymbol{\Theta}_{nb}) & \mathbf{0}_{3 \times 3} \\ \mathbf{0}_{3 \times 3} & \boldsymbol{T}(\boldsymbol{\Theta}_{nb}) \end{bmatrix}, \quad \boldsymbol{\eta} = [x^n, y^n, z^n, \phi, \theta, \psi]^\top \quad (8.6)$$

$$\boldsymbol{J}_q(\boldsymbol{\eta}) = \begin{bmatrix} \boldsymbol{R}(\boldsymbol{q}_b^n) & \mathbf{0}_{3 \times 3} \\ \mathbf{0}_{4 \times 3} & \boldsymbol{T}(\boldsymbol{q}_b^n) \end{bmatrix}, \quad \boldsymbol{\eta} = [x^n, y^n, z^n, \eta, \varepsilon_1, \varepsilon_2, \varepsilon_3]^\top \quad (8.7)$$

The system inertia matrix  $\boldsymbol{M}$  for an underwater vehicle follows the symmetry considerations in Section 8.1.4. If we consider a starboard–port symmetrical underwater vehicles with  $y_g = 0$  and  $I_{xy} = I_{yz} = 0$ , this gives

$$\boldsymbol{M} = \begin{bmatrix} m - X_{\dot{u}} & 0 & -X_{\dot{w}} & 0 & mz_g - X_{\dot{q}} & 0 \\ 0 & m - Y_{\dot{v}} & 0 & -mz_g - Y_{\dot{p}} & 0 & mx_g - Y_{\dot{r}} \\ -X_{\dot{w}} & 0 & m - Z_{\dot{w}} & 0 & -mx_g - Z_{\dot{q}} & 0 \\ 0 & -mz_g - Y_{\dot{p}} & 0 & I_x - K_{\dot{p}} & 0 & -I_{zx} - K_{\dot{r}} \\ mz_g - X_{\dot{q}} & 0 & -mx_g - Z_{\dot{q}} & 0 & I_y - M_{\dot{q}} & 0 \\ 0 & mx_g - Y_{\dot{r}} & 0 & -I_{zx} - K_{\dot{r}} & 0 & I_z - N_{\dot{r}} \end{bmatrix} \quad (8.8)$$

Consequently, it is straightforward to compute the Coriolis and centripetal matrix  $\boldsymbol{C}(\boldsymbol{\nu}_r)$  using the results in Sections 3.3 and 6.3.3 when the structure of  $\boldsymbol{M}$  has been determined. In general, the damping of an underwater vehicle moving in 6 DOF at high speed will be highly nonlinear and coupled. This could be described mathematically as

$$\boldsymbol{D}_n(\boldsymbol{\nu}_r)\boldsymbol{\nu}_r = \begin{bmatrix} |\boldsymbol{\nu}_r|^\top \boldsymbol{D}_{n1}\boldsymbol{\nu}_r \\ |\boldsymbol{\nu}_r|^\top \boldsymbol{D}_{n2}\boldsymbol{\nu}_r \\ |\boldsymbol{\nu}_r|^\top \boldsymbol{D}_{n3}\boldsymbol{\nu}_r \\ |\boldsymbol{\nu}_r|^\top \boldsymbol{D}_{n4}\boldsymbol{\nu}_r \\ |\boldsymbol{\nu}_r|^\top \boldsymbol{D}_{n5}\boldsymbol{\nu}_r \\ |\boldsymbol{\nu}_r|^\top \boldsymbol{D}_{n6}\boldsymbol{\nu}_r \end{bmatrix} \quad (8.9)$$

where  $|\boldsymbol{\nu}_r|^\top = [|u_r|, |v_r|, |w_r|, |p|, |q|, |r|]$  and  $\boldsymbol{D}_{ni}(\boldsymbol{\nu}_r)$  for  $i = 1, \dots, 6$  are  $6 \times 6$  matrices. Nevertheless, one rough approximation could be to use quadratic drag in surge and the cross-flow drag in sway and yaw (see Section 6.4.3). Alternatively, if the vehicle is performing a noncoupled motion, it makes sense to assume a diagonal structure of  $\boldsymbol{D}(\boldsymbol{\nu}_r)$  such that

$$\begin{aligned} \boldsymbol{D}(\boldsymbol{\nu}_r) = & -\text{diag}\{X_u, Y_v, Z_w, K_p, M_q, N_r\} \\ & -\text{diag}\{X_{|u|u}|u_r|, Y_{|vv|}|v_r|, Z_{|w|w}|w_r|, K_{|p|p}|p|, M_{|q|q}|q|, N_{|r|r}|r|\} \end{aligned} \quad (8.10)$$

Alternatively, the current coefficient representation in Section 6.7.1 can be used to model the damping. This can be done by replacing  $D_n(\nu_r)\nu_r$  with 6-DOF current coefficients (see Section 6.7.1)

$$\mathbf{d}(V_{rc}, \gamma_{cr}) = -\frac{1}{2}\rho V_{rc}^2 \begin{bmatrix} A_{Fc} C_X(\gamma_{rc}) \\ A_{Lc} C_Y(\gamma_{rc}) \\ A_{Fc} C_Z(\gamma_{rc}) \\ A_{Lc} H_{Lc} C_K(\gamma_{rc}) \\ A_{Fc} H_{Fc} C_M(\gamma_{rc}) \\ A_{Lc} L_{oa} C_N(\gamma_{rc}) \end{bmatrix} \quad (8.11)$$

where  $C_X, C_Y, C_Z, C_K, C_M$  and  $C_N$  are the current coefficients and  $H_{Fc}$  and  $H_{Lc}$  are the centroids above the water line of the frontal and lateral projected areas  $A_{Fc}$  and  $A_{Lc}$ , respectively.

The submerged weight of the body and buoyancy force are (see Section 4.1)

$$\mathbf{g}(\boldsymbol{\eta}) = \begin{bmatrix} (W - B) \sin(\theta) \\ -(W - B) \cos(\theta) \sin(\phi) \\ -(W - B) \cos(\theta) \cos(\phi) \\ -(y_g W - y_b B) \cos(\theta) \cos(\phi) + (z_g W - z_b B) \cos(\theta) \sin(\phi) \\ (z_g W - z_b B) \sin(\theta) + (x_g W - x_b B) \cos(\theta) \cos(\phi) \\ -(x_g W - x_b B) \cos(\theta) \sin(\phi) - (y_g W - y_b B) \sin(\theta) \end{bmatrix} \quad (8.12)$$

### 8.1.2 Equations of motion expressed in NED

For simplicity, assume that  $\boldsymbol{\nu}_c = \mathbf{0}$ . Hence, the equations of motion (8.2) when transformed to  $\{n\}$  take the following form

$$\mathbf{M}^*(\boldsymbol{\eta})\ddot{\boldsymbol{\eta}} + \mathbf{C}^*(\boldsymbol{\nu}, \boldsymbol{\eta})\dot{\boldsymbol{\eta}} + \mathbf{D}^*(\boldsymbol{\nu}, \boldsymbol{\eta})\dot{\boldsymbol{\eta}} + \mathbf{g}^*(\boldsymbol{\eta}) + \mathbf{g}_o^*(\boldsymbol{\eta}) = \boldsymbol{\tau}^* \quad (8.13)$$

where the expressions for  $\mathbf{M}^*$ ,  $\mathbf{C}^*(\boldsymbol{\nu}, \boldsymbol{\eta})$ ,  $\mathbf{D}^*(\boldsymbol{\nu}, \boldsymbol{\eta})$ ,  $\mathbf{g}^*(\boldsymbol{\eta})$ ,  $\mathbf{g}_o^*(\boldsymbol{\eta})$ ,  $\boldsymbol{\tau}^*$  and the associated kinematic transformations depend on how attitude is represented. The Euler angles and unit quaternion choices are outlined below:

- 1. Positions and Euler Angles:** The Euler angle representation (2.45) is based on the three parameters  $\phi, \theta$  and  $\psi$ . This gives

$$\mathbf{J}_\Theta(\boldsymbol{\eta}) = \begin{bmatrix} \mathbf{R}(\boldsymbol{\Theta}_{nb}) & \mathbf{0}_{3 \times 3} \\ \mathbf{0}_{3 \times 3} & \mathbf{T}(\boldsymbol{\Theta}_{nb}) \end{bmatrix}, \quad \mathbf{J}_\Theta^{-1}(\boldsymbol{\eta}) = \begin{bmatrix} \mathbf{R}^\top(\boldsymbol{\Theta}_{nb}) & \mathbf{0}_{3 \times 3} \\ \mathbf{0}_{3 \times 3} & \mathbf{T}^{-1}(\boldsymbol{\Theta}_{nb}) \end{bmatrix} \quad (8.14)$$

where  $\boldsymbol{\eta} := [x^n, y^n, z^n, \phi, \theta, \psi]^\top$ . The representation singularity at  $\theta \neq \pm\pi/2$  in the expression for  $\mathbf{T}_\Theta$  implies that the inverse matrix  $\mathbf{J}_\Theta^{-1}(\boldsymbol{\eta})$  does not exist at this value. The transformation is as follows

$$\begin{aligned} \dot{\boldsymbol{\eta}} &= \mathbf{J}_\Theta(\boldsymbol{\eta})\boldsymbol{\nu} & \iff & \boldsymbol{\nu} &= \mathbf{J}_\Theta^{-1}(\boldsymbol{\eta})\dot{\boldsymbol{\eta}} \\ \ddot{\boldsymbol{\eta}} &= \mathbf{J}_\Theta(\boldsymbol{\eta})\dot{\boldsymbol{\nu}} + \dot{\mathbf{J}}_\Theta(\boldsymbol{\eta})\boldsymbol{\nu} & \iff & \dot{\boldsymbol{\nu}} &= \mathbf{J}_\Theta^{-1}(\boldsymbol{\eta})[\ddot{\boldsymbol{\eta}} - \dot{\mathbf{J}}_\Theta(\boldsymbol{\eta})\mathbf{J}_\Theta^{-1}(\boldsymbol{\eta})\dot{\boldsymbol{\eta}}] \end{aligned}$$

and

$$\begin{aligned} \mathbf{M}^*(\boldsymbol{\eta}) &= \mathbf{J}_\Theta^{-\top}(\boldsymbol{\eta}) \mathbf{M} \mathbf{J}_\Theta^{-1}(\boldsymbol{\eta}) \\ \mathbf{C}^*(\boldsymbol{\nu}, \boldsymbol{\eta}) &= \mathbf{J}_\Theta^{-\top}(\boldsymbol{\eta}) [\mathbf{C}(\boldsymbol{\nu}) - \mathbf{M} \mathbf{J}_\Theta^{-1}(\boldsymbol{\eta}) \dot{\mathbf{J}}_\Theta(\boldsymbol{\eta})] \mathbf{J}_\Theta^{-1}(\boldsymbol{\eta}) \\ \mathbf{D}^*(\boldsymbol{\nu}, \boldsymbol{\eta}) &= \mathbf{J}_\Theta^{-\top}(\boldsymbol{\eta}) \mathbf{D}(\boldsymbol{\nu}) \mathbf{J}_\Theta^{-1}(\boldsymbol{\eta}) \\ \mathbf{g}^*(\boldsymbol{\eta}) + \mathbf{g}_o^*(\boldsymbol{\eta}) &= \mathbf{J}_\Theta^{-\top}(\boldsymbol{\eta}) [\mathbf{g}(\boldsymbol{\eta}) + \mathbf{g}_o] \\ \boldsymbol{\tau}^* &= \mathbf{J}_\Theta^{-\top}(\boldsymbol{\eta}) \boldsymbol{\tau} \end{aligned} \quad (8.15)$$

- 2. Positions and Unit Quaternions:** The unit quaternion representation (2.75) avoids the singular points  $\theta \neq \pm\pi/2$  by using four parameters  $\eta, \varepsilon_1, \varepsilon_2$  and  $\varepsilon_3$  to represent attitude

$$\mathbf{J}_q(\boldsymbol{\eta}) = \begin{bmatrix} \mathbf{R}(\mathbf{q}_b^n) & \mathbf{0}_{3 \times 3} \\ \mathbf{0}_{4 \times 3} & \mathbf{T}(\mathbf{q}_b^n) \end{bmatrix}, \quad \mathbf{J}_q^\dagger(\boldsymbol{\eta}) = \begin{bmatrix} \mathbf{R}^\top(\mathbf{q}_b^n) & \mathbf{0}_{3 \times 4} \\ \mathbf{0}_{4 \times 3} & 4 \mathbf{T}^\top(\mathbf{q}_b^n) \end{bmatrix} \quad (8.16)$$

Notice that pseudo-inverse  $\mathbf{J}_q^\dagger(\boldsymbol{\eta})$  is computed using the left *Moore–Penrose pseudo-inverse* and by exploiting the property  $\mathbf{T}^\top(\mathbf{q}_b^n) \mathbf{T}(\mathbf{q}_b^n) = 1/4 \mathbf{I}_3$ . Moreover, the left inverse of  $\mathbf{T}(\mathbf{q}_b^n)$  is

$$\begin{aligned} \mathbf{T}^\dagger(\mathbf{q}_b^n) &= (\mathbf{T}^\top(\mathbf{q}_b^n) \mathbf{T}(\mathbf{q}_b^n))^{-1} \mathbf{T}^\top(\mathbf{q}_b^n) \\ &= 4 \mathbf{T}^\top(\mathbf{q}_b^n) \end{aligned} \quad (8.17)$$

For this case,  $\boldsymbol{\eta} = [x^n, y^n, z^n, \eta, \varepsilon_1, \varepsilon_2, \varepsilon_3]^\top$  and

$$\begin{aligned} \dot{\boldsymbol{\eta}} &= \mathbf{J}_q(\boldsymbol{\eta}) \boldsymbol{\nu} & \iff & \boldsymbol{\nu} = \mathbf{J}_q^\dagger(\boldsymbol{\eta}) \dot{\boldsymbol{\eta}} \\ \ddot{\boldsymbol{\eta}} &= \mathbf{J}_q(\boldsymbol{\eta}) \dot{\boldsymbol{\nu}} + \dot{\mathbf{J}}_q(\boldsymbol{\eta}) \boldsymbol{\nu} & \iff & \dot{\boldsymbol{\nu}} = \mathbf{J}_q^\dagger(\boldsymbol{\eta}) [\ddot{\boldsymbol{\eta}} - \dot{\mathbf{J}}_q(\boldsymbol{\eta}) \mathbf{J}_q^\dagger(\boldsymbol{\eta}) \dot{\boldsymbol{\eta}}] \end{aligned}$$

and

$$\begin{aligned} \mathbf{M}^*(\boldsymbol{\eta}) &= \mathbf{J}_q^\dagger(\boldsymbol{\eta})^\top \mathbf{M} \mathbf{J}_q^\dagger(\boldsymbol{\eta}) \\ \mathbf{C}^*(\boldsymbol{\nu}, \boldsymbol{\eta}) &= \mathbf{J}_q^\dagger(\boldsymbol{\eta})^\top [\mathbf{C}(\boldsymbol{\nu}) - \mathbf{M} \mathbf{J}_q^\dagger(\boldsymbol{\eta}) \dot{\mathbf{J}}_q(\boldsymbol{\eta})] \mathbf{J}_q^\dagger(\boldsymbol{\eta}) \\ \mathbf{D}^*(\boldsymbol{\nu}, \boldsymbol{\eta}) &= \mathbf{J}_q^\dagger(\boldsymbol{\eta})^\top \mathbf{D}(\boldsymbol{\nu}) \mathbf{J}_q^\dagger(\boldsymbol{\eta}) \\ \mathbf{g}^*(\boldsymbol{\eta}) + \mathbf{g}_o^*(\boldsymbol{\eta}) &= \mathbf{J}_q^\dagger(\boldsymbol{\eta})^\top [\mathbf{g}(\boldsymbol{\eta}) + \mathbf{g}_o] \\ \boldsymbol{\tau}^* &= \mathbf{J}_q^\dagger(\boldsymbol{\eta})^\top \boldsymbol{\tau} \end{aligned} \quad (8.18)$$

### 8.1.3 Properties of the 6-DOF model

When designing feedback control systems for underwater vehicles in 6 DOF, there are clear advantages of using the matrix-vector representations. The main reasons are that system properties such as symmetry, skew-symmetry and positiveness of matrices can be incorporated into the stability analysis.

The following properties hold for the body-fixed vector representation:

**Property 8.1 (System Inertia Matrix  $M$ )**

For a rigid body the system inertia matrix is positive definite and constant, that is

$$M = M^\top > 0, \quad \dot{M} = \mathbf{0}$$

**Property 8.2 (Coriolis and Centripetal Matrix  $C$ )**

For a rigid body moving through an ideal fluid the Coriolis and centripetal matrix  $C(\nu)$  can always be parameterized such that it is skew-symmetric, that is

$$C(\nu) = -C^\top(\nu), \quad \forall \nu \in \mathbb{R}^6$$

**Proof.**  $C(\nu)$  is skew-symmetric under the assumptions that the matrices  $C_{RB}(\nu)$  and  $C_A(\nu)$  are skew-symmetric.

For the vector representation in  $\{\eta\}$  it is straightforward to show that

1.  $M^*(\eta) = M^*(\eta)^\top > 0, \quad \forall \eta$
2.  $s^\top [\dot{M}^*(\eta) - 2C^*(\nu, \eta)]s = 0, \quad \forall s \neq \mathbf{0}$
3.  $D^*(\nu, \eta) > 0, \quad \forall \nu, \eta$

since  $M = M^\top > 0$  and  $\dot{M} = \mathbf{0}$ . It should be noted that  $C^*(\nu, \eta)$  will not be skew-symmetric although  $C(\nu)$  is skew-symmetric.

**Example 8.1 (Lyapunov Analysis exploiting MIMO Model Properties)**

Consider the following 6-DOF model

$$\dot{\eta} = J_k(\eta)\nu \tag{8.19}$$

$$M\dot{\nu} + C(\nu)\nu + D(\nu)\nu + g(\eta) = \tau \tag{8.20}$$

where  $J_k(\eta)$  can be represented by  $J_\Theta(\eta)$  or  $J_q(\eta)$ . The obvious Lyapunov function candidate is based on kinetic and potential energies

$$V = \frac{1}{2}\nu^\top M\nu + \frac{1}{2}\eta^\top K_p\eta \tag{8.21}$$

where  $K_p = K_p^\top > 0$  is a constant gain matrix. Since  $M = M^\top > 0$  and  $\dot{M} = \mathbf{0}$ , it follows that

$$\begin{aligned} \dot{V} &= \nu^\top M\dot{\nu} + \eta^\top K_p\dot{\eta} \\ &= \nu^\top M\dot{\nu} + \eta^\top K_p J_k(\eta)\nu \\ &= \nu^\top [M\dot{\nu} + J_k^\top(\eta)K_p\eta] \end{aligned} \tag{8.22}$$

Substituting (8.20) into the expression for  $\dot{V}$  gives

$$\dot{V} = \nu^\top [\tau - C(\nu)\nu - D(\nu)\nu - g(\eta) + J_k^\top(\eta)K_p\eta] \tag{8.23}$$

Since  $\nu^\top C(\nu)\nu \equiv \mathbf{0}$  and  $\nu^\top D(\nu)\nu > 0$ , we can choose a PD control law with feedforward according to

$$\tau = g(\eta) - K_d\nu - J_k^\top(\eta)K_p\eta \quad (8.24)$$

with  $K_d > 0$  such that

$$\dot{V} = -\nu^\top [K_d + D(\nu)]\nu \leq 0 \quad (8.25)$$

Consequently, GAS follows from Krasowskii–LaSalle’s theorem if  $J_k(\eta)$  is nonsingular (see Appendix A.I).

### 8.1.4 Symmetry considerations of the system inertia matrix

We have seen that the 6-DOF nonlinear equations of motion, in their most general representation, require that a large number of hydrodynamic derivatives are known. From a practical point of view this is an unsatisfactory situation. However, the number of unknown parameters can be drastically reduced by using body-symmetry conditions.

In general

$$M = \begin{bmatrix} m - X_{\dot{u}} & -X_{\dot{v}} & -X_{\dot{w}} \\ -X_{\dot{v}} & m - Y_{\dot{v}} & -Y_{\dot{w}} \\ -X_{\dot{w}} & -Y_{\dot{w}} & m - Z_{\dot{w}} \\ -X_{\dot{p}} & -mz_g - Y_{\dot{p}} & my_g - Z_{\dot{p}} \\ mz_g - X_{\dot{q}} & -Y_{\dot{q}} & -mx_g - Z_{\dot{q}} \\ -my_g - X_{\dot{r}} & x_g - Y_{\dot{r}} & -Z_{\dot{r}} \\ -X_{\dot{p}} & mz_g - X_{\dot{q}} & -my_g - X_{\dot{r}} \\ -mz_g - Y_{\dot{p}} & -Y_{\dot{q}} & mx_g - Y_{\dot{r}} \\ my_g - Z_{\dot{p}} & -mx_g - Z_{\dot{q}} & -Z_{\dot{r}} \\ I_x - K_{\dot{p}} & -I_{xy} - K_{\dot{q}} & -I_{zx} - K_{\dot{r}} \\ -I_{xy} - K_{\dot{q}} & I_y - M_{\dot{q}} & -I_{yz} - M_{\dot{r}} \\ -I_{zx} - K_{\dot{r}} & -I_{yz} - M_{\dot{r}} & I_z - N_{\dot{r}} \end{bmatrix} \quad (8.26)$$

From the definitions of  $M_A$  and  $M_{RB}$  it is straightforward to verify the following cases (notice that  $m_{ij} = m_{ji}$ ):

- (i)  $xy$  plane of symmetry (bottom/top symmetry):

$$M = \begin{bmatrix} m_{11} & m_{12} & 0 & 0 & 0 & m_{16} \\ m_{21} & m_{22} & 0 & 0 & 0 & m_{26} \\ 0 & 0 & m_{33} & m_{34} & m_{35} & 0 \\ 0 & 0 & m_{43} & m_{44} & m_{45} & 0 \\ 0 & 0 & m_{53} & m_{54} & m_{55} & 0 \\ m_{61} & m_{62} & 0 & 0 & 0 & m_{66} \end{bmatrix}$$

(ii)  $xz$  plane of symmetry (port/starboard symmetry):

$$\mathbf{M} = \begin{bmatrix} m_{11} & 0 & m_{13} & 0 & m_{15} & 0 \\ 0 & m_{22} & 0 & m_{24} & 0 & m_{26} \\ m_{31} & 0 & m_{33} & 0 & m_{35} & 0 \\ 0 & m_{42} & 0 & m_{44} & 0 & m_{46} \\ m_{51} & 0 & m_{53} & 0 & m_{55} & 0 \\ 0 & m_{62} & 0 & m_{64} & 0 & m_{66} \end{bmatrix}$$

(iii)  $yz$  plane of symmetry (fore/aft symmetry):

$$\mathbf{M} = \begin{bmatrix} m_{11} & 0 & 0 & 0 & m_{15} & m_{16} \\ 0 & m_{22} & m_{23} & m_{24} & 0 & 0 \\ 0 & m_{32} & m_{33} & m_{34} & 0 & 0 \\ 0 & m_{42} & m_{43} & m_{44} & 0 & 0 \\ m_{51} & 0 & 0 & 0 & m_{55} & m_{56} \\ m_{61} & 0 & 0 & 0 & m_{65} & m_{66} \end{bmatrix}$$

(iv)  $xz$  and  $yz$  planes of symmetry (port/starboard and fore/aft symmetries):

$$\mathbf{M} = \begin{bmatrix} m_{11} & 0 & 0 & 0 & m_{15} & 0 \\ 0 & m_{22} & 0 & m_{24} & 0 & 0 \\ 0 & 0 & m_{33} & 0 & 0 & 0 \\ 0 & m_{42} & 0 & m_{44} & 0 & 0 \\ m_{51} & 0 & 0 & 0 & m_{55} & 0 \\ 0 & 0 & 0 & 0 & 0 & m_{66} \end{bmatrix}$$

More generally, the resulting inertia matrix for a body with  $ij$  and  $jk$  planes of symmetry is formed by the intersection  $M_{ij \cap jk} = M_{ij} \cap M_{jk}$ .

(v)  $xz$ ,  $yz$  and  $xy$  planes of symmetry (port/starboard, fore/aft and bottom/top symmetries):

$$\mathbf{M} = \text{diag}\{m_{11}, m_{22}, m_{33}, m_{44}, m_{55}, m_{66}\} \quad (8.27)$$

## 8.2 Longitudinal and Lateral Models for Submarines

The 6-DOF equations of motion can in many cases be divided into two noninteracting (or lightly interacting) subsystems:

- Longitudinal subsystem: states  $u_r, w_r, q$  and  $\theta$
- Lateral subsystem: states  $v_r, p, r, \phi$  and  $\psi$

This decomposition is good for slender symmetrical bodies (large length/width ratio) or so-called “flying vehicles”, as shown in Figure 8.1; typical applications are aircraft, missiles and submarines (Gertler and Hagen 1967; Feldman 1979; Tinker 1982).

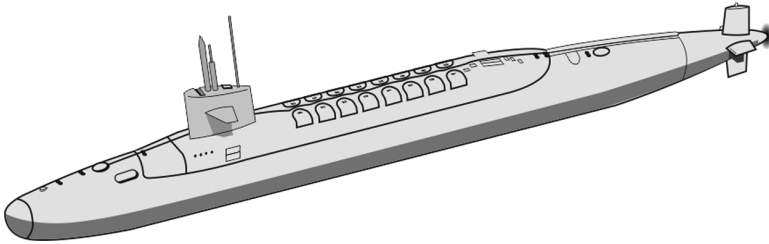


Figure 8.1: Slender body submarine (large length/width ratio).

This can also be seen from the expression of the system inertia matrix in the case of starboard–port symmetry (see Section 8.1.4)

$$\mathbf{M} = \begin{bmatrix} m_{11} & 0 & m_{13} & 0 & m_{15} & 0 \\ 0 & m_{22} & 0 & m_{24} & 0 & m_{26} \\ m_{31} & 0 & m_{33} & 0 & m_{35} & 0 \\ 0 & m_{42} & 0 & m_{44} & 0 & m_{46} \\ m_{51} & 0 & m_{53} & 0 & m_{55} & 0 \\ 0 & m_{62} & 0 & m_{64} & 0 & m_{66} \end{bmatrix} \quad (8.28)$$

which clearly confirms that the two subsystems

$$\mathbf{M}_{\text{long}} = \begin{bmatrix} m_{11} & m_{13} & m_{15} \\ m_{31} & m_{33} & m_{35} \\ m_{51} & m_{53} & m_{55} \end{bmatrix}, \quad \mathbf{M}_{\text{lat}} = \begin{bmatrix} m_{22} & m_{24} & m_{26} \\ m_{42} & m_{44} & m_{46} \\ m_{62} & m_{64} & m_{66} \end{bmatrix} \quad (8.29)$$

are decoupled.

### 8.2.1 Longitudinal subsystem

Under the assumption that the lateral states  $v, p, r, \phi$  are small, the longitudinal kinematics for surge, heave and pitch are, see (2.28) and (2.35),

$$\begin{bmatrix} \dot{z}^n \\ \dot{\theta} \end{bmatrix} = \begin{bmatrix} \cos(\theta) & 0 \\ 0 & 1 \end{bmatrix} \begin{bmatrix} w \\ q \end{bmatrix} + \begin{bmatrix} -\sin(\theta) \\ 0 \end{bmatrix} u \\ \approx \begin{bmatrix} w_r - U\theta \\ q \end{bmatrix} + \begin{bmatrix} 1 \\ 0 \end{bmatrix} w_c \quad (8.30)$$

where  $u \approx U$ ,  $w_r = w - w_c$ ,  $\sin(\theta) \approx \theta$  and  $\cos(\theta) \approx 1$ . For simplicity, it is assumed that higher-order damping terms can be neglected, that is  $\mathbf{D}_n(\boldsymbol{\nu}) = \mathbf{0}$ . Coriolis is, however, modeled by assuming that  $u \gg 0$  and that second-order terms in  $v, w, p, q$  and  $r$  are small. Hence, linearization of (3.59) about the forward speed  $U$  gives

$$\mathbf{C}_{RB}(\boldsymbol{\nu}_r)\boldsymbol{\nu}_r \approx \begin{bmatrix} 0 & 0 & 0 \\ 0 & 0 & -mU \\ 0 & 0 & mx_g U \end{bmatrix} \begin{bmatrix} u_r \\ w_r \\ q \end{bmatrix} \quad (8.31)$$

Notice that  $\mathbf{C}_{RB}(\boldsymbol{\nu}_r) \neq -\mathbf{C}_{RB}^\top(\boldsymbol{\nu}_r)$  for the decoupled model. Assuming a diagonal  $\mathbf{M}_A$  as in Example 6.2, the corresponding added mass terms are

$$\mathbf{C}_A(\boldsymbol{\nu}_r)\boldsymbol{\nu}_r = \begin{bmatrix} -Z_{\dot{w}}w_rq + Y_{\dot{v}}v_rr \\ -Y_{\dot{v}}v_rp + X_{\dot{u}}u_rq \\ (Z_{\dot{w}} - X_{\dot{u}})u_rw_r + (N_{\dot{r}} - K_p)pr \end{bmatrix} \approx \begin{bmatrix} 0 & 0 & 0 \\ 0 & 0 & X_{\dot{u}}U \\ 0(Z_{\dot{w}} - X_{\dot{u}})U & 0 & q \end{bmatrix} \begin{bmatrix} u_r \\ w_r \\ q \end{bmatrix} \quad (8.32)$$

From Section 6.5.1 and (4.6) with  $W = B$  and  $x_g = x_b$ , the dynamics becomes

$$\begin{aligned} & \begin{bmatrix} m - X_{\dot{u}} & -X_{\dot{w}} & mz_g - X_{\dot{q}} \\ -X_{\dot{w}} & m - Z_{\dot{w}} & -mx_g - Z_{\dot{q}} \\ mz_g - X_{\dot{q}} & -mx_g - Z_{\dot{q}} & I_y - M_{\dot{q}} \end{bmatrix} \begin{bmatrix} \dot{u}_r \\ \dot{w}_r \\ \dot{q} \end{bmatrix} \\ & + \begin{bmatrix} -X_u & -X_w & -X_q \\ -Z_u & -Z_w & -Z_q \\ -M_u & -M_w & -M_q \end{bmatrix} \begin{bmatrix} u_r \\ w_r \\ q \end{bmatrix} + \begin{bmatrix} 0 & 0 & 0 \\ 0 & 0 & -(m - X_{\dot{u}})U \\ 0(Z_{\dot{w}} - X_{\dot{u}})U & mx_gU \end{bmatrix} \begin{bmatrix} u_r \\ w_r \\ q \end{bmatrix} \\ & + \begin{bmatrix} 0 \\ 0 \\ W BG_z \sin(\theta) \end{bmatrix} = \begin{bmatrix} \tau_1 \\ \tau_3 \\ \tau_5 \end{bmatrix} \end{aligned} \quad (8.33)$$

This model is the basis for forward speed control (state  $u_r$ ) and depth/diving autopilot design (states  $w_r, q, \theta$ ). The speed dynamics can be removed by assuming that the speed controller stabilizes the forward speed such that  $u = u_o = \text{constant}$ . Hence, (8.33) reduces to a combined pitch and diving model where the relative surge velocity  $u_r$  is linearized about the forward speed  $U$  to give

$$\begin{aligned} & \begin{bmatrix} m - Z_{\dot{w}} & -mx_g - Z_{\dot{q}} \\ -mx_g - Z_{\dot{q}} & I_y - M_{\dot{q}} \end{bmatrix} \begin{bmatrix} \dot{w}_r \\ \dot{q} \end{bmatrix} + \begin{bmatrix} -Z_w & -Z_q \\ -M_w & -M_q \end{bmatrix} \begin{bmatrix} w_r \\ q \end{bmatrix} \\ & + \begin{bmatrix} 0 & -(m - X_{\dot{u}})U \\ (Z_{\dot{w}} - X_{\dot{u}})U & mx_gU \end{bmatrix} \begin{bmatrix} w_r \\ q \end{bmatrix} + \begin{bmatrix} 0 \\ W BG_z \sin(\theta) \end{bmatrix} = \begin{bmatrix} \tau_3 \\ \tau_5 \end{bmatrix} \end{aligned} \quad (8.34)$$

Consequently, if  $\dot{w}_r = w_r = 0$  (constant depth) and  $\theta$  is small such that  $\sin(\theta) \approx \theta$ , the linear pitch dynamics becomes

$$(I_y - M_{\dot{q}})\ddot{\theta} - M_q\dot{\theta} + W BG_z \theta = \tau_5 \quad (8.35)$$

The natural frequency and period are recognized as

$$\omega_5 = \sqrt{\frac{W BG_z}{I_y - M_{\dot{q}}}}, \quad T_5 = \frac{2\pi}{\omega_5} \quad (8.36)$$

## 8.2.2 Lateral subsystem

Under the assumption that the longitudinal states  $u, w, p, r, \phi$  and  $\theta$  are small, the lateral kinematics, see 6.5.1 and (2.36), reduce to

$$\dot{\phi} = p \quad (8.37)$$

$$\dot{\psi} = r \quad (8.38)$$

Again it is assumed that higher-order velocity terms can be neglected so that  $\mathbf{D}_n(\boldsymbol{\nu}_r) = \mathbf{0}$  and that the Coriolis terms in  $u$  are the most important, see (3.59). Hence,

$$\mathbf{C}_{RB}(\boldsymbol{\nu}_r)\boldsymbol{\nu}_r \approx \begin{bmatrix} 0 & 0 & mU \\ 0 & 0 & 0 \\ 0 & 0 & mx_g U \end{bmatrix} \begin{bmatrix} v_r \\ p \\ r \end{bmatrix} \quad (8.39)$$

Under the assumption of a diagonal  $\mathbf{M}_A$  structure as in Example 6.2, the corresponding added mass terms are

$$\begin{aligned} \mathbf{C}_A(\boldsymbol{\nu}_r)\boldsymbol{\nu}_r &= \begin{bmatrix} Z_w w_r p - X_{\dot{u}} u_r r \\ (Y_{\dot{v}} - Z_{\dot{w}}) v_r w_r + (M_{\dot{q}} - N_{\dot{r}}) qr \\ (X_{\dot{u}} - Y_{\dot{v}}) u_r v_r + (K_{\dot{p}} - M_{\dot{q}}) pq \end{bmatrix} \\ &\approx \begin{bmatrix} 0 & 0 & -X_{\dot{u}} U \\ 0 & 0 & 0 \\ (X_{\dot{u}} - Y_{\dot{v}}) U & 0 & 0 \end{bmatrix} \begin{bmatrix} v_r \\ p \\ r \end{bmatrix} \end{aligned} \quad (8.40)$$

Next, assume that  $W = B$ ,  $x_g = x_b$  and  $y_g = y_b$ . Then it follows from Section 6.5.1 that

$$\begin{aligned} &\begin{bmatrix} m - Y_{\dot{v}} & -mz_g - Y_{\dot{p}} & mx_g - Y_{\dot{r}} \\ -mz_g - Y_{\dot{p}} & I_x - K_{\dot{p}} & -I_{zx} - K_{\dot{r}} \\ mx_g - Y_{\dot{r}} & -I_{zx} - K_{\dot{r}} & I_z - N_{\dot{r}} \end{bmatrix} \begin{bmatrix} \dot{v}_r \\ \dot{p} \\ \dot{r} \end{bmatrix} + \begin{bmatrix} -Y_v & -Y_p & -Y_r \\ -K_v & -K_p & -K_r \\ -N_v & -N_p & -N_r \end{bmatrix} \begin{bmatrix} v_r \\ p \\ r \end{bmatrix} \\ &+ \begin{bmatrix} 0 & 0 & (m - X_{\dot{u}})U \\ 0 & 0 & 0 \\ (X_{\dot{u}} - Y_{\dot{v}})U & 0 & mx_g U \end{bmatrix} \begin{bmatrix} v_r \\ p \\ r \end{bmatrix} + \begin{bmatrix} 0 \\ W BG_z \sin(\phi) \\ 0 \end{bmatrix} = \begin{bmatrix} \tau_2 \\ \tau_4 \\ \tau_6 \end{bmatrix} \end{aligned} \quad (8.41)$$

For vehicles where  $\dot{p}$  and  $p$  are small (small roll motions), this reduces to

$$\begin{aligned} &\begin{bmatrix} m - Y_{\dot{v}} & mx_g - Y_{\dot{r}} \\ mx_g - Y_{\dot{r}} & I_z - N_{\dot{r}} \end{bmatrix} \begin{bmatrix} \dot{v}_r \\ \dot{r} \end{bmatrix} + \begin{bmatrix} -Y_v & -Y_r \\ -N_v & -N_r \end{bmatrix} \begin{bmatrix} v_r \\ r \end{bmatrix} \\ &+ \begin{bmatrix} 0 & (m - X_{\dot{u}})U \\ (X_{\dot{u}} - Y_{\dot{v}})U & mx_g U \end{bmatrix} \begin{bmatrix} v_r \\ r \end{bmatrix} = \begin{bmatrix} \tau_2 \\ \tau_6 \end{bmatrix} \end{aligned} \quad (8.42)$$

which is the sway–yaw maneuvering model (see Section 6.5.5). The decoupled linear roll equation under the assumption of a small  $\phi$  is

$$(I_x - K_{\dot{p}})\ddot{\phi} - K_p \dot{\phi} + W BG_z \phi = \tau_4 \quad (8.43)$$

From this it follows that the natural frequency and period are

$$\omega_4 = \sqrt{\frac{W BG_z}{I_x - K_p}}, \quad T_4 = \frac{2\pi}{\omega_4} \quad (8.44)$$

## 8.3 Decoupled Models for “Flying Underwater Vehicles”

For slender symmetrical bodies (large length/width ratio) or so-called “flying underwater vehicles” it is common to decompose the 6-DOF equations of motion into three noninteracting (or lightly interacting) subsystems:

- Forward speed subsystem: state  $u_r$
- Course subsystem: states  $v_r, p, r, \phi$  and  $\chi$
- Pitch-depth subsystem: states  $w_r, q, z$  and  $\theta$

These subsystems are used to design forward speed, course and pitch–depth control systems for AUVs.

### 8.3.1 Forward speed subsystem

For slender bodies moving at forward speed  $U \gg 0$  it is standard to assume that the surge dynamics is decoupled from the other motions of the vehicle due to the large length/width ratio. Moreover,

$$(m - X_{\dot{u}})\dot{u}_r - X_{|u|u}|u_r|u_r = T \quad (8.45)$$

where  $T$  is the thrust (see Section 9.1). The linear damping term  $X_u u_r$  is assumed to be negligible at higher speeds. The transfer function can be found by using the equivalent linearization method, see (5.66). This gives

$$X_{|u|u}|u_r|u_r \approx \frac{8A_1}{3\pi} X_{|u|u} u_r \quad (8.46)$$

where the surge velocity  $u_r = A_1 \cos(\omega t)$  is assumed to be harmonic. Hence, the surge velocity transfer function becomes

$$u(s) = \frac{K_u}{T_u s + 1} T(s) + d_u(s) \quad (8.47)$$

where  $d_u = u_c$  is a disturbance term due to ocean currents and

$$K_u = \frac{1}{-\frac{8A_1}{3\pi} X_{|u|u}}, \quad T_u = \frac{m - X_{\dot{u}}}{-\frac{8A_1}{3\pi} X_{|u|u}} \quad (8.48)$$

The value for  $X_{|u|u}$  is given by (6.71) while  $X_{\dot{u}} = -A_{11}(0)$ .

### 8.3.2 Course subsystem

Consider the linear maneuvering model (see Section 6.5.5)

$$\begin{bmatrix} m - Y_v & mx_g - Y_r \\ mx_g - Y_r & I_z - N_r \end{bmatrix} \begin{bmatrix} \dot{v}_r \\ \dot{r} \end{bmatrix} + \begin{bmatrix} -Y_v & -Y_r \\ -N_v & -N_r \end{bmatrix} \begin{bmatrix} v_r \\ r \end{bmatrix} + \begin{bmatrix} 0 & (m - X_{\dot{u}})U \\ (X_{\dot{u}} - Y_{\dot{v}})U & mx_g U \end{bmatrix} \begin{bmatrix} v_r \\ r \end{bmatrix} = \begin{bmatrix} \tau_2 \\ \tau_6 \end{bmatrix} \quad (8.49)$$

For simplicity assume that the control input is a single aft rudder (see section 9.7). This gives the following state-space representation

$$\dot{\mathbf{x}} = \mathbf{A}\mathbf{x} + \mathbf{b}u \quad (8.50)$$

$$\Updownarrow$$

$$\begin{bmatrix} \dot{v}_r \\ \dot{r} \\ \dot{\psi} \end{bmatrix} = \begin{bmatrix} a_{11} & a_{12} & 0 \\ a_{21} & a_{22} & 0 \\ 0 & 1 & 0 \end{bmatrix} \begin{bmatrix} v_r \\ r \\ \psi \end{bmatrix} + \begin{bmatrix} b_1 \\ b_2 \\ 0 \end{bmatrix} \delta_r \quad (8.51)$$

where  $\mathbf{x} = [v_r, r, \psi]^\top$  and  $u = \delta_r$  is the rudder angle.

The transfer function for heading control becomes (see Section 7.2.1)

$$\begin{aligned} \psi(s) &= \frac{K(T_3 s + 1)}{s(T_1 s + 1)(T_2 s + 1)} \delta_r(s) + d_\psi(s) \\ &\approx \frac{K}{s(Ts + 1)} \delta_r(s) + d_\psi(s) \end{aligned} \quad (8.52)$$

where  $K$  and  $T = T_1 + T_2 - T_3$  are recognized as the Nomoto gain and time constants, and  $d_\psi$  is a disturbance term representing unmodeled dynamics and ocean currents. Since,  $\chi = \psi + \beta_v$  (see (2.115)), the transfer function for course control takes the following form

$$\chi(s) = \frac{K}{s(Ts + 1)} \delta_r(s) + d_\chi(s) \quad (8.53)$$

where  $\delta_\chi = \delta_\psi + \beta_v$ .

### 8.3.3 Pitch–depth subsystem

Pitch and depth control of underwater vehicles is usually done by using control surfaces, thrusters, moving masses, spinning rotors and ballast systems. For a neutrally buoyant vehicle, stern rudders (elevators)  $\delta_e$  are effective for diving and depth changing maneuvers since they require relatively little control energy compared to thrusters (see Section 9.7). The longitudinal model (8.33) in Section 8.2 can be linearized about

the speed  $U$  to give

$$\begin{bmatrix} m - Z\dot{w} & -mx_g - Z\dot{q} \\ -mx_g - Z\dot{q} & I_y - M\dot{q} \end{bmatrix} \begin{bmatrix} \dot{w}_r \\ \dot{q} \end{bmatrix} + \begin{bmatrix} -Z_w & -Z_q \\ -M_w & -M_q \end{bmatrix} \begin{bmatrix} w_r \\ q \end{bmatrix} + \begin{bmatrix} 0 & -(m - X\dot{u})U \\ (Z\dot{w} - X\dot{u})U & mx_g U \end{bmatrix} \begin{bmatrix} w_r \\ q \end{bmatrix} + \begin{bmatrix} 0 \\ W BG_z \sin(\theta) \end{bmatrix} = \begin{bmatrix} \tau_3 \\ \tau_5 \end{bmatrix} \quad (8.54)$$

A state-space representation of this model is

$$\dot{\mathbf{x}} = \mathbf{Ax} + \mathbf{bu} \quad (8.55)$$

$\Updownarrow$

$$\begin{bmatrix} \dot{w}_r \\ \dot{q} \\ \dot{\theta} \\ \dot{z}^n \end{bmatrix} = \begin{bmatrix} a_{11} & a_{12} & 0 & 0 \\ a_{21} & a_{22} & a_{23} & 0 \\ 0 & 1 & 0 & 0 \\ 1 & 0 & -U & 0 \end{bmatrix} \begin{bmatrix} w_r \\ q \\ \theta \\ z^n \end{bmatrix} + \begin{bmatrix} b_1 \\ b_2 \\ 0 \\ 0 \end{bmatrix} \delta_e \quad (8.56)$$

where  $\mathbf{x} = [w_r, q, \theta, z^n]^\top$  and  $u = \delta_e$  is the stern rudder (elevator). The kinematic equations are based on the approximations (see Section 2.2.1)

$$\dot{\theta} = q \cos(\phi) - r \sin(\phi) \approx q \quad (8.57)$$

$$\dot{z}^n = -u \sin(\theta) + v \cos(\theta) \sin(\psi) + w \cos(\theta) \cos(\psi) \approx (w_r + w_c) - U\theta \quad (8.58)$$

for  $v = p = 0$  and small values of  $\theta$  and  $\phi$ . A further simplification could be to assume that  $\dot{w}_r$  and  $w_r$  are small during depth-changing maneuvers. This gives the transfer functions

$$z^n(s) = -\frac{U}{s}\theta(s) + d_z(s) \quad (8.59)$$

$$\theta(s) = \frac{a_3}{s^2 + a_1 s + a_2} \delta_e(s) + d_\theta(s) \quad (8.60)$$

where  $d_z(s)$  and  $d_\theta(s)$  are disturbance terms due to unmodeled dynamics and ocean currents. Consequently, the transfer function for depth control using stern rudders (elevators) as control inputs becomes

$$z^n(s) = \frac{-a_3 U}{s(s^2 + a_1 s + a_2)} \delta_e(s) + d_z(s) \quad (8.61)$$

where  $d_z(s)$  is the resulting disturbance term.

## 8.4 Cylinder-Shaped Vehicles and Myring-Type Hulls

Figure 8.2 shows a cylinder-shaped AUV. Assume that the CO is located in the center of the AUV and that  $\text{CB} = \text{CO}$  such that  $\mathbf{r}_b^b = [0, 0, 0]^\top$ . Furthermore assume that the CG is located at  $\mathbf{r}_g^b = [x_g, y_g, z_g]^\top$ . Hence, the AUV equations of motion takes the following form

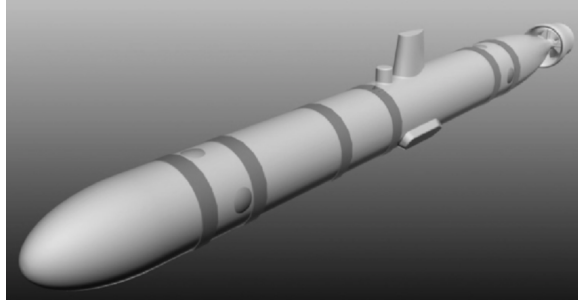


Figure 8.2: Cylinder-shaped AUV (Joung *et al.* 2012).

$$M\dot{\nu}_r + C(\nu_r)\nu_r + D\nu_r + d(\nu_r) + g(\eta) = \tau \quad (8.62)$$

Cylinder-Shaped AUVs such as the *Light Autonomous Underwater Vehicle* (LAUV) (Madureira *et al.* 2013) and the *Remote Environmental Monitoring Unit* (REMUS) AUV (Hydroid 2019; REMUS 2019) can be represented by the Myring hull profile equations (Myring 1976), which are known to produce minimum drag force for a given fineness ratio ( $L/D$ ), that is, the ratio of its length  $L$  to its maximum diameter  $D$ .

### Myring-type hull

The shapes of the nose, cylinder and tail sections of the Myring-type hull are determined by

$$r(x) = \begin{cases} \frac{1}{2}D \left(1 - \left(\frac{x-L_n}{L_n}\right)^2\right)^{1/n}, & 0 \leq x \leq L_n \\ \frac{D}{2}, & L_n < x < L_n + L_c \\ \frac{1}{2}D - \left(\frac{3D}{2L_t^2} - \frac{\tan(\alpha_t)}{L_t}\right)(x - (L_n + L_c))^2 \\ + \left(\frac{D}{L_t^3} - \frac{\tan(\alpha_t)}{L_t^2}\right)(x - (L_n + L_c))^3, & L_n + L_c \leq x \leq L \end{cases} \quad (8.63)$$

where,  $r(x)$  is the radius at a point along the  $x$  axis,  $L_n$  is the length of the noose,  $L_c$  is the length of body,  $L_t$  is the length of the tail section,  $D$  is the cylinder diameter,  $n$  is an exponential parameter which can be varied to give different body shapes, and  $\alpha_t$  is the included angle at the tip of the tail. Hence, the length of the vehicle is  $L = L_n + L_c + L_t$ .

#### 8.4.1 Spheroid approximation

An *ellipsoid* is a surface that may be obtained from a sphere by deforming it. Consider an ellipsoid totally submerged and with the origin at the center of the ellipsoid

$$\frac{x^2}{a^2} + \frac{y^2}{b^2} + \frac{z^2}{c^2} = 1 \quad (8.64)$$

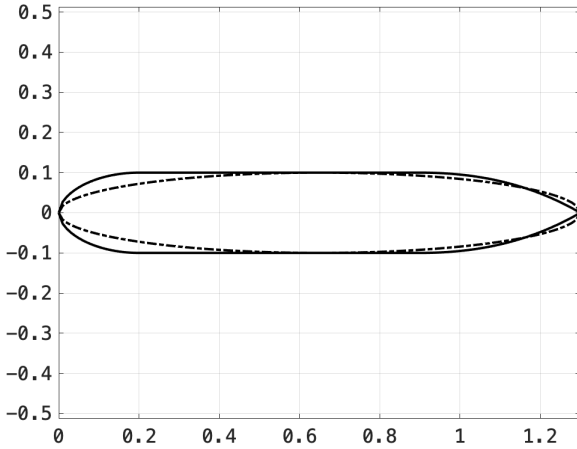


Figure 8.3: Myring-type hull (solid) for  $D = 0.2$  m,  $L = 1.3$  m,  $L_n = 0.2$  m,  $L_c = 0.7$  m,  $L_t = 0.4$  m,  $n = 1.8$ , and  $\alpha_t = 30^\circ$  approximated by a spheroid (dotted line).

where  $a$ ,  $b$  and  $c$  are the semiaxes, see Figure 8.4. A *prolate spheroid* is obtained by letting  $b = c$  and  $a > b$ . Consequently, the mass of a prolate spheroid is

$$m = \frac{4}{3}\pi\rho abc = \frac{4}{3}\pi\rho ab^2 \quad (8.65)$$

and the moments of inertia are

$$I_x = \frac{1}{5}m(b^2 + c^2) = \frac{2}{5}mb^2 \quad (8.66)$$

$$I_y = \frac{1}{5}m(a^2 + c^2) = \frac{1}{5}m(a^2 + b^2) \quad (8.67)$$

$$I_z = \frac{1}{5}m(a^2 + b^2) = I_y \quad (8.68)$$

The largest difference between a Myring-type shape and a spheroid lies in the ends of the body, see Figure 8.3. To approximate the hull with a spheroid, the method of equivalent ellipsoid is used (Korotkin 2009). This involves choosing the function  $r(x)$  such that the volumes of the spheroid and the Myring-type hull are equal

$$\int_0^L \pi r^2(x) dx = \frac{4}{3}\pi\rho ab^2 \quad (8.69)$$

Consequently, the inertia dyadic can be approximated by the formulae for the spheroid

$$\mathbf{I}_g^b = \text{diag} \left\{ \frac{2}{5}mb^2, \frac{1}{5}m(a^2 + b^2), \frac{1}{5}m(a^2 + b^2) \right\} \quad (8.70)$$

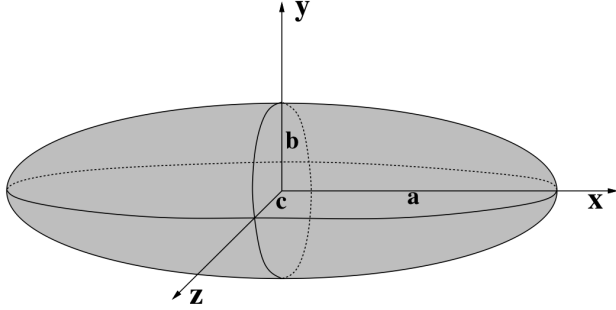


Figure 8.4: Ellipsoid with semiaxes  $a$ ,  $b$  and  $c$ .

For nonzero values of  $r_g$ , it follows from (C.18) that the rigid-body inertia matrix becomes

$$\mathbf{M}_{RB} = \mathbf{H}^\top(\mathbf{r}_g^b) \operatorname{diag} \left\{ m, m, m, \frac{2}{5}mb^2, \frac{1}{5}m(a^2 + b^2), \frac{1}{5}m(a^2 + b^2) \right\} \mathbf{H}(\mathbf{r}_g^b) \quad (8.71)$$

Fortunately, many of the added mass derivatives contained in the general expressions for added mass are either zero or mutually related when the body has various symmetries. Imlay (1961) gives the following expressions for the diagonal added mass derivatives (cross-coupling terms will be zero when CO = CB due to body symmetry about three planes)

$$X_{\dot{u}} = -\frac{\alpha_0}{2 - \alpha_0} m \quad (8.72)$$

$$Y_{\dot{v}} = Z_{\dot{w}} = -\frac{\beta_0}{2 - \beta_0} m \quad (8.73)$$

$$K_{\dot{p}} = 0 \quad (8.74)$$

$$N_{\dot{r}} = M_{\dot{q}} = -\frac{1}{5} \frac{(b^2 - a^2)^2(\alpha_0 - \beta_0)}{2(b^2 - a^2) + (b^2 + a^2)(\beta_0 - \alpha_0)} m \quad (8.75)$$

The constants  $\alpha_0$  and  $\beta_0$  can be calculated as

$$\alpha_0 = \frac{2(1 - e^2)}{e^3} \left( \frac{1}{2} \ln \frac{1 + e}{1 - e} - e \right) \quad (8.76)$$

$$\beta_0 = \frac{1}{e^2} - \frac{1 - e^2}{2e^3} \ln \frac{1 + e}{1 - e} \quad (8.77)$$

where the eccentricity is defined as

$$e := 1 - (b/a)^2 \quad (8.78)$$

An alternative representation of these mass derivatives is presented by (Lamb 1932) who defines Lamb's  $k$ -factors as

$$k_1 = \frac{\alpha_0}{2 - \alpha_0} \quad (8.79)$$

$$k_2 = \frac{\beta_0}{2 - \beta_0} \quad (8.80)$$

$$k' = \frac{e^4(\beta_0 - \alpha_0)}{(2 - e^2)[2e^2 - (2 - e^2)(\beta_0 - \alpha_0)]} \quad (8.81)$$

Hence, the added system inertia matrix can be written in terms of Lamb's k-factors

$$\begin{aligned} \mathbf{M}_A &= -\text{diag}\{X_{\dot{u}}, Y_{\dot{v}}, Z_{\dot{w}}, K_{\dot{p}}, M_{\dot{q}}, N_{\dot{r}}\} \\ &= \text{diag}\{mk_1, mk_2, mk_2, 0, k'I_y, k'I_y\} \end{aligned} \quad (8.82)$$

The final expression for the system inertia matrix then becomes  $\mathbf{M} = \mathbf{M}_{RB} + \mathbf{M}_A$ .

A more general discussion on added mass derivatives for bodies with various symmetries is found in Imlay (1961). Other useful references discussing methods for computation of the added mass derivatives are Humphreys and Watkinson (1978), and Triantafyllou and Amzallag (1984).

The Coriolis and centripetal matrix  $\mathbf{C}(\boldsymbol{\nu}_r) = \mathbf{C}_{RB}(\boldsymbol{\nu}_r) + \mathbf{C}_A(\boldsymbol{\nu}_r)$  is computed using (3.61). Moreover,

$$\mathbf{C}_{RB}(\boldsymbol{\nu}_r) = \mathbf{H}^\top(\mathbf{r}_g) \begin{bmatrix} 0 & -mr & mq & 0 & 0 & 0 \\ mr & 0 & -mp & 0 & 0 & 0 \\ -mq & mp & 0 & 0 & 0 & 0 \\ 0 & 0 & 0 & 0 & I_z r & -I_y q \\ 0 & 0 & 0 & -I_z r & 0 & I_x p \\ 0 & 0 & 0 & I_y q & -I_x p & 0 \end{bmatrix} \mathbf{H}(\mathbf{r}_g) \quad (8.83)$$

where  $I_x$ ,  $I_y$  and  $I_z$  are given by (8.66)–(8.68). From Example 6.2 it follows that

$$\mathbf{C}_A(\boldsymbol{\nu}_r) = \begin{bmatrix} 0 & 0 & 0 & 0 & -Z_{\dot{w}} w_r & Y_{\dot{v}} v_r \\ 0 & 0 & 0 & Z_{\dot{w}} w_r & 0 & -X_{\dot{u}} u_r \\ 0 & 0 & 0 & -Y_{\dot{v}} v_r & X_{\dot{u}} u_r & 0 \\ 0 & -Z_{\dot{w}} w_r & Y_{\dot{v}} v_r & 0 & -N_{\dot{r}} r & M_{\dot{q}} q \\ Z_{\dot{w}} w_r & 0 & -X_{\dot{u}} u_r & N_{\dot{r}} r & 0 & -K_{\dot{p}} p \\ -Y_{\dot{v}} v_r & X_{\dot{u}} u_r & 0 & -M_{\dot{q}} q & K_{\dot{p}} p & 0 \end{bmatrix} \quad (8.84)$$

Assume that the lift and drag coefficients  $C_L(\alpha)$  and  $C_D(\alpha)$  are known for the AUV such that the forces in FLOW axes become (see Section 2.5.2)

$$F_{\text{drag}} = \frac{1}{2} \rho V_r^2 S C_D(\alpha) \quad (8.85)$$

$$F_{\text{lift}} = \frac{1}{2} \rho V_r^2 S C_L(\alpha) \quad (8.86)$$

where  $\rho$  is the density of water and  $S$  is the area of the wetted surface of the hull. The lift and drag coefficients can be approximated as

$$C_D(\alpha) \approx C_{D_0} + C_{D_\alpha}\alpha + C_{D_{\delta_e}}\delta_e \quad (8.87)$$

$$C_L(\alpha) \approx C_{L_0} + C_{L_\alpha}\alpha + C_{L_{\delta_e}}\delta_e \quad (8.88)$$

where  $C_{D_0} = C_{L_0} = 0$  for symmetrical vehicles and  $\delta_e$  is an optional control surface (elevator) for depth-changing maneuvers. Since lift is perpendicular to the relative flow and drag is parallel, the longitudinal forces in BODY axes become

$$\begin{bmatrix} X \\ Z \end{bmatrix} = \begin{bmatrix} \cos(\alpha) & -\sin(\alpha) \\ \sin(\alpha) & \cos(\alpha) \end{bmatrix} \begin{bmatrix} -F_{\text{drag}} \\ -F_{\text{lift}} \end{bmatrix} \quad (8.89)$$

The transverse force depends on the sideslip angle according to

$$Y = \frac{1}{2}\rho V_r^2 S C_Y(\beta) \quad (8.90)$$

where

$$C_Y(\beta) \approx C_{Y_0} + C_{Y_\beta}\beta + C_{Y_{\delta_r}}\delta_r \quad (8.91)$$

Here it can be assumed that  $C_{Y_0} = 0$  for symmetrical vehicles. The rudder angle  $\delta_r$  is an optional control surface for turning maneuvers (see Section 9.7.1).

Linear damping

$$\mathbf{D} = -\text{diag}\{X_u, Y_v, Z_w, K_p, M_q, N_r\} \quad (8.92)$$

is important when operating at low speed, while the nonlinear terms

$$\mathbf{d}(\boldsymbol{\nu}_r) = \frac{1}{2}\rho V_r^2 S \begin{bmatrix} C_D(\alpha) \cos(\alpha) - C_L(\alpha) \sin(\alpha) \\ C_Y(\beta) \\ C_D(\alpha) \sin(\alpha) - C_L(\alpha) \cos(\alpha) \\ 0 \\ 0 \\ 0 \end{bmatrix} \quad (8.93)$$

dominates at higher speeds. For high-speed vehicles such as cylinder-shaped torpedos it is necessary to include hydrodynamic coefficients for the roll, pitch and yaw moments in the expression for  $\mathbf{d}(\boldsymbol{\nu}_r)$ . The procedure is similar to the method used to design small unmanned aerial vehicles (UAVs), see Beard and McLain (2012) for details.

Finally,  $\mathbf{r}_b^b = [0, 0, 0]^\top$ ,  $\mathbf{r}_g^b = [x_g, y_g, z_g]^\top$  and  $W = B$  implies that (8.12) reduces to

$$\mathbf{g}(\boldsymbol{\eta}) = \begin{bmatrix} 0 \\ 0 \\ 0 \\ z_g W \cos(\theta) \sin(\phi) - y_g W \cos(\theta) \cos(\phi) \\ z_g W \sin(\theta) + x_g W \cos(\theta) \cos(\phi) \\ x_g W \cos(\theta) \sin(\phi) - y_g W \sin(\theta) \end{bmatrix} \quad (8.94)$$

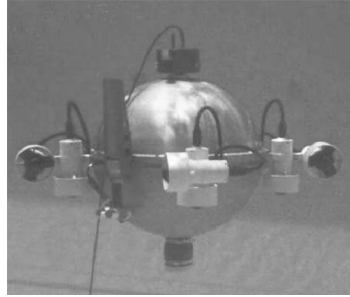


Figure 8.5: The ODIN omni-directional underwater vehicle (Choi *et al.* 2003).

## 8.5 Spherical-Shaped Vehicles

Spherical-shaped underwater vehicles are easy to model due to symmetry. An example is the Omni-Directional Intelligent Navigator (ODIN), which is an AUV that has been developed at the University of Hawaii (Choi *et al.* 2003), see Figure 8.5. Consider the 6-DOF equations of motion

$$\boldsymbol{M}\dot{\boldsymbol{\nu}}_r + \boldsymbol{C}(\boldsymbol{\nu}_r)\boldsymbol{\nu}_r + \boldsymbol{D}\boldsymbol{\nu}_r + \boldsymbol{g}(\boldsymbol{\eta}) = \boldsymbol{\tau} \quad (8.95)$$

and assume that the CO is located in the center of the sphere and that CB = CO, while CG is located a distance  $z_g$  below the CO. Hence,  $\boldsymbol{r}_b^b = [0, 0, 0]^\top$  and  $\boldsymbol{r}_g^b = [0, 0, z_g]^\top$ . For a neutrally buoyant vehicle

$$W = B = mg \quad (8.96)$$

The rigid-body system inertia matrix (3.46) takes the following form

$$\boldsymbol{M}_{RB} = \begin{bmatrix} m & 0 & 0 & 0 & mz_g & 0 \\ 0 & m & 0 & -mz_g & 0 & 0 \\ 0 & 0 & m & 0 & 0 & 0 \\ 0 & -mz_g & 0 & I_x & 0 & 0 \\ mz_g & 0 & 0 & 0 & I_y & 0 \\ 0 & 0 & 0 & 0 & 0 & I_z \end{bmatrix} \quad (8.97)$$

The moments of inertia for a sphere with radius  $R$  are computed as

$$I_x = I_y = I_z = \frac{2}{5}mR^2 \quad (8.98)$$

The added mass system inertia matrix for a spherical-shaped vehicle is given by

$$\boldsymbol{M}_A = -\text{diag}\{X_{\dot{u}}, Y_{\dot{v}}, Z_{\dot{w}}, 0, 0, 0\} \quad (8.99)$$

where the hydrodynamic derivatives are

$$X_{\dot{u}} = Y_{\dot{v}} = Z_{\dot{w}} = -\rho \frac{2}{3}\pi R^2 \quad (8.100)$$

Consequently,

$$\mathbf{M} = \mathbf{M}_{RB} + \mathbf{M}_A = \begin{bmatrix} m - X_u & 0 & 0 & 0 & mz_g & 0 \\ 0 & m - Y_v & 0 & -mz_g & 0 & 0 \\ 0 & 0 & m - Z_w & 0 & 0 & 0 \\ 0 & -mz_g & 0 & I_x & 0 & 0 \\ mz_g & 0 & 0 & 0 & I_y & 0 \\ 0 & 0 & 0 & 0 & 0 & I_z \end{bmatrix} \quad (8.101)$$

The Coriolis and centripetal matrix consists of two parts

$$\mathbf{C}(\boldsymbol{\nu}_r) = \mathbf{C}_{RB}(\boldsymbol{\nu}_r) + \mathbf{C}_A(\boldsymbol{\nu}_r) \quad (8.102)$$

where the expression for  $\mathbf{C}_{RB}(\boldsymbol{\nu}_r)$  can be derived from (3.60). This gives the formula

$$\mathbf{C}_{RB}(\boldsymbol{\nu}_r) = \begin{bmatrix} 0 & -mr & mq & mz_g r & 0 & 0 \\ mr & 0 & -mp & 0 & mz_g r & 0 \\ -mq & mp & 0 & -mz_g p & -mz_g q & 0 \\ -mz_g r & 0 & mz_g p & 0 & I_z r & -I_y q \\ 0 & -mz_g r & mz_g q & -I_z r & 0 & I_x p \\ 0 & 0 & 0 & I_y q & -I_x p & 0 \end{bmatrix} \quad (8.103)$$

From Example 6.2 it follows that

$$\mathbf{C}_A(\boldsymbol{\nu}_r) = \rho \frac{2}{3} \pi R^2 \begin{bmatrix} 0 & 0 & 0 & 0 & w_r & -v_r \\ 0 & 0 & 0 & -w_r & 0 & u_r \\ 0 & 0 & 0 & v_r & -u_r & 0 \\ 0 & w_r & -v_r & 0 & 0 & 0 \\ -w_r & 0 & u_r & 0 & 0 & 0 \\ v_r & -u_r & 0 & 0 & 0 & 0 \end{bmatrix} \quad (8.104)$$

The hydrodynamic damping matrix is chosen as

$$\mathbf{D} = -\text{diag}\{X_u, Y_v, Z_w, K_p, M_q, N_r\} \quad (8.105)$$

while (8.12) reduces to

$$\mathbf{g}(\boldsymbol{\eta}) = \text{diag}\{0, 0, 0, z_g W \cos(\theta) \sin(\phi), z_g W \sin(\theta), 0\} \quad (8.106)$$

for a neutrally buoyant vehicle  $W = B$ .

# Chapter 9

# Control Forces and Moments

This chapter discusses mathematical models for control forces and moments. The forthcoming sections discuss the following systems:

- Propellers as thrust devices
- Ship propulsion systems
- USV and underwater vehicle propulsion systems
- Thrusters
- Rudder in propeller slipstream
- Fin stabilizers
- Control surfaces
- Control moment gyroscope
- Moving mass

## 9.1 Propellers as Thrust Devices

The two main types of propellers available for ordinary merchant vessels are fixed-blade or fixed-pitch (FP) and controllable-pitch (CP) propellers. These two types are widely used as prime mover thrust devices and are also the basis for azimuth and tunnel thrusters.

### 9.1.1 Fixed-pitch propeller

A first-order approximation of the propeller thrust  $T$  and torque  $Q$  can be found from lift force calculations using a quasi-static approach (Lewis 1967) (Carlton 1994). Ships usually operate with variable forward speed. Therefore the performance of the propeller will be a function of the speed of the water in the wake of the hull (*advance speed*)  $u_a$  (m/s), propeller revolutions per second  $n$  (RPS) and propeller diameter  $D$  (m). The nondimensional open-water characteristics are defined in terms of the *open-water advance coefficient*

$$J_a = \frac{u_a}{nD} \quad (9.1)$$

The range of  $J_a$  values relevant to normal operation is quite narrow. It is only during heavy accelerations and decelerations that the propeller gets exposed to larger parts of the diagram.

The nondimensional propeller thrust and propeller torque coefficients  $K_T$  and  $K_Q$  and the thruster open-water efficiency  $\eta_0$ , that is the efficiency in undisturbed water, are given by

$$K_T = \frac{T}{\rho D^4 |n| n}, \quad K_Q = \frac{Q}{\rho D^5 |n| n}, \quad \eta_0 = \frac{J_a}{2\pi} \cdot \frac{K_T}{K_Q} \quad (9.2)$$

where  $\rho$  ( $\text{kg/m}^3$ ) is the water density and  $T$  (N) and  $Q$  (Nm) are the propeller thrust and torque, respectively. The difference between the ship speed and the average flow velocity over the propeller disc is called the wake. For a ship in transit, it is common to define the relative speed reduction by introducing the advance speed at the propeller (speed of the water going into the propeller) as

$$u_a = (1 - w) u \quad (9.3)$$

where  $w$  is the wake fraction number (typically 0.1 – 0.4) and  $u$  (m/s) is the forward speed of the ship. In practice, the wake fraction number can be determined directly from the open-water test results.

Another effect to be considered is the so-called *thrust deduction*. An increase in the flow velocity in the boundary layer behind the ship as a result of the propeller will disturb the pressure balance between the bow and stern. This phenomenon causes extra resistance on the hull which can be described by the thrust deduction number  $t$  (typically 0.05–0.2) by modifying the propeller thrust  $T$  to  $(1 - t) T$ . The thrust deduction number will strongly depend on the shape of the stern. Hence, the influence of the hull will be described by the hull efficiency

$$\eta_H = \frac{1 - t}{1 - w} \quad (9.4)$$

In practice, the ratio between the propeller thrust and torque in open water and behind the stern will differ. This effect can be described by the ratio

$$\eta_B = \frac{J_a}{2\pi} \frac{K_T}{K_{QB}} = \frac{K_Q}{K_{QB}} \quad (9.5)$$

where  $K_{QB}$  is the torque coefficient measured for a propeller behind the stern. Let the relative rotative efficiency  $\eta_R$  be defined as the ratio:  $\eta_R = \eta_B / \eta_0$ . Hence the total propeller thrust efficiency can be defined as the product

$$\eta_{\text{tot}} = \eta_0 \cdot \eta_M \cdot \eta_H \cdot \eta_B \quad (9.6)$$

where  $\eta_M$  is the mechanical efficiency (typically 0.8–0.9). The open-water test is usually performed by using a towing carriage or a cavitation tunnel. Then force and torque sensors can be applied to measure the propeller force  $T$  and torque  $Q$ , respectively. Since the speed  $u_a$  of the towing carriage or the water stream in the cavitation tunnel also can be measured,  $K_T$ ,  $K_Q$  and  $\eta_0$  can be calculated from (9.2). This is usually done by applying a nominal (design) value for  $n$ .

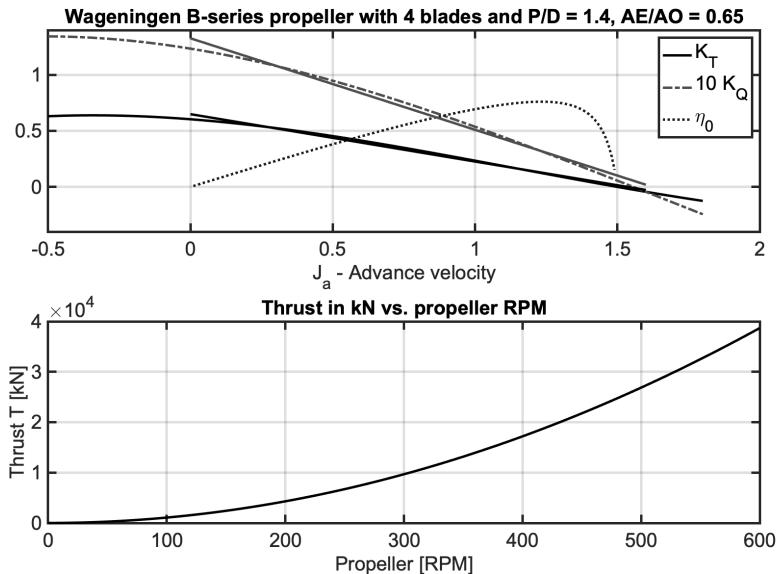


Figure 9.1: Upper plot: thrust  $K_T$ , torque  $K_Q$  and efficiency  $\eta_0$  curves (including bilinear approximations) for a propeller. Lower plot: propeller thrust  $T$  as a function of propeller speed  $n$  (see the MSS toolbox script `ExWageningen.m`).

### Bilinear thrust model

The propeller thrust and torque follow from (9.2)

$$T = \rho D^4 K_T(J_a) |n|n \quad (9.7)$$

$$Q = \rho D^5 K_Q(J_a) |n|n \quad (9.8)$$

Typical curves for  $K_T$  and  $10 \cdot K_Q$  versus  $J_a$  are shown in Figure 9.1 together with the linear approximations

$$K_T(J_a) \approx \alpha_1 - \alpha_2 J_a \quad (9.9)$$

$$K_Q(J_a) \approx \beta_1 - \beta_2 J_a \quad (9.10)$$

where  $\alpha_1, \alpha_2, \beta_1$  and  $\beta_2$  are four constants. For notational convenience let,

$$\begin{aligned} T_{|n|n} &= \rho D^4 \alpha_1, & Q_{|n|n} &= \rho D^5 \beta_1 \\ T_{|n|u_a} &= \rho D^3 \alpha_2, & Q_{|n|u_a} &= \rho D^4 \beta_2 \end{aligned} \quad (9.11)$$

such that

$$T = T_{|n|n} |n|n - T_{|n|u_a} |n|u_a \quad (9.12)$$

$$Q = Q_{|n|n} |n|n - Q_{|n|u_a} |n|u_a \quad (9.13)$$

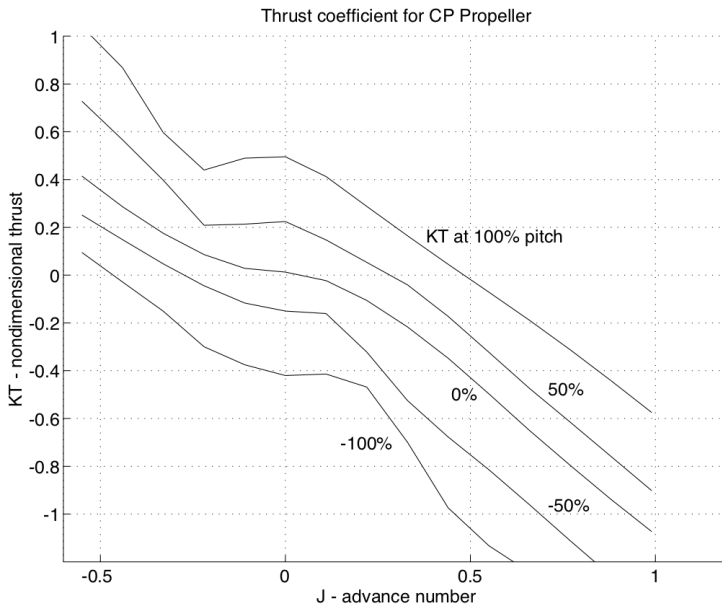


Figure 9.2:  $K_T$  characteristic for controllable pitch propeller for medium speed application. Bilinear theory is fairly accurate in steady ahead ( $u_a > 0, n > 0$ ) and astern ( $u_a < 0, n > 0$ ) cases, but not under transient conditions (Blanke 1994).

### 9.1.2 Controllable-pitch propeller

Controllable-pitch (CP) propellers are screw-blade propellers where the blades can be turned under the control of a hydraulic servo system. CP propellers are used where maneuvering properties need to be improved, where a ship has equipment that requires constant shaft speed, or with most twin-screw ships. Equipment that requires constant shaft speed includes axis generators coupled directly to the shaft via a gear, that is the generator runs with a multiple of the shaft's angular speed, and certain types of trawl drives used in the fisheries.

For the FP propeller, developed thrust and propeller shaft torque were determined by the bilinear relation with propeller turn rate  $n$  and the water velocity  $u_a$  at the propeller disc. This is also the case for a CP propeller. Consider,

$$T = T_{|n|n}(\theta) |n|n - T_{|n|u_a}(\theta) |n|u_a \quad (9.14)$$

$$Q = Q_{|n|n}(\theta) |n|n - Q_{|n|u_a}(\theta) |n|u_a \quad (9.15)$$

The coefficients  $T_{|n|n}(\theta)$ ,  $T_{|n|u_a}(\theta)$ ,  $Q_{|n|n}(\theta)$  and  $Q_{|n|u_a}(\theta)$  are complex functions of the pitch angle  $\theta$ . This is apparent from Figures 9.2 and 9.3 showing  $K_T$  and  $K_Q$  curves for a CP propeller with various values of relative pitch, between full ahead (100 %) and full astern (-100 %). On closer inspection, the curves are not too difficult to approximate, and in a simplified analysis we can assume the linear relation

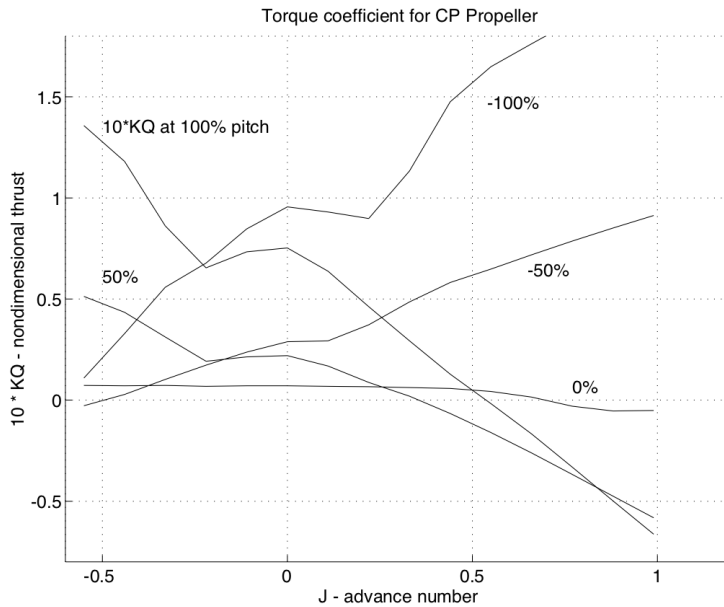


Figure 9.3:  $K_Q$  characteristic for controllable pitch propeller for medium speed application. Pitch values from  $-100\%$  to  $100\%$  are shown for positive  $n$ . Bilinear theory is seen to be fairly accurate in steady ahead and astern cases but not otherwise (Blanke 1994).

$$K_T(J_a) \approx (\alpha_1 - \alpha_2 J_a) \theta \quad (9.16)$$

for the  $K_T$  curves in Figure 9.2. This implies that  $T_{|n|n}(\theta) = T_{\theta|n|n} \theta$  and  $T_{|n|u_a}(\theta) = T_{\theta|n|u_a} \theta$ . Hence, we obtain the following thrust for the CP propeller

$$T \approx T_{\theta|n|n} \theta |n|n - T_{\theta|n|u_a} \theta |n|u_a \quad (9.17)$$

### Matlab:

The Wageningen B-series of propellers were designed and tested at the Netherlands ship model basin in Wageningen (Barnitsas *et al.* 1981). The open-water characteristics of 120 propellers were tested and fitted to polynomials. The data set is available in the MSS toolbox as `WageningData.mat`. The propellers can be configured in Matlab using:

```
% see ExWageningen.m
rho = 1025; % Density of water (kg/m^3)
D = 5; % Propeller diameter (m)
PD = 1.4; % pitch/diameter ratio
```

```

AEAO = 0.65; % blade area ratio
z = 4; % number of propeller blades

% Comput KT and KQ for advance velocites Ja
Ja = -0.8:0.01:1.8;
for i = 1:length(Ja)
    [KT(i), KQ(i)] = wageningen(Ja(i),PD,AEAO,z);
end

% Compute KT and KQ for Ja = 0 (Bollard pull)
[KT_0, KQ_0] = wageningen(0,PD,AEAO,z);

% Compute thrust [N]
n = 0:0.1:10; % propeller [RPS]
T = rho * D^4 * KT_0 * n .* abs(n); % thrust [N]

% Fit KT and KQ data to straight lines
Jdata = 0:0.01:1.6;
for i = 1:length(Jdata)
    [KTdata(i), KQdata(i)] = wageningen(Jdata(i),PD,AEAO,z);
end

alpha = polyfit(Jdata,KTdata,1) % KT = alpha(1)*Ja + alpha(2)
beta = polyfit(Jdata,KQdata,1) % KQ = beta(1) *Ja + beta(2)

```

Figure 9.1 shows the computed data graphically.

## 9.2 Ship Propulsion Systems

Marine propulsion is the mechanism or system used to generate thrust to move a ship or boat across water. There exists many different types of marine propulsion systems such as:

- Diesel engines
- Diesel-electric drives
- All-electric propulsion
- Podded propulsion
- Gas turbines
- Steam turbines
- Fuel cells
- Gas fuel
- Biodiesel fuel
- Water jets

### 9.2.1 Podded propulsion units

A podded propulsion unit consists of a FP propeller mounted on a steerable gondola (pod), which also contains the electric motor driving the propeller (see Figure 9.4). In the traditional azimuth thrusters, the propeller is driven by an electric motor or a diesel engine inside the ship's hull. The propeller is coupled to the prime mover with shafts and gears that allow rotating the propeller about a vertical axis. In a podded unit, an electric motor is mounted inside the propulsion unit and the propeller is connected directly to the motor shaft. The pod's propeller usually faces forward because in this

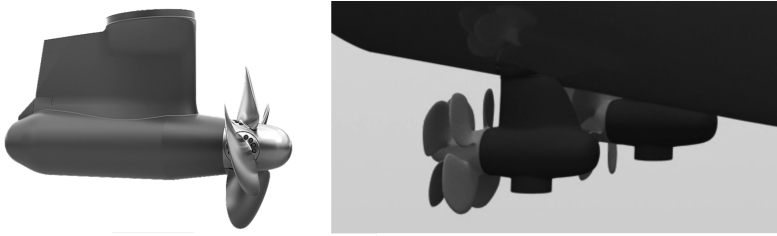


Figure 9.4: Left: podded propulsion unit. Right: two podded propulsion units aft of a ship.

pulling (or tractor) configuration the propeller is more efficient due to operation in undisturbed flow. Because it can rotate around its mount axis, the pod can apply its thrust in any direction similar to an azimuth thruster.

The thrust from a podded propulsion unit is

$$T = \rho D^4 K_T (J_a) |n| n \approx T_{|n|n} |n| n - T_{|n|u_a} (1-w) |n| u_r \quad (9.18)$$

The second term has been modified to use the relative velocity  $u_r$ . The surge, sway and yaw dynamics of a ship in transit is

$$\mathbf{M} \dot{\boldsymbol{\nu}}_r + \mathbf{C}(\boldsymbol{\nu}_r) \boldsymbol{\nu}_r + \mathbf{D}(\boldsymbol{\nu}_r) \boldsymbol{\nu}_r = \boldsymbol{\tau} + \boldsymbol{\tau}_{\text{wind}} + \boldsymbol{\tau}_{\text{wave}} \quad (9.19)$$

where  $\boldsymbol{\tau} = [\tau_1, \tau_2, \tau_6]^\top$  is the control input. Let  $\alpha$  denote the azimuth angle. For a ship, this gives the following control forces and moment in surge, sway and yaw

$$\boldsymbol{\tau} = (1-t) T_{|n|n} |n| n \begin{bmatrix} \cos(\alpha) \\ \sin(\alpha) \\ l_x \sin(\alpha) - l_y \cos(\alpha) \end{bmatrix} - \mathbf{d}_{\text{loss}}(n, \alpha) u_r \quad (9.20)$$

where  $(l_x, l_y)$  is the location of the pod with respect to CO and

$$\mathbf{d}_{\text{loss}}(n, \alpha) = (1-t)(1-w) T_{|n|u_a} |n| \begin{bmatrix} \cos(\alpha) \\ \sin(\alpha) \\ l_x \sin(\alpha) - l_y \cos(\alpha) \end{bmatrix} \quad (9.21)$$

Equation (9.21) is a dissipative propeller loss term, which vanishes for  $n = 0$ . It is possible to rewrite (9.20) as a linear control input

$$\boldsymbol{\tau} = \mathbf{B} \mathbf{u} - \mathbf{d}_{\text{loss}}(n, \alpha) u_r \quad (9.22)$$

where  $\mathbf{u} = [u_1, u_2]^\top$  and

$$u_1 = (1-t) T_{|n|n} |n| n \cos(\alpha) \quad (9.23)$$

$$u_2 = (1-t) T_{|n|n} |n| n \sin(\alpha) \quad (9.24)$$

Consequently, the input matrix becomes

$$\mathbf{B} = \begin{bmatrix} 1 & 0 & 0 \\ 0 & 1 & 0 \\ l_y & l_x & 0 \end{bmatrix} \quad (9.25)$$

and the resulting ship model becomes

$$\mathbf{M}\dot{\nu}_r + \mathbf{C}(\nu_r)\nu_r + \mathbf{D}(\nu_r)\nu_r + \mathbf{d}_{\text{loss}}(n, \alpha)u_r = \mathbf{Bu} + \boldsymbol{\tau}_{\text{wind}} + \boldsymbol{\tau}_{\text{wave}} \quad (9.26)$$

Finally, it is straightforward to design a control law for  $\mathbf{u}$  and map the control inputs to physical thruster signals

$$|n|n = \frac{1}{(1-t)T_{|n|n}} \sqrt{u_1^2 + u_2^2} \quad (9.27)$$

$$\alpha = \text{atan2}(u_2, u_1) \quad (9.28)$$

Hence, propeller RPM is computed as  $n = \text{sgn}(\tau)\sqrt{|\tau|}$  with  $\tau = |n|n$ .

### 9.2.2 Prime mover system

The section describes the rotational shaft dynamics, engine dynamics and governor of a modern ship-speed propulsion system. The dynamics of the prime mover and its control system is tightly coupled to the speed dynamics of the ship via the propeller thrust  $T$  and torque  $Q$  according to (see Figure 9.5)

$$I_m \dot{n} = Q_m - Q - Q_f \quad (9.29)$$

$$(m - X_u) \dot{u}_r = X_{|u|u} |u_r| u_r + (1-t) T + d_u \quad (9.30)$$

where

$n$	shaft speed (rad/s)
$I_m$	inertia of the rotating parts including the propeller and added inertia of the water ( $\text{kg m}^2$ )
$Q$	propeller torque (Nm)
$Q_m$	produced torque developed by the main engine (Nm)
$Q_f$	friction torque (Nm)
$u_r$	relative surge velocity (m/s)
$d_u$	unmodeled dynamics and external disturbances(N)

The transfer function  $H(s)$  from the control input  $Y(s)$  to the produced torque developed by the ship engine  $Q_m(s)$  (see Figure 9.5) can be approximated by a first-order system with time delay

$$H(s) = \frac{Q_m}{Y}(s) = \frac{K}{Ts + 1} e^{-\tau s} \quad (9.31)$$

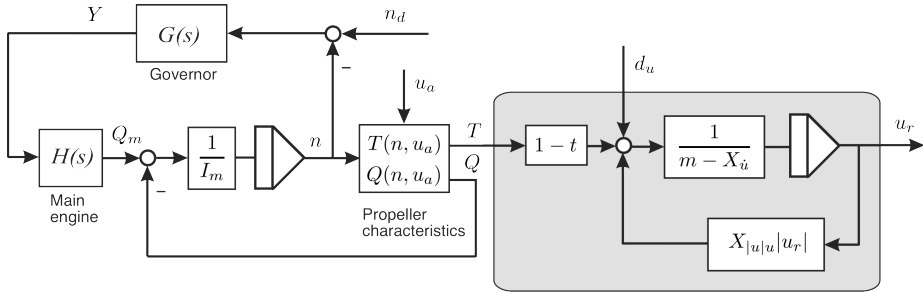


Figure 9.5: Simplified diagram showing the speed-propulsion system.

where  $\tau$  represents the time delay,  $K$  is the gain constant and  $T$  is the time constant. This model can be used to describe the dynamics of a large number of propulsion systems such as standard diesel engines, diesel-electric ship propulsion systems and all-electric ships. However, the model does not include the dynamics of the power system so it should only be used to test and verify the ship speed control system. The control input  $Y(s)$  depends on the engine system. For a diesel engine  $Y(s)$  will be the fuel pump command, while for an electric propulsion system  $Y(s)$  will represent the power needed to generate the motor torque  $Q_m$ . The control objective of the governor  $G(s)$  in Figure 9.5 is to ensure that the control loop

$$\frac{n}{n_d} \approx 1 \quad (9.32)$$

up to the frequency  $1/\tau$ , which is the bandwidth limit imposed by the engine time delay.

### Ship dynamics

The ship dynamics can be approximated by

$$(m - X_{\dot{u}}) \dot{u}_r = X_{|u|u} |u_r| u_r + (1 - t) T + d_u \quad (9.33)$$

where  $d_u$  is a disturbance term due to unmodeled dynamics and environmental forces. Equation (9.33) relates the surge acceleration  $\dot{u}$  to the propeller speed  $n$ . To see this, the expressions for relative surge velocity and acceleration (see Section 10.3)

$$u_r = u - u_c = u - V_c \cos(\beta_c) \quad (9.34)$$

$$\dot{u}_r = \dot{u} - r v_c = \dot{u} - r V_c \sin(\beta_c) \quad (9.35)$$

must be substitute into (9.33) to obtain the state-space model

$$\begin{aligned} \dot{u} = r V_c \sin(\beta_c) + \frac{1}{m - X_{\dot{u}}} & (X_{|u|u} |u - V_c \cos(\beta_c)| (u - V_c \cos(\beta_c)) \\ & + (1 - t) (T_{|n|n}(\theta) |n|n + T_{|n|V_a}(\theta) |n|u_a) + d_u) \end{aligned} \quad (9.36)$$



Figure 9.6: The two aft propellers used to control the Maritime Robotics Otter USV. Reproduced with kind permission of [www.maritimerobotics.com](http://www.maritimerobotics.com).

## 9.3 USV and Underwater Vehicle Propulsion Systems

Small USVs and underwater vehicles use propellers for propulsion, maneuvering, attitude control and dynamic positioning, see Figure 9.6. A propeller is a mechanical device, with shaped blades that turn on a shaft. It can be used to propel aircraft and ocean vehicles. For both USVs and submerged vehicles it is common to use ducted propellers to increase the efficiency at lower speeds, which allows the designer to consider smaller diameter of the blades. A duct will also protect the propeller from debris. A ducted propeller is known as a *Kort nozzle*. Ludwig Kort was a German fluid dynamicist who in the 1930s tried to reduce canal erosion and by this he discovered that directing the wake of a propeller through a short, stationary nozzle increased the thrust.

The propeller is usually driven by a DC motor, which converts direct current electrical energy into mechanical energy. This section describes mathematical models for the propeller shaft and DC motor dynamics.

### 9.3.1 Propeller shaft speed models

Yoerger *et al.* (1991) have proposed a *one-state model* with quadratic damping for propeller shaft speed. The linearized version of this model is

$$J_m \dot{n} + K_n n = Q_m - Q \quad (9.37)$$

where  $n$  is the shaft speed and  $Q_m$  is the control input (shaft torque). For ships in transit, only positive values  $u_a > 0$  are considered. A large number of marine craft, however, operate in regimes where the ambient water velocity can be both positive and negative. It is common to assume that  $u_a = 0$  during stationkeeping and low-speed maneuvering such that (9.12)–(9.13) can be simplified as (see Figure 9.7)

$$T = T_{|n|n} |n|n - T_{|n|u_a} |n|u_a \stackrel{u_a=0}{=} T_{|n|n} |n|n \quad (9.38)$$

$$Q = Q_{|n|n} |n|n - Q_{|n|u_a} |n|u_a \stackrel{u_a=0}{=} Q_{|n|n} |n|n \quad (9.39)$$

Healey *et al.* (1995) have modified the model (9.37) to describe overshoots in thrust,

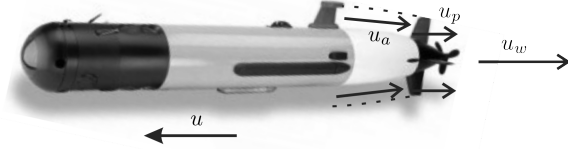


Figure 9.7: Ambient water velocity  $u_a$  (upstream), axial flow velocity in propeller disc  $u_p$  and velocity in the wake  $u_w$  (downstream) for an underwater vehicle moving at velocity  $u$ .

which are typical in experimental data. The result is a *two-state model*

$$J_m \dot{n} + K_n n = Q_m - Q \quad (9.40)$$

$$m_f \dot{u}_p + d_f (u_p - u) |u_p - u| = T \quad (9.41)$$

where  $u$  is the forward speed of the vehicle and  $u_p$  is axial flow velocity in propeller disc. This was done by modeling a control volume of water around the propeller as a mass-damper system. The mass-damper of the control volume interacts with the vehicle speed dynamics, which are also represented by a mass-damper system. Experimental verifications of the one- and two-state models are found in Whitcomb and Yoerger (1999).

The signal  $u_p$  can be measured by using a laser-Doppler velocimeter (LDV) system, a particle image velocimeter (PIV) system or an acoustic Doppler velocimeter system for instance. It is also possible to estimate  $u_p$  using Kalman filters and nonlinear observers; see Fossen and Blanke (2000) and references therein.

A more general model is the *three-state* propeller shaft speed model (Blanke *et al.* 2000b)

$$J_m \dot{n} + K_n n = Q_m - Q \quad (9.42)$$

$$m_f \dot{u}_p + d_{f0} u_p + d_f |u_p| (u_p - u_a) = T \quad (9.43)$$

$$(m - X_u) \dot{u}_r - X_u u - X_{u|u|} u_r |u_r| = (1 - t)T \quad (9.44)$$

where damping in surge is modeled as the sum of *linear laminar skin friction*,  $-X_u u_r$  and *nonlinear quadratic drag*,  $-X_{u|u|} u_r |u_r|$ . Similarly, linear damping,  $d_{f0} u_p$ , is included in the axial flow, model since quadratic damping,  $d_f |u_p| u_p$ , alone would give an unrealistic response at low speeds. Linear skin friction gives exponential convergence to zero at low speeds.

The ambient water velocity  $u_a$  in (9.43) is computed by using the steady-state condition

$$u_a = (1 - w)u \quad (9.45)$$

where  $0 < w < 1$  is the *wake fraction number* (Lewis 1989).

### 9.3.2 Motor armature current control

Consider a DC motor

$$L_a \frac{d}{dt} i_m = -R_a i_m - K_m n + V_m \quad (9.46)$$

$$Q_m = K_m i_m \quad (9.47)$$

where  $V_m$  is the armature voltage,  $i_m$  is the armature current and  $Q_m$  is the motor torque. In addition,  $L_a$  is the armature inductance,  $R_a$  is the armature resistance and  $K_m$  is the motor torque constant.

Since the electrical time constant  $T_a = L_a/R_a$  is small compared to the mechanical time constant, time scale separation suggests

$$\frac{L_a}{R_a} \frac{d}{dt} i_m \approx 0 \quad (9.48)$$

Hence, the shaft speed dynamics is given by

$$0 = -R_a i_m - K_m n + V_m \quad (9.49)$$

$$J_m \dot{n} = K_m i_m - Q \quad (9.50)$$

The motor current can be controlled by using a P controller

$$V_m = K_p(i_d - i_m), \quad K_p > 0 \quad (9.51)$$

where  $i_d$  is the desired motor current. From (9.49) we get

$$(R_a + K_p)i_m = -K_m n + K_p i_d \quad (9.52)$$

The motor dynamics (9.50) for the current controlled motor therefore takes the form

$$J_m \dot{n} + \frac{K_m^2}{R_a + K_p} n = \frac{K_m K_p}{R_a + K_p} i_d - Q \quad (9.53)$$

If a high-gain controller  $K_p \gg R_a > 0$  is used, this expression simplifies to

$$J_m \dot{n} = K_m i_d - Q \quad (9.54)$$

The desired motor torque is chosen as

$$Q_d = K_m i_d \quad (9.55)$$

From (9.53) we see that this yields the following dynamics for a torque controlled motor

$$J_m \dot{n} + \frac{K_m^2}{R_a + K_p} n = \frac{K_p}{R_a + K_p} Q_d - Q \quad (9.56)$$

which reduces to

$$J_m \dot{n} = Q_d - Q \quad (9.57)$$

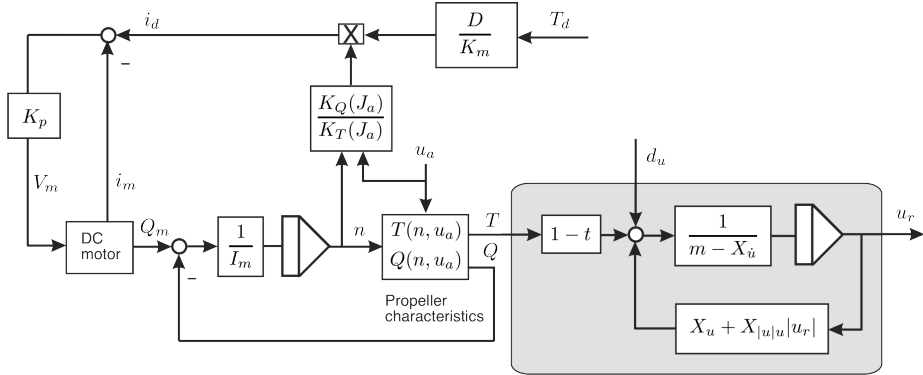


Figure 9.8: Block diagram showing DC motor controller and propeller.

for  $K_p \gg R_a > 0$ . Hence,  $Q = Q_d$  in steady state.

The current setpoint is computed by using the torque/thrust ratio

$$Q = D \frac{K_Q(J_a)}{K_T(J_a)} T \quad (9.58)$$

which follows directly from (9.7)–(9.8). The vehicle velocity can be controlled ( $u = u_d$ ) by using thrust  $T$  as control input. Hence,  $T = T_d$  and  $i_d = Q_d/K_m$ . This gives

$$i_d = \frac{D}{K_m} \frac{K_Q(J_a)}{K_T(J_a)} T_d \quad (9.59)$$

where

$$J_a = \frac{u_a}{nD} \approx 0 \quad (9.60)$$

for low-speed maneuvering and stationkeeping applications. The armature current controller (9.51) and the desired signals are shown in Figure 9.8.

### 9.3.3 Motor RPM control

In many cases it is desirable to control the propeller RPM instead of the armature current. Combining (9.49)–(9.50) gives

$$J_m \dot{n} + \frac{K_m^2}{R_a} n = \frac{K_m}{R_a} V_m - Q \quad (9.61)$$

This suggests that the RPM controller can be chosen as

$$V_m = K_p(n_d - n), \quad K_p > 0 \quad (9.62)$$

where  $n_d$  is the desired RPM, usually computed by inverting the thrust equation

$$T_d = \rho D^4 K_T(0) |n_d| n_d \quad (9.63)$$

according to

$$n_d = \text{sgn}(T_d) \sqrt{\frac{|T_d|}{\rho D^4 K_T(0)}} \quad (9.64)$$

where  $\text{sgn}(\cdot)$  is the signum function.

## 9.4 Thrusters

A thruster is a device for propelling a marine craft. It is a more complex arrangement than a single propeller. A thruster can consist of several propellers, for instance twin contra-rotating propellers (CRP). In addition, a thruster system can be podded to protect mechanical devices and reduce the resistance (energy consumption) during transit.

There exists different types of thruster systems such as:

- **Tunnel thruster** – Propeller installed in a transverse tunnel, producing a transverse force. Both bow and stern thrusters are used to dynamically position a ship or a boat.
- **Externally mounted thrusters** – Instead of a tunnel thruster, marine craft may have externally mounted thrusters. They are usually used by craft where it is impossible or undesirable to install a tunnel thruster, due to hull shape or outfitting.
- **Azimuth thruster** – Ship propellers placed in pods that can be rotated on the horizontal plane, making a rudder unnecessary. This is also referred to as thrust vectoring since both the magnitude and direction of the force can be controlled.
- **CRP thruster** – An azimuthing thruster equipped with twin contra-rotating propellers.
- **Jet thruster** – A pump arranged to take suction from beneath or close to the keel and to discharge to either side, to develop port or starboard thrust, or in many cases through  $360^\circ$ .

The forces and moments in 6 DOF corresponding to the force vector  $\mathbf{f} = [F_x, F_y, F_z]^\top$  are

$$\boldsymbol{\tau} = \begin{bmatrix} \mathbf{f} \\ \mathbf{r} \times \mathbf{f} \end{bmatrix} = \begin{bmatrix} F_x \\ F_y \\ F_z \\ l_y F_z - l_z F_y \\ l_z F_x - l_x F_z \\ l_x F_y - l_y F_x \end{bmatrix} \xrightarrow{\text{surge, sway and yaw}} \boldsymbol{\tau} = \begin{bmatrix} F_x \\ F_y \\ l_x F_y - l_y F_x \end{bmatrix} \quad (9.65)$$

where  $\mathbf{r} = [l_x, l_y, l_z]^\top$  are the moment arms.

### 9.4.1 Tunnel thrusters

Tunnel thrusters are transverse thrusters going through the hull of the craft (see Figure 9.9). The propeller unit is mounted inside a transverse tube and it produces a force

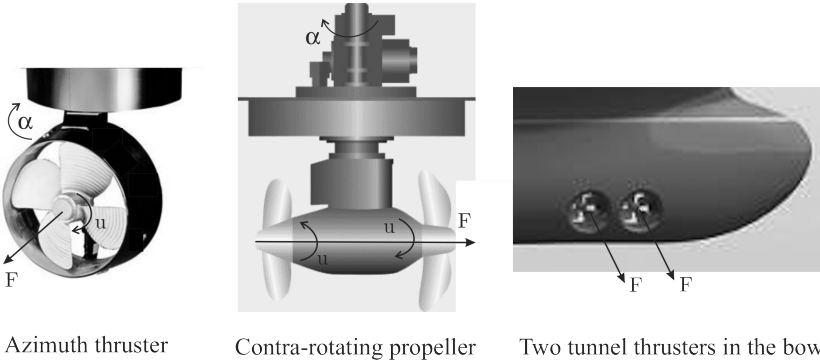


Figure 9.9: Azimuth thruster, twin contra-rotating propeller and tunnel thrusters. The force (thrust) is denoted  $F$ ,  $\alpha$  is the direction of the force and  $u = |n|n$  is the squared propeller revolution.

$F_y$  in the  $y$  direction. Tunnel thrusters are only effective at low speed which limits their use to low-speed maneuvering and stationkeeping.

The generalized control force is

$$\boldsymbol{\tau} = [0, F_y, 0, 0, 0, l_x F_y]^\top \quad (9.66)$$

where  $l_x$  is the lever arm from CO to the location of the thruster. For tunnel thrusters the advance speed  $u_a$  will be small. Hence,  $J_a \approx 0$  and the propeller produces a transverse force (see Section 9.1)

$$\text{FP propeller: } F_y = \rho D^4 K_T(0) |n|n \approx T_{|n|n} |n|n \quad (9.67)$$

$$\text{CP propeller: } F_y \approx T_{\theta|n|n} \theta |n|n \quad (9.68)$$

### 9.4.2 Azimuth thrusters

Azimuth thrusters can be rotated an angle  $\alpha$  about the  $z$  axis and produce two force components ( $F_x, F_y$ ) in the horizontal plane (see Figure 9.9). They are usually mounted under the hull of the craft and the most sophisticated units are retractable. Azimuth thrusters are frequently used in DP systems since they can produce forces in different directions. Hence, this becomes an overactuated control problem that can be optimized with respect to power and possible failure situations. The control force is

$$\boldsymbol{\tau} = [F \cos(\alpha), F \sin(\alpha), 0, 0, 0, l_x F \sin(\alpha) - l_y F \cos(\alpha)]^\top \quad (9.69)$$

where  $l_z$  is the lever arm from CO to the location of the thruster. Azimuth thrusters used for maneuvering produce a force

$$F = \rho D^4 K_T(J_a) |n|n \quad (9.70)$$

For DP applications it is common to assume that  $J_a = 0$  such that

$$\text{FP propeller: } F = \rho D^4 K_T(0) |n|n \approx T_{|n|n} |n|n \quad (9.71)$$

$$\text{CP propeller: } F \approx T_{\theta|n|n} \theta |n|n \quad (9.72)$$

For a surface vessel, an azimuth thruster will produce the following control forces and moment in the horizontal plane

$$\boldsymbol{\tau} = \begin{bmatrix} F \cos(\alpha) \\ F \sin(\alpha) \\ l_x F \sin(\alpha) - l_y F \cos(\alpha) \end{bmatrix} \quad (9.73)$$

**Example 9.1 (Thrust Configuration Matrix for a DP Vessel)**

Consider the ship in Figure 9.10, which is equipped with two azimuth thrusters  $F_1$  and  $F_3$ , two tunnel thrusters  $F_2$  and  $F_4$ , and two main propellers (forces  $F_5$  and  $F_6$ ). All thruster systems ( $i = 1, 2, \dots, 6$ ) have FP propellers and the thrust is given by (see Section 9.1)

$$F_i = \rho D_i^4 K_{T_i}(0) |n_i| n_i := K_i u_i \quad (9.74)$$

where  $K_i := \rho D_i^4 K_{T_i}(0)$  and

$$u_i := |n_i| n_i \quad (9.75)$$

The azimuth forces  $F_1$  and  $F_3$  are decomposed along the  $x$  and  $y$  axes by defining the following virtual control inputs ( $i = 1, 3$ )

$$u_{ix} := u_i \cos(\alpha_i) \quad (9.76)$$

$$u_{iy} := u_i \sin(\alpha_i) \quad (9.77)$$

such that the forces in the  $x$  and  $y$  directions become

$$F_{ix} = K_i u_{ix} \quad (9.78)$$

$$F_{iy} = K_i u_{iy} \quad (9.79)$$

The generalized force vector for motions in the surge, sway and yaw is expressed in terms of the input matrix  $\mathbf{B} \in \mathcal{R}^{3 \times 8}$  according to

$$\boldsymbol{\tau} = \mathbf{B} \mathbf{u}, \quad \mathbf{B} = \mathbf{T} \mathbf{K} \quad (9.80)$$

where  $\mathbf{u} = [u_{1x}, u_{1y}, u_2, u_{3x}, u_{3y}, u_4, u_5, u_6]^\top$  is the control input vector,  $\mathbf{T} \in \mathcal{R}^{3 \times 8}$  is the thrust configuration matrix and  $\mathbf{K} \in \mathcal{R}^{8 \times 8}$  is the thrust coefficient matrix.

Then it follows that the forces and moment  $\tau_1, \tau_2$  and  $\tau_6$  in surge, sway and yaw,

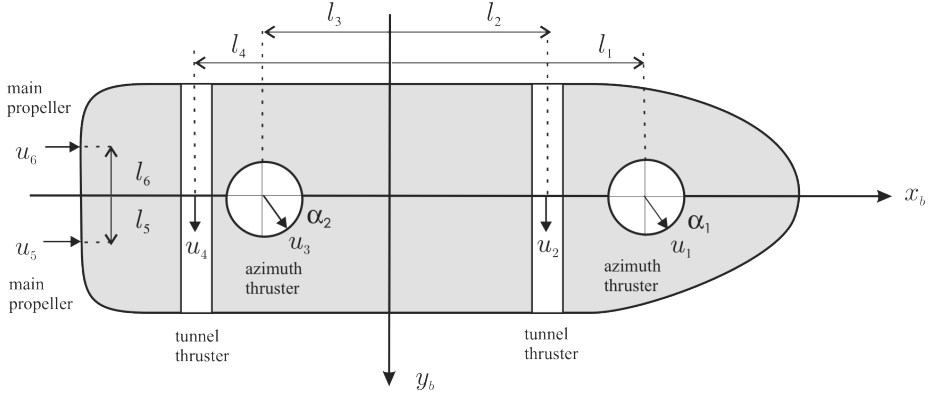


Figure 9.10: Ship equipped with two azimuth thrusters (forces  $F_1$  and  $F_3$ ), two tunnel thrusters (forces  $F_2$  and  $F_4$ ) and two main propellers (forces  $F_5$  and  $F_6$ ).

respectively for the thruster configuration shown in Figure 9.10 satisfy

$$\tau = \mathbf{T}K\mathbf{u} \quad (9.81)$$

$$\begin{array}{c} \Updownarrow \\ \left[ \begin{array}{c} \tau_1 \\ \tau_2 \\ \tau_6 \end{array} \right] = \left[ \begin{array}{ccccccc} 1 & 0 & 0 & 1 & 0 & 0 & 1 & 1 \\ 0 & 1 & 1 & 0 & 1 & 1 & 0 & 0 \\ 0 & l_1 & l_2 & 0 & l_3 & l_4 & -l_5 & -l_6 \end{array} \right] \\ \cdot \left[ \begin{array}{ccccccccc} K_1 & 0 & 0 & 0 & 0 & 0 & 0 & 0 & 0 \\ 0 & K_1 & 0 & 0 & 0 & 0 & 0 & 0 & 0 \\ 0 & 0 & K_2 & 0 & 0 & 0 & 0 & 0 & 0 \\ 0 & 0 & 0 & K_3 & 0 & 0 & 0 & 0 & 0 \\ 0 & 0 & 0 & 0 & K_3 & 0 & 0 & 0 & 0 \\ 0 & 0 & 0 & 0 & 0 & K_4 & 0 & 0 & 0 \\ 0 & 0 & 0 & 0 & 0 & 0 & K_5 & 0 & 0 \\ 0 & 0 & 0 & 0 & 0 & 0 & 0 & K_6 & 0 \end{array} \right] \left[ \begin{array}{c} u_{1x} \\ u_{1y} \\ u_2 \\ u_{3x} \\ u_{3y} \\ u_4 \\ u_5 \\ u_6 \end{array} \right] \end{array} \quad (9.82)$$

If the control input  $\mathbf{u}$  is computed using the pseudoinverse (see Section 12.3)

$$\begin{aligned} \mathbf{u} &= \mathbf{B}^\dagger \boldsymbol{\tau} \\ &= \mathbf{K}^{-1} \mathbf{T}^\dagger \boldsymbol{\tau} \end{aligned} \quad (9.83)$$

the propeller RPM commands become ( $i = 1, 2, \dots, 6$ )

$$n_i = \text{sgn}(u_i) \sqrt{|u_i|} \quad (9.84)$$

while the azimuth control inputs are derived from the pairs  $(u_{1x}, u_{1y})$  and  $(u_{3x}, u_{3y})$  according to

$$u_1 = \sqrt{u_{1x}^2 + u_{1y}^2}, \quad \alpha_1 = \text{atan2}(u_{1y}, u_{1x}) \quad (9.85)$$

$$u_3 = \sqrt{u_{3x}^2 + u_{3y}^2}, \quad \alpha_3 = \text{atan2}(u_{3y}, u_{3x}) \quad (9.86)$$

## 9.5 Rudder in Propeller Slipstream

Rudders are primary steering devices for merchant ships. Also USVs and underwater vehicles can be equipped with stern rudders as an alternative to propellers and thrusters. Rudders outside of the propeller slipstream are ineffective at small or zero ship speed (e.g. DP and berthing operations). Insufficient rudder effectiveness at slow ship speed can be temporarily increased by increasing the propeller RPM.

The main purpose of using rudders is to generate forces for course keeping and maneuvering. They can also be used for stationkeeping and emergency stops. Furthermore, rudders affect propeller thrust efficiency and total ship resistance. The performance of rudders depends on the rudder hydrodynamic characteristics, which are affected by the design choices. An overview of rudder design for the last 60 years is found in Liu and Hekkenberg (2017).

Figure 9.11 shows a conventional rudder and a flap rudder. The flap rudder is designed to improve the effective lift, which again improves the maneuverability of the craft. The flap rudder consists of two or more sections which move relative to each other as helm is applied and the angle of the main or driven section moves. Thus the shape of the rudder changes dynamically as the angle of helm is changed. Flap rudders give a much higher lift per rudder angle and a 60 to 70 % higher maximum lift compared to the conventional rudder of same shape, size and area can be expected.

### 9.5.1 Rudder forces and moment

Vertical rudders are usually placed at the vehicle's stern behind the propellers to produce a transverse force and a steering moment about the vehicle's CG by deflecting the water flow to a direction of the foil plane. Let  $A_R$  denote the area of the rudder and  $b$  the rudder height. The aspect ratio is then (see Figure 9.11)

$$\Lambda = \frac{b^2}{A_R} \quad (9.87)$$

Data for different rudder profiles are found in Bertram (2004) and references therein. The rudder normal force is expressed as (Kijima *et al.* 1990)

$$F_N = \frac{1}{2} \rho U_R^2 A_R C_N \sin(\alpha_R) \quad (9.88)$$

where the resultant rudder inflow speed  $U_R$  and effective rudder angle  $\alpha_R$  are

$$U_R = \sqrt{u_R^2 + v_R^2} \quad (9.89)$$

$$\alpha_R = \delta - \tan^{-1} \left( \frac{v_R}{u_R} \right) \approx \delta - \beta_R \quad (9.90)$$

where the ratio  $\beta_R = v_R/u_R$  is the drift angle at the position of the rudder. This value will be larger than the ship sideslip angle  $\beta$ .

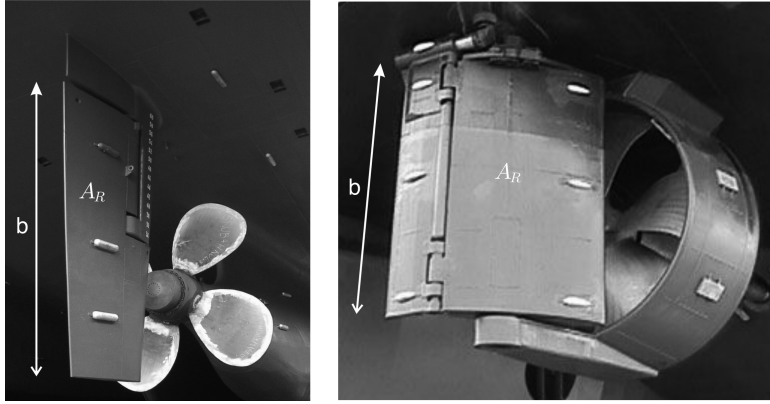


Figure 9.11: Left: Conventional stern rudder for a ship. Right: High-lift flap rudder consisting of two or more sections which move relative to each other as helm is applied.  $A_R$  denotes the area of the rudder and  $b$  is the rudder height.

According to Fujii (1960), and Fujii and Tsuda (1961, 1962),  $C_N$  can be estimated as follows

$$C_N = \frac{6.13\Lambda}{\Lambda + 2.25} \quad (9.91)$$

The inflow speed is in general complicated to compute. For simulation studies and testing of control system under normal operation of the rudder (small rudder angles  $\delta$ ) it is quite accurate to assume that  $\beta_R \approx 0$  such that  $U_r \approx u_r$  and  $\alpha_R \approx \delta$ . The *Maneuvering Modeling Group* (MMG) has proposed a standard method for ship maneuvering prediction with procedures based on captive model tests to compute the hydrodynamic coefficients including the rudder forces (Yasukawa and Yoshimura 2015). In this work the inflow surge velocity is computed as

$$u_R = \varepsilon u (1 - w_P) \sqrt{\eta \left( 1 + \kappa \left( \sqrt{1 + \frac{8K_T}{\pi J_a^2}} - 1 \right) \right)^2 + (1 - \eta)} \quad (9.92)$$

where  $u$  is the surge velocity,  $K_T$  is the thrust coefficient,  $J_a$  is the advance number,  $\varepsilon$  is the ratio of wake fraction at rudder position to that at propeller position (typically 1.09) defined by  $\varepsilon := (1 - w_R)/(1 - w_P)$  and  $\kappa$  is an experimental constant (typically 0.5). Let  $D$  denote the propeller diameter and  $b$  be the rudder height. From Yasukawa and Yoshimura (2015) it follows that  $\eta \approx D/b$ .

The rudder normal force contributes to forces in surge and sway as well as a yaw moment

$$X_R = -(1 - t_R) F_N \sin(\delta) \quad (9.93)$$

$$Y_R = -(1 + a_H) F_N \cos(\delta) \quad (9.94)$$

$$N_R = -(x_R + a_H x_H) F_N \cos(\delta) \quad (9.95)$$

where  $\delta$  is the rudder angle and  $x_R$  is the longitudinal coordinate of the rudder position (typically  $-0.5 L_{pp}$ ). The coefficient for additional drag  $t_R$  can be approximated by *Matsumoto's method* (Matsumoto and Suemitsu 1980)

$$1 - t_R = 0.28 C_B + 0.55 \quad (9.96)$$

where  $C_B = \nabla/(L_{pp}BT)$  is the block coefficient. The rudder force increase factor  $a_H$  and the longitudinal coordinate  $x_H$  of the additional lateral force are usually determined experimentally. However, Kijima *et al.* (1990) propose to use the curves in Figure 9.12 as a first estimate.

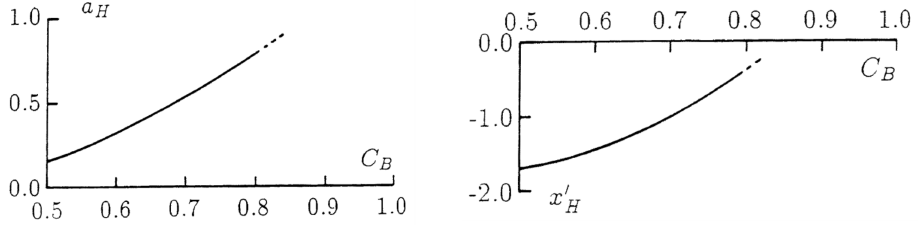


Figure 9.12: The interaction coefficients  $a_H$  and  $x'_H = x_H/L_{pp}$  as a function of  $C_B$  (Kijima *et al.* 1990).

The assumption that  $\beta_R = 0$  implies that  $\alpha_R \approx \delta$  and  $U_R \approx u_R$  such that (9.93)–(9.95) become

$$X_R = -(1 - t_R) \left( \frac{1}{2} \rho U_R^2 A_r C_N \right) \sin^2(\delta) \quad (9.97)$$

$$Y_R = -(1 + a_H) \left( \frac{1}{2} \rho U_R^2 A_r C_N \right) \frac{1}{2} \sin(2\delta) \quad (9.98)$$

$$N_R = -(x_R + a_H x_H) \left( \frac{1}{2} \rho U_R^2 A_r C_N \right) \frac{1}{2} \sin(2\delta) \quad (9.99)$$

Finally, if  $\delta$  is small, the following formulae are obtained

$$\boldsymbol{\tau}_R = \begin{bmatrix} X_R \\ Y_R \\ N_R \end{bmatrix} = \begin{bmatrix} X_{\delta\delta} \delta^2 \\ Y_\delta \delta \\ N_\delta \delta \end{bmatrix} \quad (9.100)$$

where the rudder coefficients are recognized as

$$X_{\delta\delta} = -(1 - t_R) \frac{1}{2} \rho U_R^2 A_r C_N \quad (9.101)$$

$$Y_\delta = -(1 + a_H) \frac{1}{2} \rho U_R^2 A_r C_N \quad (9.102)$$

$$N_\delta = -(x_R + a_H x_H) \frac{1}{2} \rho U_R^2 A_r C_N \quad (9.103)$$

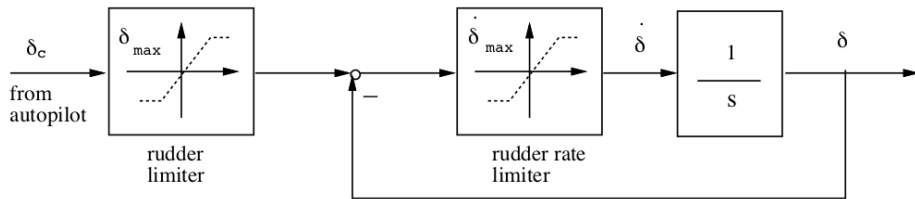


Figure 9.13: Simplified diagram of the rudder control loop (Van Amerongen 1982).

### 9.5.2 Steering machine dynamics

The steering machine, hydraulic or electric, is controlled by a feedback control system which ensures that the rudder angle  $\delta$  is close to the commanded rudder angle  $\delta_c$ . However, the steering machine is a nonlinear system with two important physical limitations: the maximum rudder angle and rudder rate. In computer simulations and when designing autopilots, (Van Amerongen 1982) suggests using a simplified representation of the steering machine where the maximum rudder angle  $\delta_{\max}$  and rudder rate  $\dot{\delta}_{\max}$  are specified, see Figure 9.13. This simplification is based on the assumption that the steering machine dynamics is being much faster than the saturated turning rate commands generated by the autopilot. Generally, the rudder angle and rudder rate limiters in Figure 9.13 will be in the ranges

$$\delta_{\max} = 35^\circ; \quad 2.3 \text{ (deg/s)} \leq \dot{\delta}_{\max}$$

for commercial ships. The requirement for minimum average rudder rate is specified by the classification societies. Typically, it is required that the rudder can be turned from  $35^\circ$  on either side to  $30^\circ$  on the other sides respectively within 28 seconds for the class notations *Tug* or *Offshore service vessel*. For the class notations for *Icebreaker* and *Pusher* the requirements are 15 and 20 seconds, respectively.

The 28 seconds requirement corresponds to the lower turning rate limit of 2.3 deg/s. Recently, much faster steering machines have been designed with rudder speeds up to 15–20 deg/s. A rudder speed of 5–20 deg/s is usually required for a rudder-roll stabilization (RRS) system to work properly.

Another model of the rudder dynamics could be (Rios-Neto and Da Cruz 1985)

$$\dot{\delta} = \begin{cases} \dot{\delta}_{\max} (1 - e^{-(\delta_c - \delta)/\Delta}) & \text{if } \delta_c - \delta \geq 0 \\ -\dot{\delta}_{\max} (1 - e^{(\delta_c - \delta)/\Delta}) & \text{if } \delta_c - \delta < 0 \end{cases} \quad (9.104)$$

The parameter  $\Delta$  will depend on the moment of inertia of the rudder. Typical values will be in the range  $3 \leq \Delta \leq 10$ .

The limitations of the rudder angle and the rudder speed can be illustrated with the following two simple examples adopted from (Van der Klugt 1987).

**Example 9.2 (Limitation of the Rudder Angle)**

Consider the rudder angle limiter in Figure 9.14 where  $\delta_c$  is the commanded rudder angle and  $\delta$  is the actual rudder angle. Let the controller output be given by

$$\delta_c = A \sin(\omega_0 t) \quad (9.105)$$

Figure 9.15 shows the actual rudder angle for three different cases;  $A = 3/4 \delta_{\max}$ ,  $A = \delta_{\max}$  and  $A = 4/3 \delta_{\max}$  where  $\delta_{\max} = 30 \text{ deg}$  and  $\omega_0 = \pi/10 \text{ rad/s}$ . It is seen from Figure 9.15 that no extra phase lag is introduced for any of the cases. However, an obvious reduction in amplitude is observed for the saturated case. Consequently, a PID controller will usually suffer from reduced performance but it will be stable.

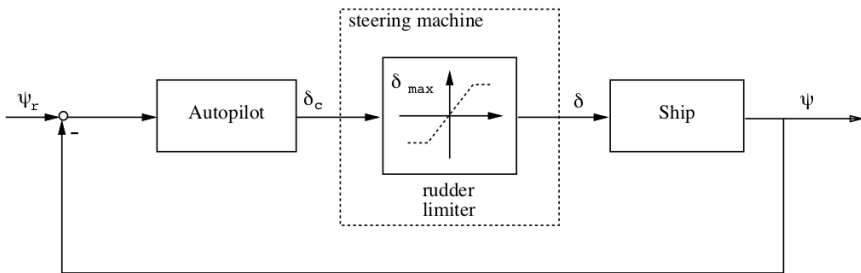


Figure 9.14: Simplified system with rudder limiter (Van der Klugt 1987).

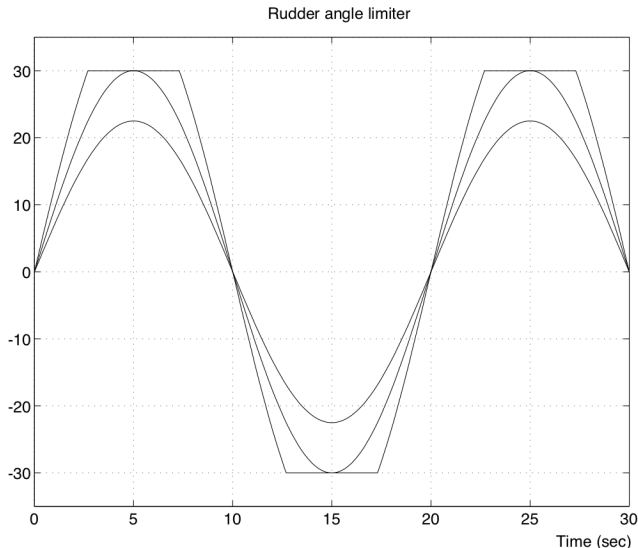


Figure 9.15: Influence of the rudder limiter (Van der Klugt 1987).

**Example 9.3 (Limitation of the Rudder Rate)**

Consider the rudder rate limiter in Figure 9.16 where  $\delta_c$  is the commanded rudder angle and  $\delta$  is the actual rudder angle. Let the controller output be given by

$$\delta_c = A \sin(\omega_0 t) \quad (9.106)$$

Figure 9.17 shows the actual and commanded rudder angle for  $\dot{\delta}_{\max} = 4 \text{ deg/s}$ ,  $A = 30 \text{ deg}$  and  $\omega_0 = \pi/10 \text{ rad/s}$ . Besides saturation we now observe that an additional phase lag has been introduced. Reduced phase margins can lead to severe stability problems for the control system. In practice, rudder rate limitations are typical in extreme weather conditions since compensation of high-frequency disturbances require a faster rudder.

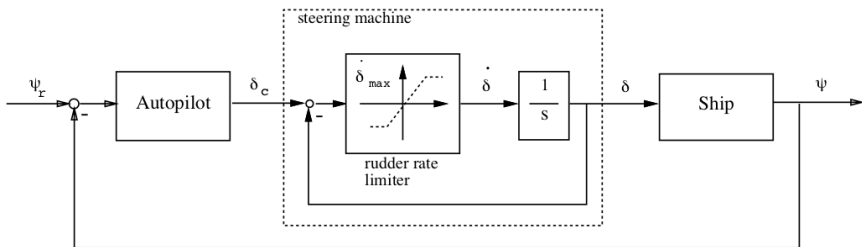


Figure 9.16: Simplified system with rudder rate limiter (Van der Klugt 1987).

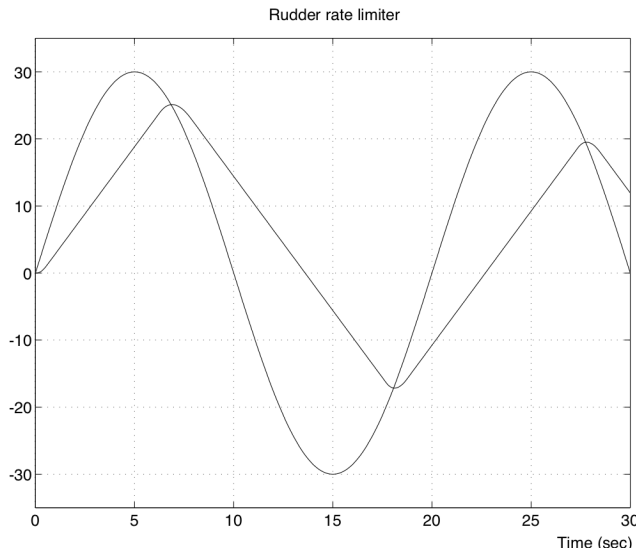


Figure 9.17: Influence of the rudder rate limiter (Van der Klugt 1987).

## 9.6 Fin Stabilizers

Fin stabilizers are primarily used for roll damping (see Figure 9.18). They provide considerable damping if the speed of the ship is not too low. The disadvantage with additional fins is increased hull resistance and high costs associated with the installation, since at least two new hydraulic systems must be installed. Retractable fins are popular, since they are inside the hull when not in use (no additional drag). It should be noted that fins are not effective at low speed and that they cause underwater noise in addition to drag.

Fin stabilizers were patented by John I. Thornycroft in 1889 and there exists a large number of commercial systems today. Modern systems are attractive for roll reduction since they are highly effective, works on a large number of ships, and they are easy to control, even for varying load conditions and actuator configurations. Fins stabilizers are effective at high speed, but at the price of additional drag and added noise. The most economical systems are retractable fins, where additional drag is avoided during normal operation, since fin stabilizers are not needed in moderate weather. Fin stabilizer can also be used in combination with rudder-roll damping systems (Källström 1981) (Roberts and Braham 1990) (Roberts 1992) (Hickey *et al.* 1997) (Hearns *et al.* 2000) (Katebi *et al.* 2000) (Perez 2005)

Some obvious benefits of fin stabilizing systems for roll damping are:

- Prevent cargo damage and to increase the effectiveness of the crew by avoiding or reducing seasickness. This is also important from a safety point of view.
- For naval ships and offshore vessels, critical marine operations like landing a helicopter, formation control and underway replenishment benefit from additional roll damping.

### 9.6.1 Fin stabilizers lift and drag forces

The water flowing past the surface of the fin exerts a force on it (see Figure 9.18). Lift is the component of this force that is perpendicular to the oncoming flow direction. It contrasts with the drag force, which is the component of the force parallel to the flow direction. Assume that the lift and drag coefficients  $C_L(\alpha_F)$  and  $C_D(\alpha_F)$  are known such that the forces in FLOW axes become

$$F_{\text{drag}} = \frac{1}{2} \rho V_r^2 A_F C_D(\alpha_F) \quad (9.107)$$

$$F_{\text{lift}} = \frac{1}{2} \rho V_r^2 A_F C_L(\alpha_F) \quad (9.108)$$

where  $\rho$  is the density of water,  $A_F$  is the fin area and  $V_r$  is the relative speed. The lift and drag coefficients depend on the angle of attack  $\alpha_F$ , which can be adjusted by the control system. Since lift is perpendicular to the relative flow and drag is parallel, the longitudinal forces in BODY axes become

$$\begin{bmatrix} F_x \\ F_z \end{bmatrix} = \begin{bmatrix} \cos(\alpha_F) & -\sin(\alpha_F) \\ \sin(\alpha_F) & \cos(\alpha_F) \end{bmatrix} \begin{bmatrix} -F_{\text{drag}} \\ -F_{\text{lift}} \end{bmatrix} \quad (9.109)$$

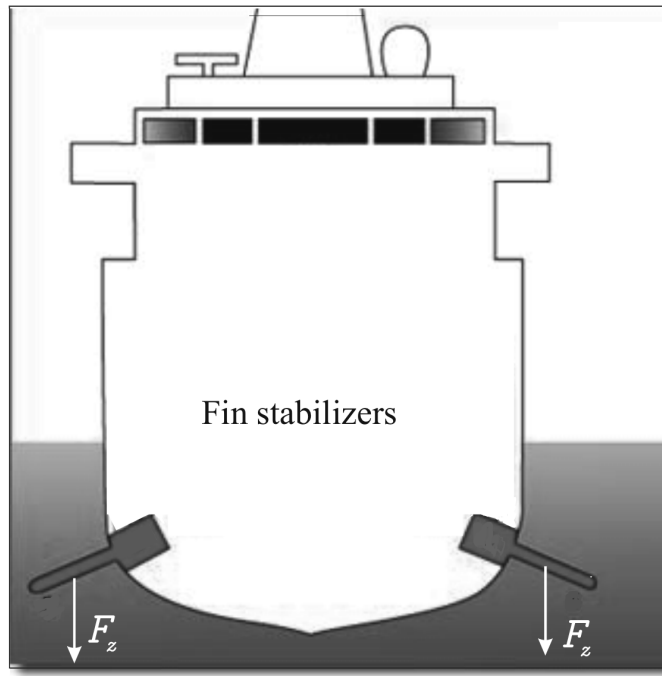


Figure 9.18: Fin stabilized ship where the vertical force  $F_z = K_\alpha \alpha_F$  is proportional to the angle  $\alpha_F$  for small deflections.

The roll moment produced by a single fin stabilizer follows from (9.65)

$$\tau_4 = l_y F_z \quad (9.110)$$

where  $(l_y, l_z)$  is the location of the fin with respect to the CO.

### 9.6.2 Linear theory for roll moment

Consider a ship with a pair of symmetrical fin stabilizers (see Figure 9.18). If the two control signals are chosen equal, the roll moment (9.110) becomes

$$\tau_4 = 2 l_y F_z \quad (9.111)$$

Expanding (9.109) gives

$$F_z = -F_{\text{drag}} \sin(\alpha_F) - F_{\text{lift}} \cos(\alpha_F) \quad (9.112)$$

The lift and drag coefficients can be approximated by

$$C_L(\alpha_F) \approx C_{L_0} + C_{L_\alpha} \alpha_F \quad (9.113)$$

$$C_D(\alpha_F) \approx C_{D_0} + C_{D_\alpha} \alpha_F \quad (9.114)$$

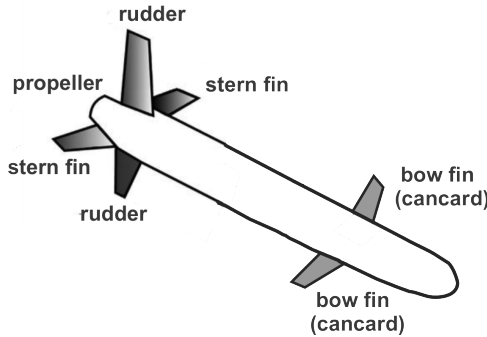


Figure 9.19: Stern: Horizontal fin and vertical rudder. This is also called cross-form rudder. Bow: *Canard*, a small fin located in front, for additional stability and lift.

Assume that  $C_{L_0} = C_{D_0} = 0$  and that  $\alpha_F$  is small such that  $\sin(\alpha_F) \approx \alpha_F$  and  $\cos(\alpha_F) \approx 1$ . Then

$$F_z \approx -\frac{1}{2}\rho V_r^2 A_F (C_{D_\alpha} \alpha_F^2 + C_{L_\alpha} \alpha_F) \quad (9.115)$$

Linear theory suggests that the second-order term  $\alpha_F^2$  can be neglected such that

$$F_z \approx -\frac{1}{2}\rho V_r^2 A_F C_{L_\alpha} \alpha_F \quad (9.116)$$

Consequently,  $\tau_4 = 2 l_y F_z$  gives the roll moment generated by a pair of fin stabilizers

$$\tau_4 = -l_y \rho A_F C_{L_\alpha} V_r^2 \alpha_F \quad (9.117)$$

## 9.7 Underwater Vehicle Control Surfaces

Control surfaces are hydrodynamic devices allowing an operator or autopilot to control the velocity and attitude of the craft. They are used on underwater vehicles such as submarines, torpedoes and AUVs. The primary control surfaces are (see Figure 9.19):

- **Rudders** – stern vertical surfaces used for turning
- **Dive planes** – bow and stern horizontal surfaces used for depth control

Figure 9.20 shows the NPS AUV II, which is a “flying vehicle.” (Healey and Lienard 1993). The vehicle is controlled by a vertical rudder, two propellers and several dive planes. The 6-DOF mathematical model is included in the MSS toolbox as a function

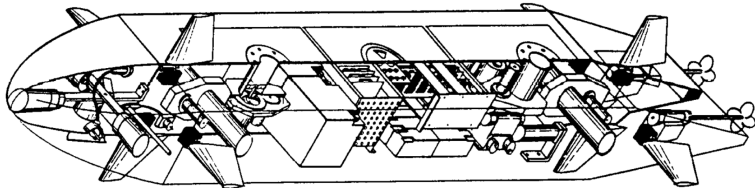


Figure 9.20: Schematic drawing of the NPS II AUV, length  $L = 5.3$  m and weight  $W = 53.4$  kN, showing the vertical rudder, propellers and dive planes (Healey and Lienard 1993).

### Matlab:

```

function [xdot,U] = npsauv(x,ui)
% States: x = [ u v w p q r x y z phi theta psi ]
% Inputs: ui = [ delta_r delta_s delta_b delta_bp delta_bs n ]
% where
%   delta_r = rudder angle                      (rad)
%   delta_s = port and starboard stern plane (rad)
%   delta_b = top and bottom bow plane          (rad)
%   delta_bp = port bow plane                   (rad)
%   delta_bs = starboard bow plane             (rad)
%   n       = propeller shaft speed            (rpm)

```

### 9.7.1 Rudder

The rudder is typically mounted aft of the vehicle as shown in Figure 9.19. The rudder can be deflected an angle  $\delta_R$ , which will force the vehicle to turn. The rudder forces are function of the rudder lift and drag coefficients  $C_L(\delta_R)$  and  $C_D(\delta_R)$

$$F_{\text{drag}} = \frac{1}{2} \rho V_r^2 A_R C_D(\delta_R) \quad (9.118)$$

$$F_{\text{lift}} = \frac{1}{2} \rho V_r^2 A_R C_L(\delta_R) \quad (9.119)$$

where  $\rho$  is the density of water,  $A_R$  is the rudder area and  $V_r$  is the relative speed. Since lift is perpendicular to the relative flow and drag is parallel, the longitudinal forces in BODY axes become

$$\begin{bmatrix} X_R \\ Y_R \end{bmatrix} = \begin{bmatrix} \cos(\delta_R) & -\sin(\delta_R) \\ \sin(\delta_R) & \cos(\delta_R) \end{bmatrix} \begin{bmatrix} -F_{\text{drag}} \\ -F_{\text{lift}} \end{bmatrix} \quad (9.120)$$

The lift and drag coefficients can be approximated by

$$C_L(\delta_R) \approx C_{L_0} + C_{L_\delta} \delta_R \quad (9.121)$$

$$C_D(\delta_R) \approx C_{D_0} + C_{D_\delta} \delta_R \quad (9.122)$$

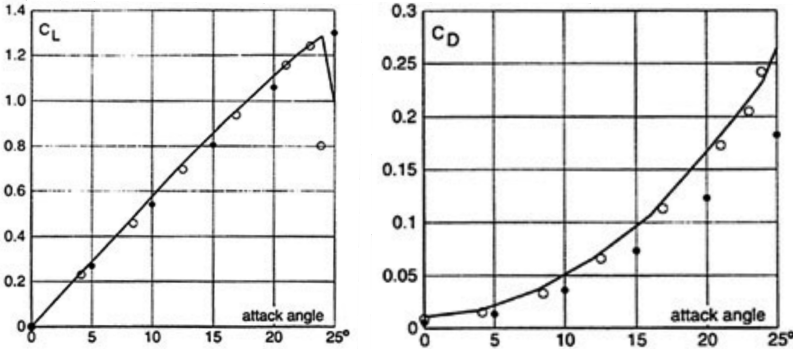


Figure 9.21: Experimental rudder lift and drag curves (circles) compared to Rans calculations (solid lines) (Söding 1990).

Figure 9.21 confirms that lift and drag can be accurately described by linear theory for small rudder angles (Söding 1990). Since underwater vehicle rudders are streamlined to produce high lift with minimum drag a standard assumption is  $F_{\text{drag}} \approx 0$ . Hence, Figure 9.21 suggest that  $C_L(\delta_R) \approx C_{L_\delta} \delta_R$  such that

$$F_{\text{lift}} \approx \frac{1}{2} \rho V_r^2 A_r C_{L_\delta} \delta_R \quad (9.123)$$

Assume that that  $\delta_R$  is small such that  $\sin(\delta_R) \approx \delta_R$  and  $\cos(\delta_R) \approx 1$ . Then the rudder forces (9.120) in the  $x$  and  $y$  directions become

$$X_R = -\frac{1}{2} \rho U_r^2 A_r C_{L_\delta} \delta_R^2 \quad (9.124)$$

$$Y_R = -\frac{1}{2} \rho U_r^2 A_r C_{L_\delta} \delta_R \quad (9.125)$$

For the AUV in Figure 9.19, the rudder is located on the centerline at  $\mathbf{r}_R = [x_R, 0, z_R]^\top$  with respect to the CO. A twin-rudder system will have two stern rudders located at  $\mathbf{r}_R = [x_{1R}, y_{1R}, z_{1R}]^\top$  and  $\mathbf{r}_R = [x_{2R}, y_{2R}, z_{2R}]^\top$  where  $x_{1R} = x_{2R}$ ,  $y_{1R} = -y_{2R}$  and  $z_{1R} = z_{2R}$ . From (9.65) it follows that the 6-DOF generalized rudder forces are

$$\tau_R \stackrel{\text{single rudder}}{=} \begin{bmatrix} X_R \\ Y_R \\ 0 \\ -z_R Y_R \\ z_R X_R \\ x_R Y_R \end{bmatrix}, \quad \tau_R \stackrel{\text{twin rudders}}{=} \begin{bmatrix} X_{1R} + X_{2R} \\ Y_{1R} + Y_{2R} \\ 0 \\ -z_{1R} Y_{1R} - z_{2R} Y_{2R} \\ z_{1R} X_{1R} + z_{2R} X_{2R} \\ x_{1R} Y_{1R} - y_{1R} X_{1R} + x_{2R} Y_{2R} - y_{2R} X_{2R} \end{bmatrix} \quad (9.126)$$

### 9.7.2 Dive planes

Dive planes are control surfaces, usually located at the stern of an underwater vehicle. They control the vehicle's pitch angle, and therefore the angle of attack and lift of the dive plane (see Figure 9.19). For aircraft dive planes are called elevators. Additional dive planes can also be located in the front of the vehicle similar to *canard* wings on an aircraft. Cancards increase the lift and pitch response of the vehicle but the downside is additional drag and fuel consumption.

Consider the vehicle in Figure 9.19, which is controlled by a stern rudder  $\delta_R$ , stern dive planes  $\delta_S$  and bow dive planes  $\delta_B$ . Assume that the dive planes are streamlined to produce high lift with minimum drag such that drag can be neglected. Hence,

$$F_{S,\text{lift}} = -\frac{1}{2}\rho V_r^2 A_S C_{L_\delta} \delta_S, \quad F_{B,\text{lift}} = -\frac{1}{2}\rho V_r^2 A_B C_{L_\delta} \delta_B \quad (9.127)$$

where  $C_{L_\delta} = \partial C_L / \partial \delta$  is the slope of the lift curve at zero angle,  $A_S$  is the stern plane area and  $A_B$  is the bow plane area. Consequently, rotating the lift force from FLOW to BODY under the assumption that the stern and bow plane angles are small give

$$X_S = -\frac{1}{2}\rho V_r^2 A_S C_{L_\delta} \delta_S^2, \quad X_B = -\frac{1}{2}\rho V_r^2 A_B C_{L_\delta} \delta_B^2 \quad (9.128)$$

$$Z_S = -\frac{1}{2}\rho V_r^2 A_S C_{L_\delta} \delta_S \quad Z_B = -\frac{1}{2}\rho V_r^2 A_B C_{L_\delta} \delta_B \quad (9.129)$$

Assume that the dive planes are located at  $\mathbf{r}_S = [x_S, y_S, z_S]^\top$  and  $\mathbf{r}_B = [x_B, y_B, z_B]^\top$ . From (9.65) it follows that the 6-DOF generalized rudder forces are

$$\boldsymbol{\tau}_S = \begin{bmatrix} X_S \\ 0 \\ Z_S \\ y_S Z_S \\ z_S X_S - x_S Z_S \\ -y_S X_S \end{bmatrix}, \quad \boldsymbol{\tau}_B = \begin{bmatrix} X_B \\ 0 \\ Z_B \\ y_B Z_B \\ z_B X_B - x_B Z_B \\ -y_B X_B \end{bmatrix} \quad (9.130)$$

## 9.8 Control Moment Gyroscope

A control moment gyroscope (CMG) is a device, which is used in spacecraft, ship and underwater vehicle attitude control systems. A CMG consists of a spinning rotor and one or more motorized gimbals that tilt the rotor's angular momentum. As the rotor tilts, the changing angular momentum causes a gyroscopic torque that rotates the craft. In this section, we will discuss applications to ships and underwater vehicles:

- Ship roll gyrostabilizer
- CMGs for underwater vehicles

Unlike rudder and fins, the gyroscope does not rely on the forward speed of the vehicle to generate roll, pitch and yaw stabilizing moments for attitude control. Hence, CMG systems can be used during stationkeeping.

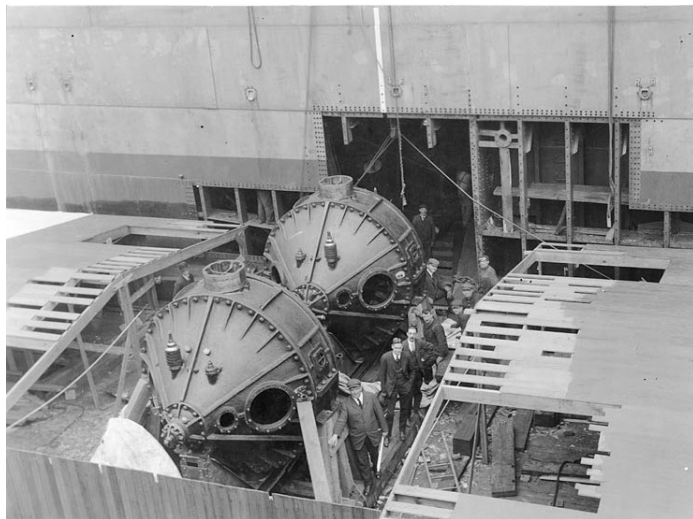


Figure 9.22: Two 25-ton roll-stabilizing gyroscopes being installed on the transport USS Henderson during construction in 1917, the first large ship to use gyroscopic stabilization. Online Library of Historical Images, US Navy Historical Center, Dept. of the Navy, Washington D.C.

### 9.8.1 Ship roll gyrostabilizer

The principle for use of dedicated spinning wheels that generate gyroscopic forces for reducing the roll motion of ships has been known for more than 100 years (Schlick 1904). The American company Sperry developed a system that addressed the problem of the Schlick gyroscope by using an electric motor and a brake to control the precession of the spinning wheel, see Figure 9.22. However, early designs of gyrostabilizer were not a success due to their relatively large size and the inability of roll damping control systems in certain sea states and sailing conditions (speed and heading relative to the waves). Today, advances in material technology, mechanical design, electrical drives, and feedback control theory have resulted in feasible systems.

The gyroscopic torque produced by a gyrostabilizer on a ship opposes the roll moment generated by the waves. The principle for the gyroscopic torque is conservation of angular momentum. The wave-pressure forces on the hull induce roll motion and an excitation torque on the gyro that is proportional to the roll rate. This excitation torque changes the angular momentum such that the spinning wheels develop precession motion. The cross product of the spin angular velocity and the precession rate induce a torque that opposes the excitation torque, and thus the roll excitation moment on the vessel. Effective ship installations require rotors having a weight of approximately 3 to 5 % of a vessel's displacement.

A mathematical model for the linear ship roll motion together with an  $n$ -spinning-wheel gyrostabilizer is (Perez and Steinmann 2009)

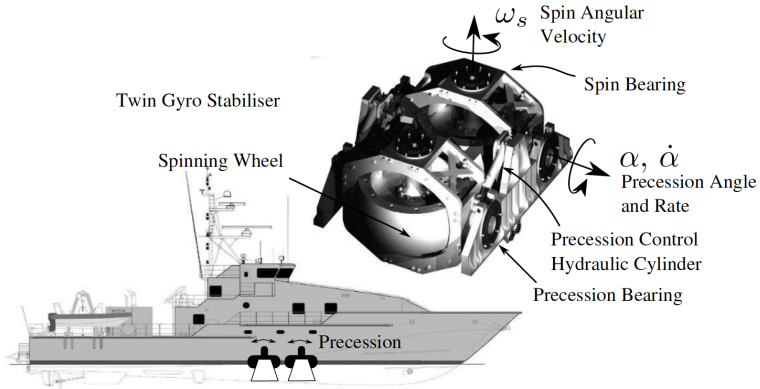


Figure 9.23: The Halcyon's twin gyrostabilizer ( $n = 2$ ). Reproduced with kind permission of Perez and Steinmann (2009).

$$(I_x - K_p + I_g) \dot{p} - K_p p + W GM_T \phi = \tau_{\text{wave}} + \tau_{\text{wind}} - nK_g \cos(\alpha) \dot{\alpha} \quad (9.131)$$

$$I_g \ddot{\alpha} + D_g \dot{\alpha} + G_g \sin(\alpha) = K_g \cos(\alpha) p + \tau_p \quad (9.132)$$

where  $\phi$  is the roll angle,  $\alpha$  is the precession angle and

- $I_x$  ship moment of inertia
- $I_g$  inertia of a single spinning wheel along the precession axis
- $K_p$  added moment of inertia coefficient caused by the ship hull (negative)
- $K_p$  linear roll damping coefficient including viscous effects (negative)
- $K_g$  spinning angular momentum, that is  $K_g = I_{\text{spin}} \omega_{\text{spin}}$
- $D_g$  damping coefficient associated with friction in the precession bearings
- $G_g$  restoring coefficient associated with the mass distribution of the spinning wheel (pendulum effect)
- $\tau_p$  precession control torque

For small precession angles  $\alpha$ , the system (9.131)–(9.132) can be approximated by a linear mass-damper-spring

$$\begin{bmatrix} I_x - K_p + I_g & 0 \\ 0 & I_g \end{bmatrix} \ddot{\mathbf{x}} + \begin{bmatrix} -K_p & nK_g \\ -K_g & D_g \end{bmatrix} \dot{\mathbf{x}} + \begin{bmatrix} W GM_T & 0 \\ 0 & G_g \end{bmatrix} \mathbf{x} = \begin{bmatrix} 0 \\ 1 \end{bmatrix} u + \begin{bmatrix} \tau_{\text{wave}} + \tau_{\text{wind}} \\ 0 \end{bmatrix} \quad (9.133)$$

where  $\mathbf{x} = [\phi, \alpha]^\top$  and  $u = \tau_p$ .

As observed by Sperry (Chalmers 1931), the gyrostabilizer can be used to generate roll rate, which again generates a roll moment. Moreover, we could design a precession torque controller such that

$$\dot{\alpha} \approx \kappa p \quad (9.134)$$

This is clearly a desired control objective since the ship roll dynamics (9.131) will experience additional roll damping for  $\kappa > 0$  as seen from

$$\dot{\phi} = p \quad (9.135)$$

$$(I_x - K_p) \dot{p} + (nK_g\kappa - K_p)p + W \text{GM}_T \phi = \tau_{\text{wave}} + \tau_{\text{wind}} \quad (9.136)$$

To achieve the control objective (9.134), a full-state feedback controller using feedback from  $\phi, p, \alpha$  and  $\dot{\alpha}$  can be designed. In a simplified decoupled design, feedback from the roll states are avoided. This suggests that the gyrostabilizer can be designed using a PD precession controller

$$\tau_p = -K_p\alpha - K_d\dot{\alpha} \quad (9.137)$$

The closed-loop transfer function is computed from (9.132)

$$\dot{\alpha} = \frac{K_g s}{s^2 I_g + (D_g + K_d)s + (G_g + K_p)} p \approx \kappa p \quad (9.138)$$

where the controller gains should be chosen such that  $\kappa$  has its maximum value for the peak frequency (wave encounter frequency) of the wave loads.

Perez and Steinmann (2009) present a case study of a navy patrol boat, for which the gyro stabilizer is a twin-wheel stabilizer with a total mass equivalent to 3.5 % of the vessel displacement. The simulation study shows that there are fundamental limitations associated with the roll reduction for certain frequency ranges, while other frequencies are well damped. This confirms that it is important to tune the controller such that maximum roll damping is achieved for frequencies where the wave loads are at their maximum. Moreover, the control system needs to adapt to changes in the sea state in order to avoid roll amplification. Adaptive and constrained control designs are methods, which can overcome these limitations in a practical design.

## 9.8.2 Control moment gyros for underwater vehicles

Internal rotors (CMGs) can control three-axis attitude of an underwater vehicle even at zero speed. The CMGs in combination with thrusters, rudders and dive planes improves controllability and maneuverability of underwater vehicles in particular at low speed. Applications to underwater robots and vehicles have been reported by Woolsey and Leonard (2002a), Thornton *et al.* (2005, 2007, 2008) and Xua *et al.* (2019).

### CMG angular momentum – pyramid configuration

A popular CMG configuration is the pyramid shown in Figure 9.24, which will generate three-axis attitude control torques for an underwater vehicle. For this configuration, the skew angle will be  $\beta = \cos^{-1}(1/\sqrt{3})$  and the four single gimbal CMGs, which will have the minimal redundancy needed to control the attitude in three directions (Thornton *et al.* 2007).

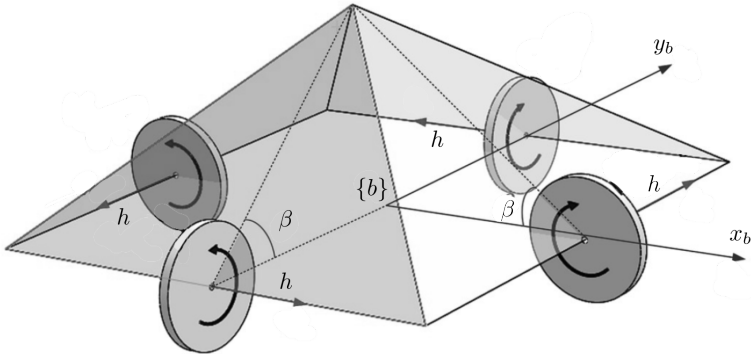


Figure 9.24: Four equal CMG units in a pyramid configuration with skew angle  $\beta = \cos^{-1}(1/\sqrt{3})$ . Each CMG produces a constant angular momentum  $h$  (Xua *et al.* 2019).

Consider four equal gyros where  $\delta_i$  ( $i = 1, 2, 3, 4$ ) are the gimbal angles. Hence, the angular momentum of the CMG system is (Kurokawa 1997)

$$\mathbf{h}_{\text{cmg}}^b(\boldsymbol{\delta}) = h \begin{bmatrix} -\cos(\beta)\sin(\delta_1) - \cos(\delta_2) + \cos(\beta)\sin(\delta_3) + \cos(\delta_4) \\ \cos(\delta_1) - \cos(\beta)\sin(\delta_2) - \cos((\delta_3)) + \cos(\beta)\sin(\delta_4) \\ \sin(\beta)(\sin(\delta_1) + \sin(\delta_2) + \sin(\delta_3) + \sin(\delta_4)) \end{bmatrix} \quad (9.139)$$

where  $h$  represents the constant angular momentum of each CMG expressed in the gimbal-fixed frame, that is  $h$  is the same for all four CMGs (see Figure 9.25). The time derivative of  $\mathbf{h}_{\text{cmg}}^b$  is

$$\dot{\mathbf{h}}_{\text{cmg}}^b = h \mathbf{A}(\boldsymbol{\delta}) \dot{\boldsymbol{\delta}} \quad (9.140)$$

where  $\mathbf{A}(\boldsymbol{\delta}) = \partial \mathbf{h}_{\text{cmg}}^b / \partial \boldsymbol{\delta} \in \mathbb{R}^{3 \times 4}$  is the Jacobian matrix

$$\mathbf{A}(\boldsymbol{\delta}) = \begin{bmatrix} -\cos(\beta)\cos(\delta_1) & \sin(\delta_2) & \cos(\beta)\cos(\delta_3) & -\sin(\delta_4) \\ -\sin(\delta_1) & -\cos(\beta)\cos(\delta_2) & \sin((\delta_3)) & \cos(\beta)\cos(\delta_4) \\ \sin(\beta)\cos(\delta_1) & \sin(\beta)\cos(\delta_2) & \sin(\beta)\cos(\delta_3) & \sin(\beta)\cos(\delta_4) \end{bmatrix} \quad (9.141)$$

The CMG gimbal angular velocity vector (see Figure 9.25)

$$\dot{\boldsymbol{\delta}} = [\dot{\delta}_1, \dot{\delta}_2, \dot{\delta}_3, \dot{\delta}_4]^\top \quad (9.142)$$

is chosen as control input.

### AUV equations of motion

Consider the cylinder-shaped AUV in Figure 8.2. Assume that the CO is located in the center of the AUV and that CB = CO such that  $\mathbf{r}_b^b = [0, 0, 0]^\top$ . Furthermore assume that the CG is located at  $\mathbf{r}_g^b = [x_g, y_g, z_g]^\top$  and  $W = B = mg$  (neutrally buoyant vehicle). The system inertia matrix  $\mathbf{M}(\boldsymbol{\delta})$  and the Coriolis and centripetal matrix

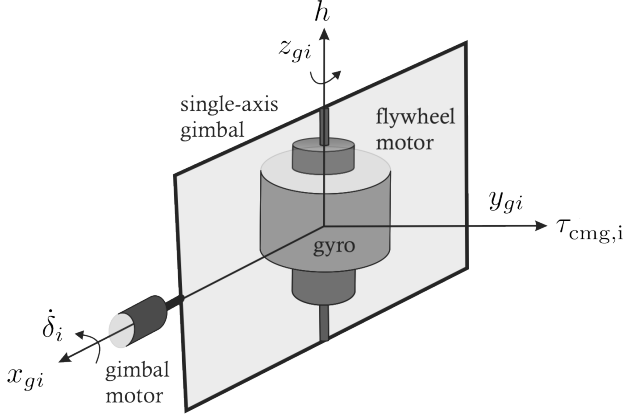


Figure 9.25: Single CMG gimbal unit: The flywheel rotates with constant angular rate and the angular rate  $\dot{\delta}_i$  of the  $i$ -th gimbal change the flywheel's angular momentum  $h$ . This produces a gyroscopic torque  $\tau_{\text{cmg},i}$ .

$C(\delta, \nu_r)$  of an CMG-actuated underwater vehicle will both depend on the gimbal angles  $\delta$ . Consequently, the resulting model will be in the following form

$$\mathbf{M}(\delta)\dot{\nu}_r + \mathbf{C}(\delta, \nu_r)\nu_r + \mathbf{D}\nu_r + \mathbf{d}(\nu_r) + \mathbf{g}(\eta) = \begin{bmatrix} \mathbf{0}_{3 \times 1} \\ \tau_{\text{cmg}} \end{bmatrix} + \boldsymbol{\tau} \quad (9.143)$$

To derive the expressions for  $M(\delta)$  and  $C(\delta, \nu_r)$  a kinetic energy approach will be applied. The kinetic energy of a rigid-body, including the CMGs and hydrodynamic added inertia, is given by (Woolsey and Leonard 2002a)

$$T = \frac{1}{2} [\nu_1^\top, \nu_2^\top] \begin{bmatrix} mI_3 + \mathbf{A}_{11} & -mS(\mathbf{r}_g^b) + \mathbf{A}_{12} \\ mS(\mathbf{r}_g^b) + \mathbf{A}_{21} & I_b^b + \mathbf{A}_{22} + \mathbf{I}_{\text{cmg}}^b(\delta) \end{bmatrix} \begin{bmatrix} \nu_1 \\ \nu_2 \end{bmatrix} \quad (9.144)$$

where  $\nu_1 = [u, v, w]^\top$  and  $\nu_2 = [p, q, r]^\top$ . The inertia dyadic of the rigid body and the CMGs are  $\mathbf{I}_b^b = I_g^b - mS^2(\mathbf{r}_g^b)$  and  $\mathbf{I}_{\text{cmg}}(\delta)$ , respectively. Hydrodynamic added mass is included by the matrices  $\mathbf{A}_{11}$ ,  $\mathbf{A}_{12} = \mathbf{A}_{21}^\top$  and  $\mathbf{A}_{22}$ . The translational and rotational dynamics can be derived from *Kirchhoff's equations*, which relates the kinetic energy  $T$  to the force vector  $\boldsymbol{\tau}_1$  and moment vector  $\boldsymbol{\tau}_2$  acting on the body. From Section 6.3.1, we have

$$\frac{d}{dt} \left( \frac{\partial T}{\partial \nu_1} \right) + S(\nu_2) \frac{\partial T}{\partial \nu_1} = \boldsymbol{\tau}_1 \quad (9.145)$$

$$\frac{d}{dt} \left( \frac{\partial T}{\partial \nu_2} \right) + S(\nu_2) \frac{\partial T}{\partial \nu_2} + S(\nu_1) \frac{\partial T}{\partial \nu_1} = \boldsymbol{\tau}_2 \quad (9.146)$$

Expanding (9.144) gives the following formula for the kinetic energy

$$T = \frac{1}{2} \nu_1^\top (mI_3 + \mathbf{A}_{11}) \nu_1 + \frac{1}{2} \nu_2^\top (I_b^b + \mathbf{I}_{\text{cmg}}^b(\delta) + \mathbf{A}_{22}) \nu_2 + \nu_1^\top (-mS(\mathbf{r}_g^b) + \mathbf{A}_{12}) \nu_2 \quad (9.147)$$

Hence,

$$\frac{\partial T}{\partial \nu_1} = (m\mathbf{I}_3 + \mathbf{A}_{11})\nu_1 + (-m\mathbf{S}(\mathbf{r}_g^b) + \mathbf{A}_{12})\nu_2 \quad (9.148)$$

$$\begin{aligned} \frac{\partial T}{\partial \nu_2} &= \mathbf{A}_{21}\nu_1 + (\mathbf{I}_b^b + \mathbf{I}_{\text{cmg}}^b(\delta) + \mathbf{A}_{22})\nu_2 + \mathbf{I}_{\text{cmg}}^b(\delta)\dot{\delta} \\ &= (m\mathbf{S}(\mathbf{r}_g^b) + \mathbf{A}_{21})\nu_1 + (\mathbf{I}_b^b + \mathbf{I}_{\text{cmg}}^b(\delta) + \mathbf{A}_{22})\nu_2 + \mathbf{h}_{\text{cmg}}(\delta) \end{aligned} \quad (9.149)$$

$$\frac{d}{dt}\left(\frac{\partial T}{\partial \nu_1}\right) = (m\mathbf{I}_3 + \mathbf{A}_{11})\dot{\nu}_1 + (-m\mathbf{S}(\mathbf{r}_g^b) + \mathbf{A}_{12})\dot{\nu}_2 \quad (9.150)$$

$$\begin{aligned} \frac{d}{dt}\left(\frac{\partial T}{\partial \nu_2}\right) &= (m\mathbf{S}(\mathbf{r}_g^b) + \mathbf{A}_{21})\dot{\nu}_1 + (\mathbf{I}_b^b + \mathbf{I}_{\text{cmg}}^b(\delta) + \mathbf{A}_{22})\dot{\nu}_2 \\ &\quad + \dot{\mathbf{I}}_{\text{cmg}}^b(\delta)\nu_2 + h\mathbf{A}(\delta)\dot{\delta} \end{aligned} \quad (9.151)$$

where  $\mathbf{h}_{\text{cmg}}(\delta) = \mathbf{I}_{\text{cmg}}(\delta)\dot{\delta}$  and  $\dot{\mathbf{h}}_{\text{cmg}}^b(\delta) = h\mathbf{A}(\delta)\dot{\delta}$ . The control torque  $\tau_{\text{cmg}}$  is applied to the four internal rotors such that

$$\dot{\mathbf{h}}_{\text{cmg}}^b(\delta) = h\mathbf{A}(\delta)\dot{\delta} = -\tau_{\text{cmg}} \quad (9.152)$$

Hence, it follows that

$$\mathbf{M}(\delta) = \begin{bmatrix} m\mathbf{I}_3 + \mathbf{A}_{11} & -m\mathbf{S}(\mathbf{r}_g^b) + \mathbf{A}_{12} \\ m\mathbf{S}(\mathbf{r}_g^b) + \mathbf{A}_{21} & \mathbf{I}_b^b + \mathbf{A}_{22} \end{bmatrix} + \mathbf{M}_{\text{cmg}}(\delta) \quad (9.153)$$

$$\begin{aligned} \mathbf{C}(\delta, \nu) &= \begin{bmatrix} m\mathbf{S}(\nu_2) \\ m\mathbf{S}(\mathbf{r}_g^b)\mathbf{S}(\nu_2) - \mathbf{S}(\mathbf{A}_{11}\nu_1 + \mathbf{A}_{12}\nu_2) \\ -m\mathbf{S}(\nu_2)\mathbf{S}(\mathbf{r}_g^b) - \mathbf{S}(\mathbf{A}_{11}\nu_1 + \mathbf{A}_{12}\nu_2) \\ \mathbf{S}(\mathbf{I}_b^b\nu_2) - \mathbf{S}(\mathbf{A}_{21}\nu_1 + \mathbf{A}_{22}\nu_2) \end{bmatrix} + \mathbf{C}_{\text{cmg}}(\delta) \end{aligned} \quad (9.154)$$

where

$$\mathbf{M}_{\text{cmg}}(\delta) = \begin{bmatrix} \mathbf{0}_{3 \times 3} & \mathbf{0}_{3 \times 3} \\ \mathbf{0}_{3 \times 3} & \mathbf{I}_{\text{cmg}}^b(\delta) \end{bmatrix} \quad (9.155)$$

$$\mathbf{C}_{\text{cmg}}(\delta) = \begin{bmatrix} \mathbf{0}_{3 \times 3} & \mathbf{0}_{3 \times 3} \\ \mathbf{0}_{3 \times 3} & \dot{\mathbf{I}}_{\text{cmg}}^b(\delta) - \mathbf{S}(\mathbf{h}_{\text{cmg}}^b(\delta)) \end{bmatrix} \quad (9.156)$$

### Singularity avoidance

When designing the control system it is important to notice that potential singularities may exist in the Jacobian  $\mathbf{A}(\delta)$  in (9.152) when transforming the control input  $\tau_{\text{cmg}}$  to desired angular rates  $\dot{\delta}$ . At least three single-axis CMGs are necessary for control of vehicle attitude. However, no matter how many CMGs the vehicle uses, gimbal motion can lead to relative orientations that produce no usable output torque along certain directions. The singularities can be monitored by computing

$$\det(\mathbf{A}(\delta)\mathbf{A}^\top(\delta)) \quad (9.157)$$

A classical solution to the singularity problem is the damped least-squares method in robotics (Nakamura and Hanafusa 1986) (Chiaverini 1993)

$$\dot{\boldsymbol{\delta}} = -\frac{1}{h} \mathbf{A}^\top(\boldsymbol{\delta}) (\mathbf{A}(\boldsymbol{\delta})\mathbf{A}^\top(\boldsymbol{\delta}) + \lambda^2 \mathbf{I}_3)^{-1} \boldsymbol{\tau}_{\text{cmg}} \quad (9.158)$$

where  $\lambda \geq 0$  is the damping factor. Notice that, when  $\lambda = 0$ , the damped least-squares solution reduces to a regular matrix inversion. Different algorithms for  $\lambda$  are reviewed by Chiaverini *et al.* (1994). A survey of steering laws for CMGs is found in Kurokawa (2007).

### Inertia dyadic for pyramid-type CMG systems

The inertia dyadic  $\mathbf{I}_{\text{cmg}}^b(\boldsymbol{\delta})$  can be modeled as (MacKunis *et al.* 2008)

$$\mathbf{I}_{\text{cmg}}^b(\boldsymbol{\delta}) = \mathbf{I}_0^b + \sum_{i=1}^4 \left( \mathbf{R}_{gi}^b(\delta_i) \mathbf{I}_{\text{cmg},i}^{gi} \mathbf{R}_{gi}^b(\delta_i)^\top - m_{\text{cmg}} \mathbf{S}^2(\mathbf{r}_i^b) \right) \quad (9.159)$$

where the parallel-axis theorem (3.35) has been applied and

$\mathbf{I}_0^b = \text{constant}$	rotational-independent inertia expressed in $\{b\}$
$\mathbf{I}_{\text{cmg},i}^{gi} = \text{diag}\{I_{x_i}, I_{y_i}, I_{z_i}\}$	inertia of CMG $i$ expressed in the gimbal-fixed frame $\{gi\}$
$\mathbf{R}_{gi}^b(\delta_i)$	rotation matrix from $\{gi\}$ to $\{b\}$
$\mathbf{r}_i^b = [x_i, y_i, z_i]^\top$	location of CMG number $i$
$m_{\text{cmg}}$	mass of one CMG

Because the gimbal and rotor are taken to be dynamically balanced, their respective inertia dyadics include no products of inertia. The rotation matrix ( $i = 1, 2, 3$ ) from the  $i$ -th gimbal-fixed frame  $\{gi\}$  to  $\{b\}$  consists of three principal rotations (Sun *et al.* 2010)

$$\mathbf{R}_{gi}^b(\delta_i) = \begin{bmatrix} 0 & -1 & 0 \\ 1 & 0 & 0 \\ 0 & 0 & 1 \end{bmatrix} \begin{bmatrix} 1 & 0 & 0 \\ 0 & \cos(\beta) & -\sin(\beta) \\ 0 & \sin(\beta) & \cos(\beta) \end{bmatrix} \begin{bmatrix} \cos(\delta_i) & -\sin(\delta_i) & 0 \\ \sin(\delta_i) & \cos(\delta_i) & 0 \\ 0 & 0 & 1 \end{bmatrix} \quad (9.160)$$

## 9.9 Moving Mass

Internal moving mass actuators as well as internal rotors (CMGs), are promising alternatives to propellers and control surfaces (Woolsey and Leonard 2002b) (Li and Shao 2008) (Li 2016). Advanced autonomous vehicles such as AUVs, gliders and USVs operating with limited battery power (see Figure 9.26). For these type of vehicles reduced power consumption is important to increase endurance and range. Unlike propeller-driven AUVs and USVs, gliders have fixed wings and tails, and use internal actuators to travel by concatenating a series of upwards and downwards glides. The endurance of underwater gliders is significantly longer than propeller-driven AUVs. Gliders, typically operate at a speed of about 0.3 m/s compared to 1.5–2.0 m/s of AUVs and 1.0–10.0 m/s of small USVs. A detailed review and overview of underwater gliders are found in Graver (2006).

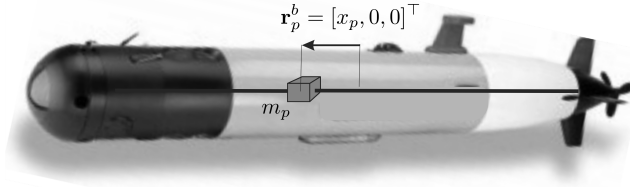


Figure 9.26: Cylinder-shaped AUV with a moving mass that can translate in the  $x$  direction.

### AUV equations of motion

Consider an underwater vehicle with constant mass  $m$  and a moving point mass  $m_p$  (see Figure 9.26). Then the total mass is

$$m_{\text{total}} = m + m_p \quad (9.161)$$

The center of gravity is given by

$$\mathbf{r}_{\text{total}}^b = \frac{m \mathbf{r}_g^b + m_p^b \mathbf{r}_p^b}{m_{\text{total}}} \quad (9.162)$$

where  $\mathbf{r}_p^b = [x_p, y_p, z_p]^\top$  is the time-varying location of the point mass expressed in  $\{b\}$ . Let  $\mathbf{v}_p^b = \dot{\mathbf{r}}_p^b$  denote the velocity of the point mass. Then the AUV kinetic energy with an internal moving mass becomes (Woolsey and Leonard 2002b)

$$T = \frac{1}{2} [(\mathbf{v}_p^b)^\top, \boldsymbol{\nu}_1^\top, \boldsymbol{\nu}_2^\top]^\top \mathbf{M}(\mathbf{r}_p^b) \begin{bmatrix} \mathbf{v}_p^b \\ \boldsymbol{\nu}_1 \\ \boldsymbol{\nu}_2 \end{bmatrix} \quad (9.163)$$

where  $\boldsymbol{\nu}_1 = [u, v, w]^\top$ ,  $\boldsymbol{\nu}_2 = [p, q, r]^\top$  and

$$\mathbf{M}(\mathbf{r}_p^b) = \mathbf{M}_{RB}(\mathbf{r}_p^b) + \mathbf{M}_A \quad (9.164)$$

The matrices are

$$\mathbf{M}_{RB}(\mathbf{r}_p^b) = \begin{bmatrix} m_p \mathbf{I}_3 & m_p \mathbf{I}_3 & -m_p \mathbf{S}(\mathbf{r}_p^b) \\ m_p \mathbf{I}_3 & (m + m_p) \mathbf{I}_3 & -m_p \mathbf{S}(\mathbf{r}_p^b) - m \mathbf{S}(\mathbf{r}_g^b) \\ m_p \mathbf{S}(\mathbf{r}_p^b) & m_p \mathbf{S}(\mathbf{r}_p^b) + m \mathbf{S}(\mathbf{r}_g^b) & \mathbf{I}_b^b - m_p \mathbf{S}^2(\mathbf{r}_p^b) \end{bmatrix} \quad (9.165)$$

$$\mathbf{M}_A = \begin{bmatrix} \mathbf{0}_{3 \times 3} & \mathbf{0}_{3 \times 3} & \mathbf{0}_{3 \times 3} \\ \mathbf{0}_{3 \times 3} & \mathbf{A}_{11} & \mathbf{A}_{12} \\ \mathbf{0}_{3 \times 3} & \mathbf{A}_{21} & \mathbf{A}_{22} \end{bmatrix} \quad (9.166)$$

The linear and angular momentums are obtained as

$$\mathbf{p}_p^b = \frac{\partial T}{\partial \mathbf{v}_p^b}, \quad \mathbf{p}^b = \frac{\partial T}{\partial \boldsymbol{\nu}_1}, \quad \mathbf{h}^b = \frac{\partial T}{\partial \boldsymbol{\nu}_2} \quad (9.167)$$

Consequently,

$$\begin{aligned} \begin{bmatrix} \mathbf{p}_p^b \\ \mathbf{p}_p^b \\ \mathbf{h}^b \end{bmatrix} &= \mathbf{M}(\mathbf{r}_p^b) \begin{bmatrix} \mathbf{v}_p^b \\ \boldsymbol{\nu}_1 \\ \boldsymbol{\nu}_2 \end{bmatrix} \\ &= \begin{bmatrix} m_p \mathbf{v}_p^b + m_p \boldsymbol{\nu}_1 - m_p \mathbf{S}(\mathbf{r}_p^b) \boldsymbol{\nu}_2 \\ m_p \mathbf{v}_p^b + (\mathbf{A}_{11} + (m + m_p) \mathbf{I}_3) \boldsymbol{\nu}_1 + (\mathbf{A}_{12} - m_p \mathbf{S}(\mathbf{r}_p^b) - m \mathbf{S}(\mathbf{r}_g^b)) \boldsymbol{\nu}_2 \\ m_p \mathbf{S}(\mathbf{r}_p^b) \mathbf{v}_p^b + (\mathbf{A}_{21} + m_p \mathbf{S}(\mathbf{r}_p^b) + m \mathbf{S}(\mathbf{r}_g^b)) \boldsymbol{\nu}_1 + (\mathbf{A}_{22} + \mathbf{I}_b^b - m_p \mathbf{S}^2(\mathbf{r}_p^b)) \boldsymbol{\nu}_2 \end{bmatrix} \end{aligned} \quad (9.168)$$

The velocity vectors are computed from the linear and angular momentums by inverting the mass matrix

$$\begin{bmatrix} \mathbf{v}_p^b \\ \boldsymbol{\nu}_1 \\ \boldsymbol{\nu}_2 \end{bmatrix} = \mathbf{M}^{-1}(\mathbf{r}_p^b) \begin{bmatrix} \mathbf{p}_p^b \\ \mathbf{p}_p^b \\ \mathbf{h}^b \end{bmatrix} \quad (9.169)$$

The kinematic equations for the point mass and the vehicle are

$$\dot{\mathbf{r}}_p^b = \mathbf{v}_p^b \quad (9.170)$$

$$\dot{\boldsymbol{\eta}} = \mathbf{J}_\Theta(\boldsymbol{\eta}) \begin{bmatrix} \boldsymbol{\nu}_1 \\ \boldsymbol{\nu}_2 \end{bmatrix} \quad (9.171)$$

Suppose that the only forces and moments which act on the AUV are due to gravity and buoyancy, and to the internal control force  $\tau_p$  used to control the position  $\mathbf{r}_p^b$  of the point mass. Furthermore, assume that the CO is located in the center of the AUV and that CB = CO such that  $\mathbf{r}_b^b = [0, 0, 0]^\top$ . Then for neutrally buoyant vehicle the restoring moments (4.5) can be expressed as

$$\mathbf{m}_g^b = \mathbf{S}(\mathbf{r}_g^b) \mathbf{R}^\top(\boldsymbol{\Theta}_{nb}) \mathbf{f}_g^n \quad (9.172)$$

$$\mathbf{m}_p^b = \mathbf{S}(\mathbf{r}_p^b) \mathbf{R}^\top(\boldsymbol{\Theta}_{nb}) \mathbf{f}_p^n \quad (9.173)$$

where  $\mathbf{f}_g^n = [0, 0, mg]^\top$  and  $\mathbf{f}_p^n = [0, 0, m_p g]^\top$  are the gravitational force of the vehicle and point mass, respectively. Hence, the state-space model in terms of linear and angular moments become (Woolsey and Leonard 2002b)

$$\dot{\mathbf{p}}_p^b = -\mathbf{S}(\boldsymbol{\nu}_2) \mathbf{p}^b + \mathbf{R}^\top(\boldsymbol{\Theta}_{nb}) \mathbf{f}_p^n + \boldsymbol{\tau}_p \quad (9.174)$$

$$\dot{\mathbf{p}}^b = -\mathbf{S}(\boldsymbol{\nu}_2) \mathbf{p}^b \quad (9.175)$$

$$\dot{\mathbf{h}}^b = -\mathbf{S}(\boldsymbol{\nu}_1) \mathbf{p}^b - \mathbf{S}(\boldsymbol{\nu}_2) \mathbf{h}^b + \mathbf{S}(\mathbf{r}_p^b) \mathbf{R}^\top(\boldsymbol{\Theta}_{nb}) \mathbf{f}_p^n + \mathbf{S}(\mathbf{r}_g^b) \mathbf{R}^\top(\boldsymbol{\Theta}_{nb}) \mathbf{f}_g^n \quad (9.176)$$

Notice the resemblance with Kirchoff's equations (3.53)–(3.54).

### Control strategies

The point mass  $m_p$  affects the angular momentum  $\mathbf{h}^b$  given by (9.176) and thus the vehicle's attitude via the gravitational force  $\mathbf{f}_p^n$ . Hence, the control strategy can be to

move the point such that attitude is stabilized. The position of the point mass  $r_p^b$  is easily controlled by means of the control force  $\tau_p$  in (9.174).

In Woolsey and Leonard (2002b) a potential-shaping control law is used to stabilize the system. The stability analysis shows that the feedback gain must be chosen sufficient large and the point mass must be big enough to influence the AUV dynamics. These conditions are derived using Lyapunov stability theory since the AUV dynamics with a moving point mass is highly nonlinear. A similar analysis is presented by Li (2016) and Li and Su (2016) who has studied the horizontal-plane motion of a cylinder-shaped AUV. In this work an LQR heading autopilot is designed using an internal moving mass to control the vehicle's heading.



## Chapter 10

# Environmental Forces and Moments

Chapters 1-9 present the marine craft equations of motion. In this chapter, complementary models for environmental disturbances are derived. The three external loads are

- Wind
- Waves
- Ocean currents

The purpose of the chapter is to offer realistic models for simulation, testing and verification of feedback control systems in varying environmental conditions. Complementary textbooks on hydrodynamic loads are Faltinsen (1990), Newman (1977) and Sarpkaya (1981).

### Superposition of wind and wave disturbances

For control system design it is common to assume the *principle of superposition* when considering wind and wave disturbances. For most marine control applications this is a good approximation. In general, the environmental forces will be highly nonlinear and both additive and multiplicative to the dynamic equations of motion. An accurate description of the environmental forces and moments are important in vessel simulators that are produced for human operators.

In Chapter 6 it was shown that the nonlinear dynamic equations of motion can be written

$$\boldsymbol{M}\dot{\boldsymbol{\nu}} + \boldsymbol{C}(\boldsymbol{\nu})\boldsymbol{\nu} + \boldsymbol{D}(\boldsymbol{\nu})\boldsymbol{\nu} + \boldsymbol{g}(\boldsymbol{\eta}) + \boldsymbol{g}_0 = \underbrace{\boldsymbol{\tau}_{\text{wind}} + \boldsymbol{\tau}_{\text{wave}}}_{\boldsymbol{w}} + \boldsymbol{\tau} \quad (10.1)$$

The principle of superposition suggests that the generalized wind- and wave-induced forces are added to the right-hand side of (10.1) by defining

$$\boldsymbol{w} := \boldsymbol{\tau}_{\text{wind}} + \boldsymbol{\tau}_{\text{wave}} \quad (10.2)$$

where  $\boldsymbol{\tau}_{\text{wind}} \in \mathbb{R}^6$  and  $\boldsymbol{\tau}_{\text{wave}} \in \mathbb{R}^6$  represent the generalized forces due to wind and waves. Computer-effective models for the simulation of generalized wind and wave forces are presented in Sections 10.1 and 10.2.

### Equations of relative motion for simulation of ocean currents

The forces on a marine craft due to ocean currents can be implemented by replacing the generalized velocity vector in the hydrodynamic terms with relative velocities

$$\boldsymbol{\nu}_r = \boldsymbol{\nu} - \boldsymbol{\nu}_c \quad (10.3)$$

where  $\boldsymbol{\nu}_c \in \mathbb{R}^6$  is the velocity of the ocean current expressed in  $\{b\}$ . The equations of motion including ocean currents become

$$\underbrace{\boldsymbol{M}_{RB}\dot{\boldsymbol{\nu}} + \boldsymbol{C}_{RB}(\boldsymbol{\nu})\boldsymbol{\nu}}_{\text{rigid-body terms}} + \underbrace{\boldsymbol{M}_A\dot{\boldsymbol{\nu}}_r + \boldsymbol{C}_A(\boldsymbol{\nu}_r)\boldsymbol{\nu}_r + \boldsymbol{D}(\boldsymbol{\nu}_r)\boldsymbol{\nu}_r}_{\text{hydrodynamic terms}} + \underbrace{\boldsymbol{g}(\boldsymbol{\eta}) + \boldsymbol{g}_o}_{\text{hydrostatic terms}} = \boldsymbol{\tau} + \boldsymbol{w} \quad (10.4)$$

Notice that the rigid-body kinetics is independent of the ocean current. A frequently used simplification is to assume that the ocean currents are *irrotational* and *constant* in  $\{n\}$ . In Section 10.3 it is shown that this assumption implies that (10.4) can be transformed to

$$\boldsymbol{M}\dot{\boldsymbol{\nu}}_r + \boldsymbol{C}(\boldsymbol{\nu}_r)\boldsymbol{\nu}_r + \boldsymbol{D}(\boldsymbol{\nu}_r)\boldsymbol{\nu}_r + \boldsymbol{g}(\boldsymbol{\eta}) + \boldsymbol{g}_0 = \boldsymbol{\tau}_{\text{wind}} + \boldsymbol{\tau}_{\text{wave}} + \boldsymbol{\tau} \quad (10.5)$$

where all mass, Coriolis–centripetal and damping terms are functions of the relative acceleration and velocity vectors only. The matrices  $\boldsymbol{M}$  and  $\boldsymbol{C}(\boldsymbol{\nu}_r)$  in this model become

$$\boldsymbol{M} = \boldsymbol{M}_{RB} + \boldsymbol{M}_A \quad (10.6)$$

$$\boldsymbol{C}(\boldsymbol{\nu}_r) = \boldsymbol{C}_{RB}(\boldsymbol{\nu}_r) + \boldsymbol{C}_A(\boldsymbol{\nu}_r) \quad (10.7)$$

In the linear case, Equation (10.5) reduces to

$$\boldsymbol{M}\dot{\boldsymbol{\nu}}_r + \boldsymbol{N}\boldsymbol{\nu}_r + \boldsymbol{G}\boldsymbol{\eta} + \boldsymbol{g}_o = \boldsymbol{\tau} + \boldsymbol{w} \quad (10.8)$$

Models for simulation of ocean currents in terms of  $\boldsymbol{\nu}_c$  are presented in Section 10.3.

## 10.1 Wind Forces and Moments

Wind is defined as the movement of air relative to the surface of the Earth. Mathematical models of wind forces and moments are used in motion control systems to improve the performance and robustness of the system in extreme conditions. Models for this are presented in the forthcoming sections.

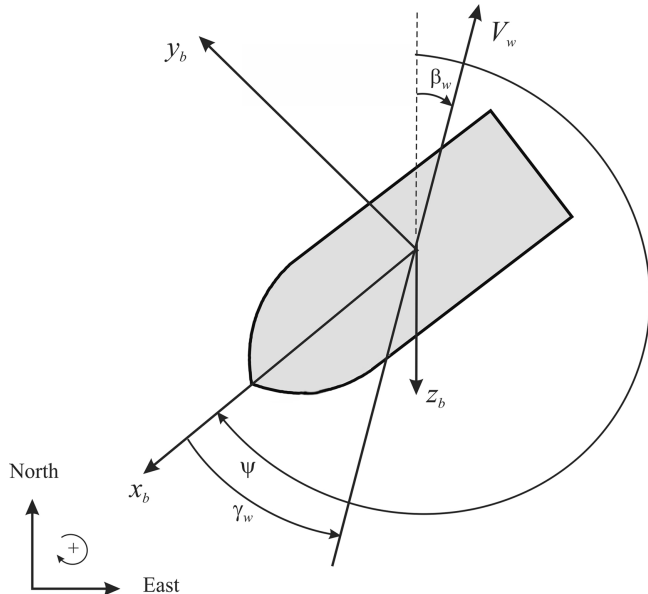


Figure 10.1: Wind speed  $V_w$ , wind direction  $\beta_w$  and wind angle of attack  $\gamma_w$  relative to the bow.

### 10.1.1 Wind forces and moments on marine craft at rest

Let  $V_w$  and  $\gamma_w$  denote the wind speed and angle of attack, respectively (see Figure 10.1). The wind forces and moments acting on a marine craft are computed using a similar approach to that of the current coefficients defined in Section 6.7.1. For zero speed it is common to write

$$X_{\text{wind}} = qC_X(\gamma_w)A_{Fw} \quad (10.9)$$

$$Y_{\text{wind}} = qC_Y(\gamma_w)A_{Lw} \quad (10.10)$$

$$Z_{\text{wind}} = qC_Z(\gamma_w)A_{Fw} \quad (10.11)$$

$$K_{\text{wind}} = qC_K(\gamma_w)A_{Lw}H_{Lw} \quad (10.12)$$

$$M_{\text{wind}} = qC_M(\gamma_w)A_{Fw}H_{Fw} \quad (10.13)$$

$$N_{\text{wind}} = qC_N(\gamma_w)A_{Lw}L_{oa} \quad (10.14)$$

where  $H_{Fw}$  and  $H_{Lw}$  are the centroids above the water line of the frontal and lateral projected areas  $A_{Fw}$  and  $A_{Lw}$ , respectively, and

$$\gamma_w = \psi - \beta_w - \pi \quad (10.15)$$

where  $\beta_w$  is the wind direction expressed in  $\{\mathbf{n}\}$  (see Figure 10.1).

The dynamic pressure of the apparent wind is

$$q = \frac{1}{2}\rho_a V_w^2 \quad (10.16)$$

Table 10.1: Air density as a function of temperature

°C	Air density, $\rho$ (kg/m <sup>3</sup> )
-10	1.342
-5	1.317
0	1.292
5	1.269
10	1.247
15	1.225
20	1.204
25	1.184
30	1.165

where  $\rho_a$  is the air density (see Table 10.1).

The mean velocity profile satisfies a boundary-layer profile (Bretschneider 1969)

$$V_w(h) = V_{10}(h/10)^\alpha \quad (10.17)$$

where  $V_{10}$  is the wind velocity 10 m above the sea surface,  $h$  is the height above the sea surface and  $\alpha = 1/7$ . The nondimensional wind coefficients  $C_X, C_Y, C_Z, C_K, C_M$  and  $C_N$  are usually computed using 10 m as reference height. To convert the nondimensional wind coefficients to a different reference height, the ratio between the dynamic pressures at the two heights are used

$$\frac{\frac{1}{2}\rho_a V_w(h_1)^2}{\frac{1}{2}\rho_a V_w(h_2)^2} = \frac{V_w(h_1)^2}{V_w(h_2)^2} = \frac{[V_{10}(h_1/10)^\alpha]^2}{[V_{10}(h_2/10)^\alpha]^2} = \left(\frac{h_1}{h_2}\right)^{2\alpha} \quad (10.18)$$

Consequently, the nondimensional wind coefficients at height  $h_1$  can be converted to height  $h_2$  by multiplying with

$$\left(\frac{h_1}{h_2}\right)^{2\alpha} \quad (10.19)$$

For surface ships it is common to assume that  $Z_{\text{wind}} = M_{\text{wind}} = 0$  while the roll moment  $K_{\text{wind}}$  is used for ships and ocean structures where large rolling angles are an issue. For semi-submersibles both  $K_{\text{wind}}$  and  $M_{\text{wind}}$  are needed in addition to the horizontal motion components  $X_{\text{wind}}, Y_{\text{wind}}$  and  $N_{\text{wind}}$ .

The wind speed is usually specified in terms of *Beaufort numbers*, as shown in Table 10.2.

### Wind coefficient approximation for symmetrical ships

For ships that are symmetrical with respect to the  $xz$  and  $yz$  planes, the wind coefficients for horizontal plane motions can be approximated by

$$C_X(\gamma_w) \approx -c_x \cos(\gamma_w) \quad (10.20)$$

$$C_Y(\gamma_w) \approx c_y \sin(\gamma_w) \quad (10.21)$$

$$C_N(\gamma_w) \approx c_n \sin(2\gamma_w) \quad (10.22)$$

Table 10.2: Definition of Beaufort numbers (Price and Bishop, 1974)

Beaufort number	Description of wind	Wind speed (knots)
0	Calm	0–1
1	Light air	2–3
2	Light breeze	4–7
3	Gentle breeze	8–11
4	Moderate breeze	12–16
5	Fresh breeze	17–21
6	Strong breeze	22–27
7	Moderate gale	28–33
8	Fresh gale	34–40
9	Strong gale	41–48
10	Whole gale	49–56
11	Storm	57–65
12	Hurricane	More than 65

which are convenient formulae for computer simulations. Experiments with ships indicate that  $c_x \in \{0.50, 0.90\}$ ,  $c_y \in \{0.70, 0.95\}$  and  $c_n \in \{0.05, 0.20\}$ . However, these values should be used with care.

### 10.1.2 Wind forces and moments on moving marine craft

For a ship moving at a forward speed, (10.9)–(10.14) should be redefined in terms of relative wind speed  $V_{rw}$  and angle of attack  $\gamma_{rw}$  according to

$$\tau_{\text{wind}} = \frac{1}{2} \rho_a V_{rw}^2 \begin{bmatrix} C_X(\gamma_{rw}) A_{Fw} \\ C_Y(\gamma_{rw}) A_{Lw} \\ C_Z(\gamma_{rw}) A_{Fw} \\ C_K(\gamma_{rw}) A_{Lw} H_{Lw} \\ C_M(\gamma_{rw}) A_{Fw} H_{Fw} \\ C_N(\gamma_{rw}) A_{Lw} L_{oa} \end{bmatrix} \quad (10.23)$$

with

$$V_{rw} = \sqrt{u_{rw}^2 + v_{rw}^2} \quad (10.24)$$

$$\gamma_{rw} = -\text{atan2}(v_{rw}, u_{rw}) \quad (10.25)$$

The relative velocities are

$$u_{rw} = u - u_w \quad (10.26)$$

$$v_{rw} = v - v_w \quad (10.27)$$

Table 10.3: Coefficients of lateral and longitudinal resistance, cross-force and rolling moment (Blendermann, 1994).

Type of vessel	$CD_t$	$CD_{l_{AF}}(0)$	$CD_{l_{AF}}(\pi)$	$\delta$	$\kappa$
1. Car carrier	0.95	0.55	0.60	0.80	1.2
2. Cargo vessel, loaded	0.85	0.65	0.55	0.40	1.7
3. Cargo vessel, container on deck	0.85	0.55	0.50	0.40	1.4
4. Container ship, loaded	0.90	0.55	0.55	0.40	1.4
5. Destroyer	0.85	0.60	0.65	0.65	1.1
6. Diving support vessel	0.90	0.60	0.80	0.55	1.7
7. Drilling vessel	1.00	0.70–1.00	0.75–1.10	0.10	1.7
8. Ferry	0.90	0.45	0.50	0.80	1.1
9. Fishing vessel	0.95	0.70	0.70	0.40	1.1
10. Liquefied natural gas tanker	0.70	0.60	0.65	0.50	1.1
11. Offshore supply vessel	0.90	0.55	0.80	0.55	1.2
12. Passenger liner	0.90	0.40	0.40	0.80	1.2
13. Research vessel	0.85	0.55	0.65	0.60	1.4
14. Speed boat	0.90	0.55	0.60	0.60	1.1
15. Tanker, loaded	0.70	0.90	0.55	0.40	3.1
16. Tanker, in ballast	0.70	0.75	0.55	0.40	2.2
17. Tender	0.85	0.55	0.55	0.65	1.1

while the components of  $V_w$  in the  $x$  and  $y$  directions are (see Figure 10.1)

$$u_w = V_w \cos(\beta_w - \psi) \quad (10.28)$$

$$v_w = V_w \sin(\beta_w - \psi) \quad (10.29)$$

The wind speed  $V_w$  and its direction  $\beta_w$  can be measured by an anemometer and a weathervane, respectively. Anemometer is derived from the Greek word *anemos*, meaning wind. Anemometers can be divided into two classes: those that measure the wind's speed and those that measure the wind's pressure. If the pressure is measured, a formula relating pressure with speed must be applied.

The wind measurements should be low-pass filtered since only the mean wind forces and moments can be compensated for by the propulsion system. In fact, since the inertia of the craft is so large, it is unnecessary for the control system to compensate for wind gust. In order to implement wind feedforward compensation for a DP vessel using (10.23), only the wind coefficients  $C_X$ ,  $C_Y$  and  $C_N$  are needed. They can be experimentally obtained by using a scale model located in a wind tunnel or computed numerically. Different models for computation of the wind coefficients for varying hull geometries will now be discussed.

### 10.1.3 Wind coefficients based on flow over a Helmholtz–Kirchhoff plate

Blendermann (1994) applies a simple load concept to compute the wind coefficients.

This is based on the *Helmholtz–Kirchhoff* plate theory. The load functions are parametrized in terms of four primary wind load parameters: longitudinal and transverse resistance  $CD_l$  and  $CD_t$ , respectively, the cross-force parameter  $\delta$  and the rolling moment factor  $\kappa$ . Numerical values for different vessels are given in Table 10.3.

The longitudinal resistance coefficient  $CD_{l_{AF}}(\gamma_w)$  in Table 10.3 is scaled according to

$$CD_l = CD_{l_{AF}}(\gamma_w) \frac{A_{F_w}}{A_{L_w}} \quad (10.30)$$

where values for two angles  $\gamma_w \in \{0, \pi\}$  are given. The value  $CD_{l_{AF}}(0)$  corresponds to head wind while  $CD_{l_{AF}}(\pi)$  should be used for tail wind. By using these two values in the regions  $|\gamma_w| \leq \pi/2$  and  $|\gamma_w| > \pi/2$ , respectively, a nonsymmetrical wind load function for surge can be computed. Moreover, this gives different wind loads for head and tail winds, as shown in Figure 10.2. Alternatively, a symmetrical wind profile is obtained by using  $CD_{l_{AF}}(0)$  or the mean of  $CD_{l_{AF}}(0)$  and  $CD_{l_{AF}}(\pi)$ .

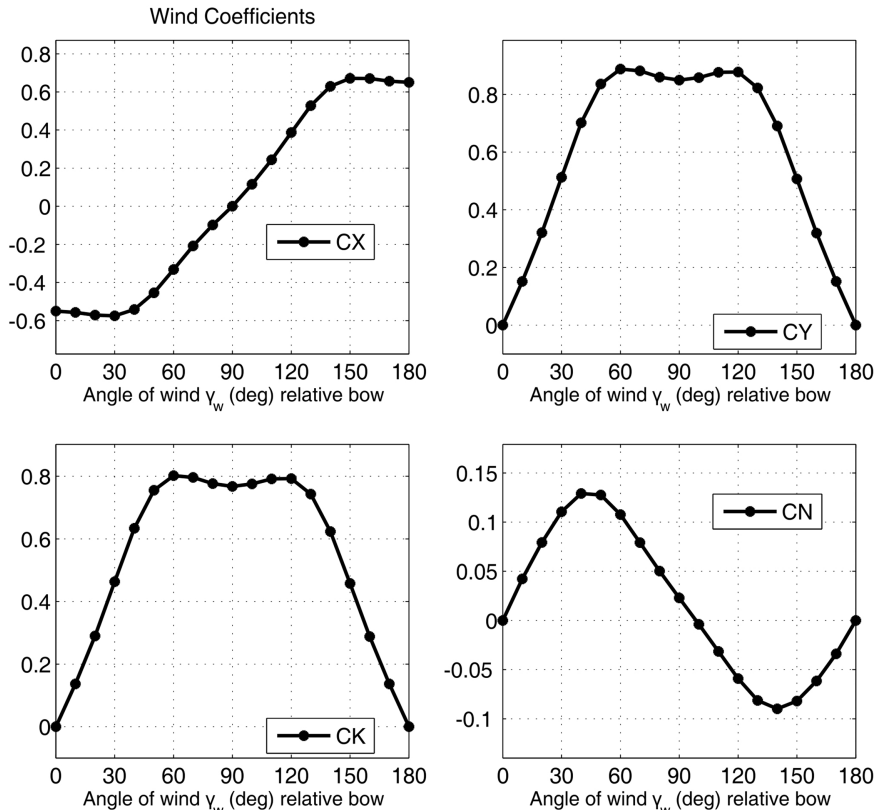


Figure 10.2: Wind coefficients for the research vessel in Table 10.3 (vessel 13).  $C_X$  is generated using  $CD_{l_{AF}}(0)$  and  $CD_{l_{AF}}(\pi)$  for  $|\gamma_w| \leq \pi/2$  and  $|\gamma_w| > \pi/2$ , respectively.

Let the mean height of the area  $A_{L_w}$  be denoted by

$$H_M = \frac{A_{L_w}}{L_{oa}} \quad (10.31)$$

and let the coordinates  $(s_L, s_H) = (s_L, H_{L_w})$  describe the centroid of the transverse project area  $A_{L_w}$  with respect to the main section and above the water line. Based on these quantities, Blädermann (1994) gives the following expressions for the wind coefficients:

$$C_X(\gamma_w) = -\underbrace{CD_t \frac{A_{L_w}}{A_{F_w}}}_{CD_{IAF}} \frac{\cos(\gamma_w)}{1 - \frac{\delta}{2} \left(1 - \frac{CD_t}{CD_t}\right) \sin^2(2\gamma_w)} \quad (10.32)$$

$$C_Y(\gamma_w) = CD_t \frac{\sin(\gamma_w)}{1 - \frac{\delta}{2} \left(1 - \frac{CD_t}{CD_t}\right) \sin^2(2\gamma_w)} \quad (10.33)$$

$$C_K(\gamma_w) = \kappa C_Y(\gamma_w) \quad (10.34)$$

$$C_N(\gamma_w) = \left[ \frac{s_L}{L_{oa}} - 0.18 \left( \gamma_w - \frac{\pi}{2} \right) \right] C_Y(\gamma_w) \quad (10.35)$$

where the expression for  $C_K(\gamma_w)$  has been modified to comply with (10.12). Notice that in Blädermann (1994)

$$C_K^{\text{Blädermann}}(\gamma_w) = \frac{s_H}{H_M} C_K(\gamma_w) \quad (10.36)$$

where  $s_H = H_{L_w}$ . The numerical values for several vessel types are given in Table 10.3.

Consider the research vessel in Table 10.3 with  $A_{F_w} = 160.7 \text{ m}^2$ ,  $A_{L_w} = 434.8 \text{ m}^2$ ,  $s_L = 1.48 \text{ m}$ ,  $s_H = 5.10 \text{ m}$ ,  $L_{oa} = 55.0 \text{ m}$ ,  $L_{pp} = 48.0 \text{ m}$  and  $B = 12.5 \text{ m}$ . For this vessel, the wind coefficients are computed in Matlab according to:

#### Matlab:

The wind coefficients are plotted in Figure 10.2 using the MSS toolbox example file `ExWindForce.m`. The data sets of Blädermann (1994) are programmed in the Matlab function:

```
[w_wind, CX, CY, CK, CN] = ...
blädermann94(gamma_r, V_r, AFw, ALw, sH, sL, Loa, vessel_no);
```

This function computes the nonsymmetrical version of  $C_X$ .

#### 10.1.4 Wind coefficients for merchant ships

Isherwood (1972) has derived a set of wind coefficients by using multiple regression techniques to fit experimental data of merchant ships. The wind coefficients are

parametrized in terms of the following eight parameters:

$L_{oa}$	length overall
$B$	beam
$A_{Lw}$	lateral projected area
$A_{Tw}$	transverse projected area
$A_{SS}$	lateral projected area of superstructure
$S$	length of perimeter of lateral projection of model excluding water line and slender bodies such as masts and ventilators
$C$	distance from bow of centroid of lateral projected area
$M$	number of distinct groups of masts or king posts seen in lateral projection; king posts close against the bridge front are not included

From regression analyses it was concluded that the measured data were best fitted to the following three equations:

$$\begin{aligned} C_X &= -\left( A_0 + A_1 \frac{2A_L}{L^2} + A_2 \frac{2A_T}{B^2} + A_3 \frac{L}{B} + A_4 \frac{S}{L} + A_5 \frac{C}{L} + A_6 M \right) \\ C_Y &= B_0 + B_1 \frac{2A_L}{L^2} + B_2 \frac{2A_T}{B^2} + B_3 \frac{L}{B} + B_4 \frac{S}{L} + B_5 \frac{C}{L} + B_6 \frac{A_{SS}}{A_L} \\ C_N &= C_0 + C_1 \frac{2A_L}{L^2} + C_2 \frac{2A_T}{B^2} + C_3 \frac{L}{B} + C_4 \frac{S}{L} + C_5 \frac{C}{L} \end{aligned}$$

where  $A_i$  and  $B_i$  ( $i = 0, \dots, 6$ ) and  $C_j$  ( $j = 0, \dots, 5$ ) are tabulated in Table 10.4, together with the *residual standard errors* (S.E.). The signs of  $C_X$  have been corrected to match the definition of  $\gamma_w$  in Figure 10.1.

#### Matlab:

The wind coefficients are plotted in Figure 10.3 using the MSS toolbox example file `ExWindForce.m`. Isherwood (1972) are programmed in the Matlab function

```
[w_wind, CX, CY, CN] = ...
    isherwood72(gamma_r, V_r, Loa, B, AFw, ALw, A_SS, S, C, M);
```

### 10.1.5 Wind coefficients for very large crude carriers

Wind loads on very large crude carriers (VLCCs) in the range 150 000 to 500 000 dwt can be computed by applying the results of OCIMF (1977). In this work the wind coefficients are scaled using the conversion factor 1/7.6 instead of 1/2. In addition, the signs in sway and yaw must be corrected such that

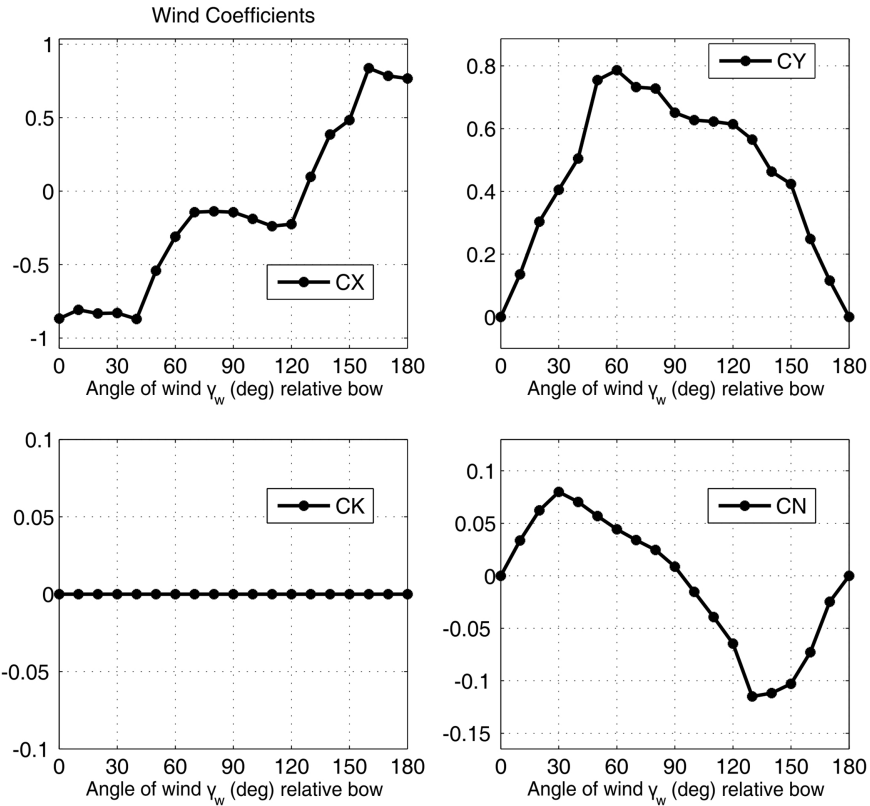


Figure 10.3: Wind coefficients for  $L_{oa} = 100$ ,  $B = 30$ ,  $A_{Lw} = 900$ ,  $A_{Fw} = 300$ ,  $A_{SS} = 100$ ,  $S = 100$ ,  $C = 50$  and  $M = 2$  using the formulae of Isherwood (1972).

$$X_{\text{wind}} = \frac{1}{7.6} C_X^{\text{OCIMF}}(\gamma_w) \rho_a V_w^2 A_{Fw} \quad (10.37)$$

$$Y_{\text{wind}} = -\frac{1}{7.6} C_Y^{\text{OCIMF}}(\gamma_w) \rho_a V_w^2 A_{Lw} \quad (10.38)$$

$$N_{\text{wind}} = -\frac{1}{7.6} C_N^{\text{OCIMF}}(\gamma_w) \rho_a V_w^2 A_{Lw} L_{oa} \quad (10.39)$$

where the wind coefficients  $C_X^{\text{OCIMF}}$ ,  $C_Y^{\text{OCIMF}}$  and  $C_N^{\text{OCIMF}}$  correspond to the plots given in OCIMF (1977); see Figures 10.4–10.6.

### 10.1.6 Wind coefficients for large tankers and medium-sized ships

For wind resistance on large tankers in the 100 000 to 500 000 dwt class the reader is advised to consult Van Berlekom *et al.* (1974). Medium-sized ships of the order 600 to 50 000 dwt are discussed by Wagner (1967).

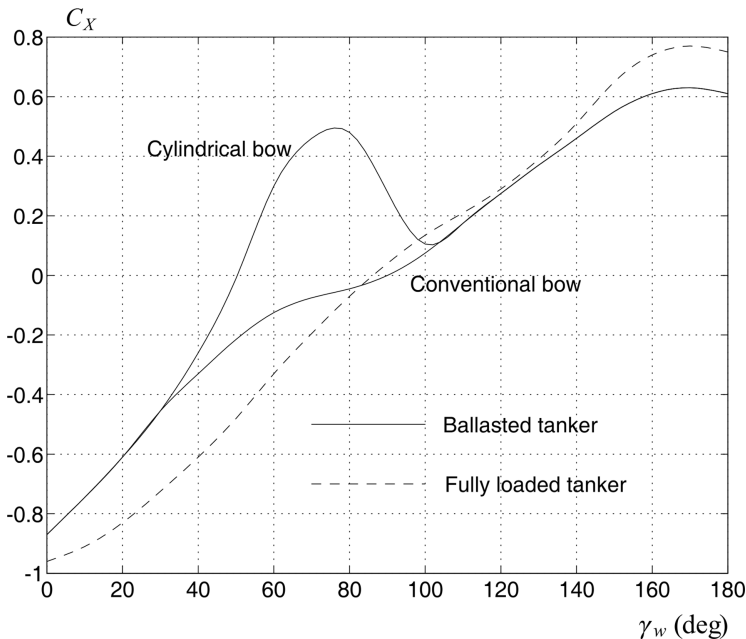


Figure 10.4: Longitudinal wind force coefficient  $C_X^{\text{OCIMF}}$  as a function of  $\gamma_w$  (OCIMF, 1977).

A detailed analysis of wind resistance using semi-empirical loading functions is given by Blendermann (1986). The data sets for seven ships are included in the report.

### 10.1.7 Wind coefficients for moored ships and floating structures

Wind loads on moored ships are discussed by De Kat and Wichers (1991) while an excellent reference for huge pontoon-type floating structures is Kitamura *et al.* (1997).

## 10.2 Wave Forces and Moments

A motion control system can be simulated under influence of wave-induced forces by separating the *first-order* and *second-order* effects:

- **First-order wave-induced forces:** wave-frequency (WF) motion observed as zero-mean oscillatory motions.
- **Second-order wave-induced forces:** wave drift forces observed as nonzero slowly-varying components.

When designing motion control systems, it is important to evaluate robustness and performance in the presence of waves. Wave forces are observed as a mean slowly

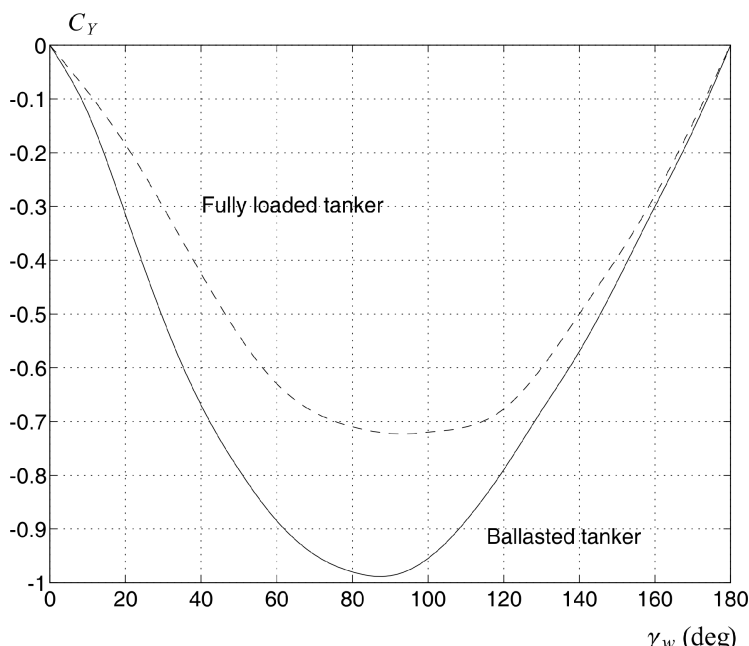
Table 10.4: Wind force parameters in surge, sway and yaw (Isherwood, 1972)

$\gamma_w$ (deg)	$A_0$	$A_1$	$A_2$	$A_3$	$A_4$	$A_5$	$A_6$	S.E.
0	2.152	-5.00	0.243	-0.164	-	-	-	0.086
10	1.714	-3.33	0.145	-0.121	-	-	-	0.104
20	1.818	-3.97	0.211	-0.143	-	-	0.033	0.096
30	1.965	-4.81	0.243	-0.154	-	-	0.041	0.117
40	2.333	-5.99	0.247	-0.190	-	-	0.042	0.115
50	1.726	-6.54	0.189	-0.173	0.348	-	0.048	0.109
60	0.913	-4.68	-	-0.104	0.482	-	0.052	0.082
70	0.457	-2.88	-	-0.068	0.346	-	0.043	0.077
80	0.341	-0.91	-	-0.031	-	-	0.032	0.090
90	0.355	-	-	-	-0.247	-	0.018	0.094
100	0.601	-	-	-	-0.372	-	-0.020	0.096
110	0.651	1.29	-	-	-0.582	-	-0.031	0.090
120	0.564	2.54	-	-	-0.748	-	-0.024	0.100
130	-0.142	3.58	-	0.047	-0.700	-	-0.028	0.105
140	-0.677	3.64	-	0.069	-0.529	-	-0.032	0.123
150	-0.723	3.14	-	0.064	-0.475	-	-0.032	0.128
160	-2.148	2.56	-	0.081	-	1.27	-0.027	0.123
170	-2.707	3.97	-0.175	0.126	-	1.81	-	0.115
180	-2.529	3.76	-0.174	0.128	-	1.55	-	0.112
						Mean S.E.		0.103

$\gamma_w$ (deg)	$B_0$	$B_1$	$B_2$	$B_3$	$B_4$	$B_5$	$B_6$	S.E.
10	0.096	0.22	—	—	—	—	—	0.015
20	0.176	0.71	—	—	—	—	—	0.023
30	0.225	1.38	—	0.023	—	-0.29	—	0.030
40	0.329	1.82	—	0.043	—	-0.59	—	0.054
50	1.164	1.26	0.121	—	-0.242	-0.95	—	0.055
60	1.163	0.96	0.101	—	-0.177	-0.88	—	0.049
70	0.916	0.53	0.069	—	—	-0.65	—	0.047
80	0.844	0.55	0.082	—	—	-0.54	—	0.046
90	0.889	—	0.138	—	—	-0.66	—	0.051
100	0.799	—	0.155	—	—	-0.55	—	0.050
110	0.797	—	0.151	—	—	-0.55	—	0.049
120	0.996	—	0.184	—	-0.212	-0.66	0.34	0.047
130	1.014	—	0.191	—	-0.280	-0.69	0.44	0.051
140	0.784	—	0.166	—	-0.209	-0.53	0.38	0.060
150	0.536	—	0.176	-0.029	-0.163	—	0.27	0.055
160	0.251	—	0.106	-0.022	—	—	—	0.036
170	0.125	—	0.046	-0.012	—	—	—	0.022

Table 10.4: (Continued)

$\gamma_w$ (deg)	$C_0$	$C_1$	$C_2$	$C_3$	$C_4$	$C_5$	S.E.
10	0.0596	0.061	—	—	—	-0.074	0.0048
20	0.1106	0.204	—	—	—	-0.170	0.0074
30	0.2258	0.245	—	—	—	-0.380	0.0105
40	0.2017	0.457	—	0.0067	—	-0.472	0.0137
50	0.1759	0.573	—	0.0118	—	-0.523	0.0149
60	0.1925	0.480	—	0.0115	—	-0.546	0.0133
70	0.2133	0.315	—	0.0081	—	-0.526	0.0125
80	0.1827	0.254	—	0.0053	—	-0.443	0.0123
90	0.2627	—	—	—	—	-0.508	0.0141
100	0.2102	—	-0.0195	—	0.0335	-0.492	0.0146
110	0.1567	—	-0.0258	—	0.0497	-0.457	0.0163
120	0.0801	—	-0.0311	—	0.0740	-0.396	0.0179
130	-0.0189	—	-0.0488	0.0101	0.1128	-0.420	0.0166
140	0.0256	—	-0.0422	0.0100	0.0889	-0.463	0.0162
150	0.0552	—	-0.0381	0.0109	0.0689	-0.476	0.0141
160	0.0881	—	-0.0306	0.0091	0.0366	-0.415	0.0105
170	0.0851	—	-0.0122	0.0025	—	-0.220	0.0057
Mean S.E.							0.0127

Figure 10.5: Lateral wind force coefficient  $C_Y^{\text{OCIMF}}$  as a function of  $\gamma_w$  (OCIMF, 1977).

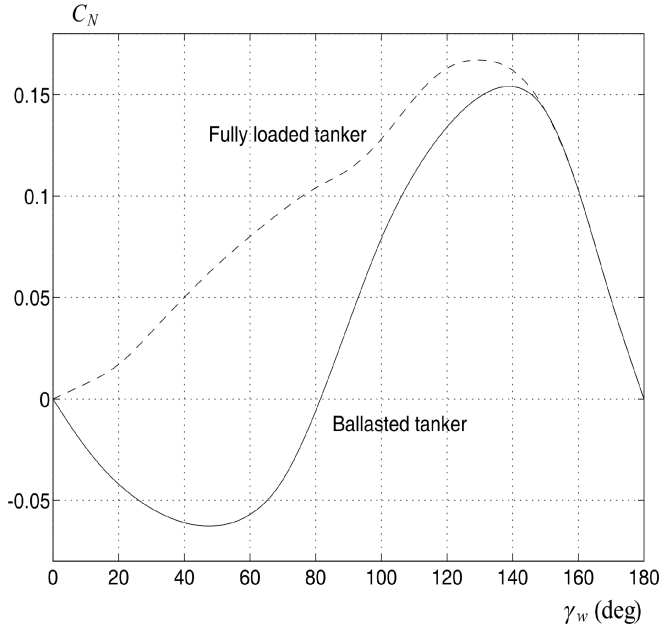


Figure 10.6: Wind moment coefficient  $C_N^{\text{OCIMF}}$  in yaw as a function of  $\gamma_w$  (OCIMF, 1977).

varying component and an oscillatory component, which need to be compensated differently by a feedback control system. For instance, the mean component can be removed by using integral action while the oscillatory component usually is removed by using a cascaded notch and low-pass filter. This is usually referred to as *wave filtering*. This section describes wave force models that can be used for prediction, observer-based wave filtering and testing of feedback control systems in the presence of waves. Both methods based on response amplitude operators (RAOs) and linear state-space models will be discussed. This includes:

1. Force RAOs
2. Motion RAOs
3. Linear state-space models (WF models)

The first two methods require that the RAO tables are computed using a hydrodynamic program (see Section 5.1) since the wave forces depend on the geometry of the craft. The last method is attractive due to its simplicity but it is only intended for the testing of robustness and performance of control systems, that is closed-loop analysis.

The resulting wave forces and moments are

$$\boldsymbol{\tau}_{\text{wave}} = \boldsymbol{\tau}_{\text{wave1}} + \boldsymbol{\tau}_{\text{wave2}} \quad (10.40)$$

This is the sum of the first- and second-order wave-induced forces and moments  $\boldsymbol{\tau}_{\text{wave1}}$

Table 10.5: Definition of sea-state (SS) codes (Price and Bishop, 1974). Notice that the percentage probability for SS codes 0, 1 and 2 is summarized.

Sea state code	Description of sea	Wave height observed (m)	Percentage probability		
			World wide	North Atlantic	Northern North Atlantic
0	Calm (glassy)	0			
1	Calm (rippled)	0–0.1	11.2486	8.3103	6.0616
2	Smooth (wavelets)	0.1–0.5			
3	Slight	0.5–1.25	31.6851	28.1996	21.5683
4	Moderate	1.25–2.5	40.1944	42.0273	40.9915
5	Rough	2.5–4.0	12.8005	15.4435	21.2383
6	Very rough	4.0–6.0	3.0253	4.2938	7.0101
7	High	6.0–9.0	0.9263	1.4968	2.6931
8	Very high	9.0–14.0	0.1190	0.2263	0.4346
9	Phenomenal	Over 14.0	0.0009	0.0016	0.0035

and  $\tau_{\text{wave}2}$ , respectively. The next sections explain how these transfer functions can be realized in a time-domain simulator.

### 10.2.1 Sea-state descriptions

For marine craft the sea states in Table 10.5 can be characterized by the following wave spectrum parameters:

- The significant wave height  $H_s$  (the mean wave height of the one-third highest waves, also denoted as  $H_{1/3}$ )
- One of the following wave periods:
  - The average wave period,  $T_1$
  - Average zero-crossing wave period,  $T_z$
  - Peak period,  $T_p$  (this is equivalent to the modal period,  $T_0$ )

To relate the different periods to each other it is necessary to define the wave spectrum moments.

#### Wave spectrum moments

A wave spectrum  $S(\omega)$ , see Figure 10.7, can be classified by means of *wave spectrum moments*

$$m_k := \int_0^\infty \omega^k S(\omega) d\omega \quad (k = 0, \dots, N) \quad (10.41)$$

For  $k = 0$ , this yields

$$m_0 = \int_0^\infty S(\omega) d\omega \quad (10.42)$$

The instantaneous wave elevation is Gaussian distributed with zero mean and variance:

$$\sigma^2 = m_0 \quad (10.43)$$

where  $\sigma$  is the root-mean-square (RMS) value of the spectrum.

The *modal frequency* (peak frequency)  $\omega_0$  is found by requiring that

$$\left( \frac{dS(\omega)}{d\omega} \right)_{\omega=\omega_0} = 0 \quad (10.44)$$

Hence, the *modal period* becomes

$$T_0 = \frac{2\pi}{\omega_0} \quad (10.45)$$

Consequently, the maximum value of  $S(\omega)$  is

$$S_{\max} = S(\omega_0) \quad (10.46)$$

Under the assumption that the wave height is Rayleigh distributed it can be shown that the significant wave height satisfies (Price and Bishop 1974)

$$H_s = 4\sigma = 4\sqrt{m_0} \quad (10.47)$$

The *average wave period* is defined as

$$T_1 := 2\pi \frac{m_0}{m_1} \quad (10.48)$$

while the *average zero-crossings period* is defined as

$$T_z := 2\pi \sqrt{\frac{m_0}{m_2}} \quad (10.49)$$

### 10.2.2 Wave spectra

The process of wave generation due to wind starts with small wavelets appearing on the water surface. This increases the drag force, which in turn allows short waves to grow. These short waves continue to grow until they finally break and their energy is dissipated. It is observed that a *developing sea*, or storm, starts with high frequencies creating a spectrum with a peak at a relatively high frequency. A storm that has lasted for a long time is said to create a *fully developed sea*. After the wind has stopped, a low-frequency decaying sea or swell is formed. These long waves form a wave spectrum with a low peak frequency.

If the swell from one storm interacts with the waves from another storm, a wave spectrum with two peak frequencies may be observed. In addition, tidal waves will

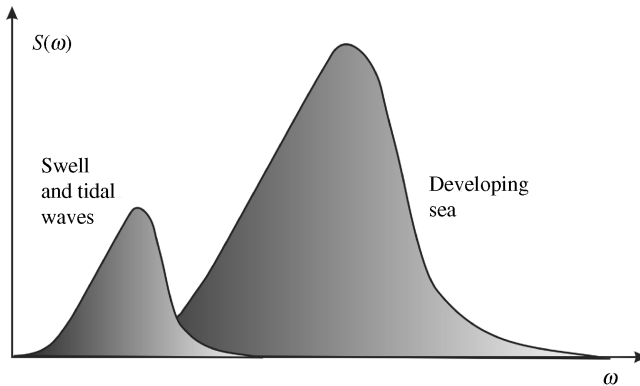


Figure 10.7: Two peaked wave spectra  $S(\omega)$  where one peak is due to swell and tidal waves and the other peak is due to a developing sea.

generate a peak at a low frequency. Hence, the resulting wave spectrum might be quite complicated in cases where the weather changes rapidly (see Figure 10.7).

The state-of-the-art wave spectra will now be presented. These models are used to derive linear approximations and transfer functions for computer simulations, autopilot wave filtering and state reconstruction, which are the topics in Part II.

### Neumann spectrum

The earliest spectral formulation is due to who proposed the *one-parameter* spectrum

$$S(\omega) = C\omega^{-6} \exp(-2g^2\omega^{-2}V^{-2}) \quad (10.50)$$

where  $S(\omega)$  in  $\text{m/s}^2$  is the wave elevation power spectral density function,  $C$  is an empirical constant,  $V$  is the wind speed and  $g$  is the acceleration of gravity. Six years later Phillips (1958) showed that the high-frequency part of the wave spectrum reached the asymptotic limit

$$\lim_{\omega \gg 1} S(\omega) = \alpha g^2 \omega^{-5} \quad (10.51)$$

where  $\alpha$  is a positive constant. This limiting function of Phillips is still used as the basis for most spectral formulations.

### Bretschneider spectrum

The spectrum of Neumann was further extended to a two-parameter spectrum by Bretschneider (1959)

$$S(\omega) = 1.25 \frac{\omega_0^4 H_s^2}{4} \omega^{-5} \exp\left[-1.25 (\omega_0/\omega)^4\right] \quad (10.52)$$

where  $\omega_0$  is the *modal* or *peak frequency* of the spectrum and  $H_s$  is the *significant wave height* (mean of the one-third highest waves). This spectrum was developed for the North Atlantic, for unidirectional seas, infinite depth, no swell and unlimited fetch.

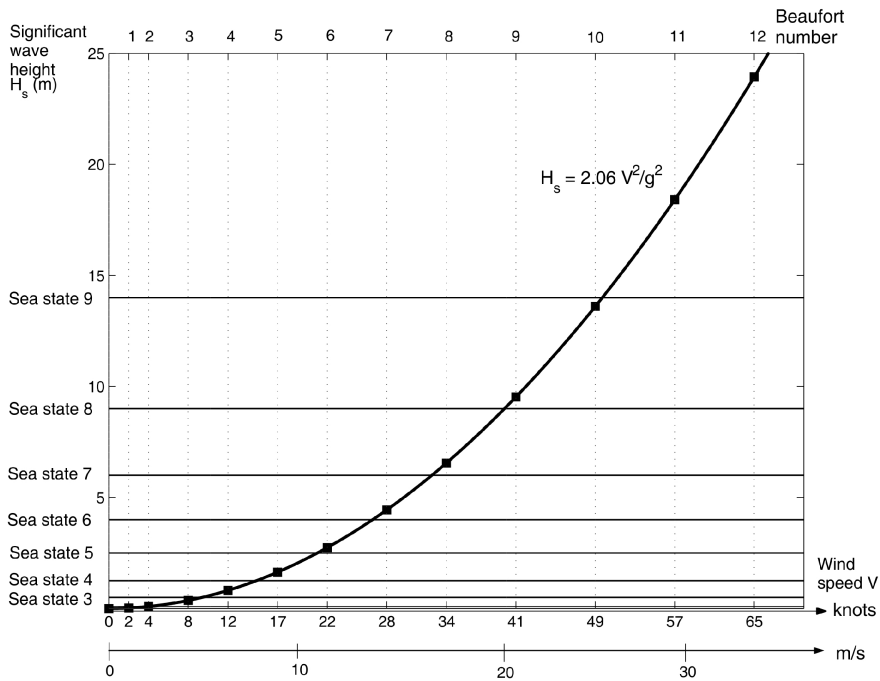


Figure 10.8: Plot showing the relationship between significant wave height, wind speed, Beaufort numbers and sea-state codes.

The significant wave height  $H_s$  is used to classify the type of sea in terms of sea-state codes 0, 1, ..., 9, as shown in Table 10.5.

### Pierson–Moskowitz spectrum

Pierson and Moskowitz (1963) have developed a two-parameter wave spectral formulation for fully developed wind-generated seas from analyses of wave spectra in the North Atlantic Ocean

$$S(\omega) = A\omega^{-5} \exp(-B\omega^{-4}) \quad (10.53)$$

which is commonly known as the *PM spectrum* (Pierson–Moskowitz spectrum). The PM spectrum is used as the basis for several spectral formulations but with different  $A$  and  $B$  values. In its original formulation, the PM spectrum is only a one-parameter spectrum since only  $B$  changes with the sea state. The parameters are

$$A = 8.1 \times 10^{-3} g^2 = \text{constant} \quad (10.54)$$

$$B = 0.74 \left( \frac{g}{V_{19.4}} \right)^4 = \frac{3.11}{H_s^2} \quad (10.55)$$

where  $V_{19.4}$  is the wind speed at a height of 19.4 m over the sea surface.

**Matlab:**

The Bretschneider and PM spectra are implemented in the MSS toolbox as wave spectra 1 and 2

```
S = wavespec(1, [A, B], w, 1);
S = wavespec(2, V20, w, 1);
```

where A and B are the spectrum parameters, V20 is wind speed at 20 m height and w is the wave frequency vector.

The relationship between  $V_{19.4}$  and  $H_s$  in (10.55) is based on the assumption that the waves can be represented by Gaussian random processes and that  $S(\omega)$  is narrow banded. From (10.55) it is seen that

$$H_s = \frac{2.06}{g^2} V_{19.4}^2 \quad (10.56)$$

This implies that the significant wave height is proportional to the square of the wind speed. This is shown in Figure 10.8 where the *sea-state codes* and *Beaufort numbers* are plotted against each other; see Tables 10.2 and 10.5.

The *modal frequency* (peak frequency)  $\omega_0$  for the PM spectrum is found by requiring that

$$\left( \frac{dS(\omega)}{d\omega} \right)_{\omega=\omega_0} = 0 \quad (10.57)$$

Solving for  $\omega_0$  in (10.53) yields

$$\omega_0 = \sqrt[4]{\frac{4B}{5}} \implies T_0 = 2\pi \sqrt[4]{\frac{5}{4B}} \quad (10.58)$$

where  $T_0$  is the *modal period*. Consequently, the maximum value of  $S(\omega)$  is

$$S_{\max} = S(\omega_0) = \frac{5A}{4B\omega_0} \exp(-5/4) \quad (10.59)$$

### Modified Pierson–Moskowitz (MPM) spectrum

In order to predict the responses of marine craft in open sea, the International Ship and Offshore Structures Congress (2nd ISSC 1964), the International Towing Tank Conferences (12th ITTC, 1969, and 15th ITTC, 1978) have recommended the use of a modified version of the PM spectrum (see Figure 10.9 where

$$A = \frac{4\pi^3 H_s^2}{T_z^4}, \quad B = \frac{16\pi^3}{T_z^4} \quad (10.60)$$

This representation of the PM spectrum has two parameters  $H_s$  and  $T_z$ , or alternatively  $T_0$  and  $T_1$  given by

$$T_z = 0.710T_0 = 0.921T_1 \quad (10.61)$$

**Matlab:**

The modified PM spectrum is implemented in the MSS toolbox as wave spectra 3 to 5

```
S = wavespec(3,[Hs,T0],w,1);
S = wavespec(4,[Hs,T1],w,1);
S = wavespec(5,[Hs,Tz],w,1);
```

where  $H_s$  is the significant wave height,  $T_0$ ,  $T_1$  and  $T_z$  are the peak, average and average zero-crossing wave periods, respectively, while  $w$  is the wave frequency vector.

The modified PM spectrum should only be used for a fully developed sea with large (infinite) depth, no swell and unlimited fetch. For nonfully developed seas the *JONSWAP* or *Torsethaugen* spectra are recommended.

**JONSWAP spectrum**

In 1968 and 1969 an extensive measurement program was carried out in the North Sea, between the island Sylt in Germany and Iceland. The measurement program is known as the *Joint North Sea Wave Project* (JONSWAP) and the results from these investigations have been adopted as an ITTC standard by the 17th ITTC (1984). Since the JONSWAP spectrum (see Figure 10.9) is used to describe *nonfully developed seas*, the spectral density function will be more peaked than those representing fully developed spectra. The proposed spectral formulation is representative for wind-generated waves under the assumption of finite water depth and limited fetch. The spectral density function is written

$$S(\omega) = 155 \frac{H_s^2}{T_1^4} \omega^{-5} \exp\left(\frac{-944}{T_1^4} \omega^{-4}\right) \gamma^Y \quad (10.62)$$

where Hasselmann et al. (1973) suggest that  $\gamma = 3.3$  and

$$Y = \exp\left[-\left(\frac{0.191\omega T_1 - 1}{\sqrt{2}\sigma}\right)^2\right] \quad (10.63)$$

where

$$\sigma = \begin{cases} 0.07 & \text{for } \omega \leq 5.24/T_1 \\ 0.09 & \text{for } \omega > 5.24/T_1 \end{cases} \quad (10.64)$$

Alternative formulations can be derived in terms of the characteristic periods like  $T_0$  and  $T_z$  by using

$$T_1 = 0.834 T_0 = 1.073 T_z \quad (10.65)$$

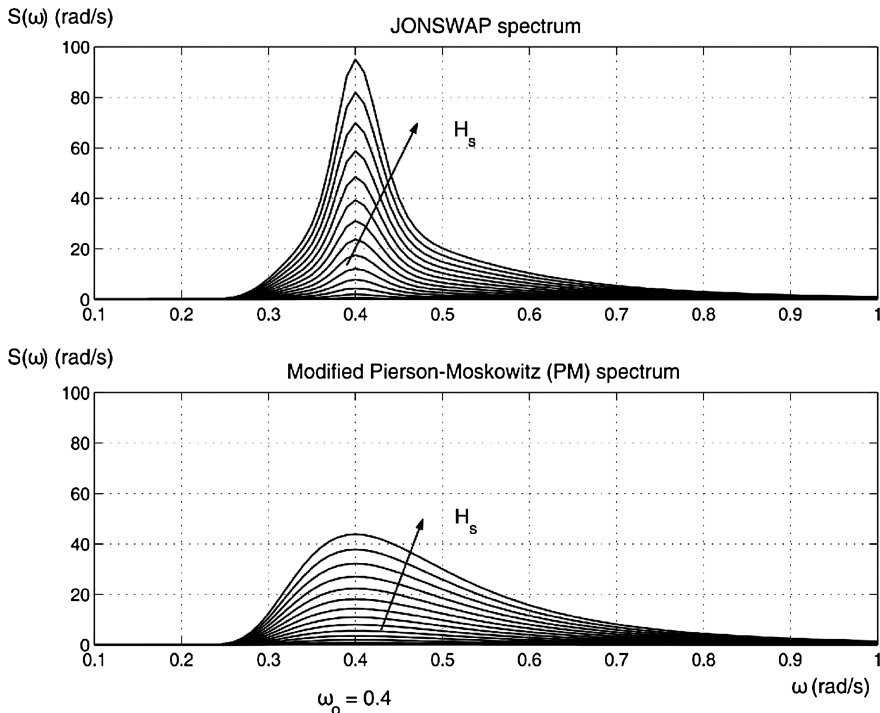


Figure 10.9: Plot showing the JONSWAP and modified Pierson–Moskowitz spectra for  $\omega_0 = 0.4$  rad/s and  $H_s = 3, 4, \dots, 14$  m.

#### Matlab:

The JONSWAP spectrum is included in the MSS toolbox as wave spectra 6 and 7

```
S = wavespec(6, [V10, fetch], w, 1);
S = wavespec(7, [Hs, w0, gamma], w, 1);
```

where V10 is the wind speed at 10 m height, Hs is the significant wave height, w0 is peak frequency and w is the wave frequency vector.

#### Torsethaugen spectrum

The *Torsethaugen spectrum* is an empirical, two-peaked spectrum, which includes the effect of swell (low-frequency peak) and newly developed waves (high-frequency peak). The spectrum was developed for Norsk Hydro (Torsethaugen 1996), and standardized under the Norsok Standard (1999). The spectrum was developed using curve fitting of experimental data from the North Sea.

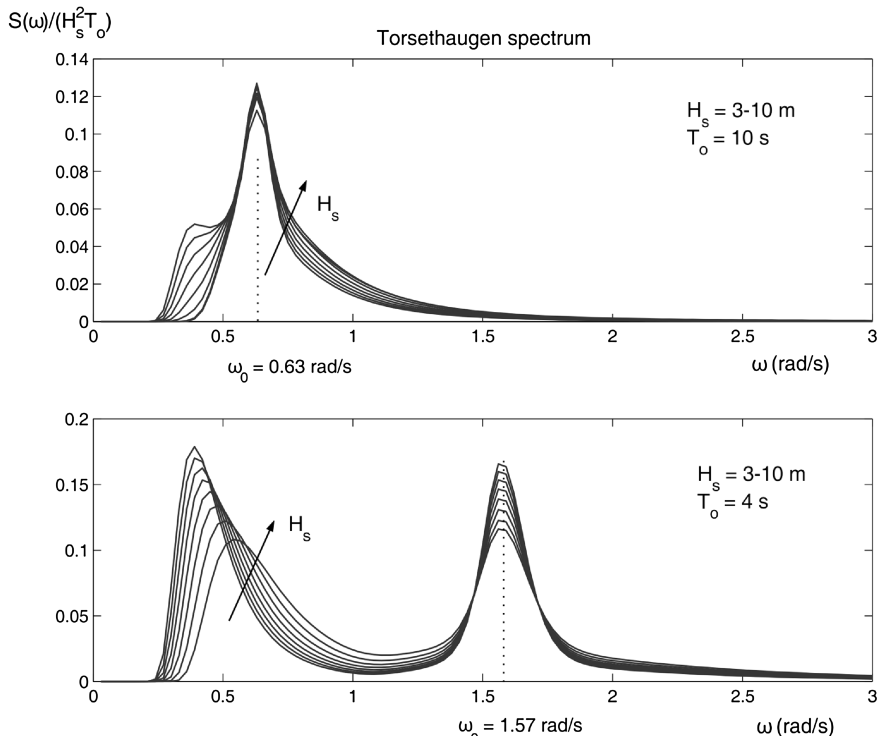


Figure 10.10: Torsethaugen spectrum: upper plot shows only one peak at  $\omega_0 = 0.63$  rad/s representing swell and developing sea while the lower plot shows low-frequency swell and newly developing sea with peak frequency  $\omega_0 = 1.57$  rad/s.

### Matlab:

The Torsethaugen spectrum is included in the MSS toolbox as wave spectrum 7

```
S = wavespec(7,[Hs,w0],w,1);
```

where  $H_s$  is the significant wave height,  $w_0$  is peak frequency and  $w$  is the wave frequency vector.

If the peak frequency  $\omega_0$  is chosen to be less than approximately 0.6 rad/s, the Torsethaugen spectrum reduces to a one-peak spectrum where swell dominates. For peak frequencies  $\omega_0 > 0.6$  rad/s the two characteristic peaks shown in Figure 10.10 clearly appear. This is due to the fact that developing waves have energy at high frequencies compared to swell. This combined effect is very common in the North Sea, and it makes DP and autopilot design a challenging task in terms of wave filtering.

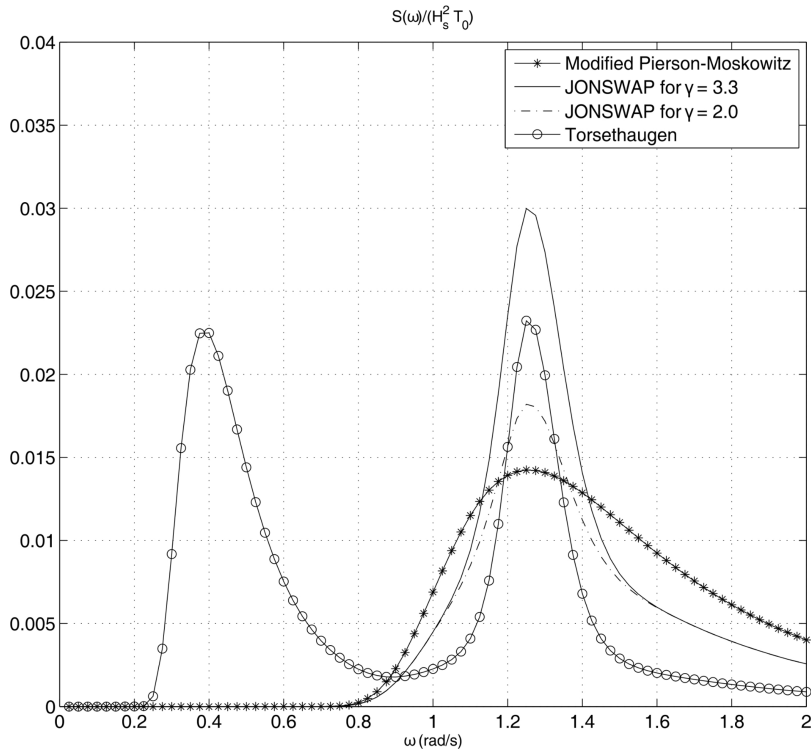


Figure 10.11: Comparison of different wave spectra.

**Matlab:**

The different wave spectra when plotted for the same wave height and peak frequency are shown in Figure 10.11. The plots are generated by using the wave demo option in the MSS toolbox:

```
gncdemo;
```

### Second-order wave transfer function approximation

The nonlinear wave spectra can be approximated by a second-order transfer function

$$h(s) = \frac{\xi}{w}(s) = \frac{K_w s}{s^2 + 2\lambda\omega_0 s + \omega_0^2} \quad (10.66)$$

where  $w$  is zero-mean Gaussian white noise and  $\xi$  is the wave elevation. It is convenient to define the gain constant according to

$$K_w = 2\lambda\omega_0\sigma \quad (10.67)$$

where  $\sigma$  is a constant describing the wave intensity,  $\lambda$  is a damping coefficient and  $\omega_0$  is the dominating wave frequency.

Consequently, substituting  $s = j\omega$  yields the frequency response

$$h(j\omega) = \frac{j 2(\lambda \omega_0 \sigma) \omega}{(\omega_0^2 - \omega^2) + j 2\lambda \omega_0 \omega} \quad (10.68)$$

The magnitude of  $h(j\omega)$  becomes

$$|h(j\omega)| = \frac{2(\lambda \omega_0 \sigma) \omega}{\sqrt{(\omega_0^2 - \omega^2)^2 + 4(\lambda \omega_0 \omega)^2}} \quad (10.69)$$

Hence, the power spectral density (PSD) function for  $\xi(s)$  can be computed as

$$P_{\xi\xi}(\omega) = |h(j\omega)|^2 P_{ww}(\omega) = |h(j\omega)|^2 \quad (10.70)$$

since  $P_{ww}(\omega) = 1$ . The ultimate goal is to design an approximation  $P_{\xi\xi}(\omega)$  to  $S(\omega)$ , for instance by means of nonlinear regression, such that  $P_{\xi\xi}(\omega)$  reflects the energy distribution of  $S(\omega)$  in the relevant frequency range. From (10.70), we obtain

$$P_{\xi\xi}(\omega) = \frac{4(\lambda \omega_0 \sigma)^2 \omega^2}{(\omega_0^2 - \omega^2)^2 + 4(\lambda \omega_0 \omega)^2} \quad (10.71)$$

### Determination of $\sigma$ and $\lambda$

Since the maximum value of  $P_{\xi\xi}(\omega)$  and  $S(\omega)$  are obtained for  $\omega = \omega_0$ , it follows that

$$\begin{aligned} P_{\xi\xi}(\omega_0) &= S(\omega_0) \\ &\Updownarrow \end{aligned} \quad (10.72)$$

$$\sigma^2 = \max_{0 < \omega < \infty} S(\omega) \quad (10.73)$$

For the PM spectrum (10.53) this implies

$$\sigma = \sqrt{\frac{A}{\omega_0^5} \exp\left(-\frac{B}{\omega_0^4}\right)} \quad (10.74)$$

while the term  $\gamma^{Y(\omega_0)}$  must be included for the JONSWAP spectrum. The damping ratio  $\lambda$  can be computed by requiring that the energy, that is the areas under  $P_{\xi\xi}(\omega)$  and  $S(\omega)$  of the spectra, be equal.

An alternative approach is to use nonlinear least-squares (NLS) to compute  $\lambda$  such that  $P_{\xi\xi}(\omega)$  fits  $S(\omega)$  in a least-squares sense; see Figure 10.13. This is demonstrated in Example 10.1 using the Matlab optimization toolbox.

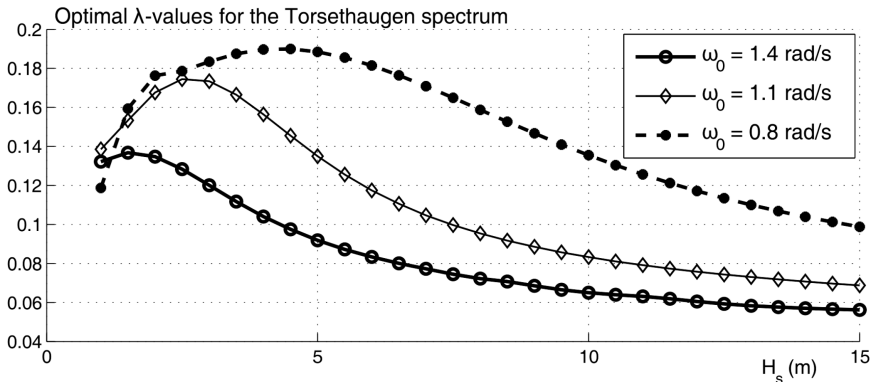


Figure 10.12: Least-squares optimal  $\lambda$  values for the Torsethaugen spectrum for varying  $H_s$  and  $\omega_0$  when a linear spectrum is fitted to the high-frequency peak of the spectrum.

### **Example 10.1 (Nonlinear Least-Squares Optimization of Linear Spectra)**

Consider the Matlab script `ExLinspec.m` for computation of  $\lambda$ . The output of the nonlinear optimization process gives the following  $\lambda$  values for the modified PM and JONSWAP spectra:

$\omega_0$	0.5	0.8	1.1	1.4	Recommended value
$\lambda$ (MPM)	0.2565	0.2573	0.2588	0.2606	0.26
$\lambda$ (JONSWAP)	0.1017	0.1017	0.1017	0.1017	0.10

The  $\lambda$  value for both these spectra are independent of the wave height  $H_s$ . For the Torsethaugen spectrum the  $\lambda$  values vary with both  $H_s$  and  $\omega_0$  as shown in Figure 10.12. The results of the curve-fitting procedure for the three different spectra are shown in Figure 10.13. Since the Torsethaugen spectrum is a two-peaked spectrum a second linear spectrum should be added to fit the swell peak at low frequencies.

#### **Matlab:**

Power spectral density function:

```

function Pyy = Slin(lambda,w)
% Pyy = Slin(lambda,w) 2nd-order linear PSD function
% w = wave spectrum frequency (rad/s)
% lambda = relative damping factor

global sigma wo
Pyy = 4*(lambda*wo*sigma)^2*w.^2 ./ ( (wo^2-w.^2).^2 + ...
4*(lambda*wo.*w).^2 );

```

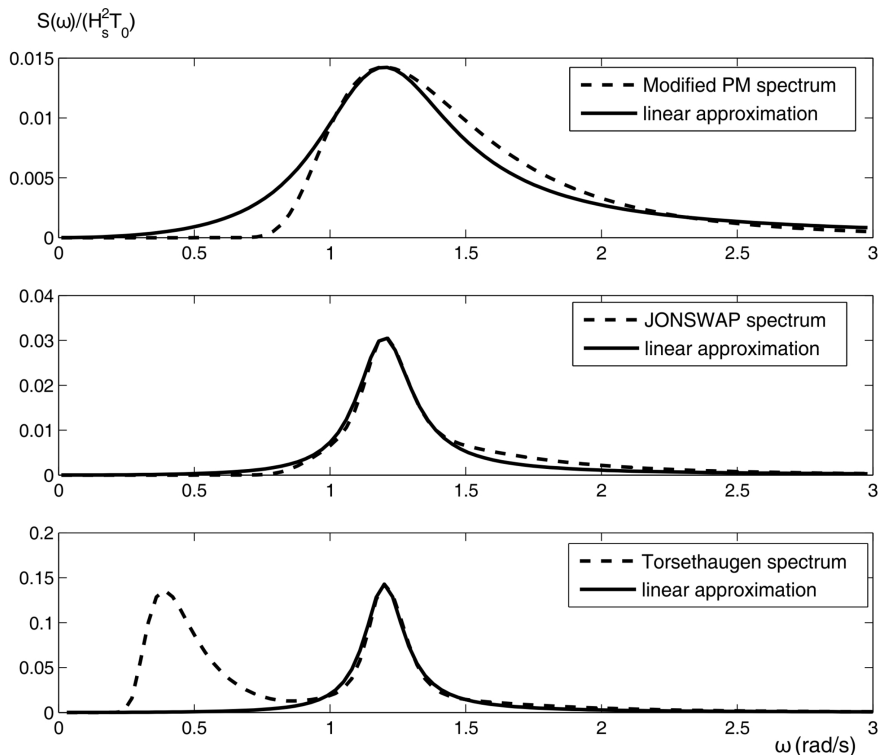


Figure 10.13: Nonlinear least-squares fit of a linear spectrum to the PM, JONSWAP and Torsethaugen spectra. Only one peak is approximated for the Torsethaugen spectrum.

**Matlab:**

Nonlinear least-squares:

```
% Script for plotting the nonlinear least-squares fit, see ...
ExLinspec.m
global sigma wo

wo = 0.8; Hs = 10; wmax = 3;
To = 2*pi/wo;
w = (0.0001:0.01:wmax)';

% Modified PM
subplot(311)
S = wavespec(3,[Hs,To],w,1); sigma = sqrt(max(S));
lambda = lsqcurvefit('Slin', 0.1, w, S)
hold on; plot(w,Slin(lambda,w),'linewidth',2); hold off;
legend('Modified PM spectrum','Linear approximation')
```

```
% JONSWAP
subplot(312)
S = wavespec(7,[Hs,wo,3.3],w,1); sigma = sqrt(max(S));
lambda = lsqcurvefit('Slin', 0.1, w, S)
hold on; plot(w,Slin(lambda,w),'linewidth',2); hold off;
legend('JONSWAP spectrum','Linear approximation')

% Torsethaugen (only one peak is fitted)
subplot(313)
S = wavespec(8,[Hs,wo],w,1); sigma = sqrt(max(S));
lambda = lsqcurvefit('Slin', 0.1, w, S)
hold on; plot(w,Slin(lambda,w),'linewidth',2); hold off;
legend('Torsethaugen spectrum','Linear approximation')
```

### 10.2.3 Wave amplitude response model

The relationship between the wave spectrum  $S(\omega_k)$  and the wave amplitude  $A_k$  for a wave component, subscript  $k$ , is (Faltinsen, 1990)

$$\frac{1}{2}A_k^2 = S(\omega_k)\Delta\omega \quad (10.75)$$

where  $\Delta\omega$  is a constant difference between the frequencies  $\omega_k$ . Formula (10.75) can be used to compute wave-induced responses in the time domain.

#### Long-crested irregular sea

The wave elevation of a *long-crested* irregular sea in the origin of  $\{s\}$  of the seakeeping reference frame under the assumption of zero speed can be written as the sum of  $N$  harmonic components

$$\begin{aligned} \xi &= \sum_{k=1}^N A_k \cos(\omega_k t + \epsilon_k) \\ &= \sum_{k=1}^N \sqrt{2S(\omega_k)\Delta\omega} \cos(\omega_k t + \epsilon_k) \end{aligned} \quad (10.76)$$

where  $\epsilon_k$  is the random phase angle of wave component number  $k$ . Since this expression repeats itself after a time  $2\pi/\Delta\omega$  a large number of wave components  $N$  are needed. However, a practical way to avoid this is to choose  $\omega_k$  randomly in the interval

$$\left[ \omega_k - \frac{\Delta\omega}{2}, \omega_k + \frac{\Delta\omega}{2} \right] \quad (10.77)$$

implying that good results can be obtained for  $N$  in the range 50–100.

The wave frequencies relate to the wave numbers through the *dispersion relation*

$$\omega^2 = kg \tanh(kh) \stackrel{kh \gg 1}{\approx} kg \quad (10.78)$$

where  $h$  is the water depth. It is possible to compute the wave elevation along the  $x$  and  $y$  axes for a given wave direction  $\beta$  (see Figure 10.14) by modifying (10.76) as

$$\xi = \sum_{k=1}^N \sqrt{2S(\omega_k)\Delta\omega} \cos(\omega_k t - k_k x \cos(\beta) - k_k y \sin(\beta) + \epsilon_k) \quad (10.79)$$

where the wave component numbers  $k_k$  are computed for each wave frequency  $\omega_k$  using (10.78).

### Short-crested irregular sea

The most likely situation encountered at sea is *short-crested* or confused waves. This is observed as irregularities along the wave crest at right angles to the direction of the wind. The effect of short-crestedness can be modeled by a 2-D wave spectrum

$$S_M(\omega, \mu) = S(\omega)M(\mu) \quad (10.80)$$

where  $\mu = 0$  is the main wave propagation direction and  $\mu$  will spread the energy over a certain angle contained within  $[-\pi/2, \pi/2]$  from the wind direction. The energy is preserved by requiring that

$$\int_{-\pi/2}^{\pi/2} M(\mu) = 1 \quad (10.81)$$

A commonly used spreading function is

$$M(\mu) = \begin{cases} \frac{2}{\pi} \cos^2(\mu), & -\pi/2 \leq \mu \leq \pi/2 \\ 0, & \text{elsewhere} \end{cases} \quad (10.82)$$

For this case (10.76) becomes

$$\xi = \sum_{k=1}^N \sum_{i=1}^M \sqrt{2S_M(\omega_k, \mu_i - \beta)\Delta\omega\Delta\mu} \cos(\omega_k t + \epsilon_{i,k}) \quad (10.83)$$

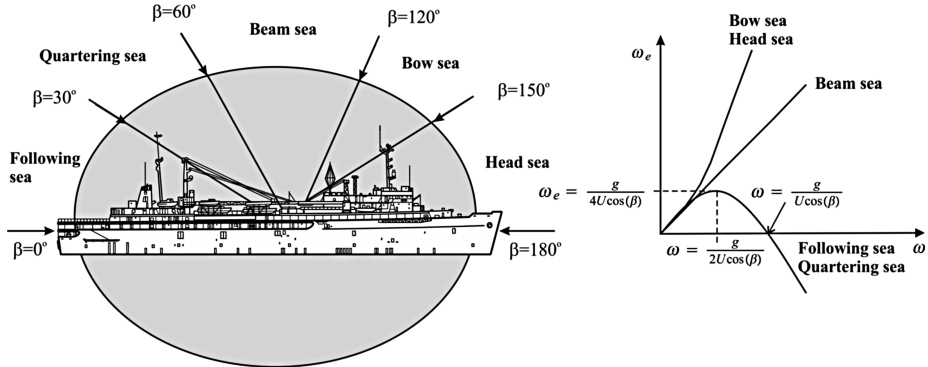
where  $\beta$  is the mean wave encounter angle and  $\mu_i$  is taken randomly in the interval

$$\left[ \mu_i - \frac{\Delta\mu}{2}, \mu_i + \frac{\Delta\mu}{2} \right] \quad (10.84)$$

These equations effectively represent the first block in Figures 10.15–10.16.

### Extension to forward speed using the frequency of encounter

For a marine craft moving at forward speed  $U$ , the peak frequency  $\omega_0$  of the spectrum will be shifted according to

Figure 10.14: Definition of encounter angle  $\beta$ .

$$\omega_e(U, \omega_0, \beta) = \left| \omega_0 - \frac{\omega_0^2}{g} U \cos(\beta) \right| \quad (10.85)$$

where

- $\omega_e$  encounter frequency (rad/s)
- $\omega_0$  wave spectrum peak frequency (rad/s)
- $g$  acceleration of gravity ( $\text{m/s}^2$ )
- $U$  total speed of ship (m/s)
- $\beta$  wave encounter angle (rad)

The definition of the encounter angle  $\beta$  is shown in Figure 10.14. The expression for the wave elevation (10.83) can be redefined in terms of the frequency of encounter  $\omega_e$  and encounter angle  $\beta$  for a ship moving at forward speed  $U > 0$ . Moreover,

$$\xi = \sum_{k=1}^N \sum_{i=1}^N \sqrt{2S_M(\omega_k, \mu_i - \beta)} \Delta\omega \Delta\mu \cos \left( \omega_k t - \frac{\omega_k^2}{g} U \cos(\mu_i - \beta) t + \epsilon_{i,k} \right) \quad (10.86)$$

This modification is particular useful for ship maneuvering.

#### 10.2.4 Force RAOs

Force RAOs can be computed for a particular craft using a hydrodynamic program where the hull geometry is specified in an input file. These programs are usually based on potential theory, as described in Section 5.1. Since the equations of motions of a moving craft are expressed in terms of Newton's second law

$$M\dot{\nu} = \sum_{i=1}^K \tau_i \quad (10.87)$$

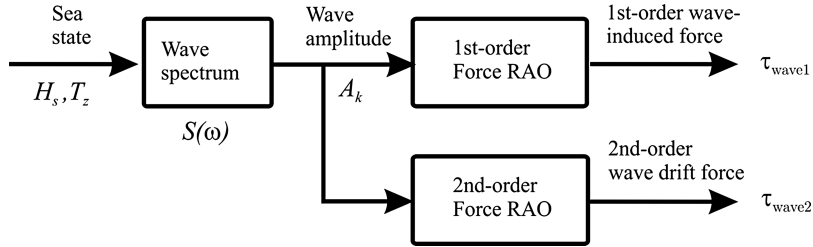


Figure 10.15: Representation of the wave-induced forces as the product of two transfer functions.

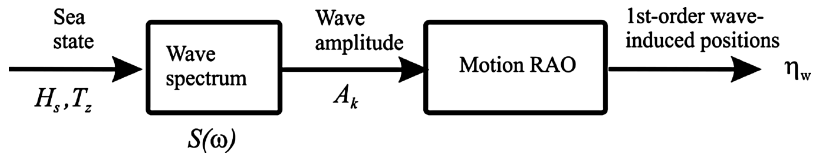


Figure 10.16: Computational setup for first-order wave-induced positions based on motion RAOs.

it is advantageous to represent the wave loads as generalized wave-induced forces

$$\tau = \tau_{\text{wave1}} + \tau_{\text{wave2}} \quad (10.88)$$

The wave force responses are computed for different sea states by using a wave spectrum  $S(\omega)$  to describe the wave amplitude components  $A_k$  as discussed in Section 10.2.3. The force RAO relates the wave amplitudes to the wave-induced force, as shown in Figure 10.15. The necessary equations that are needed to represent the force RAOs and compute the wave-induced forces in the time domain are presented now. The Simulink code for this is included in the MSS toolbox.

### Normalized force RAOs

The first- and second-order wave forces for varying wave directions  $\beta_i$  and wave frequencies  $\omega_k$  are denoted  $\tilde{\tau}_{\text{wave1}}^{\{\text{dof}\}}(\omega_k, \beta_i)$  and  $\tilde{\tau}_{\text{wave2}}^{\{\text{dof}\}}(\omega_k, \beta_i)$  where  $\text{dof} \in \{1, 2, 3, 4, 5, 6\}$ . The normalized force RAOs are complex variables (WAMIT 2010)

$$F_{\text{wave1}}^{\{\text{dof}\}}(\omega_k, \beta_i) = \left| \frac{\tilde{\tau}_{\text{wave1}}^{\{\text{dof}\}}(\omega_k, \beta_i)}{\rho g A_k} \right| e^{j\angle \tilde{\tau}_{\text{wave1}}^{\{\text{dof}\}}(\omega_k, \beta_i)} \quad (10.89)$$

$$F_{\text{wave2}}^{\{\text{dof}\}}(\omega_k, \beta_i) = \left| \frac{\tilde{\tau}_{\text{wave2}}^{\{\text{dof}\}}(\omega_k, \beta_i)}{\rho g A_k^2} \right| e^{j\angle \tilde{\tau}_{\text{wave2}}^{\{\text{dof}\}}(\omega_k, \beta_i)} \quad (10.90)$$

The output from the hydrodynamic code is usually an ASCII file containing RAOs in table format. Let us denote the imaginary and real parts of the force RAOs by two Matlab structures:  $\text{Im}_{\text{wave1}}\{\text{dof}\}(k, i)$  and  $\text{Re}_{\text{wave1}}\{\text{dof}\}(k, i)$ . The amplitudes and

phases for different frequencies  $\omega_k$  and encounter angles  $\beta_i$  for the first-order wave-induced forces can be computed according to the formulae

$$\left| F_{\text{wave1}}^{\{\text{dof}\}}(\omega_k, \beta_i) \right| = \sqrt{\text{Im}_{\text{wave1}}\{\text{dof}\}(k, i)^2 + \text{Re}_{\text{wave1}}\{\text{dof}\}(k, i)^2} \quad (10.91)$$

$$\angle F_{\text{wave1}}^{\{\text{dof}\}}(\omega_k, \beta_i) = \text{atan2}(\text{Im}_{\text{wave1}}\{\text{dof}\}(k, i), \text{Re}_{\text{wave1}}\{\text{dof}\}(k, i)) \quad (10.92)$$

The amplitudes and phases for the second-order mean forces are

$$\left| F_{\text{wave2}}^{\{\text{dof}\}}(\omega_k, \beta_i) \right| = \text{Re}_{\text{wave2}}\{\text{dof}\}(k, i) \quad (10.93)$$

$$\angle F_{\text{wave2}}^{\{\text{dof}\}}(\omega_k, \beta_i) = 0 \quad (10.94)$$

### Matlab:

The motion RAOs are processed in the MSS Hydro Matlab toolbox by using m-file commands:

```
wamit2vessel % read and process WAMIT data
veres2vessel % read and process ShipX (Veres) data
```

The data are represented in the workspace as Matlab structures:

```
vessel.forceRAO.w(k) % frequencies
vessel.forceRAO.amp{dof}(k, i, speed_no) % amplitudes
vessel.forceRAO.phase{dof}(k, i, speed_no) % phases
```

where  $\text{speed\_no} = 1$  represents  $U = 0$ . For the mean drift forces only surge, sway and yaw are considered ( $\text{dof} \in \{1, 2, 6\}$  where the third component corresponds to yaw)

```
vessel.driftfrc.w(k) % frequencies
vessel.driftfrc.amp{dof}(k, i, speed_no) % amplitudes
```

It is possible to plot the force RAOs using

```
plotTF % plot transfer function
plotWD % plot wave drift
```

## Wave forces

Since the first- and second-order wave forces are represented in terms of the complex variables  $F_{\text{wave1}}^{\{\text{dof}\}}(\omega_k, \beta_i)$  and  $F_{\text{wave2}}^{\{\text{dof}\}}(\omega_k, \beta_i)$ , the responses for sinusoidal excitations can be computed using different wave spectra. When doing this, linear superposition is employed as illustrated in Figure 10.15. Let the wave-induced forces in 6 DOF be denoted by vectors

$$\boldsymbol{\tau}_{\text{wave1}} = \left[ \tau_{\text{wave1}}^{(1)}, \tau_{\text{wave1}}^{(2)}, \tau_{\text{wave1}}^{(3)}, \tau_{\text{wave1}}^{(4)}, \tau_{\text{wave1}}^{(5)}, \tau_{\text{wave1}}^{(6)} \right]^T \quad (10.95)$$

$$\boldsymbol{\tau}_{\text{wave2}} = \left[ \tau_{\text{wave2}}^{(1)}, \tau_{\text{wave2}}^{(2)}, \tau_{\text{wave2}}^{(3)}, \tau_{\text{wave2}}^{(4)}, \tau_{\text{wave2}}^{(5)}, \tau_{\text{wave2}}^{(6)} \right]^T \quad (10.96)$$

### Wave forces (no spreading function)

For the no spreading case, the encounter angle  $\beta = \text{constant}$  such that

$$\begin{aligned}\tau_{\text{wave1}}^{\{\text{dof}\}} &= \sum_{k=1}^N \rho g \left| F_{\text{wave1}}^{\{\text{dof}\}}(\omega_k, \beta) \right| A_k \cos \left( \omega_e(U, \omega_k, \beta)t + \angle F_{\text{wave1}}^{\{\text{dof}\}}(\omega_k, \beta) + \epsilon_k \right) \\ &= \sum_{k=1}^N \rho g \left| F_{\text{wave1}}^{\{\text{dof}\}}(\omega_k, \beta) \right| \sqrt{2S(\omega_k)\Delta\omega} \\ &\quad \cos \left( \omega_e(U, \omega_k, \beta)t + \angle F_{\text{wave1}}^{\{\text{dof}\}}(\omega_k, \beta) + \epsilon_k \right)\end{aligned}\quad (10.97)$$

$$\begin{aligned}\tau_{\text{wave2}}^{\{\text{dof}\}} &= \sum_{k=1}^N \rho g \left| F_{\text{wave2}}^{\{\text{dof}\}}(\omega_k, \beta) \right| A_k^2 \\ &= \sum_{k=1}^N \rho g \left| F_{\text{wave2}}^{\{\text{dof}\}}(\omega_k, \beta) \right| 2S(\omega_k)\Delta\omega\end{aligned}\quad (10.98)$$

where

$$\omega_e(U, \omega_k, \beta) = \omega_k - \frac{\omega_k^2}{g} U \cos(\beta) \quad (10.99)$$

### Wave forces (spreading function)

The more general case, where the spreading function (10.80) is included, can be simulated by using varying wave directions  $\mu_i$  ( $i = 1, \dots, M$ ) and

$$\begin{aligned}\tau_{\text{wave1}}^{\{\text{dof}\}} &= \sum_{k=1}^N \sum_{i=1}^M \rho g \left| F_{\text{wave1}}^{\{\text{dof}\}}(\omega_k, \mu_i - \beta) \right| \sqrt{2S_M(\omega_k, \mu_i - \beta)\Delta\omega\Delta\mu} \\ &\quad \cos \left( \omega_e(U, \omega_k, \mu_i - \beta)t + \angle F_{\text{wave1}}^{\{\text{dof}\}}(\omega_k, \mu_i - \beta) + \epsilon_{i,k} \right)\end{aligned}\quad (10.100)$$

$$\tau_{\text{wave2}}^{\{\text{dof}\}} = \sum_{k=1}^N \sum_{i=1}^M \rho g \left| F_{\text{wave2}}^{\{\text{dof}\}}(\omega_k, \mu_i - \beta) \right| 2S_M(\omega_k, \mu_i - \beta)\Delta\omega\Delta\mu \quad (10.101)$$

### 10.2.5 Motion RAOs

An alternative to the force RAO representation in Section 10.2.4 is to use motion RAOs for position, velocity and acceleration to compute the wave-induced motions, see Section 5.3.3. For force RAOs the response will be generalized forces as shown in Figure 10.15. However, in a linear system it is possible to move the forces through the chain of integrators to obtain generalized position. The first-order wave-induced forces,  $\tau_{\text{wave1}}$ , are zero-mean oscillatory wave forces. Consider the linear system

$$[M_{RB} + A(\omega_e)]\ddot{\xi} + B_{\text{total}}(\omega_e)\dot{\xi} + C\xi = \tau_{\text{wave1}} \quad (10.102)$$

By assuming harmonic motions

$$\xi = \bar{\xi} e^{j\omega_e t}, \quad \tau_{\text{wave1}} = \bar{\xi} e^{j\omega_e t} \quad (10.103)$$

Equation (10.102) can be written

$$-\omega_e^2 [M_{RB} + A(\omega_e)] \bar{\xi} - j\omega_e B_{\text{total}}(\omega_e) \bar{\xi} + C \bar{\xi} = \bar{\tau}_{\text{wave1}} \quad (10.104)$$

The motion responses can be evaluated as

$$\bar{\xi} = H_v(j\omega_e) \bar{\tau}_{\text{wave1}} \quad (10.105)$$

where the *force-to-motion* transfer function

$$H_v(j\omega_e) = [-\omega_e^2 [M_{RB} + A(\omega_e)] - j\omega_e B_{\text{total}}(\omega_e) + C]^{-1} \quad (10.106)$$

is a low-pass filter representing the vessel dynamics. This expression confirms that the first-order wave-induced position can be computed by low-pass filtering the generalized forces  $\tau_{\text{wave1}}$ . Since the wave-induced forces,  $\tau_{\text{wave1}}$ , are computed using linear theory, the wave-induced positions,  $\bar{\xi}$ , are linear responses, which can be modeled by RAOs. Notice that the motion RAOs depend on the model matrices  $M_{RB}$ ,  $A(\omega_e)$ ,  $B_{\text{total}}(\omega_e)$  and  $C$  while force RAOs are only dependent on the wave excitations.

Hydrodynamic programs compute both the motion and force RAOs. Let us denote the first-order wave-induced positions in  $\{n\}$  by the vector

$$\eta_w = [\eta_w^{\{1\}}, \eta_w^{\{2\}}, \eta_w^{\{3\}}, \eta_w^{\{4\}}, \eta_w^{\{5\}}, \eta_w^{\{6\}}]^T \quad (10.107)$$

such that the total motion becomes

$$y = \eta + \eta_w \quad (10.108)$$

### Generalized position (no spreading function)

The wave-induced positions are computed according to (see Figure 10.16)

$$\begin{aligned} \eta_w^{\{\text{dof}\}} &= \sum_{k=1}^N \left| \eta_w^{\{\text{dof}\}}(\omega_k, \beta) \right| A_k \cos \left( \omega_e(U, \omega_k, \beta)t + \angle \eta_w^{\{\text{dof}\}}(\omega_k, \beta) + \epsilon_k \right) \\ &= \sum_{k=1}^N \left| \eta_w^{\{\text{dof}\}}(\omega_k, \beta) \right| \sqrt{2S(\omega_k)\Delta\omega} \cos \left( \omega_e(U, \omega_k, \beta)t + \angle \eta_w^{\{\text{dof}\}}(\omega_k, \beta) + \epsilon_k \right) \end{aligned} \quad (10.109)$$

### Generalized position (spreading function)

The spreading function (10.80) is included by using varying wave directions  $\mu_i$  ( $i = 1, \dots, M$ ) and

$$\eta_w^{\{dof\}} = \sum_{k=1}^N \sum_{i=1}^M \left| \eta_w^{\{dof\}}(\omega_k, \mu_i - \beta) \right| \sqrt{2S_M(\omega_k, \mu_i - \beta) \Delta\omega \Delta\mu} \cos \left( \omega_e(U, \omega_k, \mu_i - \beta) t + \angle \eta_w^{\{dof\}}(\omega_k, \mu_i - \beta) + \epsilon_{i,k} \right) \quad (10.110)$$

where  $|\eta_w^{\{dof\}}(\omega_k, \mu_i - \beta)|$  and  $\angle \eta_w^{\{dof\}}(\omega_k, \mu_i - \beta)$  are the motion RAO amplitude and phase for frequency  $\omega_k$  and encounter angle  $\beta_i = \mu_i - \beta$ . This expression does not contain the second-order wave-induced forces. Consequently, wave drift forces must be added manually, for instance by using the wave drift force RAO to compute  $\tau_{\text{wave2}}^{\{dof\}}$ .

### Matlab:

The motion and forces RAOs for the supply vessel in the MSS toolbox can be plotted in 6 DOF using the following commands (see Figures 10.17–10.18):

```

load supply;

for DOF = 1:6
    figure(DOF);

    % Plot motion RAO
    w      = vessel.motionRAO.w;
    amp   = vessel.motionRAO.amp;
    phase = vessel.motionRAO.phase;
    subplot(411); plotRAOamp(w,amp,DOF);
    subplot(412); plotRAOphs(w,phase,DOF);

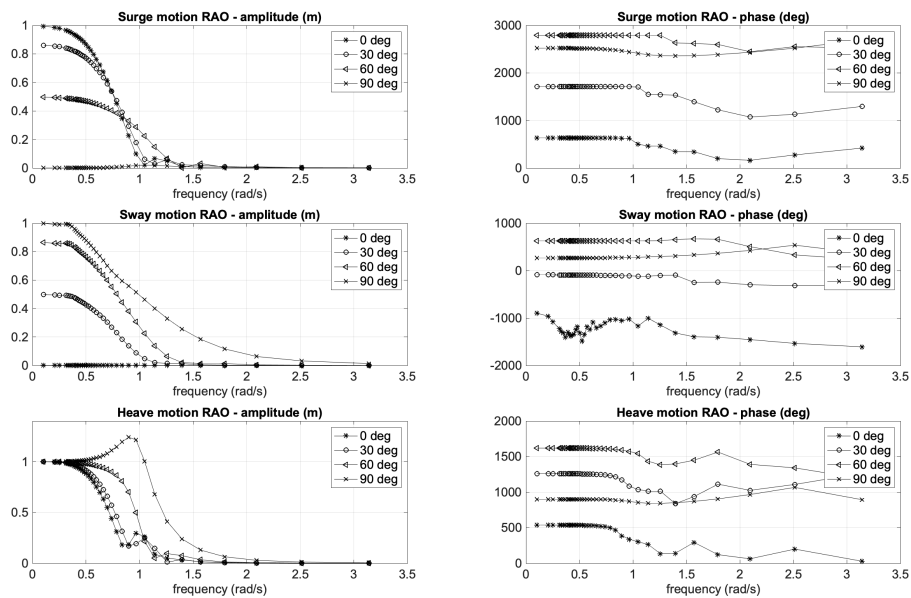
    % Plot force RAO
    w      = vessel.forceRAO.w;
    amp   = vessel.forceRAO.amp;
    phase = vessel.forceRAO.phase;
    subplot(413); plotRAOamp(w,amp,DOF);
    subplot(414); plotRAOphs(w,phase,DOF);

end

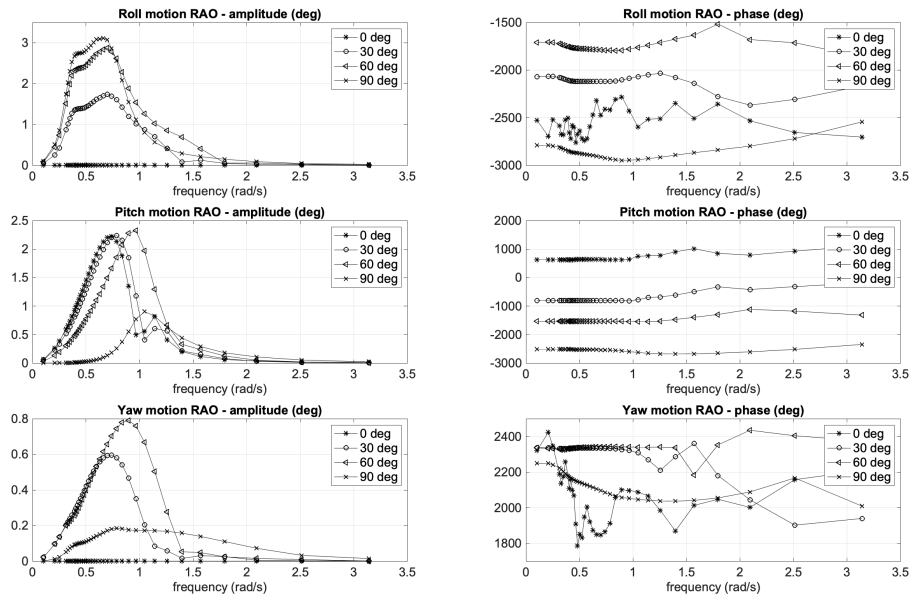
function plotRAOamp(w,amp,DOF)
    velno = 1;
    arg = amp{DOF}(:,:,velno);
    plot(w,arg(:,1),'-*k',w, arg(:,4),'-ko',w, ...
        arg(:,7),'-k<',w, arg(:,10),'-kx');
    legend('0 deg','30 deg','60 deg','90 deg');
    xlabel('wave encounter frequency (rad/s)'), grid;
end

function plotRAOphs(w,phase,DOF)
    velno = 1;
    phs = (180/pi)*unwrap(phase{DOF}(:,:,velno));
    plot(w,phs(:,1),'-*k',w, phs(:,4),'-ko',w, ...
        phs(:,7),'-k<',w, phs(:,10),'-kx');
    legend('0 deg','30 deg','60 deg','90 deg');
    xlabel('wave encounter frequency (rad/s)'), grid;
end

```

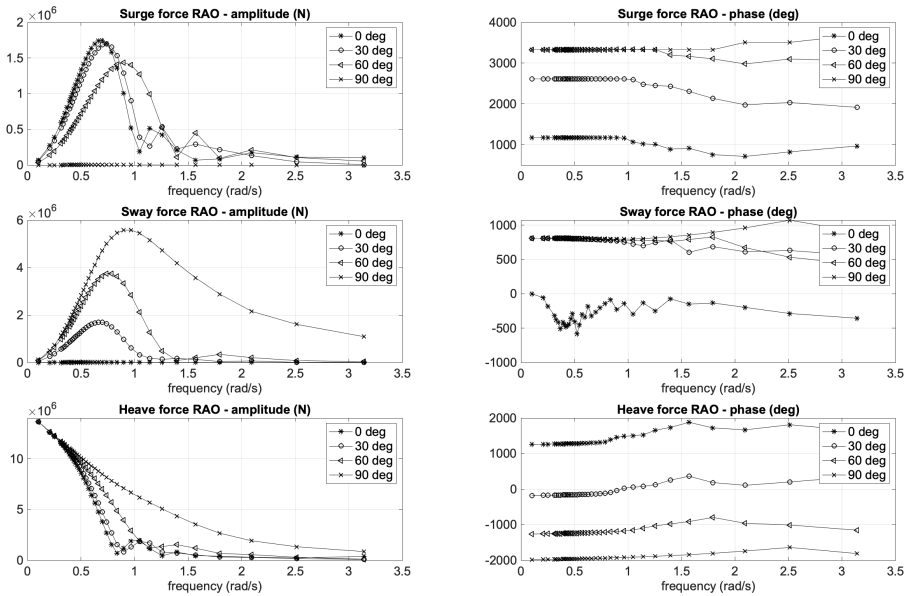


(a) Surge, sway and heave amplitudes (m) and phases (deg).

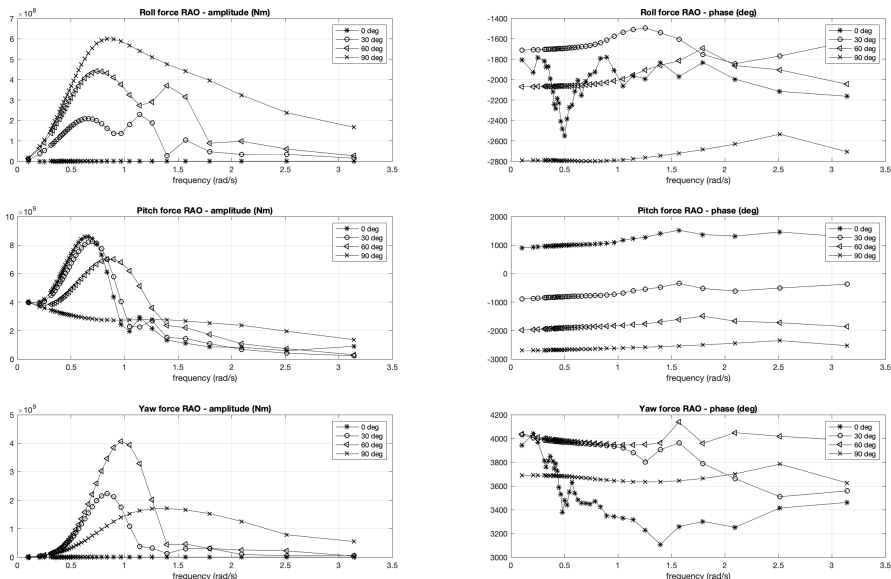


(b) Roll, pitch and yaw amplitudes (deg) and phases (deg)

Figure 10.17: Motion RAOs for the MSS supply vessel.



(a) Surge, sway and heave amplitudes (N) and phases (deg).



(b) Roll, pitch and yaw amplitudes (Nm) and phases (deg)

Figure 10.18: Force RAOs for the MSS supply vessel.

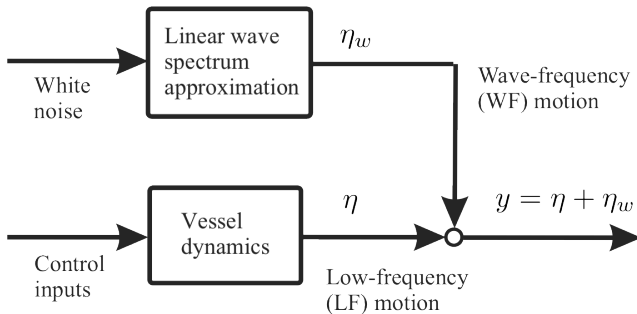


Figure 10.19: Linear approximation for computation of wave-induced positions.

### 10.2.6 State-space models for wave response simulation

When simulating and testing feedback control systems it is useful to have a simple and effective way of representing the wave-induced motions. The force RAO representation discussed in Section 10.2.4 requires that the ship geometry is known a priori and that the user has access to a hydrodynamic program for numerical computation of RAO tables. This is also the case for the motion RAO approach discussed in Section 10.2.5.

An alternative approach is to represent the motion RAO formulation in Figure 10.16 by transfer functions

$$\eta_{w,i}(s) = \frac{K_{w,i} s}{s^2 + 2\lambda\omega_e s + \omega_e^2} w_i(s) \quad (10.111)$$

where the inputs  $w_i(s)$  ( $i = 1, 2, \dots, 6$ ) are zero-mean white noise and  $K_{w,i}$  ( $i = 1, 2, \dots, 6$ ) are constant tunable gains. It is assumed that the ship is sufficiently excited such that all six DOFs oscillate at the encounter frequency  $\omega_e$ . The fixed-gain approximation produces good results in a closed-loop system where the purpose is to test robustness and performance of a feedback control system in the presence of waves. This is done by tuning of the gains until realistic results are obtained. For marine craft it is common to use position test signals  $\eta_{w,1}, \eta_{w,2}$  and  $\eta_{w,3}$  in the magnitude of  $\pm 1.0$  m and attitude test signals  $\eta_{w,4}, \eta_{w,5}$  and  $\eta_{w,6}$  of magnitudes  $\pm 5.0$ – $10.0$  degrees.

The six linear state-space models corresponding to (10.111) are ( $i = 1, 2, \dots, 6$ )

$$\dot{\mathbf{x}}_{w,i} = \mathbf{A}_{w,i} \mathbf{x}_{w,i} + \mathbf{E}_{w,i} w_i \quad (10.112)$$

$$\eta_{w,i} = \mathbf{C}_{w,i} \mathbf{x}_{w,i} \quad (10.113)$$

Expanding this expression yields

$$\dot{\mathbf{x}}_{w,i} = \begin{bmatrix} 0 & 1 \\ -\omega_e^2 & -2\lambda\omega_e \end{bmatrix} \mathbf{x}_{w,i} + \begin{bmatrix} 0 \\ K_{w,i} \end{bmatrix} w_i \quad (10.114)$$

$$\eta_{w,i} = \begin{bmatrix} 0 & 1 \end{bmatrix} \mathbf{x}_{w,i} \quad (10.115)$$

The linear wave response approximation is usually preferred by ship control systems engineers, owing to its simplicity and applicability. The first applications were

reported by Balchen *et al.* (1976) who proposed modeling the *wave-frequency* (WF) motion of a dynamically positioned ship as harmonic oscillators without damping. Later Sælid *et al.* (1983) introduced a damping term  $\lambda$  in the wave model to fit the shape of the PM spectrum better.

Since the WF model as well as the motion RAO approach only models the first-order wave-induced motions it is necessary to include second-order wave drift forces when testing integral action in a feedback control system. The state observer must also be able to handle biased measurements.

The equations of motion, including both the WF motion  $\eta_w$  and the marine craft *low-frequency* (LF) motion  $\eta$ , become (see Figure 10.19)

LF model:	$\dot{\eta} = J_{\Theta}(\eta)(\nu_r + \nu_c)$ $M\ddot{\nu}_r + C(\nu_r)\nu_r + D(\nu_r)\nu_r + g(\eta) + g_0 = \tau_{\text{wind}} + \tau_{\text{wave2}} + \tau \quad (10.116)$
WF models:	$\dot{x}_{w,i} = A_{w,i}x_{w,i} + E_{w,i}w_i, \quad (i = 1, 2, \dots, 6)$ $\eta_{w,i} = C_{w,i}x_{w,i}$
Wave drift:	$\dot{d} = w_d$ $\tau_{\text{wave2}} = d$
Measurement:	$y = \eta + \eta_w + v \quad (10.119)$

where  $v \in \mathbb{R}^6$  and  $w_d \in \mathbb{R}^6$  are zero-mean Gaussian white noise processes. The random walk process  $d \in \mathbb{R}^6$  is used to simulate slowly-varying wave drift forces. From a practical point of view, it might be necessary to saturate the  $d_i$  elements in order to avoid that the drift terms exceeds their maximum physical values. Notice that the effect of  $\tau_{\text{wave1}}$  is included in  $\eta_w$  so this signal is not needed to represent the equations of motion.

### **Example 10.2 (Linear Model for First- and Second-order Wave-Induced Forces)**

A marine control system can be tested under the influence of waves by separating the first- and second-order wave-induced forces. For a surface vessel in 3 DOF ( $i = 1, 2, 6$ ) the WF motions  $\eta_w = [\eta_{w,1}, \eta_{w,2}, \eta_{w,6}]^\top$  can be simulated using three transfer functions

$$\eta_{w,1}(s) = \frac{K_{w,1}s}{s^2 + 2\lambda\omega_e s + \omega_e^2} w_1(s) \quad (10.120)$$

$$\eta_{w,2}(s) = \frac{K_{w,2}s}{s^2 + 2\lambda\omega_e s + \omega_e^2} w_2(s) \quad (10.121)$$

$$\eta_{w,6}(s) = \frac{K_{w,6}s}{s^2 + 2\lambda\omega_e s + \omega_e^2} w_6(s) \quad (10.122)$$

where  $w_i$  ( $i = 1, 2, 6$ ) are zero-mean white noise processes. The wave drift forces

$\tau_{wave2} = [d_1, d_2, d_6]^\top$  can be modeled as slowly-varying bias terms (random walks)

$$\dot{d}_1 = w_{d,1} \quad (10.123)$$

$$\dot{d}_2 = w_{d,2} \quad (10.124)$$

$$\dot{d}_3 = w_{d,6} \quad (10.125)$$

where  $w_{d,i}$  ( $i = 1, 2, 6$ ) are zero-mean white noise processes. The amplitudes  $K_{w,1}$ ,  $K_{w,2}$  and  $K_{w,6}$  are adjusted such that the amplitudes  $\eta_{w,1}$ ,  $\eta_{w,2}$  and  $\eta_{w,6}$  represent a realistic sea state. Notice that the frequency of encounter  $\omega_e$  is used in the transfer functions since the forward speed  $U > 0$ . The wave spectrum parameter  $\lambda$  should be chosen to represent the true sea state. A good approximation is to use the  $\lambda$  values in Example 10.1 while a typical wave peak frequency is  $\omega_0 = 0.8$  rad/s. This value together with the desired wave encounter angle  $\beta$  can be used to compute the encounter frequency

$$\omega_e(U, \omega_0, \beta) = \left| \omega_0 - \frac{\omega_0^2}{g} U \cos(\beta) \right| \quad (10.126)$$

## 10.3 Ocean Current Forces and Moments

Ocean currents are horizontal and vertical circulation systems of ocean waters produced by gravity, wind friction and water density variation in different parts of the ocean. Besides *wind-generated currents*, the heat exchange at the sea surface, together with salinity changes, develop an additional sea current component, usually referred to as *thermohaline currents*. A world map showing the most major ocean surface currents is found in Defant (1961).

The oceans are conveniently divided into two water spheres, the cold and warm water spheres. Since the Earth is rotating, the Coriolis force will try to turn the major currents to the East in the northern hemisphere and West in the southern hemisphere. Finally, the major ocean circulations will also have a tidal component arising from planetary interactions like gravity. In coastal regions and fjords, tidal components can reach very high speeds, in fact speeds of 2–3 m/s or more have been measured.

### Equations of motion including ocean currents

In order to simulate ocean currents and their effect on marine craft motion, the following model can be applied (Fossen 2012)

$$\underbrace{M_{RB}\dot{\nu} + C_{RB}(\nu)\nu + g(\eta) + g_0}_{\text{rigid-body and hydrostatic terms}} + \underbrace{M_A\dot{\nu}_r + C_A(\nu_r)\nu_r + D(\nu_r)\nu_r}_{\text{hydrodynamic terms}} = \tau_{wind} + \tau_{wave} + \tau \quad (10.127)$$

where  $\nu_r = \nu - \nu_c$  is the relative velocity vector. The generalized ocean current

velocity of an irrotational fluid is

$$\boldsymbol{\nu}_c = \underbrace{[u_c, v_c, w_c]}_{\boldsymbol{v}_c^b}, [0, 0, 0]^\top \quad (10.128)$$

where  $u_c, v_c$  and  $w_c$  are expressed in  $\{b\}$ . Moreover,  $\boldsymbol{v}_c^b = [u_c, v_c, w_c]^\top$ . The ocean current velocity vectors in  $\{n\}$  and  $\{b\}$  satisfy

$$\boldsymbol{v}_c^n = \mathbf{R}(\Theta_{nb})\boldsymbol{v}_c^b \quad (10.129)$$

**Definition 10.1 (Irrotational Constant Ocean Current)**

An irrotational constant ocean current in  $\{n\}$  is defined by

$$\dot{\boldsymbol{v}}_c^n = \dot{\mathbf{R}}(\Theta_{nb})\boldsymbol{v}_c^b + \mathbf{R}(\Theta_{nb})\dot{\boldsymbol{v}}_c^b := \mathbf{0} \quad (10.130)$$

where

$$\dot{\mathbf{R}}(\Theta_{nb}) = \mathbf{R}(\Theta_{nb})\mathbf{S}(\boldsymbol{\omega}_{nb}^b) \quad (10.131)$$

Consequently,

$$\dot{\boldsymbol{v}}_c^b = -\mathbf{S}(\boldsymbol{\omega}_{nb}^b)\boldsymbol{v}_c^b \quad (10.132)$$

**Property 10.1 (Irrotational Constant Ocean Currents)**

If the Coriolis and centripetal matrix  $\mathbf{C}_{RB}(\boldsymbol{\nu}_r)$  is parametrized independent of linear velocity  $\boldsymbol{\nu}_1 = [u, v, w]^\top$ , for instance by using (3.60), and the ocean current is irrotational and constant (Definition 10.1), the rigid-body kinetics satisfies (Hegrenæs 2010)

$$\mathbf{M}_{RB}\dot{\boldsymbol{\nu}} + \mathbf{C}_{RB}(\boldsymbol{\nu})\boldsymbol{\nu} = \mathbf{M}_{RB}\dot{\boldsymbol{\nu}}_r + \mathbf{C}_{RB}(\boldsymbol{\nu}_r)\boldsymbol{\nu}_r \quad (10.133)$$

with

$$\boldsymbol{\nu}_r = \begin{bmatrix} \boldsymbol{v}^b - \boldsymbol{v}_c^b \\ \boldsymbol{\omega}_{nb}^b \end{bmatrix} \quad (10.134)$$

**Proof.** Since the Coriolis and centripetal matrix represented by (3.60) is independent of linear velocity  $\boldsymbol{\nu}_1 = [u, v, w]^\top$ , it follows that  $\mathbf{C}_{RB}(\boldsymbol{\nu}_r) = \mathbf{C}_{RB}(\boldsymbol{\nu})$ . The property

$$\mathbf{M}_{RB}\dot{\boldsymbol{\nu}}_c + \mathbf{C}_{RB}(\boldsymbol{\nu}_r)\boldsymbol{\nu}_c = \mathbf{0} \quad (10.135)$$

is easily verified by expanding the matrices  $\mathbf{M}_{RB}$  and  $\mathbf{C}_{RB}(\boldsymbol{\nu}_r)$  and corresponding acceleration and velocity vectors according to

$$\begin{bmatrix} m\mathbf{I}_3 & -m\mathbf{S}(\boldsymbol{r}_g^b) \\ m\mathbf{S}(\boldsymbol{r}_g^b) & \mathbf{I}_b \end{bmatrix} \begin{bmatrix} -\mathbf{S}(\boldsymbol{\omega}_{nb}^b)\boldsymbol{v}_c^b \\ \mathbf{0}_{3 \times 1} \end{bmatrix} + \begin{bmatrix} m\mathbf{S}(\boldsymbol{\omega}_{nb}^b) & -m\mathbf{S}(\boldsymbol{\omega}_{nb}^b)\mathbf{S}(\boldsymbol{r}_g^b) \\ m\mathbf{S}(\boldsymbol{r}_g^b)\mathbf{S}(\boldsymbol{\omega}_{nb}^b) & -\mathbf{S}(\mathbf{I}_b\boldsymbol{\omega}_{nb}^b) \end{bmatrix} \begin{bmatrix} \boldsymbol{v}_c^b \\ \mathbf{0}_{3 \times 1} \end{bmatrix} = \mathbf{0}$$

Finally, it follows that

$$\begin{aligned} \mathbf{M}_{RB}\dot{\boldsymbol{\nu}} + \mathbf{C}_{RB}(\boldsymbol{\nu})\boldsymbol{\nu} &= \mathbf{M}_{RB}[\dot{\boldsymbol{\nu}}_r + \dot{\boldsymbol{\nu}}_c] + \mathbf{C}_{RB}(\boldsymbol{\nu}_r)[\boldsymbol{\nu}_r + \boldsymbol{\nu}_c] \\ &= \mathbf{M}_{RB}\dot{\boldsymbol{\nu}}_r + \mathbf{C}_{RB}(\boldsymbol{\nu}_r)\boldsymbol{\nu}_r \end{aligned} \quad (10.136)$$

### State-space model for relative velocity

Property 10.1 can be used to simplify the the equations of motion (10.127). Moreover,

$$\dot{\boldsymbol{\eta}} = \mathbf{J}_\Theta(\boldsymbol{\eta}) [\boldsymbol{\nu}_r + \boldsymbol{\nu}_c] \quad (10.137)$$

$$\dot{\boldsymbol{\nu}}_r = \mathbf{M}^{-1} (\boldsymbol{\tau}_{\text{wind}} + \boldsymbol{\tau}_{\text{wave}} + \boldsymbol{\tau} - \mathbf{C}(\boldsymbol{\nu}_r)\boldsymbol{\nu}_r - \mathbf{D}(\boldsymbol{\nu}_r)\boldsymbol{\nu}_r - \mathbf{g}(\boldsymbol{\eta}) - \mathbf{g}_0) \quad (10.138)$$

where

$$\mathbf{M} = \mathbf{M}_{RB} + \mathbf{M}_A \quad (10.139)$$

$$\mathbf{C}(\boldsymbol{\nu}_r) = \mathbf{C}_{RB}(\boldsymbol{\nu}_r) + \mathbf{C}_A(\boldsymbol{\nu}_r) \quad (10.140)$$

### State-space model for absolute velocity

The 6-DOF equations of motion (10.138) can also be expressed in terms of absolute velocities

$$\dot{\boldsymbol{\eta}} = \mathbf{J}_\Theta(\boldsymbol{\eta})\boldsymbol{\nu} \quad (10.141)$$

$$\dot{\boldsymbol{\nu}} = \begin{bmatrix} -\mathbf{S}(\boldsymbol{\omega}_{nb}^b)\boldsymbol{v}_c^b \\ \mathbf{0}_{3 \times 1} \end{bmatrix} + \mathbf{M}^{-1} (\boldsymbol{\tau} + \boldsymbol{\tau}_{\text{wind}} + \boldsymbol{\tau}_{\text{wave}} - \mathbf{C}(\boldsymbol{\nu}_r)\boldsymbol{\nu}_r - \mathbf{D}(\boldsymbol{\nu}_r)\boldsymbol{\nu}_r - \mathbf{g}(\boldsymbol{\eta}) - \mathbf{g}_0) \quad (10.142)$$

where  $\boldsymbol{\nu}_r = \boldsymbol{\nu} - [u_c, v_c, w_c, 0, 0, 0]^\top$ . For 3-DOF horizontal-plane (surge, sway and yaw) applications this expression simplifies to

$$\dot{\boldsymbol{\eta}} = \mathbf{R}(\psi)\boldsymbol{\nu} \quad (10.143)$$

$$\dot{\boldsymbol{\nu}} = \begin{bmatrix} rv_c \\ -ru_c \\ 0 \end{bmatrix} + \mathbf{M}^{-1} (\boldsymbol{\tau} + \boldsymbol{\tau}_{\text{wind}} + \boldsymbol{\tau}_{\text{wave}} - \mathbf{C}(\boldsymbol{\nu}_r)\boldsymbol{\nu}_r - \mathbf{D}(\boldsymbol{\nu}_r)\boldsymbol{\nu}_r) \quad (10.144)$$

where  $\boldsymbol{\nu}_r = \boldsymbol{\nu} - [u_c, v_c, 0]^\top$ . A further simplification could be to assume that  $r \approx 0$  (straight-line motion or stationkeeping) such that

$$\dot{\boldsymbol{\nu}} = \mathbf{M}^{-1} (\boldsymbol{\tau} + \boldsymbol{\tau}_{\text{wind}} + \boldsymbol{\tau}_{\text{wave}} - \mathbf{C}(\boldsymbol{\nu}_r)\boldsymbol{\nu}_r - \mathbf{D}(\boldsymbol{\nu}_r)\boldsymbol{\nu}_r) \quad (10.145)$$

We will now turn our attention to simulation models for  $\boldsymbol{\nu}_c$ .

### Current speed and direction

The ocean current speed is denoted by  $V_c$  while its direction relative to the moving craft is conveniently expressed in terms of two angles: *current angle of attack*  $\alpha_c$  and *current sideslip angle*  $\beta_c$  as shown in Figure 2.10 in Section 2.5. For computer simulations the ocean current velocity can be generated by using a first-order *Gauss–Markov process*

$$\dot{V}_c + \mu V_c = w \quad (10.146)$$

where  $w$  is Gaussian white noise and  $\mu \geq 0$  is a constant. If  $\mu = 0$ , this model reduces to a *random walk*, corresponding to time integration of *white noise*. A saturating element is usually used in the integration process to limit the current speed to

$$V_{\min} \leq V_c(t) \leq V_{\max} \quad (10.147)$$

The direction of the current can be fixed by specifying constant values for  $\alpha_c$  and  $\beta_c$ . Time-varying ocean current directions can easily be simulated by associating dynamics to  $\alpha_c$  and  $\beta_c$ .

### 10.3.1 3-D irrotational ocean current model

A 3-D ocean current model is obtained by transforming the current speed  $V_c$  from FLOW axes to NED velocities

$$\mathbf{v}_c^n = \mathbf{R}_{y,\alpha_c}^\top \mathbf{R}_{z,-\beta_c}^\top \begin{bmatrix} V_c \\ 0 \\ 0 \end{bmatrix} \quad (10.148)$$

where the rotation matrices  $\mathbf{R}_{y,\alpha_c}$  and  $\mathbf{R}_{z,-\beta_c}$  are defined in Section 2.5. Expanding (10.148) yields

$$\mathbf{v}_c^n = \begin{bmatrix} V_c \cos(\alpha_c) \cos(\beta_c) \\ V_c \sin(\beta_c) \\ V_c \sin(\alpha_c) \cos(\beta_c) \end{bmatrix} \quad (10.149)$$

which can be transformed to BODY using the Euler angle rotation matrix. Consequently,

$$\begin{bmatrix} u_c \\ v_c \\ w_c \end{bmatrix} = \mathbf{R}^\top(\Theta_{nb}) \mathbf{v}_c^n \quad (10.150)$$

and

$$\boldsymbol{\nu}_c = [u_c, v_c, w_c, 0, 0, 0]^\top \quad (10.151)$$

### 10.3.2 2-D irrotational ocean current model

For the 2-D case (motions in the horizontal plane), the 3-D equations (10.149) with  $\alpha_c = 0$  reduce to

$$\mathbf{v}_c^n = \begin{bmatrix} V_c \cos(\beta_c) \\ V_c \sin(\beta_c) \\ 0 \end{bmatrix} \quad (10.152)$$

Hence, from (10.150) it follows that

$$u_c = V_c \cos(\beta_c - \psi), \quad v_c = V_c \sin(\beta_c - \psi) \quad (10.153)$$

Notice that

$$V_c = \sqrt{u_c^2 + v_c^2} \quad (10.154)$$

**Example 10.3 (Maneuvering Model including Ocean Currents)**

Consider the linearized maneuvering model

$$\begin{bmatrix} m_{11} & m_{12} & 0 \\ m_{21} & m_{22} & 0 \\ 0 & 0 & 1 \end{bmatrix} \begin{bmatrix} \dot{v} - \dot{v}_c \\ \dot{r} \\ \dot{\psi} \end{bmatrix} + \begin{bmatrix} d_{11} & d_{12} & 0 \\ d_{21} & d_{22} & 0 \\ 0 & -1 & 0 \end{bmatrix} \begin{bmatrix} v - v_c \\ r \\ \psi \end{bmatrix} = \begin{bmatrix} b_1 \\ b_2 \\ 0 \end{bmatrix} \delta + \begin{bmatrix} Y_{\text{wind}} \\ N_{\text{wind}} \\ 0 \end{bmatrix} + \begin{bmatrix} Y_{\text{wave}} \\ N_{\text{wave}} \\ 0 \end{bmatrix} \quad (10.155)$$

where  $v$  is the sway velocity,  $r$  is the yaw rate,  $\psi$  is the yaw angle,  $\delta$  is the rudder angle and  $(u_c, v_c)$  are the current velocities given by

$$u_c = V_c \cos(\beta_c - \psi) \quad (10.156)$$

$$v_c = V_c \sin(\beta_c - \psi) \quad (10.157)$$

The transverse current acceleration is

$$\dot{v}_c = -ru_c \quad (10.158)$$

Assume that the current speed  $V_c$  is a Gauss–Markov process (10.146) and the wave direction  $\beta_c = \text{constant}$ . The resulting state-space model is

$$\begin{bmatrix} \dot{v} \\ \dot{r} \\ \dot{\psi} \\ \dot{V}_c \end{bmatrix} = \begin{bmatrix} rV_c \sin(\beta_c - \psi) \\ -rV_c \cos(\beta_c - \psi) \\ 0 \\ 0 \end{bmatrix} + \begin{bmatrix} m_{11} & m_{12} & 0 & 0 \\ m_{21} & m_{22} & 0 & 0 \\ 0 & 0 & 1 & 0 \\ 0 & 0 & 0 & 1 \end{bmatrix}^{-1} \left( \begin{bmatrix} b_1 \\ b_2 \\ 0 \\ 0 \end{bmatrix} \delta + \begin{bmatrix} Y_{\text{wind}} \\ N_{\text{wind}} \\ 0 \\ 0 \end{bmatrix} \right) + \begin{bmatrix} Y_{\text{wave}} \\ N_{\text{wave}} \\ 0 \\ 0 \end{bmatrix} + \begin{bmatrix} -d_{11} & -d_{12} & 0 & 0 \\ -d_{21} & -d_{22} & 0 & 0 \\ 0 & 1 & 0 & 0 \\ 0 & 0 & 0 & -\mu \end{bmatrix} \begin{bmatrix} v \\ r \\ \psi \\ V_c \end{bmatrix} + \begin{bmatrix} d_{11}V_c \sin(\beta_c - \psi) \\ d_{21}V_c \sin(\beta_c - \psi) \\ 0 \\ 0 \end{bmatrix} + \begin{bmatrix} 0 \\ 0 \\ 0 \\ 1 \end{bmatrix} w \quad (10.155)$$

Notice that the state-space model is nonlinear in  $\psi$ ,  $V_c$  and  $\beta_c$  even though the ship model (10.155) was linear.



# Appendices

DRAFT MANUSCRIPT

## Appendix A

# Nonlinear Stability Theory

This appendix briefly reviews some useful results from nonlinear stability theory. The methods are classified according to

- Lyapunov stability of nonlinear *autonomous* systems  $\dot{\mathbf{x}} = \mathbf{f}(\mathbf{x})$ , that is systems where  $\mathbf{f}(\mathbf{x})$  does not explicitly depend on the time  $t$ .
- Lyapunov stability of nonlinear *nonautonomous* systems  $\dot{\mathbf{x}} = \mathbf{f}(\mathbf{x}, t)$ , that is systems where  $\mathbf{f}(\mathbf{x}, t)$  does depend on  $t$  explicitly.

### A.1 Lyapunov Stability for Autonomous Systems

Before stating the main Lyapunov theorems for *autonomous* systems, the concepts of stability and convergence are briefly reviewed (Khalil 2002).

#### A.1.1 Stability and convergence

Consider the nonlinear time-invariant system

$$\dot{\mathbf{x}} = \mathbf{f}(\mathbf{x}), \quad \mathbf{x}(0) = \mathbf{x}_0 \quad (\text{A.1})$$

where  $\mathbf{x} \in \mathbb{R}^n$  and  $\mathbf{f} : \mathbb{R}^n \rightarrow \mathbb{R}^n$  is assumed to be *locally Lipschitz* in  $\mathbf{x}$ ; that is for each point  $\mathbf{x} \in D \subset \mathbb{R}^n$  there exists a neighborhood  $D_0 \in D$  such that

$$\|\mathbf{f}(\mathbf{x}) - \mathbf{f}(\mathbf{y})\| \leq L \|\mathbf{x} - \mathbf{y}\|, \quad \forall \mathbf{x}, \mathbf{y} \in D_0 \quad (\text{A.2})$$

where  $L$  is called the Lipschitz constant on  $D_0$ .

Let  $\mathbf{x}_e$  denote the equilibrium point of (A.1) given by

$$\mathbf{f}(\mathbf{x}_e) = \mathbf{0} \quad (\text{A.3})$$

The solutions  $\mathbf{x}(t)$  of (A.1) are:

Table A.1: Classification of theorems for stability and convergence

Autonomous systems	$V > 0, \dot{V} < 0$	Lyapunov's direct method	GAS/GES
	$V > 0, \dot{V} \leq 0$	Krasovskii–LaSalle's theorem	GAS
Nonautonomous systems	$V > 0, \dot{V} < 0$	LaSalle–Yoshizawa's theorem	UGAS
	$V \geq 0, \dot{V} \leq 0$	Barbalat's lemma	Convergence

- *bounded*, if there exists a nonnegative function  $0 < \gamma(\mathbf{x}(0)) < \infty$  such that

$$\|\mathbf{x}(t)\| \leq \gamma(\mathbf{x}(0)), \quad \forall t \geq 0 \quad (\text{A.4})$$

In addition, the equilibrium point  $\mathbf{x}_e$  of (A.1) is:

- *stable*, if, for each  $\epsilon > 0$ , there exists a  $\delta(\epsilon) > 0$  such that

$$\|\mathbf{x}(0)\| < \delta(\epsilon) \Rightarrow \|\mathbf{x}(t)\| < \epsilon, \quad \forall t \geq 0 \quad (\text{A.5})$$

- *unstable*, if it is not stable.

- *attractive*, if, for each  $r > 0, \epsilon > 0$ , there exists a  $T(r, \epsilon) > 0$  such that

$$\|\mathbf{x}(0)\| \leq r \Rightarrow \|\mathbf{x}(t)\| \leq \epsilon, \quad \forall t \geq T(r, \epsilon) \quad (\text{A.6})$$

Attractivity implies convergence, that is  $\lim_{t \rightarrow \infty} \|\mathbf{x}(t)\| = 0$ .

- (*locally*) *asymptotically stable (AS)*, if the equilibrium point  $\mathbf{x}_e$  is stable and attractive.
- *globally stable (GS)*, if the equilibrium point  $\mathbf{x}_e$  is stable and  $\delta(\epsilon)$  can be chosen to satisfy  $\lim_{\epsilon \rightarrow \infty} \delta(\epsilon) = \infty$ .
- *global asymptotically stable (GAS)*, if the equilibrium point  $\mathbf{x}_e$  is stable for all  $\mathbf{x}(0)$  (region of attraction  $\mathbb{R}^n$ ).
- (*locally*) *exponentially stable (ES)*, if there exist positive constants  $\alpha, \lambda$  and  $r$  such that

$$\|\mathbf{x}(0)\| < r \Rightarrow \|\mathbf{x}(t)\| < \alpha e^{-\lambda t} \|\mathbf{x}(0)\|, \quad \forall t \geq 0 \quad (\text{A.7})$$

- *globally exponentially stable (GES)*, if there exist positive constants  $\alpha, \lambda$  and  $r$  such that for all  $\mathbf{x}(0)$  (region of attraction  $\mathbb{R}^n$ ):

$$\|\mathbf{x}(t)\| < \alpha e^{-\lambda t} \|\mathbf{x}(0)\|, \quad \forall t \geq 0 \quad (\text{A.8})$$

Different theorems for investigation of stability and convergence will now be presented. A guideline for which theorem that should be applied is given in Table A.1 whereas the different theorems are listed in the forthcoming sections.

Notice that for nonautonomous systems GAS is replaced by *uniform global asymptotic stability (UGAS)* since uniformity is a necessary requirement in the case of time-varying nonlinear systems.

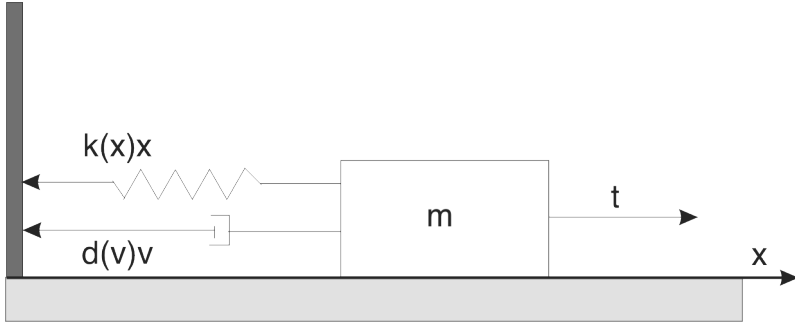


Figure A.1: Mass–damper–spring system.

### A.1.2 Lyapunov's direct method

**Theorem A.1 (Lyapunov's Direct Method)**

Let  $x_e$  be the equilibrium point of (A.1) and assume that  $f(x)$  is locally Lipschitz in  $x$ . Let  $V : \mathbb{R}^n \rightarrow \mathbb{R}_+$  be a continuously differentiable function  $V(x)$  satisfying

$$(i) V(x) > 0 \text{ (positive definite) and } V(0) = 0 \quad (\text{A.9})$$

$$(ii) \dot{V}(x) = \frac{\partial V(x)}{\partial x} f(x) \leq -W(x) \leq 0 \quad (\text{A.10})$$

$$(iii) V(x) \rightarrow \infty \text{ as } \|x\| \rightarrow \infty \text{ (radially unbounded)} \quad (\text{A.11})$$

Then the equilibrium point  $x_e$  is GS if  $W(x) \geq 0$  (positive semidefinite) and GAS if  $W(x) > 0$  (positive definite) for all  $x \neq 0$ .

**Proof.** Khalil (2002).

The requirement that  $W(x) > 0$  such that  $\dot{V}(x) < 0$  is in many cases difficult to satisfy. This is illustrated in the following example.

**Example A.1 (Stability of a Mass–Damper–Spring System)**

Consider the nonlinear mass–damper–spring system

$$\dot{x} = v \quad (\text{A.12})$$

$$m\dot{v} + d(v)v + kx^2 = 0 \quad (\text{A.13})$$

where  $m > 0, d(v) > 0, \forall v$  and  $k > 0$ , see Figure A.1. Let us choose  $V(x)$  as the sum of kinetic energy  $(1/2)mv^2$  and potential energy  $(1/2)kx^2$  such that

$$V(x) = \frac{1}{2} (mv^2 + kx^2) = \frac{1}{2} \mathbf{x}^\top \begin{bmatrix} m & 0 \\ 0 & k \end{bmatrix} \mathbf{x} \quad (\text{A.14})$$

where  $\mathbf{x} = [v, x]^\top$  results in

$$\begin{aligned}\dot{V}(\mathbf{x}) &= mv\dot{v} + kx\dot{x} \\ &= v(m\dot{v} + kx) \\ &= -d(v)v^2 \\ &= -\mathbf{x}^\top \begin{bmatrix} d(v) & 0 \\ 0 & 0 \end{bmatrix} \mathbf{x}\end{aligned}\tag{A.15}$$

Hence, only stability can be concluded from Theorem A.1, since  $\dot{V}(\mathbf{x}) = 0$  for all  $v = 0$ . However, GAS can in many cases also be proven for systems with a negative semidefinite  $\dot{V}(\mathbf{x})$  thanks to the invariant set theorem of Krasovskii–LaSalle; see LaSalle and Lefschetz (1961) and LaSalle (1966).

### A.1.3 Krasovskii–LaSalle’s theorem

The theorem of Krasovskii–LaSalle can be used to check a nonlinear *autonomous* system for GAS in the case of a negative semidefinite  $\dot{V}(\mathbf{x})$ .

**Theorem A.2 (Krasovskii–LaSalle’s Theorem)**

Let  $V : \mathbb{R}^n \rightarrow \mathbb{R}_+$  be a continuously differentiable positive definite function such that

$$V(\mathbf{x}) \rightarrow \infty \text{ as } \|\mathbf{x}\| \rightarrow \infty\tag{A.16}$$

$$\dot{V}(\mathbf{x}) \leq 0, \forall \mathbf{x}\tag{A.17}$$

Let  $\Omega$  be the set of all points where  $\dot{V}(\mathbf{x}) = 0$ , that is

$$\Omega = \left\{ \mathbf{x} \in \mathbb{R}^n \mid \dot{V}(\mathbf{x}) = 0 \right\}\tag{A.18}$$

and  $M$  be the largest invariant set in  $\Omega$ . Then all solutions  $\mathbf{x}(t)$  converge to  $M$ . If  $M = \{\mathbf{x}_e\}$  then the equilibrium point  $\mathbf{x}_e$  of (A.1) is GAS.

**Proof.** LaSalle (1966).

**Example A.2 (Continued Example A.1: Stability of a Mass–Damper–Spring System)**

Again consider the mass–damper–spring system of Example A.1. The set  $\Omega$  is found by requiring that

$$\dot{V}(\mathbf{x}) = -d(v)v^2 \equiv 0\tag{A.19}$$

which is true for  $v = 0$ . Therefore,

$$\Omega = \{(x \in \mathbb{R}, v = 0)\}\tag{A.20}$$

Now,  $v = 0$  implies that  $m\dot{v} = -kx$ , which is nonzero when  $x \neq 0$ . Hence, the system cannot get “stuck” at a point other than  $x = 0$ . Since the equilibrium point of the mass–damper–spring system is  $(x, v) = (0, 0)$ , the largest invariant set  $M$  in  $\Omega$  contains only one point, namely  $(x, v) = (0, 0)$ . Hence, the equilibrium point of (A.1) is GAS according to Theorem A.2.

### A.1.4 Global exponential stability

The following theorem is useful to guarantee global exponential stability.

**Theorem A.3 (Global Exponential Stability)**

Let  $\mathbf{x}_e$  be the equilibrium point of (A.1) and assume that  $\mathbf{f}(\mathbf{x})$  is locally Lipschitz in  $\mathbf{x}$ . Let  $V : \mathbb{R}^n \rightarrow \mathbb{R}_+$  be a continuously differentiable and radially unbounded function satisfying

$$V(\mathbf{x}) = \mathbf{x}^\top \mathbf{P} \mathbf{x} > 0, \quad \forall \mathbf{x} \neq \mathbf{0} \quad (\text{A.21})$$

$$\dot{V}(\mathbf{x}) \leq -\mathbf{x}^\top \mathbf{Q} \mathbf{x} < 0, \quad \forall \mathbf{x} \neq \mathbf{0} \quad (\text{A.22})$$

with constant matrices  $\mathbf{P} = \mathbf{P}^\top > 0$  and  $\mathbf{Q} = \mathbf{Q}^\top > 0$ . Then the equilibrium point  $\mathbf{x}_e$  is GES and the state vector satisfies

$$\|\mathbf{x}(t)\|_2 \leq \sqrt{\frac{\lambda_{\max}(\mathbf{P})}{\lambda_{\min}(\mathbf{P})}} e^{-\alpha t} \|\mathbf{x}(0)\|_2 \quad (\text{A.23})$$

where

$$\alpha = \frac{\lambda_{\min}(\mathbf{Q})}{2\lambda_{\max}(\mathbf{P})} > 0 \quad (\text{A.24})$$

is a bound on the convergence rate.

**Proof.** Since  $V(\mathbf{x})$  is bounded by

$$0 < \lambda_{\min}(\mathbf{P}) \|\mathbf{x}(t)\|_2^2 \leq V(\mathbf{x}) \leq \lambda_{\max}(\mathbf{P}) \|\mathbf{x}(t)\|_2^2, \quad \forall \mathbf{x} \neq \mathbf{0} \quad (\text{A.25})$$

it is seen that

$$-\|\mathbf{x}(t)\|_2^2 \leq -\frac{1}{\lambda_{\max}(\mathbf{P})} V(\mathbf{x}) \quad (\text{A.26})$$

Hence, it follows from (A.22) that

$$\begin{aligned} \dot{V}(\mathbf{x}) &\leq -\mathbf{x}^\top \mathbf{Q} \mathbf{x} \\ &\leq -\lambda_{\min}(\mathbf{Q}) \|\mathbf{x}(t)\|_2^2 \\ &\leq -\underbrace{\frac{\lambda_{\min}(\mathbf{Q})}{\lambda_{\max}(\mathbf{P})}}_{2\alpha} V(\mathbf{x}) \end{aligned} \quad (\text{A.27})$$

Integration of  $\dot{V}(\mathbf{x}(t))$  yields

$$V(\mathbf{x}(t)) \leq e^{-2\alpha t} V(\mathbf{x}(0)) \quad (\text{A.28})$$

Finally, (A.25) implies

$$\lambda_{\min}(\mathbf{P}) \|\mathbf{x}(t)\|_2^2 \leq e^{-2\alpha t} \lambda_{\max}(\mathbf{P}) \|\mathbf{x}(0)\|_2^2 \quad (\text{A.29})$$

$$\|\mathbf{x}(t)\|_2 \leq \sqrt{\frac{\lambda_{\max}(\mathbf{P})}{\lambda_{\min}(\mathbf{P})}} e^{-\alpha t} \|\mathbf{x}(0)\|_2 \quad (\text{A.30})$$

This shows that  $\|\mathbf{x}(t)\|_2$  will converge exponentially to zero with convergence rate  $\alpha$ .

## A.2 Lyapunov Stability of Nonautonomous Systems

In this section several useful theorems for convergence and stability of time-varying nonlinear systems

$$\dot{\mathbf{x}} = \mathbf{f}(\mathbf{x}, t), \quad \mathbf{x}(0) = \mathbf{x}_0 \quad (\text{A.31})$$

where  $\mathbf{x} \in \mathbb{R}^n$ ,  $t \in \mathbb{R}_+$  and  $\mathbf{f} : \mathbb{R}^n \times \mathbb{R}_+ \rightarrow \mathbb{R}^n$  is assumed to be *locally Lipschitz* in  $\mathbf{x}$  and uniformly in  $t$ , are briefly reviewed.

### A.2.1 Barbălat's lemma

**Lemma A.1 (Barbălat's Lemma)**

Let  $\phi : \mathbb{R}_+ \rightarrow \mathbb{R}$  be a uniformly continuous function and suppose that  $\lim_{t \rightarrow \infty} \int_0^t \phi(\tau) d\tau$  exists and is finite; then

$$\lim_{t \rightarrow \infty} \phi(t) = 0 \quad (\text{A.32})$$

**Proof.** Barbălat (1959).

Notice that *Barbălat's lemma* only guarantees *global convergence*. This result is particularly useful if there exists a uniformly continuous function  $V : \mathbb{R}^n \times \mathbb{R}_+ \rightarrow \mathbb{R}$  satisfying

- (i)  $V(\mathbf{x}, t) \geq 0$
- (ii)  $\dot{V}(\mathbf{x}, t) \leq 0$
- (iii)  $\dot{V}(\mathbf{x}, t)$  is uniformly continuous

Hence, according to Barbălat's lemma,  $\lim_{t \rightarrow \infty} \dot{V}(\mathbf{x}, t) = 0$ . The requirement that  $\dot{V}$  should be uniformly continuous can easily be checked by using

$$\ddot{V}(\mathbf{x}, t) \text{ is bounded} \implies \dot{V}(\mathbf{x}, t) \text{ is uniformly continuous}$$

### A.2.2 LaSalle–Yoshizawa's theorem

For nonautonomous systems the following theorem of LaSalle (1966) and Yoshizawa (1968) is quite useful

**Theorem A.4 (LaSalle–Yoshizawa's Theorem)**

Let  $\mathbf{x}_e = \mathbf{0}$  be the equilibrium point of (A.31) and assume that  $\mathbf{f}(\mathbf{x}, t)$  is locally Lipschitz in  $\mathbf{x}$ . Let  $V : \mathbb{R}^n \times \mathbb{R}_+ \rightarrow \mathbb{R}_+$  be a continuously differentiable function  $V(\mathbf{x}, t)$  satisfying

$$(i) \quad V(\mathbf{x}, t) > 0 \text{ (positive definite) and } V(0) = 0 \quad (\text{A.33})$$

$$(ii) \quad \dot{V}(\mathbf{x}, t) = \frac{\partial V(\mathbf{x}, t)}{\partial t} + \frac{\partial V(\mathbf{x}, t)}{\partial \mathbf{x}} \mathbf{f}(\mathbf{x}, t) \leq -W(\mathbf{x}) \leq 0 \quad (\text{A.34})$$

$$(iii) \quad V(\mathbf{x}, t) \rightarrow \infty \text{ as } \|\mathbf{x}\| \rightarrow \infty \text{ (radially unbounded)} \quad (\text{A.35})$$

where  $W(\mathbf{x})$  is a continuous function. Then all solutions  $\mathbf{x}(t)$  of (A.31) are uniformly globally bounded and

$$\lim_{t \rightarrow \infty} W(\mathbf{x}(t)) = 0 \quad (\text{A.36})$$

In addition, if  $W(\mathbf{x}) > 0$  (positive definite), then the equilibrium point  $\mathbf{x}_e = \mathbf{0}$  of (A.31) is UGAS.

*Proof.* LaSalle (1966) and Yoshizawa (1968).

### A.2.3 UGAS when backstepping with integral action

When designing industrial control systems it is important to include integral action in the control law in order to compensate for slowly varying and constant disturbances. This is necessary to avoid steady-state errors both in regulation and tracking. The integral part of the controller can be provided by using *adaptive backstepping* (Krstic *et al.* 1995) under the assumption of constant disturbances (see Section 13.3.4). Unfortunately, the resulting error dynamics in this case often becomes nonautonomous, which again implies that *Krasovskii–LaSalle’s theorem* cannot be used. An alternative theorem for this case will be stated by considering the nonlinear system

$$\dot{\mathbf{x}} = \mathbf{f}(\mathbf{x}, \mathbf{u}, \boldsymbol{\theta}, t) \quad (\text{A.37})$$

where  $\mathbf{x} \in \mathbb{R}^n$ ,  $\mathbf{u} \in \mathbb{R}^n$  and  $\boldsymbol{\theta} \in \mathbb{R}^p$  ( $p \leq n$ ) is a constant *unknown* parameter vector. Furthermore, assume that there exists an adaptive control law

$$\mathbf{u} = \mathbf{u}(\mathbf{x}, \mathbf{x}_d, \hat{\boldsymbol{\theta}}) \quad (\text{A.38})$$

$$\dot{\hat{\boldsymbol{\theta}}} = \phi(\mathbf{x}, \mathbf{x}_d) \quad (\text{A.39})$$

where  $\mathbf{x}_d \in C^r$  and  $\hat{\boldsymbol{\theta}} \in \mathbb{R}^p$ , such that the error dynamics can be written

$$\dot{\mathbf{z}} = \mathbf{h}(\mathbf{z}, t) + \mathbf{B}(t)\tilde{\boldsymbol{\theta}} \quad (\text{A.40})$$

$$\dot{\tilde{\boldsymbol{\theta}}} = -\mathbf{P}\mathbf{B}(t)^\top \left( \frac{\partial W(\mathbf{z}, t)}{\partial \mathbf{z}} \right)^\top, \quad \mathbf{P} = \mathbf{P}^\top > 0 \quad (\text{A.41})$$

where  $W(\mathbf{z}, t)$  is a suitable  $C^1$  function and  $\tilde{\boldsymbol{\theta}} = \hat{\boldsymbol{\theta}} - \boldsymbol{\theta}$  is the parameter estimation error. The parameter estimate  $\hat{\boldsymbol{\theta}}$  can be used to compensate for a constant disturbance, that is integral action. Hence, the conditions in the following theorem can be used to establish UGAS when backstepping with integral action. The conditions are based on Loria *et al.* (1999) or alternatively Fossen *et al.* (2001).

#### Theorem A.5 (UGAS/ULES when Backstepping with Integral Action)

The origin of the system (A.40)–(A.41) is UGAS if  $\mathbf{B}^\top(t)\mathbf{B}(t)$  is invertible for all  $t$ ,  $\mathbf{P} = \mathbf{P}^\top > 0$ , there exists a continuous, nondecreasing function  $\rho : \mathbb{R}_+ \rightarrow \mathbb{R}_+$  such that

$$\max \left\{ \|\mathbf{h}(\mathbf{z}, t)\|, \left\| \frac{\partial W(\mathbf{z}, t)}{\partial \mathbf{z}} \right\| \right\} \leq \rho(\|\mathbf{z}\|) \|\mathbf{z}\| \quad (\text{A.42})$$

and there exist class- $\mathcal{K}_\infty$  functions  $\alpha_1$  and  $\alpha_2$  and a strictly positive real number  $c > 0$  such that  $W(\mathbf{z}, t)$  satisfy

$$\alpha_1(\|\mathbf{z}\|) \leq W(\mathbf{z}, t) \leq \alpha_2(\|\mathbf{z}\|) \quad (\text{A.43})$$

$$\frac{\partial W(\mathbf{z}, t)}{\partial t} + \frac{\partial W(\mathbf{z}, t)}{\partial \mathbf{z}} \mathbf{h}(\mathbf{z}, t) \leq -c \|\mathbf{z}\|^2. \quad (\text{A.44})$$

If, in addition,  $\alpha_2(s) \propto s^2$  for sufficiently small  $s$  then the origin is ULES.

**Proof.** Fossen et al. (2001).

Theorem A.5 implies that both  $z \rightarrow 0$  and  $\tilde{\theta} \rightarrow 0$  when  $t \rightarrow \infty$ . The following example illustrates how a UGAS integral controller can be derived:

**Example A.3 (UGAS Integral Controller)**

Consider the nonautonomous system

$$\dot{x} = -a(t)x + \theta + u \quad (\text{A.45})$$

$$u = -K_p x - \hat{\theta} \quad (\text{A.46})$$

$$\dot{\hat{\theta}} = px \quad (\text{A.47})$$

where  $0 < a(t) \leq a_{\max}$ ,  $\theta = \text{constant}$ ,  $K_p > 0$  and  $p > 0$ . This is a PI controller since

$$u = -K_p x - p \int_0^t x(\tau) d\tau \quad (\text{A.48})$$

Choosing  $z = x$ , the error dynamics can be written

$$\dot{z} = -(a(t) + K_p)z - \tilde{\theta} \quad (\text{A.49})$$

$$\dot{\tilde{\theta}} = pz \quad (\text{A.50})$$

which is in the form (A.40)–(A.41) with  $W(z) = \frac{1}{2}z^2$  and  $B = 1$ . Since  $B^\top B = 1 > 0$  and

$$\max \{|a(t)z + K_p z|, |z|\} \leq \rho|z| \quad (\text{A.51})$$

with  $\rho = a_{\max} + K_p$ , the equilibrium point  $z = 0$  is UGAS according to Theorem A.5. Notice that the LaSalle–Yoshizawa theorem fails for this case since

$$V(z, t) = W(z) + \frac{1}{2p}\tilde{\theta}^2 \quad (\text{A.52})$$

$$\begin{aligned} \dot{V}(z, t) &= z\dot{z} + \frac{1}{p}\tilde{\theta}\dot{\tilde{\theta}} \\ &= -[a(t) + K_p]z^2 \\ &\leq 0 \end{aligned} \quad (\text{A.53})$$

which by LaSalle–Yoshizawa only shows UGS and  $z(t) \rightarrow 0$ , but not  $\tilde{\theta} \rightarrow 0$ .

## Appendix B

# Numerical Methods

From a physical point of view, marine craft kinematics and kinetics are most naturally derived in the continuous-time domain using *Newtonian* or *Lagrangian* dynamics. In the implementation of a control law, it is desirable to represent the nonlinear dynamics in discrete time. This chapter discusses methods for discretization of linear and nonlinear systems, numerical integration and differentiation.

## B.1 Discretization of Continuous-Time Systems

This section discusses discretization of linear state-space models with extensions to nonlinear systems. For notational simplicity, let  $t_k = kt$  such that  $\mathbf{x}[k] = \mathbf{x}(t_k)$  and  $\mathbf{x}[k+1] = \mathbf{x}(t_k + h)$  where  $h$  is the sampling time. The *forward shift operator*  $z$  is defined by

$$\mathbf{x}[k+1] := z\mathbf{x}[k] \quad (\text{B.1})$$

### B.1.1 State-space models

Consider the linear continuous-time model

$$\dot{\mathbf{x}} = \mathbf{A}\mathbf{x} + \mathbf{B}\mathbf{u} \quad (\text{B.2})$$

Assume that  $\mathbf{u}$  is piecewise constant over the sampling interval  $h$  and equal to  $\mathbf{u}[k]$ . Hence, the solution of (B.2) is

$$\mathbf{x}[k+1] = e^{\mathbf{A}h}\mathbf{x}[k] + \left( \int_{kh}^{(k+1)h} e^{\mathbf{A}[(k+1)h-\tau]} \mathbf{B} d\tau \right) \mathbf{u}[k] \quad (\text{B.3})$$

where we have moved the constant term  $\mathbf{u}[k]$  outside the integral. The integral can be solved by changing the variables

$$\lambda = (k+1)h - \tau, \quad \lambda = \begin{cases} 0, & \tau = (k+1)h \\ h, & \tau = kh \end{cases} \quad (\text{B.4})$$

Consequently,

$$\int_{kh}^{(k+1)h} e^{\mathbf{A}[(k+1)h-\tau]} \mathbf{B} d\tau = \int_h^0 e^{\mathbf{A}\lambda} \mathbf{B} (-d\lambda) = \int_0^h e^{\mathbf{A}\lambda} \mathbf{B} d\lambda \quad (\text{B.5})$$

The discrete-time state-space model becomes

$$\mathbf{x}[k+1] = \mathbf{A}_d \mathbf{x}[k] + \mathbf{B}_d \mathbf{u}[k] \quad (\text{B.6})$$

where

$$\mathbf{A}_d = e^{\mathbf{A}h} \quad (\text{B.7})$$

$$\mathbf{B}_d = \int_0^h e^{\mathbf{A}\tau} \mathbf{B} d\tau \quad (\text{B.8})$$

### Matlab:

The matrices  $\mathbf{A}_d$  and  $\mathbf{B}_d$  can be computed in Matlab as

```
[Ad, Bd] = c2d(A, B, h)
```

The function `c2d.m` discretizes the continuous-time dynamic system model using zero-order hold on the inputs.

### Explicit solution

Consider the state-transition matrix

$$\Phi = e^{\mathbf{A}h} \quad (\text{B.9})$$

If the inverse matrix  $\mathbf{A}^{-1}$  for the system (B.3) exists, an explicit solution of (B.8) is found

$$\mathbf{A}_d = \Phi \quad (\text{B.10})$$

$$\mathbf{B}_d = \mathbf{A}^{-1}(\Phi - \mathbf{I})\mathbf{B} \quad (\text{B.11})$$

### Example B.1 (Discretization of a First-Order Linear System)

Consider the SISO linear system

$$\dot{x} = ax + bu \quad (\text{B.12})$$

$$y = cx + du \quad (\text{B.13})$$

Application of (B.10)–(B.11) yields

$$x[k+1] = e^{ah}x[k] + \frac{b}{a}(e^{ah} - 1)u[k] \quad (\text{B.14})$$

$$y[k] = cx[k] + du[k] \quad (\text{B.15})$$

### B.1.2 Computation of the transition matrix

The transition matrix  $\Phi$  can be computed numerically as

$$\Phi = e^{\mathbf{A}h} = \mathbf{I} + \mathbf{A}h + \frac{1}{2!}\mathbf{A}^2h^2 + \cdots + \frac{1}{n!}\mathbf{A}^nh^n + \cdots \quad (\text{B.16})$$

Hence,

$$\mathbf{A}_d = \Phi = \mathbf{I} + \mathbf{A}h + \frac{1}{2!}\mathbf{A}^2h^2 + \cdots + \frac{1}{n!}\mathbf{A}^nh^n + \cdots \quad (\text{B.17})$$

$$\mathbf{B}_d = \mathbf{A}^{-1}(\Phi - \mathbf{I})\mathbf{B} = h + \frac{1}{2!}\mathbf{A}h^2 + \cdots + \frac{1}{n!}\mathbf{A}^{n-1}h^n + \cdots \quad (\text{B.18})$$

#### Matlab:

The transition matrix can be computed in Matlab as

```
PHI = exp(A *h);
```

Consequently, a first-order approximation (Euler discretization) is obtained by

$$\mathbf{A}_d \approx \mathbf{I} + \mathbf{A}h \quad (\text{B.19})$$

$$\mathbf{B}_d \approx Bh \quad (\text{B.20})$$

## B.2 Numerical Integration Methods

In this section numerical solutions to the nonlinear time-varying system

$$\dot{\mathbf{x}} = \mathbf{f}(\mathbf{x}, \mathbf{u}, t) \quad (\text{B.21})$$

where the control input  $\mathbf{u}$  is assumed to be constant over the sampling interval  $h$  (zero-order hold), are discussed. Four different methods will be presented.

### B.2.1 Euler's method

A frequently used method for numerical integration is forward Euler

$$\mathbf{x}[k+1] = \mathbf{x}[k] + h\mathbf{f}(\mathbf{x}[k], \mathbf{u}[k], t_k) \quad (\text{B.22})$$

The global truncation error for Euler's method is of order  $O(h)$ .

Applying Euler's method to a second-order system

$$\dot{x} = v \quad (\text{B.23})$$

$$m\ddot{v} + dv + kx = \tau \quad (\text{B.24})$$

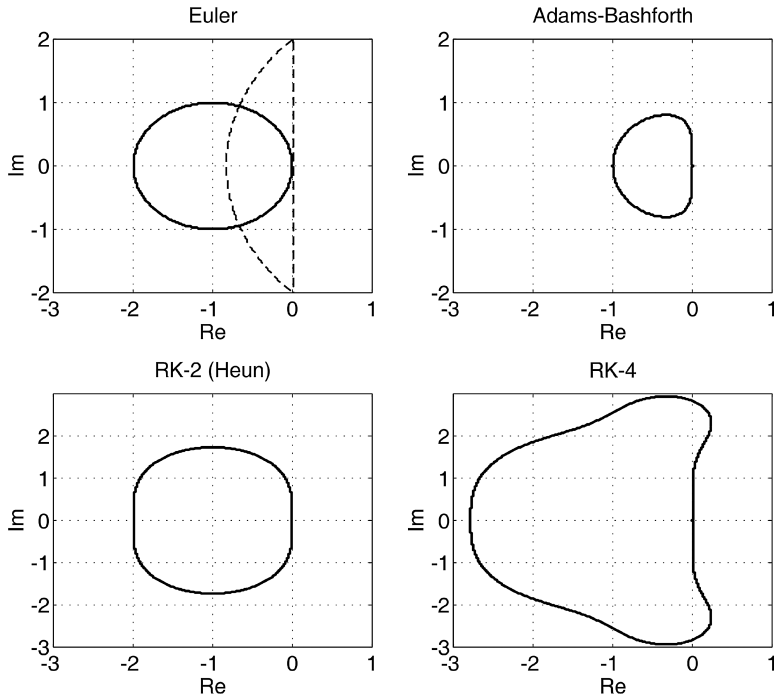


Figure B.1: Stability regions for the Euler, Adams–Bashford, RK-2 and RK-4 methods.

yields

$$v[k+1] = v[k] + h \left( \frac{1}{m} \tau[k] - \frac{d}{m} v[k] - \frac{k}{m} x[k] \right) \quad (\text{B.25})$$

$$x[k+1] = x[k] + hv[k] \quad (\text{B.26})$$

It should be noted that Euler's method should only be applied to a well-damped second-order system and not an undamped oscillator. In fact an undamped oscillator will yield an unstable solution, as seen from Figure B.1, where the circle in the upper left-hand plot represents the stable region. An undamped oscillator will have eigenvalues on the imaginary axis, which clearly lie outside the circle.

### Forward and backward Euler integration

A stable method for the undamped second-order system can be obtained by combining the *forward* and *backward* methods of Euler (dotted line in the upper left-hand plot in Figure B.1) according to

Forward Euler:	$v[k+1] = v[k] + h \left( \frac{1}{m} \tau[k] - \frac{d}{m} v[k] - \frac{k}{m} x[k] \right)$	(B.27)
----------------	--	--------

Backward Euler:	$x[k+1] = x[k] + hv[k+1]$	(B.28)
-----------------	---------------------------	--------

### Extension to nonlinear systems

The methods of Euler can be extended to the more general nonlinear system

$$\dot{\nu} = M^{-1} [Bu - C(\nu)\nu - D(\nu)\nu - g(\eta)] \quad (\text{B.29})$$

$$\dot{\eta} = J_\Theta(\eta)\nu \quad (\text{B.30})$$

by the following set of discrete-time equations

$$\nu[k+1] = \nu[k] + hM^{-1} (Bu[k] - C(\nu[k])\nu[k] - D(\nu[k])\nu[k] - g(\eta[k])) \quad (\text{B.31})$$

$$\eta[k+1] = \eta[k] + hJ_\Theta(\eta[k])\nu[k+1] \quad (\text{B.32})$$

### B.2.2 Adams–Bashford’s second-order method

Adams–Bashford integration is more computationally intensive than the schemes of Euler. For instance, the two-step Adams–Bashford integration

$$x[k+1] = x[k] + h \left[ \frac{3}{2}f(x[k], u[k], t_k) - \frac{1}{2}f(x[k-1], u[k-1], t_{k-1}) \right] \quad (\text{B.33})$$

implies that the old value

$$\dot{x}[k-1] = f(x[k-1], u[k-1], t_{k-1}) \quad (\text{B.34})$$

must be stored. The global truncation error for this method is of order  $O(h^2)$ . The advantage with this method compared to Euler integration is seen from Figure B.1.

### B.2.3 Runge–Kutta second-order method

Heun’s integration method or Runge–Kutta’s second-order method (RK-2) is implemented as

$$\begin{aligned} k_1 &= f(x[k], u[k], t_k) \\ k_2 &= f(x[k] + hk_1, u[k], t_k + h) \end{aligned} \quad (\text{B.35})$$

$$x[k+1] = x[k] + \frac{h}{2}(k_1 + k_2)$$

The global truncation error for Heun’s method is of order  $O(h^2)$ .

### B.2.4 Runge–Kutta fourth-order method

An extension of Heun’s integration method to the fourth order (RK-4) is

$$\begin{aligned} \mathbf{k}_1 &= h \mathbf{f}(\mathbf{x}[k], \mathbf{u}[k], t_k) \\ \mathbf{k}_2 &= h \mathbf{f}(\mathbf{x}[k] + \mathbf{k}_1/2, \mathbf{u}[k], t_k + h/2) \\ \mathbf{k}_3 &= h \mathbf{f}(\mathbf{x}[k] + \mathbf{k}_2/2, \mathbf{u}[k], t_k + h/2) \\ \mathbf{k}_4 &= h \mathbf{f}(\mathbf{x}[k] + \mathbf{k}_3/2, \mathbf{u}[k], t_k + h) \\ \mathbf{x}[k+1] &= \mathbf{x}[k] + \frac{1}{6}(\mathbf{k}_1 + 2\mathbf{k}_2 + 2\mathbf{k}_3 + \mathbf{k}_4) \end{aligned} \quad (\text{B.36})$$

The global truncation error for the RK-4 method is of order  $O(h^4)$ .

## B.3 Numerical Differentiation

Numerical differentiation is usually sensitive to noisy measurements. Nevertheless, a reasonable estimate  $\dot{\eta}_f$  of the time derivative  $\dot{\eta}$  of a signal  $\eta$  can be obtained by using a *filtered differentiation*. The simplest filter is obtained by the first-order low-pass structure

$$\dot{\eta}_f(s) = \frac{T_s}{T_s + 1} \eta(s) \quad (\text{B.37})$$

corresponding to the continuous-time system

$$\dot{x} = ax + bu \quad (\text{B.38})$$

$$y = cx + du \quad (\text{B.39})$$

with  $u = \eta$ ,  $y = \dot{\eta}_f$ ,  $a = -1/T$ ,  $b = 1/T$ ,  $c = -1$  and  $d = 1$ . Using the results from Example B.1, the following discrete-time filter equations can be used to differentiate a time-varying signal

$$x[k+1] = e^{-h/T} x[k] - (e^{-h/T} - 1) u[k] \quad (\text{B.40})$$

$$y[k] = -x[k] + u[k] \quad (\text{B.41})$$

## Appendix C

# Model Transformations

When deriving the equations of motion it is convenient to represent inertia, damping, gravitational and buoyancy forces in different coordinate origins to exploit structural properties of the model. The main tool for this is the *system transformation matrix*, which will be derived below.

### C.1 Transforming the Equations of Motion to an Arbitrarily Point

The rigid-body translational and rotational parts of the system inertia matrix is decoupled if the coordinate system is located in the CG. Hence, it is convenient to express the rigid-body kinetics in the CG. However, it is common to compute hydrodynamic added mass and damping in the CF or the CO (see Section 2.1.1). Since the model matrices and vectors are computed in several coordinate origins such as the CG, CF and CO it is necessary to transform the data between the different origins such that the resulting model can be expressed in CO. This creates a need for a common framework for systematic transformation of model matrices and vectors to a common coordinate origin.

#### C.1.1 System transformation matrix

The system transformation matrix is used to transform the generalized velocities, accelerations and forces between two points in the BODY frame. It will be assumed that

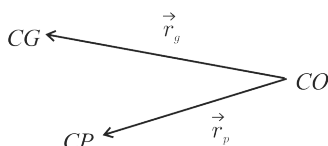


Figure C.1: Definitions of vectors and coordinate systems.

NED is an inertial frame when deriving the transformation. For notational simplicity, we will define  $\mathbf{r}_p^b := \mathbf{r}_{bp}^b$  and  $\mathbf{r}_g^b := \mathbf{r}_{bg}^b$  (see Figure C.1). The system transformation matrix is derived from (3.15) for an arbitrarily point CP according to

$$\begin{aligned}\mathbf{v}_{np}^b &= \mathbf{v}_{nb}^b + \boldsymbol{\omega}_{nb}^b \times \mathbf{r}_p^b \\ &= \mathbf{v}_{nb}^b - \mathbf{S}(\mathbf{r}_p^b) \boldsymbol{\omega}_{nb}^b \\ &= \mathbf{v}_{nb}^b + \mathbf{S}^\top(\mathbf{r}_p^b) \boldsymbol{\omega}_{nb}^b\end{aligned}\quad (\text{C.1})$$

where  $\mathbf{r}_p^b = [x_p, y_p, z_p]^\top$  is the vector from CO to CP expressed in  $\{b\}$  and  $\boldsymbol{\omega}_{np}^b = \boldsymbol{\omega}_{nb}^b$ .

### Definition C.1 (System Transformation Matrix)

The system transformation matrix

$$\mathbf{H}(\mathbf{r}_p^b) = \begin{bmatrix} \mathbf{I}_3 & \mathbf{S}^\top(\mathbf{r}_p^b) \\ \mathbf{0}_{3 \times 3} & \mathbf{I}_3 \end{bmatrix}, \quad \mathbf{H}^{-1}(\mathbf{r}_p^b) = \begin{bmatrix} \mathbf{I}_3 & \mathbf{S}(\mathbf{r}_p^b) \\ \mathbf{0}_{3 \times 3} & \mathbf{I}_3 \end{bmatrix} \quad (\text{C.2})$$

transforms the linear and angular velocity vectors between the two points CO and CP in the  $\{b\}$  frame according to

$$\begin{bmatrix} \mathbf{v}_{np}^b \\ \boldsymbol{\omega}_{np}^b \end{bmatrix} = \mathbf{H}(\mathbf{r}_p^b) \begin{bmatrix} \mathbf{v}_{nb}^b \\ \boldsymbol{\omega}_{nb}^b \end{bmatrix} \quad (\text{C.3})$$

⇓

$$\boldsymbol{\nu}_{np} = \mathbf{H}(\mathbf{r}_p^b) \boldsymbol{\nu} \quad (\text{C.4})$$

where  $\boldsymbol{\nu} := \boldsymbol{\nu}_{nb}$ . Hence,

$$\boldsymbol{\nu} = \mathbf{H}^{-1}(\mathbf{r}_p^b) \boldsymbol{\nu}_{np} \quad (\text{C.5})$$

The generalized force vector  $\boldsymbol{\tau}$  can be transformed from CO to an arbitrary point CP by

$$\begin{bmatrix} \mathbf{f}_b^b \\ \mathbf{m}_b^b \end{bmatrix} = \begin{bmatrix} \mathbf{f}_p^b \\ \mathbf{r}_p^b \times \mathbf{f}_p^b + \mathbf{m}_p^b \end{bmatrix} = \begin{bmatrix} \mathbf{I}_3 & \mathbf{0}_{3 \times 3} \\ \mathbf{S}(\mathbf{r}_p^b) & \mathbf{I}_3 \end{bmatrix} \begin{bmatrix} \mathbf{f}_p^b \\ \mathbf{m}_p^b \end{bmatrix} \quad (\text{C.6})$$

⇓

$$\boldsymbol{\tau} = \mathbf{H}^\top(\mathbf{r}_p^b) \boldsymbol{\tau}^p \quad (\text{C.7})$$

### Matlab:

The system transformation matrix is implemented in the MSS toolbox as

```
function H = Hmtrx(r)
% H = Hmtrx(r) 6x6 system transformation matrix

S = Smtrx(r);
H = [ eye(3)      S'
      zeros(3,3)  eye(3) ];
```

### C.1.2 Equations of motion about an arbitrarily point

Definition C.1 implies that the equations of motion can be represented at an arbitrary defined point CP by using the transformation matrix  $\mathbf{H}(\mathbf{r}_p^b)$ . Consider the nonlinear equations of motion expressed in  $\{\mathbf{b}\}$  with coordinate origin CO

$$\mathbf{M}\dot{\mathbf{v}} + \mathbf{C}(\boldsymbol{\nu})\mathbf{v} + \mathbf{D}(\boldsymbol{\nu})\mathbf{v} + \mathbf{g}(\boldsymbol{\eta}) = \boldsymbol{\tau} \quad (\text{C.8})$$

This expression can be transformed to a point CP in  $\{\mathbf{b}\}$  by substituting (C.5) into (C.8) and premultiply both sides of (C.8) with  $\mathbf{H}^{-\top}(\mathbf{r}_p^b)$  to obtain

$$\underbrace{\mathbf{H}^{-\top}(\mathbf{r}_p^b)\mathbf{M}\mathbf{H}^{-1}(\mathbf{r}_p^b)}_{\mathbf{M}^p}\dot{\mathbf{v}}_{np} + \underbrace{\mathbf{H}^{-\top}(\mathbf{r}_p^b)\mathbf{C}(\boldsymbol{\nu})\mathbf{H}^{-1}(\mathbf{r}_p^b)}_{\mathbf{C}^p(\boldsymbol{\nu})}\mathbf{v}_{np} + \underbrace{\mathbf{H}^{-\top}(\mathbf{r}_p^b)\mathbf{D}(\boldsymbol{\nu})\mathbf{H}^{-1}(\mathbf{r}_p^b)}_{\mathbf{D}^p(\boldsymbol{\nu})}\mathbf{v}_{np} + \underbrace{\mathbf{H}^{-\top}(\mathbf{r}_p^b)\mathbf{g}(\boldsymbol{\eta})}_{\mathbf{g}^p(\boldsymbol{\eta})} = \underbrace{\mathbf{H}^{-\top}(\mathbf{r}_p^b)\boldsymbol{\tau}}_{\boldsymbol{\tau}^p} \quad (\text{C.9})$$

### C.1.3 Matrix and vector transformations

The result (C.9) implies that a matrix  $\mathbf{A}$  and a vector  $\boldsymbol{\tau}$  can be transformed from CO to an arbitrarily coordinate origin CP in  $\{\mathbf{b}\}$  by

$$\mathbf{A}^p = \mathbf{H}^{-\top}(\mathbf{r}_p^b)\mathbf{A}\mathbf{H}^{-1}(\mathbf{r}_p^b) \quad (\text{C.10})$$

$$\boldsymbol{\tau}^p = \mathbf{H}^{-\top}(\mathbf{r}_p^b)\boldsymbol{\tau} \quad (\text{C.11})$$

The superscript  $p$  denotes quantities that have been transformed to the coordinate origin CP, while quantiles in the default coordinate origin CO are written without the superscript  $b$  to simplify the notation. Consequently, the inverse transformation from CP to CO becomes

$$\mathbf{A} = \mathbf{H}^\top(\mathbf{r}_p^b)\mathbf{A}^p (\mathbf{r}_p^b) \quad (\text{C.12})$$

$$\boldsymbol{\tau} = \mathbf{H}^\top(\mathbf{r}_p^b)\boldsymbol{\tau}^p \quad (\text{C.13})$$

The matrices and vectors in (C.9) are recognized as

$$\mathbf{M}^p = \mathbf{H}^{-\top}(\mathbf{r}_p^b)\mathbf{M}\mathbf{H}^{-1}(\mathbf{r}_p^b) \quad (\text{C.14})$$

$$\mathbf{C}^p(\boldsymbol{\nu}) = \mathbf{H}^{-\top}(\mathbf{r}_p^b)\mathbf{C}(\boldsymbol{\nu})\mathbf{H}^{-1}(\mathbf{r}_p^b) \quad (\text{C.15})$$

$$\mathbf{D}^p(\boldsymbol{\nu}) = \mathbf{H}^{-\top}(\mathbf{r}_p^b)\mathbf{D}(\boldsymbol{\nu})\mathbf{H}^{-1}(\mathbf{r}_p^b) \quad (\text{C.16})$$

$$\mathbf{g}^p(\boldsymbol{\eta}) = \mathbf{H}^{-\top}(\mathbf{r}_p^b)\mathbf{g}(\boldsymbol{\eta}) \quad (\text{C.17})$$

The inverse transformation from CP to CO becomes

$$\mathbf{M} = \mathbf{H}^\top(\mathbf{r}_p^b)\mathbf{M}^p\mathbf{H}(\mathbf{r}_p^b) \quad (\text{C.18})$$

$$\mathbf{C}(\boldsymbol{\nu}) = \mathbf{H}^\top(\mathbf{r}_p^b)\mathbf{C}^p(\boldsymbol{\nu})\mathbf{H}(\mathbf{r}_p^b) \quad (\text{C.19})$$

$$\mathbf{D}(\boldsymbol{\nu}) = \mathbf{H}^\top(\mathbf{r}_p^b)\mathbf{D}^p(\boldsymbol{\nu})\mathbf{H}(\mathbf{r}_p^b) \quad (\text{C.20})$$

$$\mathbf{g}(\boldsymbol{\eta}) = \mathbf{H}^\top(\mathbf{r}_p^b)\mathbf{g}^p(\boldsymbol{\eta}) \quad (\text{C.21})$$



## Appendix D

# Nondimensional Equations of Motion

When designing ship control systems it is often convenient to make the equations of motion nondimensional such that the model parameters can be treated as constants with respect to the instantaneous speed  $U$  defined by

$$U = \sqrt{u^2 + v^2} = \sqrt{(u_0 + \Delta u)^2 + \Delta v^2} \quad (\text{D.1})$$

where  $u_0$  is the *service speed* and  $\Delta u$  and  $\Delta v$  are small perturbations in the surge and sway velocities, respectively. Hence,

$$U \approx u_0 \quad (\text{D.2})$$

During course-changing maneuvers the instantaneous speed will decrease due to increased resistance during the turn.

### D.1 Nondimensionalization

Nondimensionalization is the partial or full removal of units from an equation involving physical quantities by a suitable substitution of variables. The most commonly used methods for marine craft are the *Prime system* of SNAME (1950) and the *Bis system* of Norrbin (1970).

**Prime System:** This system uses the craft's instantaneous speed  $U$ , the length  $L = L_{pp}$  (the length between the fore and aft perpendiculars), the time unit  $L/U$  and the mass unit  $1/2\rho L^3$  or  $1/2\rho L^2 T$  as normalization variables. The latter is inspired by wing theory, where the reference area  $A = LT$  is used instead of  $A = L^2$ . The prime system cannot be used for low-speed applications such as dynamic ship positioning, since normalization of the velocities  $u$ ,  $v$  and  $w$  implies dividing by the cruise speed  $U$ , which can be zero for a dynamically positioned ship. As a consequence, the prime system is mostly used in ship maneuvering.

Table D.1: Prime and Bis system variables used for nondimensionalization.

Unit	Prime system I	Prime system II	Bis system
Length	$L$	$L$	$\bar{L}$
Mass	$\frac{1}{2}\rho L^3$	$\frac{1}{2}\rho L^2 T$	$\mu\rho\nabla$
Inertia moment	$\frac{1}{2}\rho L^5$	$\frac{1}{2}\rho L^4 T$	$\mu\rho\nabla L^2$
Time	$\frac{L}{U}$	$\frac{L}{U}$	$\sqrt{L/g}$
Reference area	$L^2$	$L T$	$\mu \frac{2\nabla}{L}$
Position	$L$	$L$	$L$
Angle	1	1	1
Linear velocity	$U$	$U$	$\sqrt{Lg}$
Angular velocity	$\frac{U}{L}$	$\frac{U}{L}$	$\sqrt{g/L}$
Linear acceleration	$\frac{U^2}{L}$	$\frac{U^2}{L}$	$g$
Angular acceleration	$\frac{U^2}{L^2}$	$\frac{U^2}{L^2}$	$\frac{g}{L}$
Force	$\frac{1}{2}\rho U^2 L^2$	$\frac{1}{2}\rho U^2 LT$	$\mu\rho g\nabla$
Moment	$\frac{1}{2}\rho U^2 L^3$	$\frac{1}{2}\rho U^2 L^2 T$	$\mu\rho g\nabla L$

**Bis System:** This system can be used for zero speed as well as high-speed applications since division of speed  $U$  is avoided. The bis system is based on the use of the length  $L = L_{pp}$ , with the time unit  $\sqrt{L/g}$  such that speed becomes  $\sqrt{Lg} > 0$ . In addition, the body mass density ratio  $\mu = m/\rho\nabla$ , where  $m$  is the mass unit and  $\nabla$  is the hull contour displacement, is applied. The density ratio  $\mu$  takes the following values:

- $\mu < 1$  Underwater vehicles (ROVs, AUVs and submarines)
- $\mu = 1$  Floating ships/rigs and neutrally buoyant underwater vehicles
- $\mu > 1$  Heavy torpedoes (typically  $\mu = 1.3\text{--}1.5$ )

The prime and bis system variables used for nondimensionalization are given in Table D.1. The nondimensional quantities will be distinguished from those with dimension by applying the notation  $(\cdot)'$  for the prime system and  $(\cdot)''$  for the bis system.

### D.1.1 Nondimensional hydrodynamic coefficients

The procedure making a hydrodynamic coefficient dimensionless is easiest illustrated by an example. For instance, the hydrodynamic coefficient  $Y_r$  can be made nondimensional by using the prime and bis systems. First, let us determine the dimension of  $Y_r$ . Consider

$$\underbrace{Y}_{[N=\text{kgm/s}^2]} = \underbrace{Y_r}_{[\text{unknown}]} \underbrace{r}_{[\text{rad/s}]}$$

Hence, the unknown dimension must be kg m/s since rad is a nondimensional unit. The nondimensional values  $Y'_r$  and  $Y''_r$  are found by using kg, m and s from Table D.1.

Consequently,

$$Y'_r = \frac{Y_r}{\frac{[\frac{1}{2}\rho L^3][L]}{[L/U]}} = \frac{1}{\frac{1}{2}\rho L^3 U} Y_r \quad (\text{D.3})$$

$$Y''_r = \frac{Y_r}{\frac{[\mu\rho\nabla][L]}{\sqrt{L/g}}} = \frac{1}{\mu\rho\nabla\sqrt{Lg}} Y_r \quad (\text{D.4})$$

For a floating ship,  $Y''_r$  can be further simplified since  $\mu = 1$  and  $m = \rho\nabla$ . Hence,

$$Y''_r = \frac{1}{m\sqrt{Lg}} Y_r \quad (\text{D.5})$$

### D.1.2 Nondimensional Nomoto models

The gain and time constants in Nomoto's first- and second-order models can be made invariant with respect to  $U$  and  $L$  by using

$$K' = (L/U) K \quad (\text{D.6})$$

$$T' = (U/L) T \quad (\text{D.7})$$

This suggests that the first-order Nomoto model

$$T\dot{r} + r = K\delta \quad (\text{D.8})$$

can be expressed as

$$(L/U) T' \dot{r} + r = (U/L) K' \delta \quad (\text{D.9})$$

or

$$\dot{r} = -\left(\frac{U}{L}\right) \frac{1}{T'} r + \left(\frac{U}{L}\right)^2 \frac{K'}{T'} \delta \quad (\text{D.10})$$

This representation is quite useful since the nondimensional gain and time constants will typically be in the range  $0.5 < K' < 2$  and  $0.5 < T' < 2$  for most ships. An extension to Nomoto's second-order model is given by

$$(L/U)^2 T'_1 T'_2 \psi^{(3)} + (L/U) (T'_1 + T'_2) \ddot{\psi} + \dot{\psi} = (U/L) K' \delta + K' T'_3 \dot{\delta} \quad (\text{D.11})$$

where the nondimensional time constants  $T'_i$  are defined as  $T'_i = T_i (U/L)$  for  $i = 1, 2, 3$  and the nondimensional gain constant is  $K' = (L/U) K$ .

### D.1.3 Nondimensional maneuvering models

Consider the linear maneuvering model (6.123) in nondimensional form

$$\mathbf{M}' \dot{\boldsymbol{\nu}}' + \mathbf{N}'(u'_0) \boldsymbol{\nu}' = \mathbf{b}' \delta' \quad (\text{D.12})$$

Transforming the states  $\boldsymbol{\nu}'$  and control input  $\delta'$  to dimensional quantities yields

$$(\mathbf{T} \mathbf{M}' \mathbf{T}^{-1}) \dot{\boldsymbol{\nu}} + \frac{U}{L} (\mathbf{T} \mathbf{N}'(u'_0) \mathbf{T}^{-1}) \boldsymbol{\nu} = \frac{U^2}{L} \mathbf{T} \mathbf{b}' \delta \quad (\text{D.13})$$

where

$$\mathbf{T} = \text{diag}\{1, 1/L\} \quad (\text{D.14})$$

Notice that  $\delta = \delta'$ . Expanding (D.13) yields

$$\begin{bmatrix} m'_{11} & Lm'_{12} \\ \frac{1}{L}m'_{21} & m'_{22} \end{bmatrix} \begin{bmatrix} \dot{v} \\ \dot{r} \end{bmatrix} + \frac{U}{L} \begin{bmatrix} n'_{11} & Ln'_{12} \\ \frac{1}{L}n'_{21} & n'_{22} \end{bmatrix} \begin{bmatrix} v \\ r \end{bmatrix} = \frac{U^2}{L} \begin{bmatrix} b'_1 \\ \frac{1}{L}b'_2 \end{bmatrix} \delta \quad (\text{D.15})$$

where  $m'_{ij}$ ,  $d'_{ij}$  and  $b'_i$  are defined according to prime systems I or II in Table D.1.

## D.2 6-DOF Procedure for Nondimensionalization

A systematic procedure for nondimensionalization of 6-DOF models is found by defining the transformation matrix

$$\mathbf{T} = \text{diag}\left\{1, 1, 1, \frac{1}{L}, \frac{1}{L}, \frac{1}{L}\right\} \quad (\text{D.16})$$

$$\mathbf{T}^{-1} = \text{diag}\{1, 1, 1, L, L, L\} \quad (\text{D.17})$$

Consider the nondimensional model

$$\mathbf{M}' \dot{\boldsymbol{\nu}}' + \mathbf{N}' \boldsymbol{\nu}' + \mathbf{G}' \boldsymbol{\eta}' = \boldsymbol{\tau}' \quad (\text{D.18})$$

When designing marine craft simulators and gain-scheduled controllers it is convenient to perform the numerical integration in real time using dimensional time. Consequently, it is convenient to use the nondimensional hydrodynamic coefficients as input to the simulator or controller, while the states  $\boldsymbol{\nu}$ ,  $\boldsymbol{\eta}$  and input  $\boldsymbol{\tau}$  should have their physical dimensions. For the *prime system* this is obtained by applying the following transformation to (D.18)

$$\mathbf{M}' \left( \frac{L}{U^2} \mathbf{T}^{-1} \dot{\boldsymbol{\nu}} \right) + \mathbf{N}' \left( \frac{1}{U} \mathbf{T}^{-1} \boldsymbol{\nu} \right) + \mathbf{G}' \left( \frac{1}{L} \mathbf{T}^{-1} \boldsymbol{\eta} \right) = \frac{1}{\frac{1}{2}\rho U^2 L^2} \mathbf{T} \boldsymbol{\tau} \quad (\text{D.19})$$

such that

$$(\mathbf{T} \mathbf{M}' \mathbf{T}^{-1}) \dot{\boldsymbol{\nu}} + \left( \frac{U}{L} \right) (\mathbf{T} \mathbf{N}' \mathbf{T}^{-1}) \boldsymbol{\nu} + \left( \frac{U}{L} \right)^2 (\mathbf{T} \mathbf{G}' \mathbf{T}^{-1}) \boldsymbol{\eta} = \frac{1}{\frac{1}{2}\rho L^3} \mathbf{T}^2 \boldsymbol{\tau} \quad (\text{D.20})$$

Hence,

$$\mathbf{M} = \frac{\rho L^3}{2} \mathbf{T}^{-2} (\mathbf{T} \mathbf{M}' \mathbf{T}^{-1}) \quad (\text{D.21})$$

$$\mathbf{N} = \frac{\rho L^2 U}{2} \mathbf{T}^{-2} (\mathbf{T} \mathbf{N}' \mathbf{T}^{-1}) \quad (\text{D.22})$$

$$\mathbf{G} = \frac{\rho L U^2}{2} \mathbf{T}^{-2} (\mathbf{T} \mathbf{G}' \mathbf{T}^{-1}) \quad (\text{D.23})$$

Table D.2: Variables used for nondimensionalization of 6-DOF models.

	Prime system	Bis system
Acceleration	$\dot{\nu} = \frac{U^2}{L} \mathbf{T} \dot{\nu}'$	$\dot{\nu} = g \mathbf{T} \dot{\nu}''$
Velocity	$\nu = U \mathbf{T} \nu'$	$\nu = \sqrt{Lg} \mathbf{T} \nu''$
Position/attitude	$\eta = L \mathbf{T} \eta'$	$\eta = L \mathbf{T} \eta''$
Control forces/momenta	$\tau = \frac{1}{2} \rho U^2 L^2 \mathbf{T}^{-1} \boldsymbol{\tau}'$	$\tau = \mu \rho g \nabla \mathbf{T}^{-1} \boldsymbol{\tau}''$

Notice that  $\nu$ ,  $\eta$  and the input vector  $\boldsymbol{\tau}$  now have physical dimensions while  $M'$ ,  $N'$  and  $G'$  are nondimensional. Similarly, *bis system* scaling with  $\mu = 1$  gives

$$(\mathbf{T} M'' \mathbf{T}^{-1}) \dot{\nu} + \sqrt{\frac{g}{L}} (\mathbf{T} N'' \mathbf{T}^{-1}) \nu + \frac{g}{L} (\mathbf{T} G'' \mathbf{T}^{-1}) \eta = \frac{1}{m} \mathbf{T}^2 \boldsymbol{\tau} \quad (\text{D.24})$$

Consequently,

$$\mathbf{M} = m \mathbf{T}^{-2} (\mathbf{T} M'' \mathbf{T}^{-1}) \quad (\text{D.25})$$

$$\mathbf{N} = m \sqrt{\frac{g}{L}} \mathbf{T}^{-2} (\mathbf{T} N'' \mathbf{T}^{-1}) \quad (\text{D.26})$$

$$\mathbf{G} = m \frac{g}{L} \mathbf{T}^{-2} (\mathbf{T} G'' \mathbf{T}^{-1}) \quad (\text{D.27})$$

The 6-DOF nondimensionalization procedure is summarized in Table D.2.



# References

DRAFT MANUSCRIPT

# References

- 2nd ISSC (1964). Report of the Seakeeping Committee. In: *Proceedings of the 2nd International Ship and Offshore Structures Congress*. Delft, August 1964. p. 19.
- 12th ITTC (1969). Report of the Seakeeping Committee. In: *Proceedings of the 12th International Towing Tank Conference*. Rome, September 1969. pp. 775–779.
- 14th ITTC (1975). Discussion and Recommendations for an ITTC 1975 Maneuvering Trial Code. In: *Proceedings of the 14th International Towing Tank Conference*. Ottawa, September 1975. pp. 348–365.
- 15th ITTC (1978). Report of the Seakeeping Committee. In: *Proceedings of the 15th International Towing Tank Conference*. The Hague, Netherlands, September 1978. pp. 55–70.
- 17th ITTC (1984). Report of the Seakeeping Committee. In: *Proceedings of the 17th International Towing Tank Conference*. The Hague, Netherlands, September 1984. pp. 531–534.
- Aarset, M. F., J. P. Strand and T. I. (1998). Nonlinear Vectorial Observer Backstepping With Integral Action and Wave Filtering for Ships. In: *Proceedings of the IFAC Conference on Control Applications in Marine Systems (CAMS'98)*. pp. 83–89.
- Abkowitz, M. A. (1964). Lectures on Ship Hydrodynamics – Steering and Maneuverability. Technical Report Hy-5. Hydro- and Aerodynamic's Laboratory. Lyngby, Denmark.
- Acheson, D. J. (1990). *Elementary Fluid Dynamics*. Oxford Applied Mathematics and Computing Science Series. Clarendon Press, Oxford.
- Allensworth, T. (1999). A Short History of Sperry Marine. Internet. <<http://www.sperry-marine.com/pages/history.html>> [Accessed October 1, 2010].
- Aranda, J., J. M. de-la-Cruz, J. M. Diaz, B. de-Andres, P. Ruiperez, S. Esteban and J. M. Giron (2000). Modelling of a High Speed Craft by a Nonlinear Least Squares Method with Constraints. In: *Proceedings of the 5th IFAC Conference on Maneuvering and Control of Marine Craft (MCMC'2000)*. Aalborg, Denmark. pp. 227–232.

- Arimoto, S. and F. Miyazaki (1984). Stability and Robustness of PID Feedback Control for Robot Manipulators of Sensory Capability. In: *Proceedings of the 1st International Symposium on Robotics Research* (M. Brady and R. Paul, Eds). pp. 783–799. MIT Press.
- Arstein, Z. (1983). Stabilization with Relaxed Controls. *Nonlinear Analysis* TMA-7, 1163–1173.
- Asare, H. and D. Wilson (1986). Design of Computed Torque Model Reference Adaptive Control for Space-Based Robotic Manipulators. ASME, Winter Annual Meeting (WAM), pp. 195–204.
- Athans, M. and Falb, P. L. (Eds) (1966). *Optimal Control*. McGraw-Hill Book Company. New York, NY.
- Bailey, P. A., W. G. Price and P. Temarel (1998). A Unified Mathematical Model Describing the Maneuvering of a Ship Travelling in a Seaway. *Transactions of the Royal Institute of Naval Architects* Transactions RINA-140, 131–149.
- Baitis, A. E. (1980). The Development and Evaluation of a Rudder Roll Stabilization System for the WHEC Hamiltonian Class. Technical Report DTNSRDC. Naval Ship Research and Development Center. Bethesda, MD.
- Baitis, E., D. A. Woolaver and T. A. Beck (1983). Rudder Roll Stabilization for Coast Guards Cutters and Frigates. *Naval Engineers Journal*, pp. 267–282.
- Baitis, E., D. A. Woolaver and T. A. Beck (1989). Ship Roll Stabilization in the U.S. Navy. *Naval Engineers Journal*, 43–53.
- Balchen, J. G., N. A. Jenssen and S. Sælid (1976). Dynamic Positioning Using Kalman Filtering and Optimal Control Theory. In: *Proceedings of the IFAC/IFIP Symposium on Automation in Offshore Oil Field Operation*. Bergen, Norway. pp. 183–186.
- Balchen, J. G., N. A. Jenssen and S. Sælid (1980a). Dynamic Positioning of Floating Vessels Based on Kalman Filtering and Optimal Control. In: *Proceedings of the 19th IEEE Conference on Decision and Control*. New York, NY. pp. 852–864.
- Balchen, J. G., N. A. Jenssen, E. Mathisen and S. Sælid (1980b). Dynamic Positioning System Based on Kalman Filtering and Optimal Control. *Modeling, Identification and Control* MIC-1(3), 135–163.
- Barbălat (1959). Systèmes d'Équations Différentielles d'Oscillations Non Linéaires. *Revue de Mathématiques Pures et Appliquées* Vol. 4(2), 267–270. Académie de la République Populaire Roumaine (in French).
- Barbier, C., P. Sen and M. Downie (1994). Parallel Dynamic Programming and Ship Voyage Management. *Concurrency: Practice and Experience* CPE-6(8), 673–696.
- Barbour, N. and G. Schmidt (1998). Inertial Sensor Technology Trends. In: *Proceedings of the Workshop on Autonomous Underwater Vehicles*. pp. 52–55.

- Barnitsas, M. M., Ray, D. and Kinley, P. (1981). *KT, KQ and Efficiency Curves for the Wageningen B-Series Propellers*. <Open Access: <http://deepblue.lib.umich.edu/handle/2027.42/3557>>.
- Beard, R. W. and T. W. McLain (2012). *Small Unmanned Aircraft. Theory and Practice*. Princeton University Press.
- Bech, M. I. (1968). The Reversed Spiral Test as Applied to Large Ships. In: *Shipping World and Shipbuilder*. pp. 1753–1754.
- Bech, M. I. and L. Wagner Smith (1969). Analogue Simulation of Ship Maneuvers. Technical Report Hy-14. Hydro- and Aerodynamics Laboratory. Lyngby, Denmark.
- Bennet, S. (1979). *A History of Control Engineering 1800–1930*. Peter Peregrinus. London.
- Bennett, S. (1991). Ship Stabilization: History. In: *Concise Encyclopedia of Traffic and Transportation Systems* (Markos Papageorgiou, Ed.). pp. 454–459. Pergamon Press.
- Berge, S. P. and T. I. Fossen (1997). Robust Control Allocation of Overactuated Ships: Experiments With a Model Ship. In: *Proceedings of the 4th IFAC Conference on Manoeuvring and Control of Marine Craft*. Brijuni, Croatia. pp. 166–171.
- Berge, S. P. and T. I. Fossen (2000). On the Properties of the Nonlinear Ship Equations of Motion. *Journal of Mathematical and Computer Modelling of Dynamical Systems* JMCMDS-6(4), 365–381.
- Bertram, V. (2004). *Practical Ship Hydrodynamics*. Butterworth Heinemann.
- Bhat, S. P. and D. S. Bernstein (2000). A Topological Obstruction to Continuous Global Stabilization of Rotational Motion and the Unwinding Phenomenon. *Systems and Control Letters* SCL-39(1), 63–70.
- Bhattacharyya, R. (1978). *Dynamics of Marine Vehicles*. John Wiley & Sons, Inc. New York, NY.
- Blanke, M. (1981). Ship Propulsion Losses Related to Automated Steering and Prime Mover Control. PhD thesis. The Technical University of Denmark, Lyngby.
- Blanke, M. (1994). Optimal Speed Control for Cruising. In: *Proceedings of the 3rd Conference on Marine Craft Maneuvering and Control*, Southampton, UK.
- Blanke, M. (1996). Uncertainty Models for Rudder-Roll Damping Control. In: *Proceedings of the IFAC World Congress*. Vol. Q. Elsevier. San Francisco, CA. pp. 285–290.
- Blanke, M. and A. Christensen (1993). Rudder-Roll Damping Autopilot Robustness due to Sway-Yaw-Roll Couplings. In: *Proceedings of the 10th International Ship Control Systems Symposium (SCSS'93)*. Ottawa, Canada. pp. A.93–A.119.

- Blanke, M. and A. G. Jensen (1997). Dynamic Properties of Container Vessel with Low Metacentric Height. *Transactions of the Institute of Measurement and Control* TIMC-19(2), 78–93.
- Blanke, M. and A. Tiano (1997). Multivariable Identification of Ship Steering and Roll Motions. *Transactions of the Institute of Measurement and Control* TIMC-19(2), 62–77.
- Blanke, M., P. Haals and K. K. Andreasen (1989). Rudder Roll Damping Experience in Denmark. In: *Proceedings of the IFAC Workshop on Expert Systems and Signal Processing in Marine Automation*. Lyngby, Denmark. pp. 149–160.
- Blanke, M., Adrian, K.-E. Larsen and J. Bentsen (2000a). Rudder Roll Damping in Coastal Region Sea Conditions. In: *Proceedings 5th IFAC Conference on Manoeuvring and Control of Marine Craft (MCMC'00)*. Aalborg, Denmark, 23–25 August, pp. 39–44.
- Blanke, M., K. P. Lindegaard and T. I. Fossen (2000b). Dynamic Model for Thrust Generation of Marine Propellers. In: *Proceedings of the IFAC Conference of Manoeuvring of Marine Craft (MCMC'00)*, Aalborg, Denmark, 23–25 August.
- Blendermann, W. (1986). Die Windkräfte am Schiff. Technical Report Bericht Nr. 467. Institut für Schiffbau der Universität Hamburg (in German).
- Blendermann, W. (1994). Parameter Identification of Wind Loads on Ships. *Journal of Wind Engineering and Industrial Aerodynamics* JWEIA-51, 339–351.
- Bordignon, K. A. and W. C. Durham (1995). Closed-Form Solutions to Constrained Control Allocation Problem. *Journal of Guidance, Control and Dynamics* JGCD-18(5), 1000–1007.
- Børhaug, E. and K. Y. Pettersen (2006). LOS Path Following for Underwater Underactuated Vehicles. In: *Proceedings of the IFAC MCMC'07*. Lisbon, Portugal.
- Breivik, M. (2010). Topics in Guided Motion Control. PhD thesis. Department of Engineering Cybernetics, Norwegian University of Science and Technology, Trondheim, Norway.
- Breivik, M. and T. I. Fossen (2004a). Path following for marine surface vessels. In: *Proceedings of the OTO'04*. Kobe, Japan.
- Breivik, M. and T. I. Fossen (2004b). Path Following of Straight Lines and Circles for Marine Surface Vessels. In: *Proceedings of the IFAC CAMS'04*. Ancona, Italy.
- Breivik, M. and T. I. Fossen (2005a). A Unified Concept for Controlling a Marine Surface Vessel Through the Entire Speed Envelope. In: *Proceedings of the IEEE MED'05*. Cyprus.
- Breivik, M. and T. I. Fossen (2005b). Principles of guidance-based path following in 2D and 3D. In: *Proceedings of the CDC-ECC'05*. Seville, Spain.

- Breivik, M. and T.I. Fossen (2009). Guidance Laws for Autonomous Underwater Vehicles. In: *Intelligent Underwater Vehicles* (A. V. Inzartsev, Ed.). Chap. 4. I-Tech Education and Publishing. <Open Access: <http://books.i-techonline.com>>. ISBN 978-953-7619-49-7.
- Breivik, M. and G. Sand (2009). Jens Glad Balchen: A Norwegian Pioneer in Engineering Cybernetics. *Modeling, Identification and Control* MIC-30(3), 101–125.
- Breivik, M., J. P. Strand and T. I. Fossen (2006). Guided Dynamic Positioning for Fully Actuated Marine Surface Vessels. In: *Proceedings of the 7th IFAC MCMC'06*. Lisbon, Portugal.
- Breivik, M., V. E. Hovstein and T. I. Fossen (2008). Ship formation control: A guided leader-follower approach. In: *Proceedings of the 17th IFAC World Congress*. Seoul, Korea.
- Bretschneider, C. L. (1959). Wave Variability and Wave Spectra for Wind Generated Gravity Waves. Technical Report. Beach Erosion Board, Corps. of Engineers. 118 (Technical Memo).
- Bretschneider, C. L. (1969). *Wave and Wind Loads. Section 12 of Handbook of Ocean and Underwater Engineering*. McGraw-Hill. New York, NY.
- Brian, Adrian (2003). *Ship Hydrostatics and Stability*. Butterworth-Heinemann. Oxford, UK.
- Brian, D., O. Andersen and J. B. Moore (1989). *Optimal Control: Linear Quadratic Methods*. Prentice Hall. London.
- Britting, K. R. (1971). *Inertial Navigation Systems Analysis*. Wiley Interscience.
- Brown, R. G. and Y. C. Hwang (1998). *Introduction to Random Signals and Applied Kalman Filtering*. John Wiley & Sons, Inc. New York, NY.
- Burger, W. and A. G. Corbet (1960). *Ship Stabilizers. Their Design and Operation in Correcting the Rolling of Ships. A Handbook for Merchant Navy Officers*. Pergamon Press Ltd. London.
- Byrnes, C. I. and A. Isidori (1989). New Results and Examples in Nonlinear Feedback Stabilization. *Systems and Control Letters* SCL-12, 437–442.
- Byrnes, C. I., A. Isidori and J. C. Willems (1991). Passivity, Feedback Equivalence, and the Global Stabilization of Minimum Phases Nonlinear Systems. *IEEE Transactions on Automatic Control* TAC-36, 1228–1240.
- Calvert, S. (1989). Optimal Weather Routing Procedures for Vessels on Oceanic Voyages. PhD thesis. Institute of Marine Studies, Polytechnic South West, UK.
- Carley, J. B. (1975). Feasibility Study of Steering and Stabilizing by Rudder. In: *Proceedings of the 4th International Ship Control Systems Symposium (SCSS'75)*. The Hague, Netherlands.

- Carlton, J. S. (1994). *Marine Propellers and Propulsion*. Oxford, U.K., Butterworth-Heinemann Ltd.
- Chislett, M. S. and J. Strøm-Tjøsen (1965a). Planar Motion Mechanism Tests and Full-Scale Steering and Maneuvering Predictions for a Mariner Class Vessel. Technical Report Hy-5. Hydro- and Aerodynamics Laboratory. Lyngby, Denmark.
- Chislett, M. S. and J. Strøm-Tjøsen (1965b). Planar Motion Mechanism Tests and Full-Scale Steering and Maneuvering Predictions for a Mariner Class Vessel. Technical Report Hy-6. Hydro- and Aerodynamics Laboratory. Lyngby, Denmark.
- Chalmers, T. W. (1931). The Automatic Stabilisation of Ships. Chapman and Hall, London.
- Chiaverini, S. (1993). *Estimate of the two Smallest Singular Values of the Jacobian Matrix: Application to Damped Least-Squares Inverse Kinematics*, *Journal of Robotic Systems*, 10(8), 991-ÅŠ1008.
- Chiaverini, S., B. Siciliano and O. Egeland (1994). *Review of the Damped Least-Squares Inverse Kinematics with Experiments on an Industrial Robot Manipulator* 2(2), 123-134.
- Choi, H. T., A. Hanai, S. K. Choi and J. Yuh (2003). Development of an Underwater Robot, ODIN-III. Proc. of the 2003 IEEURSJ International Conference on Intelligent Robots and Systems Las Vegas, Nevada. October 2003.
- Chou, J. C. K. (1992). Quaternion Kinematic and Dynamic Differential Equations. *IEEE Transactions on Robotics and Automation* RA-8(1), 53-64.
- Clarke, D. (2003). The foundations of steering and manoeuvring. In: *Proceedings of the IFAC Conference on Maneuvering and Control of Marine Craft (MCMC'03)*. Girona, Spain.
- Clarke, D. and J. R. Horn (1997). Estimation of hydrodynamic derivatives. In: *Proceedings of the 11th Ship Control Systems Symposium, Southampton, Volume 2, 14th-19th April 1997*. pp. 275-289.
- Cowley, W. E. and T. H. Lambert (1972). The Use of Rudder as a Roll Stabilizer. In: *Proceedings of the 3rd International Ship Control Systems Symposium (SCSS'72)*. Bath, UK.
- Cowley, W. E. and T. H. Lambert (1975). Sea Trials on a Roll Stabilizer Using the Ship's Rudder. In: *Proceedings of the 4th International Ship Control Systems Symposium (SCSS'75)*. The Hague, Netherlands.
- Craig, J. J. (1989). *Introduction to Robotics*. Addison-Wesley. Reading, MA.
- Cristi, R., F. A. Papoulias and A. J. Healey (1990). Adaptive Sliding Mode Control of Autonomous Underwater Vehicles in the Dive Plane. *IEEE Journal of Oceanic Engineering* OE-15(3), 152-160.

- Cummins, W. E. (1962). The Impulse Response Function and Ship Motions. Technical Report 1661. David Taylor Model Basin. Hydrodynamics Laboratory, USA.
- Davidson, K. S. M. and L. I. Schiff (1946). Turning and Course Keeping Qualities. *Transactions of SNAME*.
- Defant, A. (1961). *Physical Oceanography*. Pergamon Press. London.
- De Kat, J. O. and J. E. W. Wicher (1991). Behavior of a Moored Ship in Unsteady Current, Wind and Waves. *Marine Technology* 28(5), 251–264.
- de-la-Cruz, J. M., J. Aranda, P. Ruiperez, J. M. Diaz and A. Maron (1998). Identification of the Vertical Plane Motion Model of a High Speed Craft by Model Testing in Irregular Waves. In: *Proceedings of the IFAC Conference on Control Applications in Marine Systems (CAMS'98)*. Fukuoka, Japan. pp. 257–262.
- Dieudonné, J. (1953). Collected French Papers on the Stability of Route of Ships at Sea, 1949–1950 (Translated by H. E. Saunders and E. N. Labouvie). Technical Report DTMB-246. Naval Ship Research and Development Center. Washington D.C.
- DnV (1990). *Rules for Classification of Steel Ships: Dynamic Positioning Systems, Part 6, Chapter 7*. Det norske Veritas, Veritasveien 1, N-1322 Høvik, Norway.
- Donha, D. C., D. S. Desanj, M. R. Katebi and M. J. Grimble (1998).  $H_\infty$  adaptive Controller for Autopilot Applications. *Spesial Issue on Marine Systems of the International Journal of Adaptive Control and Signal Processing* IJACSP-12(8), 623–648.
- Draper, C. S. (1971). Guidance is Forever. *Navigation* 18(1), 26–50.
- Dubins, L. (1957). On Curves of Minimal Length with a Constraint on Average Curvature and with Prescribed Initial and Terminal Positions and Tangents. *American Journal of Mathematics* 79, 497–516.
- Durham, W. C. (1993). Constrained Control Allocation. *Journal of Guidance, Control and Dynamics* JGCD-16(4), 717–725.
- Durham, W. C. (1994a). Attainable Moments for the Constrained Control Allocation Problem. *Journal of Guidance, Control and Dynamics* JGCD-17(6), 1371–1373.
- Durham, W. C. (1994b). Constrained Control Allocation: Three Moment Problem. *Journal of Guidance, Control and Dynamics* JGCD-17(2), 330–336.
- Durham, W. C. (1999). Efficient, Near-Optimal Control Allocation. *Journal of Guidance, Control and Dynamics* JGCD-22(2), 369–372.
- Dyne, G. and P. Trägårdh (1975). Simuleringsmodell för 350 000 tdw tanker i fullast- och ballastkonditioner på djupt vatten. Technical Report 2075-1. Swedish State Shipbuilding Experimental Tank (SSPA). Gothenburg, Sweden.
- Egeland, O. and J. T. Gravdahl (2002). *Modeling and Simulation for Automatic Control*. Marine Cybernetics. Trondheim, Norway.

- Encarnacao, P. and A. Pascoal (2001). Combined Trajectory Tracking and Path Following for Marine Craft. In: *Proceedings of the 9th Mediterranean Conference on Control and Automation*. Dubrovnik, Croatia.
- Encarnacao, P., A. Pascoal and M. Arcak (2000). Path Following for Autonomous Marine Craft. In: *Proceedings of the 5th MCMC'00*. Aalborg, Denmark. pp. 117–122.
- Esteban, S., J. M. de-la-Cruz, J. M. Giron-Sierra, B. de-Andres, J. M. Diaz and J. Aranda (2000). Fast Ferry Vertical Accelerations Reduction with Active Flaps and T-foil. In: *Proceedings of the 5th Conference on Maneuvering and Control of Marine Craft (MCMC'2000)*. Aalborg, Denmark. pp. 233–238.
- Euler, L. (1776). Novi Commentarii Academiae Scientiarum Imperialis Petropolitane. - Vol. XX, 189.
- Faltinsen, O. M. (1990). *Sea Loads on Ships and Offshore Structures*. Cambridge University Press.
- Faltinsen, O. M. (2005). *Hydrodynamic of High-Speed Marine Vehicles*. Cambridge University Press.
- Faltinsen, O. M. and B. Sortland (1987). Slow Drift Eddy Making Damping of a Ship. *Applied Ocean Research* AOR-9(1), 37–46.
- Farrell, J. A. (2008). *Aided Navigation: GPS with High Rate Sensors*. McGraw-Hill. New York, NY.
- Farrell, J. A. and M. Barth (1998). *The Global Positioning System and Inertial Navigation*. McGraw-Hill. New York, NY.
- Fathi, D. (2004). *ShipX Vessel Responses (VERES)*. Marintek AS, Trondheim, Norway. <http://www.sintef.no/>.
- Fedyaevsky, K. K. and G. V. Sobolev (1963). Control and Stability in Ship Design. State Union Shipbuilding House.
- Feldman, J. (1979). DTMSRDC Revised Standard Submarine Equations of Motion. Technical Report DTNSRDC-SPD-0393-09. Naval Ship Research and Development Center. Washington D.C.
- Fjellstad, O. E. and T. I. Fossen (1994). Quaternion Feedback Regulation of Underwater Vehicles. In: *Proceedings of the 3rd IEEE Conference on Control Applications (CCA'94)*. Glasgow. pp. 857–862.
- Fjellstad, O. E., T. I. Fossen and O. Egeland (1992). Adaptive Control of ROVs with Actuator Dynamics and Saturation. In: *Proceedings of the 2nd International Offshore and Polar Engineering Conference (ISOPE)*. San Francisco, CA.
- Forssell, B. (1991). *Radio Navigation Systems*. Prentice Hall. Englewood Cliffs, NJ.

- Fossen, T. I. (1991). Nonlinear Modeling and Control of Underwater Vehicles. PhD thesis. Department of Engineering Cybernetics, Norwegian University of Science and Technology. Trondheim, Norway.
- Fossen, T. I. (1993). Comments on “Hamiltonian Adaptive Control of Spacecraft”. *IEEE Transactions on Automatic Control* TAC-38(4), 671–672.
- Fossen, T. I. (1994). *Guidance and Control of Ocean Vehicles*. John Wiley & Sons. Ltd. ISBN 0-471-94113-1.
- Fossen, T. I. (2000a). A Survey on Nonlinear Ship Control: From Theory to Practice. In: *Proceedings of the IFAC Conference on Maneuvering and Control of Marine Craft* (G. Roberts, Ed.). Elsevier Science. Netherlands. pp. 1–16. Plenary Talk.
- Fossen, T. I. (2000b). Recent Developments in Ship Control Systems Design. In *World Superyacht Review*. Sterling Publications Limited, London pp. 115–116.
- Fossen, T. I. (2005). Nonlinear Unified State-Space Model for Ship Maneuvering and Control in a Seaway. *International Journal of Bifurcation and Chaos* IJBC-15(9), 2717–2746. Also in the Proceedings of the ENOC’05 (Plenary Talk), Eindhoven, Netherlands, August 2005, pp. 43–70.
- Fossen, T. I. (2012). How to Incorporate Wind, Waves and Ocean Currents in the Marine Craft Equations of Motion. In: *Proceedings of the IFAC Conference on Maneuvering and Control of Marine Craft (MCMC’12)*, 19-21 September, Arenzano, Italy 2012.
- Fossen, T. I. and M. Blanke (2000). Nonlinear Output Feedback Control of Underwater Vehicle Propellers using Feedback from Estimated Axial Flow Velocity. *IEEE Journal of Oceanic Engineering*, JOE-25(2), 241–255.
- Fossen, T. I. and S. P. Berge (1997). Nonlinear Vectorial Backstepping Design for Global Exponential Tracking of Marine Vessels in the Presence of Actuator Dynamics. In: *Proceedings of the IEEE Conference on Decision and Control (CDC’97)*. San Diego, CA. pp. 4237–4242.
- Fossen, T. I. and O. E. Fjellstad (1995). Nonlinear Modelling of Marine Vehicles in 6 Degrees of Freedom. *International Journal of Mathematical Modelling of Systems* JMMS-1(1), 17–28.
- Fossen, T. I. and Å. Grøvlen (1998). Nonlinear Output Feedback Control of Dynamically Positioned Ships Using Vectorial Observer Backstepping. *IEEE Transactions on Control Systems Technology* TCST-6(1), 121–128.
- Fossen, T. I. and T. A. Johansen (2006). A Survey of Control Allocation Methods for Ships and Underwater Vehicles. In: *Proceedings of the 14th IEEE Mediterranica Conference on Control and Automation*. Ancona, Italy.
- Fossen, T. I. and T. Lauvdal (1994). Nonlinear Stability Analysis of Ship Autopilots in Sway, Roll and Yaw. *Proceedings of the Conference on Marine Craft Maneuvering and Control (MCMC’94)*. Southampton, UK.

- Fossen, T. I. and M. Paulsen (1992). Adaptive Feedback Linearization Applied to Steering of Ships. In: *Proceedings of the 1st IEEE Conference on Control Applications*. Dayton, Ohio. pp. 1088–1093.
- Fossen, T. I. and T. Perez (2009). Kalman Filtering for Positioning and Heading Control of Ships and Offshore Rigs. *IEEE Control Systems Magazine* CST-29(6), 32–46.
- Fossen, T. I. and S. I. Sagatun (1991). Adaptive Control of Nonlinear Systems: A Case Study of Underwater Robotic Systems. *Journal of Robotic Systems* JRS-8(3), 393–412.
- Fossen, T. I. and Ø. N. Smogeli (2004). Nonlinear Time-Domain Strip Theory Formulation for Low-Speed Maneuvering and Station-Keeping. *Modelling, Identification and Control* MIC-25(4), 201–221.
- Fossen, T. I. and J. P. Strand (1998). Nonlinear Ship Control (Tutorial Paper). In: *Proceedings of the IFAC CAMS'98*. Fukuoka, Japan. pp. 1–75.
- Fossen, T. I. and J. P. Strand (1999a). A Tutorial on Nonlinear Backstepping: Applications to Ship Control. *Modelling, Identification and Control* MIC-20(2), 83–135.
- Fossen, T. I. and J. P. Strand (1999b). Passive Nonlinear Observer Design for Ships Using Lyapunov Methods: Experimental Results with a Supply Vessel. *Automatica* AUT-35(1), 3–16.
- Fossen, T. I. and J. P. Strand (2000). Position and Velocity Observer Design. In: *The Ocean Engineering Handbook* (F. El-Hawary, Ed.). Chap. 3, pp. 189–206. CRC Press.
- Fossen, T. I. and J. P. Strand (2001). Nonlinear Passive Weather Optimal Positioning Control (WOPC) System for Ships and Rigs: Experimental Results. *Automatica* AUT-37(5), 701–715.
- Fossen, T. I., S. I. Sagatun and A. J. Sørensen (1996). Identification of Dynamically Positioned Ships. *Journal of Control Engineering Practice* CEP-4(3), 369–376.
- Fossen, T. I., A. Loria and A. Teel (2001). A Theorem for UGAS and ULES of (Passive) Nonautonomous Systems: Robust Control of Mechanical Systems and Ships. *International Journal of Robust and Nonlinear Control* JRNC-11, 95–108.
- Fossen, T. I., M. Breivik and R. Skjetne (2003). Line-of-Sight Path Following of Underactuated Marine Craft. In: *Proceedings of the IFAC MCMC'03*. Girona, Spain.
- Fossen, T. I., T. A. Johansen and T. Perez (2009). A Survey of Control Allocation Methods for Underwater Vehicles. In: *Underwater Vehicles* (A. V. Inzartsev, Ed.). Chap. 7, pp. 109–128. In-Tech Education and Publishing.
- Fotakis, J., M. J. Grimble and B. Kouvaritakis (1982). A Comparison of Characteristic Locus and Optimal Designs for Dynamic Ship Positioning Systems. *IEEE Transactions on Automatic Control* TAC-27(6), 1143–1157.

- Frenet, F. (1847). Sur les Courbes à Double Courbure, Thèse, Toulouse. *Journal de Mathématiques*. Viewed November 19, 2009, <[http://portail.mathdoc.fr/JMPA/PDF/JMPA\\_1852\\_1\\_17\\_A22\\_0.pdf](http://portail.mathdoc.fr/JMPA/PDF/JMPA_1852_1_17_A22_0.pdf)>.
- Freund, E. (1973). Decoupling and Pole Assignment in Nonlinear Systems. *Electronics Letter*.
- Fung, P. T-K. and M. J. Grimble (1981). Self-Tuning Control of Ship Positioning Systems. In: *Self-Tuning and Adaptive Control: Theory and Applications* (C. J. Harris and S. A. Billings, Eds.). pp. 308–331. Peter Peregrinus Ltd. on behalf of IEE.
- Fung, P. T-K. and M. J. Grimble (1983). Dynamic Ship Positioning Using a Self Tuning Kalman Filter. *IEEE Transactions on Automatic Control* TAC-28(3), 339–349.
- Fujii, H. (1960). Experimental Researches on Rudder Performance (1) [in Japanese]. *J Zosen Kiokai*, 107, 105–111.
- Fujii, H. and T. Tsuda (1961). Experimental Researches on Rudder Performance (2). [in Japanese]. *J Zosen Kiokai*, 110, 31–42.
- Fujii, H. and T. Tsuda (1962). Experimental Researches on Rudder Performance (3). [in Japanese]. *J Zosen Kiokai*, 111, 51–58.
- Gade, K. The Seven Ways to Find Heading. *The Royal Institute of Navigation* RIN-69, 955–970.
- Gelb, A. and W. E. Vander Velde (1968). *Multiple-Input Describing Functions and Nonlinear System Design*. McGraw-Hill Book Company.
- Gelb, A., J. F. Kasper, Jr., R. A. Nash, Jr., C. F. Price and A. A. Sutherland, Jr. (1988). *Applied Optimal Estimation*. MIT Press. Boston, MA.
- Gertler, M. and S. C. Hagen (1960). Handling Criteria for Surface Ships. Technical Report DTMB-1461. Naval Ship Research and Development Center. Washington D.C.
- Gertler, M. and G. R. Hagen (1967). Standard Equations of Motion for Submarine Simulation. Technical Report DTMB-2510. Naval Ship Research and Development Center. Washington D.C.
- Giron-Sierra, J. M., S. Esteban, B. De Andres, J. M. Diaz and J. M. Riola (2001). Experimental Study of Controlled Flaps and T-foil for Comfort Improvements of a Fast Ferry. In: *Proceedings of the IFAC Conference on Control Applications in Marine Systems (CAMS'01)*. Glasgow, UK.
- Goldstein, H. (1980). *Classical Mechanics*. Addison-Wesley. Reading, MA.
- Graver, J. G. (2006). *Underwater Gliders: Dynamics, Control and Design*. PhD thesis. Princeton University, New Jersey, USA.

- Grewal, M. S., L. R. Weill and A. P. Andrews (2001). *Global Positioning Systems, Inertial Navigation and Integration*. John Wiley & Sons, Inc. New York, NY.
- Grimble, M. J. (1978). Relationship Between Kalman and Notch Filters Used in Dynamic Ship Positioning Systems. *Electronics Letters* EL-14(13), 399–400.
- Grimble, M. J. and M. A. Johnson (1989). *Optimal Control and Stochastic Estimation. Theory and Applications*. John Wiley & Sons, Ltd, Chichester, UK.
- Grimble, M. J., R. J. Patton and D. A. Wise (1979). The Design of Dynamic Positioning Systems using Extended Kalman Filtering Techniques. In: *Proceedings of OCEANS'79*. pp. 488–497.
- Grimble, M. J., R. J. Patton and D. A. Wise (1980). The Design of Dynamic Positioning Control Systems Using Stochastic Optimal Control Theory. *Optimal Control Applications and Methods* OCAM-1, 167–202.
- Grimble, M. J., R. J. Patton and D. A. Wise (1980b). Use of Kalman Filtering Techniques in Dynamic Ship Positioning Systems. *IEE Proceedings* 127D(3), 93–102.
- Grip, H. F., T. I. Fossen, T. A. Johansen and A. Saberi (2011). Attitude Estimation Based on Time-Varying Reference Vectors with Biased Gyro and Vector Measurements. In: *Proceedings of the 2011 IFAC World Congress*. Milan, Italy.
- Grøvlen, Å. and T. I. Fossen (1996). Nonlinear Control of Dynamic Positioned Ships Using Only Position Feedback: An Observer Backstepping Approach. In: *Proceedings of the 35th IEEE Conference on Decision and Control (CDC'96)*. pp. 3388–3393.
- Hagiwara, H. (1989). Weather Routing of Sail-Assisted Motor Vessels. PhD thesis. University of Delft, Netherlands.
- Harvey, A. C. (1989). *Forecasting Structural Time Series Models and the Kalman Filter*. Cambridge University Press.
- Hasselmann *et al.* (1973). Measurements of Wind-Wave Growth and Swell Decay during the Joint North Sea Wave Project (JONSWAP). *Deutschen Hydrographischen Zeitschrift*.
- Hauser, J. and R. Hindmann (1995). Maneuvering Regulation from Trajectory Tracking: Feedback Linearizable Systems. In: *Proceedings IFAC Symposium on Nonlinear Control Systems Design*. Lake Tahoe, CA. pp. 595–600.
- Healey, A. J. and D. Lienard (1993). Multivariable Sliding Mode Control for Autonomous Diving and Steering of Unmanned Underwater Vehicles. *IEEE Journal of Ocean Engineering*, OE-18(3), 327–339.
- Healey, A. J. and D. B. Marco (1992). Slow Speed Flight Control of Autonomous Underwater Vehicles: Experimental Results with the NPS AUV II. In: *Proceedings of the 2nd International Offshore and Polar Engineering Conference (ISOPe)*. San Francisco, CA. pp. 523–532.

- Healey, A. J., S. M Rock, S. Cody, D. Miles and J. P. Brown. Toward an Improved Understanding of Thruster Dynamics for Underwater Vehicles. *IEEE Journal of Oceanic Engineering*, JOE-29(4), 354–361, 1995.
- Hearns, G. and M. Blanke (1998). Quantitative Analysis and Design of a Rudder Roll Damping Controller. In: *Proceedings IFAC Conference on Control Applications in Marine Systems (CAMS'98)*. pp. 115–120. Fukuoka, Japan.
- Hearns, E., R. Katebi and M. Grimble (2000). Robust Fin Roll Stabilizer Controller Design. In: *Proceedings of the 5th IFAC Conference on Maneuvering and Control of Marine Craft*. Aalborg, Denmark. pp. 81–86.
- Hegrenæs, Øyvind (2010). Autonomous Navigation for Underwater Vehicles. PhD thesis. Department of Engineering Cybernetics, Norwegian University of Science and Technology, Trondheim, Norway.
- Heiskanen, W. A. and H. Moritz (1967). *Physical Geodesy*. Freeman. London.
- Hickey, N. A., M. J. Grimble, M. A. Johnson, M. R. Katebi and R. Melville (1997). Robust Fin Roll Stabilization of Surface Ships. In: *Proceedings of the IEEE Conference on Decision and Control (CDC'97)*. Vol. 5. pp. 4225–4230.
- Hickey, N. A., M. A. Johnson, M. R. Katebi and M. J. Grimble (2000). PID Controller Optimization for Fin Roll Stabilization. In: *Proceedings of the IEEE Conference of Control Applications (CCA'2000)*. Hawaii, HI. pp. 1785–1790.
- Hoerner, S. F. (1965). *Fluid Dynamic Drag*. Hartford House.
- Hofmann-Wellenhof, B., H. Lichtenegger and J. Collins (1994). *Global Positioning System: Theory and Practice*. 3rd ed. Springer Verlag. New York, NY.
- Holzhüter, T. (1992). On the Robustness of Course Keeping Autopilots. In: *Proceedings of IFAC Workshop on Control Applications in Marine Systems (CAMS'92)*. Genova, Italy. pp. 235–244.
- Holzhüter, T. (1997). LQG Approach for the High-Precision Track Control of Ships. *IEE Proceedings on Control Theory and Applications* 144(2), 121–127.
- Holzhüter, T. and R. Schultze (1996). On the Experience with a High-Precision Track Controller for Commercial Ships. *Control Engineering Practice* CEP-4(3), 343–350.
- Holzhüter, T. and H. Strauch (1987). A Commercial Adaptive Autopilot for Ships: Design and Experimental Experience. In: *Proceedings of the 10th IFAC World Congress*. July 27–31, Munich, Germany. pp. 226–230.
- Hooft, J. P. (1994). The cross-flow drag on manoeuvring ship. *Oceanic Engineering* OE-21(3), 329–342.
- Hua, M.-D (2010). Attitude Estimation for Accelerated Vehicles using GPS/INS Measurements. *Control Engineering Practice* CEP-18, 723–732.

- Hughes, P. C. (1986). *Spacecraft Attitude Dynamics*. John Wiley & Sons, Inc. New York, NY.
- Humphreys, D. E. and K. W. Watkinson (1978). Prediction of the Acceleration Hydrodynamic Coefficients for Underwater Vehicles from Geometric Parameters. Technical Report NCSL-TR-327-78. Naval Coastal System Center. Panama City, Florida.
- Hydroid Inc. (2019). Marine Robots (AUVs) <[www.hydroid.com](http://www.hydroid.com)>. Retrieved 12 June 2019.
- Ikeda, Y., K. Komatsu, Y. Himeno and N. Tanaka (1976). On Roll Damping Force of Ship: Effects of Friction of Hull and Normal Force of Bilge Keels. *Journal of the Kansai Society of Naval Architects* JKSNA-142, 54–66.
- Imlay, F. H. (1961). The Complete Expressions for Added Mass of a Rigid Body Moving in an Ideal Fluid. Technical Report DTMB 1528. David Taylor Model Basin. Washington D.C.
- Ingram, M. J., R. C. Tyce and R. G. Allen (1996). Dynamic Testing of State of the Art Vertical Reference Units. In: *Proceedings of the Oceans 96 MTS/IEEE*. IEEE. pp. 1533–1538.
- Isherwood, R. M. (1972). Wind Resistance of Merchant Ships. *RINA Transcripts* 115, 327–338.
- Isidori, A. (1989). *Nonlinear Control Systems*. Springer-Verlag. Berlin.
- ISO 2631-1 (1997). Mechanical Vibration and Shock. Evaluation of Human Exposure to Whole-Body Vibration – Part 1: General Requirements.
- ISO 2631-3 (1985). Evaluation of Human Exposure to Whole-Body Vibration – Part 3: Evaluation of Whole Body  $z$ -axis Vertical Vibration in the Frequency Range 0.1 to 0.63 Hz.
- Jacobson, D. H. (1977). *Extensions to Linear-Quadratic Control, Optimization and Matrix Theory*. Academic Press. New York, NY.
- Jensen, J. J., A. E. Mansour and A. S. Olsen. Estimation of Ship Motions using Closed-Form Expressions *Ocean Engineering* OE-31, 61–85.
- Johansen, T. A., T. I. Fossen and S. P. Berge (2004). Constraint Nonlinear Control Allocation with Singularity Avoidance using Sequential Quadratic Programming. *IEEE Transactions on Control Systems Technology* TCST-12, 211–216.
- Johansen, T. A., T. I. Fossen and P. Tøndel (2005). Efficient Optimal Constrained Control Allocation via Multi-Parametric Programming. *AIAA Journal of Guidance, Control and Dynamics* 28, 506–515.
- Jouffroy, J. and T. I. Fossen (2010). A Tutorial on Incremental Stability Analysis using Contraction Theory. *Modelling, Identification and Control* MIC-31(3), 93–106.

- Joung, T.-H., K. Sammut, F. He and S.-K. Lee (2012). Shape Optimization of an Autonomous Underwater Vehicle with a Ducted Propeller using Computational Fluid Dynamics Analysis. *International Journal of Naval Architecture and Ocean Engineering*, 4:44–56.
- Journée, J. M. J. and L. J. M. Adegeest (2003). *Theoretical Manual of Strip Theory Program SEAWAY for Windows*. Delft University of Technology, Delft, Netherlands. <http://www.ocp.tudelft.nl/mt/journee>.
- Journée, J.M.J. and W.W. Massie (2001). *Offshore Hydrodynamics*. Delft University of Technology.
- Jurdjevic, V. and J. P. Quinn (1978). Controllability and Stability. *Journal of Differential Equations* JDE-28, 381–389.
- Källström, C. G. (1981). Control of Yaw and Roll by Rudder/Fin Stabilization System. In: *Proceedings of the 6th International Ship Control Systems Symposium (SCSS'81)*, Vol. 2. Paper F2 3-1. Ottawa, Canada.
- Källström, C. G. (1987). Improved Operational Effectiveness of Naval Ships by Rudder Roll Stabilization. In: *NAVAL'87, Asian Pacific Naval Exhibition and Conference*. Singapore.
- Källström, C. G. and W. L. Schultz (1990). An Integrated Rudder Control System for Roll Damping and Maintenance. In: *Proceedings of the 9th International Ship Control Systems Symposium (SCSS'90)*. Bethesda, MD. pp. 3.278–3.296.
- Källström, C. G. and K. Theoren (1994). Rudder-Roll Stabilization an Improved Control Law. In: *Proceedings of the IEEE Conference on Control Applications*. New York, NY, pp. 1099–1105.
- Källström, C. G., P. Wessel and S. Sjölander (1988). Roll Reduction by Rudder Control. In: *Proceedings of the SNAME Spring Meeting/STAR Symposium*. Pittsburg, PE. pp. 67–76.
- Kalman, R. E. (1960). A New Approach to Linear Filtering and Prediction Problems. *ASME Transactions, Series D: Journal of Basic Engineering* JBE-82, 35–42.
- Kalman, R. E. and R. S. Bucy (1961). New Results in Linear Filtering and Prediction Theory. *ASME Transactions, Series D: Journal of Basic Engineering* JBE-83, 95–108.
- Kane, T. R., P. W. Likins and D. A. Levinson (1983). *Spacecraft Dynamics*. McGraw-Hill. New York, NY.
- Kanellakopoulos, I., P. V. Kokotovic and A. S. Morse (1992). A Toolkit for Nonlinear Feedback Design. *Systems and Control Letters* SCL-18, 83–92.

- Katebi, M. R., D. K. K. Wong and M. J. Grimble (1987). LQG Autopilot and Rudder Roll Stabilization Control System Design. In: *Proceedings of the 8th International Ship Control Systems Symposium (SCSS'87)*. The Hague, Netherlands. pp. 3.69–3.84.
- Katebi, M. R., M. J. Grimble and Y. Zhang (1997a).  $H_\infty$  Robust Control Design for Dynamic Ship Positioning. In: *IEE Proceedings on Control Theory and Applications*. Vol. 144 2. pp. 110–120.
- Katebi, M. R., Y. Zhang and M. J. Grimble (1997b). Nonlinear Dynamic Ship Positioning. In: *Proceedings of the 13th IFAC World Congress*. Vol. Q. pp. 303–308.
- Katebi, M. R., N. A. Hickey and M. J. Grimble (2000). Evaluation of Fin Roll Stabilizer Controller Design. In: *Proceedings of the 5th IFAC Conference on Maneuvering and Control of Marine Craft*. Aalborg, Denmark. pp. 69–74.
- Kayton, M. and W. L. Fried (1997). *Avionics Navigation Systems*. John Wiley & Sons, Inc. New York, NY.
- Kempf, G. (1932). Measurements of the Propulsive and Structural Characteristic of Ships. In: *Transactions of SNAME* 40, 42–57.
- Kempf, G. (1944). Manöveriernorm für Schiffe. In: *Hansa, Deutsche Schiffahrtszeitschrift*, Heft 27/28. pp. 372–276 (in German).
- Khalil, H. K. (2002). *Nonlinear Systems*. Macmillan. New York, NY.
- Kijima, K., T. Katsuno, Y. Nakiri and Y. Furukawa (1990). On the Manoeuvring Performance of a Ship with the Parameter of Loading Condition. *J. Society of Naval Architects of Japan*. 168, 141–148.
- Kirchhoff, G. (1869). *Über die Bewegung eines Rotationskörpers in einer Flüssigkeit*. Crelle's Journal, No. 71, pp. 237–273 (in German).
- Kitamura, F., H. Sato, K. Shimada and T. Mikami (1997). Estimation of Wind Force Acting on Huge Floating Ocean Structures. In: *Proceedings of the Oceans '97. MTS/IEEE Conference*. Vol. 1. pp. 197–202.
- Koditschek, D. E. (1987). Adaptive Techniques for Mechanical Systems. In: *Proceedings of the 5th Yale Workshop on Adaptive Systems*. New Haven, CT. pp. 259–265.
- Kokotovic, P. V. (1991). The Joy of Feedback: Nonlinear and Adaptive. *IEEE Control Systems Magazine* ICSM-12, 7–17. Bode Price Lecture.
- Kokotovic, P. V. and H. J. Sussmann (1989). A Positive Real Condition for Global Stabilization of Nonlinear Systems. *Systems and Control Letters* SCL-13, 125–133.
- Korotkin, A. I. Added Masses of Ship Structures. (2009). Springer Science.
- Kostov, V. and E. Degtiariova-Kostova (1993). Suboptimal Paths in the Problem of a Planar Motion with Bounded Derivative of the Curvature. Technical Report. Research Report 2051, INRIA, France.

- Koyama, T. (1967). *On the Optimum Automatic Steering System of Ships at Sea.* J.S.N.A., Vol. 122.
- Kristiansen, E. and O. Egeland (2003). Frequency Dependent Added Mass in Models for Controller Design for Wave Motion Damping. In: *Proceedings of the IFAC Conference on Maneuvering and Control of Marine Craft (MCMC'03)*. Girona, Spain.
- Kristiansen, E., A. Hjulstad and O. Egeland (2005). State-Space Representation of Radiation Forces in Time-Domain Vessel Models. *Oceanic Engineering* OE-32, 2195–2216.
- Krstic, M. and H. Deng (1998). *Stabilization of Nonlinear Uncertain Systems.* Springer-Verlag. Berlin.
- Krstic, M., I. Kanellakopoulos and P. V. Kokotovic (1995). *Nonlinear and Adaptive Control Design.* John Wiley & Sons, Inc. New York, NY.
- Kurokawa, H. (1997). Constrained Steering Law of Pyramid-Type Control Moment Gyros and Ground Tests. *AIAA Journal of Guidance, Control and Dynamics* 20(3), 445–449.
- Kurokawa, H. (1997). Survey of Theory and Steering Laws of Single-Gimbal Control Moment Gyros. *AIAA Journal of Guidance, Control and Dynamics* 30(5), 1331–1340.
- Kvasnica, M., P. Grieder and M. Baotic (2004). Multi-Parametric Toolbox (MPT). Viewed December 26, 2009, <[www.control.ee.ethz.ch/~mpt](http://www.control.ee.ethz.ch/~mpt)>.
- Lamb, H. (1932). *Hydrodynamics.* Cambridge University Press. London.
- Landau, Y. D. (1979). *Adaptive Control – The Model Reference Approach.* Marcel Dekker Inc. New York, NY.
- Lapierre, L. and D. Soetanto (2007). Nonlinear Path-Following Control of an AUV. *Ocean Engineering* OE-34, 1734–1744.
- LaSalle, J. P. (1966). Stability Theory for Ordinary Differential Equations. *Journal of Differential Equations* JDE-4, 57–65.
- LaSalle, J. and S. Lefschetz (1961). *Stability by Lyapunov's Direct Method.* Academic Press. Baltimore, MD.
- Laувдал, Т. and Т. И. Фоссен (1997). Nonlinear Rudder-Roll Damping of Non-Minimum Phase Ships Using Sliding Mode Control. In: *Proceedings of the European Control Conference.* Brussels, Belgium.
- Laувдал, Т. and Т. И. Фоссен (1998). Rudder Roll Stabilization of Ships Subject to Input Rate Saturation Using a Gain Scheduled Control Law. In: *Proceedings of the IFAC Conference on Control Applications in Marine Systems (CAMS'98).* pp. 121–127. Fukuoka, Japan.

- Leick, A. (1995). *GPS: Satellite Surveying*. Chap. Appendix G, pp. 534–537. John Wiley & Sons, Ltd.
- Leite, A .J. P., J. A. P. Aranha, C. Umeda and M. B. de Conti (1998). Current Forces in Tankers and Bifurcation of Equilibrium of Turret Systems: Hydrodynamic Model and Experiments. *Applied Ocean Research* AOR-20, 145–156.
- Lewandowski, E. M. (2004). *The Dynamics of Marine Craft: Maneuvering and Seakeeping*. World Scientific. Washington D. C.
- Lewis, F. M. (1967). The Motion of Ships in Waves. In: *Principles of Naval Architecture* (J. P. Comstock, Ed.). pp. 669–692. Society of Naval Architects and Marine Engineers, 601 Pavonia Avenue, Jersey City, NJ 07306.
- Lewis, E. V. (Ed.) (1989). *Principles of Naval Architecture*. 2nd ed. Society of Naval Architects and Marine Engineers (SNAME).
- Li, B. (2016). *Dynamics and Control of Autonomous Underwater Vehicles with Internal Actuators*. PhD thesis. Faculty of College of Engineering and Computer Science, Florida Atlantic University, Boca Raton, FL, USA.
- Li, B. and T.-C. Su (2016). Nonlinear Heading Control of an Autonomous Underwater Vehicle with Internal Actuators. *Ocean Engineering*, OE-125, 103–112.
- Li, J.-W. and C. Shao (2008). Tracking Control of Autonomous Underwater Vehicles with Internal Moving Mass. *Acta Automatica Sinica* 34(10), 1319–1323.
- Lin, Ching-Fang (1992). *Modern Navigation, Guidance and Control Processing*. Prentice-Hall Inc. Englewood Cliffs, New Jersey 07632.
- Lindgaard, K.-P. (2003). *Acceleration Feedback in Dynamic Positioning Systems*. PhD thesis. Department of Engineering Cybernetics, Norwegian University of Science and Technology. Trondheim, Norway.
- Lindgaard, K. P. and T. I . Fossen (2001a). A Model Based Wave Filter for Surface Vessels using Position, Velocity and Partial Acceleration Feedback. In: *Proceedings of the IEEE Conference on Decision and Control (CDC'2001)*. IEEE. Orlando, FL. pp. 946–951.
- Lindgaard, K. P. and T. I. Fossen (2001b). On Global Model Based Observer Designs for Surface Vessels. In: *5th IFAC Conference on Control Applications in Marine Systems (CAMS'2001)*. Elsevier Science.
- Lindgaard, K.-P. and T. I. Fossen (2003). Fuel Efficient Control Allocation for Surface Vessels with Active Rudder Usage: Experiments with a Model Ship. *IEEE Transactions on Control Systems Technology* 11, 850–862.
- Lindfors, I. (1993). Thrust Allocation Method for the Dynamic Positioning System. In: *10th International Ship Control Systems Symposium (SCSS'93)*. Ottawa, Canada. pp. 3.93–3.106.

- Liu, J. and R. Hekkenberg (2017). Sixty Years of Research on Ship Rudders: Effects of Design Choices on Rudder Performance. *Ships and Offshore Structures*, 12:4, 495–512.
- Ljung, L. (1999). *System Identification: Theory for the User*. Prentice Hall. Englewood Cliffs, New Jersey.
- Lloyd, A. E. J. M. (1975). Roll Stabilization by Rudder. In: *Proceedings of the 4th International Ship Control Systems Symposium (SCSS'75)*. The Hague, Netherlands.
- Lloyd, A. R. J. M. (1989). Seakeeping; Ship Behavior in Rough Water. Ellis Horwood Ltd.
- Lo, H. (1991). Dynamic Ship Routing through Stochastic, Spatially Dependent Ocean Currents. PhD thesis. The Ohio State University, Columbus, OH.
- Lo, H. K. and M. R. McCord (1995). Routing through Dynamic Ocean Currents: General Heuristics and Empirical Results in the Gulf Stream Region. *Transportation Research Part B: Methodological* 29(2), 109–124.
- Lo, H. K. and M. R. McCord (1998). Adaptive Ship Routing through Stochastic Ocean Currents: General Formulations and Empirical Results. *Transportation Research Part A: Policy and Practice* 32(7), 547–561.
- Loria, A., T. I. Fossen and A. Teel (1999). UGAS and ULES of Non-Autonomous Systems: Applications to Integral Action Control of Ships and Manipulators. In: *Proceedings of the 5th European Control Conference (ECC'99)*. Karlsruhe, Germany.
- Loria, A., T. I. Fossen and E. Panteley (2000). A Separation Principle for Dynamic Positioning of Ships: Theoretical and Experimental Results. *IEEE Transactions on Control Systems Technology* TCST-8(2), 332–343.
- Lozano, R., B. Brogliato and I. D. Landau (1992). Passivity and Global Stabilization of Cascaded Nonlinear Systems. *IEEE Transactions on Automatic Control* TAC-37, 1386–1388.
- Lozano, R., B. Brogliato, O. Egeland and B. Maschke (2000). *Dissipative Systems Analysis and Control. Theory and Applications*. Springer Verlag.
- Lyapunov, M. A. (1907). Problème Général de la Stabilité de Mouvement. *Ann. Fac. Sci. Toulouse* 9, 203–474. (Translation of a paper published in Comm. Soc. Math. Kharkow 1893, reprinted in Annual Math Studies, Vol. 17, Princeton, 1949).
- Lyshevski, S. E. (2001). Autopilot Design for Highly Maneuverable Multipurpose Underwater Vehicles. In: *Proceedings of the American Control Conference*. Arlington, VA. pp. 131–136.
- MacKunis, W., K. Dupree, N. Fitz-Coy and W. E. Dixon (2008). *Adaptive Satellite Attitude Control in the Presence of Inertia and CMG Gimbal Friction Uncertainties*. *Journal of the Astronautical Sciences* 56(1), 121–134.

- Madureira, L., A. Sousa, J. Braga, P. Calado, P. Dias, R. Martins, J. Pinto and J. Sousa (2013). The Light Autonomous Underwater Vehicle: Evolutions and Networking (2013). In: *Proceedings of 2013 MTS/IEEE OCEANS*. Bergen, Norway, 10–14 June 2013.
- Matsumoto, K. and K. Suemitsu (1980). The Prediction of Manoeuvring Performances by Captive Model Tests. *Journal of the Kansai Society of Naval Architects*, No. 176.
- McCord, M. and S. Smith (1995). Beneficial Voyage Characteristics for Routing through Dynamic Currents. *Transportation Research Record* 1511, 19–25.
- McGee, T. G., S. Spry and J. K. Hedrick (2006). Optimal Path Planning in a Constant Wind with a Bounded Turning Rate. In: *Proceedings AIAA Conference on Guidance, Navigation and Control*. Ketstone, CO. pp. 4261–4266.
- McGookin, E. W., D. J. Murray-Smith, Y. Lin and T. I. Fossen (2000a). Experimental Results from Supply Ship Autopilot Optimisation Using Genetic Algorithms. *Transactions of the Institute of Measurement and Control* TIMC-22(2), 141–178.
- McGookin, E. W., D. J. Murray-Smith, Y. Lin and T. I. Fossen (2000b). Ship Steering Control System Optimisation Using Genetic Algorithms. *Journal of Control Engineering Practise* CEP-8, 429–443.
- Mahony, R., T. Hamel and J.M. Pflimlin (2008). Nonlinear Complementary Filters on the Special Orthogonal Group. *IEEE Transactions on Automatic Control* TAC-53(5), 1203–1218.
- Matrosov, V. M. (1962). On the Stability of Motion. *Prikl. Mat. Meh.* PMM-26, 885–895.
- Maybeck, P. S. (1979). *Stochastic Models, Estimation and Control*. Academic Press. New York, NY.
- Meirovitch, L. (1990). *Dynamics and Control of Structures*. Wiley Interscience. New York, NY.
- Meirovitch, L. and M. K. Kwak (1989). State Equations for a Spacecraft with Flexible Appendages in Terms of Quasi-Coordinates. *Applied Mechanics Reviews* 42(11), 161–170.
- Micaelli, A. and C. Samson (1993). Trajectory Tracking for Unicycle-Type and Two-Steering-Wheels Mobile Robots. Internal Report 2097. INRIA. Sophia-Antipolis, France.
- Minorsky, N. (1922). Directional Stability of Automatic Steered Bodies. *Journal of the American Society of Naval Engineers* 34(2), 280–309.
- Morgan, J. M. (Ed.) (1978). *Dynamic Positioning of Offshore Vessels*. Petroleum, Tulsa, OK.

- Fossen, T. I. and T. Perez (2004). Marine Systems Simulator (MSS). <<https://github.com/cybergalactic/MSS>>.
- Munk, T. and M. Blanke (1987). Simple Command of a Complex Ship. In: *Proceedings of the 8th Ship Control Systems Symposium*. The Hague, Netherlands.
- Myring, D. F. (1976). A Theoretical Study of Body Drag in Subcritical Axisymmetric Flow. *Aeronautical Quarterly*, 27(3), pp. 186–94.
- Nakamura, Y. and H. Hanafusa (1986). Inverse Kinematic Solutions with Singularity Robustness for Robot Manipulator Control. *Journal of Dynamic Systems, Measurements and Control* 108(3), 163–171.
- Narendra, K. S. and A. M. Annaswamy (1989). *Stable Adaptive Systems*. Prentice Hall Inc. Boston, MA.
- NASA (2013). Mission Planning and Analysis Division. Euler Angles, Quaternions, and Transformation Matrices. NASA. Retrieved 12 January 2013.
- Nelson, R. C. (1998). *Flight Stability and Automatic Control*. McGraw-Hill Int.
- Neumann, G. (1952). *On Wind-Generated Ocean Waves with Special Reference to the Problem of Wave Forecasting*. New York University, College of Engineering Research Division, Department of Meteorology and Oceanography. Prepared for the Naval Res.
- Newman, J. N. (1977). *Marine Hydrodynamics*. MIT Press. Cambridge, MA.
- Nocedal, J. and S. J. Wright (1999). *Numerical Optimization*. Springer-Verlag, New York, NY.
- Nomoto, K., T. Taguchi, K. Honda and S. Hirano (1957). On the Steering Qualities of Ships. Technical Report. International Shipbuilding Progress, Vol. 4.
- Norrbin, N. H. (1963). On the Design and Analyses of the Zig-Zag Test on Base of Quasi Linear Frequency Response. Technical Report B 104-3. The Swedish State Shipbuilding Experimental Tank (SSPA). Gothenburg, Sweden.
- Norrbin, N. H. (1965). Zig-Zag Provets Teknik och Analys. Technical Report 12. The Swedish State Shipbuilding Experimental Tank (SSPA). Gothenburg, Sweden (in Swedish).
- Norrbin, N. H. (1970). Theory and Observation on the Use of a Mathematical Model for Ship Maneuvering in Deep and Confined Waters. In: *Proceedings of the 8th Symposium on Naval Hydrodynamics*. Pasadena, CA.
- Norrbin, N. H. (1972). On the Added Resistance due to Steering on a Straight Course. In: *Proceedings of the 13th ITTC*. Berlin, Hamburg, Germany.
- Norsok Standard (1999). Actions and Actions Effects Rev. 1.0. N-003.

- OCIMF (1977). Prediction of Wind and Current Loads on VLCCs. Oil Companies International Marine Forum, London, pp. 1–77.
- Oda, H. *et al.* (1992). Rudder Roll Stabilization Control System through Multivariable Auto Regressive Model. In: *Proceedings of IFAC Workshop on Control Applications in Marine Systems (CAMS'92)*. Genova, Italy. pp. 113–127.
- Oda, H., K. Ohtsu and T. Hotta (1996). Statistical Analysis and Design of a Rudder-Roll Stabilization System. *Control Engineering Practice* CEP-4(3), 351–358.
- Oda, H., K. Igarashi and K. Ohtsu (1997). Simulation Study and Full-Scale Experiment of Rudder-Roll Stabilization Systems. In: *Proceedings of the 11th Ship Control Systems Symposium*. Southampton, UK. pp. 299–313.
- Ogilvie, T. F. (1964). Recent Progress Towards the Understanding and Prediction of Ship Motions. In: *Proceedings of the 5th Symposium on Naval Hydrodynamics*. pp. 3–79.
- O'Hanlon, J. F. and M. E. McCauley (1974). Motion Sickness Incidence as a Function of Vertical Sinusoidal Motion. *Aerospace Medicine* AM-45(4), 366–369.
- Ortega, R. (1991). Passivity Properties for Stabilization of Cascaded Nonlinear Systems. *Automatica* AUT-27, 423–424.
- Ortega, R., A. Loria, P. J. Nicklasson and H. Sira-Ramirez (1998). *Passivity-Based Control of Euler–Lagrange Systems: Mechanical, Electrical and Electromechanical Applications*. Springer Verlag.
- Padadakis, N. A. and A. N. Perakis (1990). Deterministic Minimal Time Vessel Routing. *Operations Research* OR-38(3), 416–438.
- Panteley, E. and A. Loria (1998). On Global Uniform Asymtotic Stability of Nonlinear Time-Varying Noautonomous Systems in Cascade. *System Control Letters* SCL-33(2), 131–138.
- Papoulias, F. A. (1991). Bifurcation analysis of line of sight vehicle guidance using sliding modes. *International Journal of Bifurcation and Chaos* 1(4), 849–865.
- Parkinson, B. W. and Spilker, J. J. (Eds) (1995). *Global Positioning System: Theory and Applications*. American Institute of Aeronautics and Astronautics Inc. Washington D. C.
- Parks, P. C. (1966). Lyapunov Redesign of Model Reference Adaptive Control Systems. *IEEE Transactions on Automatic Control* TAC-11, 362–367.
- Perez, T. (2005). *Ship Motion Control: Course Keeping and Roll Reduction using Rudder and Fins*. Advances in Industrial Control Series. Springer-Verlag, London, UK.
- Perez, T. and T. I. Fossen (2007). Kinematic Models for Seakeeping and Manoeuvring of Marine Vessels. *Modeling, Identification and Control* MIC-28(1), 19–30. Open source, <http://www.mic-journal.no>.

- Perez, T. and T. I. Fossen (2008). Time- vs. Frequency-domain Identification of Parametric Radiation Force Models for Marine Structures at Zero Speed. *Modeling, Identification and Control* MIC-29(1), 1–19. Open source, <http://www.mic-journal.no>.
- Perez, T. and T. I. Fossen (2009). A Matlab Toolbox for Parametric Identification of Radiation-Force Models of Ships and Offshore Structures. *Modeling, Identification and Control* MIC-30(1), 1–15. Open source, <http://www.mic-journal.no>.
- Perez, T. and T. I. Fossen (2011). Practical Aspects of Frequency-Domain Identification of Dynamic Models of Marine Structures from Hydrodynamic Data. *IEEE Journal of Oceanic Engineering*.
- Perez, T. and P. D. Steinmann (2007). Modelling and Performance of an Active Heave Compensator for Offshore Operations. In: *Proceedings of the IFAC Conference on Control Applications in Marine Systems CAMS'09*. Bol, Croatia. pp. 30–36.
- Perez, T. and P. D. Steinmann (2009). Analysis of Ship Roll Gyrostabiliser Control. In: *Proceedings of the 8th IFAC International Conference on Manoeuvring and Control of Marine Craft MCMC'09*. Guaruja (SP), Brazil. pp. 30–36.
- Phillips, O. M. (1958). The Equilibrium Range in the Spectrum of Wind Generated Waves. *Journal of Fluid Mechanics* JFM-4(4), 426–434.
- Pierson, W. J. and L. Moskowitz (1963). A Proposed Spectral Form for Fully Developed Wind Seas Based on the Similarity Theory of S. A. Kitaigorodsku. U.S. Naval Oceanographic Office Contract 62306-1042.
- Pinkster, J. (1971). Dynamic Positioning of Vessels at Sea. International Centre for Mechanical Structures, Udine, Italy.
- Pinkster, J. A. and U. Nienhuis (1986). Dynamic Positioning of Large Tankers at Sea. In: *Proceedings of the Offshore Technology Conference (OTC'86)*. Houston, TX.
- Price, W. G. and R. E. D. Bishop (1974). *Probabilistic Theory of Ship Dynamics*. Chapman and Hall. London.
- Reid, R. E., A. K. Tugcu and B. C. Mears (1984). The Use of Wave Filter Design in Kalman Filter State Estimation of the Automatic Steering Problem of a Tanker in a Seaway. *IEEE Transactions on Automatic Control* TAC-29(7), 577–584.
- REMUS (2019). Woods Hole Oceanographic Institution <<http://www.whoi.edu/>>. Retrieved 12 June 2019.
- Rios-Neto, A. and J. J Da Cruz (1985). A Stochastic Rudder Control Law for Ship Path-Following Autopilots, *Automatica* 21(4), 371–384.
- Roberts, G. N. (1992). Ship Roll Damping Using Rudder and Stabilizing Fins. In: *Proceedings of the IFAC Workshop on Control Applications in Marine Systems (CAMS'92)*. Genova, Italy. pp. 129–138.

- Roberts, G. N. (1993). A Method to Determine the Applicability of Rudder Roll Stabilization for Ships. In: *Proceedings of the 12th IFAC World Congress*. pp. 1009–1012.
- Roberts, G. N. and S. W. Braham (1990). Warship Roll Stabilization Using Integrated Rudder and Fins. In: *9th International Ship Control Systems Symposium (SCSS'90)*. Bethesda, MD. pp. 1.234–1.248.
- Robertson, A. and R. Johansson (1998). Comments on “Nonlinear Output Feedback Control of Dynamically Positioned Ships Using Vectorial Observer Backstepping”. *IEEE Transactions on Control Systems Technology* TCST-6(3), 439–441.
- Ross, A. (2008). Nonlinear Manoeuvring Models for Ships: a Lagrangian Approach. PhD thesis. Department of Engineering Cybernetics, Norwegian University of Science and Technology.
- Ross, A. and T. I. Fossen (2005). Identification of Frequency-Dependent Viscous Damping. In: *Proceedings of OCEANS'05 MTS/IEEE*. Washington D.C.
- Ross, A., T. Perez and T. I. Fossen (2006). Clarification of the Low-Frequency Modelling Concept for Marine Craft. In: *Proceedings of MCMC'06*. Lisbon.
- Routh, E. J. (1877). *A Treatise on The Stability on Motion*. Macmillan. London, UK.
- Saberi, A., P. V. Kokotovic and H. J. Sussmann (1990). Global Stabilization of Partially Linear Composite Systems. *SIAM J. Control Opt.* SJCO-28, 1491–1503.
- Sælid, S. and N. A. Jenssen (1983). Adaptive Ship Autopilot with Wave Filter. *Modeling, Identification and Control* MIC-4(1), 33–46.
- Sælid, S., N. A. Jenssen and J. G. Balchen (1983). Design and Analysis of a Dynamic Positioning System Based on Kalman Filtering and Optimal Control. *IEEE Transactions on Automatic Control* TAC-28(3), 331–339.
- Sagatun, S. I. and T.I. Fossen (1991). Lagrangian Formulation of Underwater Vehicles’ Dynamics. In: *Proceedings of the IEEE International Conference on Systems, Man and Cybernetics*. Charlottesville, VA. pp. 1029–1034.
- Sagatun, S. I., T. I. Fossen and K.-P. Lindegaard (2001). Inertance Control of Underwater Installations. In: *Proceedings of the 5th IFAC Conference on Control Applications in Marine Systems CAMS'2001*. Glasgow, UK.
- Salcudean, S. (1991). A Globally Convergent Angular Velocity Observer for Rigid Body Motion. *IEEE Transaction on Automatic Control* TAC-36(12), 1493–1497.
- Samson, C. (1992). Path Following and Time-Varying Feedback Stabilization of a Wheeled Mobile Robot. In: *Proceedings of ICARV*. pp. RO–13.1.
- Sargent, J. S. and P. N. Cowgill (1976). Design Considerations for Dynamically Positioned Utility Vessels. In: *Proceedings of the 8th Offshore Technology Conference*. Dallas, TX.

- Sarpkaya, T. (1981). *Mechanics of Wave Forces on Offshore Structures*. Van Nostrand Reinhold Company. New York, NY.
- Savage, P. G. (1990). Strapdown Inertial Navigation. Lecture Notes. Strapdown Associates Inc., Minnetonka, MN.
- Scheuer, A. and C. Laugier (1998). Planning Sub-Optimal and Continuous-Curvature Paths for Car-Like Robots. In: *Proceedings IEEE-RSJ International Conference on Intelligent Robots and Systems*.
- Schlick, O. (1904). Gyroscopic Effects of Flying Weels on Board Ships. Transactions of The Institution of Naval Architects INA, 1904.
- Sciavicco, L. and B. Siciliano (1996). *Modeling and Control of Robot Manipulators*. McGraw-Hill Companies Inc.
- Sellars, F. H. and J. P. Martin (1992). Selection and Evaluation of Ship Roll Stabilization Systems. *Marine Technology* MT-29(2), 84–101.
- Sepulchre, R., M. Jankovic and P. Kokotovic (1997). *Constructive Nonlinear Control*. Springer-Verlag. Berlin.
- Serret, J. A. (1851). Sur Quelques Formules Relatives à la Théorie des Courbes À Double Courbure. *Journal de Mathématiques*. Viewed November 19, 2009, <[http://portail.mathdoc.fr/JMPA/PDF/JMPA\\_1843\\_1\\_8\\_A32\\_0.pdf](http://portail.mathdoc.fr/JMPA/PDF/JMPA_1843_1_8_A32_0.pdf)>.
- Sharif, M. T., G. N. Roberts and R. Sutton (1995). Sea-Trial Experimental Results of Fin/Rudder Roll Stabilization. *Control Engineering Practice* CEP-3(5), 703–708.
- Sharif, M. T., G. N. Roberts and R. Sutton (1996). Final Experimental Results of Full Scale Fin/Rudder Roll Stabilization Sea Trials. *Control Engineering Practice* CEP-4(3), 377–384.
- Shepperd, S. W. (1978). Quaternion from Rotation Matrix. *Journal of Guidance and Control* JGC-1(3), 223–224.
- Shneydor, N. A. (1998). *Missile Guidance and Pursuit: Kinematics, Dynamics and Control*. Horwood Publishing Ltd.
- Siouris, G. M. (2004). *Missile Guidance and Control Systems*. Springer-Verlag New York, NY.
- Skejic, R., M. Breivik, T. I. Fossen and O. M. Faltinsen (2009). Modeling and Control of Underway Replenishment Operations in Calm Water. In: *Proceedings of the IFAC MCMC'09*. Sao Paulo, Brazil.
- Skjetne, R. and T. I. Fossen (2004). On Integral Control in Backstepping: Analysis of Different Techniques. In: *Proceedings of the 2004 American Control Conference*. Boston, MA. pp. 1899–1904.

- Skjetne, R., T. I. Fossen and P. V. Kokotovic (2002). Output Maneuvering for a Class of Nonlinear Systems. In: *Proceedings of the IFAC World Congress*. Barcelona, Spain.
- Skjetne, R., T. I. Fossen and P. V. Kokotovic (2004). Robust Output Maneuvering for a Class of Nonlinear Systems. *Automatica*.
- Slotine, J. J. E. and M. D. Di Benedetto (1990). Hamiltonian Adaptive Control of Spacecraft. *IEEE Transactions on Automatic Control* AC-35(7), 848–852.
- Slotine, J. J. E. and W. Li (1987). Adaptive Manipulator Control. A Case Study.. In: *Proceedings of the 1987 IEEE Conference on Robotics and Automation*. Raleigh, North Carolina. pp. 1392–1400.
- Slotine, J. J. E. and W. Li (1991). *Applied Nonlinear Control*. Prentice-Hall International Englewood Cliffs, New Jersey 07632.
- Smith, J. E. (1977). *Mathematical Modeling and Digital Simulation for Engineers and Scientists*. John Wiley & Sons, Inc. New York, NY.
- SNAME (1950). The Society of Naval Architects and Marine Engineers. Nomenclature for Treating the Motion of a Submerged Body Through a Fluid. In: *Technical and Research Bulletin No. 1–5*.
- SNAME (1989). The Society of Naval Architects and Marine Engineers. Guide For Sea Trials. In: *Technical and Research Bulletin No. 3–47*.
- Son, K. H. and K. Nomoto (1981). On the Coupled Motion of Steering and Rolling of a High Speed Container Ship. J.S.N.A., Japan, Vol. 150, pp. 232–244 (in Japanese).
- Son, K. H. and K. Nomoto (1982). On the Coupled Motion of Steering and Rolling of a High Speed Container Ship. *Naval Architect of Ocean Engineering* 20, 73–83. From J.S.N.A., Japan, Vol. 150, 1981.
- Sontag, E. D. and H. J. Sussmann (1988). Further Comments on the Stabilizability of the Angular Velocity of a Rigid Body. *Systems and Control Letters* SCL-12, 437–442.
- Sontag, E. D. (1983). A Lyapunov-like Characterization of Asymptotic Controllability. *SIAM Journal of Control and Optimization* JCO-21, 462–471.
- Sørdalen, O. J. (1997a). Full Scale Sea Trials with Optimal Thrust Allocation. In: *Proceedings of the 4th IFAC Conference on Manoeuvring and Control of Marine Craft (MCMC'97)*. Brijuni, Croatia. pp. 150–155.
- Sørdalen, O. J. (1997b). Optimal Thrust Allocation for Marine Vessels. *Control Engineering Practice* CEP-5(9), 1223–1231.
- Sørensen, A. J. and J. P. Strand (1998). Positioning of Semi-submersible with Roll and Pitch Damping. In: *Proceedings of the IFAC Conference on Control Applications in Marine Systems (CAMS'98)*. Fukuoka, Japan. pp. 67–73.

- Sørensen, A. J. and J. P. Strand (2000). Positioning of Small-Waterplane-Area Marine Constructions with Roll and Pitch Damping. *Journal of Control Engineering in Practice* CEP-8(2), 205–213.
- Sørensen, A. J., S. I. Sagatun and T. I. Fossen (1995). The Design of a Dynamic Positioning System Using Model Based Control. In: *Proceedings of the IFAC Workshop on Control Applications in Marine Systems (CAMS'95)*. Trondheim, Norway. pp. 16–26.
- Sørensen, A. J., S. I. Sagatun and T. I. Fossen (1996). Design of a Dynamic Positioning System Using Model Based Control. *Journal of Control Engineering Practice* CEP-4(3), 359–368.
- Sørensen, A. J., T. I. Fossen and J. P. Strand (2000). Design of Controllers for Positioning of Marine Vessels. In: *The Ocean Engineering Handbook* (F. El-Hawary, Ed.). Chap. 3, pp. 207–218. CRC Press, USA.
- Sørensen, A. J., B. Leira, J. P. Strand and C. M. Larsen (2001). Optimal Setpoint Chasing in Dynamic Positioning of Deep-Water Drilling and Intervention Vessels. *International Journal of Robust and Nonlinear Control* IJRNC-11, 1187–1205.
- Spjøtvold, J. (2008). Parametric Programming in Control Theory. PhD thesis. Department of Engineering Cybernetics, Norwegian University of Science and Technology, Trondheim.
- Stevens, B. L. and F. Lewis (1992). *Aircraft Control and Simulation*. John Wiley & Sons, Ltd.
- Stoustrup, J., H. H. Niemann and M. Blanke (1995). A Multi-Objective  $H_\infty$  Solution to the Rudder Roll Damping Problem. In: *Proceedings of the IFAC Workshop on Control Applications in Marine Systems (CAMS'95)*. pp. 238–246.
- Strand, J. P. (1999). Nonlinear Position Control Systems Design for Marine Vessels. PhD thesis. Department of Engineering Cybernetics, Norwegian University of Science and Technology, Trondheim, Norway.
- Strand, J. P. and T. I. Fossen (1999). Nonlinear Passive Observer for Ships with Adaptive Wave Filtering. In: *New Directions in Nonlinear Observer Design* (H. Nijmeijer and T. I. Fossen, Eds.). Chap. I-7, pp. 113–134. Springer-Verlag, London.
- Strand, J. P. and A. J. Sørensen (2000). Marine Positioning Systems. In: *Ocean Engineering Handbook* (F. El-Hawary, Ed.). Chap. 3, pp. 163–176. CRC Press, USA.
- Strand, J. P., A. J. Sørensen and T. I. Fossen (1998). Design of Automatic Thruster Assisted Position Mooring Systems for Ships. *Modeling, Identification and Control* MIC-19(2), 61–75.
- Sun, Z., L. Zhang, G. Jin and X. Yang (2010). Analysis of Inertia Dyadic Uncertainty for Small Agile Satellite with Control Moment Gyros. In: *Proceedings of the 2010 IEEE International Conference on Mechatronics and Automation*, August 4–7, Xi'an, China.

- Söding, H. (1999). Limits of Potential Theory in Rudder Flow Predictions In: *Twenty-Second Symposium on Naval Hydrodynamics* Chapter: 10 Weinblum Lecture. , pp. 622–637. The National Academies Press, USA.
- Techy, L. and C. A. Woolsey (2009). Minimum-Time Path Planning for Unmanned Aerial Vehicles in Steady Uniform Winds. *AIAA Journal of Guidance, Control, and Dynamics* JGCD-32(6), 1736–1746.
- Techy, L. and C. A. Woolsey (2010). Planar Path Planning for Flight Vehicles in Wind with Turn Rate and Acceleration Bounds. In: *Proceedings AIAA Conference on Guidance, Navigation and Control*. Anchorage, AK.
- Thienel, J. and R. M. Sanner (2003). A Coupled Nonlinear Spacecraft Attitude Controller and Observer with an Unknown Constant Gyro Bias and Gyro Noise. *IEEE Transactions on Automatic Control* TAC-48(11), 2011–2015.
- Tinker, S. J. (1982). Identification of Submarine Dynamics from Free-Model Test. In: *Proceedings of the DRG Seminar*. Netherlands.
- Titterton, D. H. and J. L. Weston (1997). *Strapdown Inertial Navigation Technology*. IEE. London, UK.
- Thornton, B., T. Ura, Y. Nose and S. Turnock (2005). Internal Actuation of Underwater Robots Using Control Moment Gyros. In: *Proceedings Oceans 2005-Europe*. pp. 591–598.
- Thornton, B., T. Ura, Y. Nose and S. Turnock (2007). Zero-G Class Underwater Robots: Unrestricted Attitude Control Using Control Moment Gyros. *IEEE Journal of Oceanic Engineering* 32(3), 565–583.
- Thornton, B., T. Ura and Y. Nose, Y. (2008). Combined Energy Storage and Three-Axis Attitude Control of a Gyroscopically Actuated AUV. In: *Proceedings Oceans*. Quebec City, QC, Canada.
- Tøndel, P., T. A. Johansen and A. Bemporad (2003a). An algorithm for multi-parametric quadratic programming and explicit MPC solutions. *Automatica* 39, 489–497.
- Tøndel, P., T. A. Johansen and A. Bemporad (2003b). Evaluation of Piecewise Affine Control via Binary Search Tree. *Automatica* 39, 743–749.
- Torsethaugen, K. (1996). Model for a Doubly Peaked Wave Spectrum. Technical Report STF22 A96204. SINTEF, Trondheim, Norway. Prepared for Norsk Hydro.
- Triantafyllou, M. S. and A. M. Amzallag (1984). A New Generation of Underwater Unmanned Tethered Vehicles Carrying Heavy Equipment at Large Depths. Technical Report MITSG 85-30TN. MIT Sea Grant. Boston, MA.
- Triantafyllou, M. S. and F. S. Hover (2002). Maneuvering and Control of Marine Vehicles. Internet. <<http://ocw.mit.edu/13/13.49/f00/lecture-notes/>>[Accessed November 15, 2002].

- Triantafyllou, M. S., M. Bodson and M. Athans (1983). Real Time Estimation of Ship Motions Using Kalman Filtering Techniques. *IEEE Journal of Ocean Engineering* JOE-8(1), 9–20.
- Tsinias, J. (1989). Sufficient Lyapunov-Like Conditions for Stabilization. *Mathematics of Control, Signals and Systems* MCSS-2, 343–357.
- Tsourdos, A., B. White and M. Shanmugavel (2010). Cooperative Path Planning of Unmanned Aerial Vehicles. John Wiley & Sons, Ltd.
- Tzeng, C. Y. (1998a). Analysis of the Pivot Point for a Turning Ship. *Journal of Marine Science and Technology* JMST-6(1), 39–44.
- Tzeng, C. Y. (1998b). Optimal Control of a Ship for a Course-Changing Maneuver. *Journal of Optimization Theory and Applications* JOTA-97(2), 281–297.
- Utkin, V. I. (1977). Variable Structure Systems with Sliding Modes. *IEEE Transactions on Automatic Control* TAC-22(2), 212–222.
- Utkin, V. I. (1992). *Sliding Modes in Control and Optimization*. Springer-Verlag, Berlin.
- Van Amerongen, J. (1982). Adaptive Steering of Ships – A Model Reference Approach to Improved Maneuvering and Economical Course Keeping. PhD thesis. Delft University of Technology, Netherlands.
- Van Amerongen, J. (1984). Adaptive Steering of Ships – A Model Reference Approach. *Automatica* AUT-20(1), 3–14.
- Van Amerongen, J. and H. R. Van Nauta Lemke (1978). Optimum Steering of Ships with an Adaptive Autopilot. In: *Proceedings of the 5th Ship Control Systems Symposium*. Annapolis, MD.
- Van Amerongen, J. and H. R. Van Nauta Lemke (1980). Criteria for Optimum Steering of Ships. In: *Proceedings of Symposium on Ship Steering Automatic Control*. Genova, Italy.
- Van Amerongen, J. and H. R. Van Nauta Lempke (1987). Adaptive Control Aspects of a Rudder Roll Stabilization System. In: *Proceedings of the 10th IFAC World Congress*. Munich, Germany. pp. 215–219.
- Van Amerongen, J., P. G. M. Van der Klugt and J. B. M. Pieffers (1987). Rudder Roll Stabilization – Controller Design and Experimental Results. In: *Proceedings of the 8th International Ship Control Systems Symposium (SCSS'87)*. The Hague, Netherlands. pp. 1.120–1.142.
- Van Berlekom, W. B., P. Trägårdh and A. Dellhag (1974). Large Tankers – Wind Coefficients and Speed Loss Due to Wind and Sea. In: *Meeting at the Royal Institution of Naval Architects, April 25, 1974*. London. pp. 41–58.

- Van der Klugt, P. G. M. (1987). Rudder Roll Stabilization. PhD thesis. Delft University of Technology, Delft, Netherlands.
- Vik, B. (2000). Nonlinear Design and Analysis of Integrated GPS and Inertial Navigation Systems. PhD thesis. Department of Engineering Cybernetics, Norwegian University of Science and Technology. Trondheim, Norway.
- Vik, B. and T. I. Fossen (2001). Nonlinear Observer Design for Integration of GPS and Inertial Navigation Systems. In: *Proceedings of the Conference on Decision and Control (CDC'2001)*. Orlando, FL.
- Vik, B., A. Shiriaev and T. I. Fossen (1999). Nonlinear Observer Design for Integration of DGPS and INS. In: *New Directions in Nonlinear Observer Design* (H. Nijmeijer and T. I. Fossen, Eds). Chap. I-8, pp. 135–160. Springer-Verlag. London.
- Wagner, Von B. (1967). Windkräfte an Überwasserschiffen. In: *Schiff und Hafen, Heft 12, 19. Jahrgang*. pp. 894–900. (in German).
- WAMIT (2010). WAMIT User Manual. <[www.wamit.com](http://www.wamit.com)>.
- Webster, W. C. and J. Sousa (1999). Optimum Allocation for Multiple Thrusters. In: *Proceedings of the International Society of Offshore and Polar Engineers Conference (ISOPe'99)*. Brest, France.
- Wendel, K. (1956). Hydrodynamic Masses and Hydrodynamic Moments of Inertia. Technical Report. TMB Translation 260.
- Wilson, P. A. (2018). *Basic Naval Architecture. Ship Stability*. Springer Nature Switzerland AG.
- Whitcomb, L. L. and D. Yoerger. Development, Comparison, and Preliminary Experimental Validation of Nonlinear Dynamic Thruster Models. *IEEE Journal of Oceanic Engineering*, JOE-24(4), 481–494.
- Woolsey, C. A. and N. E. Leonard (2002a). Stabilizing Underwater Vehicle Motion using Internal Rotors. *Automatica* AUT-38, 2053–2062.
- Woolsey, C. A. and N. E. Leonard (2002b). Moving Mass Control for Underwater Vehicles In: *Proceedings of the American Control Conference*, Anchorage, AK, USA, May 8-10.
- World Geodetic System (1984). Its Definition and Relationships with Local Geodetic Systems. DMA TR 8350.2, 2nd ed., Defense Mapping Agency, Fairfax, VA.
- Yakubovich, V. A. (1973). A Frequency Theorem in Control Theory. *Siberian Mathematical Journal* SMJ-14(2), 384–420.
- Yang, C. and M. Blanke (1997). A Robust Roll Damping Controller. In: *Proceedings of the IFAC Conference on Manoeuvring and Control (MCMC'97)*. Croatia.

- Yang, C. and M. Blanke (1998). Rudder-Roll Damping Controller Design Using Mu Synthesis. In: *Proceedings IFAC Conference on Control Applications in Marine Systems (CAMS'98)*. pp. 127–132. Fukuoka, Japan.
- Yanushevsky, R. (2008). *Modern Missile Guidance*. CRC Press.
- Yasukawa., H. and Y. Yoshimura (2015). Introduction of MMG Standard Method for Ship Maneuvering Predictions. *Journal of Marine Science Technology*, 20:37–52.
- Yoerger, D. R. and J. J. E. Slotine (1985). Robust Trajectory Control of Underwater Vehicles. *IEEE Journal of Oceanic Engineering* JOE-10(4), 462–470.
- Yoerger, D. R., J. G. Cooke and J.- J. E. Slotine (1991). The Influence of Thruster Dynamics on Underwater Vehicle Behavior and their Incorporation into Control System Design, *IEEE Journal of Oceanic Engineering*, JOE-15(3), 167–178.
- Yoshizawa, T. (1968). *Stability Theory by Lyapunov's Second Method*. The Mathematical Society of Japan.
- Yu, Z. and J. Falnes (1995). Spate-Space Modelling of a Vertical Cylinder in Heave. *Applied Ocean Research* 17, 265–275.
- Yu, Z. and J. Falnes (1998). Spate-Space Modelling of Dynamic Systems in Ocean Engineering. *Journal of Hydrodynamics, China Ocean Press*, 1–17.
- Zhou, W. W. (1990). A New Approach for Adaptive Rudder Roll Stabilization Control. In: *9th International Ship Control Systems Symposium (SCSS'90)*. Bethesda, MD. pp. 1.115–1.125.
- Zhu, J. (1993). Exact Conversion of Earth-Centered Earth-Fixed Coordinates to Geodetic Coordinates. *AIAA Journal of Guidance, Control and Dynamics* 162(2), 389–391.
- Xua, R., G. Tanga, L. Hana and D. Xiea (2019). Trajectory Tracking Control for a CMG-Based Underwater Vehicle with Input Saturation in 3D Space. *Ocean Engineering* 173, 587–598.



DRAFT MANUSCRIPT

# **Index**

DRAFT MANUSCRIPT

# Index

- 1st-order wave forces and moments, 251
- 2nd-order modulus functions, 151
- 2nd-order modulus terms, 145
- 2nd-order wave forces and moments, 251
- 3-DOF maneuvering model, 131
- 4 DOF maneuvering model, 155
- 6-DOF equations of motion, 181
- Abkowitz's model, 152
- Adams–Bashforth's integration method, 613
- adaptive control, 175
- added mass, 107
  - definition, 108
  - energy approach, 135
  - forces and moments, 137
  - potential coefficient, 129
  - property of the system inertia matrix, 136
  - system inertia matrix, 136
- advance speed, 202
- anemometer, 246
- angle of attack, definition, 45
- angular velocity transformation, 27, 32
- Archimedes, 65
- asymptotic stability, 601
- attitude
  - dynamics, 54
- automatic pretrimming, 94
- autonomous systems, 601
- autopilot, 169
  - nondimensional models, 619
- autopilot, definition, 169, 171
- AUV, 236
  - CMG controlled, 232
- AUV, autonomous underwater vehicle, 1
- average wave period, 256
- average zero-crossings period, 256
- azimuth thruster, 215
- ballast systems, 89
  - semisubmersible, 92
- Barbălat's lemma, 606
- Beaufort number, 244, 259
- Bech's reverse spiral maneuver, 177
- Bernoulli equation, 100
- bilinear thrust, 203
- Bis system, 619
- boat, definition, 1
- BODY, body-fixed reference frame, 18
- body-fixed vector representation, 181
- Bretschneider spectrum, 257
- buoyancy, 65
  - buoyancy force
    - floating vessels, 68
    - submerged vehicle, 65
- CB, center of buoyancy, 19
- center of buoyancy (CB), 19, 65
- center of flotation (CF), 19, 76
- center of gravity (CG), 19
- centripetal forces, 59
- CF, center of flotation, 19
- CG, center of gravity, 19
- CMG, 229, 232
  - pyramid configuration, 232
- CO, body axes coordinate origin, 18
- control design model, 6
- control moment gyroscope, 229
- controllable-pitch propeller, 204
- convergence, 601
- coordinate
  - form, 20
  - free vector, 20
  - generalized, 20

- systems, 16  
 transformation matrix, 22
- Coriolis and centripetal forces  
 maneuvering, 133  
 seakeeping, 117
- Coriolis and centripetal matrix  
 definition, 59  
 property, 60, 185
- course  
 autopilot model, 172
- course angle, definition, 43
- course control, 172
- crab angle, definition, 44
- craft, 1
- cross-flow drag, 144, 149, 166
- cross-product operator, 22
- Cummins equation, 115
- current angle of attack, 166
- current coefficients  
 area-based, 167  
 DP, 163  
 relationship to cross-flow drag and surge  
 resistance, 166  
 surge damping, 145
- D'Alambert's paradox, 140
- damped least-squares, 236
- damping  
 frequency-dependent, 111  
 matrix, 141
- DC motor, 212
- degrees-of-freedom  
 model classification, 3  
 notation, 15
- density  
 air, 244
- describing function, 112
- diesel engine, 206, 208
- Dieudonné's spiral maneuver, 177
- dimensionless parameter, 620
- discretization of continuous-time systems,  
 609
- dispersion relation, 267
- displacement vessel, 2
- DP  
 linearized model, 168
- nonlinear model, 163  
 drag coefficient, 145  
 drift angle, definition, 45  
 ducted propeller, 210
- Earth rotation, 53
- ECEF, Earth-centered Earth-fixed frame, 17
- ECI, Earth-centered inertial frame, 17
- effective metacentric height, 82
- ellipsoidal height, 37
- energy dissipation, 140
- environmental forces, 241
- equations of motion  
 3 DOF, 146  
 4 DOF, 155  
 6 DOF, 181  
 classical model, 6  
 DP, 163  
 expressed in BODY, 181  
 expressed in NED, 183  
 lateral, 189  
 longitudinal, 188  
 maneuvering, 127, 146  
 nondimensional, 619  
 nonlinear, 181  
 rigid-body, 58  
 seakeeping, 114  
 vectorial representation, 12
- equations of relative motion, 242
- equilibrium heading, 103
- equivalent linearization, 112
- Euler  
 angles, 24  
 backward, 612  
 equation, 99  
 forward, 611  
 parameters, 30
- Euler angles from a unit quaternion, 35
- Euler's  
 axioms, 52  
 integration method, 611  
 theorem on rotation, 23
- fixed-blade propeller, 201  
 fixed-pitch propeller, 201

- flat Earth navigation, 18  
flow  
  axes, 42  
  control, 91  
  irrotational, 99  
  potential, 99  
fluid  
  kinetic energy, 136  
  memory effects, 97, 114, 122  
  viscous, 99  
force RAO, 270  
forced oscillations, 107  
forward shift operator, 609  
forward speed model, 154  
free-surface  
  correction, 82  
  effect, 82  
frequency  
  encounter, 268  
frequency-domain model, 106  
frequency-independent  
  model, 131  
  potential coefficients, 129  
frictional forces, 140  
Froude number, definition, 2  
FSC, free-surface correction, 82  
gain scheduling, 175  
GAS, 601  
Gauss-Markov process, 281  
generalized  
  coordinates, 134  
  eigenvalue problem, 78  
generalized coordinates, 20  
geodetic latitude, 37  
GES, 601  
gimbal, 232  
gliders, 236  
global exponential stability, 605  
GM, metacenter height, 73  
governor, 207, 209–211, 213  
gravitational force  
  floating vessels, 68  
  submerged vehicle, 65  
gyroscope, 229  
gyrostabilizer, 230  
harmonic oscillator, 83  
heading  
  autopilot model, 173  
heading angle, definition, 43  
heading control, 173  
heave  
  period, 80  
heave, definition, 15  
Helmholtz-Kirchhoff plate, 246  
Heun's integration method, 613  
Hoerner's curve, 145  
hull efficiency, 202  
Huygens–Steiner theorem, 57  
hydrodynamic  
  code, 100  
  Coriolis and centripetal matrix, property, 138  
  damping, 140  
  derivatives, 136  
  forces, 145  
  system inertia matrix, property, 136  
hydrodynamics  
  computation programs, 100  
  potential theory, 98  
hydrostatics, 65  
  box-shaped vessels, 70  
  floating vessels, 68  
  semisubmersibles, 68  
  ships, 68  
  submerged vehicles, 65  
IKEDA damping, 112  
incompressible fluid, 98  
inertia dyadic, definition, 55  
internal actuators, 236  
internal rotor, 232  
irrotational  
  flow, 99  
  ocean currents, 121  
irrotational ocean currents, 62, 127  
ITTC resistance, 142  
JONSWAP, Joint North Sea Wave Project spectrum, 260  
kinematic viscosity, 140

- kinematics, 15  
 kinetics, 15, 51  
 Kirchhoff's equations, 60, 135  
 Kort nozzle, 210  
 KrasovskiiâŠLaSalleâŽs theorem, 604
- Lagrange equations, 134  
 Lamb's k-factors, 196  
 Laplace equation, 99  
 LaSalle–Yoshizawa's theorem, 606  
 lateral model, 187  
 latitude, definition, 36  
 LCF, 71  
 LCF, longitudinal center of flotation, 19  
 lift and drag, 140  
 linear velocity transformation, 24, 31  
 linear viscous damping, 141  
 linearized  
     Coriolis and centripetal forces, 63  
     DP model, 168  
     equations of motion, 63  
     maneuvering model, 153  
 load condition, 75  
 long-crested irregular sea, 267  
 longitude, definition, 36  
 longitudinal model, 187  
 Lyapunov's direct method, 603
- maneuvering  
     coefficients, 145  
     equations, 145  
     kinematics, 102  
     theory, 8, 97, 127  
     zero-frequency model, 131
- maneuvering model  
     2nd-order modulus, 149  
     3 DOF, 146  
     4 DOF, 155  
     including ocean currents, 283  
     ITTC and cross-flow drag, 149  
     linearized, 153  
     odd functions, 151  
     potential theory representation, 154
- marine craft, 1  
 mariner class vessel  
     Nomoto models, 176
- pivot point, 180  
 mass  
     moving, 236  
 mean wave drift force, 114  
 mechanical efficiency, 202  
 metacenter height  
     lateral, 73  
     transverse, 73  
 metacenter stability, definition, 74  
 metacenter, definition, 68  
 modal  
     frequency, 256  
     period, 256  
 modal analysis, 77  
 model representations, 8  
 model transformation, 615  
 models, 5  
 modified Pierson–Moskowitz spectrum, 259  
 moments of inertia, 55  
 Moore–Penrose pseudo-inverse, 92  
 Moore–Penrose pseudoinverse, 184  
 Morison's equation, 140  
 Morriss's formula, 74  
 motion  
     RAO, 272  
 motor control, 212  
 moving mass, 236  
 Munk moment, 155  
 Munro-Smith formula, 73
- natural  
     frequency, 76, 132  
     period, 76
- Navier-Stokes equation, 99  
 NED, North-East-Down reference frame, 18  
 Neumann spectrum, 257  
 neutrally buoyant, 67  
 Newton's second law, 52  
 Newton–Euler formulation, 52  
 Nomoto model  
     1st-order, 175  
     2nd-order, 175  
     dimensionless, 621  
     nonlinear extension, 177  
 nonautonomous systems, 601

- nondimensional equations of motion, 619
- nondimensionalization, 619
- numerical
  - differentiation, 614
  - integration, 611
- observer
  - design model, 6
- ocean currents, 242
  - 2-D, 282
  - 3-D, 282
  - direction, 281
  - equations of relative motion, 279
  - irrotational, 280
  - models, 279
  - speed, 281
  - wind generated, 279
- odd functions, 151
- open-water advance coefficient, 201
- orthogonal matrix, 22
- panel methods, 101
- parallel-axis theorem, 57
- peak period, 255
- period
  - peak, 255
  - wave, 255
  - zero-crossing, 255
- perturbation coordinates, 103
- pitch
  - definition, 15
  - period, 81, 189
- pitch propeller, 204
- pivot point, definition, 179
- planning vessel, 3
- PM spectrum, 258
- PMM, 10, 153
- potential
  - coefficients, 108, 129
  - damping, 107, 129, 140
  - theory, 98
- potential coefficients
  - properties, 120
  - speed-dependent, 119
  - zero-speed, 118
- precession, 230
- pretrimming, 91
- prime mover dynamics, 206, 208
- Prime system, 619
- principal rotation, 24
- principle of superposition, 241
- products of inertia, 55
- projected area, 243
- propeller, 201, 210
  - propeller characteristics, 201, 203
  - propeller control systems, 210
  - propeller thrust coefficient, 202
  - propeller thrust efficiency, 202
  - propeller torque coefficient, 202
- quadratic
  - drag, 140
- quaternions
  - definition, 30
  - from Euler angles, 34
  - from rotation matrix, 34
- radiation force, 107
- radius of gyration, 80
- RAO, 113
  - force, 254, 269
  - motion, 254, 272
- reference frame
  - body-fixed, 18
  - Earth-centered Earth-fixed, 17
  - Earth-centered inertial, 17
  - flow axes, 42
  - North-East-Down, 18
  - seakeeping, 102
- relative
  - speed, 44
  - velocity, 242
- relative rotative efficiency, 202
- resonance, 84
- resonant frequency, 84
- response amplitude operator, 113
- response amplitude operator (RAO), 254
- restoring
  - forces, 65
  - matrix, 77
- retardation functions, 10, 106, 115
- Reynolds number, 140, 143

- rig, 92  
 rigid-body kinetics  
     maneuvering, 128  
     Newton–Euler, 52  
     seakeeping, 106  
 roll  
     definition, 15  
     period, 81, 190  
 roll and sway-yaw subsystems, 157  
 roll damping, 230  
 rotation matrix, 22, 34  
 rotation matrix differential equation, 28  
 rotational motion, 54, 57  
 ROV, remotely operated vehicle, 1  
 rudder-roll damping, 157  
 Runge–Kutta integration methods, 613  
 screw propeller, 201  
 sea state  
     codes, 258  
     definition, 255  
 seakeeping  
     coordinates, 103  
     equations of motion, 113  
     kinematics, 102  
     theory, 10, 97  
 seakeeping analysis, 75  
 semi-displacement vessel, 2  
 semi-empirical methods, 102  
 semisubmersible  
     ballast control, 93  
 service speed, 619  
 ship  
     definition, 1  
 ship propulsion, 206  
 ship roll gyrostabilizer, 230  
 ShipX, 101  
 short-crested irregular sea, 268  
 sideslip angle, definition, 45  
 significant wave height, 255, 257  
 simple rotation, definition, 23  
 simulation model, 5  
 singularity, 28, 236  
 skew-symmetry, 22  
 skin friction, 140  
 slack tank, 82  
 SNAME notation, 15  
 Son and Nomoto’s model, 161  
 special orthogonal group, 22  
 spectrum  
     Bretschneider, 257  
     JONSWAP, 260  
     modified Pierson–Moskowitz, 259  
     Neumann, 257  
     Pierson–Moskowitz, 258  
     Torsethaugen, 261  
 spreading function, 268  
 SS(3), set of skew-symmetric matrices, 23  
 stability  
     axes, 47  
 steering and roll, 161  
 steering machine, 221  
 strip theory, 100  
 submarine  
     definition, 1  
     model, 187  
 submerged vehicles  
     hydrostatics, 65  
     model, 187  
 superposition, 241  
 surface vessels  
     hydrostatics, 68  
 surge  
     damping, 142  
     definition, 15  
     resistance, 142, 149, 166  
 sway, definition, 15  
 symmetry properties of inertia, 186  
 system inertia matrix  
     property, 185  
 system inertia matrix, definition, 58  
 system transformation matrix, 615  
 system transformation matrix, definition,  
     616  
 tanks, 91  
 Taylor series, 151  
 thrust deduction, 202  
 thrust devices, 201  
 thruster open-water efficiency, 202  
 time differentiation, moving reference frame,  
     53

- Torsethaugen spectrum, 261  
 translational motion, 53, 56  
 tunnel thruster, 214
- underwater vehicle  
     added mass and damping, 132  
     definition, 1  
     lateral model, 189  
     longitudinal model, 188  
     restoring forces, 65
- unified  
     model, 121  
     theory, 11
- unit quaternions, 30  
     normalization, 33
- USV, 236
- UVU, unmanned underwater vehicle, 1
- vectorial mechanics, 51
- velocity transformation  
     angular, 27, 32  
     linear, 24, 31
- VERES, 101
- vessel, definition, 1
- viscous  
     damping, 107, 140  
     damping matrix, 111
- volume of displaced fluid, 65
- WAMIT, 101, 270
- water tanks, 91
- waterplane area coefficient, 74
- waterplane area moment, 71
- wave  
     1st-order forces and moments, 251  
     2nd-order forces and moments, 251  
     force, 271  
     force RAO, 270  
     models, 256  
     period, 255  
     response, 277  
         state-space model, 278
- wave amplitude response model, 267
- wave drift damping, 140
- wave excitation force, 114
- wave spectrum
- Bretschneider, 257  
 JONSWAP, 260  
 maximum value, 259  
 modified Pierson–Moskowitz, 259  
 Neumann, 257  
 Torsethaugen, 261
- wave spectrum moments  
     moments, 255
- wave-frequency motion, 251, 277
- wave-induced forces, 241
- weight, 65, 66
- WF, wave-frequency motion, 251
- WGS-84, World Geodetic System, 18
- wind  
     angle of attack, 243  
     axes, 47  
     coefficients, 243  
     container ship, 246  
     direction, 243  
     forces on marine craft at rest, 243  
     forces on moving craft, 245  
     large tankers, 250  
     merchant ships, 248  
     models, 242  
     moored ships and floating structures, 251  
     offshore vessels, 246  
     relative angle of attack, 245  
     relative speed, 245  
     speed, 243  
     tunnel, 246  
     wind-generated waves, 256
- yaw, definition, 15
- zero-frequency model, definition, 131  
 zero-speed model, 121